



**TECHNICAL REPORT 0-7042-1**  
TXDOT PROJECT NUMBER 0-7042

# Larger-Diameter Shear Studs for Composite Steel Bridges

Xianjue Deng  
Lu Wan  
Yucel Alp  
Michael Engelhardt  
Todd Helwig  
Eric Williamson  
Ioannis Koutromanos  
Jeonghwa Lee

October 2023  
Published December 2023

<https://library.ctr.utexas.edu/ctr-publications/0-7042-1.pdf>



Technical Report Documentation Page

1. Report No. FHWA/TX-24/0-7042-1	2. Government Accession No.	3. Recipient's Catalog No.
4. Title and Subtitle Larger-Diameter Shear Studs for Composite Steel Bridges		5. Report Date October 31, 2023
7. Author(s) Xianjue Deng, Lu Wan, Yucel Alp, Michael Engelhardt, Todd Helwig, Eric Williamson, Ioannis Koutromanos, Jeonghwa Lee		6. Performing Organization Code 8. Performing Organization Report No. 0-7042-1
9. Performing Organization Name and Address Center for Transportation Research The University of Texas at Austin 3925 W. Braker Lane, 4 <sup>th</sup> Floor Austin, TX 78759		10. Work Unit No. (TR AIS) 11. Contract or Grant No. 0-7042
12. Sponsoring Agency Name and Address Texas Department of Transportation Research and Technology Implementation Division 125 E. 11 <sup>th</sup> Street Austin, TX 78701		13. Type of Report and Period Covered Technical Report January 2020 – October 2023 14. Sponsoring Agency Code
15. Supplementary Notes Project performed in cooperation with the Texas Department of Transportation and the Federal Highway Administration.		
16. Abstract <p>Composite steel bridge girders are typically constructed using 7/8" diameter shear studs. A large number of shear studs is often needed to satisfy AASHTO shear stud fatigue and strength requirements. Using a larger-diameter shear stud can significantly reduce the required number of shear studs which in turn can improve construction worker safety, expedite the girder fabrication process, and facilitate the use of partial depth precast concrete deck panels (PCPs). The overall objective of this research project was to evaluate the feasibility of shear stud diameters greater than 7/8" for composite steel bridge construction. The research initially considered both 1-1/8" and 1-1/4" diameter shear studs, but the majority of testing and finite element analysis ultimately focused on 1-1/8" studs. The research considered the use of 1-1/8" studs in two types of bridge deck systems. The first was a deck constructed using 8.5" full-depth cast-in place (CIP) concrete. The second was a deck constructed using 4" thick precast concrete deck panels (PCPs) with a 4.5" CIP concrete topping.</p> <p>The research included preliminary design studies to quantify the reduction in the number of shear studs that can be achieved with larger-diameter shear studs. The reduction in the number of shear studs was found to be significant when larger-diameter shear studs are used. Compared to 7/8" shear studs, the reduction in the number of studs was found to be on the order of 40%, and 50% for 1-1/8" and 1-1/4" diameter shear studs, respectively.</p> <p>In an extensive investigation of stud welding, it was found that larger-diameter shear studs can be welded with consistent good quality using commercially available stud welding equipment. However, the welding of 1-1/4" studs was quite sensitive to the selected welding parameters and base metal conditions, and conducting a bend test on 1-1/4" studs was much more difficult than for 1-1/8" studs. Based on the results of the stud welding investigations, the decision was made to proceed with the use of 1-1/8" studs for the remainder of this research project.</p> <p>Push-out tests were conducted to evaluate the static and fatigue performance of 1-1/8" studs. The results of the static push-out tests showed excellent performance of 1-1/8" shear studs. The ultimate strength of 1-1/8" shear studs exceeded the stud ultimate strength requirements of both the 9<sup>th</sup> Ed. AASHTO LRFD Bridge Design Specifications and the proposed 10<sup>th</sup> Ed. AASHTO LRFD Bridge Design Specifications. For decks with PCPs,</p>		



the ultimate strength of both 7/8" and 1-1/8" shear studs was less than the corresponding specimens constructed with full-depth CIP decks. In the fatigue push-out tests, all specimens exhibited fatigue lives that exceeded the requirements of both the 9<sup>th</sup> Ed. AASHTO and the proposed 10<sup>th</sup> Ed. AASHTO S-N curves.

Parametric finite element studies were conducted to extend information developed in the static push-out test program. A focus of these studies was the behavior of 7/8" and 1-1/8" studs in bridge decks constructed using PCPs. Based on these studies, recommendations were developed for minimum penetration distance of the stud into the bridge deck and minimum clear distance between the stud and the PCP needed to achieve stud strength that satisfies the 9<sup>th</sup> Ed. AASHTO and the proposed 10<sup>th</sup> Ed. AASHTO.

Two large-scale composite beams were constructed in the laboratory and tested to failure to evaluate the performance of bridge girders constructed using 1-1/8" shear studs. The large-scale beam tests showed satisfactory strength and ductility of 1-1/8" shear studs.

The results of this research project demonstrated that 1-1/8" shear studs can be safely used in composite steel bridges in Texas. Design recommendations are included in this report.

17. Key Words composite steel girders, shear studs, stud welding, partial-depth precast concrete deck panels		18. Distribution Statement No restrictions. This document is available to the public through the National Technical Information Service, Alexandria, Virginia 22312; www.ntis.gov.	
19. Security Classif. (of report) Unclassified	20. Security Classif. (of this page) Unclassified	21. No. of pages: 408	22. Price

Form DOT F 1700.7 (8-72) Reproduction of completed page authorized



**THE UNIVERSITY OF TEXAS AT AUSTIN  
CENTER FOR TRANSPORTATION RESEARCH**

## **Larger-Diameter Shear Studs for Composite Steel Bridges**

Xianjue Deng  
Lu Wan  
Yucel Alp  
Michael Engelhardt  
Todd Helwig  
Eric Williamson  
Ioannis Koutromanos  
Jeonghwa Lee

---

CTR Technical Report:	0-7042-1
Report Date:	October 31, 2023
Project:	0-7042
Project Title:	Use of Larger Diameter Shear Studs for Composite Steel Bridges
Sponsoring Agency:	Texas Department of Transportation
Performing Agency:	Center for Transportation Research at The University of Texas at Austin

Project performed in cooperation with the Texas Department of Transportation and the Federal Highway Administration.

Center for Transportation Research  
The University of Texas at Austin  
3925 W. Braker Lane, 4<sup>th</sup> floor  
Austin, TX 78759

<http://ctr.utexas.edu/>

## **Disclaimers**

---

**Author's Disclaimer:** The contents of this report reflect the views of the authors, who are responsible for the facts and the accuracy of the data presented herein. The contents do not necessarily reflect the official view or policies of the Federal Highway Administration or the Texas Department of Transportation (TxDOT). This report does not constitute a standard, specification, or regulation.

**Patent Disclaimer:** There was no invention or discovery conceived or first actually reduced to practice in the course of or under this contract, including any art, method, process, machine manufacture, design or composition of matter, or any new useful improvement thereof, or any variety of plant, which is or may be patentable under the patent laws of the United States of America or any foreign country.

## **Engineering Disclaimer**

---

NOT INTENDED FOR CONSTRUCTION, BIDDING, OR PERMIT PURPOSES.

Project Engineer: Michael D. Engelhardt  
Professional Engineer License State and Number: Texas No. 88934  
P.E. Designation: Research Supervisor

## **Acknowledgments**

---

The authors express appreciation to the TxDOT Project Manager Jadé Adediwura. The authors gratefully acknowledge the advice, guidance and support of the following TxDOT Project Monitoring Committee members: Jamie Farris, Doug Beer, Igor Kafando, Paul Rollins, Addisu Tilahun, and Greg Turko. The authors also gratefully acknowledge the following individuals for their advice and support: Clark Champney and Ian Houston of Nelson Stud Welding, John Holt of Modjeski and Masters, Ronnie Medlock of High Steel Structures, Dennis Noernberg of W&W-Afco Steel, Randy Rogers of Williams Brothers Construction, and Karl Frank, Consultant and UT Austin Professor Emeritus.

## Table of Contents

---

Chapter 1. Introduction .....	1
1.1. Background .....	1
1.2. Research Goal and Objectives .....	3
1.3. Project Scope and Report Organization .....	4
Chapter 2. Background and Literature Review.....	7
2.1. Introduction.....	7
2.2. Review of Shear Stud Requirements in Bridge Standards.....	7
2.3. Shear Stud Test Methods .....	10
2.3.1. Push-out Tests.....	10
2.3.2. Beam Tests.....	12
2.4. Shear Stud Behavior under Static Loading.....	13
2.4.1. Load- Slip Curves and Stud Failure Modes .....	14
2.4.2. Development of Equations to Predict Shear Stud Strength .....	15
2.4.3. Ductility of Shear Studs .....	20
2.4.4. Tests on Larger-diameter Shear Studs .....	24
2.5. Larger-diameter Shear Studs under Fatigue Loading .....	31
2.6. Bridges Constructed with Larger-diameter Shear Studs.....	34
2.6.1. Gering Bridge.....	34
2.6.2. Skyline Bridge .....	35
2.6.3. Current Status of Bridges.....	35
2.7. Summary .....	35
Chapter 3. Preliminary Design Studies.....	38
3.1. Introduction.....	38
3.2. Description of the Bridges .....	38
3.2.1. Guadalupe River Bridge .....	39
3.2.2. US 83 Overpass Bridge.....	40
3.2.3. IH 610 Tub Girder Bridge.....	40
3.2.4. Comment on Shear Stud Length.....	41
3.3. Shear Stud Design based on 9 <sup>th</sup> Ed. AASHTO.....	42
3.4. Evaluation of the Original Designs.....	49
3.4.1. Guadalupe River Bridge .....	49
3.4.2. US 83 Overpass Bridge.....	53
3.4.3. IH 610 Tub Girder Bridge.....	56

3.5. Redesign with Larger-diameter Shear Studs using the 9 <sup>th</sup> Ed. AASHTO .	59
3.5.1. Guadalupe River Bridge .....	60
3.5.2. US 83 Overpass Bridge.....	61
3.5.3. IH 610 Tub Girder Bridge.....	62
3.6. Redesign with Larger-diameter Shear Studs using Proposed 10 <sup>th</sup> Ed. AASHTO .....	63
3.6.1. Guadalupe River Bridge .....	64
3.6.2. US 83 Overpass Bridge.....	65
3.6.3. IH 610 Tub Girder Bridge.....	67
3.7. Summary and Conclusions .....	68
Chapter 4. Stud Welding Investigations .....	70
4.1. Introduction.....	70
4.2. Background on Stud Welding.....	70
4.3. Welding Parameters Used in Previous Larger-diameter Shear Stud Research.....	76
4.4. Shear Studs used in Welding Investigation .....	76
4.4.1. Shear Stud Dimensions .....	78
4.4.1. Material Characterization Tests .....	78
4.5. Stud Weld Quality Evaluation Methods .....	86
4.5.1. Visual Inspection .....	87
4.5.2. 90° Bend Tests .....	89
4.5.3. Tension Test on Welded Stud.....	89
4.5.4. Macro Etch Weld Test .....	90
4.6. Stud Welding Equipment and Initial Welding Parameters .....	90
4.7. Verification of 7/8" Diameter Stud Weld Quality .....	91
4.8. Welding Investigation for 1" Diameter Studs.....	94
4.9. Welding Investigation for 1-1/8" Diameter Shear Studs .....	96
4.9.1. Investigation of Welds on Steel Plate.....	96
4.9.2. Investigation of Welds on Steel Girders .....	101
4.9.3. Summary of Welding Investigations of 1-1/8" Studs.....	107
4.10. Welding Investigation on 1-1/4" Diameter Shear Studs.....	108
4.10.1. Investigation of Welds on Steel Plate .....	108
4.10.2. Investigation of Welds on Steel Girders .....	114
4.10.3. Summary of Welding Investigations on 1-1/4" Studs .....	116
4.11. Conclusions and Recommended Welding Parameters .....	116

4.12. Selection of Shear Stud Diameter for Subsequent Research Tasks .....	117
Chapter 5. Static Push-Out Tests .....	119
5.1. Introduction.....	119
5.2. Test Specimens .....	120
5.2.1. Overview.....	120
5.2.2. Standard Test Specimens .....	120
5.2.3. Remainder of Test Specimens .....	125
5.3. Test Setup, Specimen Fabrication, and Instrumentation .....	133
5.3.1. Test Setup.....	133
5.3.2. Specimen Fabrication.....	136
5.3.3. Instrumentation .....	139
5.4. Material Properties.....	144
5.4.1. Shear Studs.....	144
5.4.2. Steel Reinforcement and Steel Girders .....	145
5.4.3. Concrete Material Properties .....	147
5.5. Test Procedures and Observations .....	148
5.5.1. Specimen No. 1, Three 7/8" Studs Per Row, CIP.....	149
5.5.2. Specimen No. 2, Three 7/8" Studs Per Row, PCP.....	151
5.5.3. Specimen No. 3, One 1-1/8" Stud Per Row, No Stagger, CIP.....	152
5.5.4. Specimen No. 4, One 1-1/8" Stud Per Row, No Stagger, PCP.....	154
5.5.5. Specimen No. 5, One 1-1/8" Stud Per Row, Staggered, CIP.....	155
5.5.6. Specimen No. 6, One 1-1/8" Stud Per Row, Staggered, PCP.....	156
5.5.7. Specimen No. 7, Two 1-1/8" Studs Per Row, CIP .....	158
5.5.8. Specimen No. 8, Two 1-1/8" Studs Per Row, CIP, Half Transverse Reinforcement.....	159
5.5.9. Specimen No. 9, Two 1-1/8" Studs Per Row, CIP, 5" Long Shear Studs.....	162
5.5.10. Specimen No. 10, Two 1-1/8" Studs Per Row, CIP, 1" Haunch ....	163
5.5.11. Specimen No. 11, Two 1-1/8" Studs Per Row, CIP, W14×99 .....	164
5.5.12. Summary of Test Observations.....	166
5.6. Test Results and Discussion.....	168
5.6.1. Load-Slip Response .....	168
5.6.2. Discussion of Results.....	173
5.7. Conclusions.....	181
Chapter 6. Fatigue Push-Out Tests .....	184



6.1. Introduction.....	184
6.2. Test Specimens .....	184
6.3. Test Setup, Specimen Fabrication, Instrumentation and Closed-Loop Control .....	185
6.3.1. Test Setup and Specimen Fabrication.....	185
6.3.2. Instrumentation .....	185
6.3.3. Closed-Loop Control .....	186
6.4. Material Properties.....	188
6.4.1. Shear Studs.....	188
6.4.2. Concrete Material Properties .....	188
6.5. Test Procedures and Observations .....	188
6.5.1. Cyclic Loading Observations.....	190
6.5.2. Monotonic Loading Observations.....	194
6.6. Fatigue Test Results.....	196
6.6.1. S-N Results .....	196
6.6.2. Slip Versus Number of Cycles.....	197
6.6.3. Comparison with AASHTO S-N Curves .....	200
6.7. Residual Static Strength Results .....	202
6.8. Conclusions.....	204
Chapter 7. Finite Element Studies: Static Push-Out Behavior .....	206
7.1. Introduction.....	206
7.2. FE Model Description and Validation .....	206
7.2.1. Model Geometry and Components .....	206
7.2.2. Material Properties.....	209
7.2.3. Constraints and Contact Conditions.....	224
7.2.4. Element Formulation and Mesh.....	226
7.2.5. Boundary Conditions .....	231
7.2.6. Solver and Large Deformation Algorithm.....	232
7.2.7. Validation Results and Discussion.....	234
7.2.8. Discussion on Selected Modeling Parameters .....	242
7.3. Parametric Studies .....	245
7.3.1. Stud Penetration into Concrete Deck.....	246
7.3.2. Haunch Depth .....	250
7.3.3. Beam Flange Width .....	255
7.3.4. Clear Distance Between Stud and PCP with 7/8" Studs.....	257

7.3.5. PCP Overlap on Steel Beam Flange with 1-1/8" Studs .....	259
7.3.6. Bedding Strip Size .....	260
7.3.7. Transverse Reinforcement Ratio with 1-1/8" Studs .....	261
7.4. Development of Design Recommendations Based on FE Studies of Push-out Tests .....	262
7.4.1. Fully CIP Concrete Decks .....	262
7.4.2. Concrete Decks with PCPs .....	264
7.5. Conclusions.....	269
Chapter 8. Large-Scale Beam Tests.....	271
8.1. Introduction.....	271
8.2. Beam Specimens.....	272
8.2.1. Span Arrangements.....	272
8.2.2. Specimen Cross-Sections.....	274
8.2.3. Stud Layouts .....	276
8.2.4. Deck Reinforcement .....	278
8.2.5. Precast Concrete Panels .....	280
8.3. Test Setup.....	284
8.3.1. Girder Supports.....	284
8.3.2. Loading Towers .....	284
8.3.3. Lateral Restraints .....	286
8.3.4. End Braces .....	287
8.4. Specimen Construction .....	287
8.4.1. Erection of Steel Girder .....	287
8.4.2. Formwork.....	289
8.4.3. Shear Stud Welding .....	291
8.4.4. Placement of Deck Reinforcement .....	294
8.4.5. PCP Placement.....	295
8.4.6. Concrete Placement .....	298
8.5. Material Properties.....	300
8.5.1. Shear Studs.....	300
8.5.2. Steel Girders – Material Properties and Section Dimensions.....	302
8.5.3. Concrete .....	305
8.5.4. Reinforcement.....	306
8.6. Instrumentation .....	308
8.6.1. Applied Loads and Girder Reactions.....	308

8.6.2. Vertical deflection.....	308
8.6.3. Slip.....	309
8.6.4. Strain.....	310
8.7. Loading Procedures .....	313
8.7.1. Two-Span Tests .....	313
8.7.2. Single-Span Tests.....	314
8.8. Beam Specimen No. 1 – Test Results, Analysis, and Discussion.....	315
8.8.1. Two-Span Test.....	315
8.8.2. Single-Span Test.....	320
8.9. Beam Specimen No. 2 – Test Results, Analysis and Discussion.....	332
8.9.1. Two-Span Test.....	332
8.9.2. Single-Span Test.....	336
8.10. Summary and Conclusions .....	345
Chapter 9. Summary, Key Findings, and Recommendations.....	348
9.1. Introduction.....	348
9.2. Summary of Research Tasks and Key Findings .....	349
9.2.1. Background and Literature Review .....	349
9.2.2. Preliminary Design Studies.....	350
9.2.3. Stud Welding Investigations.....	350
9.2.4. Static Push-Out Tests.....	352
9.2.5. Fatigue Push-Out Tests.....	353
9.2.6. Finite Element Studies of Static Push-Out Behavior.....	354
9.2.7. Large-Scale Composite Beam Tests.....	355
9.3. Recommendations.....	357
9.3.1. General Recommendations.....	357
9.3.2. Welding of 1-1/8" Shear Studs .....	357
9.3.3. Head Dimensions for 1-1/8" Studs .....	359
9.3.4. Design of 1-1/8" Studs for Ultimate Strength and Fatigue.....	359
9.3.5. Stud Penetration into Deck and Clear Distance to PCP for 7/8" and 1-1/8" Studs.....	359
9.3.6. Additional Detailing Recommendations for 1-1/8" Studs.....	363
9.3.7. Effects of PCPs on Composite Steel Girders.....	364
9.4. Proposed Changes to the AASHTO LRFD Bridge Design Specifications .....	366
9.5. Proposed Changes to the AASHTO/AWS D1.5 Bridge Welding Code..	368

9.6. Value of Research .....	369
References.....	372

## List of Tables

---

Table 1.1 - Potential Reduction in Shear Studs .....	3
Table 2.1 - Mechanical Property Requirements for Studs in AWS D1.5 .....	8
Table 2.2 - Standard Dimensions for Shear Studs in AWS D1.5 .....	8
Table 2.3 - Detailing Requirements for Shear Studs .....	9
Table 2.4 - Shear Stud Fatigue and Ultimate Strength Requirements in 9th Ed. AASHTO and Proposed 10th Ed. AASHTO .....	10
Table 2.5 - Stud Diameters in Millimeters and in Inches .....	24
Table 3.1 - Pitch of 7/8" Shear studs on Exterior Girder of Guadalupe River Bridge.....	51
Table 3.2 - Arrangement of 7/8" Shear Stud Pitch (Grouping) on Exterior Girder of Guadalupe River Bridge .....	52
Table 3.3 - Pitch of 7/8" Shear Studs on Girder 1 of the US 83 Overpass Bridge	55
Table 3.4 - Arrangement of 7/8" shear Stud Pitch (Grouping) on Girder 1 of US 83 Overpass Bridge.....	55
Table 3.5 - Pitch of 7/8" Shear Studs on Exterior Girders of IH 610 Tub Girder Bridge.....	59
Table 3.6 - Arrangement of 7/8" Shear Stud Pitch (Grouping), Eight Studs per Row, on each Girder of the IH 610 Tub Girder Bridge .....	59
Table 3.7 - Pitch of 1" Shear Studs on Exterior Girders of Guadalupe River Bridge Using One Stud per Row .....	60
Table 3.8 - Arrangement of 1" Shear Stud Pitch (Grouping) on Exterior Girders of Guadalupe River Bridge Using One Stud per Row .....	61
Table 3.9 - Redesign Results for Guadalupe River Bridge using 9 <sup>th</sup> Ed. AASHTO .....	61
Table 3.10 - Redesign Results for US 83 Overpass Bridge using 9th Ed. AASHTO .....	62
Table 3.11 - Pitch of 1" Shear studs, Two Studs per Row (One Stud per Flange), on Exterior Girders of IH 610 Tub Girder Bridge .....	62
Table 3.12 - Arrangement of 1" Shear Stud Pitch (Grouping), Two Studs per Row (One Stud per Flange), on Exterior Girders of IH 610 Tub Girder Bridge .....	63
Table 3.13 - Redesign Results for IH 610 Tub Girder Bridge using 9 <sup>th</sup> Ed. AASHTO .....	63
Table 3.14 - Pitch of 1" Shear Studs on Exterior Girders of Guadalupe River Bridge using Proposed 10 <sup>th</sup> Ed. AASHTO .....	64

Table 3.15 - Arrangement of 1" Shear Stud Pitch (Grouping) on Exterior Girders of Guadalupe River Bridge using Proposed 10 <sup>th</sup> Ed. AASHTO.....	65
Table 3.16 - Redesign Results for Guadalupe River Bridge using Proposed 10 <sup>th</sup> Ed. AASHTO.....	65
Table 3.17 - Pitch of 1" Shear Studs on Girder 1 of US 83 Overpass Bridge using Proposed 10 <sup>th</sup> Ed. AASHTO.....	66
Table 3.18 - Arrangement of 1" Shear Stud Pitch (Grouping) on Girder 1 of US 83 Overpass Bridge using Proposed 10 <sup>th</sup> Ed. AASHTO.....	66
Table 3.19 - Redesign Results for US 83 Overpass Bridge using Proposed 10 <sup>th</sup> Ed. AASHTO.....	67
Table 3.20 - Pitch of 1" Shear Studs, Two Studs per Row (One Stud per Flange), on Exterior Girder of IH 610 Tub Girder Bridge using Proposed 10 <sup>th</sup> Ed. AASHTO.....	67
Table 3.21 - Arrangement of 1" Shear Stud Pitch (Grouping), Two Studs per Row (One Stud per Flange), on Exterior Girder of IH 610 Tub Girder Bridge using Proposed 10 <sup>th</sup> Ed. AASHTO.....	68
Table 3.22 - Redesign Result for IH 610 Tub Girder Bridge using Proposed 10 <sup>th</sup> Ed. AASHTO.....	68
Table 4.1 - Welding Information from Previous Studies on Larger-diameter Shear Studs.....	77
Table 4.2 - Geometry of Shear Studs in Stud Welding Investigations.....	79
Table 4.3 - Tension Coupon Test Results.....	83
Table 4.4 - Shear Strength Test Results.....	85
Table 4.5 - Charpy-V-Notch Test Results.....	86
Table 4.6 - Suggested Stud Length Reduction from Chambers (2001).....	88
Table 4.7 - Initial Welding Parameters.....	91
Table 4.8 - Summary of Welding Investigations for 1-1/8" Studs.....	108
Table 4.9 - 1-1/4" Studs Welded Using 2275 Amp, 1/4" Lift, S Polarity, One Clockwise Loop, Surface Preparation, and Various Welding Times.....	110
Table 4.10 - 1-1/4" Studs Welded Using 2275 Amp, 1/4" Lift, Reverse Polarity, One Counterclockwise Loop, Surface Preparation, and Various Welding Times.....	112
Table 4.11 - Summary of Welding Trials for 1-1/4" Studs on 1'×1' Steel Plate.....	113
Table 4.12 - Recommended Welding Parameters.....	117
Table 5.1 – Static Push-Out Specimens.....	121
Table 5.2 - Total Number of Studs in Each Push-Out Specimen.....	132
Table 5.3 - Stud Welding Parameters used for Push-out Specimens.....	136

Table 5.4 - Dimensions of Shear Studs Used in Push-Out Specimens .....	144
Table 5.5 - Tension Coupon Test Results for Studs Used in Push-out Specimens .....	145
Table 5.6 - Tensile Properties for Reinforcement Used in Push-Out Specimens	147
Table 5.7 - Tensile Properties for Steel Girders (From Certified Mill Test Reports) .....	147
Table 5.8 - Concrete Strength for Push-Out Specimens .....	148
Table 5.9 – Failure Modes of Push-Out Specimens .....	167
Table 5.10 - Key Values in Load-Slip Curves .....	173
Table 5.11 - Load Per Stud from Push-Out Tests and AASHTO Stud Factored Shear Resistance .....	173
Table 6.1 – Fatigue Push-Out Specimens .....	185
Table 6.2 - Concrete Strength for Fatigue Specimens .....	188
Table 6.3 - Load and Stress Ranges for Fatigue Specimens.....	189
Table 6.4 - Fatigue Test Results .....	197
Table 6.5 – Maximum Load in Monotonic Loading Cycle and Residual Strength .....	203
Table 6.6 – Load Per Stud and AASHTO Stud Factored Resistance .....	204
Table 7.1 - FE Models for Validation.....	207
Table 7.2 - Dimensions of Weld Collars .....	208
Table 7.3 - Ductile and Shear Damage Model Parameters .....	223
Table 7.4 - Strength Comparisons Between FE Models and Experiments.....	238
Table 7.5 - Slip Comparisons Between FE Models and Experiments .....	238
Table 7.6 - Average Error for Different Concrete Tensile Strengths .....	244
Table 7.7 - Parametric Study Matrix.....	246
Table 7.8 - Concrete Compressive Strength and Stud Tensile Strength Used in FE Models and to Compute AASHTO Stud Strength (Unless Noted Otherwise)...	247
Table 8.1 – Stud Welding Parameters used for Beam Specimens .....	291
Table 8.2 – Gaps Between PCP Panels.....	297
Table 8.3 – Tensile Properties of 1-1/8" Studs Used in Beam Tests .....	302
Table 8.4 – CVN Test Results for 1-1/8" Studs Used in Beam Tests.....	303
Table 8.5 – Tension Coupon Test Results for Beam Specimen No. 1.....	304
Table 8.6 - Tension Coupon Test Results for Beam Specimen No. 2 .....	304
Table 8.7 – Measured Cross-Section Dimensions .....	305

Table 8.8 – Concrete Compressive Strength for Beam Specimen No. 1 .....	306
Table 8.9 – Concrete Compressive Strength for Beam Specimen No. 2 .....	306
Table 8.10 – Reinforcing Bar Tensile Test Results for Beam Specimen No. 1 .	307
Table 8.11 - Reinforcing Bar Tensile Test Results for Beam Specimen No. 2 ..	307
Table 8.12 – Loading Sequence for Two-Span Test of Beam Specimen No. 1 .	313
Table 8.13 - Loading Sequence for Two-Span Test of Beam Specimen No. 2..	314
Table 8.14 – Beam Specimen No. 1 - Maximum Crack Width under Different Load Levels.....	319
Table 8.15 – Shear Stud Failure Modes – Beam Specimen No 1 .....	323
Table 8.16 – Slip Just Prior to Specimen Failure.....	327
Table 8.17 – Maximum Moment Sustained by Beam Specimen No. 1 .....	328
Table 8.18 – Computed Full Composite Moment Capacity of Beam Specimen No. 1.....	329
Table 8.19 – AASHTO Factored Shear Resistance for 1-1/8" Studs in Beam Specimen No. 1 .....	332
Table 8.20 – Beam Specimen No. 2 – Maximum Crack Width under Different Loads.....	336
Table 8.21 - Maximum Moment Sustained by Beam Specimen No. 2 .....	343
Table 8.22 – Computed Full Composite Moment Capacity for Beam Specimen No. 2.....	343
Table 9.1 – Recommendations for Stud Penetration into Concrete Deck and Clear Distance Between Stud Head and PCP for Decks Constructed with PCPs .....	361

## List of Figures

---

Figure 1.1 - Steel Bridge Girders with Shear Studs.....	1
Figure 1.2 - Typical Cross-Section of a Composite Steel Bridge Girder with a Full-Depth Cast-in-Place Deck.....	2
Figure 1.3 - Typical Cross-Section of a Composite Steel Bridge Girder Using PCPs.....	2
Figure 2.1 - Typical Push-out Test Setup (Patel 2013).....	11
Figure 2.2 - One-Sided Push-out Specimen with a Single Shear Stud and Load Applied to Steel (Kayir 2006).....	12
Figure 2.3 - One-Sided Push-out Specimen with Load Applied to Concrete (Badie, Tadros, et al. 2002).....	12



Figure 2.4 - Example of Laboratory Test of a Composite Beam (Kwon, et al. 2007) .....	13
Figure 2.5 - Qualitative Load-Slip Curve from Push-out Test .....	14
Figure 2.6 - Example of Shear Stud Fracture in a Push-out Test (Xue, et al. 2012) .....	15
Figure 2.7 - Example of Concrete Embedment Failure at Shear Stud (Ollgaard, Slutter and Fisher, Shear Strength of Stud Connectors in Lightweight and Normal-Weight Concrete 1971) .....	16
Figure 2.8 - Close of View of Right Shear Stud in Figure 2.7 (Ollgaard, Slutter and Fisher, Shear Strength of Stud Connectors in Lightweight and Normal-Weight Concrete 1971) .....	17
Figure 2.9 - Normalized Moment versus Beam End Slip for Two Beam Tests (Driscoll and Slutter 1961).....	21
Figure 2.10 - Composite Beam Specimens tested by Chapman and Balakrishnan (1964).....	22
Figure 2.11 - End slip versus applied moment for two beams tested by Badie et al. (2011).....	23
Figure 2.12 - Average Load-Slip Curves Derived by Ollgaard et al. (1971).....	24
Figure 2.13 - Specimen Using Precast Concrete Slab with Shear Pocket (Wang, et al. 2018); Specimen on the Right has no Reinforcement in the Pocket.....	28
Figure 2.14 - Cracking Pattern for Normal Strength Concrete Specimen with Shear Pocket (Wang, et al. 2018).....	28
Figure 2.15 - Summary of static strength data for larger-diameter shear studs....	30
Figure 2.16 - Fatigue Test Results for 7/8" and 1-1/4" Shear Studs by Badie et al. (2002).....	32
Figure 2.17 - Fatigue Test Results for 25mm (0.98"), 27mm (1.06") and 30mm (1.18") Shear Studs by Lee et al. (2005).....	32
Figure 2.18 - Fatigue Test Results for 7/8" and 1-1/4" Shear Studs by Mundie (2011).....	33
Figure 2.19 - Comparison of Fatigue Test Data with 9th E. AASHTO and Proposed 10th Ed. AASHTO S-N Curves .....	34
Figure 3.1 - Typical Cross-Section for Guadalupe River Bridge. (Taken from TxDOT Design Drawings).....	39
Figure 3.2 - Typical Cross-Section for US 83 Overpass Bridge (Taken from TxDOT Design Drawings).....	40
Figure 3.3 - Typical Cross-Section for IH 610 Tub Girder Bridge (Taken from TxDOT Design Drawings).....	41
Figure 3.4 - CSI Output for Unfactored $V_f$ ( $V_2$ in CSI Convention) .....	44

Figure 3.5 - CSi Bridge Output for Unfactored $M_f$ ( $M_3$ in CSI Convention) .....	45
Figure 3.6 - Section Divisions for Shear Stud Strength Limit State Check in a Three-Span Bridge where Negative Moment Region is Designed Non-Composite .....	46
Figure 3.7 - Shear Stud Strength Limit State Check for Straight Bridge when Negative Moment Region is Designed Non-Composite: Studs are Checked in Red Regions and $P=P_p$ .....	47
Figure 3.8 - Section Division for Shear Stud Strength Limit State Check in a Three-Span Bridge where Negative Moment Region is Designed Composite.....	48
Figure 3.9 - Shear Stud Strength Limit State Check when Negative Moment Region is Designed Composite: Studs are Checked in Red Region with Corresponding $P$ .....	49
Figure 3.10 - Guadalupe River Bridge Model in CSiBridge .....	50
Figure 3.11 CSiBridge $V_f$ Results for Guadalupe River Bridge on Exterior Girder .....	50
Figure 3.12 - US 83 Overpass Bridge Model in CSiBridge .....	53
Figure 3.13 - CSiBridge $V_f$ Results for US 83 Overpass Bridge Girder 1 .....	54
Figure 3.14 - CSiBridge $M$ Results for US 83 Overpass Bridge Girder 1 .....	54
Figure 3-15 - IH 610 Tub Girder Bridge Model in CSiBridge .....	56
Figure 3-16 - CSiBridge Output for Unfactored Torsion Along the Exterior Girder of the IH 610 Tub Girder Bridge .....	57
Figure 3-17 - CSiBridge $V_{sr}$ Results for IH 610 Tub Girder Bridge Exterior Girders.....	58
Figure 4.1 - Stud Welding Equipment (AWS 1991).....	71
Figure 4.2 - Details of Stud Welding Process (ISO 2017b).....	72
Figure 4.3 - Stud Welding Gun (Chambers 2001).....	73
Figure 4.4 - Cross-Section of a Welded Stud (Chambers 2001).....	73
Figure 4.5 - Arc Blow Effect (Nelson Stud Welding 2008a) .....	74
Figure 4.6 - Weld Collar Under Arc Blow Effect (Illustration on the Left: ISO 2017b).....	75
Figure 4.7 - Cable Looping Around the Welding Point.....	75
Figure 4.8 Shear Studs and Welding Ferrules of Various Diameter.....	79
Figure 4.9 - Tension Coupon Dimensions .....	80
Figure 4.10 - Tension Coupon Test Setup .....	80
Figure 4.11 - Stress-Strain Curves for 7/8" Studs.....	81
Figure 4.12 – Stress-Strain Curves for 1" studs.....	81

Figure 4.13 – Stress-Strain Curves for 1-1/8" studs .....	82
Figure 4.14 - Stress-Strain Curves for 1-1/4" studs .....	82
Figure 4.15 - Shear Strength Test Setup .....	83
Figure 4.16 - Photos of Shear Studs After Shear Fracture Tests .....	84
Figure 4.17 - Arrangement of CVN Coupons within Shear Studs .....	85
Figure 4.18 - Photos of a Good Stud Weld and Common Problematic Stud Welds (pictures on top: Chambers (2001), pictures on bottom: Midwest Fasteners Inc. (2019)).....	87
Figure 4.19 - Unsuccessful Stud Weld .....	88
Figure 4.20 - Shear Studs Passing 90° Bend Test.....	89
Figure 4.21- Weld Tension Test Setup and a Successful Test.....	89
Figure 4.22 - Macro Etch Weld Test. (a) Welds Are Cut in the Middle and Polished, (b) Cross-Section of a Weld Treated with Nitric Acid .....	90
Figure 4.23 Welding Gun Chucks for Various Diameter Shear Studs .....	91
Figure 4.24 - Appearance of 7/8" Stud Welds. (a) Welded on 1" Thick Plate for Tension Test, (b) Welded on 2" Thick Plate for Macro Etch Weld Test, (c) Welded on 2" Thick Plate for Bend Test .....	92
Figure 4.25 - Weld Tension Tests for 7/8" Studs .....	92
Figure 4.26 - 90° Bend Test on 7/8" Studs. (a) Test for Stud Welded on 1" Thick Plate. (b) Test for Studs Welded on 2" Thick Plate .....	93
Figure 4.27 – Macro Etch Weld Tests for 7/8" Studs. (a) Studs Welded on 1" Thick Plate, (b) Studs Welded on 2" Thick Plate .....	93
Figure 4.28 - Appearance of 1" Stud Welds. (a) Welded on 1" Thick Plate for Tension Test, (b) Welded on 2" Thick Plate for Weld Tension Test, (c) Welded on 1" Thick Plate for Bend Test.....	94
Figure 4.29 - Four 1" Diameter Shear Studs Passing Weld Tension Test. (a)(b)(c) Stud Welded on 1" Thick Plate, (d) Stud Welded on 2" Thick Plate .....	95
Figure 4.30 - Macro Etch Weld Test for 1" Diameter Shear Stud Welded on 1" Thick Plate .....	95
Figure 4.31 - 1" Diameter Shear Stud Welded Without Surface Preparation.....	96
Figure 4.32 - Appearance of 1-1/8" Diameter Shear Studs Welds. (a) Welded on 1" Thick Plate for Weld Tension Test (b) Welded on 2" Thick Plate for Weld Tension Test (c) Welded on 1" Plate for Macro Etch Weld Test .....	97
Figure 4.33 - Four 1-1/8" Studs Passing Weld Tension Tests. (a)(b) Stud Welded on 1" Thick Plate (c)(d) Stud Welded on 2" Thick Plate.....	97
Figure 4.34 - 90° Bend Test Results for 1-1/8" Diameter Shear Studs. (a) Studs Welded on 1" Thick Plate (b) Studs Welded on 2" Thick Plate .....	98

Figure 4.35 - Macro Etch Weld Test Results for 1-1/8" Shear Studs. (a) Studs Welded on 1" Thick Plate (b) Studs Welded on 2" Thick Plate .....	98
Figure 4.36 - 1-1/8" Studs Welded Without Cable Looping .....	99
Figure 4.37 - 1-1/8" Studs Welded Without Surface Preparation and Without Cable Looping. (a) lift is 1/8" (b) Lift is 3/16". .....	100
Figure 4.38 - Failed Bend Test for 1-1/8" Studs Using Counterclockwise Cable Loop, Straight Polarity, and No Surface Preparation .....	101
Figure 4.39 - Arc Blow Effect on 1-1/8" Diameter Shear Studs Close to Ground and Free Edges .....	101
Figure 4.40 - 1-1/8" Studs Welded Using 2050A, 1.3s, S Polarity, One Clockwise Loop, and Surface Preparation on a W14×132 Girder. Weld Collar (left photos) and Fracture Surfaces After Bend Test (center and right photos) .....	102
Figure 4.41 - 1-1/8" Studs Welded Using 2150A, 1.4s, S Polarity (right side of photo) and R Polarity (left side of photo) on W14×132 Girder. Some Studs on the Left are Welded Without Cable Looping and Surface Preparation. ....	103
Figure 4.42 - 1-1/8" Studs Welded Using 2150A, 1.4s, R Polarity, No Surface Preparation, No Cable Looping on a W14×500 Girder with 3-1/2" Thick Flange. 90° Bend Test Results .....	104
Figure 4.43 - 1-1/8" Studs Welded Using 2250A, 1.55s, R Polarity, No Surface Preparation, No Cable Looping on a W14×500 Girder with 3-1/2" Thick Flange. 90° Bend Test Results .....	105
Figure 4.44 - 1-1/8" Studs Welded Using 2250A, 1.55s, R Polarity, No Surface Preparation, No Cable Looping on a W14×132 girder. 90° Bend Test Results..	105
Figure 4.45 - 1-1/8" Studs Welded Using 2250A, 1.55s, R Polarity, No surface Preparation, No Cable Looping on a W14×99 Girder. 90° Bend Test Results...	106
Figure 4.46 - 1-1/8" Studs Welded Using 2250A, 1.55s, R Polarity, No Surface Preparation, No Cable Looping on 1" Thick Plate. Appearance of Weld Collars (left) and 90° Bend Test Results (right). .....	106
Figure 4.47 - 1-1/8" Studs Welded Using 2250A, 1.55s, R Polarity, No Surface Preparation, No Cable Looping on 2" Thick Plate. Appearance of Weld Collars (left) and 90° Bend Test Results. ....	107
Figure 4.48 - 1-1/4" Studs Welded Using 2200A, 1.4s, S Polarity, Surface Preparation, One Clockwise Cable Loop on 1" Plate. Appearance of Weld Collar (left) and Cross-Section (right). .....	109
Figure 4.49 - 1-1/4" Studs Welded Using 2275A, 1.45s, S Polarity, Surface Preparation, One Clockwise Cable Looping on 1" Plate. Fracture Section of Failed Bend Tests.....	110
Figure 4.50 - 1-1/4" Studs Welded Using 2275 Amp, 2.0s, 1/4" Lift, S Polarity, One Clockwise Loop, Surface Preparation and With Counter Arc Blow Measures. Unsuccessful Hot Welds. ....	111

Figure 4.51 - 1-1/4" Studs on Girder with 1" Thick Flange Welded Using 2500 amps, 2s, R Polarity, No Cable Looping, No Surface Preparation.....	115
Figure 4.52 - 1-1/4" Studs on Girders with 3.5" Thick Flange Welded Using 2500 amps, 2 s, R Polarity, No Cable Looping, No Surface Preparation.....	116
Figure 5.1 - 3D Schematic of Typical Push-Out Specimen Used in this Study .	120
Figure 5.2 – CIP Standard Push-Out Specimen (Specimen No. 7) (a) 3D Schematic (b) View with CIP Concrete Slab Omitted.....	123
Figure 5.3 - Details of CIP Standard Push-Out Specimen (Specimen No. 7) ....	123
Figure 5.4 - PCP Standard Push-Out Specimen (Specimen No. 4) (a) 3D Schematic (b) View with Cast-in-Place Concrete Omitted .....	124
Figure 5.5 - Details of PCP Standard Push-Out Specimen (Specimen No. 4) (Reinforcement in PCP is Omitted) .....	124
Figure 5.6 - Details of PCPs .....	124
Figure 5.7 - Photo of (a) PCPs (b) PCP Standard Specimen Before Casting ....	125
Figure 5.8 - Shear Studs Bent Inward in Specimen No. 2 .....	126
Figure 5.9 - Details for Specimen No. 1, Three 7/8" Studs Per Row, Fully CIP	127
Figure 5.10 - Details for Specimen No. 2, Three 7/8" Studs Per Row, PCP .....	127
Figure 5.11 - Details for Specimen No. 3, One 1-1/8" Stud Per Row, No Stagger, Fully CIP.....	127
Figure 5.12 - Details for Specimen No. 5, One 1-1/8" Stud Per Row, Staggered Layout, Fully CIP.....	128
Figure 5.13 - Details for Specimen No. 6, One 1-1/8" stud Per Row, Staggered Layout, PCP .....	128
Figure 5.14 - Steel Girder for Specimen No. 5 with Staggered Layout of Shear Studs.....	129
Figure 5.15 - Comparison of Standard CIP Specimen (Specimen No. 7, Left) with Specimen No. 8 (Right) .....	130
Figure 5.16 - Comparison of Standard CIP Specimen (Specimen No. 7, Left) with Specimen No. 9 (Right) .....	130
Figure 5.17 - Photos of (a) Specimen No. 9 (5" Long Stud) Before Casting (b) Standard CIP Specimen (7" Long Stud) Before Casting .....	131
Figure 5.18 Comparison of Standard CIP Specimen (Specimen No. 7, Left) with Specimen No. 10 (Right) .....	131
Figure 5.19 - Comparison of Standard CIP Specimen (Specimen No. 7, Left) with Specimen No. 11 (Right) .....	132
Figure 5.20 - 3D Schematic of Test-Setup and the Components.....	133

Figure 5.21 - Photo of Specimens in the Test Setup with Enlarged View of the Haunch Bottom - Safety Measures for Load Assembly Can Be Seen (With Arrows) Between 4" Thick Load Spreader Plate and W30×211 Load Beam ....	134
Figure 5.22 - Epoxy is Used to Fill the Gap Between Actuators and Lateral Support.....	135
Figure 5.23 - Air Powered Hydraulic Pump .....	136
Figure 5.24 - 90° Bend Tests on (a) 7/8" Studs on 1'×1' Plate (b) 1-1/8" Studs on W14×132 girder Flange .....	137
Figure 5.25 - 3D Schematic of Casting Formwork.....	138
Figure 5.26 - Fabrication Process for Specimen (1) Steel Beam and Reinforcement Placed in the Formwork (2) Concrete Being Cast and Vibrated (3) Concrete Being Cured Inside the Formwork (4) Specimens Removed from the Formwork.....	138
Figure 5.27 - Location of LPs and Wood Blocks on Specimen No. 5 and Specimen No. 6.....	140
Figure 5.28 - Location of LPs and Wood Blocks on Specimens other than Specimen No. 5 and No. 6. ....	140
Figure 5.29 - Photo of LPs and the Wood Blocks on Specimen No. 11.....	141
Figure 5.30 - Strain Gauge Locations and Notations for Specimen No. 1 .....	142
Figure 5.31 - Strain Gauge Locations and Notations for Specimen No. 3 .....	142
Figure 5.32 - Strain Gauge Locations and Notations for Specimen No. 5 .....	143
Figure 5.33 - Strain Gauge Locations and Notations for Specimen No. 7 and No. 9 .....	143
Figure 5.34 - Strain Gauge Locations and Notations for Specimen No. 8 .....	143
Figure 5.35 - Stress-Strain Curves for 5" Long 1-1/8" Diameters Stud Coupons .....	145
Figure 5.36 - Reinforcing Bars Used in Push-Out Specimens.....	146
Figure 5.37 - Stress-Displacement Curves for Reinforcing Bars .....	146
Figure 5.38 - Surface Notations on Push-Out Specimens.....	149
Figure 5.39 - Concrete Damage on Specimen No. 1 .....	150
Figure 5.40 - Specimen No. 1: Concrete Deck After Failure with Enlarged Photos of the Stud Identified by the Arrow (a) Taken from Concrete Side (b) Taken from Steel Beam Flange Side .....	150
Figure 5.41 - Concrete Damage on Specimen No. 2. Location of Photos (a) and (b) are Shown in the Left Diagram .....	151
Figure 5.42 - Concrete Crack Mapping on Specimen No. 2.....	152
Figure 5.43 - Concrete Crack Mapping on Specimen No. 3.....	153

Figure 5.44 - Specimen No. 3: Concrete Deck After Failure with Enlarged Photos of the Stud Identified by the Arrow (a) Taken from Concrete Side (b) Taken from Steel Beam Flange Side .....	153
Figure 5.45 - Concrete Damage on Specimen No. 4. Locations of Photos are Shown in the Left Diagram.....	154
Figure 5.46 - Concrete Crack Mapping on Specimen No. 4.....	155
Figure 5.47 - Concrete Crack Mapping on Specimen No. 5.....	156
Figure 5.48 Specimen No. 5: Concrete Deck After Failure with Enlarged Photos of Stud Identified by the Arrow (a) Taken from Concrete Side (b) Taken from Steel Beam Flange Side .....	157
Figure 5.49 - Concrete Damage on Specimen No. 6. Locations of Photos Shown in the Left Diagram.....	157
Figure 5.50 - Concrete Crack Mapping on Specimen No. 6.....	158
Figure 5.51 - Concrete Crack Mapping on Specimen No. 7.....	159
Figure 5.52 - Specimen No. 7: Concrete Deck After Failure with Enlarged Photos of Stud Identified by the Arrow (a) Taken from Concrete Side (b) Taken from Steel Beam Flange Side .....	160
Figure 5.53 - Concrete Deck Cracking on Specimen No. 8. Locations of Photos are Shown in Left Diagram.....	161
Figure 5.54 - Concrete Crack Mapping on Specimen No. 8.....	161
Figure 5.55 - Concrete Crack Mapping and Photo After Test on Specimen No. 9 .....	162
Figure 5.56 - Concrete Crack Mapping and Photo of Spalled Concrete on Specimen No. 10.....	163
Figure 5.57 - Specimen No. 10: Concrete Deck After Failure with Enlarged Photos of Stud Identified by Arrow (a) Taken from Concrete Side (b) Taken from Steel Beam Flange Side .....	164
Figure 5.58 - Concrete Crack Mapping and Photo of Vertical Crack on Specimen No. 11.....	165
Figure 5.59 - Specimen No. 11: Concrete Deck After Failure with Enlarged Photos of Stud Identified by Arrow (a) Taken from Concrete Side (b) Taken from Steel Beam Flange Side .....	166
Figure 5.60 – Deformation of Studs After Testing.....	168
Figure 5.61 - Load-Slip Curves for Static Push-Out Tests.....	170
Figure 5.62 - Initial Portion of Load-Slip Curve for Specimen No. 5.....	171
Figure 5.63 - Comparison Between Special Detail Specimens and the Standard CIP Specimen.....	174

Figure 5.64 - Push-Out Test results Comparison: PCPs Versus Full-Depth CIP Decks.....	177
Figure 5.65 - Comparison Between Different Layouts for 1-1/8" Shear Studs..	178
Figure 5.66 - Peak Strain in the Middle of the Transverse Reinforcement for Specimen No. 1 .....	179
Figure 5.67 - Peak Strain in the Longitudinal Reinforcement for Specimen No. 1 .....	179
Figure 5.68 - Strain Development at the Same Location in Specimen No. 8 and Specimen No. 7 .....	180
Figure 5.69 - Strain Development in Specimen Nos. 3, 5, and 7.....	180
Figure 6.1 – Location of Linear Potentiometers on Fatigue Push-Out Specimens .....	186
Figure 6.2 - Flow Chart of the Closed-Loop Control System.....	187
Figure 6.3 – Sinusoidal Loading Pattern for Specimen No. 2F .....	189
Figure 6.4 - Specimen No.2F: Photo of Separation Between Steel Flange and Concrete After Failure .....	191
Figure 6.5 - Specimen No.2F: Concrete Deck After Failure with Enlarged Photos of Studs .....	191
Figure 6.6 - Specimen No.3F: Crack Mapping After Runout.....	192
Figure 6.7 - Specimen No.4F: Photo of the Separation and Crack Mapping After Failure .....	193
Figure 6.8 - Specimen No.4F: Concrete Deck After Failure with Enlarged Photos of Studs .....	193
Figure 6.9 - Specimen No.1F: Photo of the Separation Between Steel Beam Flange and Concrete After Failure Under Monotonic Loading.....	194
Figure 6.10 - Specimen No.1F: Concrete Deck After Failure Under Monotonic Loading with Enlarged Photos of Studs.....	195
Figure 6.11 - Specimen No.3F: Photo of the Separation Between the Steel Beam Flange and Concrete After Failure.....	195
Figure 6.12 - Specimen No.3F: Concrete Deck After Failure with Enlarged Photos of Studs .....	196
Figure 6.13 – Slip Versus Number of Cycles for Specimen No. 1F.....	197
Figure 6.14 – Slip Versus Number of Cycles for Specimen No. 2F.....	198
Figure 6.15 – Slip Versus Number of Cycles for Specimen No. 3F.....	198
Figure 6.16 – Slip Versus Number of Cycles for Specimen No. 4F.....	199
Figure 6.17 – Slip Versus Number of Cycles for All Specimens .....	200



Figure 6.18 – 9 <sup>th</sup> Ed. AASHTO S-N Curve for Shear Studs and Fatigue Test Results.....	201
Figure 6.19 - Comparison of 9 <sup>th</sup> Ed. and Proposed 10 <sup>th</sup> Ed. AASHTO S-N Curves and Fatigue Results for 1-1/8" Studs Tested in TxDOT 0-7042 Research Project .....	202
Figure 6.20 – Load-Slip Curve for Specimen No. 1F for Final Monotonic Loading .....	203
Figure 6.21 - Load-Slip Curve for Specimen No. 3F for Final Monotonic Loading .....	203
Figure 7.1 - FE Model No. 6.....	208
Figure 7.2 - FE Model No. 7.....	208
Figure 7.3 - Enlarged View of FE Model of Shear Stud .....	209
Figure 7.4 - Von Mises Yield Surface in 2D Principal Stress Space and 3D Principal Stress Space.....	210
Figure 7.5 - CDP Yield Surface for Different Values of K in 3D Principal Space .....	211
Figure 7.6 - Rectangular Bar Model (a) Boundary Conditions (b) Two Different Mesh Schemes (c) Stress-Strain Behavior for Each Element.....	212
Figure 7.7 - FE Results for Bar Under Tension (a) When Bar Reaches the Peak Tensile Strength (b) When Bar Starts Softening.....	213
Figure 7.8 - Axial Load versus Axial Displacement for Two Mesh Schemes with the Same Stress-Strain Input.....	213
Figure 7.9 - Bar Analysis Results After Regularization of Tensile Softening Rule .....	215
Figure 7.10 - Uniaxial Stress-Strain Behavior of Concrete .....	216
Figure 7.11 - FE Models and Parametric Study on Impact of Dilation Angle $\psi$ (Dara 2015).....	218
Figure 7.12 - Effect of Eccentricity on Plastic Potential Surface (Wosatko, et al. 2019).....	218
Figure 7.13 - True Stress-Strain Curve for Stud Material .....	220
Figure 7.14 – FE analysis of steel tension coupon and comparison with experiments.....	220
Figure 7.15 - Stress-strain curve for material with ductile damage (Abaqus 2016) .....	221
Figure 7.16 - Element Removal at the Weld of Shear Stud.....	221
Figure 7.17 - Relationship Between Fracture Energy and Plastic Equivalent Displacement at Failure .....	223

Figure 7.18 - Surface Interactions in Model No. 4 .....	225
Figure 7.19 - Surface Penetration Between Master and Slave Surfaces (Abaqus 2016) .....	225
Figure 7.20 - PCP Reinforcement Embedment Interaction .....	227
Figure 7.21 - Abaqus Elements Used in FE Model (Abaqus 2016) .....	227
Figure 7.22 – Mesh for Model No. 3 .....	228
Figure 7.23 - Mesh Schemes for Sensitivity Study on Model No. 3 .....	229
Figure 7.24 - Load-Slip Response for Different Mesh Sizes for Model No. 3... ..	229
Figure 7.25 - Mesh Schemes for Sensitivity Study for Model No. 1.....	230
Figure 7.26 - Load-Slip Response for (A) With and Without Mass Scaling for 0.1" Mesh Scheme (B) Under Different Mesh Sizes for Model No. 1.....	230
Figure 7.27 - Deformation of Steel Beam Flange When One Element Is Used Through the Thickness.....	231
Figure 7.28 - Strain Localization in Top Layer of Elements in Steel Beam.....	231
Figure 7.29 - Boundary Conditions for Model No. 7 .....	232
Figure 7.30 - Slip Measurement in Model No. 5 .....	235
Figure 7.31 - Load-Slip Curves for FE Models and Corresponding Experiments .....	237
Figure 7.32 - Comparison Between Maximum Principal Strain Contours in FE Model No. 5 and Cracks Observed in Experiment .....	240
Figure 7.33 - Comparison Between Minimum Principal Strain Contours in FE Model No. 3 and Compression Damage Observed in Experiment.....	240
Figure 7.34 - Maximum Principal Strain Contours for (a) Model No. 7, (b) Model No. 2, (c) Model No. 4, and (d) Model No. 6 .....	241
Figure 7.35 - (a) Maximum Principal Strain Contour on Model No. 8 Concrete Deck, and (b) Photo of Specimen No. 8 Concrete Deck after the Test .....	241
Figure 7.36 - Element Removal at Base of Shear Studs at Different Analysis Steps .....	242
Figure 7.37 - Model No. 7 Results Using Various Friction Coefficients .....	243
Figure 7.38 - Load-Slip Curves for Model No. 2 Using Various Values of Concrete Tensile Strength.....	244
Figure 7.39 - Load-Slip Curves for Model No. 7 Using Various Values of Concrete Compressive Strength.....	245
Figure 7.40 - FE Models with Different Stud Penetrations into a Fully CIP Concrete Deck.....	247

Figure 7.41 - Parametric Study on Penetration of 7/8" Studs into Fully CIP Concrete Deck.....	248
Figure 7.42 - Parametric Study on Penetration of 1-1/8" Studs into Fully CIP Concrete Deck.....	249
Figure 7.43 - FE Models with PCP and with Different Stud Penetrations .....	249
Figure 7.44 - Parametric Study on Penetration of 1-1/8" Studs into Concrete Deck with PCP .....	250
Figure 7.45 - FE Models with Different Haunch Depths and with Fixed Stud Length of 7" .....	251
Figure 7.46 - Parametric Study on Haunch Depth for 1-1/8" Studs in Fully CIP Concrete Deck and with Fixed Stud Length of 7" .....	251
Figure 7.47 - Parametric Study on Haunch Depth for 1-1/8" Studs in Fully CIP Concrete Deck, Using UF PI from Model No. 10.....	252
Figure 7.48 - FE Models with Different Haunch Depths and with Stud Penetration Fixed at 4" .....	253
Figure 7.49 - Parametric Study on Haunch Depth for 1-1/8" Studs in Fully CIP Concrete Deck and with a Fixed Deck Penetration Of 4" .....	254
Figure 7.50 - Parametric Study on Haunch Depth for 1-1/8" Studs in Fully CIP Concrete deck and with a Fixed Stud Penetration of 2" .....	254
Figure 7.51 - FE Models with Different Haunch Depths; Concrete Deck Has PCP and Stud Length Is Fixed at 7".....	255
Figure 7.52 - Parametric Study on Haunch Depth for 1-1/8" Studs in Concrete Deck with PCP and with a Fixed Stud Length of 7" .....	255
Figure 7.53 - FE Models with Different Beam Flange Widths.....	256
Figure 7.54 - Parametric Study on Steel Beam Flange Width for Fully CIP Concrete Deck and 1-1/8" Studs.....	256
Figure 7.55 - Parametric Study on Steel Beam Flange Width for Concrete Deck with PCP and 1-1/8" Studs.....	257
Figure 7.56 - FE Models with Different Clear Distances Between Stud Head and PCP (CIP Concrete Omitted from View).....	258
Figure 7.57 - Parametric Study on Clear Distance Between 7/8" Stud and PCP	258
Figure 7.58 - FE Models with Different PCP Overlap Distance with Steel Beam Flange.....	259
Figure 7.59 - Parametric Study on PCP Overlap Distance with Steel Beam Flange for 1-1/8" Studs.....	259
Figure 7.60 - FE Models with Different Size of Bedding Strips .....	260
Figure 7.61 - Parametric Study on Size of Bedding Strips.....	260

Figure 7.62 - FE Models with Different Transverse Reinforcement Ratios.....	261
Figure 7.63 - Parametric Study on Transverse Reinforcement Ratio .....	262
Figure 7.64 - Re-analysis for FE Models with 3" Penetration Using $f_c = 4.0$ ksi.....	263
Figure 7.65 - Parametric Study Results on Stud Penetration and Clear Distance .....	264
Figure 7.66 - Additional Parametric Study Results on Stud Penetration and Clear Distance.....	265
Figure 7.67 - Classification and Boundary Equation for 1-1/8" Studs using Linear SVM.....	266
Figure 7.68 - Classification and Boundary Equation for 7/8" Studs using Linear SVM.....	267
Figure 7.69 - Additional Parametric Study Results on Stud Penetration and Clear Distance with $f_c=4.0$ ksi (proposed 10 <sup>th</sup> Ed. AASHTO).....	268
Figure 7.70 - Classification and Boundary Equation for 1-1/8" Stud using Linear SVM (proposed 10 <sup>th</sup> Ed. AASHTO).....	269
Figure 8.1 – Two-Span Loading Arrangement for Beam Specimen Nos. 1 and 2 .....	273
Figure 8.2 – Single-Span Loading Arrangement for Beam Specimen No. 1 .....	273
Figure 8.3 – Single-Span Loading Arrangement for Beam Specimen No. 2 .....	274
Figure 8.4 – Overhang Lengths of Beam Specimens .....	274
Figure 8.5 – Cross-Section of Beam Specimen No. 1 (Deck Reinforcement Shown for Negative Moment Region).....	275
Figure 8.6 – Cross-Section of Beam Specimen No. 2 (Deck Reinforcement Shown for Negative Moment Region).....	276
Figure 8.7 – Shear Stud Dimensions.....	277
Figure 8.8 – Shear Stud Layout for Beam Specimen No. 1.....	277
Figure 8.9 – Shear Stud Layout for Beam Specimen No. 2.....	277
Figure 8.10 – Layout of Studs.....	278
Figure 8.11 – Plan View of Top Mat of Reinforcing Bars for Beam Specimen No. 1.....	279
Figure 8.12 – Plan View of Bottom Mat of Reinforcing Bars for Beam Specimen No. 1.....	279
Figure 8.13 – Location of Splices in #4 Longitudinal Reinforcing Bars for Beam Specimen No. 1 .....	280
Figure 8.14 – Plan View of Longitudinal Reinforcing Bars for Beam Specimen No. 2.....	281

Figure 8.15 – Dimensions of a PCP Panel.....	281
Figure 8.16 – U-Bar Dimensions .....	282
Figure 8.17 – Formwork and Reinforcing for PCPs.....	282
Figure 8.18 – Broom Finishing of Top Surface of PCPs.....	283
Figure 8.19 – Finished PCP Panels.....	283
Figure 8.20 – Girder Supports (From Left to Right: North, Interior, South).....	284
Figure 8.21 – Photos of Loading Tower .....	285
Figure 8.22 – Location of Loading Towers for Two-Span Test on Beam Specimen Nos. 1 and 2 .....	285
Figure 8.23 – Location of Loading Towers for Single-Span Test on Beam Specimen No. 1 .....	286
Figure 8.24 – Location of Loading Tower for Single-Span Test on Beam Specimen No. 2.....	286
Figure 8.25 – Beam Specimen Lateral Restraint .....	286
Figure 8.26 – Beam Specimen End Braces.....	287
Figure 8.27 – Unloading and Erection of Steel Girder .....	288
Figure 8.28 – Welded Splice Detail.....	288
Figure 8.29 – Photos of Welded Splice .....	289
Figure 8.30 - 3D Sketch of the Formwork.....	289
Figure 8.31 - Cross-Section of Formwork .....	290
Figure 8.32 – Assembled Formwork .....	290
Figure 8.33 – Shear Stud Welding Gun with Stud Installed.....	292
Figure 8.34 – Welding Studs on Beam Specimen No. 2 .....	292
Figure 8.35 – 30 Degree Bend Tests of Studs on Beam Specimen No. 1 .....	293
Figure 8.36 – 90 Degree Bend Tests of Studs on Beam Specimen No. 2 .....	293
Figure 8.37 – Examples of Weld Collars.....	293
Figure 8.38 – Finished Deck Reinforcement for Beam Specimen No. 1 .....	294
Figure 8.39 – Finished Deck Reinforcement for Beam Specimen No. 2 .....	294
Figure 8.40 – PCP Panels Prior to Placement.....	295
Figure 8.41 – Foam Bedding Strips .....	296
Figure 8.42 – Reinforcing Bar Protruding from PCP Bent to Avoid Shear Stud	296
Figure 8.43 – Location of Panels and Corresponding Concrete Truck Numbers	297
Figure 8.44 – Examples of Gaps Between PCP Panels .....	298

Figure 8.45 – Concrete Placement for Beam Specimen No. 1 .....	299
Figure 8.46 – Concrete Placement for Beam Specimen No. 2 .....	299
Figure 8.47 – Beam Specimen No. 1: Sections of Concrete Deck Cast from Different Concrete Trucks .....	300
Figure 8.48 – Beam Specimen No. 2: Sections of CIP Portion of Deck Cast from Different Trucks.....	300
Figure 8.49 – Tension Test on Coupon Machined for 1-1/8" Stud.....	301
Figure 8.50 – Tensile Coupons from 1-1/8" Studs Before and After Testing ....	301
Figure 8.51 – Stress-Strain Curves for 1-1/8" Stud Tension Coupons .....	302
Figure 8.52 – Location of Tension Coupons in W40x199 Sections.....	304
Figure 8.53 – Cross-Section Measurement Locations .....	305
Figure 8.54 - Typical Reinforcement Tensile Test Results for Beam Specimen No. 1.....	307
Figure 8.55 – Locations of Vertical Deflection Measurements (Top: Two-Span Test; Bottom: Single Span Test).....	308
Figure 8.56 - String Potentiometers at the Quarter Point and at Midspan.....	309
Figure 8.57 – Location of Slip Measurements.....	309
Figure 8.58 – Linear Potentiometers and Dial Gauges Used to Measure Slip ...	310
Figure 8.59 – Specimen Cross-Sections with Strain Gauges.....	310
Figure 8.60 - Strain Gauge Locations in Positive Moment Region (Sections A, C, D) .....	311
Figure 8.61 - Strain Gauge Locations in Negative Moment Region (Section B)	311
Figure 8.62 - Strain Gauge Locations in Negative Moment Region (Section E)	312
Figure 8.63 - Strain Gauge Locations to Estimate Shear Stud Forces.....	312
Figure 8.64 – Beam Specimen No. 1 – Overall View During Two-Span Test...	315
Figure 8.65 – Beam Specimen No. 1 - Portion of Deck over Interior Support Prepared for Tracking Cracks .....	316
Figure 8.66 – Beam Specimen No. 1 - Crack Distribution after 7 Cycles of 50 kips Load per Ram.....	316
Figure 8.67 - Beam Specimen No. 1 - Crack Distribution after 7 Cycles of 150 kips Load per Ram .....	317
Figure 8.68 - Beam Specimen No. 1 - Crack Distribution after 7 Cycles of 225 kips Load per Ram .....	317
Figure 8.69 - Beam Specimen No. 1 - Crack Distribution after 7 Cycles of 300 kips Load per Ram .....	318

Figure 8.70 – Beam Specimen No. 1 - Crack Distribution After Completion of Two-Span Test.....	318
Figure 8.71 – Beam Specimen No. 1 – Maximum Crack Width under 450 kips per Ram and After Unloading.....	319
Figure 8.72 – Beam Specimen No. 1 Prior to Single-Span Test.....	321
Figure 8.73 – Beam Specimen No. 1 – Total Load vs. Midspan Deflection .....	321
Figure 8.74 – Beam Specimen No. 1 After Completion of Single-Span Test....	322
Figure 8.75 – Beam Specimen No. 1 – View of Top Flange for South Half of the Girder After Removal of Concrete Deck .....	322
Figure 8.76 – Beam Specimen No. 1 – Shear Studs on North Half of Beam After Removal of Concrete Deck.....	323
Figure 8.77 – Photos of Shear Stud Failure Modes for Beam Specimen No. 1..	324
Figure 8.78 – Macro-Etch Test Results for Shank Failure Mode .....	324
Figure 8.79 - Macro-Etch Test Results for Bright Spot Failure Mode .....	325
Figure 8.80 – Macro-Etch Test Results for Flat Fracture Failure Mode .....	325
Figure 8.81 – Macro-Etch Test Results for Deep Fracture Failure Mode .....	325
Figure 8.82 – Macro-Etch Test Results for Wide Crater Failure Mode .....	326
Figure 8.83 – Deformed Shape of Fractured Shear Studs .....	326
Figure 8.84 - Typical Load Slip Curve for Beam Specimen No. 1 (LP5) .....	328
Figure 8.85 – Cross-Section of FE Model of Beam Specimen No. 1 .....	330
Figure 8.86 – FE Model of Beam Specimen No. 1 Under Load .....	331
Figure 8.87 – FE and Experimental Load-Deflection Responses for Beam Specimen No. 1 .....	331
Figure 8.88 – Beam Specimen No. 2 Prior to Two-Span Test .....	333
Figure 8.89 - Beam Specimen No. 2 - Portion of Deck over Interior Support Prepared for Tracking Cracks .....	333
Figure 8.90 – Beam Specimen No. 2 – Crack Distribution after 7 Cycles of 50 kips Load per Ram .....	334
Figure 8.91 - Beam Specimen No. 2 - Crack Distribution after 7 Cycles of 150 kips Load per Ram .....	334
Figure 8.92 - Beam Specimen No. 2 - Crack Distribution after 7 Cycles of 225 kips Load per Ram .....	335
Figure 8.93 - Beam Specimen No. 2 - Crack Distribution after 7 Cycles of 300 kips Load per Ram .....	335
Figure 8.94 - Beam Specimen No. 2 - Crack Distribution After Completion of Two-Span Test and Boundaries of the PCPs .....	336

Figure 8.95 – Beam Specimen No. 2 Prior to Single-Span Test.....	337
Figure 8.96 – Beam Specimen No. 2 – Load vs Midspan Deflection .....	338
Figure 8.97 – Beam Specimen No. 2 After Completion of Single-Span Test ....	338
Figure 8.98 – Beam Specimen No. 2 – View Looking Down on Crushed Section of Deck.....	339
Figure 8.99 – Beam Specimen No. 2 – East Side of Crushed Section of Deck..	339
Figure 8.100 – Beam Specimen No. 2 -West Side of Crushed Section of Deck	339
Figure 8.101 – Beam Specimen No. 2 – View Looking Up at the Bottom Side of Deck Showing Crushing at Boundary of PCPs.....	340
Figure 8.102 – Beam Specimen No. 2 – Photos of Studs After Concrete Deck Removal .....	340
Figure 8.103 – Beam Specimen No. 2 – Section Cut Through Slab Near Shear Stud .....	341
Figure 8.104 – Beam Specimen No. 2 – Section of Slab Cut Near End of Beam .....	341
Figure 8.105 – Load-Slip Curve at LP7 for Beam Specimen No. 2 .....	342
Figure 8.106 – Mesh of FE Model for Beam Specimen No. 2 .....	344
Figure 8.107 - FE and Experimental Load-Deflection Responses for Beam Specimen No. 2.....	344
Figure 9.1 – Recommended Stud Penetration into Deck for Full-Depth Cast-in- Place Decks.....	360
Figure 9.2 – Recommended Stud Penetration into Deck and Clear Distance from Stud to PCP for Decks with PCPs.....	362
Figure 9.3 – Plan View of Girder Top Flange with Staggered Stud Arrangement .....	363
Figure 9.4 – Idealized Representation of the Compressive Stress Block in a Bridge Deck with PCPs .....	365



# Chapter 1. Introduction

## 1.1. Background

Efficient steel bridge girder design makes use of composite action between the concrete deck and the steel girders. Composite action is achieved by welding shear studs to the top flange of the steel girder during fabrication or erection. The shear stud diameter most commonly used in steel bridge construction in Texas and throughout most of the U.S. is 7/8". The design of composite steel girder bridges and requirements for shear studs are specified in the 9<sup>th</sup> Ed. AASHTO LRFD Bridge Design Specifications (AASHTO 2020) and in the 2020 AASHTO/AWS D1.5 Bridge Welding Code (AWS 2020). The number and placement of studs must satisfy both the strength and fatigue requirements in AASHTO. Fatigue normally controls the required number of shear studs, and many shear studs are typically needed to satisfy AASHTO fatigue requirements. The photos in Figure 1.1 show the large number of shear studs typically used on steel I girder and tub girder bridges. Both photos are of bridges under construction in Texas.



*Figure 1.1 - Steel Bridge Girders with Shear Studs*

The large number of shear studs creates a safety hazard for workers during erection and early stages of construction due to limited space to walk or stand on the flange. The large number of studs can also increase the cost of fabrication.

Decks for steel girder bridges in Texas have typically been constructed using full-depth cast-in-place concrete slabs formed on permanent metal deck forms. Figure 1.2 shows a cross-section of a composite bridge girder with a full-depth cast-in-place deck (permanent metal deck forms not shown). However, there is increasing interest in using partial depth precast concrete deck panels (PCPs) on steel girder bridges in Texas to increase the speed and reduce the cost of construction. Figure 1.3 shows a typical cross-section when PCPs are used. The PCPs span between steel girders and are supported on the edge of the steel girders on foam bedding strips. Densely placed shear studs can impede the placement of the PCPs. When multiple shear studs are used across the

width of the beam flange, the space left for placing the PCP is limited. The use of larger-diameter shear studs can reduce the number of shear studs on a girder, thereby improving safety and facilitating the use of PCPs.

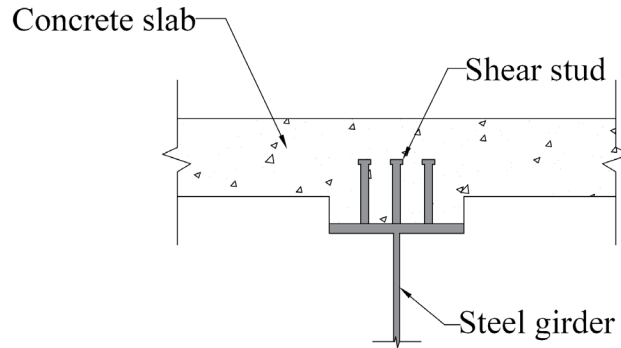


Figure 1.2 - Typical Cross-Section of a Composite Steel Bridge Girder with a Full-Depth Cast-in-Place Deck

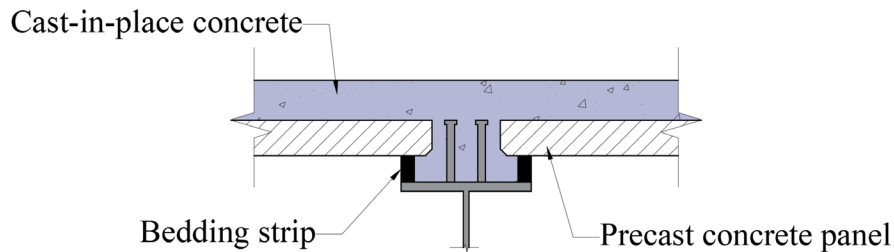


Figure 1.3 - Typical Cross-Section of a Composite Steel Bridge Girder Using PCPs

Based on current AASHTO rules, the capacity of a shear stud, both for fatigue and for ultimate strength, is proportional to the cross-sectional area of the stud. Table 1.1 lists the areas of shear studs ranging from 7/8" to 1-1/4". The last column in this table shows the number of studs needed for larger-diameter shear studs compared to 7/8" shear studs. For 1-1/4" shear studs, the required number of studs is about 50 percent of the required number of 7/8" studs. For 1-1/8" shear studs, the required number of studs is about 60 percent of the required number of 7/8" studs. It is clear that using larger-diameter shear studs can significantly reduce the required number of shear studs.

**Table 1.1 - Potential Reduction in Shear Studs**

Stud Diameter	Stud Area	$A_{stud} / A_{7/8\text{ stud}}$	No. of studs / No. of 7/8" studs
7/8"	0.60 in <sup>2</sup>	1.0	100 %
1"	0.79 in <sup>2</sup>	1.31	76 %
1-1/8"	0.99 in <sup>2</sup>	1.65	61 %
1-1/4"	1.23 in <sup>2</sup>	2.04	49 %

The 9<sup>th</sup> Ed. AASHTO (AASHTO 2020) does not specify an upper limit of stud diameter. However, the 9<sup>th</sup> Ed. AASHTO requires that stud dimensions and mechanical properties conform to the requirements in the AWS D1.5 Bridge Welding Code (AWS 2020). AWS D1.5 specifies dimensions and mechanical properties for studs up to and including 1" diameter. Consequently, the 9<sup>th</sup> Ed. AASHTO indirectly limits shear stud diameter to 1" by reference to AWS D1.5. Further, a review of stud manufacturers' websites and literature indicates that shear stud diameters greater than 1" are not commercially available as "off-the-shelf" products. However, shear studs with a diameter great than 1" can currently be provided by stud manufacturers on a custom order basis.

## 1.2. Research Goal and Objectives

Texas Department of Transportation (TxDOT) Research Project 0-7042 – *Use of Larger Diameter Shear Studs for Composite Steel Bridges* was undertaken with the overall goal of evaluating the feasibility of using larger-diameter shear studs in composite steel bridges. As described above, shear stud diameters up to and including 1" are currently permitted in steel bridge construction by AASHTO and AWS D1.5. Consequently, for the research undertaken in TxDOT Research Project 0-7042, the term *larger-diameter* shear studs refer to studs with a diameter greater than 1". More specifically, 1-1/8" and 1-1/4" shear studs were considered in this research.

Specific objectives of TxDOT Project 0-7042 included the following:

- Determine if larger-diameter shear studs can be welded with consistently good quality using commercially available stud welding equipment.
- Determine if current equations in the AASHTO LRFD Bridge Design Specifications for stud ultimate strength and fatigue strength can be safely used for larger-diameter shear studs, or if modifications to these equations are needed.
- Determine if larger-diameter shear studs cause excessive cracking of the concrete deck under service level loading.

At the time this research was conducted and at the time this report was prepared, the governing version of the AASHTO LRFD Bridge Design Specifications was the 9<sup>th</sup> Edition (AASHTO 2020). The shear stud ultimate strength and fatigue strength equations in the 9<sup>th</sup> Edition AASHTO are essentially the same as those in earlier versions of AASHTO, going back for many years. However, significant changes have been proposed to the provisions for computing both ultimate strength and fatigue strength of shear studs for the upcoming 10<sup>th</sup> Ed. AASHTO, expected to be released in 2024. At the time this report was prepared, the proposed changes to shear stud provisions (AASHTO 2021) have been successfully balloted. Thus, when evaluating larger-diameter shear studs in this research project, the performance of the studs will be compared to both the current 9<sup>th</sup> Ed. AASHTO (AASHTO 2020) as well as the upcoming 10<sup>th</sup> Ed. AASHTO requirements (AASHTO 2021). A summary of all shear stud design and detailing requirements in the 9<sup>th</sup> Ed. AASHTO and proposed 10<sup>th</sup> Ed. AASHTO is provided in Chapter 2 of this report.

### 1.3. Project Scope and Report Organization

---

This report summarizes the research conducted under TxDOT Project 0-7042. The following major tasks were undertaken in this project:

#### Background and Literature Review

A literature review was conducted on previous research on shear studs, in general, and more specifically on larger-diameter shear studs. This includes previous work both on stud ultimate strength and on stud fatigue strength. In addition, all design and detailing requirements for shear studs were summarized, including those in the 9<sup>th</sup> Ed. AASHTO, the proposed 10<sup>th</sup> Ed. AASHTO, AWS D1.5, and in pertinent TxDOT standards and guidance documents. This work is summarized in Chapter 2.

#### Preliminary Design Studies

In this task, three existing TxDOT bridges constructed with 7/8" diameter shear studs were redesigned using 1", 1-1/8", and 1-1/4" shear studs. The purpose of these redesigns was to quantify the reduction in the number of shear studs that can be achieved when using larger-diameter studs for realistic bridges. An additional purpose of this exercise was to determine if existing stud geometric requirements (minimum and maximum pitch, transverse spacing requirements, minimum and maximum stud length requirements, etc.) may be problematic for larger diameter shear studs. These studies are summarized in Chapter 3.

## Stud Welding Investigations

The purpose of this task was to determine if larger-diameter shear studs can be welded with consistent quality using commercially available stud welding equipment. As part of this task, hundreds of trial welds were made using a variety of welding parameters and then evaluated for quality using a variety of evaluation and testing methods. Trial welds were made on small plates as well as on girders with various flange thicknesses. Welding trials were conducted both on 1-1/8" and 1-1/4" studs. The stud welding investigations are documented in Chapter 4. Chapter 4 concludes with a selection of the shear stud diameter for further testing and analysis in this research project. The remaining tasks of this project involved extensive large-scale testing, including both push-out tests and composite girder tests. Because of the cost and time required for these tests, a single shear stud diameter was selected for investigation in the remainder of this research project. Based on the stud welding investigations as well as on the findings of the preliminary design studies, 1-1/8" shear studs were selected for further investigation. The reasoning for this selection is described in Chapter 4.

## Push-out Tests

A series of push-out tests were conducted to study the static loading behavior of 1-1/8" shear studs. These tests characterized the overall load-slip response of the studs and quantified stud ultimate strength and slip capacity. Some push-out tests were also conducted using 7/8" studs for comparison. The stud static push-out tests explored a number of design variables, including stud layout, stud penetration depth into the deck, deck type (full-depth cast-in-place versus PCPs), and others. In addition, a series of push-out fatigue tests were conducted to investigate the fatigue performance of 1-1/8" studs. The static push-out tests are described in Chapter 5 and the fatigue push-out tests are described in Chapter 6.

## Finite Element Analysis of Static Push-out Behavior of 1-1/8" Studs

Detailed finite element models were developed for the experimental static push-out tests. The modeling techniques were validated with the experimental results. The validated finite element models were then used to conduct an extensive parametric study of the static push-out behavior of 1-1/8" studs. These parametric studies investigated a wide range of variables that may affect stud static loading behavior. The results of these parametric finite element studies were then used to guide the development of design recommendations for the ultimate strength of 1-1/8" studs. The finite element studies of static push-out behavior are summarized in Chapter 7.

## Large-scale Composite Beam Tests

To further investigate the static loading performance of 1-1/8" shear studs, two large-scale composite beam specimens were tested. The first specimen used a full-depth cast-in-place deck and the second specimen used a deck constructed using PCPs. The large-scale beam tests

included some supporting finite element analysis to help in interpreting the test results. The large-scale composite beam tests and supporting finite element analysis are described in Chapter 8.

### Major Findings and Design Recommendations

A summary of all research conducted in this project and the major findings for each task is provided in Chapter 9. Chapter 9 also provides design recommendations for the use of 1-1/8" shear studs in composite steel bridge girders, and draft specification language for possible adoption in the AASHTO LRFD Bridge Design Specifications and the AASHTO/AWS D1.5 Bridge Welding Code.

## Chapter 2. Background and Literature Review

### 2.1. Introduction

---

This chapter begins with a review of shear stud requirements in the AASHTO LRFD Bridge Design Specifications, in the AWS Bridge Welding Code, and in pertinent TxDOT standards and preferred practices. This is followed by a review of past research on shear studs, with an emphasis on past research on larger-diameter shear studs. This includes information on shear stud test methods, shear stud behavior under static loading, and shear stud behavior under fatigue loading. Previous data on static and fatigue strength of larger-diameter shear studs is summarized and compared to static and fatigue strength requirements in AASHTO. The chapter concludes with information on two bridges constructed in Nebraska using 1-1/4" shear studs.

### 2.2. Review of Shear Stud Requirements in Bridge Standards

---

This section provides a summary of shear stud design and detailing requirements pertinent to Texas bridges, in the following standards and guidelines:

- 9<sup>th</sup> Ed. AASHTO LRFD Bridge Design Specifications (AASHTO 2020) – hereinafter referred to as the *9<sup>th</sup> Ed. AASHTO*.
- Proposed shear stud requirements in the upcoming 10<sup>th</sup> Ed. AASHTO LRFD Bridge Design Specifications (AASHTO 2021) – hereinafter referred to as the *proposed 10<sup>th</sup> Ed. AASHTO*.
- AWS D1.5 Bridge Welding Code (AWS 2020) – hereinafter referred to as *AWS D1.5*.
- TxDOT *Preferred Practices for Steel Bridge Design, Fabrication and Erection* (TxDOT 2021).
- TxDOT *Bridge Design Manual* (TxDOT 2023).
- TxDOT *Miscellaneous Details – Steel Girders and Beams – SGMD* (TxDOT 2019).
- TxDOT *Prestressed Concrete Panel Fabrication Details – PCP-FAB* (TxDOT 2015).

Minimum mechanical requirements for welded shear studs for use in bridges are specified in AWS D1.5 and are reproduced in Table 2.1. Shear studs used in composite beams are required to be Type B. A footnote to this table in AWS D1.5 states that Type B studs are limited in diameter from 1/2" through 7/8". No reference is made to 1" studs which are currently allowed in bridge construction. It appears that the 7/8" limit in the footnote is an oversight, and should likely be 1".

**Table 2.1 - Mechanical Property Requirements for Studs in AWS D1.5**

Property	Type A	Type B
Tensile Strength	55 ksi min.	60 ksi min.
Yield Strength (0.2% offset)	-	50 ksi min.
Elongation (% in 2 in.)	17% min.	20% min.
Reduction of Area	50% min.	50% min.

Dimensions and tolerances for shear studs are also specified in AWS D1.5 and are reproduced in Table 2.2.

**Table 2.2 - Standard Dimensions for Shear Studs in AWS D1.5**

Standard Shear Stud Dimensions (in.)			
Shank Diameter	Length Tolerance	Head Diameter	Minimum Head Height
0.5	±1/16	1 ± 1/64	0.28
0.625	±1/16	1.25 ± 1/64	0.28
0.75	±1/16	1.25 ± 1/64	0.38
0.875	±1/16	1.375 ± 1/64	0.38
1	±1/16	1.625 ± 1/64	0.50

A review of the 9<sup>th</sup> Ed. AASHTO, the proposed 10<sup>th</sup> Ed. AASHTO, and AWS D1.5 indicates there is no explicit limit specified for shear stud diameter for bridges. However, the absence of specified dimensions for shear studs greater than 1" diameter implies that shear studs greater than 1" diameter are not permitted in AWS D1.5, and by reference to AWS D1.5 in AASHTO, are also not permitted by AASHTO.

Dimensions and mechanical properties for shear studs used in building applications are specified in AWS D1.1 – *Structural Welding Code Steel* (AWS 2020). AWS D1.1 specifies a minimum tensile strength for shear studs in composite beams equal to 65 ksi, in comparison with 60 ksi in AWS D1.5. A review of stud manufacturers' websites and a discussion with a stud manufacturer suggests that all shear studs for use in composite beams, whether for buildings or bridges, and whether specified to be in accordance with AWS D1.1 or D1.5, are all supplied with a minimum tensile strength of 65 ksi. Table 2.3 summarizes various detailing requirements for shear studs in the 9<sup>th</sup> Ed. AASHTO, in the proposed 10<sup>th</sup> Ed. AASHTO, and in various TxDOT standards and guidelines.



**Table 2.3 - Detailing Requirements for Shear Studs**

Item	9 <sup>th</sup> Ed. AASHTO	Proposed 10 <sup>th</sup> Ed. AASHTO	TxDOT Standards and Guidelines
Stud length to diameter ratio	≥ 4.0	≥ 5.0* ≥ 7.0**	Minimum stud length = 5" (TxDOT 2019)
Minimum longitudinal pitch	6d	4d	4" (TxDOT 2021) 4d (TxDOT 2023)
Maximum longitudinal pitch	48" (w <sub>d</sub> ≥ 24") 24" (w <sub>d</sub> < 24")		24" (TxDOT 2023)
Transverse pitch	≥ 4d		≥ 3.5" (TxDOT 2019) ≥ 4d (TxDOT 2021)
Clear distance (beam flange edge/stud)	≥ 1"		-
Clear distance (PCP edge/stud head)	-		≥ 5/8" (TxDOT 2019, TxDOT 2021)
Top clear cover above stud	≥ 2"		≥ 2.5" (TxDOT 2019)
Stud penetration into concrete deck	≥ 2"		≥ 2"

Notes: \* = normal weight concrete  
 \*\* = lightweight concrete  
 d = stud diameter  
 w<sub>d</sub> = depth of girder web  
 - = not specified

The changes in stud detailing requirements between the 9<sup>th</sup> Ed. AASHTO and the proposed 10<sup>th</sup> Ed. AASHTO are in the required stud length to diameter ratio (discussed in Section 2.3.2) and in the minimum longitudinal pitch, which is reported to be based on a study by Provines et al. (Provines, Ocel and Zmetra 2019).

Table 2.4 summarizes key provisions for computing stud shear strength and stud fatigue resistance in the 9<sup>th</sup> Ed. AASHTO and in the proposed 10<sup>th</sup> Ed. AASHTO.

**Table 2.4 - Shear Stud Fatigue and Ultimate Strength Requirements in 9th Ed. AASHTO and Proposed 10th Ed. AASHTO**

Item	9 <sup>th</sup> Ed. AASHTO	Proposed 10 <sup>th</sup> Ed. AASHTO
Critical $(ADTT)_{SL}$	1090	11320
Fatigue resistance of one stud, $Z_r$ (kips)	Fatigue I: $5.5d^2$	Fatigue I: $(\Delta F)_{TH}A_{sc}$ where: $(\Delta F)_{TH} = 7$ ksi
	Fatigue II: $(34.5-4.28 \log N)d^2$	Fatigue II: $(\frac{A}{N})^{\frac{1}{m}}A_{sc}$ where: $A = 1040 \times 10^8$ ksi <sup>5</sup> $m = 5$
Strength resistance factor, $\phi_{sc}$	0.85	1.00
Nominal shear resistance of one stud, $Q_n$	$0.5A_{sc}\sqrt{f'_cE_c} \leq A_{sc}F_u$	$0.7A_{sc}F_u$

Notes:  $d$  = diameter of stud (in)  
 $A_{sc}$  = area of shear stud (in<sup>2</sup>)  
 $F_u$  = tensile strength of shear stud material (ksi)  
 $f'_c$  = minimum 28-day compressive strength of concrete (ksi)  
 $E_c$  = modulus of elasticity of concrete (ksi)  
 $(ADTT)_{SL}$  = average single-lane daily truck traffic  
 $(\Delta F)_{TH}$  = constant amplitude fatigue threshold (ksi)  
 $N$  = number of cycles  
 $A$  = fatigue detail category constant (ksi<sup>m</sup>)  
 $m$  = fatigue growth constant

As described in Chapter 1, there are significant changes to both the stud shear resistance and fatigue resistance calculations in going from the 9<sup>th</sup> Ed. AASHTO to the proposed 10<sup>th</sup> Ed. AASHTO. In regard to the stud ultimate strength, both the nominal shear resistance calculation and the resistance factor changed, based largely on the work by Pallares and Hajjar (2010) as discussed in Section 2.3.2. The change in fatigue requirements were based on a reevaluation of stud fatigue test data and reformatting to include stud fatigue resistance in Table 6.6.1.2.3-1 of AASHTO, thus making fatigue design of shear studs similar to fatigue design of other steel bridge components (AASHTO 2021).

## 2.3. Shear Stud Test Methods

To investigate shear stud behavior under static and fatigue loading, there are mainly two categories of test methods in previous studies. The first is push-out tests and the second is beam tests. This section will introduce these test methods and discuss their advantages and disadvantages in investigating shear stud performance.

### 2.3.1. Push-out Tests

Push-out tests are the most common method for investigating shear stud behavior. A typical push-out test setup is composed of two nominally identical concrete slabs, a steel wide flange

beam and several shear connectors, as shown in Figure 2.1. The force is usually applied on the top of the steel section and transferred to the two concrete slabs through the shear studs.

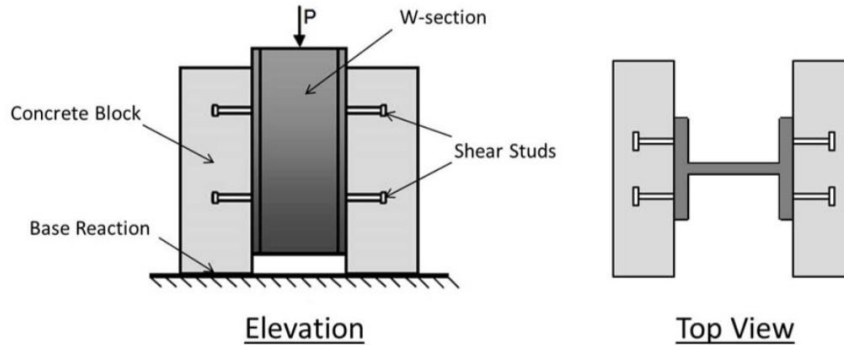


Figure 2.1 - Typical Push-out Test Setup (Patel 2013)

This test setup has the advantage of economy compared to beam tests and has been used in numerous past studies. Eurocode 4 (CEN 2004) specifies a standard push-out specimen that has been used in a number of past studies. However, a majority of past studies have not used the Eurocode 4 standard specimen. The details of the push-out test specimen have varied considerably among researchers. There are variations in the dimensions of the concrete slabs, reinforcing details used in the concrete slabs, the number and layout of the shear studs, support conditions at the bottom of the concrete slabs, and the use of mechanisms to prevent outward movement of the concrete slabs away from the steel section. While commonly used, the push-out specimen has some disadvantages when used to investigate the behavior of shear studs. Stud fatigue performance has been observed to be different than what has been measured in more realistic beam tests (Ghiami Azad 2016). Push-out tests appear to provide a lower bound for fatigue strength compared to beam tests (Slutter and Fisher 1966). Due to the limited specimen size, only a few studs can be installed in the slabs, which leads to limited load redistribution among studs and thus potentially earlier failure compared with actual bridge girders. It can be difficult to obtain consistent properties of the concrete in the two slabs. If the slabs are cast in the vertical position, there can be a variation in concrete properties over the height of the slab. The push-out test setup also introduces load eccentricity. The distance from the reaction force to the steel-concrete interface will cause a moment that can cause additional tension force in the studs that may not be present in an actual bridge girder.

A variation on the typical push-out specimen shown in Figure 2.1 is a one-sided push-out specimen. Many variations of one-sided push-out specimens are possible. One variation is shown in Figure 2.2 in which a single shear stud can be tested. Another variation of a one-sided push-out specimen is shown in Figure 2.3. This setup was used in a previous study on 1-1/4" shear studs.

One potential advantage of the one-sided test is that a test can be conducted on a single shear stud. The push-out test requires at least two studs (one in each slab) and usually includes more. Thus, the one-sided tests may allow more accurately characterizing the load-slip behavior or fatigue strength of a single stud. When multiple studs are tested in a single specimen, the resulting behavior reflects some redistribution of load among the shear studs. Although the one-sided push-out test, also sometimes referred to as a direct shear test, is intended to minimize load eccentricities, researchers have observed bending of the steel plate during load application (Kayir 2006). This problem was addressed by using various devices to clamp down the plate. Based on information in the literature, there is no clear conclusion or consensus on which type of test setup, i.e., the conventional push-out test or the one-sided push-out test, is preferable for establishing the static and fatigue properties of shear studs. Nonetheless, the conventional push-out test is the most common testing approach used and is the primary basis for shear stud requirements in AASHTO (2021).

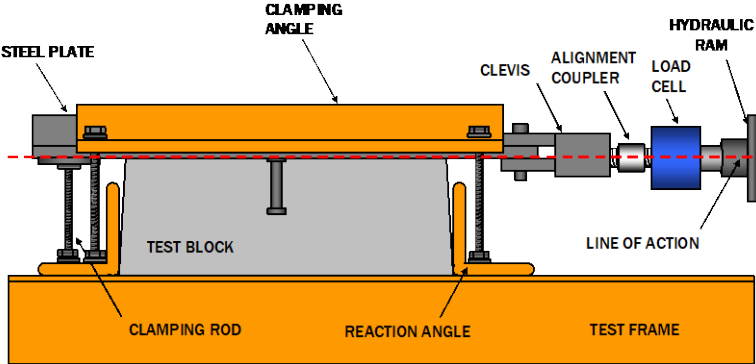


Figure 2.2 - One-Sided Push-out Specimen with a Single Shear Stud and Load Applied to Steel (Kayir 2006)

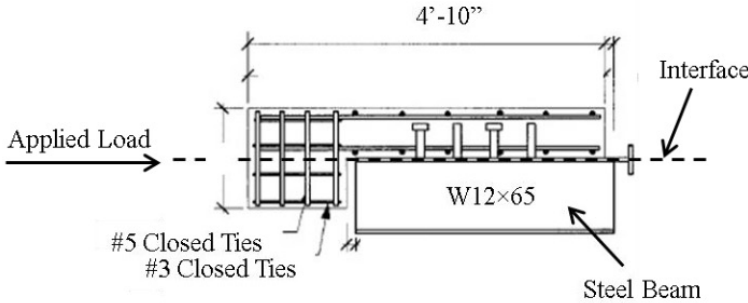


Figure 2.3 - One-Sided Push-out Specimen with Load Applied to Concrete (Badie, Tadros, et al. 2002)

### 2.3.2. Beam Tests

Beam tests have the advantage of replicating the geometry and loading conditions of shear connectors in an actual beam in the most accurate way. An example of a laboratory test of a composite bridge girder is shown in Figure 2.4.



*Figure 2.4 - Example of Laboratory Test of a Composite Beam (Kwon, et al. 2007)*

However, compared to component tests, beam tests are costly and time consuming. In addition, it is difficult to capture the behavior of a single shear stud. For example, it is difficult to measure the shear force resisted by any particular shear stud in a beam test, although some researchers have attempted to do this (Kreitman, et al. 2016). Another challenge with beam tests is identifying individual connector failure sequence and their failure modes. An additional limitation is that laboratory beam tests typically use span lengths on the order of about 30 ft. to 40 ft. (Kwon, et al. 2007, Badie, Tadros, et al. 2002); significantly shorter than typical steel bridge spans. Nevertheless, beam tests represent the most realistic tests of shear studs and composite behavior that can be achieved in a laboratory.

## **2.4. Shear Stud Behavior under Static Loading**

---

The behavior of shear studs under static loading has been studied since the 1950's by numerous investigators. These studies can be broadly divided into two categories: studs in solid concrete slabs and studs in concrete slabs with metal floor decking. The studies with metal floor decking are largely aimed at building applications, where metal floor decking running over the beams is commonly used. For bridge applications, studies of studs in solid concrete slabs (i.e., no metal decking running over beams) are of primary interest, since metal decking running over bridge girders is not normally used. While permanent metal deck forms are often used in bridge construction, these forms run between girders but do not run over the top of the girders.

Consequently, the metal deck forms do not impact the behavior of the shear studs. This section briefly reviews previous research on the static loading behavior of shear studs in solid concrete slabs. Section 2.5 reviews the behavior of shear studs under fatigue loading in solid concrete slabs.

### 2.4.1. Load- Slip Curves and Stud Failure Modes

As described earlier, stud behavior has typically been studied using push-out tests. This includes both conventional push-out tests as well as one-sided push-out tests. The primary result of a push-out test is a load-slip curve. A qualitative load slip curve is illustrated in Figure 2.5

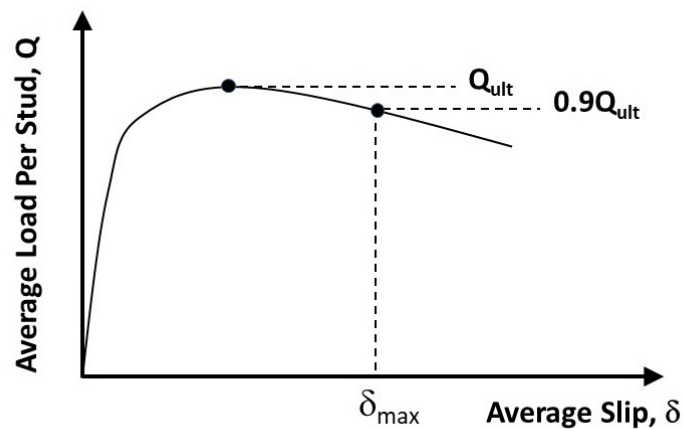


Figure 2.5 - Qualitative Load-Slip Curve from Push-out Test

On the vertical axis is the average load per stud. This is determined by taking the total load applied to the specimen, for example the load  $P$  shown in Figure 2.1, and dividing by the number of studs in the specimen. On the horizontal axis is the average slip between the steel and the concrete. The slip is typically determined by instruments measuring the relative displacement between the steel and concrete, at the steel-concrete interface. Several displacement transducers are normally placed at various locations along the steel-concrete interface, and the readings from these transducers are averaged to obtain the average slip.

The peak of the load slip curve, shown as  $Q_{ult}$  in Figure 2.5, is taken as the ultimate capacity of the shear studs in the test. The ductility of the studs is also of interest in characterizing the static behavior, and this is normally represented by the slip capacity, shown as  $\delta_{max}$  in Figure 2.5. Different investigators have used various definitions of slip capacity, but a common definition is that the slip capacity is taken as the slip when the stud resistance reduces to 90 percent of its peak value as adopted in Eurocode 4 (CEN 2004), as illustrated in Figure 2.5. The load-slip curve, in addition to providing data on stud ultimate strength and slip capacity, can also be used in finite element models of composite beams to represent shear stud behavior.



Also of interest in a push-out test is the observed failure mode of the studs. Failure modes have been described by investigators as either failure in the concrete, fracture of the shear stud, or a mixed failure where the shear stud has fractured but the concrete also shows significant distress. A common failure mode is fracture of the shear stud, either through the shank of the stud a short distance above the weld or a fracture passing through or close to the weld region. An example of stud fracture is shown in Figure 2.6 from push-out tests on 7/8" studs reported by Xue, et al. (2012).



*Figure 2.6 - Example of Shear Stud Fracture in a Push-out Test (Xue, et al. 2012)*

The studs shown in this figure were extracted from the concrete slabs after testing. The highly localized shear deformations at the fractures are apparent.

The failure mode in a push-out test can also be associated with failure of the concrete. Various types of concrete failures and distress have been described by investigators, including embedment failure, splitting cracks in the concrete, crushing of the concrete and others. A common concrete failure mode appears to be embedment failure, sometimes also referred to as pry-out failure. Figure 2.7 and Figure 2.8 show an example of an embedment failure in tests by Ollgaard et al (1971).

#### **2.4.2. Development of Equations to Predict Shear Stud Strength**

Many investigators, dating back to the 1950's, have proposed equations to predict the strength of shears studs, based primarily on push-out tests. One of the earliest investigations of shear studs using push-out tests was conducted by Viest (1956). These tests considered stud diameters ranging from 1/2" to 1-1/4". Based on results of 12 push-out tests, the equation proposed by Viest considered stud strength in solid concrete slabs as a function of stud diameter and concrete compressive strength, as shown in Eq. 2-1. It should be noted this research focused on elastic

design of composite structures. Stud strength,  $Q_n$ , predicted by Eq. 2-1 reflects small inelastic deformations in the structure and provides considerably smaller strength values compared to more recent stud strength equations.

$$Q_n = \begin{cases} 5.25 d^2 f_c' \sqrt{\frac{4000}{f_c'}} & \text{for } d < 1 \text{ in.} \\ 5 d f_c' \sqrt{\frac{4000}{f_c'}} & \text{for } d \geq 1 \text{ in.} \end{cases} \quad (2-1)$$

where:

- $Q_n$  = shear stud capacity, lbs;
- $d$  = shear stud diameter, in;
- $f_c'$  = concrete compressive strength, psi.

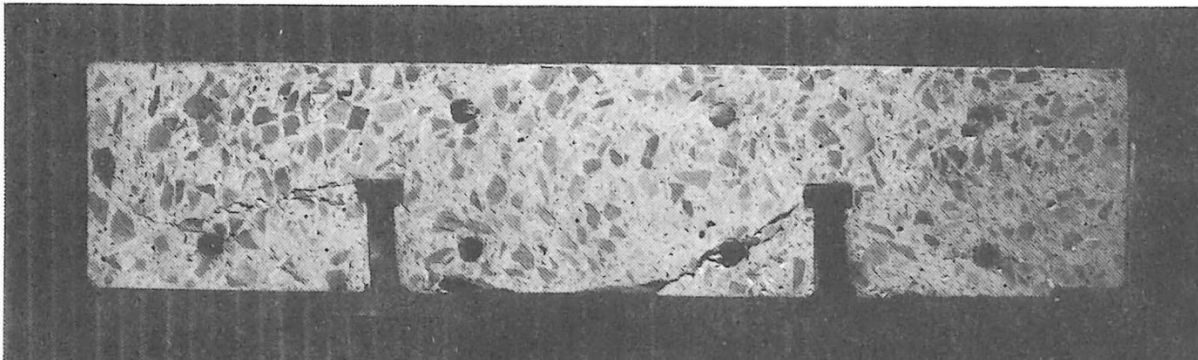


Figure 2.7 - Example of Concrete Embedment Failure at Shear Stud (Ollgaard, Slutter and Fisher, Shear Strength of Stud Connectors in Lightweight and Normal-Weight Concrete 1971)

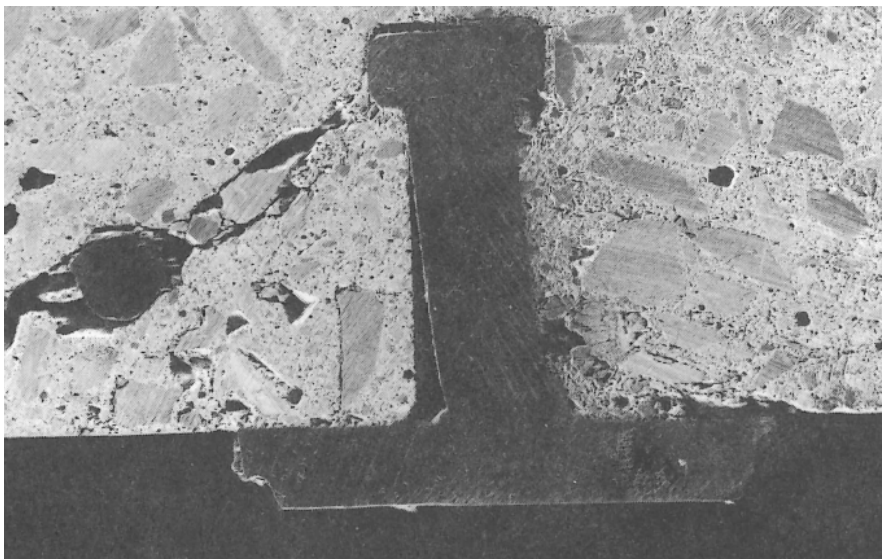




Figure 2.8 - Close of View of Right Shear Stud in Figure 2.7 (Ollgaard, Slutter and Fisher, *Shear Strength of Stud Connectors in Lightweight and Normal-Weight Concrete* 1971)

Based on push-out tests conducted by Viest (1956) and by Thurlimann (1959), Driscoll and Slutter (1961) modified Eq. 2-1 and proposed the stud strength equation shown in Eq. 2-2. Shear stud diameters considered by Driscoll and Slutter were between 1/2" and 1-1/4". It was reported that when the stud had a height to diameter ratio less than 4.2 (short stud), concrete cracking failure may occur. When the stud had a height to diameter ratio larger than 4.2 (long stud), shear stud fracture was the dominant failure mode. Thus, the strength of short studs is smaller than that of long studs, which is reflected in Eq. 2-2. Furthermore, Driscoll and Slutter observed that the stud can develop the full tensile fracture strength in push-out tests rather than just the shear fracture strength. It was reported that stud tensile strength should be used to predict the strength of a long stud even though this is not reflected in Eq. 2-2.

$$Q_n = \begin{cases} 222 h d \sqrt{f'_c} & \text{for } h/d < 4.2 \\ 932 d^2 \sqrt{f'_c} & \text{for } h/d \geq 4.2 \end{cases} \quad (2-2)$$

where:

- $Q_n$  = shear stud capacity, lbs;
- $d$  = shear stud diameter, in;
- $h$  = shear stud height, in;
- $f'_c$  = concrete compressive strength, psi.

Equation 2-2 allows for more inelastic deformation in shear studs at ultimate strength. Shear stud strength calculated is much larger than that from Eq. 2-1. For example, consider a 7/8" stud with a height greater than 4.2 times its diameter, and a concrete compressive strength of 4000 psi. The stud strength  $Q_n$  is 16,080 lb. according to Eq. 2-1 and is 45,130 lb. according to Eq. 2.2.

As reported by Pallares and Hajjar (2010) and Bonilla et al. (2018), later equations for stud strength proposed during the 1960's took failure mode into consideration in an explicit way. Failure modes considered in these equations include stud fracture, concrete failure, and flange pull out failure. For stud fracture, stud strength is a function of cross-section area and the stud steel tensile strength. For failure caused by concrete, stud strength is related to stud diameter, stud height, and concrete compressive strength.

Goble (1968) performed 41 push-out tests using steel girders with thin flanges. Shear studs of 1/2" to 3/4" diameter and a solid concrete slab were considered. It was reported that to avoid failure caused by pull out of the steel beam flange, the stud diameter must be smaller than 2.7 times the flange thickness. Based on the work by Goble, the 2022 AISC *Specification for Structural Steel Buildings* (AISC 2022), hereinafter referred to as AISC 2022, requires that the stud diameter shall not be greater than 2.5 time the thickness of the flange unless welded to a flange directly over the web. This same limit has been included in AISC Specifications for

several decades. Note that this limit has no practical implications for bridge construction, even for larger-diameter shear studs. For example, for 1-1/4" studs, the minimum flange thickness is  $1.25"/2.5 = 0.50"$ . TxDOT *Preferred Practices for Steel Bridge Design, Fabrication, and Erection* (TxDOT 2021) states that the preferred minimum flange thickness in plate girders is 3/4" for straight girders and 1" for curved girders. Consequently, flange pull out failure need not be considered in bridge girder design.

Ollgaard et al. (1971) performed 48 push-out tests using 5/8" and 3/4" diameter shear studs in solid concrete slabs. Predictive equations for shear stud strength were developed by curve fitting the test data. It was found that in addition to stud cross-section area, the average measured static ultimate strength of a shear stud correlated not only to the concrete compressive strength but also to the concrete modulus of elasticity. The best fit equation developed by Ollgaard was as follows.

$$Q_n = 1.106 A_{sc} f_c'^{0.3} E_c^{0.44} \quad (2-3)$$

where:

- $Q_n$  = shear stud capacity, kips;
- $A_{sc}$  = cross-sectional area of stud, in<sup>2</sup>;
- $f_c'$  = concrete compressive strength, ksi;
- $E_c$  = concrete modulus of elasticity, ksi.

A design-oriented simplified version of Eq. 2-3 is shown in Eq. 2-4, in which an upper limit is given as stud cross-section area multiplied by material tensile strength. Ollgaard performed a comparison study between Eq. 2-3 and the first part of Eq. 2-4 and showed that the two equations were similarly accurate in predicting the test data.

$$Q_n = 0.5 A_{sc} \sqrt{f_c' E_c} \leq A_{sc} F_u \quad (2-4)$$

where:

- $Q_n$  = shear stud capacity, kips;
- $A_{sc}$  = cross-sectional area of stud, in<sup>2</sup>;
- $f_c'$  = concrete compressive strength, ksi;
- $E_c$  = concrete modulus of elasticity, ksi;
- $F_u$  = tensile strength of shear stud material, ksi.

Eq. 2-5 was later adopted both by AASHTO and by AISC since the 1990's. In AISC 2022, the steel tensile strength term ( $A_{sc}F_u$ ) is further reduced by factors accounting for reduction of stud strength when a floor system with ribbed metal deck is used. When a shear stud is directly welded on a steel beam without metal deck, the steel tensile strength term ( $A_{sc}F_u$ ) is multiplied by a factor of 0.75. In design, the nominal strength of the stud,  $Q_n$ , is multiplied by a resistance factor  $\phi$  accounting for variability and uncertainty in strength. The resistance factor is 0.85 in the 9<sup>th</sup> Ed. AASHTO and 1.0 in AISC 2022.

Pallares and Hajjar (2010) conducted a comprehensive evaluation of Eq. 2-4 and compared it with design equations including the one from Eurocode 4 (CEN 2004). In their study, the resistance factor for Eq. 2-4 was set to be 1.0 and no strength reduction on the steel tensile strength term ( $A_{sc}F_u$ ) was considered. The Eurocode 4 equation specifying the design strength of a shear stud in a solid concrete slab is given in Eq. 2-5. Eurocode 4 specifies that the strength given by Eq. 2-5 be further multiplied by a resistance factor of 0.8.

$$Q_n = 0.37 A_{sc} \sqrt{f'_c E_c} \leq 0.8 A_{sc} F_u \quad (2-5)$$

where:

- $Q_n$  = shear stud capacity, kips;
- $A_{sc}$  = cross-sectional area of stud, in<sup>2</sup>;
- $f'_c$  = concrete compressive strength, ksi;
- $E_c$  = concrete modulus of elasticity, ksi;
- $F_u$  = tensile strength of shear stud material; ksi.

Eq. 2-5 from Eurocode 4 applies to shear studs with length to diameter ratios larger than 4.0, which is required in both the 9<sup>th</sup> Ed. AASHTO and AISC 2022. Note that the Eurocode 4 equation gives a lower prediction of stud strength compared to Eq. 2-4.

Pallares and Hajjar (2010) compared a total of 391 stud push-out test results in solid concrete slabs with Eq. 2-4 and Eq. 2-5 when no resistance factor is considered. Results from this evaluation showed that Eq. 2-4 was not conservative for 60% of the tests. As a comparison, the Eurocode 4 equation (Eq. 2-5) was not conservative for 21% of the tests. When failure mode was specifically considered, Eq. 2-5 was conservative for steel-controlled failure but unconservative for concrete controlled failure. Eq. 2-4 was shown to be unconservative for both steel-controlled failure and concrete controlled failure, but especially for the concrete controlled failure mode. When the resistance factor is considered, Eq. 2-5 becomes conservative for both steel failure mode and concrete failure mode. Since the authors took the resistance factor for Eq. 2-4 as 1.0, thus, Eq. 2-4 is still unconservative for both failure modes. Similar arguments were made in another review study conducted by Bonilla et al. (2018), in which additional tests on larger-diameter shear studs were included. Both Eq. 2-4 and Eq. 2-5 were shown to be not conservative for larger-diameter shear studs when no resistance factor is considered.

Based on the observations above, Pallares and Hajjar (2010) proposed a new resistance factor  $\phi$  of 0.65 for Eq. 2-4, which is smaller than the 0.85 resistance factor currently used in the 9<sup>th</sup> Ed. AASHTO. In other words, the 9<sup>th</sup> Ed. AASHTO tends to overestimate stud strength based on the evaluation performed by Pallares and Hajjar.

Another important observation made by Pallares and Hajjar is that when the stud height to diameter ratio ( $h/d$ ) is more than 5, stud strength can be checked with the steel tensile strength term ( $A_{sc}F_u$ ) only. This is because 84% of tests using normal strength concrete failed in the steel-

controlled mode when the stud  $h/d$  ratio is more than 5. For the remaining 16% of tests with concrete-controlled failure, the strength could be safely predicted using the steel tensile strength equation with a resistance factor of 0.65. It should be noted that haunch depth is not mentioned by Pallares and Hajjar when calculating  $h/d$  ratio.

The work by Pallares and Hajjar (2010) is the basis for proposed new stud ultimate strength provisions in the proposed 10<sup>th</sup> Ed. AASHTO (AASHTO 2021). The stud requirements in the proposed 10<sup>th</sup> Ed. AASHTO increase the minimum stud  $h/d$  ratio from 4.0 to 5.0. Further, stud ultimate strength is computed only using by the steel-controlled strength term, which is taken as  $0.7A_{sc}F_u$  with a resistance factor of 1.0. This is close to the value of  $0.65A_{sc}F_u$  recommended by Pallares and Hajjar. Once again, the proposed 10<sup>th</sup> Ed. AASHTO does not specify how to calculate  $h$  when a haunch exists. That is, it is unclear if  $h$  should be measured from the top of the steel girder or from the top of the haunch.

To summarize, following are the stud shear strength equations in the 9<sup>th</sup> Ed. AASHTO and in the proposed 10<sup>th</sup> Ed. AASHTO:

$$Q_r = \phi_{sc} Q_n \quad (2-6)$$

where:

$Q_r$  = factored shear resistance of one shear connector, kips;

$\phi_{sc}$  = resistance factor for shear connectors;

$Q_n$  = nominal shear resistance of one stud shear connector, kips.

9<sup>th</sup> Ed. AASHTO (for  $h/d \geq 4$ ):

$$Q_n = 0.5 A_{sc} \sqrt{f'_c E_c} \leq A_{sc} F_u \quad (2-7a)$$

$$\phi_{sc} = 0.85 \quad (2-7b)$$

Proposed 10<sup>th</sup> Ed. AASHTO (for  $h/d \geq 5$ ):

$$Q_n = 0.7 A_{sc} F_u \quad (2-8a)$$

$$\phi_{sc} = 1.0 \quad (2-8b)$$

These equations are also listed in Table 2.4.

### 2.4.3. Ductility of Shear Studs

Typical design of shear studs for composite beams for ultimate strength implicitly rely on redistribution of forces among shear studs to develop the full composite flexural strength of the beam. Consequently, shear studs must be able to sustain some post yielding deformation before losing shear resistance. This is because the longitudinal shear flow along the length of the bridge is not constant. Shear studs at locations of high shear (e.g., close to points of zero moment) will yield first and must maintain their shear resistance as forces are redistributed to other studs.

Shear studs must therefore exhibit some ductility. As described in Section 2.4.1, the ductility of studs is typically assessed by evaluating slip capacity.

Two issues related to stud slip are considered. One is the maximum slip at a stud when the composite beam reaches its ultimate flexural capacity. That is, what is the slip demand on a stud in a composite beam? The other issue is the actual slip capacity of shear studs. The slip capacity of shear studs must be larger than the maximum slip demand in order to develop the ultimate capacity of the composite beam.

The slip demand can be studied by large-scale beam tests or by analysis. Driscoll and Slutter (1961) reported two 15 ft. long simply supported composite beam tests where one has an adequate number of shear studs to develop the full composite strength of the beam and the other one used only half as many studs. Results from the two tests show that the beam with an adequate number of shear studs (B5) developed about 0.02" (0.5mm) end slip at peak strength. The beam with half the number of shear studs (B6), i.e., a partially composite beam, developed 82% of the plastic bending capacity of B5. However, the slip at the end of the beam was about 6 times higher than B5 when the peak strength was reached, as shown in Figure 2.9, which means the slip was 0.12" (3mm) to develop the ultimate strength in the partial composite case. This finding means stud ductility is more important for structures with less composite action (partial composite beams) since there will be a higher slip demand.

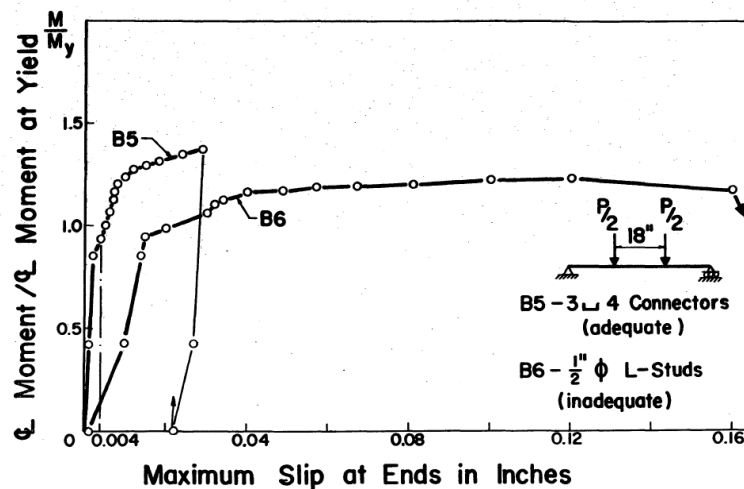
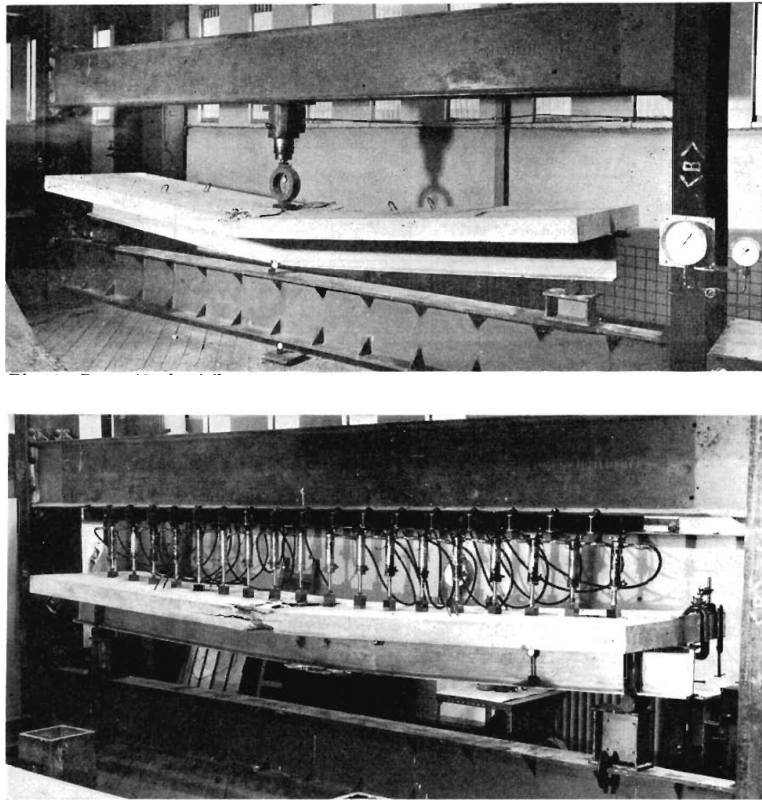


Figure 2.9 - Normalized Moment versus Beam End Slip for Two Beam Tests (Driscoll and Slutter 1961)

Chapman and Balakrishnan (1964) performed 16 beam tests. The length of the beam specimens was 18 ft. Shear studs of 3/4" diameter and 1/2" diameter were used in the beams with different layouts. The load on the beam was either a point load at midspan or a uniformly distributed load using 18 hydraulic jacks. Figure 2.10 illustrate test specimens from this research. The slip

between the concrete deck and the steel girder was measured at the left and right ends and also at the left and right quarter points. The maximum slip at the ultimate load capacity for the 16 beams ranged from 0mm to 3.8mm (0.15").



*Figure 2.10 - Composite Beam Specimens tested by Chapman and Balakrishnan (1964)*

Badie et al. (2011) tested two composite beam specimens using 1-1/4" diameter shear studs. The two beams were 30 ft. long simple spans and full-depth precast concrete panels were used in deck. Shear studs were used in clusters. In each cluster, either 4 or 8 shear studs were closely welded. The longitudinal spacing between each cluster of studs was 24" for Beam 1 and 48" for Beam 2. Slip versus applied moment is shown in Figure 2.11. Due to limitations of the loading device, the beams did not reach their ultimate capacity but considerable slip was recorded. It can be seen that, to reach 90% of the ultimate moment capacity, the slip capacity of the studs must be larger than 0.12" (3mm). The reference to "Steel Tubes" and "Closed Ties" in Figure 2.11 indicates how confinement was provided for the studs in the grout pockets of the precast deck panels.

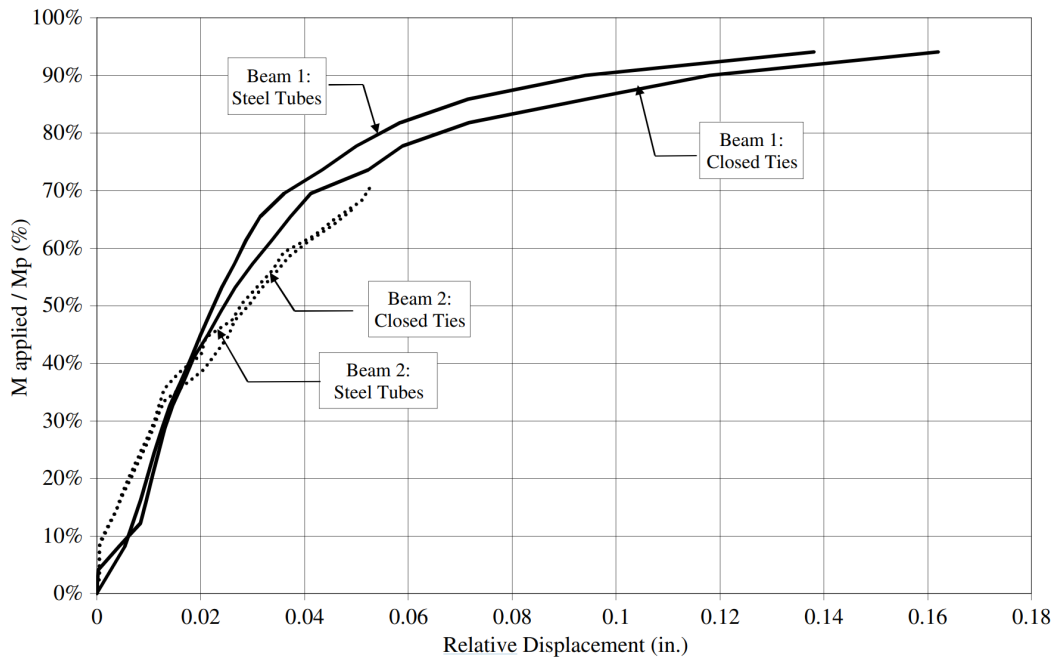


Figure 2.11 - End slip versus applied moment for two beams tested by Badie et al. (2011)

Zona and Ranzi (2014) conducted an extensive study on slip demands on shear studs in composite beams with solid slabs using finite element analysis. They considered a wide range of design parameters in their study, including construction method (shored versus unshored), span length, shear connection ratio (full versus partially composite), steel beam and concrete slab cross-section properties, and other variables. In their study, they considered span lengths up to 130 ft. which far exceeds the span lengths for typical laboratory beam tests. Their analysis showed that slip demand increased with span length. For fully composite beams with unshored construction and a 130 ft. span, they predicted slip demands up to approximately 4mm (0.16").

Eurocode 4 (CEN 2004) specifies slip requirements for shear studs. To be specific, in standard Eurocode 4 push-out test, when a shear stud loses 10% of its shear resistance (see Figure 2.5), the slip must be larger than 6.67mm (0.26"). Studs satisfying this requirement will accommodate all beam tests and finite element studies mentioned above. However, it is noticed that in most previous research, Eurocode 4 slip requirement have been interpreted as 6mm (0.24") slip at 10% load drop. Driscoll and Slutter (1961) reviewed multiple push-out test and full-scale beam test results and observed that slip at failure in push-out tests is usually larger than the maximum slip in beams at ultimate capacity. Therefore, they claimed that the ductility of shear studs is sufficient. Average load-slip curves obtained by Ollgaard et al. (1971) for shear studs in normal strength concrete and in lightweight concrete is shown in Figure 2.12. This curve is based on 48 push-out tests using 5/8" and 3/4" diameter shear studs. It can be noticed that the slip at peak strength is about 0.23" and the slip at 10% load drop is more than 0.3", which satisfies the Eurocode 4 requirements.

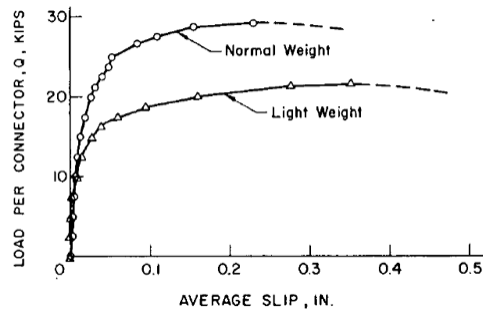


Figure 2.12 - Average Load-Slip Curves Derived by Ollgaard et al. (1971)

Based on the limited information mentioned above, shear studs of normal diameter are shown to have adequate ductility. On the other hand, the laboratory beam tests described above were conducted on beam sizes and span lengths typical of building construction, and not representative of the larger beam sizes and span lengths typical of bridge construction. Research, either experimental or analytical, evaluating slip demands on shear studs in bridge girders, where spans can reach several hundred feet, was not identified in this literature review. Additional information on the slip capacity of larger-diameter shear studs, determined from push-out tests, is provided in the next section.

#### 2.4.4. Tests on Larger-diameter Shear Studs

This section provides a review of previous static loading tests on larger-diameter shear studs. A number of these tests were conducted outside of the U.S. where shear stud diameter is measured in millimeters (mm). Stud diameters considered in these studies included 22mm, 25mm, 27mm, 30mm and 32mm. Table 2.5 provides the equivalent diameter in inches.

**Table 2.5 - Stud Diameters in Millimeters and in Inches**

Stud Diameter in mm	Equivalent Stud Diameter in inches
22 mm	0.87"
25 mm	0.98"
27 mm	1.06"
30 mm	1.18"
32 mm	1.26"

As described earlier, Viest (1956) performed push-out tests to study the static ultimate strength of shear studs with diameters ranging from 1/2" to 1-1/4". Two or four shear studs were stud-welded on each steel beam flange. The transverse spacing of studs was either 2" or 4" and the height for all studs was 4". A solid concrete slab of 30"×24"×7" (length×width×thickness, hereinafter L×W×T) was used with a single layer of "4×4-10/10" reinforcement, which is



assumed to be #4@10" in orthogonal directions. The average compressive strength for most concrete slabs was relatively low in this study and was only 3.4 ksi for the 1-1/4" stud specimen. Concrete failure controlled specimens with studs of 1" diameter or higher. The test results showed that the strength of the stud was proportional to the square root of the concrete compressive strength and was proportional to the diameter of shear stud when the stud diameter is larger than 1", as indicated by Eq. 2-1. Larger-diameter shear studs had significantly higher static strength than normal diameter (< 1") studs. As noted in Section 2.4.2, this study also proposed one of the first equations predicting the "critical" strength of shear studs. The "Critical" strength of the shear stud was obtained when the push-out specimen has an arbitrary residual slip of 0.003", which corresponds to a state where the structure has minimal inelastic deformation.

Badie et al. (2002) studied the static and fatigue behavior of larger-diameter shear studs. Larger-diameter shear studs of 1-1/4" diameter and 5" length were investigated. Badie used the one-sided push-out specimen shown in Figure 2.3. Four studs in one column were welded to the steel beam by stud welding. The concrete slab had a dimension of 58"×20"×8" (L×W×T). The longitudinal reinforcement ratio was 1% and the transverse reinforcement ratio varied from 0.5% to 1.8% among specimens. A few specimens were built with a mixture of normal headed shear studs and headless shear studs. It was observed that for specimens with the 0.5% transverse reinforcement ratio, the static strength for 1-1/4" diameter studs was considerably smaller compared to that predicted by design equations in AASHTO LRFD 1998 (Eq. 2-7) and the failure was a combination of stud fracture and concrete splitting cracking. When transverse reinforcement ratio increased to 1.8%, the strength of 1.25" stud increased to a comparable value as predicted by AASHTO LRFD 1998 (Eq. 2-7). Slip at failure of the 1-1/4" shear studs was about 30% less than that of the 7/8" studs and smaller than the Eurocode 4 (CEN 2004) ductile criteria of 6mm. A few specimens were first subjected to two million fatigue cycles and then test statically. It was observed that the previous fatigue cycles had no detrimental effect on the static performance. However, the stress range sustained in the fatigue cycles by those specimens was not reported. The strength of specimens using a mixture of headless studs and headed studs was found to be 17% smaller than that of specimens using headed studs only.

Shim et al. (2004) and Lee et al. (2005) performed static and fatigue push-out tests on 25mm, 27mm, and 30mm diameter shear studs. The standard push-out specimen design from EC-4 (CEN 2004) was adopted in this research, which has a concrete slab of 600mm×600mm×200mm (≈24"×24"×8", L×W×T). The stud welding process was used to attach the studs to the steel beam. Four studs were welded in two rows on the steel beam. The transverse reinforcement ratio in the concrete slabs was at least 1.5% in all specimens. Grease was applied between the steel beam flange and the concrete to reduce friction. All static tests achieved an ultimate slip larger than 6mm, which was taken by researchers as the criterion for ductile behavior. Stud fracture failure was observed in the 25mm diameter stud specimens. A failure mode referred to by the researchers as concrete embedment failure was observed in specimens with 27mm and 30mm diameter shear studs. As a result, the 27mm and 30mm diameter stud specimens were tested with

a thicker concrete slab of 220mm (8.66") thickness, and stud fracture failure modes were achieved. However, fracture was not observed in the shank of the stud. Instead, weld fracture and steel beam flange tear off were observed. The static strength of the larger-diameter shear studs was compared with AASHTO LRFD 2004 (Eq. 2-7) and most of tests had a strength lower than AASHTO predictions, regardless of the diameter. The Eurocode 4 stud strength equations (Eq. 2-5) were found to be able to safely predict the strength of the studs. Therefore, the researchers recommended using Eurocode 4 equations to predict the static strength of larger-diameter shear studs.

Lin and Liu (2015) tested the static behavior of 22mm, 25mm, and 30mm diameter shear studs using push-out tests. The concrete slab had dimensions of 460mm×460mm×400mm ( $\approx 18''\times 18''\times 16''$ , L×W×T). The longitudinal and transverse reinforcement ratios were 1.0% and 1.4%, respectively. Two studs in a single row were welded to the steel beam flange without reporting the welding method. Friction between the steel beam and concrete was reduced by applying lubricants. All specimens failed by shear stud fracture above the weld. Local crushing was noticed on concrete directly below the stud. The ultimate strength of the large studs was found to be larger than predictions from AASHTO LRFD 2007 (Eq. 2-7), Eurocode 4 (Eq. 2-5), and the Chinese code. The failure slip, which was defined as the slip when strength reduced 10% from the peak strength, of 22mm diameter studs varied from 5.6mm to 6.7mm. The failure slip of 25mm diameter shear studs was 11% larger than that of 22mm studs. However, the failure slip for 30mm diameter shear studs was 6% smaller than that of 22mm studs.

Wang et al. (2019) conducted push-out tests on 22mm and 30mm diameter shear studs in normal strength concrete (NSC) and ultra-high-performance concrete (UHPC). Two studs were welded to the steel beam flange in a single row by fillet welds, which is allowed by AWS D1.5 as an alternative to the more conventional stud welding process. No information was provided by the researchers concerning the impact of using fillet welds for the studs. The transverse spacing between the studs was 120mm (4.72"). The concrete slab had dimensions of 500mm×400mm×150mm ( $\approx 20''\times 16''\times 6''$ , L×W×T). The reinforcement ratios were 0.79% and 0.67% for longitudinal and transverse reinforcement, respectively. It was observed that when 30mm studs were used with NSC, the failure was a combined mode of stud fracture and concrete cracking. However, the strength of 30mm studs was found to be higher than predicted by AASHTO LRFD 2014 (Eq. 2-7). The ultimate slip of the 30mm studs was 8.2mm (0.32"), which was larger than that of 22mm studs for NSC specimens. Therefore, this study showed that the static strength of 30mm studs could be safely predicted using AASHTO LRFD 2014, and that these studs had adequate ductility based on the slip criteria of 6mm (0.24"). All other specimens in this study showed stud fracture failure. At the same load, the slip of the UHPC specimens was significantly smaller than that of NSC specimens. This research also investigated the influence of stud height and concrete slab thickness when UHPC is used. The stud height varied from 70mm (2.76") to 120mm (4.72") for 30mm studs and was found to have no effect on the load-slip

response. The same observation was made for slab thickness when it varied from 100mm (3.94") to 150mm (5.91").

Hu et al. (2020) conducted static push-out tests on 30mm diameter shear studs. Specimens were built with either NSC or UHPC. Two layouts of shear studs were investigated, namely one row of two studs and three rows of two studs. The concrete slab was the same as the one used in Wang et al. (2019) described above, including the reinforcement ratio. Transverse and longitudinal spacing between studs were 120mm (4.72") and 150mm (5.91"). The failure mode of the NSC specimens was a mixture of concrete cracking and stud fracture. No concrete cracking was observed in specimens using UHPC but local crushing was noticed. The strength of the shear studs was 12% lower when NSC was used in lieu of UHPC. This decrease is not significant considering the cube compressive strength of UHPC is 2.5 times higher than that of the NSC. This suggests that the contribution of concrete strength to the stud strength has an upper limit. The strength difference between specimens using different layouts was negligible. The researchers reported that all specimens showed a ductile slip response with the smallest ultimate slip obtained in test program equal to 6.7mm (0.26"). The ultimate slip for the NSC specimens was 12.6% higher than that of UHPC specimens. The UHPC specimens using one row of studs has an ultimate slip that was 11% higher than that of UHPC specimen using three rows of studs. The static strength of each specimen was compared with Eurocode 4 (Eq. 2-5), AASHTO LRFD 2014 (Eq. 2-7), and the Chinese code. It was observed that the strength of the studs in NSC was smaller than the prediction from AASHTO while larger than the prediction from Eurocode 4 and the Chinese code. The strength of studs in UHPC was higher than predicted by any of these three codes.

Wang et al. (2018) conducted static push-out tests of 30mm diameter shear studs in fully cast-in-place slabs and in full-depth precast concrete slabs with shear pockets. Figure 2.13 shows the precast specimen with a shear pocket. Specimens using NSC and UHPC were constructed. The reinforcement ratio in the concrete slab was 0.78% for the longitudinal reinforcement and 0.64% for the transverse reinforcement. The concrete slabs had dimensions of 1150mm×660mm×250mm ( $\approx 45''\times 26''\times 10''$ , L×W×T). The shear pockets had the same reinforcement ratio as the slab but there was one specimen having no reinforcement in the shear pocket, as Figure 2.13 shows. The pocket was infilled with different materials to study their influence. Two layouts of shear studs were used, namely one row of two studs and three rows of two studs. Test results showed all specimens ultimately failed by stud fracture. The specimen using NSC developed extensive cracking of the concrete. The static ultimate strength of each specimen was higher than AASHTO LRFD 2012 (Eq. 2-7) and Eurocode 4 (Eq. 2-5). The ultimate slip for the NSC specimens was more than 6mm (0.24") and was regarded as ductile. On the other hand, most of the UHPC specimens had an ultimate slip less than 6mm (0.24"). The authors attribute the low slip in UHPC specimens to the high integrity and high confinement effect of the UHPC that did not allow the stud to deform extensively before fracture. Results between the two stud layouts showed that the strength was slightly smaller when three rows were

used, regardless of the concrete strength. However, the ultimate slip for three row specimens was 13% to 27% higher than the one row specimens, which is opposite the observations in research conducted by Hu et al. (2020). Comparison between fully CIP specimens and precast specimens showed that when NSC is used for both precast panel and infill material, the precast specimen had a 10% reduction in the ultimate strength but a higher ultimate slip. The precast specimen showed a unique concrete cracking pattern after the test wherein a crack initiated from the corner of interface between precast concrete and the shear pocket infill, as shown in Figure 2.14. It was reported that the strength of the specimen decreased 16% when lower strength infill material was used. The compressive strength of the lower strength infill material was 50Mpa (7252psi), compared to high strength infill of 125Mpa (18130psi). However, the slip at failure for the lower strength infill specimen was doubled compared to that of the high strength infill specimen. The research also studied the reinforcement in the shear pocket. Since UHPC was used for both precast and infill parts in this case study, the specimens with or without reinforcement in the shear pocket showed essentially the same load-slip response.

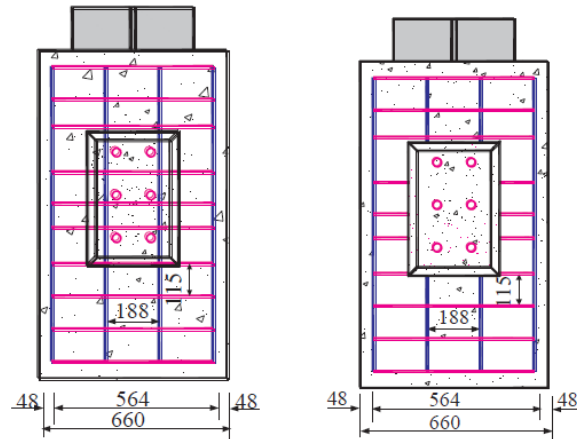


Figure 2.13 - Specimen Using Precast Concrete Slab with Shear Pocket (Wang, et al. 2018); Specimen on the Right has no Reinforcement in the Pocket

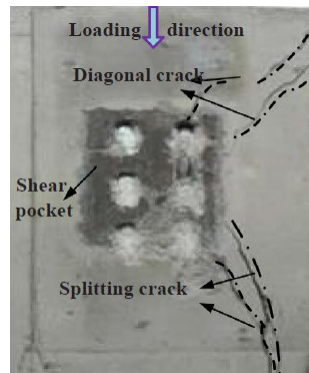


Figure 2.14 - Cracking Pattern for Normal Strength Concrete Specimen with Shear Pocket (Wang, et al. 2018)

A summary of static push-out test strength results for studs with diameters of 25mm and larger is given in Figure 2.15 below. The vertical axis is the ratio between static ultimate strength of studs reported in the literature ( $Q_{test}$ ) and the strength predicted by 9<sup>th</sup> Ed. AASHTO and 10<sup>th</sup> Ed. AASHTO ( $Q_{LRFD}$ ), respectively. Material properties reported in the literature were used for calculation. As the figure shows, when the 0.85 resistance factor is considered, 20 out of 51 (39%) tests in the literature showed an ultimate strength lower than the 9<sup>th</sup> Ed. AASHTO equation. When the 0.85 resistance factor is not considered, 27 out 51 (53%) tests show an ultimate strength lower than the 9<sup>th</sup> Ed. AASHTO equations. These observations are comparable to the conclusion made by Pallares and Hajjar (2010). The 10<sup>th</sup> Ed. AASHTO is shown to be more conservative and 9 out 51 (18%) tests have stud ultimate strength lower than the 10<sup>th</sup> Ed. AASHTO equation. Bonilla et al. (2018) reviewed stud strength equations in AASHTO 2014, AISC 2010, Eurocode 4, Chinese standard GB 2003, Japanese standard JSCE 2007, and Australia & New Zealand standard AS/NZS 2327 for predicting larger-diameter shear stud static strength (25mm, 27mm, 30mm). It was reported that none of the equations provided consistently conservative predictions.

The literature review from past static push-out tests indicates that larger-diameter studs have exhibited highly variable strength and ductility. Contradictory conclusions regarding the strength and ductility are reported in the literature. Test results have shown strength values both well above and well below predictions from the AASHTO LFRD design equations. The ductility of larger-diameter shear studs is commonly reported as better than that of 7/8" studs, but lower ductility is also reported. On the other hand, data on the impact of factors such as deck reinforcement ratio and stud penetration into the deck on the strength and ductility of larger-diameter shear studs is limited.

Nonetheless, there are some trends that can be observed from the literature. When higher strength concrete is used, a higher ultimate strength and a lower ductility capacity of studs is usually reported. Transverse reinforcement ratio of the concrete slab is shown to be important for strength and ductility development of large shear studs. This is because transverse reinforcement delayed or eliminated the splitting cracking of the concrete slab. Specimens with larger size concrete slabs appear to have higher stud strength in push-out tests. Large shear studs are shown to cause more cracks on normal strength concrete when ultimate static strength is reached.

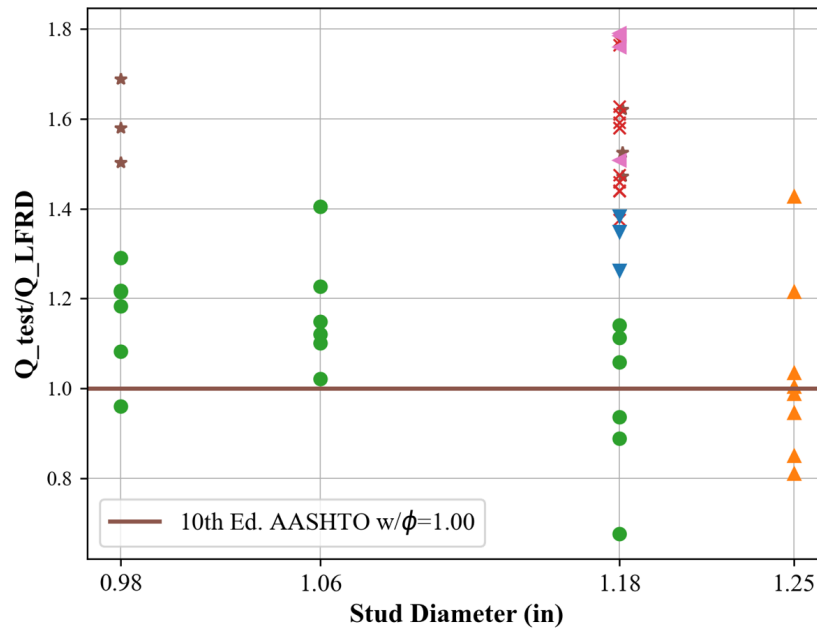
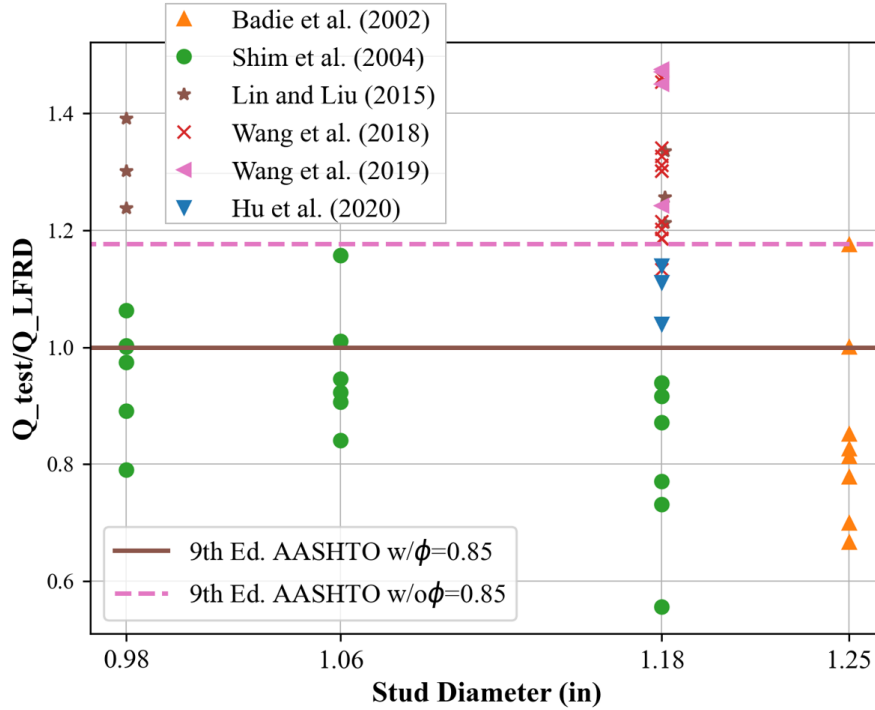


Figure 2.15 - Summary of static strength data for larger-diameter shear studs

Based on the available data, the suitability of larger-diameter shear studs for use in composite steel bridges is unclear. Additional testing and analysis are needed to establish the performance

of larger-diameter shear studs more clearly in bridge decks representative of Texas bridge design standards and practices.

## 2.5. Larger-diameter Shear Studs under Fatigue Loading

---

A number of past research studies in the U.S. and internationally have evaluated the fatigue performance of larger-diameter shear studs embedded in solid concrete slabs, typically using push-out tests. Results of fatigue experiments are normally presented in a plot of the applied stress range,  $S_r$ , versus the number of cycles to failure,  $N$ . This section reviews key results from past research and compares experimentally observed fatigue performance with the stud fatigue resistance equations in the 9<sup>th</sup> Ed. AASHTO (AASHTO 2020) and in the proposed 10<sup>th</sup> Ed. AASHTO (AASHTO 2021). As described in 2.2, changes were made to stud fatigue requirements in going from the current 9<sup>th</sup> Ed. AASHTO to the proposed 10<sup>th</sup> Ed. AASHTO. Stud fatigue requirements, both for the 9<sup>th</sup> Ed. AASHTO and the proposed 10<sup>th</sup> Ed. AASHTO are summarized in Table 2.4. Some of the previous research compared test results to editions of the AASHTO LRFD Bridges Design Specifications earlier than the 9<sup>th</sup> Edition. For all of the earlier versions of AASHTO referenced below, the fatigue requirements for shear studs are the same as in the 9<sup>th</sup> Ed. AASHTO.

Badie et al. (2002) conducted 25 fatigue tests using push-out specimens; 14 specimens with 1-1/4" studs, and 11 specimens with 7/8" studs. The applied stress ranges varied from 10 ksi to 25 ksi. Results of the fatigue tests are plotted in Figure 2.16. These results showed that the fatigue performance of 1-1/4" studs was similar but somewhat better than that of 7/8" studs. The researchers concluded that the 1998 AASHTO LRFD stud fatigue resistance equations can be safely used for 1-1/4" studs.

Lee et al. (2005) conducted 12 fatigue push-out tests with stud diameters of 25mm, 27mm and 30mm. By comparing test results with AASHTO LRFD and Eurocode 4 as shown in Figure 2.17, the researchers concluded that the fatigue life of larger-diameter studs was reasonably and somewhat conservatively predicted by AASHTO LRFD.

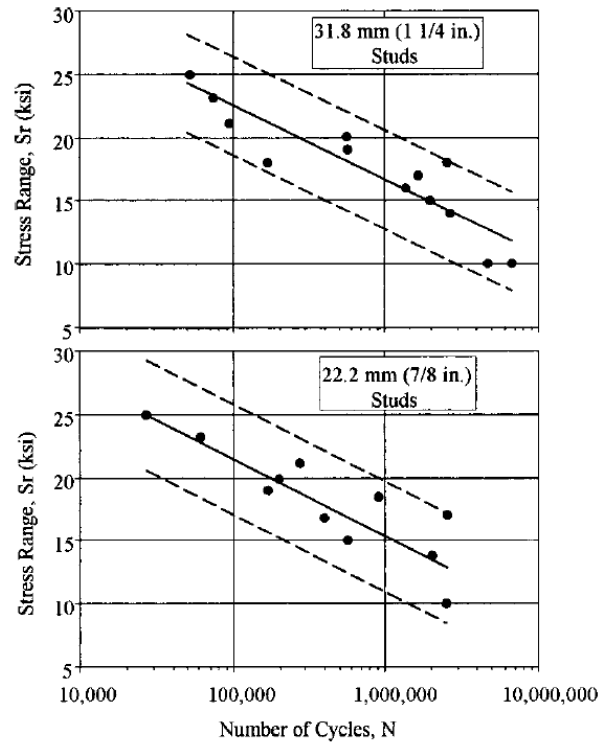


Figure 2.16 - Fatigue Test Results for 7/8" and 1-1/4" Shear Studs by Badie et al. (2002)

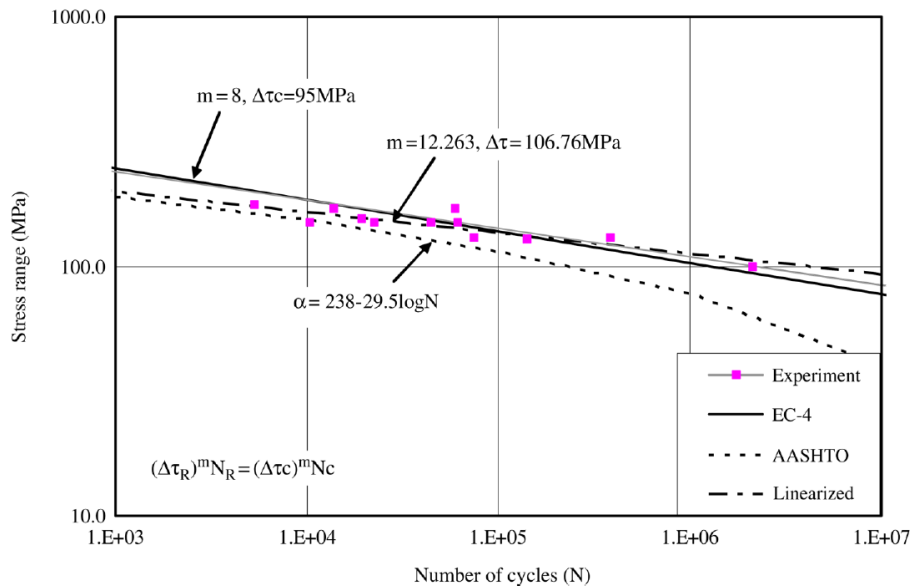


Figure 2.17 - Fatigue Test Results for 25mm (0.98"), 27mm (1.06") and 30mm (1.18") Shear Studs by Lee et al. (2005)

Fatigue tests on larger-diameter shear stud were also conducted by Mundie (2011). This study evaluated the fatigue life of 7/8" studs and 1-1/4" studs. Stress ranges used in the tests were 18,



22, and 26 ksi. The results, plotted in Figure 2.18, show very similar fatigue lives for the 7/8" and 1-1/4" studs. This plot also shows the stud fatigue limits from various design codes, including AASHTO LRFD. This comparison indicates that the AASHTO LRFD fatigue provisions for shear studs can be safely used for 1-1/4" studs.

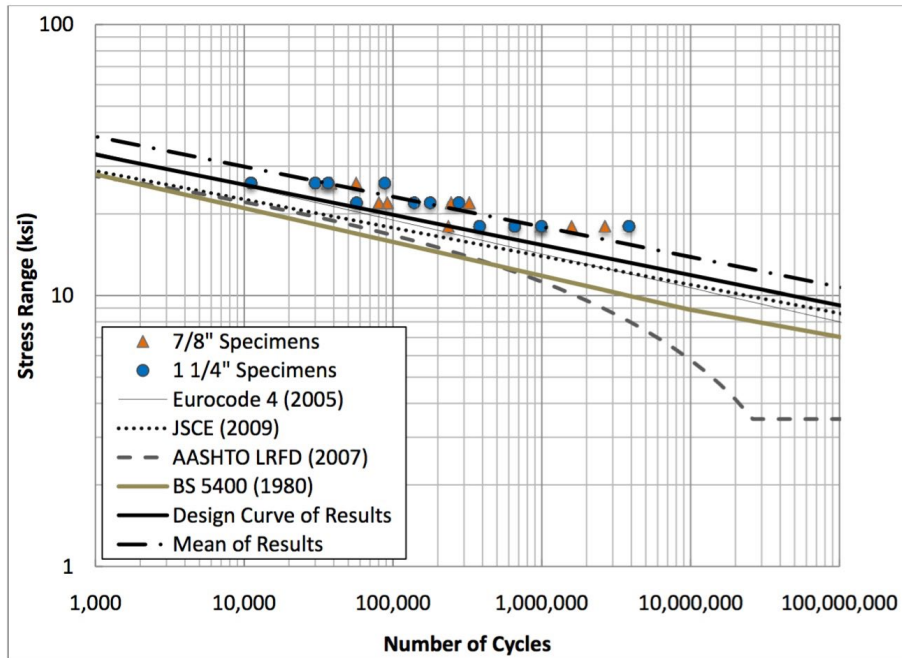


Figure 2.18 - Fatigue Test Results for 7/8" and 1-1/4" Shear Studs by Mundie (2011)

Kakish (1997) evaluated the fatigue performance of 1-1/4" studs in eight push-out specimens. They concluded 1-1/4" shear studs had a higher fatigue resistance than predicted by AASHTO LRFD. For instance, at 2,000,000 cycles, the allowable stress range for 1-1/4 in. studs based on Kakish's tests results was 18 ksi, while the stress range calculated from AASHTO LRFD was 11.7 ksi. Kakish also compared 1-1/4" stud fatigue test data with fatigue data from Slutter and Fisher (1966) for 3/4" and 7/8" studs. This comparison showed that 1-1/4" studs have higher fatigue resistance than 3/4" and 7/8" studs.

Figure 2.19 shows a comparison of fatigue test data reported in literature with the S-N curves in the 9<sup>th</sup> E. AASHTO and proposed 10<sup>th</sup> Ed. AASHTO. This data indicates that shear stud diameter does not have a significant effect on fatigue life. Further, the data indicates that larger-diameter shear studs can be safely designed for fatigue using either the 9<sup>th</sup> Ed. AASHTO or the proposed 10<sup>th</sup> Ed. AASHTO.

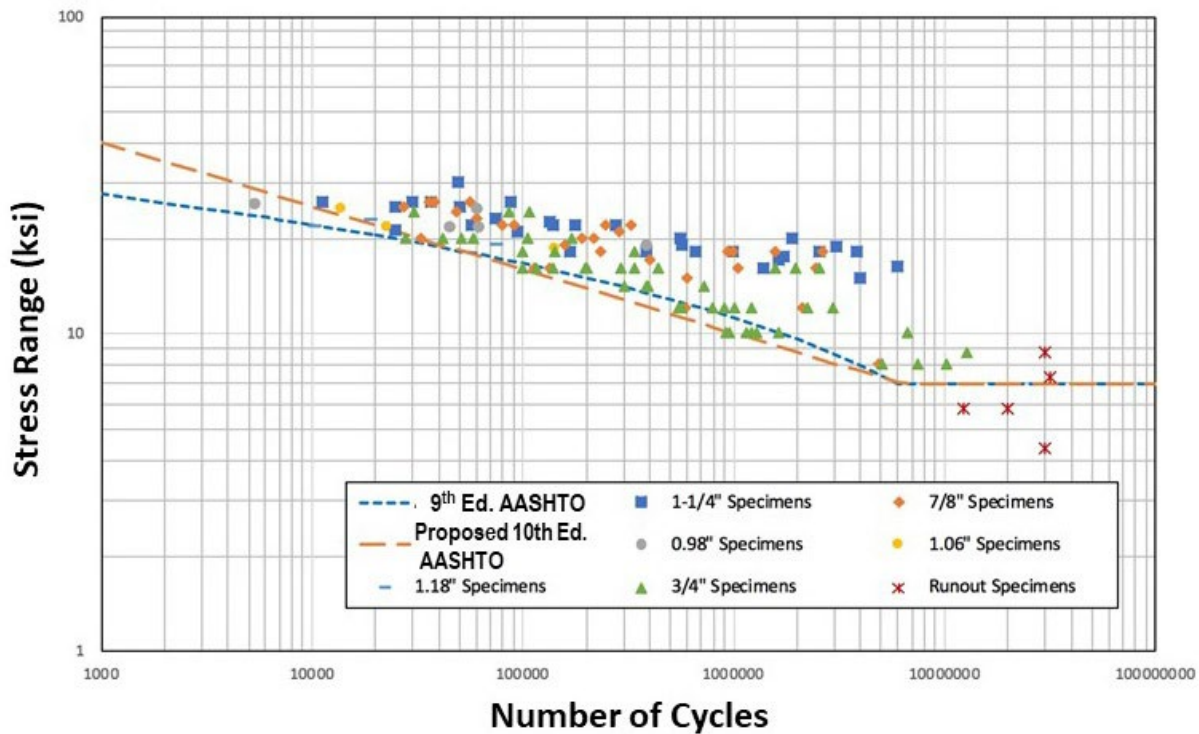


Figure 2.19 - Comparison of Fatigue Test Data with 9th E. AASHTO and Proposed 10th Ed. AASHTO S-N Curves

## 2.6. Bridges Constructed with Larger-diameter Shear Studs

A review of the literature identified two bridges in the U.S. that were constructed with larger-diameter shear studs. Both bridges were constructed in Nebraska using 1-1/4" shear studs. The bridges are referred to in the literature as the Gering Bridge and the Skyline Bridge. Information on these bridges is reported by Badie et al. (2007) and by Fallaha et al. (2004). These two bridges were constructed as demonstration projects in conjunctions with research on 1-1/4" studs conducted at the University of Nebraska (Badie, Tadros, et al. 2002, Badie, Girgis, et al. 2007, Badie, Morgan Girgis, et al. 2011, Kakish 1997).

### 2.6.1. Gering Bridge

The Gering Bridge is on Highway 71 in Gering, Nebraska and was constructed in 1999. The bridge consists of three continuous spans (45 ft. – 60 ft. – 45 ft.) with W30x99 rolled beams spaced at 8ft.-9in. and with a 7.5" thick full-depth cast-in-place deck. 1-1/4" studs were used on the south span of the bridge, with the studs welded in a single row directly over the web with a pitch of 7 to 10 inches. The other 2 spans used 7/8" studs with three studs per row and a pitch of 10 to 16 inches. After completion, the bridge was loaded with a dump truck in each span. Both exterior spans (one exterior span with 1-1/4" studs and the other exterior span with 7/8" studs)

showed the same deflection. Badie et al. (2007) report that continuous visual inspection (presumably from the end of construction in 1999 to 2007) showed no cracks or distress on the south span where the 1-1/4" studs were used.

### 2.6.2. Skyline Bridge

The Skyline Bridge (Fallaha, et al. 2004) is located on Skyline Drive and passes over US 6 in Omaha, Nebraska, and was completed in 2004. The bridge consists of two continuous spans of 89 ft. and 125 ft. with a 25° skew and with five steel plate girders spaced at 10 ft.-10 in. A full-depth precast concrete deck system was used for the bridge. The precast panels have a continuous opening over the girders. 1-1/4" studs were welded in a single line over the web of the girder within this opening, which was subsequently filled with grout.

### 2.6.3. Current Status of Bridges

The research team for TxDOT Project 0-7042 conducted a meeting with an engineer with the Nebraska DOT on April 13, 2020 to learn the current status of the two bridges built with 1-1/4" shear studs. According to the Nebraska DOT engineer, periodic visual inspection of the bridge decks has shown no unusual deck cracking or distress on the spans where the 1-1/4" studs were used. They also noted that after the construction of Skyline Bridge in 2004, no additional bridges were constructed in Nebraska with 1-1/4" shear studs. This was not attributed to any problems with the 1-1/4" studs during construction or in-service. Rather, the absence of any additional bridges constructed using 1-1/4" studs was believed to be the result of market driven factors, most notably that 1-1/4" studs are not commercially available, and therefore implementing 1-1/4" studs on a bridge project would require custom manufacturing of the studs, which is costly.

## 2.7. Summary

---

This chapter has reviewed previous research on larger-diameter shear studs under both static and fatigue loading. A summary was provided of shear stud design and detailing requirements in the AASHTO LRFD Bridge Design Specifications and in pertinent TxDOT standards and guideline documents. Information was provided on two bridges constructed in Nebraska using 1-1/4" shear studs. Following are key observations from this chapter:

- Shear stud strength and fatigue requirements in the current 9<sup>th</sup> Ed. AASHTO are essentially the same as those found in previous versions of AASHTO going back for many years. However, significant changes to shear stud strength and fatigue requirements have been proposed for the upcoming 10<sup>th</sup> Ed. AASHTO. A summary of the proposed changes is provided in Table 2.3 and Table 2.4. In the remainder of this report, when evaluating the feasibility of using larger-diameter shear studs, both the current 9<sup>th</sup> Ed. AASHTO and proposed 10<sup>th</sup> Ed. AASHTO shear stud requirements will be considered.

- A limited number of studies were identified that experimentally evaluated the static and fatigue loading behavior of larger-diameter shear studs. This includes research conducted in the U.S. at the University of Nebraska and at Auburn University, as well as research conducted in Korea and China.
- The literature review from past static push-out tests indicates that larger-diameter studs have exhibited highly variable strength and ductility. Contradictory conclusions regarding the strength and ductility are reported in the literature. Test results have shown strength values both well above and well below predictions from the AASHTO LFRD design equations (both 9<sup>th</sup> Ed. AASHTO and proposed 10<sup>th</sup> Ed. AASHTO). The ductility of larger-diameter shear studs is commonly reported as better than that of 7/8" studs, but lower ductility is also reported. On the other hand, data on the impact of factors such as deck reinforcement ratio and stud penetration into the deck on the strength and ductility of larger-diameter shear studs is limited. Based on the available data on static loading behavior, the suitability of larger-diameter shear studs for use in composite steel bridges is unclear. Additional testing and analysis are needed to establish the performance of larger-diameter shear studs more clearly in bridge decks representative of Texas bridge design standards and practices.
- The literature review from past fatigue push-out tests have shown consistently good fatigue performance for larger-diameter shear studs. This data indicates that shear stud diameter does not have a significant effect on fatigue life. The fatigue resistance exhibited by larger-diameter shear studs has been similar to and often better than that of 7/8" studs. Essentially all fatigue tests on larger-diameter shear studs have shown performance that satisfies both the 9<sup>th</sup> Ed. AASHTO and the proposed 10<sup>th</sup> Ed. AASHTO S-N curves.
- No previous studies were identified that evaluated the behavior of shear studs of any diameter in concrete decks constructed using partial depth precast concrete panels with a cast-in-place topping (see Figure 1.3) as used in Texas bridges.
- A review of the literature identified two bridges in the U.S. that were constructed with larger-diameter shear studs. Both bridges were constructed in Nebraska using 1-1/4" shear studs. The first bridge was constructed in 1999 with a full-depth cast-in-place deck. The second bridge was constructed in 2004 using a full-depth precast concrete deck system. Based on recent information obtained from the Nebraska Department of Transportation, the decks of both bridges are performing well

Based on the literature review, there is considerable uncertainty on whether equations for stud strength in the 9<sup>th</sup> Ed. AASHTO and the proposed 10<sup>th</sup> Ed. AASHTO can safely be used with larger-diameter shear studs. Consequently, the major emphasis of the experimental studies in this research project will be on the strength and slip capacity of larger-diameter shear studs under

static loading. This will be the case both for the push-out test program reported in Chapter 5 and the large-scale beam test program reported in Chapter 7. Further, the push-out test program and the large-scale beam test program will consider both full-depth cast-in-place decks and decks with PCPs, since no previous research on shear stud behavior in decks with PCPs was identified.

Previous research has shown that larger-diameter shear studs consistently exhibit fatigue behavior that is at least as good as that of 7/8" studs. Consequently, there will be less emphasis on the experimental fatigue behavior of larger diameter shear studs in this research project. Nonetheless, a limited number of fatigue tests will be conducted on larger-diameter shear studs to confirm their fatigue performance. These fatigue tests are reported in Chapter 6 of this report.

An important issue not covered in this chapter is background on stud welding and the stud welding details used in previous research projects on larger-diameter shear studs. This background information on stud welding is provided in Chapter 4 of this report.

The next chapter describes preliminary design studies where three existing TxDOT bridges constructed with 7/8" diameter shear studs are redesigned using 1", 1-1/8", and 1-1/4" shear studs. The purpose of these redesigns is to quantify the reduction in the number of shear studs that can be achieved when using larger-diameter studs for realistic bridges.

## Chapter 3. Preliminary Design Studies

### 3.1. Introduction

---

Three real bridges were redesigned using larger-diameter shear studs to evaluate the potential benefits of using larger-diameter shear studs. These three bridges used 7/8" shear studs in their original designs, as is typical of current practice. The purpose of the redesigns using larger-diameter shear studs was to estimate the reduction in the number of shear studs that can be achieved by using larger-diameter shears studs, and to determine if any shear stud requirements in the AASHTO LRFD Bridge Design Specifications or in Texas Department of Transportation standards and recommend practices might be problematic for larger-diameter shear studs. Original design drawings and calculations of the three bridges were provided by TxDOT. These original designs were based on the 6<sup>th</sup> Ed and 8<sup>th</sup> Edition AASHTO LRFD Bridge Design Specifications. The 6<sup>th</sup> Ed. And 8<sup>th</sup> Ed. AASHTO and the current 9<sup>th</sup> Ed. AASHTO (AASHTO 2020) have the same requirements with respect to shear studs. As described in Chapters 1 and 2, the upcoming 10<sup>th</sup> Ed. AASHTO has significant changes to shear stud static and fatigue strength requirements (AASHTO 2021). Consequently, the redesign of the three bridges using larger-diameter shear studs will consider both the 9<sup>th</sup> Ed. AASHTO and the proposed 10<sup>th</sup> Ed. AASHTO stud shear stud requirements. The redesigns will also consider pertinent TxDOT standards and preferred practices ( (TxDOT 2019, TxDOT 2021, TxDOT 2023).

In this study, it was assumed that shear stud design and detailing requirements in AASHTO and in the TxDOT documents noted above are valid for larger-diameter shear studs. The three bridges were redesigned with 1", 1-1/8", and 1-1/4" diameter shear studs. The number of 7/8" shear studs in the original design is compared with the number of larger-diameter shear studs after the redesign. Thus, the reduction in the number of shear studs can be quantified. The redesigns can also help clarify whether using larger-diameter shear studs conflicts with any existing geometric or other detailing requirements in AASHTO or in TxDOT standards and preferred practices.

### 3.2. Description of the Bridges

---

TxDOT provided the research team drawings and design calculations for three bridges for use in this study, as follows:

1. Guadalupe River Bridge – Yoakum District – Straight Continuous Plate Girder
2. US 83 E-WB Overpass at BUs 83- Pharr District – Curved Continuous Plate Girder
3. IH 610 at IH 69 Connector C – Houston District – Straight Single Span Tub Girder

Bridges 1 and 3 were designed in accordance with the 8<sup>th</sup>. Ed. AASHTO and Bridge 2 was designed in accordance with the 6<sup>th</sup> Ed. AASHTO. As noted above, the shear stud requirements in these editions of AASHTO are the same as in the 9<sup>th</sup> E. AASHTO.

### 3.2.1. Guadalupe River Bridge

The first bridge is a composite steel bridge located in DeWitt County and crosses the Guadalupe River. This bridge is referred to as the “Guadalupe River Bridge” herein. Design drawings of this bridge are dated 2019. The Guadalupe River Bridge is a three-span continuous straight I-girder bridge with normal supports (i.e., no skew). The span configuration is 236'-300'-236' and the overall bridge width is 42'. ASTM A709-50W grade steel is used for all steel components except reinforcement in the concrete slab, which has a specified yielding strength of 60 ksi. Five identical steel I-girders equally spaced at 9' are used. The girder webs are 90" in depth and 0.75" in thickness along their entire length, except for the dapped ends where web depth decreases to 54". All flange plates are 24" wide and vary in thickness from 1" to 3". Concrete with a nominal compressive strength of 4 ksi is used. A full-depth cast-in-place 8.5" thick deck slab thickness is specified. The effective width of the concrete deck is 90" and 108" for the exterior and interior girders, respectively. Design calculations indicate that 1% deck reinforcement is used in negative moment regions for two orthogonal directions. 7/8" shear studs are placed over the entire length of the Guadalupe River Bridge including negative moment regions. According to TxDOT (2021), studs in negative flexure are provided not for achieving composite action but for crack width control. At each location of shear studs, three studs are provided across the width of the beam flange. The  $(ADTT)_{SL}$  is given as 3200. Figure 3.1 shows a typical cross-section of the bridge.

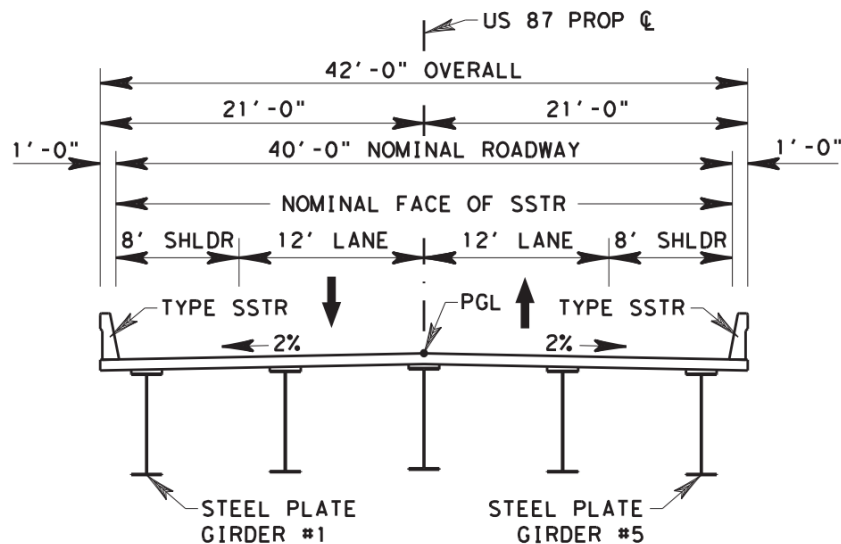


Figure 3.1 - Typical Cross-Section for Guadalupe River Bridge. (Taken from TxDOT Design Drawings)

### 3.2.2. US 83 Overpass Bridge

The second bridge in this study, located in Hidalgo County, is a continuous curved bridge which is referred to herein as “US 83 Overpass Bridge”. The design drawings of the bridge were completed in 2015. The US 83 Overpass Bridge is a two-span continuous curved steel plate I-girder bridge with no skew. The total length of the bridge is 400' with two-equal spans. The out-to-out bridge width is 40', and the radius of the bridge is 1065'. AASHTO M270-50W grade steel is used for steel components, for slab reinforcing steel, Grade 60 steel is used, and the specified compressive strength of concrete is 4 ksi. The bridge consists of five I-girders spaced at 8'-6". Since the bridge is a curved bridge, the total length of each girder is different. While different flange thicknesses are used along the length of the girders, all flange plates are 24" wide, and all web plates are 84" deep and 0.75" thick. The total slab thickness is 8.5" and the effective width of the concrete deck for the exterior and interior girders is 87" and 102" respectively. Design calculations indicate that 1% deck reinforcement ratio is used in negative moment regions in two orthogonal directions. The  $(ADTT)_{SL}$  is 7940. Figure 3.2 shows a typical cross-section of the bridge.

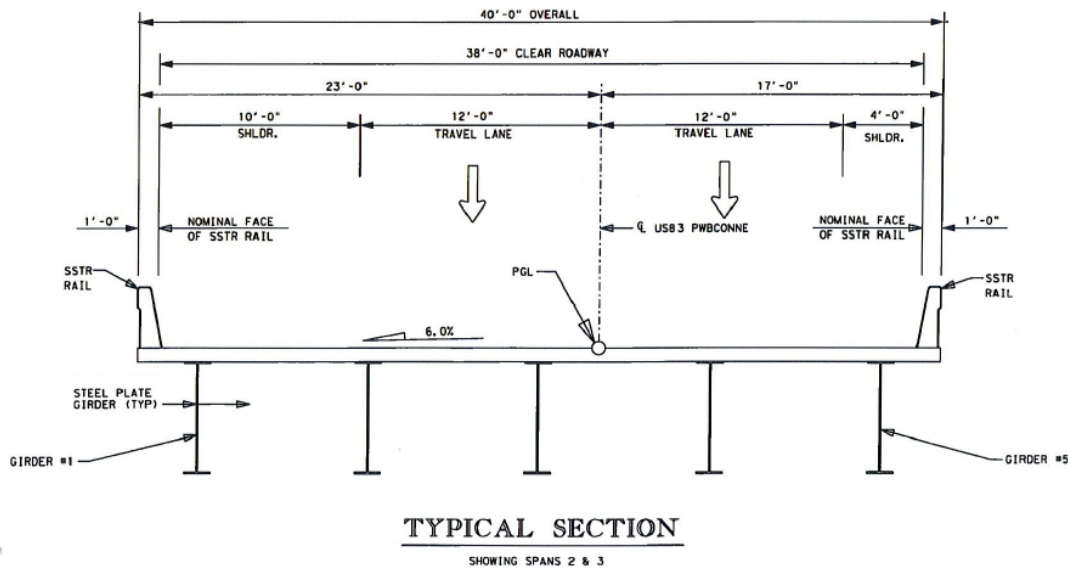


Figure 3.2 - Typical Cross-Section for US 83 Overpass Bridge (Taken from TxDOT Design Drawings)

### 3.2.3. IH 610 Tub Girder Bridge

The third bridge considered in this study is a steel tub girder bridge used as a direct connector between IH 610 and IH 69 in Houston, referred to herein as the “IH 610 Tub Girder Bridge”. The bridge design drawings were dated 2020. The IH 610 Tub Girder Bridge is a straight simply supported one-span bridge with no skew. With three steel tub girders equally spaced at 12'-9", this bridge has a length of 203.25' and an overall width of 38'-5". The steel and concrete used in the design has a specified yield strength of 50 ksi and a compressive strength of 4 ksi, respectively. No information about the yielding strength of reinforcing steel is available from



design documents and is assumed to be 60 ksi. The three girders share the same cross-section configuration. Webs of the box section have a thickness of 9/16" and a 14.04-degree angle with respect to the vertical. The clear vertical distance between the bottom of the top flange and the top of the bottom flange is 84", thus, the actual length of each web can be determined as 86.6" along the inclined direction. The two top flanges are each 24" wide, and the thickness varies from 1.25" to 2" along the span. The bottom flange has a width of 30" while the thickness varies from 1.5" to 2.5" along the length. The full-depth cast-in-place concrete slab has a thickness of 8.5". Design drawings specified the stud spacing along the length of the bridge and noted eight shear studs are used per location (four studs per flange). The typical center-to-center transverse distance between shear studs is given in the design drawings as 6". The reported  $(ADTT)_{SL}$  is 2400. Figure 3.3 shows a typical cross-section of the bridge.

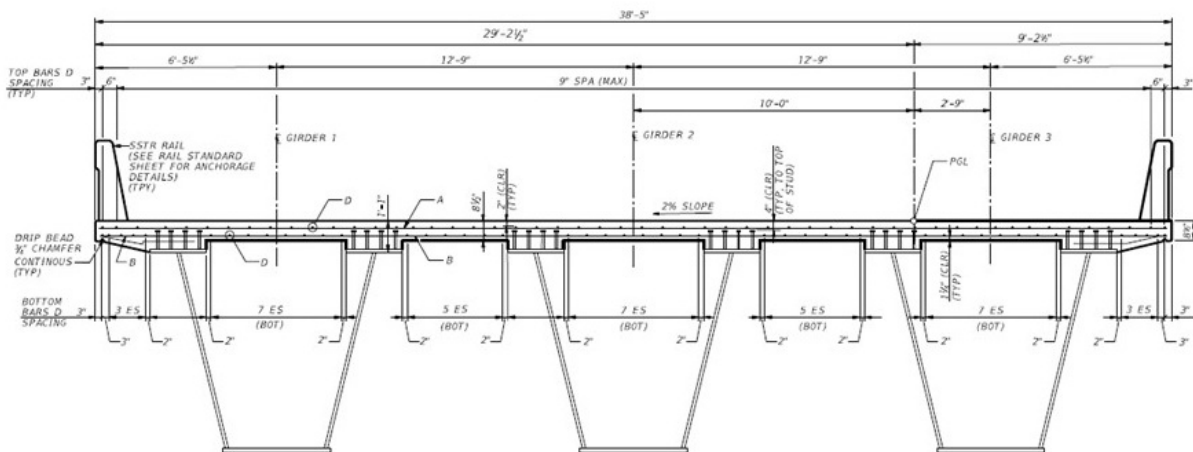


Figure 3.3 - Typical Cross-Section for IH 610 Tub Girder Bridge (Taken from TxDOT Design Drawings)

### 3.2.4. Comment on Shear Stud Length

The design calculations for the three bridges described above typically included a reference to the shear stud length. For example, the design calculations for Bridge No. 1 noted the length of the shear studs is 5". However, no shear stud lengths were noted on any of the design drawings. Limits on the minimum and maximum length of shear studs is controlled by the AASHTO and by TxDOT standards, as listed in Table 2.3. Discussions with TxDOT engineers indicated that shear stud lengths are typically chosen by fabricators working within the bounds of the limits listed in Table 2.3. Consequently, it appears that the stud heights noted in the design calculations do not necessarily reflect what was actually used in the bridges. Since the actual shear stud lengths were not specified in the design drawings and no additional information on shear stud lengths was available to the research team, the review of the stud designs for the three bridges did not include an evaluation of shear stud length. Note that if the shear stud length falls within

the minimum and maximum permissible limits in Table 2.3, the shear stud length has no influence on the calculated static or fatigue strength in AASHTO.

### 3.3. Shear Stud Design based on 9<sup>th</sup> Ed. AASHTO

The general shear stud design procedure based on the 9<sup>th</sup> Ed. AASHTO (AASHTO 2020) is summarized in this section. The first step is to select the shear stud geometry, including stud diameter, and number of studs per row. In this re-design study, the target diameter of the shear studs is set as 1", 1-1/8", and 1-1/4". For each diameter, one and two studs per row are considered in the designs. The height of shear studs has no influence on stud fatigue or ultimate strength calculations, although stud height must conform with minimum length to diameter ratio, minimum penetration requirements, and minimum clear cover requirements (which establishes the maximum height) in AASHTO and in TxDOT design standards, as described below.

The next step is to check shear stud geometry requirements. Information regarding this can be found in the 9<sup>th</sup> Ed. AASHTO and TxDOT *Miscellaneous Details – Steel Girders and Beams – SGMD* (TxDOT 2019). TxDOT *SGMD* specifies that the stud must penetrate at least 2" into the concrete deck. TxDOT *SGMD* also specifies a minimum clear cover of 2.5" from the top of the stud to the top surface of the concrete deck, which is 0.5" more than that in 9<sup>th</sup> Ed. AASHTO. The 9<sup>th</sup> Ed. AASHTO specifies a minimum stud height equal to four times the diameter. These requirements can only be checked once the stud height, concrete deck thickness, and haunch depth are known. For the three bridges considered in this study, using 7" long studs satisfies all the requirements regardless of stud diameter, assuming a minimum 1" haunch depth.

The next step is to find the fatigue-based longitudinal spacing between studs, also referred to as the pitch. As per 9<sup>th</sup> Ed. AASHTO, the fatigue-based longitudinal pitch,  $p$ , in inches of shear studs is determined according to Eq. 3-1.

$$p \leq \frac{nZ_r}{V_{sr}} \quad (3-1)$$

where:

- $Z_r$  = fatigue resistance of an individual shear connector, kips;
- $N$  = number of shear connectors at a cross-section;
- $V_{sr}$  = horizontal fatigue shear range per unit length, kip/in, determined with Eq. 3-2.

$$\sqrt{(V_{fat})^2 + (F_{fat})^2} \quad (3-2)$$

where:

- $V_{fat}$  = longitudinal fatigue shear range per unit length, kip/in;
- $F_{fat}$  = radial fatigue shear range per unit length, kip/in.

Expressions for  $V_{fat}$  and  $F_{fat}$  are given in Eq. 3-3 and Eq. 3-4.

$$V_{fat} = \frac{V_f Q}{I} \quad (3-3)$$

$$F_{fat} = \max \left[ \frac{A_{bot} \sigma_{flg} l}{w R_p}, \frac{F_{rc}}{w} \right] \quad (3-4)$$

where:

- $V_f$  = vertical shear force range under the appropriate fatigue load combination with the fatigue live load, kips;
- $Q$  = first moment of the transformed short-term area of the concrete deck about the neutral axis of the short-term composite section, in<sup>3</sup>;
- $I$  = moment of inertia of the short-term composite section, in<sup>4</sup>;
- $A_{bot}$  = area of the bottom flange, in<sup>2</sup>;
- $\sigma_{flg}$  = range of longitudinal fatigue stress in the bottom flange without consideration of flange lateral bending, ksi;
- $L$  = distance between brace points, ft;
- $W$  = effective width of the deck, in;
- $R_p$  = minimum girder radius within the panel, ft;
- $F_{rc}$  = net range of cross-frame or diaphragm force at the top flange, kips.

Most parameters in Eq. 3-3 and Eq. 3-4 can be derived with hand calculation once the geometry of the bridge and shear studs is determined. However, calculation of  $V_f$ ,  $\sigma_{flg}$ , and  $F_{rc}$  are more involved, and are usually obtained from bridge analysis software.

$V_f$  is the vertical shear force range in the bridge cross-section under fatigue truck loading and can be output by most commercial bridge analysis software. For example, Figure 3.4 depicts CSiBridge (CSI 2022) outputs for unfactored  $V_f$  ( $V_2$  in CSI convention). For a straight bridge, AASHTO allows taking  $F_{fat}$  equal to zero. Therefore, Eq. 3-1 can be simplified as:

$$p \leq \frac{nZ_r}{V_{sr}} = \frac{nZ_r}{V_{fat}} = \frac{nZ_r I}{V_f Q} \quad (3-5)$$

Thus, once  $V_f$  is obtained,  $V_{sr}$  can be derived and the fatigue-based pitch of shear studs can be determined.

For a curved bridge,  $F_{fat}$ , the radial fatigue shear range per unit length, should be calculated to obtain  $V_{sr}$ .  $F_{fat}$  has two components, and the second component of  $F_{fat}$  may be taken equal to zero for a bridge with no skew because the first component generally governs if there is no torsion effect due to the skew. Thus, in this case:

$$F_{fat} = \frac{A_{bot} \sigma_{flg} l}{w R_p} \quad (3-6)$$

Once  $\sigma_{flg}$  is derived,  $F_{fat}$  can be calculated using Eq. 3-6.  $\sigma_{flg}$  is expressed as follows:

$$\sigma_{flg} = \frac{M_f}{S_{bottom}} \quad (3-7)$$

where:

$M_f$  = fatigue moment range (kip-ft);

$S_{bottom}$  = short term composite section modulus to the bottom flange ( $\text{in}^3$ ).

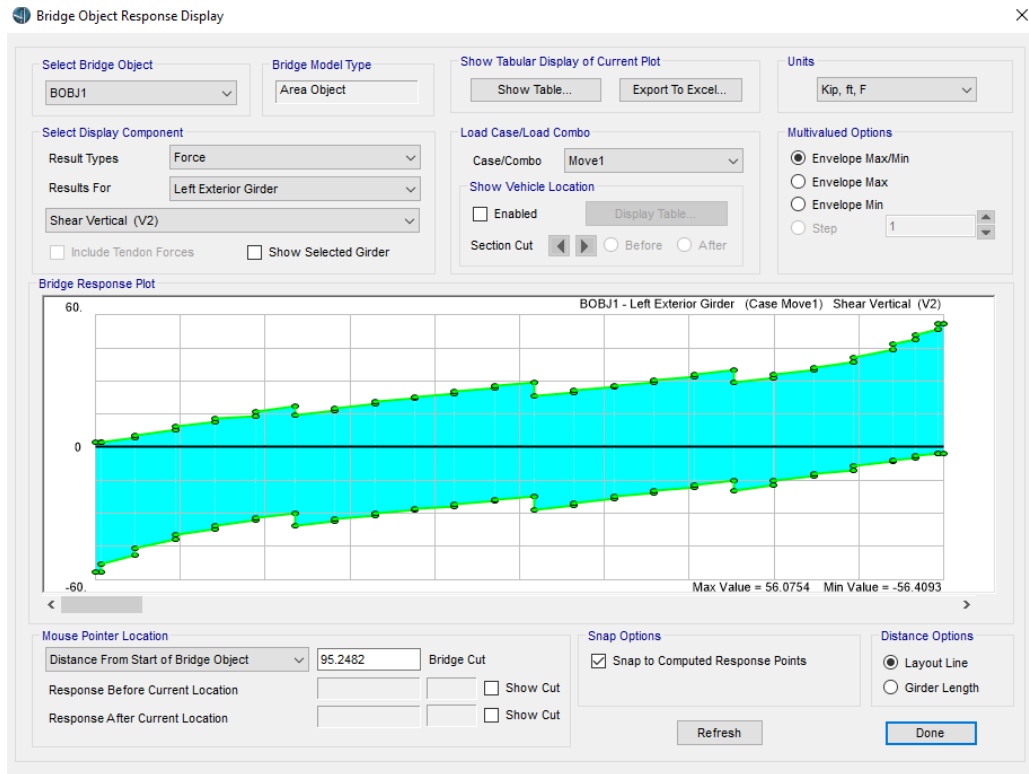


Figure 3.4 - CSI Output for Unfactored  $V_f$  ( $V_2$  in CSI Convention)

$M_f$  ( $M_3$  in CSI convention) can be obtained from the bridge analysis software such as MDX or CSiBridge. The output generated by CSiBridge can be seen in Figure 3.5.

In a continuous bridge, special consideration must be given for shear studs around contraflexure points. As per 8<sup>th</sup> Ed. AASHTO Article 6.10.10.3, the shear stud pitch in transition regions between negative and positive moment must decrease in the event that the negative moment region is designed as non-composite. The decrease of shear stud pitch is based on the additional shear stud number  $n_{ac}$  of Eq. 3-8.

$$n_{ac} = \frac{A_s f_{sr}}{Z_r} \quad (3-8)$$

where:

- $A_s$  = total area of longitudinal reinforcement over the interior support within the effective concrete deck width, in<sup>2</sup>;  
 $f_{sr}$  = stress range in the longitudinal reinforcement over the interior support under the applicable fatigue load combination, ksi.

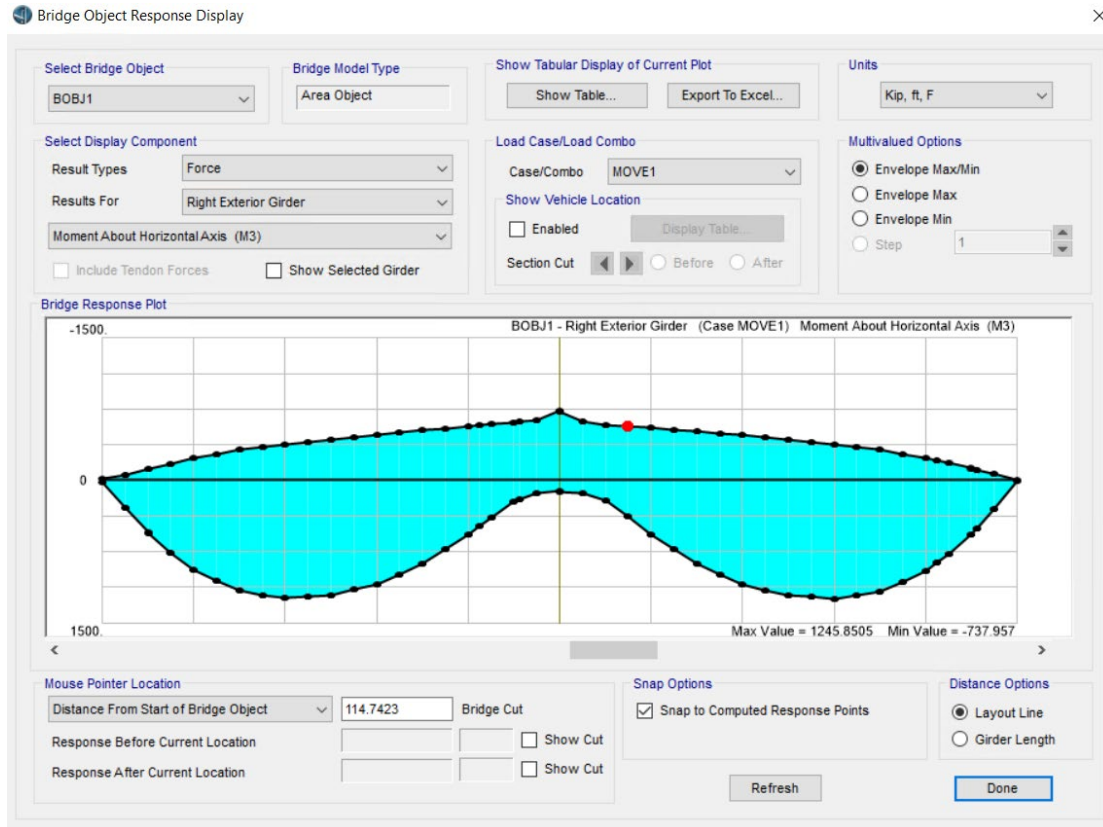


Figure 3.5 - CSI Bridge Output for Unfactored  $M_f$  ( $M_3$  in CSI Convention)

The length of the region for placing additional shear studs is given as one-third of the effective concrete slab width,  $b_s$ , on each side of contraflexure points. Since the minimum allowable longitudinal pitch of studs is 6 times the diameter in the 9th Ed. AASHTO, the pitch of shear studs in the transition region can be calculated using Eq. 3-9.

$$p_{ac} = \max \left[ \frac{2b_s}{3n_{ac}}, 6d \right] \quad (3-9)$$

where:

- $d$  = shear stud diameter, in.

The pitch determined based on the process described above only satisfies the fatigue requirements and must be checked against the strength limit state requirement per 9<sup>th</sup> Ed.

AASHTO Article 6.10.10.4.1. Eq. 3-10 is used to obtain the number of shear studs needed for the strength limit state.

$$n_s = \frac{P}{Q_r} \quad (3-10)$$

where:

$P$  = nominal shear force, kips;

$Q_r$  = factored shear resistance of one shear connector, kips.

According to the 9<sup>th</sup> Ed. AASHTO, a continuous bridge shall be divided into several sections and in each section, the value of  $P$  is calculated independently. If a continuous bridge is designed as non-composite in the negative moment region, the bridge shall be divided at contraflexure points under dead load and points of maximum live load plus impact positive moment. Figure 3.6 qualitatively illustrates the sections to be checked for shear stud strength requirements for a three-span continuous bridge.

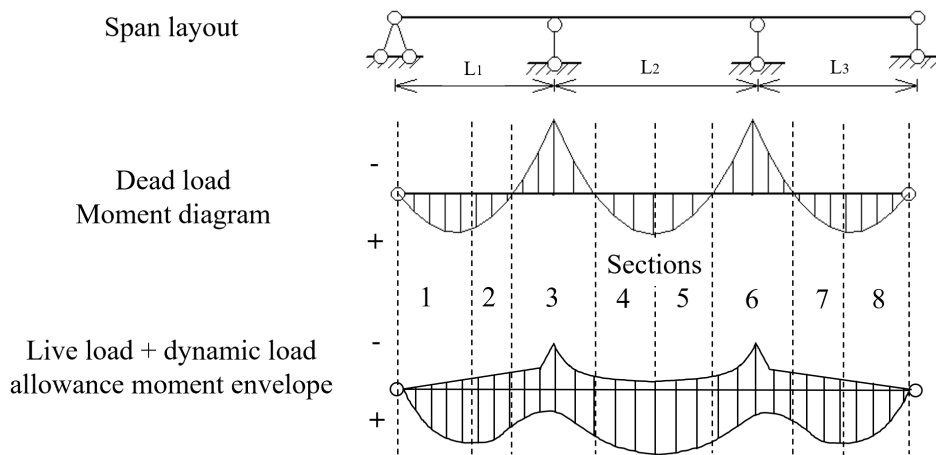


Figure 3.6 - Section Divisions for Shear Stud Strength Limit State Check in a Three-Span Bridge where Negative Moment Region is Designed Non-Composite

In the region of negative moment (sections 3 and 6 in Figure 3.6), the 9<sup>th</sup> Ed. AASHTO does not specify how to determine  $P$ . In other words, the 9<sup>th</sup> Ed. AASHTO only requires the shear stud strength limit state check in the positive moment region when the bridge is designed as non-composite for negative flexure. The nominal shear force  $P$  for sections other than negative flexure (sections 1, 2, 4, 5, 7, and 8 in Figure 3.6) are given in Eq. 3-11.

$$P = \sqrt{P_p^2 + F_p^2} \quad (3-11)$$

where:

- $P_p$  = total longitudinal force in the concrete deck at the point of maximum live load plus impact positive moment, kips;  
 $F_p$  = total radial force in the concrete deck at the point of maximum live load plus impact positive moment, kips.

$P_p$  and  $F_p$  can be determined by using Eq. 3-12 if the yielding strength over the cross-section of the steel girder is uniform, which is valid for the bridges considered in the present study.

$$\begin{cases} P_p = \text{Min}[0.85f'_c b_s t_s, F_y A_g] \\ F_p = P_p \frac{L_p}{R} \end{cases} \quad (3-12)$$

where:

- $f'_c$  = compressive strength of the concrete deck, ksi;  
 $b_s$  = effective concrete slab width, in;  
 $t_s$  = concrete deck thickness, in;  
 $F_y$  = yielding strength of the steel girder, in;  
 $A_g$  = cross-sectional area of the steel girder, in;  
 $L_p$  = arc length between an end of the girder and an adjacent point of maximum live load plus impact positive moment, ft;  
 $R$  = minimum girder radius over the length  $L_p$ , ft.

It can be observed from above definitions that, for a straight bridge, the nominal shear force  $P$  is equal to  $P_p$ . Eq. 3-10 can therefore be written as  $n_s = \frac{P_p}{Q_r}$  for a straight bridge. Figure 3.7 provides a diagram illustrating the shear stud strength limit state check on a straight bridge with non-composite negative moment design.

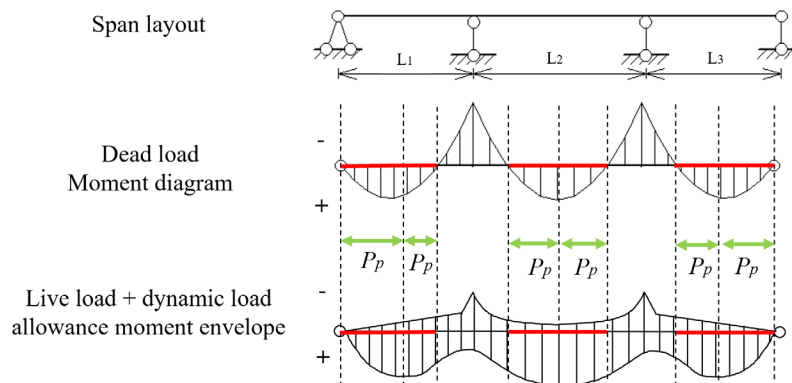


Figure 3.7 - Shear Stud Strength Limit State Check for Straight Bridge when Negative Moment Region is Designed Non-Composite: Studs are Checked in Red Regions and  $P=P_p$

On the other hand, if the bridge is designed as composite in negative moment regions, the bridge is divided at maximum live load plus impact positive moment points and interior support centerlines as depicted in Figure 3.8.

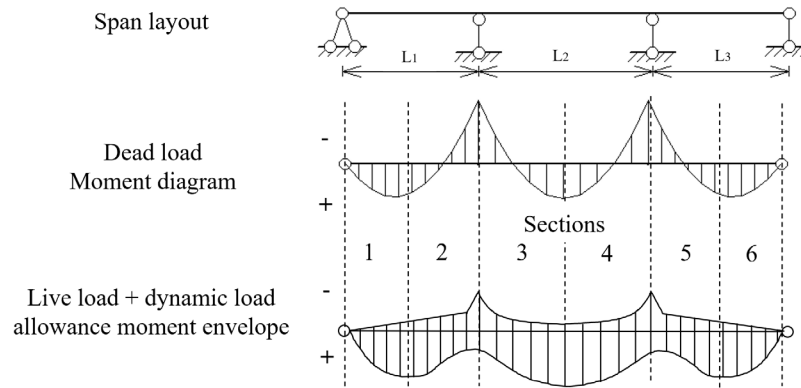


Figure 3.8 - Section Division for Shear Stud Strength Limit State Check in a Three-Span Bridge where Negative Moment Region is Designed Composite

For this case, the 9<sup>th</sup> Ed. AASHTO requires the strength check of shear studs over the entire bridge including the negative moment regions. However, the nominal shear force  $P$  is different on the two sides of points of maximum live load plus impact positive moment. From the end of the bridge to the maximum live load plus impact positive moment location (sections 1 and 6 in Figure 3.8),  $P$  is given by Eq. 3-11. From the maximum live load plus impact positive moment point to the interior support center line (sections 2, 3, 4, and 5 in Figure 3.8),  $P$  is determined per Eq. 3-13.

$$P = \sqrt{P_T^2 + F_T^2} \quad (3-13)$$

where:

$P_T$  = total longitudinal force in the concrete deck between the point of maximum live load plus impact positive moment and the centerline of an adjacent interior support, kips, taken as  $P_T = P_p + P_n$ ;

$F_T$  = total radial force in the concrete deck between the point of maximum live load plus impact positive moment and the centerline of an adjacent interior support, kips.

Expressions for  $P_n$  and  $F_T$  are given below in Eq. 3-14.

$$\begin{cases} P_n = \text{Min}[0.45f'_c b_s t_s, F_y A_g] \\ F_T = P_T \frac{L_p}{R} \end{cases} \quad (3-14)$$



Similarly, for a straight bridge,  $F_T$  is zero and Eq. 3-10 can be rewritten as  $n_s = \frac{P_p}{Q_r}$  for exterior sections and  $n_s = \frac{P_T}{Q_r}$  for interior sections. Figure 3.9 is a diagram illustrating the stud strength limit state check on a straight bridge for composite negative moment design.

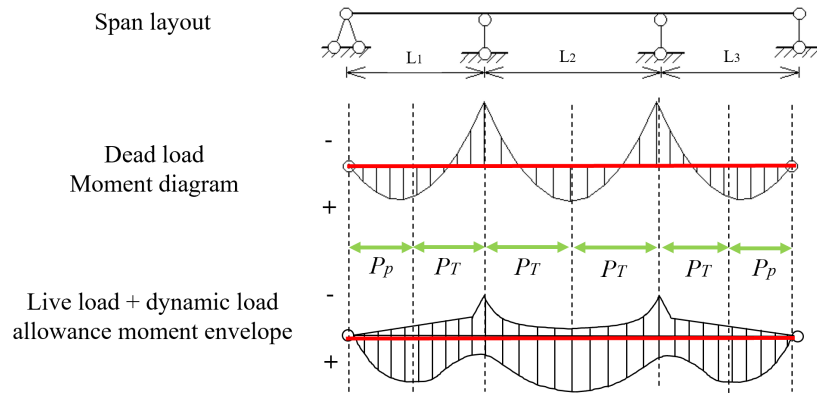


Figure 3.9 - Shear Stud Strength Limit State Check when Negative Moment Region is Designed Composite: Studs are Checked in Red Region with Corresponding P

### 3.4. Evaluation of the Original Designs

The number of shear stud in a steel bridge is controlled by the longitudinal pitch. Evaluation of the original designs for the three bridges focuses on the process of obtaining the stud longitudinal pitch, in which important design parameters such as  $V_{sr}$  are obtained from bridge analysis and design software. Since the numerical bridge models in original design were not available, the three bridges were modeled again in this study using CSiBridge (CSI 2022) to reproduce and evaluate key parameters like  $V_{sr}$ . At the same time, design conventions and common practices were learned by evaluating the original designs and by communicating with TxDOT engineers. Following the same design practices as closely as possible, the final number of 7/8" shear studs was computed and compared with that in original designs.

#### 3.4.1. Guadalupe River Bridge

The Guadalupe River Bridge was modeled and analyzed using the program MDX in the original TxDOT design. Figure 3.10 illustrates the CSI model. A modeling approach referred to as a “grid” model is implemented in MDX, which is understood as all elements in the model are represented by line elements assigned with section properties. Therefore, the similar “frame” modeling scheme in CSiBridge was used, where all girders were modeled by beam elements but the deck is modeled by shell elements. Rigid link connections are applied between the two.

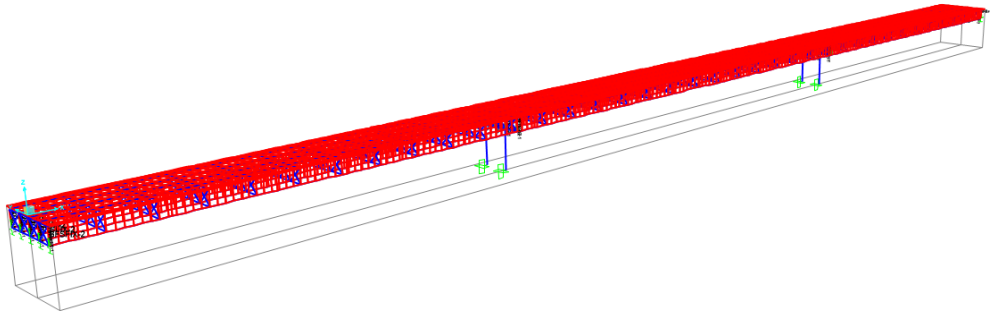


Figure 3.10 - Guadalupe River Bridge Model in CSiBridge

As per 9<sup>th</sup> Ed. AASHTO Article 3.6.1.4, the fatigue truck loading is one design truck with a fixed back axle distance of 30' acting anywhere on the bridge deck regardless of actual design lanes. Thus, in the CSI model, one single fatigue design truck was placed on the bridge with access to the entire deck width within barriers. An influence surface method was utilized for the fatigue load analysis. CSiBridge can automatically consider the dynamic allowance of the fatigue truck. When the analysis is complete,  $V_2$  obtained from CSiBridge only needs to be multiplied by the load factor to get the final fatigue shear effect  $V_f$ . As noted in Section 3.3, in a straight I-girder steel bridge,  $V_{sr} = V_{fat} = V_f (Q/I)$ . The pitch of the shear studs can be derived by Eq. 3-5 once  $V_{sr}$  is determined. Figure 3.11 plots the distribution of  $V_f$  over the length of one exterior girder from the CSiBridge model, which agrees well with the  $V_f$  values reported in the original design.

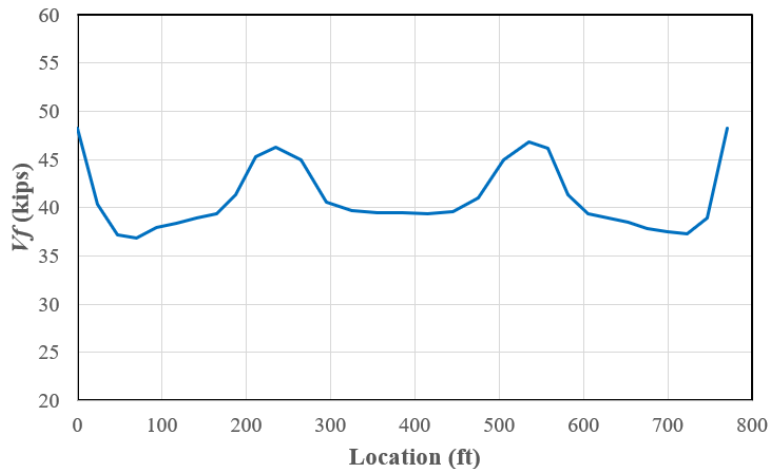


Figure 3.11 CSiBridge  $V_f$  Results for Guadalupe River Bridge on Exterior Girder

Following the determination of  $V_f$ , the pitch satisfying the fatigue limit state can be obtained by using Eq. 3-5. Table 3.1 shows pitches at various control points on the exterior girder when 7/8"

shear studs are used. The location of control points is the distance from the simply supported end of the girder. Since results from CSiBridge generally agreed with the original design,  $V_f$  values from the original design were used in Table 3.1. Original  $Q$  and  $I$  values from the TxDOT design were also adopted in Table 3.1. It was found that in positive moment regions,  $Q$  and  $I$  were determined by considering the concrete slab and steel girder but not including the haunch or deck reinforcement. In negative moment regions,  $Q$  and  $I$  were calculated based on the steel girders and on the reinforcement in the concrete slab. This calculation of  $Q$  and  $I$  is different from the method given in *Steel Bridge Design Handbook* (NSBA 2022) design examples and is believed to be an artifact of the MDX software. These design examples considered the concrete slab in negative moment region for  $Q$  and  $I$  calculations. As per 9<sup>th</sup> Ed. AASHTO Article 10.10.1.2, the upper limit of shear stud pitch is 48" when girder web depth is larger than 24", otherwise, the pitch shall not exceed 24". However, in the original design, a 24" maximum pitch is used regardless of girder web depth. The TxDOT *Bridge Design Manual* (TxDOT 2023) specified that all bridges use 24" maximum pitch. The lower limit for shear stud pitch is six times the stud diameter, which is 5.25" for 7/8" studs. Similar tables of shear stud pitches were developed for all girders in the bridge.

**Table 3.1 - Pitch of 7/8" Shear studs on Exterior Girder of Guadalupe River Bridge**

Location (ft)	$V_f$ (kips)	$Q$ (in <sup>3</sup> )	$I$ (in <sup>4</sup> )	Studs per row	$V_{fat}$ (kip/in)	$Z_r$ (kips)	$p$ (in)
0	73.28	2628.8	277609	3	0.69	4.21	18.20
23.5	62.16	2628.8	277609	3	0.59	4.21	21.46
94	59.98	2983.7	331684	3	0.54	4.21	23.41
141	62.09	2983.7	331684	3	0.56	4.21	22.62
188	62.72	371.2	268365	3	0.09	4.21	24.00
235	75.62	374.8	377643	3	0.08	4.21	24.00
265	69.05	371.2	268365	3	0.10	4.21	24.00
355	65.04	2983.7	331684	3	0.59	4.21	21.59
385	82.85	2983.7	331684	3	0.75	4.21	16.95
445	67.36	2628.8	277609	3	0.64	4.21	19.80
505	65.36	371.2	268365	3	0.09	4.21	24.00
535	81.24	374.8	377643	3	0.08	4.21	24.00
582	60.18	371.2	268365	3	0.08	4.21	24.00
629	61.89	2983.7	331684	3	0.56	4.21	22.69
676	60.13	2983.7	331684	3	0.54	4.21	23.35
723	58.44	2983.7	331684	3	0.53	4.21	24.00
770	73.32	2628.8	277609	3	0.69	4.21	18.20

The location-based pitch results in Table 3.1 can be organized in a way such that nearby control points with similar pitches are combined into a single region where shear studs are uniformly distributed. This process is called “grouping” in TxDOT design documents. No formal guidance of the grouping procedure was found and it appears to be based on engineering judgement. However, some principles about grouping of shear studs are summarized based on evaluation of the original designs:

1. Value of pitch should be an integer.
2. Pitch in grouping region should be smaller but no more than 1” less compared to the smallest fatigue-based pitch in that region.
3. Arrangement of groupings should be symmetric over the bridge length if possible.
4. The difference in shear stud longitudinal pitches should at least be 2” in nearby grouping regions to avoid difficulties in construction.
5. The interface of two grouping regions should be controlled by the one with smaller pitches.

Based on these principles, the 7/8” shear stud pitches (grouping) can be determined. Results are presented in Table 3.2, which matches the results in the TxDOT design calculations. The grouping in Table 3.2 assumes that the first and the last row of shear studs are located at zero distance from the support, which is unrealistic in practice. In the design drawings, the first and last row of shear studs are placed 6” from the bearing centerline. However, this difference only results a slight change in the final number of shear studs. Thus, the stud numbers given in Table 3.2 are used for estimating the total number of shear studs. Similar tables of shear stud groupings and resulting shear stud numbers were developed for the other girders in Guadalupe River Bridge.

**Table 3.2 - Arrangement of 7/8" Shear Stud Pitch (Grouping) on Exterior Girder of Guadalupe River Bridge**

Location (ft)	Pitch (in)	Number of rows	Studs per row	Number of studs
0-24	18	17	3	51
24-189	20	100	3	297
189-265	24	39	3	114
265-505	16	181	3	540
505-581	24	39	3	114
583-746	20	100	3	297
746-770	18	17	3	48

A final step in the shear stud design is checking the strength limit state. The Guadalupe River Bridge shear studs were checked by the strength limit state over the entire span in the original

TxDOT design, which means the bridge was designed as composite in negative moment regions. Communication with TxDOT design engineers confirmed this point. Results from strength limit state check show that the fatigue-based pitch controls the required number of shear studs over the entire span.

The total number of shear studs can now be determined. For the two exterior girders, each need 1461 studs. For the three interior girders, each need 1188 studs. Thus, for the five girders in total, 6486 studs are required. Nonetheless, the original design calculations further simplified the grouping results that the same number and arrangement of shear studs are used in all five girders. In addition, the design drawings show that only five grouping regions with 18", 24", and 16" pitches were used over the entire length of the bridge. If similar simplifications are followed, it was determined that the total number of shear studs for this bridge to be 7710, which is very close to the 7680 reported in the original design calculations.

### 3.4.2. US 83 Overpass Bridge

The US 83 Overpass Bridge was also modeled and analyzed using the MDX software in the original TxDOT. CSiBridge was used to evaluate the design parameters of this bridge such as  $V_{sr}$  by the research team to evaluate the original design and to redesign the bridge with larger-diameter shear studs.

The US 83 Overpass Bridge was modeled in CSi Bridge using a combination of shell and beam element. The concrete deck and girder webs were modeled using shell elements, and the flanges were modeled by beam elements, and there is a rigid link between the top flange beam element and the concrete deck. The CSiBridge model is shown in Figure 3.12.

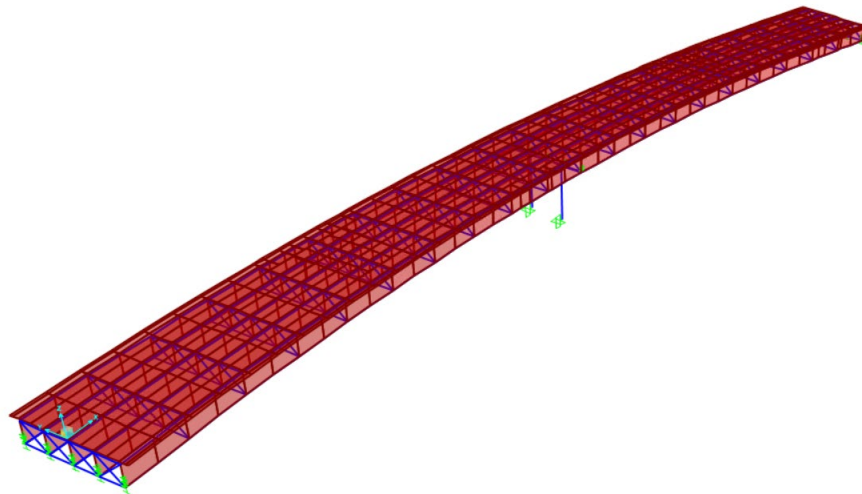


Figure 3.12 - US 83 Overpass Bridge Model in CSiBridge

Since the US 83 Overpass Bridge is a curved plate girder bridge, unlike the Guadalupe Bridge, the radial component of fatigue shear range,  $F_{fat}$ , is taken into account to compute  $V_{sr}$ . After analysis is completed, by obtaining the values of  $M_f$  and  $V_f$  from CSiBridge,  $F_{fat}$  and  $V_{fat}$  can be computed as described in Section 3.3. Therefore,  $V_{sr}$  can be determined using Eq. 3-2 to compute the required stud pitch.

To determine the stud pitches,  $M_f$  and  $V_f$  are obtained from CSiBridge, and the results are shown in Figure 3.13 and Figure 3.14 for a single girder.

Analysis results showed good agreement with TxDOT results. Since the analysis results represented the TxDOT design results closely, the original  $M_f$  and  $V_f$  results were used to compute  $V_{sr}$  which was then used to determine the pitches listed in Table 3.3. Also, because MDX has a slightly different methodology as explained in the previous section to calculate  $Q$  and  $I$  values rather than following the *Steel Bridge Design Handbook* (NSBA 2022) design examples, the research team decided to use original  $Q$  and  $I$  results in the TxDOT design. According to 9<sup>th</sup> Ed. AASHTO Article 6.10.10.1.2 and TxDOT practices, while maximum center-to-center pitch is 24", the pitch must not be less than six shear stud diameters which is 5.25" for 7/8" shear studs.

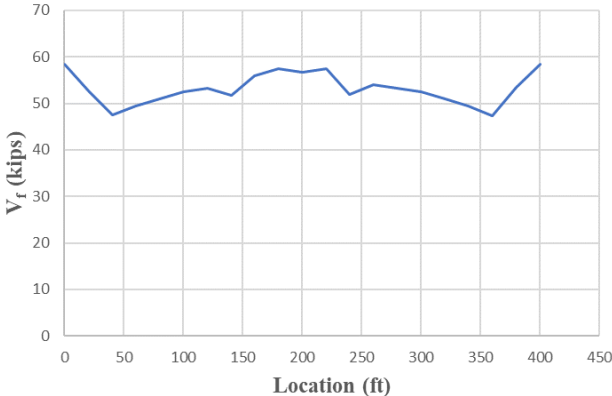


Figure 3.13 - CSiBridge  $V_f$  Results for US 83 Overpass Bridge Girder 1

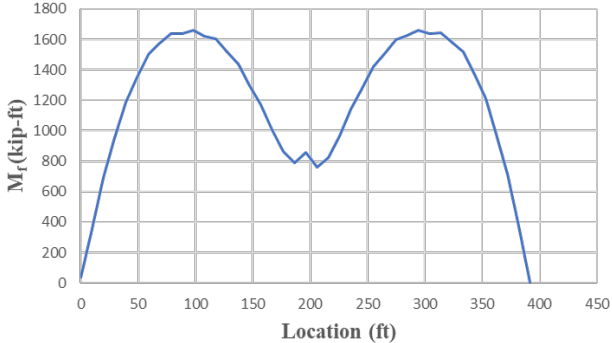


Figure 3.14 - CSiBridge  $M$  Results for US 83 Overpass Bridge Girder 1

The next step is grouping of the shear studs, which was done by following the same principles explained in the previous section. Results are listed in Table 3.4, which matches the TxDOT design. As indicated in this table, a pitch of 24" was used over the full length of the girder. Similar results were obtained for the other girders of this bridge.

**Table 3.3 - Pitch of 7/8" Shear Studs on Girder 1 of the US 83 Overpass Bridge**

Location (ft)	$V_f$ (kips)	$Q$ (in <sup>3</sup> )	$I$ (in <sup>4</sup> )	Studs per row	$V_{sr}$ (kip/in)	$Z_r$ (kips)	$p$ (in)
0	63.07	2506.8	265696	3	0.60	4.21	21.22
19.52	53.44	2506.8	265696	3	0.51	4.21	24.00
39.05	48.63	2506.8	265696	3	0.47	4.21	24.00
58.57	52.34	2506.8	265696	3	0.51	4.21	24.00
78.1	53.5	2506.8	265696	3	0.53	4.21	23.82
97.62	54.15	2506.8	265696	3	0.53	4.21	23.71
117.15	54.78	2506.8	265696	3	0.53	4.21	23.69
136.67	55.29	2506.8	265696	3	0.53	4.21	23.71
156.2	55.66	2506.8	265696	3	0.53	4.21	23.79
175.72	55.54	2506.8	265696	3	0.53	4.21	24.00
195.24	69.52	2677.8	322790	3	0.58	4.21	21.85
214.77	57.66	2506.8	265696	3	0.55	4.21	23.13
234.29	55.07	2506.8	265696	3	0.53	4.21	24.00
253.82	56.19	2506.8	265696	3	0.54	4.21	23.35
273.34	55.46	2506.8	265696	3	0.54	4.21	23.42
292.87	54.54	2506.8	265696	3	0.54	4.21	23.38
312.39	53.64	2506.8	265696	3	0.53	4.21	23.80
331.39	52.44	2506.8	265696	3	0.52	4.21	24.00
351.44	51.1	2506.8	265696	3	0.50	4.21	24.00
370.96	49.82	2506.8	265696	3	0.47	4.21	24.00
390.49	63.08	2506.8	265696	3	0.60	4.21	21.20

**Table 3.4 - Arrangement of 7/8" shear Stud Pitch (Grouping) on Girder 1 of US 83 Overpass Bridge**

Location (ft)	Pitch (in)	Number of rows	Studs per row	Number of Studs
0-390.49	21	224	3	672

As per 9<sup>th</sup> Ed. AASHTO Article 6.10.10.4, the number of shear studs based on the fatigue limit state should be checked against the strength limit state. In consideration of composite design in

both negative and positive bending regions, shear stud pitches were controlled by the fatigue limit state for this bridge.

In the TxDOT design, the total number 7/8" shear studs used for US 83 Overpass Bridge is 3445. The total number of studs determined by the research team was 3411 which is very similar to the TxDOT design.

### 3.4.3. IH 610 Tub Girder Bridge

The IH 610 Tub Girder Bridge was modeled and analyzed using the program DESCUS II version 8.3 in the original design. The DESCUS model showed an effective slab width of 102" for all three girders. However, based on the design drawings and AASHTO rules for effective slab width, the effective slab width for the exterior girders and the interior girder should be 154" and 153", respectively. CSiBridge was used in this research to evaluate the original design. CSiBridge does not require input of effective slab width since the cross-section of bridge is explicitly modeled. There were some minor differences between the definition of diaphragms between the CSiBridge model and original model due to software capabilities. However, it is believed that such modeling differences have negligible influence on live load effects.

Figure 3-15 illustrates the CSiBridge model. A 3D model was created where the box girder webs, bottom flanges, and concrete deck were modeled by shell elements. The top flanges of the girders were modeled by beam elements. A rigid link was applied between the top flange beam element and the concrete deck to enforce composite action. DESCUS uses a 2-D grillage analysis, where the steel girders and their associated effective width of the concrete deck are represented by beam elements. The cross-sectional properties of the beam elements include the effect of composite action between the steel girders and the concrete deck. The DESCUS model was therefore more simplified than the CSiBridge model.

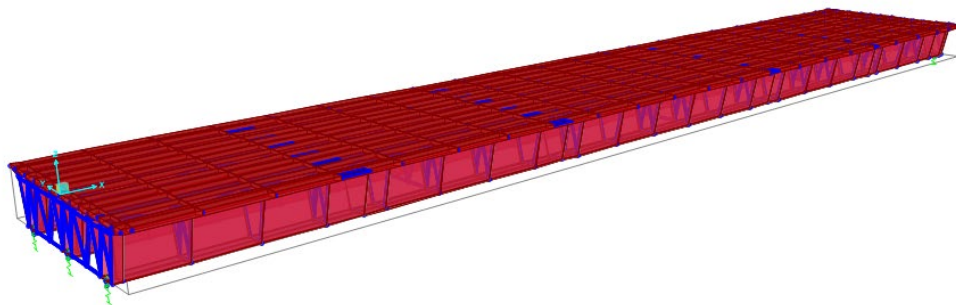


Figure 3-15 - IH 610 Tub Girder Bridge Model in CSiBridge



As per the 9<sup>th</sup> Ed. AASHTO Article 6.11.10,  $V_{sr}$  of composite box girders shall be the vector sum of  $V_{fat}$  and the torsional fatigue shear range in the concrete deck. On the other hand, AASHTO specifies that for box girder bridges satisfying geometry requirements in Article 6.11.2.3, the torsional shear can be neglected. The IH 610 Tub Girder Bridge satisfied those requirements.

Preliminary analysis results from the CSiBridge model showed that  $V_{sr}$  obtained without considering torsional effects is around 20% smaller than the value provided by the DESCUS model. In addition, the original design showed calculations of St. Venant torsional shear and warping stress under maximum live load. Based on these observations, it is assumed torsional effects were included in original design and should be considered in this evaluation study. The torsional effect is given by St. Venant torsional shear flow,  $f$  (kips/in.), per Eq. 3-15.

$$f = \frac{T}{2A_0} \quad (3-15)$$

where:

$A_0$  = enclosed area within the box section, in<sup>2</sup>;

$T$  = internal torque due to the factored fatigue loads, kip-in.

Figure 3-16 shows the internal torque,  $T$ , output from CSiBridge for one exterior girder. Once the above-mentioned parameters were obtained,  $V_{sr}$  under both flexural and torsional shear is given in Eq. 3-16.

$$\sqrt{V_{fat}^2 + f^2} \quad (3-16)$$

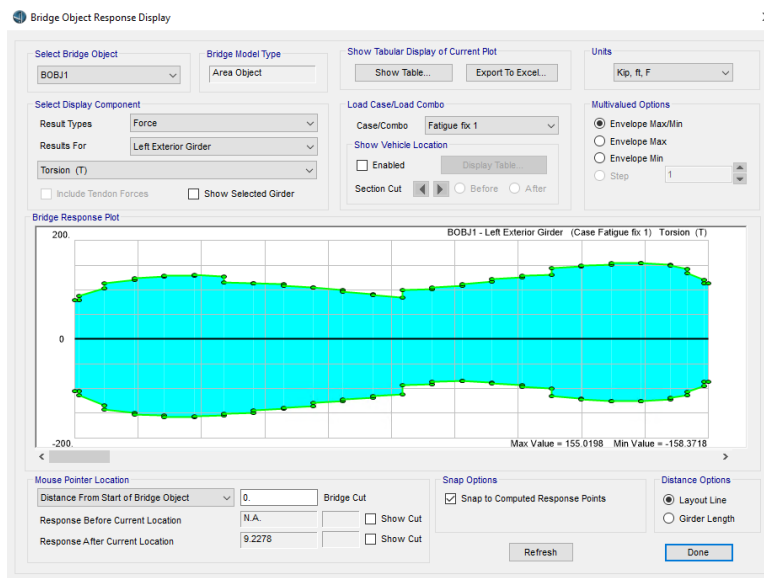


Figure 3-16 - CSiBridge Output for Unfactored Torsion Along the Exterior Girder of the IH 610 Tub Girder Bridge

Figure 3-17 shows  $V_{sr}$  obtained from the CSiBridge model. The results were generally with 15-percent of the DESCUS values. Considering the significant differences between the modeling approaches used in the CSiBridge model and the DESCUS model, these differences were considered acceptable.

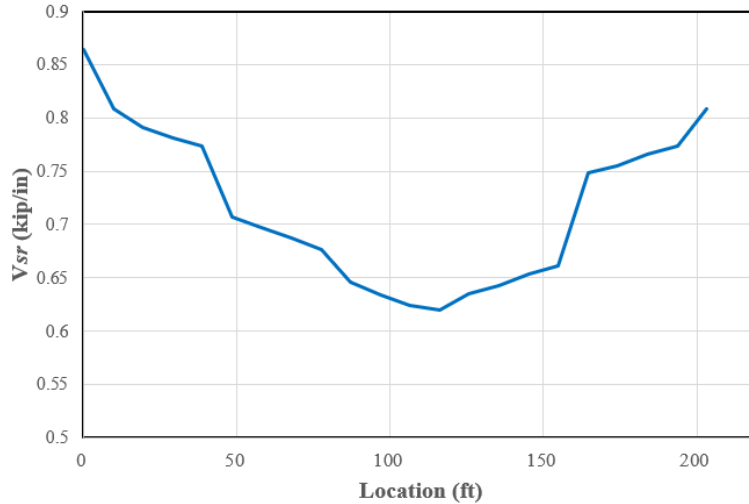


Figure 3-17 - CSiBridge  $V_{sr}$  Results for IH 610 Tub Girder Bridge Exterior Girders

Table 3.5 provides the fatigue-based pitch at control points for exterior girders for 7/8" shear studs. Since  $V_{sr}$  from the CSiBridge and from the DESCUS models showed reasonable agreement, the  $V_{sr}$  values from the original design calculations were used in Table 3.5. Table 3.5 omits parameters like  $V_{fat}$  and  $f$  because they were not available in the original design calculations. Unlike the first bridge, evaluation of  $Q$  and  $I$  shows that they were calculated with consideration of the haunch. It can be noticed that, since eight shear studs are used at one cross-section location, the pitch is always controlled by the upper limit of 24". Similar calculations for shear stud pitch were developed for the interior girder of this three-girder bridge and showed that the maximum pitch limit of 24" also controlled.

A strength limit state check was performed and showed that the pitch given in Table 3.5 also satisfied strength requirements.

The arrangement of shear studs on the bridge (grouping) was simple since the entire bridge has a uniform pitch of 24". The design drawings for the IH 610 Tub Girder Bridge showed that more shear studs were placed at the end regions of the girders with a pitch of 12". The length of the reduced-pitch region is approximately the same as the length of the girders' dapped ends. The reason for the reduced pitch at the bridge ends was not clear. The first row of shear studs is aligned with the first diaphragm, which is 15" away from the end of the tub girder. Table 3.6 below gives the grouping of 7/8" shear stud with the consideration of reduced pitch at end regions.

**Table 3.5 - Pitch of 7/8" Shear Studs on Exterior Girders of IH 610 Tub Girder Bridge**

Location (ft)	Q (in <sup>3</sup> )	I (in <sup>4</sup> )	V <sub>sr</sub> (kips/in)	Studs per row	Z <sub>r</sub> (kips)	p (in)
0	4092.2	494949	0.76	8	4.21	24.00
19.36	4092.2	494949	0.85	8	4.21	24.00
38.72	4092.2	494949	0.89	8	4.21	24.00
58.07	4490.0	628306	0.75	8	4.21	24.00
77.43	4490.0	628306	0.71	8	4.21	24.00
96.79	4572.3	674899	0.66	8	4.21	24.00
116.15	4572.3	674899	0.69	8	4.21	24.00
135.51	4490.0	628306	0.74	8	4.21	24.00
154.86	4490.0	628306	0.77	8	4.21	24.00
174.22	4092.2	494949	0.86	8	4.21	24.00
193.58	4092.2	494949	0.81	8	4.21	24.00
203.26	4092.2	494949	0.77	8	4.21	24.00

**Table 3.6 - Arrangement of 7/8" Shear Stud Pitch (Grouping), Eight Studs per Row, on each Girder of the IH 610 Tub Girder Bridge**

Location (ft)	Pitch (in)	Number of rows	Studs per row	Number of studs
0-19	12	69	8	160
19-184.26	24	47	8	656
184.26-203.26	12	78	8	160

Ultimately, based on discussion above, the total number of 7/8" shear studs on the IH 610 Tub Girder Bridge was determined as 976 for one girder and 2928 for the three girders, which is very close to that of TxDOT design of 968 per girder and 2904 in total.

### 3.5. Redesign with Larger-diameter Shear Studs using the 9<sup>th</sup> Ed. AASHTO

The existing designs using 7/8" diameter shear studs have been evaluated in the previous section. This section will utilize results obtained in the evaluation process to redesign the shear studs using 1", 1-1/8", and 1-1/4" diameter studs. As noted earlier, for the purposes of the redesigns, it

was assumed all equations and requirements from the 9<sup>th</sup> Ed. AASHTO and TxDOT standards are applicable for shear studs of a diameter larger than 7/8".

### 3.5.1. Guadalupe River Bridge

The redesigns considered two cases: one stud per row and two studs per row. Since every parameter needed for determining stud longitudinal pitch was been evaluated in Section 3.4.1, shear stud pitches satisfying fatigue requirements can be easily obtained following the same procedures shown in Table 3.1 and Table 3.2. Table 3.7 lists pitches when 1" shear studs with one stud per row are used on the exterior girders. A similar table was developed for 1" studs with two studs per row. Further, similar tables were developed for 1-1/8" and 1-1/4" studs for one stud per row and two studs per location.

**Table 3.7 - Pitch of 1" Shear Studs on Exterior Girders of Guadalupe River Bridge Using One Stud per Row**

Location (ft)	$V_f$ (kips)	$Q$ (in <sup>3</sup> )	$I$ (in <sup>4</sup> )	Studs per row	$V_{fat}$ (kip/in)	$Z_r$ (kips)	$p$ (in)
0	73.28	2628.8	277609	1	0.69	5.5	7.93
23.5	62.16	2628.8	277609	1	0.59	5.5	9.34
94	59.98	2983.7	331684	1	0.54	5.5	10.19
141	62.09	2983.7	331684	1	0.56	5.5	9.85
188	62.72	371.2	268365	1	0.09	5.5	24.00
235	75.62	374.8	377643	1	0.08	5.5	24.00
265	69.05	371.2	268365	1	0.10	5.5	24.00
355	65.04	2983.7	331684	1	0.59	5.5	9.40
385	82.85	2983.7	331684	1	0.75	5.5	7.38
445	67.36	2628.8	277609	1	0.64	5.5	8.62
505	65.36	371.2	268365	1	0.09	5.5	24.00
535	81.24	374.8	377643	1	0.08	5.5	24.00
582	60.18	371.2	268365	1	0.08	5.5	24.00
629	61.89	2983.7	331684	1	0.56	5.5	9.88
676	60.13	2983.7	331684	1	0.54	5.5	10.17
723	58.44	2983.7	331684	1	0.53	5.5	10.46
770	73.32	2628.8	277609	1	0.69	5.5	7.92

The strength check of the fatigue-controlled pitches showed that in regions of negative moment, the strength limit state requires a stud pitch of 17", which is smaller than the 24" fatigue-based pitch. Therefore, shear stud pitches at these locations were controlled by the strength limit state. Table 3.8 lists the arrangement of stud pitches (grouping) along the span.

**Table 3.8 - Arrangement of 1" Shear Stud Pitch (Grouping) on Exterior Girders of Guadalupe River Bridge Using One Stud per Row**

Location (ft)	Pitch (in)	Number of rows	Studs per row	Number of studs
0-24	7	42	1	42
23-188	9	220	1	219
188-265	17	55	1	54
265-505	7	413	1	412
505-582	17	55	1	54
582-747	9	221	1	220
747-770	7	42	1	40

The final redesign results using 1", 1-1/8", and 1-1/4" diameter shear studs are summarized in Table 3.9. By using larger-diameter shear studs instead of 7/8" studs, there is a significant decrease in the number of studs, which is approximately 25%, 40%, and 50% for 1", 1-1/8", and 1-1/4" studs, respectively. The number of 7/8" studs listed in Table 3.9 is the grouping results from Section 3.4.1 without considering the additional simplifications in the original design calculation. This is because all redesign results do not include the additional simplification.

**Table 3.9 - Redesign Results for Guadalupe River Bridge using 9<sup>th</sup> Ed. AASHTO**

Stud diameter (in)	Studs per row	Total number of studs used	Number of studs/Number of 7/8" studs
7/8	3	6486	100%
1	1	4827	74.4%
	2	4690	72.3%
1-1/8	1	4018	61.9%
	2	4092	63.1%
1-1/4	1	3244	50.0%
	2	3864	59.6%

### 3.5.2. US 83 Overpass Bridge

In the redesign process of the Guadalupe River Bridge, one and two larger-diameter shear studs per row were considered. By following the same methodology explained in the previous section, the redesign of the US 83 Overpass Bridge for 1", 1-1/8", and 1-1/4" studs was completed. Redesign results are presented in Table 3.10. The reduction in the number of studs, when using larger-diameter shear studs, is very similar to the Guadalupe River Bridge.

**Table 3.10 - Redesign Results for US 83 Overpass Bridge using 9th Ed. AASHTO**

Stud diameter (in)	Studs per row	Total number of studs used	Number of studs/Number of 7/8" studs
7/8	3	3411	100%
1	1	2628	77%
	2	2537	74%
1-1/8	1	2076	61%
	2	2074	61%
1-1/4	1	1689	50%
	2	2010	59%

### 3.5.3. IH 610 Tub Girder Bridge

Like the redesign of the previous two bridges, one or two larger-diameter shear studs per row were used in the redesign of the IH 610 Tub Girder Bridge. For the tub girder, there are two top flanges. Thus, the total number of shear studs per row is either two or four. Table 3.11 illustrates the redesign results for 1" shear studs on exterior girders when two studs per row are used. The pitch arrangement along the girder length (grouping) can be found in Table 3.12. Similar tables were developed for 1-1/8" and 1-1/4" studs and four studs per row.

**Table 3.11 - Pitch of 1" Shear studs, Two Studs per Row (One Stud per Flange), on Exterior Girders of IH 610 Tub Girder Bridge**

Location (ft)	Studs per row	$V_{sr}$ (kip/in)	$Z_r$ (kips)	$p$ (in)
0.00	2	0.76	5.5	14.47
19.36	2	0.85	5.5	12.94
38.72	2	0.89	5.5	12.36
77.43	2	0.71	5.5	15.49
96.79	2	0.66	5.5	16.67
116.15	2	0.69	5.5	15.94
135.51	2	0.74	5.5	14.86
154.86	2	0.77	5.5	14.29
174.22	2	0.86	5.5	12.79
193.58	2	0.81	5.5	13.58
203.26	2	0.77	5.5	14.29

**Table 3.12 - Arrangement of 1" Shear Stud Pitch (Grouping), Two Studs per Row (One Stud per Flange), on Exterior Girders of IH 610 Tub Girder Bridge**

Location (ft)	Pitch (in)	Number of rows	Studs per row	Number of studs
0-68	12	69	2	138
68-126	15	47	2	92
126-202.5	12	78	2	154

All numbers presented in Table 3.12 satisfied the strength limit state check and therefore the fatigue limit state controlled the pitch at every location.

Final results are presented in Table 3.13 below. The advantage of using larger-diameter shear studs is found to be significant. By using larger-diameter shear studs, the number of studs is reduced approximately 55%, 60%, and 65% for 1", 1-1/8", and 1-1/4" studs, respectively, compared with 7/8" studs. The large decrease in stud numbers is mainly due to eight studs per row in the original 7/8" stud design, which resulted in more studs than needed. Results for two studs per row and four studs per row are considerably different for 1-1/8" and 1-1/4" shear studs. This is mainly due to the fact when four studs per row is used, the 24" maximum pitch requirement will control the entire span and the total number of studs could not be smaller than 1224.

**Table 3.13 - Redesign Results for IH 610 Tub Girder Bridge using 9<sup>th</sup> Ed. AASHTO**

Stud diameter (in)	Studs per location (Studs per row)	Total number of studs used	Number of studs/Number of 7/8" studs
7/8	4 (8)	2904	100%
1	1 (2)	1214	41.8%
	2 (4)	1268	43.7%
1-1/8	1 (2)	956	32.9%
	2 (4)	1224	42.1%
1-1/4	1 (2)	766	26.4%
	2 (4)	1224	42.1%

### 3.6. Redesign with Larger-diameter Shear Studs using Proposed 10<sup>th</sup> Ed. AASHTO

The proposed 10<sup>th</sup> Ed. AASHTO (AASHTO 2021) will include significant changes to shear stud requirements. Table 2.3 and Table 2.4 summarize key changes to shear stud requirements between the 9<sup>th</sup> Ed. AASHTO and the proposed 10<sup>th</sup> Ed. AASHTO.

To evaluate the potential impact of these changes on the required number of larger-diameter shear studs, redesigns were also performed based on the proposed 10<sup>th</sup> Ed. AASHTO using 1", 1-

1/8", and 1-1/4" diameter shear studs. Similar to the prior sections in this chapter, all equations and requirements from the proposed 10<sup>th</sup> Ed. AASHTO are assumed to be valid for larger diameter shear studs.

### 3.6.1. Guadalupe River Bridge

Using the proposed 10<sup>th</sup> Ed. AASHTO, the Fatigue II load combination controls for the Guadalupe River Bridge. The  $Z_r$  value for shear studs will be different at different locations along the bridge as the number of stress range cycles per truck passage varies along the length. Table 3.14 lists the fatigue-based pitches for 1" studs on an exterior girder using one stud per row. Similar tables were developed for 1-1/8" and 1-1/4" studs and two studs per row.

The strength limit state check showed that within negative moment regions, the required pitch is 14", which is smaller than the 24" fatigue-based pitch. Consequently, the strength-based pitch controlled at those locations. Table 3.15 is the grouping of shear stud pitches that satisfies both fatigue and strength limit states. Similar tables were developed for 1-1/8" and 1-1/4" studs for one and two studs per row.

**Table 3.14 - Pitch of 1" Shear Studs on Exterior Girders of Guadalupe River Bridge using Proposed 10<sup>th</sup> Ed. AASHTO**

Location (ft)	$V_f$ (kips)	$Q$ (in <sup>3</sup> )	$I$ (in <sup>4</sup> )	Studs per row	$V_{fat}$ (kip/in)	$Z_r$ (kips)	$p$ (in)
0	73.28	2628.8	277609	1	0.35	3.2	9.16
23.5	62.16	2628.8	277609	1	0.29	3.2	10.80
94	59.98	2983.7	331684	1	0.27	3.2	11.78
141	62.09	2983.7	331684	1	0.28	3.2	11.38
188	62.72	371.2	268365	1	0.04	3.2	24.00
235	75.62	374.8	377643	1	0.04	2.9	24.00
265	69.05	371.2	268365	1	0.05	2.9	24.00
355	65.04	2983.7	331684	1	0.32	3.2	10.02
385	82.85	2983.7	331684	1	0.29	3.2	10.87
445	67.36	2628.8	277609	1	0.37	3.2	8.53
505	65.36	371.2	268365	1	0.32	2.9	9.97
535	81.24	374.8	377643	1	0.05	2.9	24.00
582	60.18	371.2	268365	1	0.04	2.9	24.00
629	61.89	2983.7	331684	1	0.04	3.2	24.00
676	60.13	2983.7	331684	1	0.28	3.2	11.42
723	58.44	2983.7	331684	1	0.27	3.2	11.75
770	73.32	2628.8	277609	1	0.26	3.2	12.09



**Table 3.15 - Arrangement of 1" Shear Stud Pitch (Grouping) on Exterior Girders of Guadalupe River Bridge using Proposed 10<sup>th</sup> Ed. AASHTO.**

Location (ft)	Pitch (in)	Number of rows	Studs per row	Number of studs
0-24	9	33	1	33
23-188	10	198	1	197
188-264	14	66	1	65
264-505	8	363	1	362
505-582	14	66	1	65
582-747	10	199	1	198
747-770	9	32	1	31

The final redesign results using the proposed 10<sup>th</sup> Ed. AASHTO are summarized in Table 3.16. Although there are significant changes to shear stud design provisions in the proposed 10<sup>th</sup> Ed. AASHTO, the reduction in the number of shear stud numbers is similar to the 9<sup>th</sup> Ed. AASHTO, as the number of 1", 1-1/8", and 1-1/4" studs reduced about 30%, 40%, and 45%, respectively, compared to 7/8" studs. Using one stud per row versus two studs per row had some impact on the required number of studs, as seen in Table 3.16.

**Table 3.16 - Redesign Results for Guadalupe River Bridge using Proposed 10<sup>th</sup> Ed. AASHTO**

Stud diameter (in)	Studs per row	Total number of studs used	Number of studs/Number of 7/8" studs
7/8	3	6018	100%
1	1	4389	72.9%
	2	4310	71.6%
1-1/8	1	3414	56.7%
	2	3876	64.4%
1-1/4	1	2742	45.6%
	2	3860	59.5%

### 3.6.2. US 83 Overpass Bridge

Using the proposed 10<sup>th</sup> Ed. AASHTO, the Fatigue II load combination controls for the US 83 Overpass Bridge. Table 3.17 and Table 3.18 show the redesign results for Girder 1 for 1" studs and one stud per row. A similar table was developed for 1" studs with two studs per row, as well as for 1-1/8" and 1-1/4" studs with one and two studs per row. The Fatigue limit state controlled the pitch of all shear studs for this girder.

A summary of redesign results based on the proposed 10<sup>th</sup>. Ed AASHTO are shown in Table 3.19.

For 7/8" shear studs with 3 studs per row, the proposed 10<sup>th</sup> Ed. AASHTO results in approximately a 3-percent reduction in the number studs compared to the 9<sup>th</sup> Edition AASHTO. The reduction in the number of studs when using 1", 1-1/8" and 1-1/4" studs is substantial and is similar to the reductions obtained using the 9<sup>th</sup> Edition of AASHTO.

**Table 3.17 - Pitch of 1" Shear Studs on Girder 1 of US 83 Overpass Bridge using Proposed 10th Ed. AASHTO**

Location (ft)	$V_f$ (kips)	$Q$ (in <sup>3</sup> )	$I$ (in <sup>4</sup> )	Studs per Row	$V_{sr}$	$Z_r$ (kips)	$p$ (in)
					(kip/in)		
0	63.07	2506.8	265696	1	0.27	2.70	9.91
19.52	53.44	2506.8	265696	1	0.23	2.70	11.61
39.05	48.63	2506.8	265696	1	0.22	2.70	12.48
58.57	52.34	2506.8	265696	1	0.24	2.70	11.47
78.1	53.5	2506.8	265696	1	0.24	2.70	11.13
97.62	54.15	2506.8	265696	1	0.24	2.70	11.08
117.15	54.78	2506.8	265696	1	0.24	2.70	11.07
136.67	55.29	2506.8	265696	1	0.24	2.70	11.08
156.2	55.66	2506.8	265696	1	0.24	2.70	11.11
175.72	55.54	2506.8	265696	1	0.24	2.49	10.34
195.24	69.52	2677.8	322790	1	0.26	2.49	9.41
214.77	57.66	2506.8	265696	1	0.25	2.49	9.96
234.29	55.07	2506.8	265696	1	0.24	2.70	11.23
253.82	56.19	2506.8	265696	1	0.25	2.70	10.91
273.34	55.46	2506.8	265696	1	0.25	2.70	10.94
292.87	54.54	2506.8	265696	1	0.25	2.70	10.92
312.39	53.64	2506.8	265696	1	0.24	2.70	11.12
331.39	52.44	2506.8	265696	1	0.24	2.70	11.43
351.44	51.1	2506.8	265696	1	0.23	2.70	11.92
370.96	49.82	2506.8	265696	1	0.22	2.70	12.44
390.49	63.08	2506.8	265696	1	0.27	2.70	9.90

**Table 3.18 - Arrangement of 1" Shear Stud Pitch (Grouping) on Girder 1 of US 83 Overpass Bridge using Proposed 10th Ed. AASHTO**

Location (ft)	Pitch (in)	Number of rows	Studs per row	Number of studs
0-390.49	9	521	1	521

**Table 3.19 - Redesign Results for US 83 Overpass Bridge using Proposed 10th Ed. AASHTO**

Stud diameter (in)	Studs per row	Total number of studs used	Number of studs/Number of 7/8" studs
7/8	3	3303	100%
1	1	2592	78%
	2	2537	77%
1-1/8	1	1996	60%
	2	2032	62%
1-1/4	1	1637	50%
	2	1988	60%

### 3.6.3. IH 610 Tub Girder Bridge

Using the proposed 10<sup>th</sup> Ed. AASHTO, the Fatigue II load combination controls for the IH 610 Tub Girder Bridge. Unlike the previous two bridges,  $Z_r$  for shear studs is constant along the length of the girder for a simply supported bridge. Table 3.20 and Table 3.21 show the redesign results for 1" stud, two studs per row (one stud per flange), on an exterior girder. Similar tables were developed 1" studs with four studs per row, as well as for 1-1/8" and 1-1/4" studs with two and four studs per row.

**Table 3.20 - Pitch of 1" Shear Studs, Two Studs per Row (One Stud per Flange), on Exterior Girder of IH 610 Tub Girder Bridge using Proposed 10<sup>th</sup> Ed. AASHTO.**

Location (ft)	Studs per row	$V_{sr}$ (kip/in)	$Z_r$ (kips)	$p$ (in)
0.00	2	0.76	3.43	9.02
19.36	2	0.85	3.43	8.06
38.72	2	0.89	3.43	7.70
58.07	2	0.75	3.43	9.14
77.43	2	0.71	3.43	9.66
96.79	2	0.66	3.43	10.39
116.15	2	0.69	3.43	9.93
135.51	2	0.74	3.43	9.26
154.86	2	0.77	3.43	8.90
174.22	2	0.86	3.43	7.97
193.58	2	0.81	3.43	8.46
203.26	2	0.77	3.43	8.90

**Table 3.21 - Arrangement of 1" Shear Stud Pitch (Grouping), Two Studs per Row (One Stud per Flange), on Exterior Girder of IH 610 Tub Girder Bridge using Proposed 10<sup>th</sup> Ed. AASHTO.**

Location (ft)	Pitch (in)	Number of rows	Studs per row	Stud number
0-58	7	101	2	202
58-145	9	116	2	230
145-203	7	101	2	200

The fatigue-based pitch was checked against the strength limit state requirements. It was found that the fatigue pitch controlled over the entire bridge.

A summary of the redesign results using the proposed 10<sup>th</sup> Ed. AASHTO is presented in Table 3.22. The reduction in the number of studs is about 35%, 45%, and 55% for 1", 1-1/8", and 1-1/4" shear studs, respectively, compared with the 7/8" shear stud design. The percentage reduction in the number of studs is somewhat less compared to the redesigns based on 9<sup>th</sup> Ed. AASHTO, but were still substantial. Note that the number of shear studs is similar for two studs per row and four studs per row.

**Table 3.22 - Redesign Result for IH 610 Tub Girder Bridge using Proposed 10<sup>th</sup> Ed. AASHTO.**

Stud diameter (in)	Studs per row (Studs per flange)	Total number of studs used	Number of studs/Number of 7/8" studs
7/8	8 (4)	3048	100%
1	2 (1)	2052	67.3%
	4 (2)	2020	66.3%
1-1/8	2 (1)	1624	53.3%
	4 (2)	1664	54.6%
1-1/4	2 (1)	1246	40.9%
	4 (2)	1488	48.8%

### 3.7. Summary and Conclusions

In this chapter, three real bridges were studied to determine the required number of shear studs for 7/8", 1", 1-1/8", and 1-1/4" diameter studs. The three bridges were a straight three-span continuous I-girder bridge, a curved two-span continuous I-girder bridge, and a straight simple span tub girder bridge. The bridges were first evaluated to determine the required number of 7/8" studs, and compared to the number of 7/8" studs used in the original designs. By using similar strategies in the grouping as used in the original design, it was possible to closely replicate the number of studs specified in the original design. Similar practices in the original design like the grouping strategy were used to redesign with larger-diameter shear studs of 1", 1-1/8", and 1-1/4" diameters. The redesigns assumed equations and specifications in AASHTO and TxDOT

standards applied to the larger-diameter shear studs. The redesigns considered both the current 9<sup>th</sup> Ed. AASHTO as well as the proposed 10<sup>th</sup> Ed. AASHTO. The number of 7/8" diameter shear studs used in the original designs was compared to the required number of 1", 1-1/8" and 1-1/4" studs in the redesigns to evaluate the potential benefits of using larger-diameter shear studs.

It was found that the redesign process for larger diameter shear studs was very similar to that of 7/8" diameter shear studs. Stud diameter up to 1-1/4" can be successfully designed without violating any geometric requirements or limitations in the 9<sup>th</sup> Ed. AASHTO, the proposed 10<sup>th</sup> Ed. AASHTO, or TxDOT specifications. The reduction in the number of shear studs was found to be significant when larger-diameter shear studs are used. The actual percentage reduction in the required number of studs varied somewhat based on which of the three bridges was considered, based on the stud diameter, and based on the number of studs per row used in the design. However, compared to 7/8" shear studs, the reduction in the number of studs was found to be on the order of 25%, 40%, and 50% for 1", 1-1/8", and 1-1/4" diameter shear studs, respectively, for both the current 9<sup>th</sup> Ed. AASHTO and the proposed 10<sup>th</sup> Ed. AASHTO. This matches closely with the ratio of the area of a 7/8" stud to the area of the larger-diameter studs, listed in Table 1.1. Since both stud ultimate strength and stud fatigue strength based on AASHTO equations are directly proportional to stud area, the final results of this study are not surprising. However, the reduction in the number of studs, in addition to being related to stud area, also depends on factors such as maximum permissible pitch and minimum number of studs per row used in a design. Nonetheless, the design study presented in this chapter confirmed that using larger-diameter shear studs can lead to a significant reduction in the number of shear studs required on a composite steel girder.

# Chapter 4. Stud Welding Investigations

## 4.1. Introduction

---

This chapter describes an investigation undertaken to determine if larger-diameter shear studs can be welded to achieve consistently good quality, and if so, establish stud welding procedures and parameters to be used in the push-out tests and large-scale beam tests to be conducted in other phases of this study. This chapter starts with details of the shear studs used in the welding investigation. This is followed by a brief introduction to stud welding and a review of stud welding parameters used in previous research on larger-diameter shear studs. The process and details of the welding investigation are described next, and a recommended welding procedure for large diameter shear studs is given at the end of the chapter.

## 4.2. Background on Stud Welding

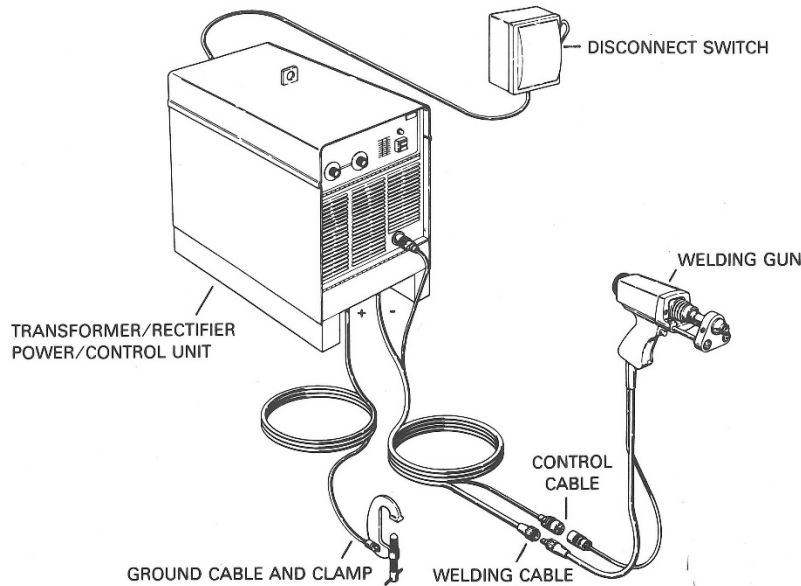
---

Stud welding, also referred to as arc stud welding, is an electric arc welding process for attaching a steel shear stud to a steel member. A description of stud welding can be found in several references, including the *AWS Welding Handbook* (1991), Linnert (1965), and Chambers (2001). Stud welding is classified as an electric arc welding process, as the heat to melt steel is provided by an electric arc. In the case of stud welding, the electric arc is formed between the tip of the stud and the base metal, melting both the tip of the stud and the base metal directly beneath the stud. Unlike most other electric arc welding processes, no external filler metal is used in stud welding. A ceramic ferrule is placed at the base of the stud during welding to restrict air flow into the weld, thereby serving as shielding for the weld. The ferrule also confines the molten steel in the region beneath the stud and is removed after welding is complete. An aluminum ball is pressed into the tip of the stud and serves flux to deoxidize the weld (ISO 2017a).

An illustration of stud welding equipment is shown in Figure 4.1. Components in the setup include the welding gun, the weld control unit, cables, and a ground. The weld control unit generates electric current into the circuit. The amperage and duration of electric current can be specified in the welding control unit. The welding gun is used for holding the shear stud and controls the movement of the stud during the welding process. The ground is attached to the steel to which the stud is being welded.

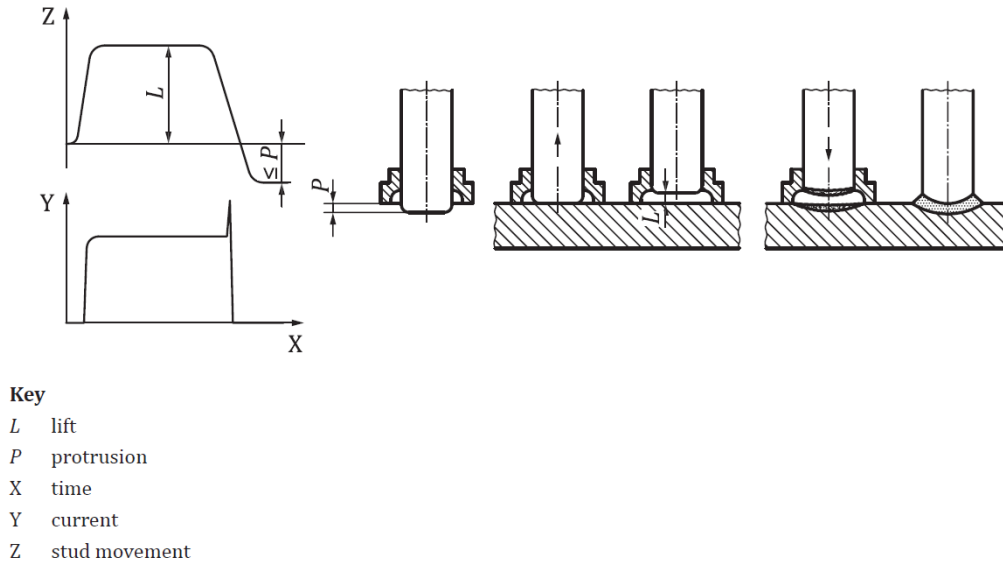
Details of the stud welding process are illustrated in Figure 4.2. Welding a shear stud begins with loading the shear stud in the welding gun and pushing the stud against the base material. The ceramic ferrule needs to be placed around the stud base at this time. When the trigger of the welding gun is pulled, the welding gun will pull the stud away from base metal to create an air gap. An electric current will be generated from the weld control unit at the same time. The distance the stud is pulled away from the base metal is called the “lift”. Electric current will

break-through the air gap (lift), creating a bright arc and producing a large amount of heat. The larger the lift, the stronger the electric current will be needed to break the gap, and therefore more heat is generated. Heat generated by the arc is confined by the ceramic ferrule to melt the base of the shear stud as well as some of the base material in close proximity. The ferrule also works with the aluminum flux tip on the shear stud to reduce the formation of oxidation. The duration of the electric current is the same as the duration that the welding gun lifts the stud away from the base metal. Too small of a weld time or too small of a lift will not produce enough heat and leads to low quality cold welds. However, too much welding time is reported to be likely to introduce defects in the weld as well (Chambers 2001). When the specified weld time is reached, the welding gun will push the stud down into the molten pool by a distance referred to as the “plunge” and the melted stud base will be merged with melted base material to create a pool of mixed melted metal. Once the mixed melted metal cools down and hardens, the stud is connected to the base metal. Finally, the ceramic ferrule is removed.



*Figure 4.1 - Stud Welding Equipment (AWS 1991)*

Figure 4.3 shows a welding gun loaded with a stud. The chuck has the same diameter as the stud head and needs to be changed when different diameter shear studs are used. The plunge is the distance between the base of the ferrule and the base of the stud excluding the aluminum flux tip. The leg of the welding gun can be extended or shortened to give the desired plunge. An additional adjustment on the welding gun is referred to as “free travel”. Free travel controls the point when the welding gun engages the dampener in the gun, thereby controlling the force used to plunge the stud into the molten weld pool.



*Figure 4.2 - Details of Stud Welding Process (ISO 2017b)*

Figure 4.4 shows the cross-section of a stud welded on metal. Part A and E in this figure are the original stud and original base material, respectively, which are called parent materials. Part B and D are called heat-affected zones (HAZ). They are the boundary between melted metal in part C weld zone and un-melted parent material. Material in the HAZ does not melt during welding but its micro-structure is permanently changed due to the exposure to high temperature and subsequent cooling. When the cooling rate of the base material is high, martensite will form in the HAZ, which makes the HAZ to be a brittle region. Preheating the base metal is usually used in welding to reduce cooling rates and therefore reduce the formation of martensite. Since stud arc welding generates a large amount of heat and preheating is not used, it is believed that the presence of brittle HAZ is very likely. According to AWS D1.5, when the temperature of the base metal is below  $-20^{\circ}\text{C}$  ( $0^{\circ}\text{F}$ ), stud welding should not be performed and when base metal temperature is below  $0^{\circ}\text{C}$  ( $32^{\circ}\text{F}$ ), additionally bend tests should be performed on the shear stud. These requirements reflect the increased formation of martensite in the HAZ at colder temperatures, which cause more rapid cooling of the weld.

During welding, some of the molten steel extends beyond the shank of the stud and is contained within the ferrule, forming what is referred to as weld flash or a weld collar. The stud is shorter after welding because some of the stud material forms the weld collar around the base of the welded stud. The length reduction of shear stud for a good quality weld is equal to or larger than the plunge.



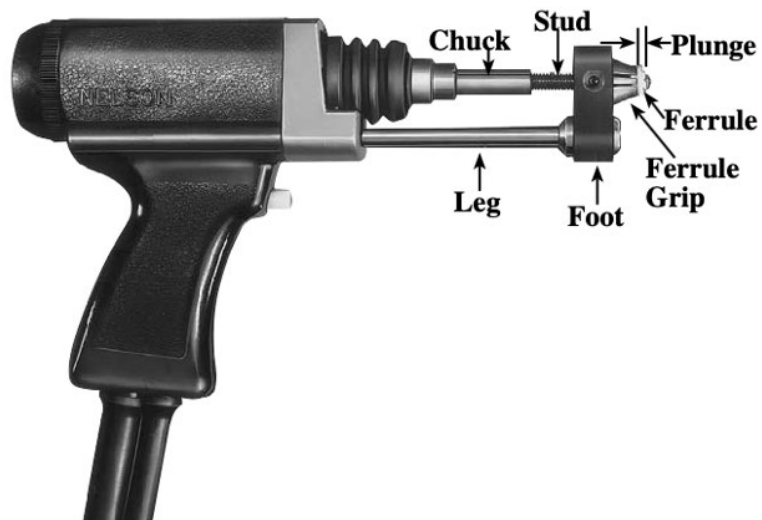


Figure 4.3 - Stud Welding Gun (Chambers 2001)

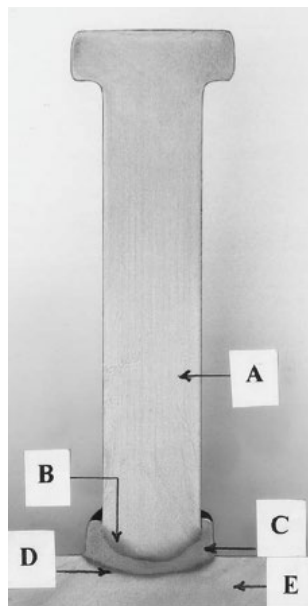


Figure 4.4 - Cross-Section of a Welded Stud (Chambers 2001)

There are two different paths for electric current to go through the welding circuit.

- Straight polarity: Weld control unit → Welding gun → Shear stud → Base metal → Ground → Welding control unit.
- Reverse polarity: Weld control unit → Ground → Base metal → Shear stud → Welding gun → Welding control unit.

As described later, it was observed in the welding investigation that the length reduction of the welded stud under straight polarity was larger than that under reverse polarity. However, the heat produced under straight polarity is less than that under reverse polarity. It is believed that the stud will be attracted towards the moving direction of electric current. When straight polarity is used, electric current moves from stud to the base metal and facilitates the downward movement of the shear stud, thus pushing the stud deeper into the melted metal pool and giving a larger length reduction. And when reverse polarity is used, the stud will be attracted by the upstream electric current from base metal. This will make the lift of the stud slightly bigger and create more heat.

Since electric current of high amperage ( $\geq 1700$  Amp) is used in stud welding, the effect of electromagnetic induction should be considered on weld quality. There are two practices in arc welding that relate to electromagnetic induction. The first one is to weld the stud away from the ground or free edge of the base material. The second is to loop the cable clockwise around the stud under straight polarity and counterclockwise for reverse polarity. The center of the cable loop should be the stud welding location. The first one is to minimize problems caused by arc blow and the second one is to facilitate weld quality using the magnetic field.

Figure 4.5 illustrates the effect of arc blow. The International Organization for Standardization (ISO) *Welding – Arc Stud Welding of Metallic Material* (ISO 2017b) defines arc blow as the magnetic deflection of the arc from the axial direction of the stud. To be specific, electric current in the circuit will impose forces on the arc. This force will push the arc away from the ground and free edge and attract the arc toward the large mass of steel. The results of arc blow, shown in Figure 4.6, are that an uneven weld collar will be produced and the quality of weld is impacted. To minimize the effect of arc blow, the stud should be welded away from the ground or free edges of the base metal or counter measurements specified in ISO 2017b should be considered.

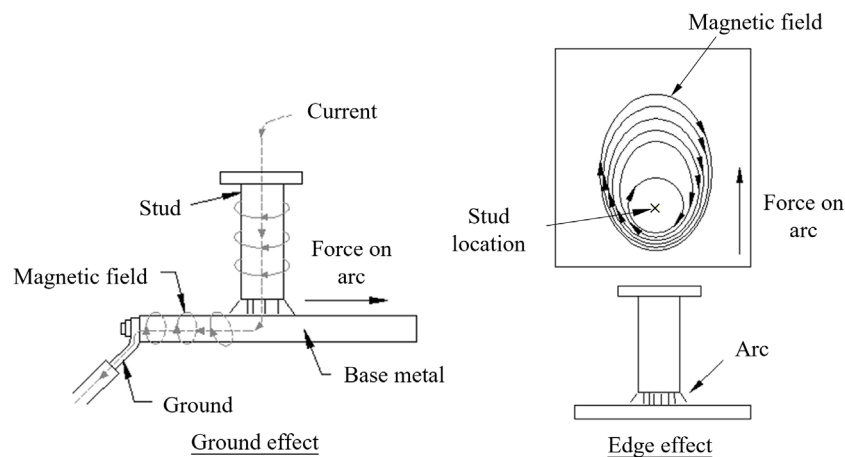
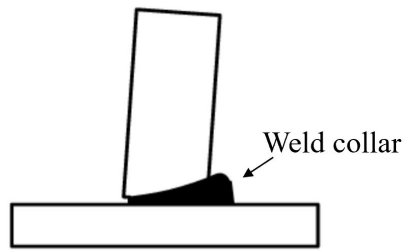


Figure 4.5 - Arc Blow Effect (Nelson Stud Welding 2008a)



*Figure 4.6 - Weld Collar Under Arc Blow Effect (Illustration on the Left: ISO 2017b)*

Figure 4.7 is a photo showing cable looping around the stud welding location. The purpose of cable looping is to use the magnetic field generated by the electric current to facilitate the stud welding process. When straight polarity is used, the magnetic field generated will push the stud down if the cable is looped clockwise. This will provide a larger stud penetration. When reverse polarity is used, the cable looped counterclockwise will have the same effect on the stud. Cable looping is not normally required for welding normal diameter shear studs (7/8", 3/4"). However, Nelson recommended this procedure if welding larger-diameter shear stud proved difficult. The effect of cable looping is investigated in the welding investigation described later.



*Figure 4.7 - Cable Looping Around the Welding Point*

Based on the information presented above and in the literature, the following parameters can be identified as affecting the stud welding process and the stud weld quality:

- welding current;
- welding time;
- lift;
- plunge;
- polarity;
- free travel (welding gun damper);
- location of ground cable attachment(s);
- addition of steel mass to control arc blow;
- use of cable looping;
- surface preparation.

### **4.3. Welding Parameters Used in Previous Larger-diameter Shear Stud Research**

---

As described in the literature review in Chapter 2, there have been a number of past investigations on the behavior of larger-diameter shear studs, both in the U.S. and internationally. These past studies generally involved conducting push-out tests, and required welding of larger-diameter shear studs to steel plates or beams. These past studies were reviewed to determine the information that was reported on the welding process and parameters used in the research. These past studies and stud welding-related information reported by the researchers is summarized in Table 4.1.

As can be observed from Table 4.1, previous researchers did not report extensive details of the welding variables employed in their studies, although some reported the welding current and welding time. However, as described in the previous section, there are numerous other variables that control the stud welding process and stud weld quality including polarity, lift, plunge, and others. Thus, information on welding of larger-diameter shear studs from previous research is not sufficient to establish welding parameters for this research project. Consequently, an extensive investigation was undertaken in this research on welding of larger-diameter shear studs, as described in the remainder of this chapter.

### **4.4. Shear Studs used in Welding Investigation**

---

AWS D1.5 (AWS 2020) does not currently recognize studs with a diameter greater than 1". Further, a review of the websites of stud manufacturers indicates that shear studs with diameters up through 1" are listed in their catalogs of available products. However, no manufacturer was found that offered shear studs with diameters greater than 1". Further, since stud diameters

greater than 1" are not available in the market, it is unclear if commercially available stud welding equipment is capable of welding shear studs with a diameter greater than 1".

Nelson Stud Welding Company specially manufactured 1-1/8" and 1-1/4" diameter shear studs and ferrules for use in this research project in addition to supplying 7/8" and 1" diameter "off the shelf" studs and ferrules. Nelson also assisted with providing technical advice on stud welding. Stud welding in this research was done using a Nelson Nelweld 6000 stud welding machine (Nelson Stud Welding 2008a). Nelson provided the equipment needed to modify the stud welding gun of this machine to accommodate the larger-diameter studs.

**Table 4.1 - Welding Information from Previous Studies on Larger-diameter Shear Studs**

Reference	Shear Stud Diameters Investigated	Reported Welding Parameters
Shim et al. (2004) And Lee et al. (2005)	25 mm (0.98") 27 mm (1.06") 30 mm (1.18")	<u>25 mm and 27 mm studs:</u> welding current: 2200 amps welding time: 1.3 sec. <u>30 mm studs:</u> welding current: 2400 amps welding time: 1.3 sec.
Lin and Liu (2015)	22 mm (0.87") 25 mm (0.98") 30 mm (1.18")	No welding information was reported
Wang et al. (2019)	22 mm (0.87") 30 mm (1.18")	Studs welded using all-around fillet welds (arc stud welding process not used)
Hu et al. (2020)	30 mm (1.18")	No welding information was reported
Wang et al. (2018)	30 mm (1.18")	No welding information was reported
Badie et al. (2002)	1-1/4"	Reported that a power source with a minimum amperage of 2400 was adequate to weld studs, but provided no additional details
Kakish (1997)	1-1/4"	Reported that a power source with 3000 amps was needed to weld, but provided no additional details
Mundie (2011)	1-1/4"	Welding was done using a Pro-Weld Arc 3000 welder; welding current: 2702 amps welding time: 1.812 sec.

### 4.4.1. Shear Stud Dimensions

Figure 4.8 is a photo showing the shear studs and welding ferrules used in the stud welding investigation. From the left to the right, the stud diameter is 1-1/4", 1-1/8", 1", and 7/8". Table 4.2 lists the measured dimensions of each type of shear stud. The nominal length of the shear studs after welding was 7". The actual length before welding, shown in Table 4.2, is longer than that to consider the length reduction during welding. For the 7/8" and 1" diameter studs, the head diameter and height listed in Table 4.2 conform with the dimensions specified in AWS D1.5. AWS D1.5 does not provide head dimensions for stud diameters greater than 1". The head dimensions of the 1-1/8" and 1-1/4" diameter studs, listed in Table 4.2, were selected by Nelson. The basis for the selected head dimensions is unclear. However, information provided by Nelson indicates that for stud diameters of 3/4" and larger, the head area is approximately equal to 2.5 times the shank area. The head areas of the 1-1/8" and 1-1/4" studs supplied by Nelson were 2.78 and 2.56 times the respective shank areas, thereby satisfying this guideline. No information was available on guidelines for stud head height. However, it is noted that for the studs supplied by Nelson, the head height was 0.5 times the shank diameter for the 1", 1-1/8" and 1-1/4" studs. A review of various standards did not identify general requirements for head dimensions as a function of stud diameter, although AISC 2022 (AISC 2022) requires that the head diameter must be at least 1.6 times the stud diameter when studs are subjected to tension or combined shear and tension. The head diameters listed in Table 4.2 satisfy this requirement.

### 4.4.1. Material Characterization Tests

To obtain data on mechanical properties of the studs used in the welding investigation, tension coupon tests and shear strength tests were conducted. In addition, Charpy V-notch tests were conducted to see whether larger-diameter shear stud have significantly different CVN properties compared with 7/8" studs.

#### 4.4.1.1. Tension Coupon Tests

Tension coupons were machined from the studs using coupon dimensions specified in ASTM A370 (ASTM 2022), as shown in Figure 4.9. The coupons had a total length of 6.625" (all on the shank part), a gage length of 2", a reduced area diameter of 0.5", a grip diameter of 0.75", and a fillet radius of 0.375". The length of 6.625" was chosen to make the most use of the available shank lengths of all diameter shear studs for a longer grip.



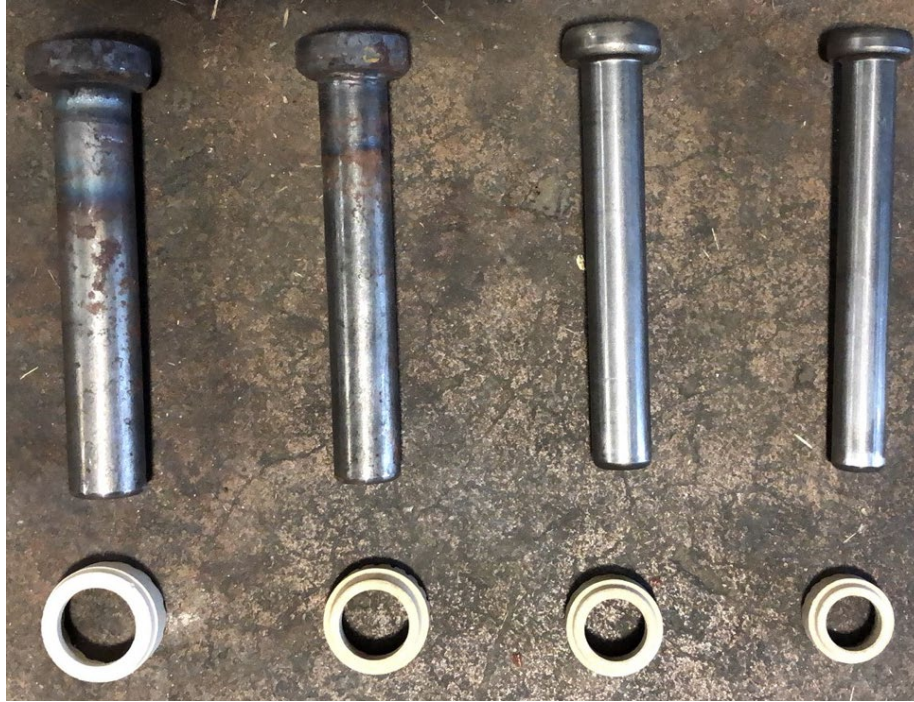


Figure 4.8 Shear Studs and Welding Ferrules of Various Diameter

Table 4.2 - Geometry of Shear Studs in Stud Welding Investigations

Stud diameter (in)	Stud total length before welding (in)	Stud head diameter (in)	Stud head height (in)
7/8	7-3/16	1-3/8	7/16
1	7-1/4	1-5/8	1/2
1-1/8	7-5/16	1-7/8	9/16
1-1/4	7-3/8	2	5/8

The tension coupon tests were conducted at Ferguson Structural Engineering Laboratory at University of Texas at Austin. Tension coupons were loaded to fracture by a 22-kip MTS test machine. Figure 4.10 illustrates the test setup. The extensometer remained on the coupon through fracture to obtain the entire stress-strain curve. The cross-head loading rate was 0.02 in. per minute for the entire duration of the test. However, the cross-heads were periodically stopped and held at constant displacement for at least 2 minutes to obtain static yield and tensile strength values. The static yielding strength was obtained from the interconnection of points of 0.2% line and the regression curve of first three pause points in the stress-strain curve. The static ultimate strength was obtained from the regression curve.

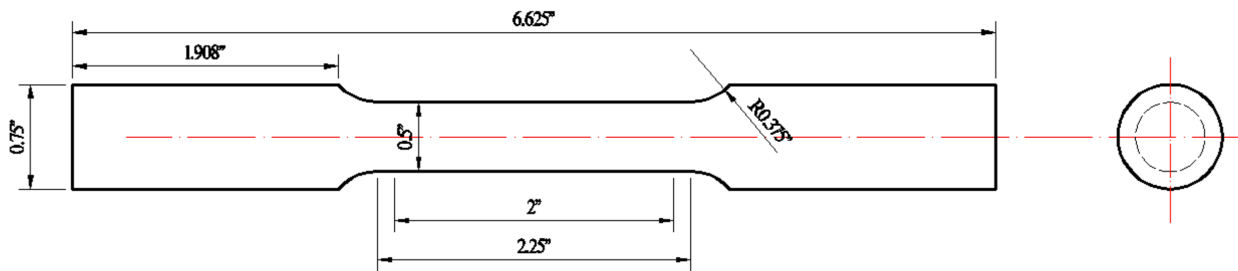


Figure 4.9 - Tension Coupon Dimensions



Figure 4.10 - Tension Coupon Test Setup

The stress strain curves for the four different stud diameters are shown in Figure 4.11 to Figure 4.14. For each stud diameter, at least four tension tests were conducted. The curves of each diameter shear stud match well with each other except the curves of 1" diameter shear studs where the curve of specimen 1 has significant difference with other three specimens. This was likely caused by errors during the test and was discarded.

The measured tensile strengths and yield strengths are shown in Table 4.3. As can be seen from the table, the static yield strength is very close to the dynamic yielding strength. The static ultimate strength is 6% - 9% smaller than the dynamic ultimate strength. The dynamic yield and ultimate strength refer to the values measured while the machine cross-heads were in motion at the rate of 0.02 inches per minute. Note that the tension coupons exhibited an ultimate strength (static and dynamic) greater than 60 ksi, as required by AWS D1.5. However, none of the studs satisfied the elongation (failure strain) requirement of 20 percent specified in AWS D1.5.



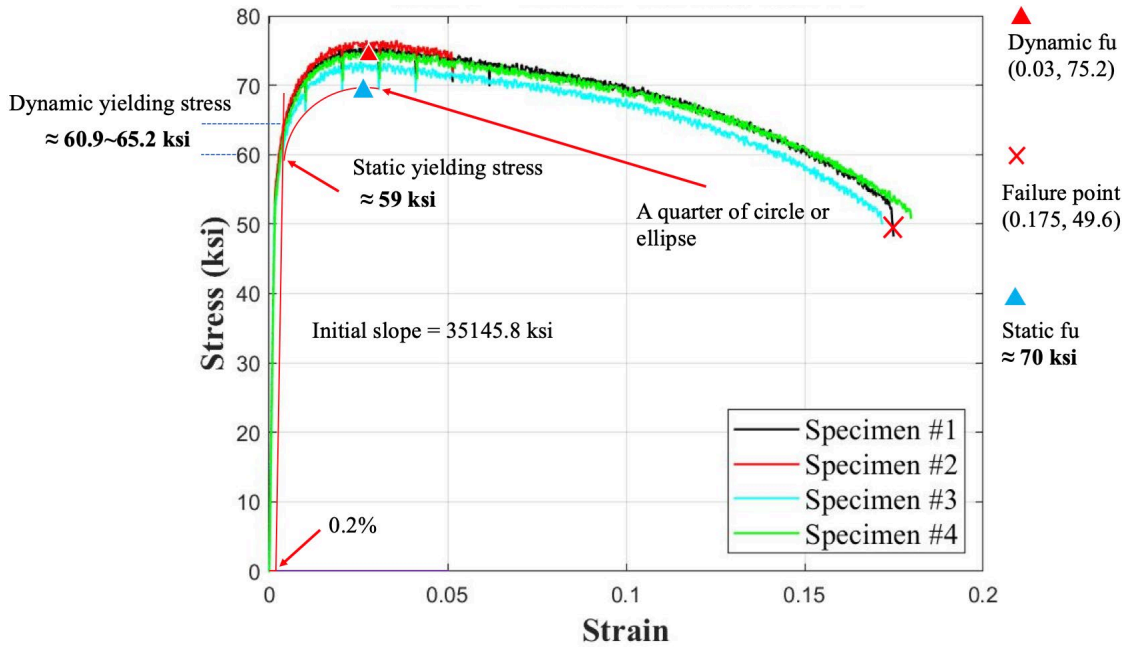


Figure 4.11 - Stress-Strain Curves for 7/8" Studs

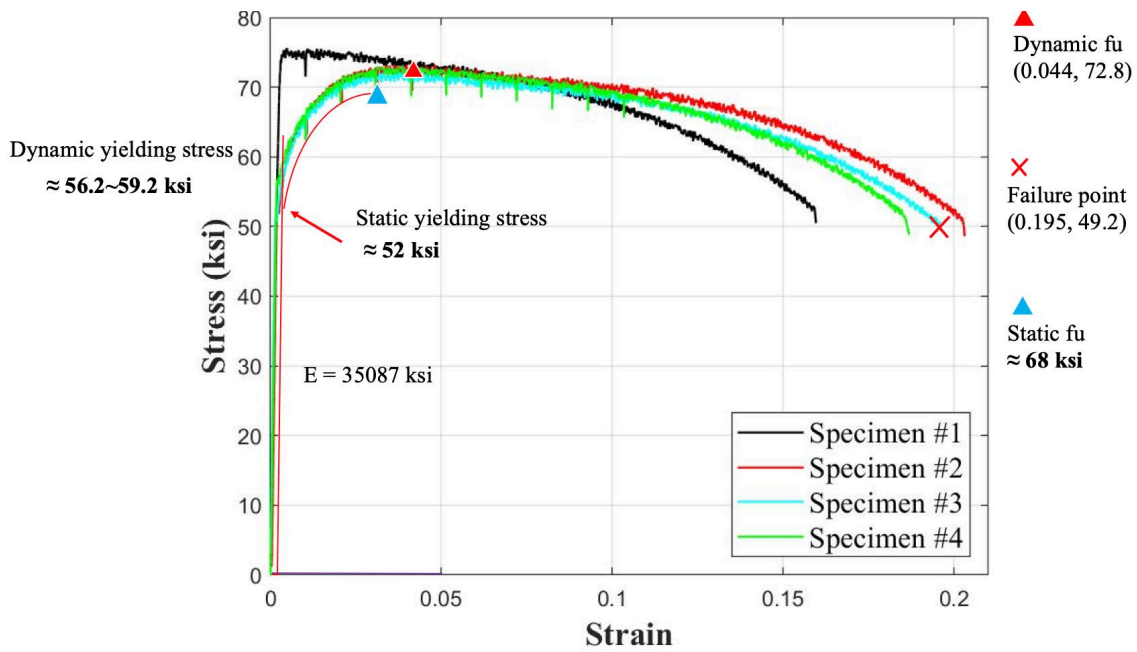


Figure 4.12 - Stress-Strain Curves for 1" studs

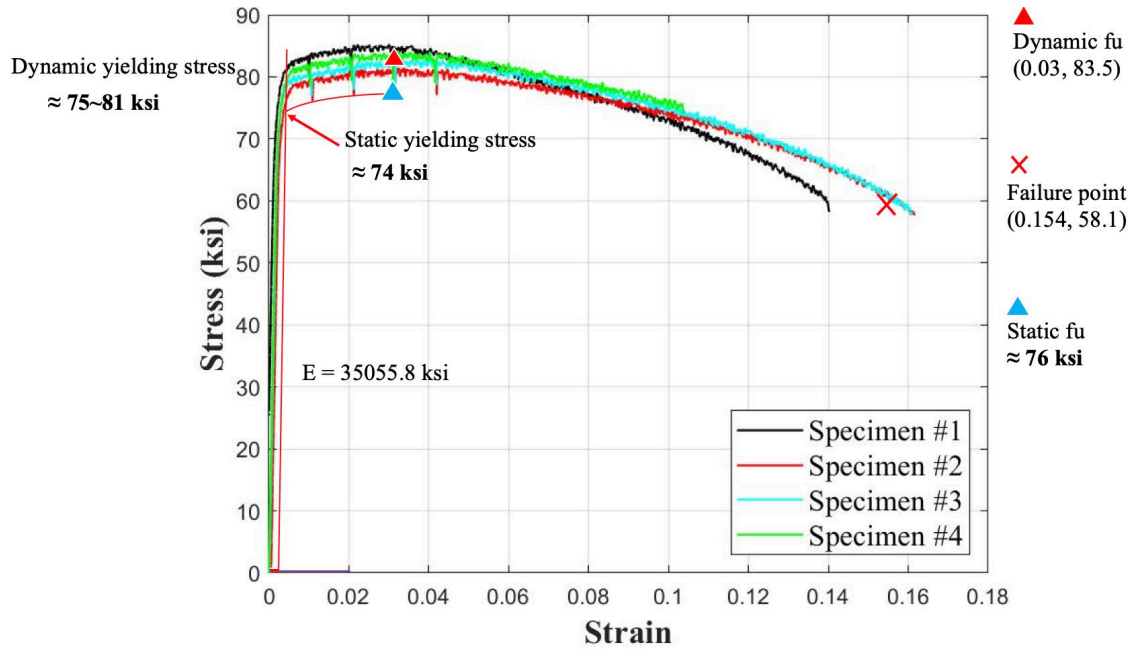


Figure 4.13 – Stress-Strain Curves for 1-1/8" studs

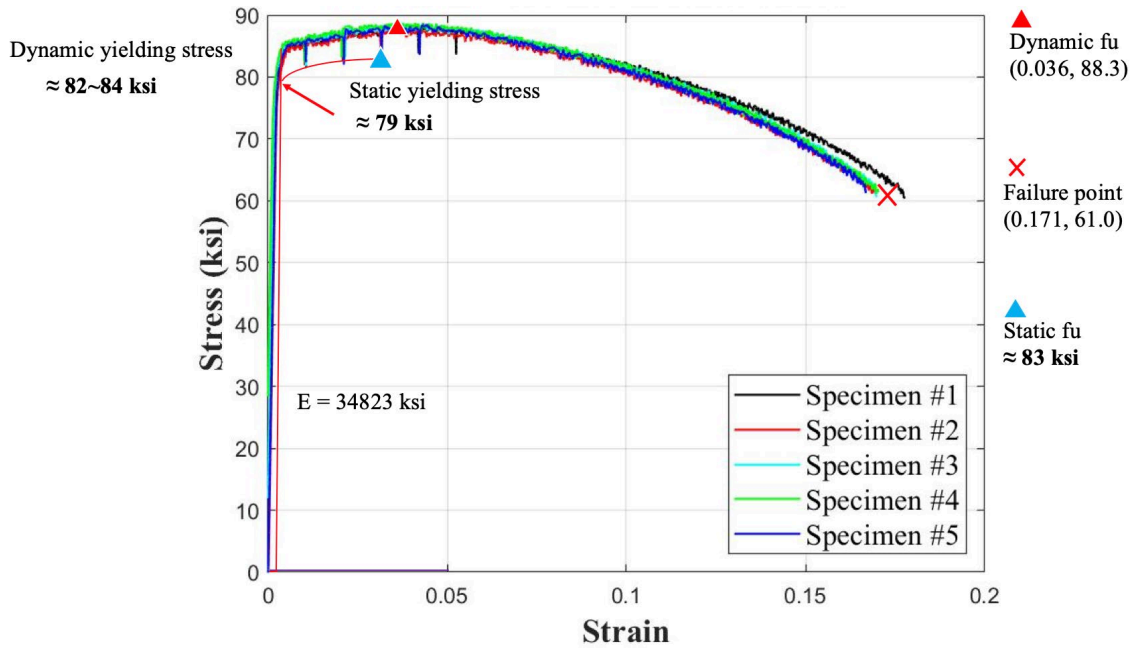


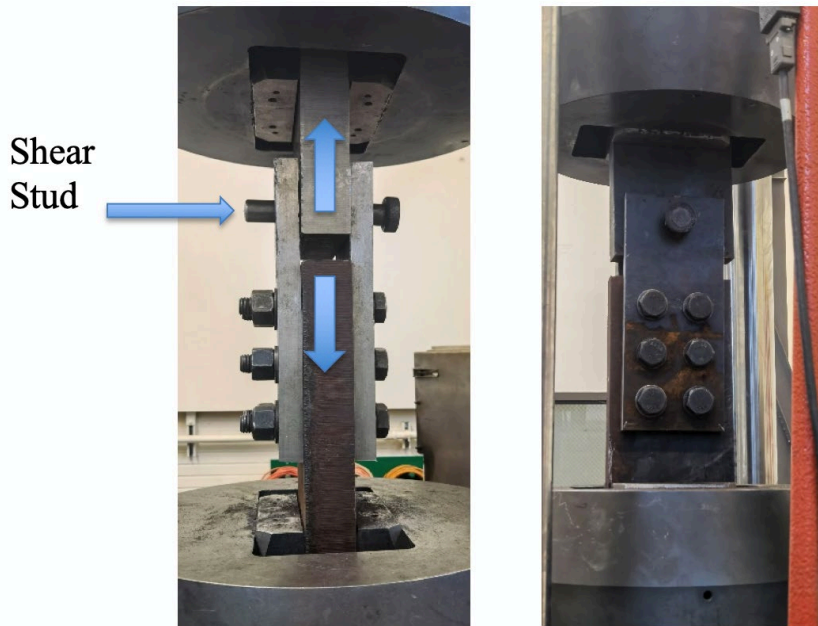
Figure 4.14 - Stress-Strain Curves for 1-1/4" studs

**Table 4.3 - Tension Coupon Test Results**

Diameter (in)	Number of Specimens	Dynamic Yield $F_y$ (ksi)	Static Yield $F_y'$ (ksi)	$F_y'/F_y$ (%)	Dynamic Ultimate Strength $F_u$ (ksi)	Static Ultimate Strength $F_u'$ (ksi)	$F_u/F_u'$ (ksi)	Strain at Fracture (%)
7/8	4	61	59	96.7	75.2	70	93.1	17.5
1	4	56	52	92.9	72.8	68	93.4	19.5
1-1/8	4	75	74	98.7	83.5	76	91.0	15.4
1-1/4	5	82	79	96.3	88.3	83	94.0	17.1

#### 4.4.1.2. Shear Strength Tests

To obtain data on the shear strength of the studs, 4 shear tests of each stud diameter were conducted by fracturing the studs in a double-shear test setup. Full-size studs were tested, i.e., the studs were not machined to a smaller size as was the case with the tension coupon tests. The average shear strength was calculated after the four tests. The test setup is shown in Figure 4.15.



*Figure 4.15 - Shear Strength Test Setup*

Results of the shear strength tests are summarized in Table 4.4 with photos of the studs after testing shown in Figure 4.16 Two series of shear tests were conducted In Series 1, the holes in the plates for the studs was 1/8" larger than the stud diameter. Shear studs tested using these larger holes exhibited significant bending deformation, which is marked as Series 1 in Figure 4.16 and Table 4.4. To reduce the amount of bending in the studs, new plates were prepared with holes with a diameter just slightly larger than the stud diameter, and these are marked as "Series

2” in Figure 4.16 and Table 4.4. It is observed that the studs with less bending deformation had higher shear resistance. Based on the Series 2 data, the shear fracture strength of the studs is in the range of 65 to 70-percent of the tensile fracture strength. Tests on high strength bolts (Kulak, Fisher and Struik 2001) showed the shear strength of bolts was approximately 62-percent of the tensile strength, when tested in a jig subjected to tension, similar to what was used for the shear studs, whereas tests on rivets showed a ratio of shear strength to tensile strength ranging from 67-percent to 83-percent. The ratio of shear to tensile strength measured for the shear studs in this research program is within the range of what has been measured previously for bolts and rivets.

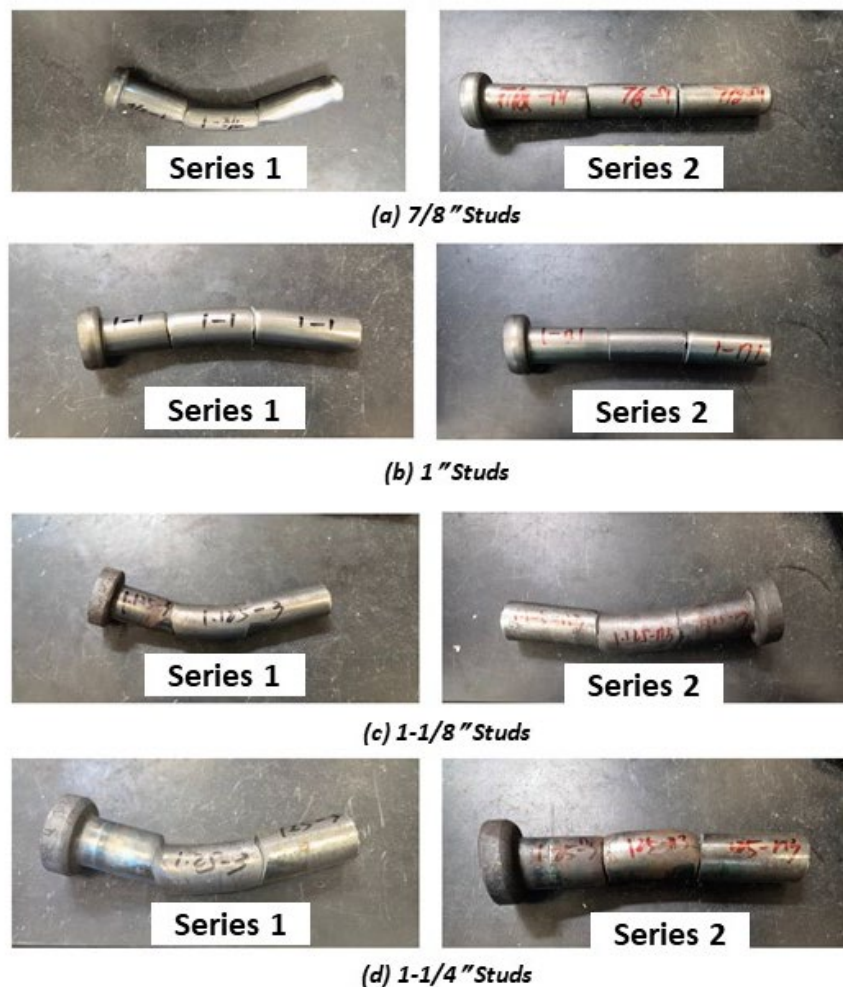


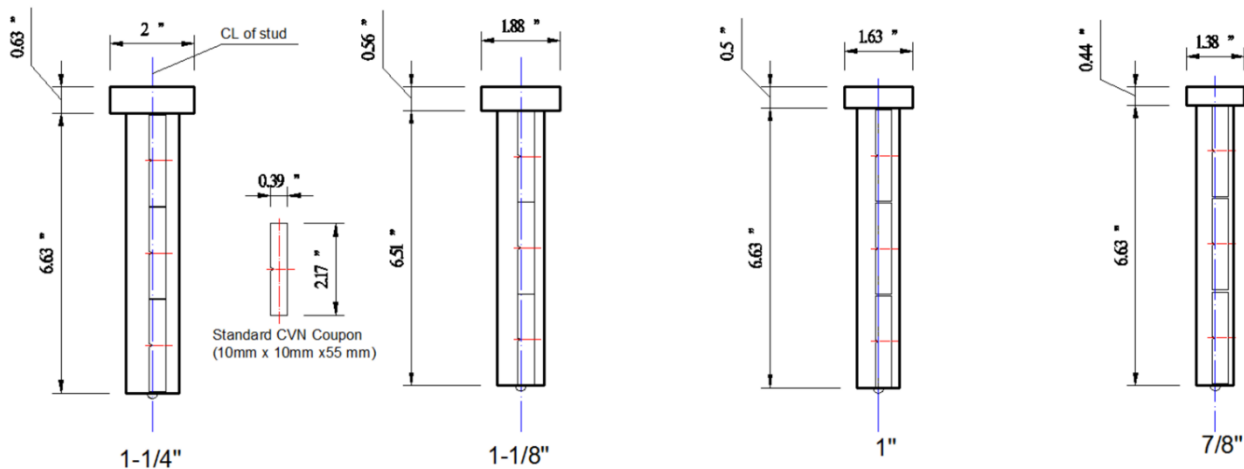
Figure 4.16 - Photos of Shear Studs After Shear Fracture Tests

**Table 4.4 - Shear Strength Test Results**

Diameter (in)	Max Shear Strength $F_s$ (ksi) [Series 1]	Max Shear Strength $F_s'$ (ksi) [Series 2]	Dynamic Tensile Strength $F_u$ (ksi)	$F_s/F_u$ (%) [Series 1]	$F_s'/F_u$ (%) [Series 2]
0.875	46.1	49.2	75.2	61.30	65.40
1	46.7	50.9	72.8	64.10	69.90
1.125	49.3	53.6	83.5	59.00	64.2
1.25	52.1	53.8	88.3	59.00	60.90

#### 4.4.1.3. Charpy V-Notch Tests

In addition to tension coupon tests and shear strength tests, Charpy V-notch (CVN) tests were conducted on samples machined from the studs. The CVN tests were conducted by Chicago Spectro Service Laboratory, Inc. The tests were performed at four temperatures: -30 deg. F , 0 deg F, 30 deg. F and 70 deg. F. At each temperature, three Charpy V-notch tests were performed for each stud diameter. The three Charpy V-notch coupons in a set were machined from a single shear stud. The standard Charpy V-notch coupon and the arrangement of the coupons within the shear studs are shown in Figure 4.17.



*Figure 4.17 - Arrangement of CVN Coupons within Shear Studs*

Table 4.5 presents the results of the CVN tests. From the table, the larger-diameter shear studs (1", 1-1/8" and 1-1/4") showed similar CVN values compared to the 7/8" studs at test temperatures of -30 deg. F and 0 deg. F. At 30 deg. F and 70 deg. F, the CVN values for the larger-diameter shear studs was somewhat less than that for the 7/8" studs. There is no indication

that there have been problems with brittle fracture of 7/8" studs in bridges. Neither AWS D1.5 (AWS 2020) nor AASHTO (AASHTO 2020) specify CVN requirements for shear studs.

**Table 4.5 - Charpy-V-Notch Test Results**

Temperature [°F]	Absorbed Energy [ft-lbs]			
	7/8"	1"	1-1/8"	1-1/4"
-30	7	5	3	5
-30	4	7	4	7
-30	4	6	3	3
Avg. at -30	5	6	3	5
0	9	6	5	14
0	8	7	6	10
0	8	6	6	6
Avg. at 0	8	6	6	10
30	15	9	5	17
30	6	19	10	33
30	48	15	9	9
Avg. at 30	23	14	8	20
70	89	83	13	30
70	95	65	76	57
70	78	67	74	42
Avg. at 70	87	72	54	43

## 4.5. Stud Weld Quality Evaluation Methods

In the stud welding investigation, trial welds were produced using various welding parameters. It was then necessary to evaluate the quality of the welds. This section discusses the methods used to assess stud weld quality in this investigation.

A good welding practice produces consistent high-quality welds. AWS D1.5 (AWS 2020) requires shear stud welds to pass manufacturer's stud base qualification tests, special condition application qualification tests, and preproduction tests. This welding investigation followed the application qualification test procedure and additional tests were included. More specifically, visual inspection, 90° bend tests, weld tension tests, and macro etch weld tests were used in this study. Macro etch weld tests are not required in AWS D1.5 to check the quality of welds but are specified in ISO (2017b). AWS D1.5 specifies that in the application qualification test, for a given welding parameter, 10 studs that are welded consecutively must pass either a bend test, torque test or tension test. In this welding investigation, for each diameter shear stud, four studs



were subjected to a 90° bend test, four studs were subjected to tension tests, and four studs were subjected to macro etch testing. Welding parameters and practices that were able to pass all tests were selected for welding studs in the subsequent push-out and large-scale beam tests.

#### 4.5.1. Visual Inspection

Figure 4.18 provides photos of a good stud weld along with some common problematic welds. A good stud weld should have even weld collar formation around the stud base and a shiny (bluish) weld collar surface. The weld collar should have enough height (see picture of “Normal Weld” in Figure 4.18), and no indications of holes or disconnections between the stud and base metal.

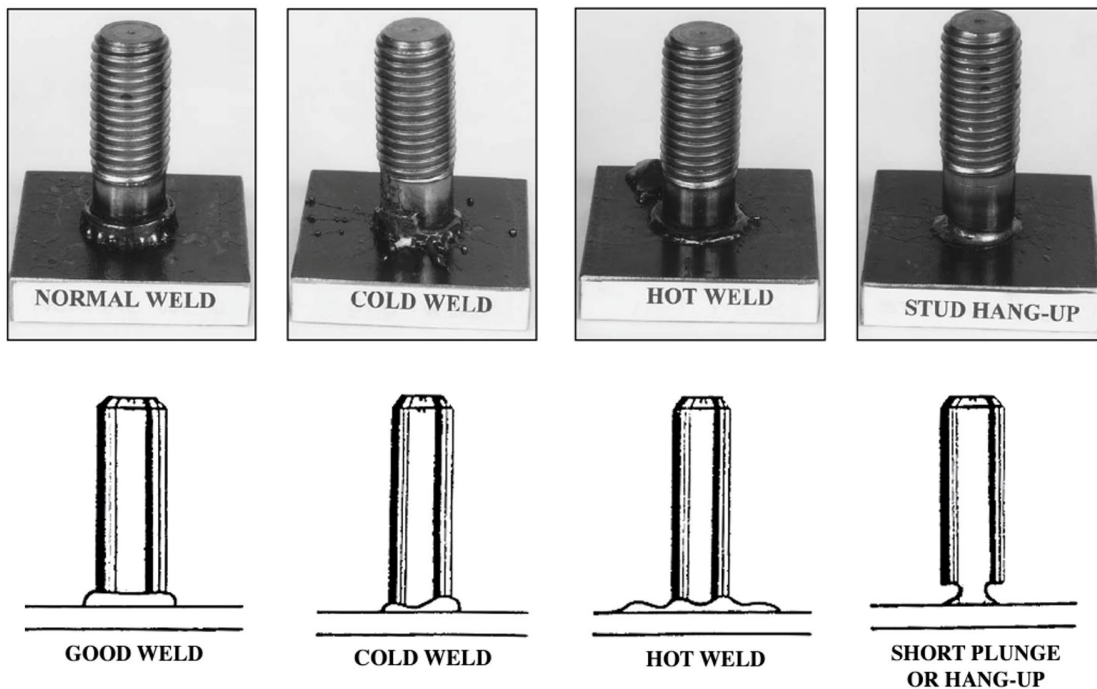


Figure 4.18 - Photos of a Good Stud Weld and Common Problematic Stud Welds (pictures on top: Chambers (2001), pictures on bottom: Midwest Fasteners Inc. (2019))

Cold welds were the most commonly seen welding problem for larger-diameter shear studs in the welding investigation. Formation of a cold weld is mainly due to insufficient weld time and/or current amperage. Cold welds exhibit a low and uneven weld collar and the weld collar surface shows a dull grayish color. In the photo of Figure 4.18, “spider legs” can be found around a cold weld. However, the spider legs are not only observed in cold welds. The spider legs are the hardened speckles expelled from melted metal pool. For welding on untreated surfaces and hot welds, considerable specking can also occur and spider legs are formed.

A hot weld is caused by excessive heat produced during welding. Common observations for hot welds include excessive splatter, an unformed weld collar, undercutting of the stud, unsuccessful

stud welding, and burn through the base metal. Undercutting means there is no weld collar and no length reduction after the weld. Severe undercutting leads to stud hang-up appearance or even unsuccessful welding, where the shear stud is not connected to the base metal after welding. In the welding investigation, hot welds for larger-diameter shear stud typically resulted in unsuccessful welding as illustrated in Figure 4.19. Besides hot welds, it is reported that stud hang-up can be caused by misalignment of the shear stud with respect to the base metal, and inadequate lift Lienert et al. (2011).



Figure 4.19 - Unsuccessful Stud Weld

Visual inspection can also be done quantitatively by measuring the stud length reduction after welding. In the welding investigation, length reduction was found to be a very effective indicator of the overall integrity of the weld. Studs with sufficient length reduction usually passed the mechanical tests. Length reduction is a sensitive variable whose influencing factors include welding power, plunge, the electromagnetic induction effect, and the friction between stud and ferrule/ferrule grip. Chambers (2001) suggested length reduction for shear studs of various diameter, which is shown in the Table 4.6. AWS D1.5 requires the length reduction to be in the range of 1/8" to 3/16" and larger-diameter stud require higher length reductions. Based on these references and communication with Nelson, the target length reduction of 7/8", 1", and 1-1/8" diameter shear stud was set to be 3/16". For 1-1/4" diameter shear stud, the target length reduction was set to be 1/4".

Table 4.6 - Suggested Stud Length Reduction from Chambers (2001)

Stud Diameter (in)	Length Reduction (in)
3/16 – 1/2	3/32 – 1/8
5/8 – 7/8	5/32 – 3/16
≥1	3/16 – 1/4



### 4.5.2. 90° Bend Tests

According to AWS D1.5, in application qualification tests, a shear stud should be bent 90° from its original axis without fracture in the weld. For preproduction tests, which are performed at the construction site, only two shear studs need to be bent 30°, and when the temperature is low, the bend degree is reduced to 15° and hammer striking should be avoided. Nevertheless, in this welding investigation, 90° bend tests were always performed and done by striking the stud with a hammer. Figure 4.20 shows pictures of shear studs after bend testing.



*Figure 4.20 - Shear Studs Passing 90° Bend Test*

### 4.5.3. Tension Test on Welded Stud

Figure 4.21 illustrates the setup of a stud weld tension test and a successful test. The shear stud was first welded to a 1'×1' plate and the plate was bolted to a T-shape section for gripping in a tension test machine. The head of the stud was removed to allow gripping of the top of the stud in the test machine. A 220-kip MTS machine was used for the tension tests. AWS D1.5 specifies that a shear stud pass the weld tension test if the final fracture occurred at the stud shank rather than weld or if the maximum stress developed in the shear stud in the test is higher than 60 ksi. These criteria were adopted in this study for weld tension tests.



*Figure 4.21- Weld Tension Test Setup and a Successful Test*

#### 4.5.4. Macro Etch Weld Test

Macro etch weld testing is a visual inspection of the weld cross-section. The stud weld is first cut into two half pieces, as it shown in Figure 4.22 (a). Then the cross-section is polished using a series of sandpaper grinders. Finally, 10% Nitric acid solution is applied on the cross-section to help reveal the HAZ and other regions in the weld. Figure 4.22 (b) shows the cross-section of a sound weld in a macro etch weld test. It can be seen that the HAZ is in a darker color compared to the weld zone and parental materials under the Nitric acid. The acceptance criteria for macro etch weld tests is given in ISO (2017b), which states that an imperfection of 0.5mm or smaller should be discarded if the nearest imperfection is at least 0.5mm away. The total length of visible imperfections in a cross-section should be smaller than 20% of the width of the weld zone. If undercut is present, the undercut should be less than 5% of the total width of the weld zone and the bend test should be performed. These criteria were adopted in this study for macro-etch testing.



Figure 4.22 - Macro Etch Weld Test. (a) Welds Are Cut in the Middle and Polished, (b) Cross-Section of a Weld Treated with Nitric Acid

#### 4.6. Stud Welding Equipment and Initial Welding Parameters

All stud welds in this research project were made using a Nelson Nelweld 6000 control unit (Nelson Stud Welding 2008a) and a Nelson NS20 heavy duty welding gun (Nelson Stud Welding 2008b). The Nelson Nelweld 6000 is a commercially available stud welding unit with a rated output of up to 2500 amps. Nelson supplied specialized chucks for the welding gun to accommodate 1-1/8" and 1-1/4" studs, in addition to the "off-the-shelf" chucks for 7/8" and 1" studs. The first modification needed in the weld setup was the chuck for welding gun. Figure 4.23 is a photo of chucks of different stud.

Table 4.7 lists the initial welding parameters used for the welding investigation, based on recommendations from Nelson. These parameters were ultimately modified for the 1-1/8" and 1-1/4" studs based on the weld parameter investigations.

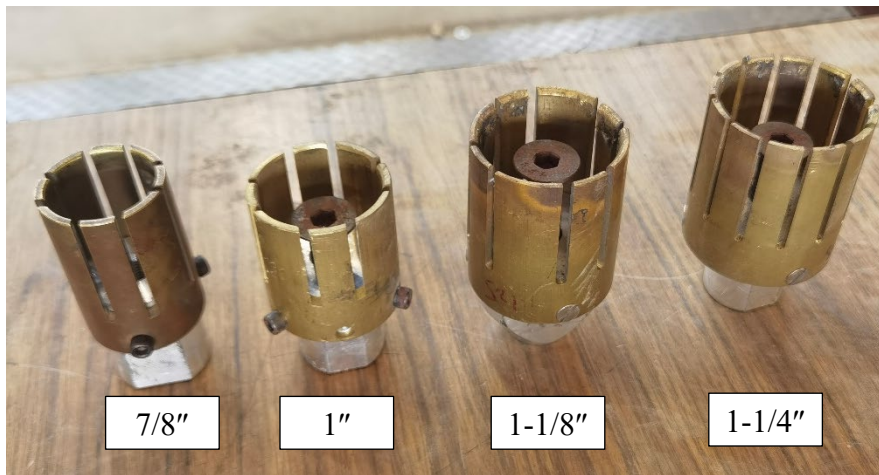


Figure 4.23 Welding Gun Chucks for Various Diameter Shear Studs

Table 4.7 - Initial Welding Parameters

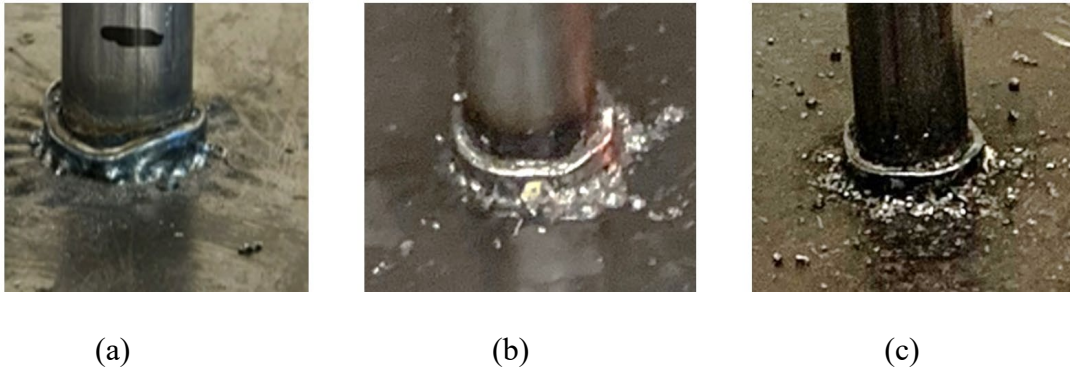
Diameter (in)	Current (Amp)	Time (s)	Plunge (in)	Lift (in)
7/8	1700	1.0	1/4	1/8
1	1900	1.4	1/4	1/8
1-1/8	2050	1.3	5/16	1/8
1-1/4	2200	1.4	3/8	3/16

Note: Straight polarity for all stud diameters

## 4.7. Verification of 7/8" Diameter Stud Weld Quality

The purpose of the welding investigation was to identify proper welding parameters and practices for larger-diameter shear studs. However, all weld quality tests were performed on 7/8" studs used in this project as well. For the weld quality tests, 7/8" studs were welded to 1'×1' plates of 1" and 2" thickness using the suggested weld parameters from Nelson in Table 4.7. Straight polarity, no surface preparation, and no cable looping were used when welding the 7/8" studs. Steel for the plates was ASTM A709 Grade 50W.

Figure 4.24 shows the typical weld collar appearance of the 7/8" studs. It can be seen that the weld collar generally satisfied the criteria for passing visual inspection. The height of weld collar was not completely uniform but sufficient height was developed. Blueish and shiny surfaces can be noticed. The length reduction of 7/8" studs were checked in selected shear studs and were sufficient.

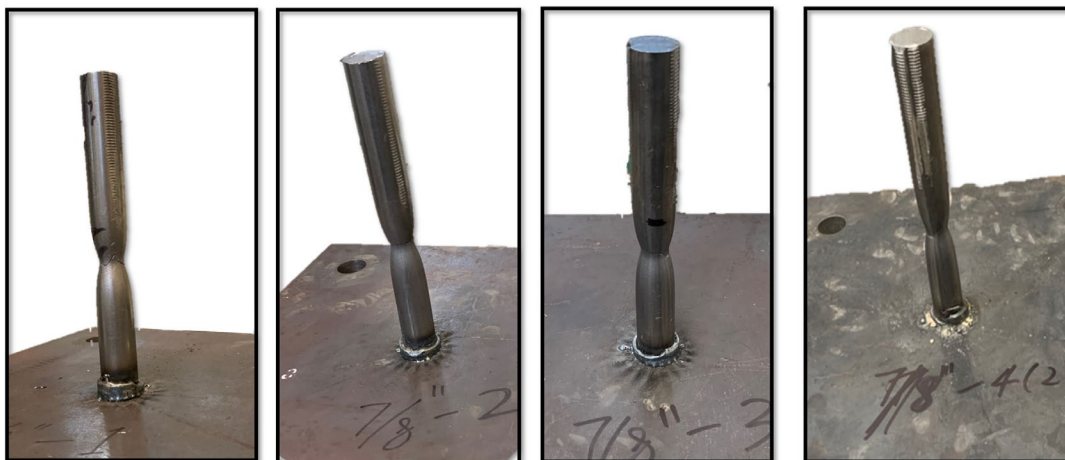


*Figure 4.24 - Appearance of 7/8" Stud Welds. (a) Welded on 1" Thick Plate for Tension Test, (b) Welded on 2" Thick Plate for Macro Etch Weld Test, (c) Welded on 2" Thick Plate for Bend Test*

Four 7/8" studs were tested in a weld tension test, in which three studs were welded on 1" thick plate and one was welded on 2" thick plate. Results of the weld tension tests showed that all shear studs fractured in the stud shank. The average tensile strength of four weld tension tests was 73.5 ksi, which is larger than the AWS D1.5 requirement of 60 ksi. Figure 4.25 shows the studs after testing. Fracture can be seen in the stud shank at necking region and the weld is intact.

Four 7/8" studs were subjected to 90° bend testing, in which two studs were welded on 1" thick plate and two were welded on 2" thick plate. Figure 4.26 shows the results of 90° bend tests. All four shear studs passed the test without fracture.

The last test was the macro etch weld test. Results of two macro etch weld tests are presented in Figure 4.27. It was observed that the cross-sections of welds were sound and intact. The liquid on the cross-section in the photo is the 10% Nitric acid solution. No porosity was visible. Parent material, the weld zone and the HAZ can be clearly seen.



*Figure 4.25 - Weld Tension Tests for 7/8" Studs*



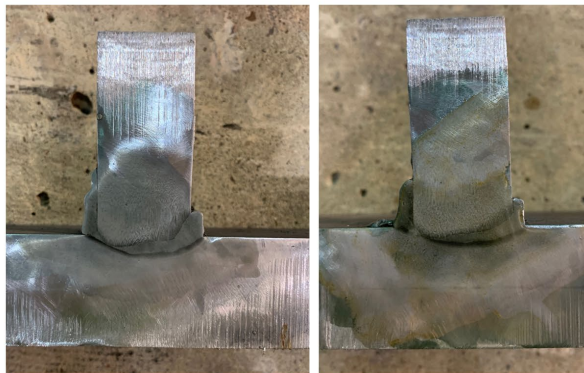


(a)

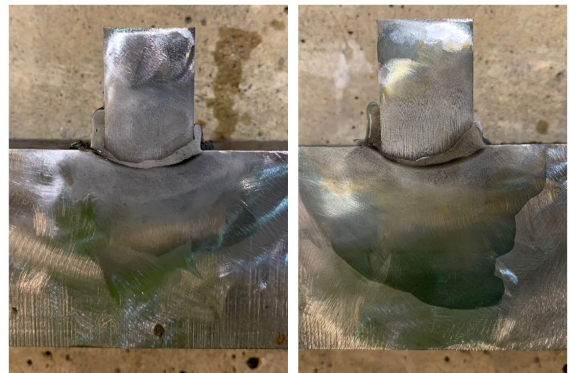


(b)

*Figure 4.26 - 90° Bend Test on 7/8" Studs. (a) Test for Stud Welded on 1" Thick Plate. (b) Test for Studs Welded on 2" Thick Plate*



(a)



(b)

*Figure 4.27 – Macro Etch Weld Tests for 7/8" Studs. (a) Studs Welded on 1" Thick Plate, (b) Studs Welded on 2" Thick Plate*

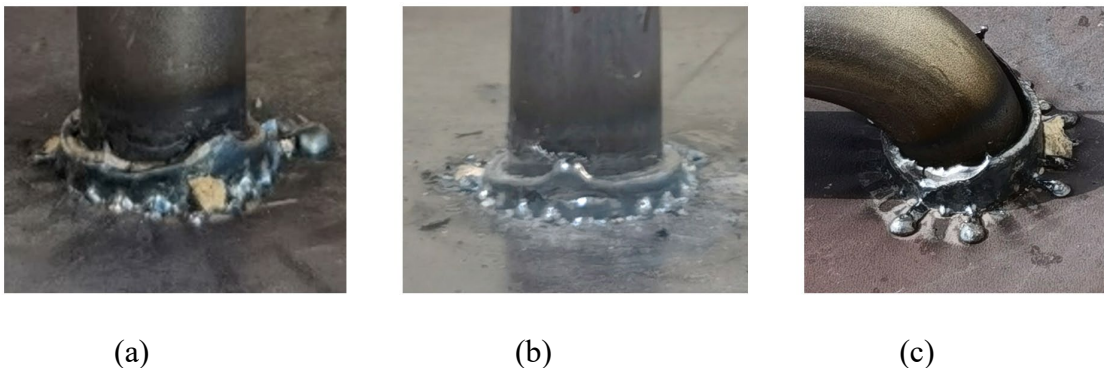
In summary, twelve 7/8" welded shear studs were tested by weld tension tests, 90° bend tests, and macro etch weld tests. Welding parameters given in Table 4.7 produced consistent good weld quality for 7/8" diameter shear studs on 1'×1' plate of 1" and 2" thickness using ASTM A709 Grade 50W steel. No special consideration was needed for surface preparation of the base metal and no cable looping was used.

Even though good results were obtained in these quality tests, when welding 7/8" studs on W14×132 girders in the push-out test study described in Chapter 6, additional 90° bend tests were performed and all shear studs passed these tests. During this process, a higher lift of 3/16" was used and it had no influence on the weld quality.

## 4.8. Welding Investigation for 1" Diameter Studs

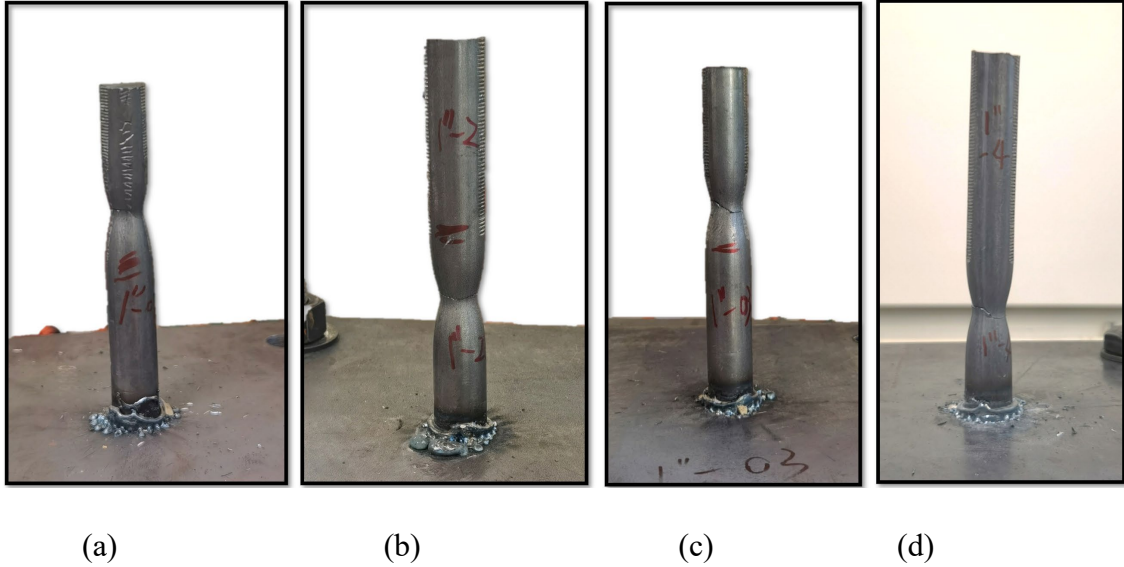
Studs of 1" diameter are the maximum diameter stud commercially available "off-the-shelf." In this study, welding parameters given in Table 4.7 were used for welding 1" diameter shear studs. Like 7/8" studs, 1" diameter shear studs were welded on 1'×1' plate of 1" and 2" thickness of ASTM A709 Grade 50W steel. Straight polarity and no cable looping was used during the welding. Surface preparation of the base metal was considered for 1" diameter shear studs in the weld quality tests. A steel brush wire grinder was used to remove the mill scale and rust and an Acetone solution was used to remove grease or oil. This surface preparation was done because initial trial welds showed a high rate of unsuccessful welds on the untreated base metal surface.

Figure 4.28 shows the typical appearance of 1" stud weld collars when surface preparation was done on the base metal. It can be seen that the weld collar was uneven in height but sufficient height was formed. Shiny and bright color was observed on the surface of the weld collar. In Figure 4.28 (c), "spider legs" are observed but no cold weld issue was seen. The length reduction of 1" studs was checked in selected studs and was sufficient.



*Figure 4.28 - Appearance of 1" Stud Welds. (a) Welded on 1" Thick Plate for Tension Test, (b) Welded on 2" Thick Plate for Weld Tension Test, (c) Welded on 1" Thick Plate for Bend Test*

Four 1" studs were subjected to weld tension tests and all of them passed the test with fracture occurring at the stud shank. Three studs were welded on 1" thick plate and one stud was welded on 2" thick plate. Figure 4.29 shows the four shear studs after the weld tension tests. The average tensile strength measured in the weld tension test was 72.9 ksi, satisfying the minimum required strength of 60 ksi.



*Figure 4.29 - Four 1" Diameter Shear Studs Passing Weld Tension Test. (a)(b)(c) Stud Welded on 1" Thick Plate, (d) Stud Welded on 2" Thick Plate*

Four 1" diameter shear studs were subjected to 90° bend testing, in which three studs were welded on 1" thick plate and one was welded on 2" thick plate. All studs passed the bend test without any fracture in the stud weld.

The last test was the macro etch weld test. Two studs were welded on 1" thick plate and another two studs were welded on 2" thick plate for this test. A typical cross-section of 1" stud weld is shown in Figure 4.30. No porosity was visually detectable and the cross-section was sound and intact with clear formation of HAZ.



*Figure 4.30 - Macro Etch Weld Test for 1" Diameter Shear Stud Welded on 1" Thick Plate*

Based on observations and findings in the 12 weld quality tests, the welding parameters suggested by Nelson (Table 4.7) produced consistent good welds for 1" diameter shear studs on 1'×1' plate of 1" and 2" thickness using ASTM A709 Grade 50W steel with surface preparation. It was found that successful welding on untreated steel plate surfaces was also possible. Figure 4.31 illustrates the weld when no surface preparation was performed. The appearance of weld is close to that with surface preparation and length reduction for two welds in Figure 4.31 are 1/4". However, surface preparation is recommended to reduce the unsuccessful weld rate. No cable looping was needed to obtain sound and good quality welds. A later study showed a larger lift of 3/16" can also be used for welding 1" studs. Weld quality was not sensitive to this change.



*Figure 4.31 - 1" Diameter Shear Stud Welded Without Surface Preparation*

1" diameter shear studs were not used in the later push-out tests and large-scale beam tests, because 1-1/8" diameter stud was ultimately selected for these tests. Thus, the 1" diameter studs were not welded on steel girders in this study. Conclusions based on investigation on steel plate may not be applicable for welding on steel girders.

## **4.9. Welding Investigation for 1-1/8" Diameter Shear Studs**

---

### **4.9.1. Investigation of Welds on Steel Plate**

Starting with the recommended welding parameters from Nelson in Table 4.7, shear studs were welded on 1'×1' plate of 1" and 2" thickness of ASTM A709 Grade 50W steel. Initially, surface preparation, cable looping, and straight polarity were all used. The surface preparation procedure was the same as that used for welding 1" diameter shear studs, as described in the previous section. The cable was looped clockwise into one circle of approximate 20" diameter with the center being the welding position.

Studs welded using these procedures resulted in acceptable weld collar appearance. Figure 4.32 shows the weld collar appearance for 1-1/8" diameter shear studs. The weld collar showed a blueish shiny surface, with uniform height. Selected shear studs were checked for length reduction and the acceptance criteria of 3/16" was met.



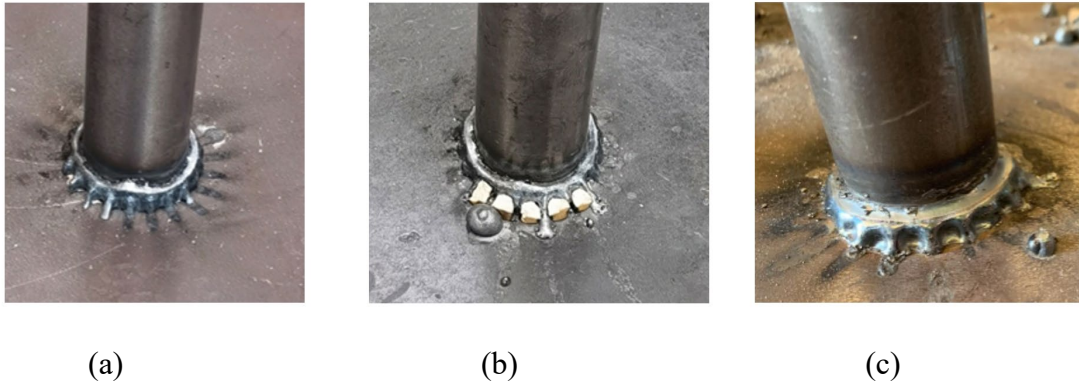


Figure 4.32 - Appearance of 1-1/8" Diameter Shear Studs Welds. (a) Welded on 1" Thick Plate for Weld Tension Test (b) Welded on 2" Thick Plate for Weld Tension Test (c) Welded on 1" Plate for Macro Etch Weld Test

Four 1-1/8" studs were subjected to weld tension tests, of which two were welded on 1" thick plate and two were welded on 2" thick plate. The results of the weld tension tests are shown in Figure 4.33. Three of the studs fractured in the stud shank and one stud fractured at the weld. A grayish dull color can be seen at the fracture surface, which suggests fracture occurred in the HAZ (ISO 2017b). However, the average tensile strength of the four weld tension tests was 83.8 ksi. The stud that fractured at the weld had the smallest tensile strength among the four and was equal to 81.8 ksi, which is larger than the acceptance criterion of 60 ksi. Therefore, the weld tension tests were deemed successful.

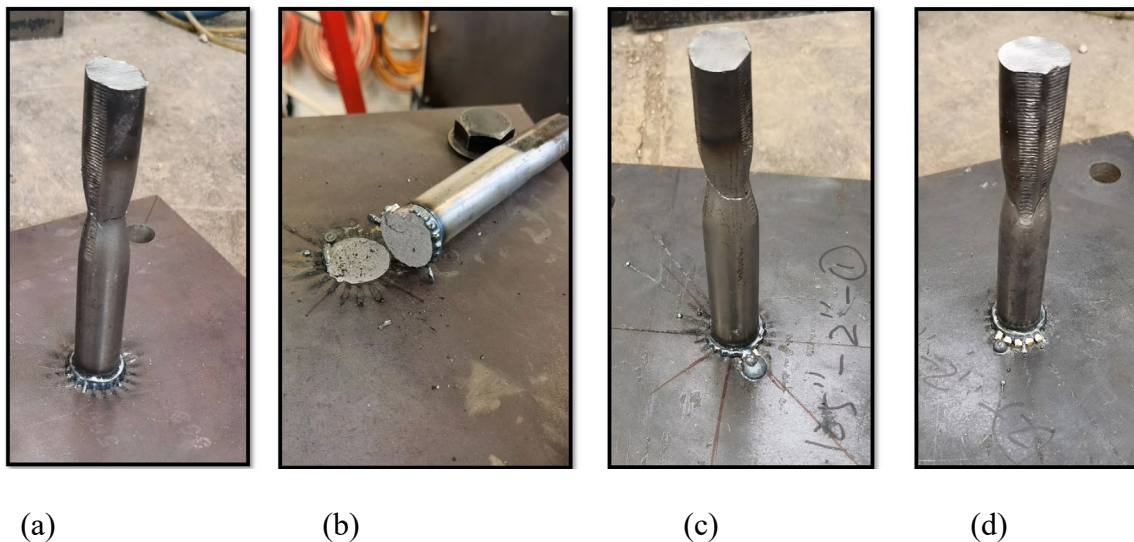
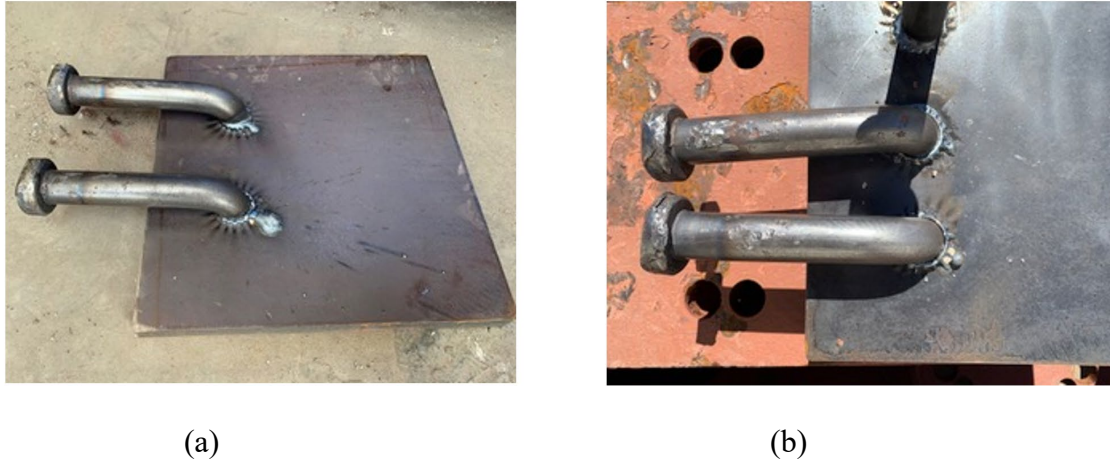


Figure 4.33 - Four 1-1/8" Studs Passing Weld Tension Tests. (a)(b) Stud Welded on 1" Thick Plate (c)(d) Stud Welded on 2" Thick Plate

Four studs underwent 90° bend tests. Two studs were welded to 1" thick plate and two studs were welded to 2" thick plate for the bend tests. All four studs passed the bend tests without fracture. Figure 4.34 shows the 90° bend test results.



*Figure 4.34 - 90° Bend Test Results for 1-1/8" Diameter Shear Studs. (a) Studs Welded on 1" Thick Plate  
(b) Studs Welded on 2" Thick Plate*

Four macro etch weld tests were performed and the cross-sections satisfied the ISO (2017b) acceptance criteria. Figure 4.35 shows the test results. The cross-section for studs welded on 2" thick plate showed minor porosity. However, none of these imperfections violated the ISO (2017b) macro section requirements.



*Figure 4.35 - Macro Etch Weld Test Results for 1-1/8" Shear Studs. (a) Studs Welded on 1" Thick Plate  
(b) Studs Welded on 2" Thick Plate*

The good quality 1-1/8" diameter shear stud welds described above were made using surface preparation and cable looping. However, surface preparation and cable looping increase the time required to complete the entire stud welding process. Further investigation was therefore performed to study the influence of these two factors. The first step was to try welding without cable looping while keeping all other aspects unchanged. Photos of the welds and cross-sections

(no Nitric acid solution applied) of the welds made without cable looping are shown in Figure 4.36. It can be seen that uneven weld collars of reduced height were formed. Length reductions were  $1/8''$ , which is smaller than the  $3/16''$  target. Nonetheless, the cross-section of weld was intact and sound.



*Figure 4.36 - 1-1/8" Studs Welded Without Cable Looping*

The second step was to skip surface preparation. Figure 4.37 shows the weld collar when no surface preparation and no cable loop was used. The studs could be successfully welded on to the plate. Weld collars of smaller and uneven height were formed and the length reduction was only  $1/8''$ . To get increased length reduction, the lift of the welding gun was increased from  $1/8''$  to  $3/16''$  to incorporate more heat in the welding process. Sufficient length reduction was obtained after this change. Figure 4.37 (b) shows the weld collar under  $3/16''$  lift, which had no significant visual difference from  $1/8''$  lift in Figure 4.37 (a). No mechanical tests or any cross-section inspection was performed under this setting.





(a)

(b)

*Figure 4.37 - 1-1/8" Studs Welded Without Surface Preparation and Without Cable Looping. (a) lift is 1/8" (b) Lift is 3/16".*

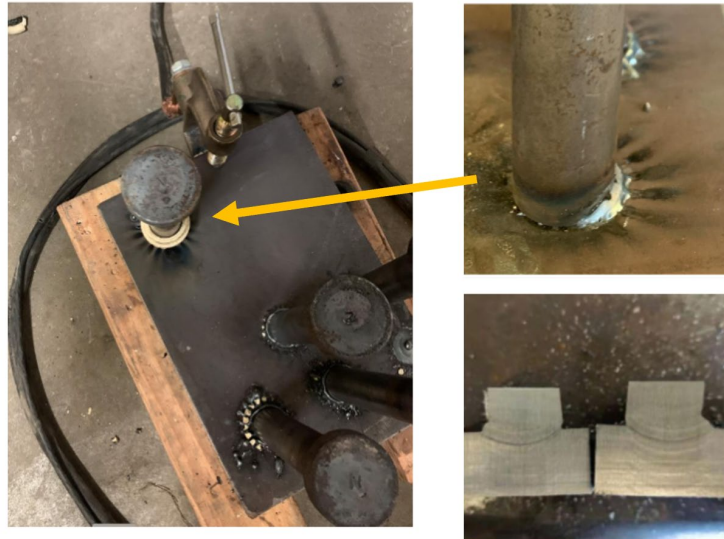
To further study the influence of electromagnetic induction, a cable loop of opposite direction was used. That is for straight polarity, the cable was looped counterclockwise. The magnetic field will be likely to restrain the downward movement of the shear stud under this condition. It was observed that the weld quality decreased significantly. Four studs were welded on 1" plate under this setting, and only 50% passed the 90° bend test. Figure 4.38 shows the fractured surfaces of the welds after the bend test. Large porosity was observed in the weld and a bright fracture surface was noticed. ISO (2017b) attributes this issue to low welding power or unclean surface.

Another aspect of electromagnetic induction is arc blow. To study this, 1-1/8" studs were intentionally welded at locations very close to the ground and free edge while correct cable looping and surface preparation were used. Figure 4.39 illustrates a stud welded close to the ground and provides photos for typical weld appearance and cross-sections under the arc blow effect. The arc blow strongly influenced the weld collar formation. In Figure 4.39, a biased weld collar is visible but the cross-section is free of defects. In some other welds under arc blow, no weld collar or stud hang up was observed. Thus, sufficient distance from the ground location and free edge is beneficial for good quality stud welding.

In conclusion, the 1-1/8" studs were successfully welded on steel plate with the parameters suggested from Nelson (Table 4.7). Proper cable looping was deemed necessary to have sufficient length reduction. If no cable looping is used, an increased lift of 3/16" should be used. Using the incorrect direction of cable looping will significantly diminish the weld quality. Surface preparation was shown to be not needed. The arc blow effect on 1-1/8" when welding on 1'×1' plate was strong. The welding location should be carefully selected or counter arc blow measures like adding a steel mass between the ground and the weld (ISO 2017b) should be used.



*Figure 4.38 - Failed Bend Test for 1-1/8" Studs Using Counterclockwise Cable Loop, Straight Polarity, and No Surface Preparation*



*Figure 4.39 - Arc Blow Effect on 1-1/8" Diameter Shear Studs Close to Ground and Free Edges*

## **4.9.2. Investigation of Welds on Steel Girders**

In addition to evaluating stud welding procedures on small steel plates, as described above, additional welding trials were conducted wherein shear studs were welded to girder flanges. For this purpose, a 30' long W14×132 girder was used. The beam flange thickness for the W14×132 girder is 1" and the material for the steel girder is ASTM A992. This same girder cross-section was used later in this research program for push-out testing. Unlike the steel plate, the only mechanical weld quality test that can conveniently be performed for a stud on steel girder is the 90° bend test.

The welding investigation of studs on a steel girder started with the best welding practice learned from welding on steel plate, as follows:

*2050 Amp, 1.3s, 3/16" lift, straight polarity, one clockwise loop, surface preparation.*

This set of welding parameters were adopted from Table 4.7 for 1-1/8" diameter studs, except that a 3/16" lift was used instead of 1/8" since it was found to give better length reduction on steel plate. One loop of clockwise cable and surface preparation was used. The welding location was far away from the ground or free edge. However, using these settings, poor weld quality was obtained. Figure 4.40 shows the picture of weld collar and failed bend test under these settings.



*Figure 4.40 - 1-1/8" Studs Welded Using 2050A, 1.3s, S Polarity, One Clockwise Loop, and Surface Preparation on a W14×132 Girder. Weld Collar (left photos) and Fracture Surfaces After Bend Test (center and right photos)*

The weld collar exhibited typical cold weld appearance and the fractured weld showed a large amount of porosity. Based on ISO (2017b), these observations lead to the conclusion that the welding power is too low. Increasing the welding time and current amperage is the most direct way to increase welding power. Therefore, a series of welding trials using higher current and a longer welding time were performed. A larger lift was also used since this can provide more heat as well. One set of parameters that were used in those welding trials were as follows:

*2150 Amp, 1.4s, 1/4" lift, straight polarity, one clockwise loop, surface preparation.*

Figure 4.41 (right) shows the bend test results for welds using these parameters. It can be seen that many of the studs still did not pass the 90° bend test. The welding power under these settings is significantly greater than that used with steel plate. It was realized that solely increasing the welding current and time was not the most effective approach. Based on advice from Nelson, instead of further increasing the amperage and time, changing from straight to reverse polarity



was attempted. The cable looping direction changed accordingly from clockwise to counterclockwise. Thus, the parameters that were used were as follows:

*2150 Amp, 1.4s, 1/4" lift, reverse polarity, one counterclockwise loop, surface preparation.*

Weld quality obtained using these parameters was checked with visual inspection and 90° bend testing and all studs passed the test, as seen in the photo on the left side of Figure 4.41. These results indicate that reverse polarity provides higher welding energy on a steel girder comparing to straight polarity.

Next, additional trials were conducted using the following parameters:

*2150 Amp, 1.4s, 1/4" lift, reverse polarity, no loop, no surface preparation.*

The results (left side of Figure 4-32) showed that high quality stud welds can be achieved without surface preparation and without cable looping.



*Figure 4.41 - 1-1/8" Studs Welded Using 2150A, 1.4s, S Polarity (right side of photo) and R Polarity (left side of photo) on W14×132 Girder. Some Studs on the Left are Welded Without Cable Looping and Surface Preparation.*

Thus, the best welding practice for 1-1/8" studs on a W14×132 girder significantly changed from that on 1'×1' plate. Higher welding current amperage, longer welding time, and reverse polarity instead of straight polarity was used. These results indicate that more welding power is needed for welding larger-diameter shear studs on a bigger piece of base metal. Further, the increased welding power makes the surface preparation and cable looping unnecessary on steel girders, which will facilitate the application of larger-diameter shear studs in actual construction. This is counter intuitive since the electromagnetic induction effect should be stronger under higher

electric current. However, it is believed the enlarged pieces of base metal dissipates the electromagnetic induction effect.

The studies so far indicate that the optimal welding parameters may vary with the type and thickness of the base metal. To further explore this issue, the best welding practice obtained from the W14×132 girder was attempted on girder with a thicker flange. Figure 4.42 shows 90° bend tests on a 6' long W14×500 girder which has a 3-1/2" flange thickness. A total of four studs were welded and tested and only half of them passed the test. Once again, bright spots and porosity were observed on the fracture surface, indicating a deficiency of welding power. This led to another cycle of trials of increasing welding power.



*Figure 4.42 - 1-1/8" Studs Welded Using 2150A, 1.4s, R Polarity, No Surface Preparation, No Cable Looping on a W14×500 Girder with 3-1/2" Thick Flange. 90° Bend Test Results*

For the next welding trials, the following parameters were used:

*2250 Amp, 1.55s, 1/4" lift, reverse polarity, no loop, no surface preparation.*

The results of these trials are shown in Figure 4.43. Seven consecutive welds were made using these settings, and all passed the 90° bend test.

Based on these observations, welding parameters working on a girder with a thin flange may not work on girder with a thicker flange. This means girders of different flange thickness may need different welding parameters for larger-diameter shear studs. Next, an investigation was carried out to learn if welding parameters working on a thicker flange will work on a girder with a thinner flange.

First, the welding parameters successfully used on the W14×500 girder with 3-1/2" thick flange were used on the W14×132 girder with 1" thick flange. Results are shown in Figure 4.44. Six consecutive welds were subjected to a 90° bend test and all of them passed the test. Visual inspection showed the length reduction for all studs was more than 1/4", which exceeds the 3/16" requirement.





Figure 4.43 - 1-1/8" Studs Welded Using 2250A, 1.55s, R Polarity, No Surface Preparation, No Cable Looping on a W14×500 Girder with 3-1/2" Thick Flange. 90° Bend Test Results



Figure 4.44 - 1-1/8" Studs Welded Using 2250A, 1.55s, R Polarity, No Surface Preparation, No Cable Looping on a W14×132 girder. 90° Bend Test Results

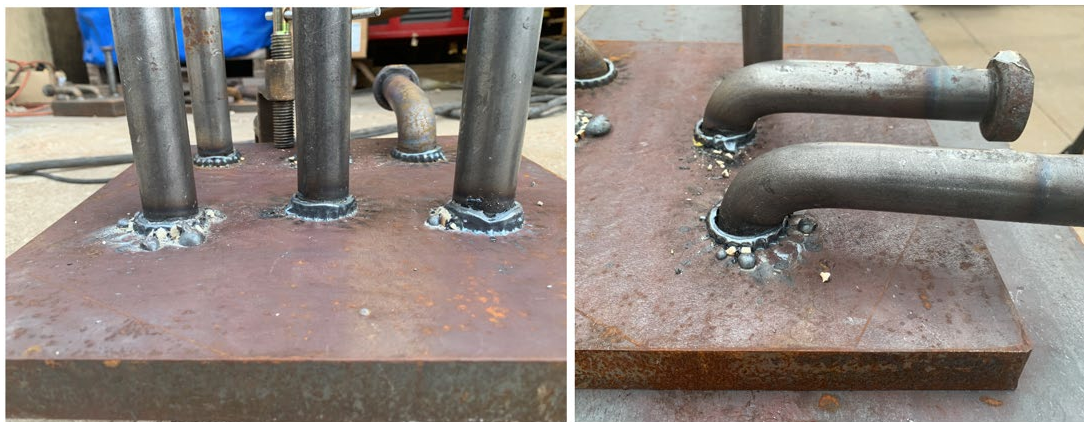
Next, these parameters were used on a girder with an even thinner flange. A 20' long W14×99 girder with 3/4" thick flange was used. Three 1-1/8" studs were consecutively welded and tested. Visual inspection showed that the length reduction for all satisfied the 3/16" criterion and all of them passed the 90° bend test. During bend test, there was no evidence that the 3/4" thick flange had any excessive deformation when the studs deformed in the bend test. Figure 4.45 shows the weld appearance and the bend test results on a 3/4" thick flange girder.



*Figure 4.45 - 1-1/8" Studs Welded Using 2250A, 1.55s, R Polarity, No surface Preparation, No Cable Looping on a W14x99 Girder. 90° Bend Test Results*

These test results showed that the acceptable welding parameters for a 3-1/2" thick flange can be used on thinner flanges at least to 3/4" thick. This range of flange thickness covers the most common flange thicknesses used on steel bridge girders.

One last question is if these same welding parameters can be used on steel plate and produce consistent good quality welds. Therefore, three studs were welded using these settings on 1'x1' plate of 1" and 2" thickness. Visual inspection and 90° bend tests were performed. Figure 4.46 and Figure 4.47 show the test results and all studs had adequate length reduction and passed the bend test. This indicates that higher welding power is desirable for larger-diameter shear studs.



*Figure 4.46 - 1-1/8" Studs Welded Using 2250A, 1.55s, R Polarity, No Surface Preparation, No Cable Looping on 1" Thick Plate. Appearance of Weld Collars (left) and 90° Bend Test Results (right).*



*Figure 4.47 - 1-1/8" Studs Welded Using 2250A, 1.55s, R Polarity, No Surface Preparation, No Cable Looping on 2" Thick Plate. Appearance of Weld Collars (left) and 90° Bend Test Results.*

### **4.9.3. Summary of Welding Investigations of 1-1/8" Studs**

A summary of the welding investigations of 1-1/8" studs is provided in Table 4.8 below. It should be noted that the plunge of 5/16" is unchanged during the entire study.

High welding power settings provided the best results for 1-1/8" diameter shear studs. The use of 2250 amps plus 1.55 seconds welding time provided the highest amount of welding energy among all welding parameters attempted, and reverse polarity helped to produce even more heat at the weld. Unlike other settings, this highest-power setting worked well on every single base metal tested in this study and no surface preparation or cable looping was required. The 90° bend test and visual inspection (weld collar appearance and length reduction) are the only tests performed for this high-power setting but all welds under this setting passed the two tests regardless of the base metal. In this study, welding on the girders was generally several feet from the ground. Welding close to a free edge did not show significant arc blow effect. It appears welding on large piece of steel is less sensitive to arc blow compared to welding on a small plate.



**Table 4.8 - Summary of Welding Investigations for 1-1/8" Studs**

Current (Amp)	Time (s)	Lift (in)	Polarity	Surface Preparation/Cable looping	1'x1' plate	Girder Flange Thickness		
						1"	3.5"	0.75"
2050	1.3	1/8	S	Y/C	✓ <sup>+</sup>	-		
				Y/N	✓ <sup>-</sup>			
				Y/CC	✗			
				N/N	✓ <sup>-</sup>			
		3/16		N/N	✓			
				Y/C	✓	✗	-	
2150	1.4	1/4	S	Y/C	-	✗	-	
			R	Y/CC	-	✓		
		Y/N		-	✓			
		N/N		-	✓	✗	-	
2250	1.55	1/4	R	N/N	✓	✓	✓	✓

Notes: S: Straight polarity. R: Reverse polarity. Y/C: with surface preparation and with clockwise cable loop. Y/N: with surface preparation and no cable loop. Y/CC: with surface preparation and with counterclockwise cable loop. N/N: no surface preparation and no cable loop. ✓<sup>+</sup>: passed visual inspection, weld tension test, 90° bend test, and macro etch test. ✓<sup>-</sup>: passed 90° bend test and visual inspection, no other test performed. ✓<sup>-</sup>: failed length reduction check but passed macro etch tests (no Nitric acid solution in some cases), no other test performed. -: no test data available. ✗: failed 90° bend test.

## 4.10. Welding Investigation on 1-1/4" Diameter Shear Studs

### 4.10.1. Investigation of Welds on Steel Plate

Like all other diameter shear studs in this study, the 1-1/4" diameter shear studs were welded on 1'x1' plate of 1" and 2" thickness using ASTM A709 Grade 50W steel for weld quality tests. To begin with, two studs were welded using the settings listed in Table 4.7 for 1-1/4" studs. Surface preparation, straight polarity, and one clockwise cable loop were used. Figure 4.48 shows the weld collar and macro etch cross-sections (no Nitric acid solution). The weld collars developed enough height and a shiny surface. However, the length reduction was only 1/8", which is smaller than the acceptance criteria of 1/4" (see Table 4.6). The cross-section of the weld shows large amounts of porosity. By visual inspection, the total length of imperfections is clearly more than 20% of the total width of the weld which is unacceptable per ISO (2017b).



(a)

(b)

*Figure 4.48 - 1-1/4" Studs Welded Using 2200A, 1.4s, S Polarity, Surface Preparation, One Clockwise Cable Loop on 1" Plate. Appearance of Weld Collar (left) and Cross-Section (right).*

The amount of imperfection in the weld indicates deficiency in welding power. The next setting attempted was as follows:

*2275 Amp, 1.45s, 3/16" lift, straight polarity, one clockwise loop, surface preparation.*

Studs welded using these settings gave an acceptable weld collar appearance but an unacceptable length reduction. The length reduction was only 3/16", less than the 1/4" target. Four studs were subjected to a 90° bend test and only two of them passed. In conducting the bend tests, it was found that bending a 1-1/4" diameter shear stud with a hammer was much more difficult than for a 1-1/8" diameter shear stud. The fracture surface at a failed bend test is shown in Figure 4.49. Each fracture surface exhibited two regions with different appearances. There was a region of dull grayish color and a region of densely distributed small and bright porosities. The first region is an indication of HAZ fracture and the second region is evidence of insufficient weld power. Based on ISO (2017b), both issues can be addressed with a longer welding time. Therefore, a series of trials was conducted to find the best welding time, using the following settings:

*2275 Amp, 1.6s~2.4s, 1/4" lift, straight polarity, one clockwise loop, surface preparation.*




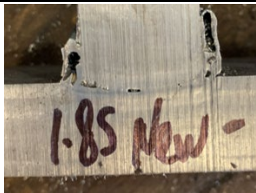

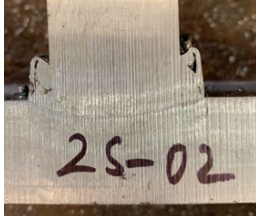
Welding times of 1.6s, 1.8s, 2.0s, 2.2s, and 2.4s were used. For each weld time case, at least two studs were welded and macro etch sections were prepared for visual inspection (no Nitric acid solution). A higher lift was also used in these trials. All these trials are performed on 1" plate with surface preparation.



Figure 4.49 - 1-1/4" Studs Welded Using 2275A, 1.45s, S Polarity, Surface Preparation, One Clockwise Cable Looping on 1" Plate. Fracture Section of Failed Bend Tests.

Table 4.9 presents the typical weld collar and cross-section for each welding time. It can be seen that the quality of the weld collar and cross-section was improved with longer welding times. Welding times larger than 2.0s were able to produce sound and intact weld cross-sections and sufficient length reduction.

Table 4.9 - 1-1/4" Studs Welded Using 2275 Amp, 1/4" Lift, S Polarity, One Clockwise Loop, Surface Preparation, and Various Welding Times

Welding Time (s)	Number of Studs Welded	Typical Weld Collar	Typical Cross-Section	Length Reduction (in)
1.6	2			3/16
1.8	4			3/16 (1), 1/4 (3)
2.0	8 (3 unsuccessful welds)			1/4 (2), 5/16 (2), 3/8 (1)

2.2	2			3/16, 1/4
2.4	2 (1 unsuccessful welds)			1/4

However, a high rate of unsuccessful hot welds was seen with weld times of 2.0s or higher. Figure 4.50 shows three unsuccessful hot welds using a 2.0s weld time. This phenomenon was especially common when welding a 1-1/4" stud on an empty plate without any existing studs welded on it. Welding on plate without surface preparation likely also increased the rate of unsuccessful hot welds. A total of six 1-1/4" studs were welded on untreated 1" plate with a welding time of 2.0s. Half of them were unsuccessful. This observation indicates the presence of prior shear studs on a small steel plate can influence the weld power on later shear studs. Surface preparation of steel plate is likely also needed to reduce the hot weld issue.

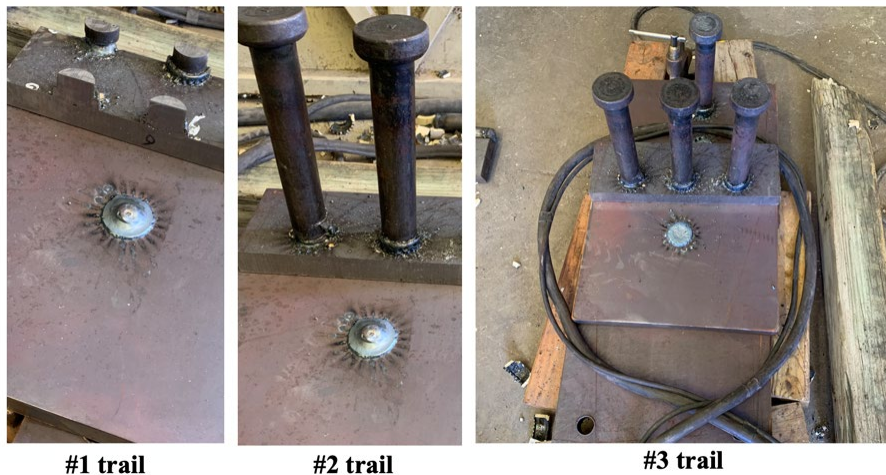


Figure 4.50 - 1-1/4" Studs Welded Using 2275 Amp, 2.0s, 1/4" Lift, S Polarity, One Clockwise Loop, Surface Preparation and With Counter Arc Blow Measures. Unsuccessful Hot Welds.






As discussed earlier, the use of reverse polarity improved the weld quality of 1-1/8" studs. Accordingly, a series of trials were performed with reverse polarity, and with the corresponding change in loop direction to counterclockwise. The settings used for these trials were as follows:

*2275 Amp, 1.45s~2.0s, 1/4" lift, reversed polarity, one counterclockwise loop, surface preparation.*



For this series of trial welds, both 1" thick plate and 2" thick plate was used. For most cases, only visual inspection and length reduction were checked. Table 4.10 summarizes the results.

**Table 4.10 - 1-1/4" Studs Welded Using 2275 Amp, 1/4" Lift, Reverse Polarity, One Counterclockwise Loop, Surface Preparation, and Various Welding Times**

Welding Time (s)	Number of Studs Welded	Typical Weld Collar	Typical Cross-Section	Length Reduction (in)
<b>On 1" Thick Plate</b>				
1.45	4 (1 unsuccessful weld)		-	1/8 (2), 3/16 (1)
1.8	5 (2 passed bend test)			3/16 (3), 1/4 (2)
<b>On 2" Thick Plate</b>				
1.8	4		-	0 (2), 1/8 (1), 3/16 (1)
1.9	3		-	1/8 (2), 1/4 (1)
2.0	1 (unsuccessful)	-	-	-

On 1" thick plate, using a 1.8 second weld time produced sound and intact cross-sections with minor imperfections. A 90° bend test was carried out for two studs under this setting and both of them passed the test. However, the same welding parameters produced lower quality welds with an unacceptable weld collar on 2" thick plate. Length reduction was also decreased. This observation indicates that base metals of different thickness require different welding parameters,



which was also encountered in the welding investigation of 1-1/8" studs. However, 1-1/4" studs appear to be more sensitive to changes in base metal thickness. Welding trials on 2" thick plate were performed with higher welding times up to 2.0s and but consistent good welds could be not obtained.

Discussion with Nelson suggested that modifying the "free travel" of the weld gun may be helpful. Thus, sixty 1-1/4" shear studs were welded using a modified free travel with various values of electric current amperage, weld time, and different welding practices. Weld tension tests, bend tests, and macro etch weld tests were performed on selected studs with good visual appearance and length reduction. However, consistent good quality welds still could not be obtained. Table 4.11 provides a summary of the welding investigation 1-1/4" diameter shear stud on steel plate. It should be noted that the plunge for all 1-1/4" stud trial welds was kept constant at 3/8".

**Table 4.11 - Summary of Welding Trials for 1-1/4" Studs on 1'x1' Steel Plate**

Current (Amp)	Time (s)	Lift (in)	Polarity	Modified "free travel"	Surface Preparation/Cable Looping	Length Reduction (in)	1'x1' plate (1" thick/2" thick)
2200	1.4	3/16	S	N	Y/C	0~1/8	x/-
	2.0		R	N	Y/C	N.A.	x/-
2275	1.45	3/16	S	N	Y/CC	N.A.	x/x
			R	N	Y/C	N.A.	x/x
2275	1.45	3/16	S	N	Y/C	1/8~1/4	x/-
		1/4			Y/C	0~1/4	x/x
					Y/N	1/8	Welded on girder flange
	1.6	1/4	S	N	Y/C	3/16	x/-
	1.8				Y/C	3/16~1/4	x/-
	2.0				Y/C	1/4~3/8	✓/-
					N/C	1/8~5/16	⊙/-
	2.2				Y/C	3/16~1/4	✓/-
	2.4				Y/C	1/4	✓/-
	1.45				1/4	R	N
	1.8	Y/CC	0~1/4	✓+/⊙			
	1.9	Y/CC	1/8~1/4	-/--			
	2.0	Y/CC	0	-/⊙			
	1.45	1/4	S	Y	Y/C	1/8~5/16	-/--

	1.45				N/C	0~5/16	--/⊙
	1.8				Y/C	3/16	⊙/-
	1.9	1/4	S	Y	Y/C	1/4	⊙/-
			R		N/C	1/8	--/-
					Y/CC	1/8~5/16	*/*
2400	1.3	1/4	S	Y	Y/C	3/16~5/16	--/--
			R		Y/CC	1/8~3/16	-/--
	2.0	3/16	R	N	Y/C	0	⊙/-
2500	1.27	1/4	S	Y	Y/C	3/16~1/4	⊙/-
	2.0	3/16	R	Y	Y/C	N.A.	⊙/-

Notes: S: Straight polarity. R: Reverse polarity. Y/C: with surface preparation and with clockwise cable loop. N/C: no surface preparation and with clockwise cable loop. Y/CC: with surface preparation and with counterclockwise \* : failed either 90° bend test or cross-section inspection. \* -: failed either 90° bend test or cross-section inspection and high rate of unsuccessful weld. ✓ -: passed cross-section inspection but high rate of unsuccessful weld, no other test performed. ✓ : passed cross-section inspection, no other test performed. ✓ +: passed cross-section inspection plus 90° bend test. ⊙: no test performed and high rate of unsuccessful welds. -: no weld on this plate. - -: only length reduction check, no other test performed.

More than two hundred 1-1/4" diameter shear studs were welded and tested and Table 4.11 only lists a portion of these. Some studs encountered strong arc blow effect and remedies were later implemented. Those results are not included. Some welding results only underwent length reduction checks because the weld collar was not acceptable. Like 1-1/8" studs, the effect of cable looping was studied by using a counterclockwise loop under straight polarity and a clockwise under reverse polarity. Welds with higher porosity were obtained compared to those with the correct cable looping direction.

Unfortunately, no single group of welding parameters was identified that could give consistent good weld quality on 1'x1' plate of 1" thickness and 2" thickness. For some parameters that were able to produce high quality welds on 1" thick plate, a high rate of unsuccessful welds was seen when welding on 2" thick plate. No parameters were identified that provided consistent good weld quality on 2" thick plate. A strong arc blow effect was frequently observed. Welding 1-1/4" stud on small plates was extremely sensitive not only to the welding parameters but also to practices related to arc blow and magnetic field.

#### 4.10.2. Investigation of Welds on Steel Girders

Similar to the 1-1/8" studs, a number of weld trials of 1-1/4" studs were attempted on steel girders. The weld trials included girders with a 1" thick flange and a girder with a 3.5" thick flange. After a number of trials, consistent good quality welds for the 1-1/4" studs on these

girders was achieved using a welding current of 2500 amps, a welding time of 2 seconds, reverse polarity, no cable looping, no surface preparation and without a modified free travel on the welding gun. Figure 4.51 shows photos of the successful stud welds on girders with a 1" thick flange. Figure 4.52 shows photos of successful stud welds on girders with a 3.5" thick flange.



(a) Weld Collar Appearance



(b) 90° Bend Tests

*Figure 4.51 - 1-1/4" Studs on Girder with 1" Thick Flange Welded Using 2500 amps, 2s, R Polarity, No Cable Looping, No Surface Preparation*



Figure 4.52 - 1-1/4" Studs on Girders with 3.5" Thick Flange Welded Using 2500 amps, 2 s, R Polarity, No Cable Looping, No Surface Preparation

### 4.10.3. Summary of Welding Investigations on 1-1/4" Studs

Welding of 1-1/4" studs proved more problematic than for 1-1/8" studs. The welding trials conducted on 1'×1' plate of 1" and 2" thickness did not identify a single set of welding parameters that provided consistent good quality welds on both plate thicknesses. However, subsequent welding trials on girders with 1" and 3.5" thick flanges did identify a single set of welding parameters that resulted in consistent good quality welds on both flange thicknesses. The parameters that resulting in consistent good quality welds on girders were: welding current of 2500 amps, welding time of 2 seconds, reverse polarity, no cable looping, no surface preparation and without a modified free travel on the welding gun.

## 4.11. Conclusions and Recommended Welding Parameters

In this chapter, welding of shear studs of 7/8", 1", 1-1/8", and 1-1/4" diameter was investigated through an extensive series of trial welds on 1'×1' steel plate. Welding of 1-1/8" and 1-1/4" studs was further explored by a series of trial welds on steel girders of various flange thickness. The shear studs and the arc welding equipment, along with technical advice on welding, was provided by Nelson Stud Welding Company. Stud weld quality was assessed using visual inspection, weld tension tests, 90° bend tests, and macro etch weld tests following requirements in AWS D1.5, ISO (ISO 2017b), and suggestions from Nelson. The impact of welding parameters, electromagnetic induction effects, and base metal thickness/preparation were extensively explored. This welding investigation showed that as stud diameter increased beyond 7/8", weld quality became more sensitive to the parameters mentioned above. The welding parameters and procedures for large diameter shear studs need to be carefully controlled to obtain consistent high-quality welds. Further, it was found that 90° bend tests conducted using a

hammer on 1-1/4" shear studs were substantially more difficult and physically demanding on the operator, than for studs with a smaller diameter than 1-1/4".

The recommended welding parameters and practices for each diameter shear stud used in this study is shown in Table 4.12 . For 1" diameter shear studs, the recommended weld settings were verified on 1'×1' steel plate of 1" and 2" thickness using ASTM A709 Grade 50W steel. For 7/8" and 1-1/8" diameter shear studs, the recommended parameters in Table 4.12 were verified on both 1'×1' steel plate and steel girder flanges. For 1-1/4" diameter shear studs, the recommended welding parameters were only verified on steel girder flanges.

**Table 4.12 - Recommended Welding Parameters**

Stud Diameter (in)	Current (Amp)	Time (s)	Plunge (in)	Lift (in)	Polarity	Surface Preparation/Cable Looping
7/8	1700	1.0	1/4	3/16	S	N/N
1	1900	1.4	1/4	3/16	S	
1-1/8	2250	1.55	5/16	1/4	R	
1-1/4	2500	2.5	3/8	1/4	R	

Surface preparation is not necessary but should be considered in case the base metal has excessive mill scale or rust. Cable looping is not required but opposite looping should be avoided since it is shown to be detrimental to the weld quality. Arc blow is especially prominent in welding with the high amperage needed for larger-diameter shear studs and should be considered, especially on small base metal like the 1'×1' plate used in this study.

## 4.12. Selection of Shear Stud Diameter for Subsequent Research Tasks

Based on the results of the preliminary design studies described in Chapter 3 and the welding investigations described in this chapter, the decision was made to proceed with the use of 1-1/8" studs for the remainder of this research project. Consequently, the push-out test program described in Chapters 5 and 6, the finite element studies described in Chapter 7, and the large-scale beam tests described in Chapter 8 will all use 1-1/8" studs, and there will be no further consideration of 1-1/4" studs in these subsequent research tasks. The reasons for this choice are as follows:

- Based on the welding investigations, the welding of 1-1/4" studs appears to be quite sensitive to the selected welding parameters and base metal conditions. The welding of 1-1/8" studs, on the other hand, appears to be more robust with a single set of welding parameters providing consistent good quality welds over a wide range base metal



conditions (welding on small plates versus girders, various thicknesses of plates and girder flanges). Thus, it is believed that the use of 1-1/8" studs is more likely to provide consistent good quality stud welds in actual bridge construction.

- A common technique used to verify weld quality is conducting bend tests on welded studs. This includes 90° bend tests as used in this chapter to verify weld quality as well as 30° bend tests used in the field for routine quality control. For 7/8" studs, bend tests can be conducted using a pipe section placed over the stud to bend the stud, or by striking the stud with a hammer. For the 1-1/8" and 1-1/4" studs used in this research project, using a pipe to bend the studs was not feasible due to the significantly higher strength of these studs compared to 7/8" studs. Consequently, the bend tests on 1-1/8" and 1-1/4" studs was done by striking them with a heavy sledge hammer. In conducting the bend tests, it was found that bending a 1-1/4" diameter shear stud with a hammer was much more difficult and physically demanding than for a 1-1/8" diameter shear stud. Thus, it is believed that conducting bend tests in the field will be more feasible for 1-1/8" studs than for 1-1/4" studs.
- Based on the preliminary design studies in Chapter 3, using 1-1/4" studs results in reducing the number of studs in a bridge by about 50-percent compared to 7/8" studs. Using 1-1/8" studs results in reducing the number of studs in a bridge by about 40-percent. Consequently, using 1-1/8" studs still results in a very significant reduction in the number of shear studs in a bridge. As described in Chapter 1, the primary reasons for considering larger-diameter shear studs are to improve construction safety and to facilitate the use of PCPs. The 40-percent reduction in the number of studs provided by 1-1/8" studs still satisfies these objectives.

The decision to proceed with 1-1/8" shear studs was made collectively by the research team, TxDOT personnel, and by the project's Industry Advisory Group. Future research may show greater feasibility for the use of 1-1/4" shear studs in bridges. However, based on currently available information from this research and from previous research, it is believed that using 1-1/8" shear studs is the most practical and implementable choice at this time.

# Chapter 5. Static Push-Out Tests

## 5.1. Introduction

---

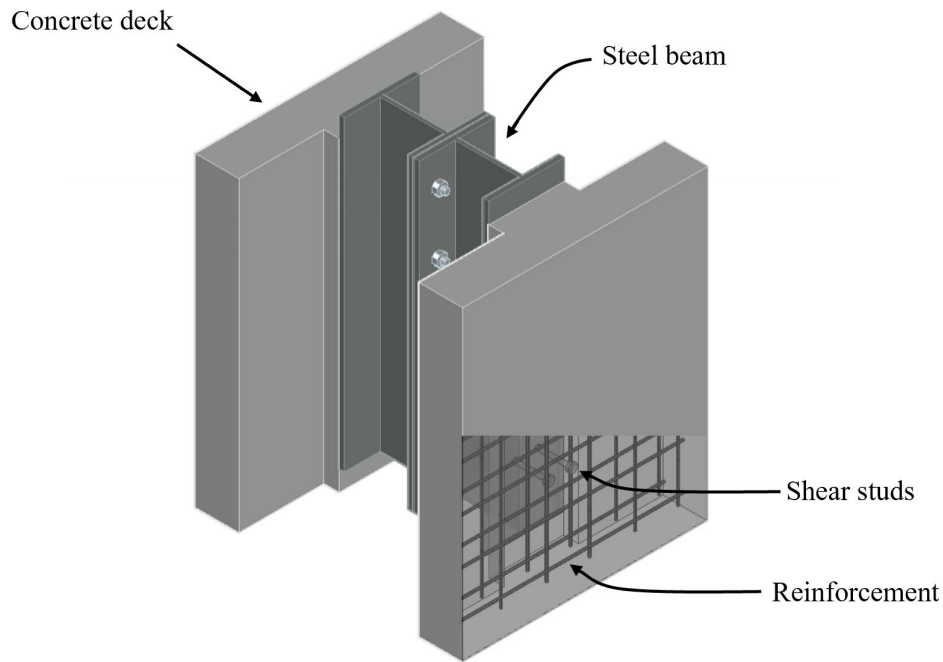
This chapter provides a detailed description of a series of static push-out tests conducted to obtain data on the strength and deformation capacity of larger-diameter shear studs. Based on the discussion in Section 4.11, 1-1/8" diameter shear studs were selected for the push-out test program. For comparison, several push-out tests were also conducted using conventional 7/8" diameter shear studs. In addition to the static push-out tests described in the chapter, fatigue tests on 1-1/8" studs were also performed on push-out specimens. The fatigue push-out tests are described in Chapter 6.

As described in Chapter 2, push-out tests are very commonly used to study shear stud behavior, and many of the design provisions for shear stud design, both for buildings and bridges, are based on push-out tests. Figure 5.1 shows a schematic view of the typical push-out test specimen used in this research. The specimen consists of a steel beam, shear studs, and concrete slab with reinforcement. The actual specimen has two slabs and therefore two steel concrete interfaces with shear studs, as is typical of most push-out specimens used in past research. When load is applied on top of the steel beams, the steel beams move relative to the concrete slabs. The relative movement between the steel and concrete is the slip. Shear studs will deform and the concrete will crush and crack as the slip increases. Eventually the specimen will lose its load resistance due to either stud fracture and/or concrete failure. A more detailed description of the push-out test specimens used in this research is provided later in this chapter.

Past research has suggested that the static strength as well as fatigue behavior of shear studs in push-out tests is conservative compared to beam tests (Slutter and Fisher 1966). There are some disadvantages of push-out tests, including the limited number of shear studs in one specimen, which confines the distribution of load among studs and may cause early failure compared to a full-scale beam test. Load eccentricity caused by the moment arm between the reaction force at the base of the slab and the applied force at the top of the steel beam may not be representative of the forces which may exist in actual composite beam. Nonetheless, push-out tests are considered to provide important information on shear stud behavior, and as noted earlier, are the basis for most shear stud design provisions for buildings and bridges, including those in the AASHTO LRFD Bridge Design Specifications (AASHTO 2020, AASHTO 2021).

An additional objective of this push-out test program is to assess if equations for shear stud static strength provided in the AASHTO *LRFD Bridge Design Specifications* can be safely used for 1-1/8" studs, or if modifications to these equations appear to be needed. In this regard, consideration is given to the shear stud static strength equations both in the current 9<sup>th</sup> Ed. of AASHTO (AASHTO 2020) as well as in the proposed 10<sup>th</sup> Ed. AASHTO (AASHTO 2021). The differences between the two for shear stud static strength are described in Chapter 2.

This chapter reports the experimental program in detail. The following sections are included: design of the push-out specimens and test matrix, fabrication of test setup and specimens, mechanical property tests for materials used in the specimens, test procedures and observations, and the push-out test results and discussion. All tests were carried out at the Ferguson Structural Engineering Laboratory (FSEL) at the University of Texas at Austin.



*Figure 5.1 - 3D Schematic of Typical Push-Out Specimen Used in this Study*

## 5.2. Test Specimens

---

### 5.2.1. Overview

A total of eleven push-out specimens were constructed and tested. Table 5.1 provides an overview of the key characteristics of each specimen. The following sections provide more detailed descriptions of each specimen.

### 5.2.2. Standard Test Specimens

The “Standard” specimens are the design prototypes in the push-out test program. Other specimens in the test matrix are based on the design of the standard specimens, with modifications from the standard specimens to investigate the influence of that modification on stud performance. There are two standard specimens: one for cast-in-place (CIP) specimens and the other for precast-concrete-panel (PCP) specimens.



**Table 5.1 – Static Push-Out Specimens**

Spec. No.	Stud Diameter	Deck Type	Haunch Depth	Stud Length After Welding	Stud Arrangement	Beam Size	Comments
1	7/8"	CIP	3"	7"	3 studs/row × 3 rows	W14×132	Reference
2		PCP	3"	7"	3 studs/row × 3 rows	W14×132	
3	1-1/8"	CIP	3"	7"	1 stud/row; no stagger × 3 rows	W14×132	
4		PCP	3"	7"	1 stud/row; no stagger × 3 rows	W14×132	PCP Standard Specimen
5		CIP	3"	7"	1 stud/row; staggered × 4 rows	W14×132	
6		PCP	3"	7"	1 stud/row; staggered × 4 rows	W14×132	
7		CIP	3"	7"	2 studs/row × 3 rows	W14×132	CIP Standard Specimen
8		CIP	3"	7"	2 studs/row × 3 rows	W14×132	Reduced Transverse Reinforcement
9		CIP	3"	5"	2 studs/row × 3 rows	W14×132	Min. Stud Penetration
10		CIP	1"	7"	2 studs/row × 3 rows	W14×132	Min. Top Cover
11		CIP	3"	7"	2 studs/row × 3 rows	W14× 99	Min. Flange Thickness

**5.2.2.1. Cast-In-Place (CIP) Standard Specimen**

Specimen No. 7 in Table 5.1 is the CIP standard specimen. This specimen is intended to represent a full-depth cast-in-place bridge deck. Figure 5.2 shows 3D schematic views of the CIP standard specimen. In Figure 5.2 (b), the concrete deck in the front is omitted to reveal the shear studs and deck reinforcement.

Figure 5.3 shows details of the CIP standard specimen. The design of the CIP standard specimen reflects typical full-depth cast-in-place decks used for composite steel bridges in Texas. References for this design are the TxDOT Bridge Design Manual (TxDOT 2023), TxDOT standard drawing SGMD (TxDOT 2019a), and the real bridge designs reported in Chapter 3.

The specimen consists of two W14×132 steel beams, and two fully cast-in-place 60" high × 48" wide × 8.5" thick concrete decks. In each deck, two layers of #4@9" reinforcing bars in orthogonal directions are used. The two steel beams are bolted together by ten A490 bolts. The W14×132 section has a flange width of 14-3/4" and a flange thickness of 1". Steel bridge plate girders normally have flange widths in the range of 18 to 24-inches and flange thicknesses in the range 0.75 to 3-inches. The W14×132 was selected based on practical limitations of what could be accommodated within the project budget and within laboratory limitations.

On each steel beam, six 1-1/8" diameter shear studs were welded in three rows, two studs per row. The shear studs were 7" long after welding. Longitudinal and transverse spacing of studs were 12" and 4.5" (four times the diameter), respectively. The haunch has the same width as the steel beam flange and a depth of 3". The penetration of shear studs into the concrete deck is 4". The top of the shear stud is 2.75" above the bottom layer of reinforcement. The top concrete cover above the studs is 4.5". The steel beam has a 4" vertical offset with respect to the concrete at the top of the specimen for load application purposes.

As noted above, the specimen was constructed using two W14×132 beams. This was done so that the concrete slabs could be cast in a horizontal position with the same batch of concrete used for both concrete slabs. A more detailed discussion on the construction of the specimens is provided later.

### **5.2.2.2. Precast-Concrete-Panel (PCP) Standard Specimen**

Specimen No. 4 in Table 5.1 is the PCP standard specimen. This specimen is intended to represent a bridge deck constructed using 4" thick PCPs with a 4.5" CIP topping. Figure 5.4 provides 3D schematics of the PCP standard specimen. In Figure 5.4 (b), the CIP concrete in the front is omitted to reveal the PCP details, reinforcement in the CIP concrete, and the shear studs. Figure 5.5 shows details for PCP standard specimen, in which the CIP part of the concrete is in blue shading and the reinforcement from the PCP is omitted.

Overall, the PCP standard specimen shares a similar design with the CIP standard specimen. The specimen has two 60" × 48" × 8.5" concrete slabs, in which PCPs are used. Two W14 × 132 steel beams were bolted together by ten A490 bolts. Three rows of single 1-1/8" diameter shear studs were welded in the center of each steel beam, directly over the web.

The presence of the PCPs creates a narrow transition region between the cast-in-place haunch and the cast-in-place 60" × 48" × 4.5" topping. The narrowest portion in the transition region is 7.7" wide and can only accommodate one 1-1/8" stud per row. The only reinforcement in the transition region is the short bars extending from the PCPs, as shown in Figure 5.7 (b). One layer of orthogonal #4@9" reinforcement is embedded in the CIP topping. The head of the shear stud

is at the same level as the top surface of the PCPs. Therefore, shear studs in the PCP standard specimen have no penetration into any layer of continuous reinforcement.

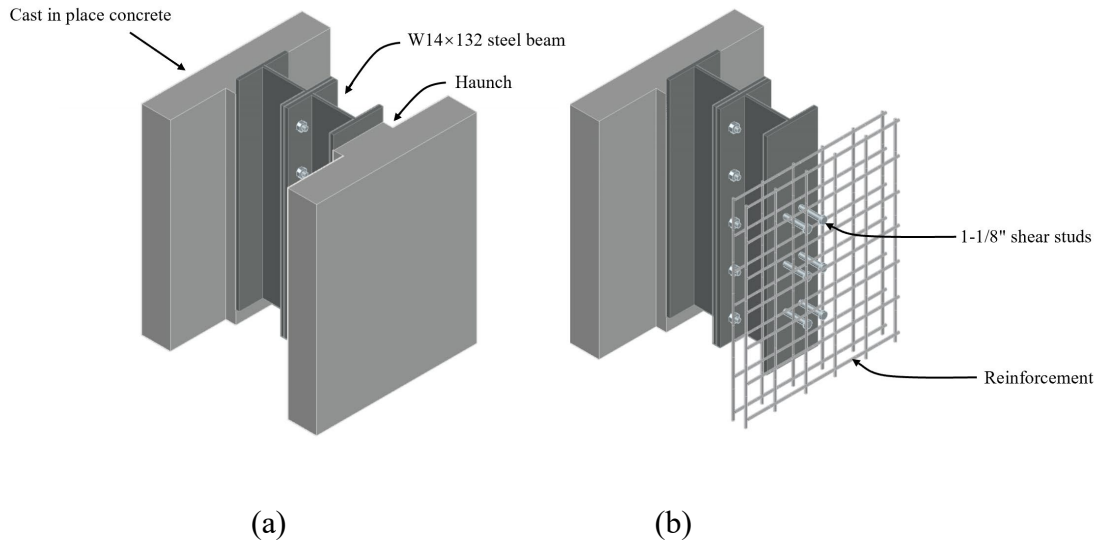


Figure 5.2 – CIP Standard Push-Out Specimen (Specimen No. 7) (a) 3D Schematic (b) View with CIP Concrete Slab Omitted

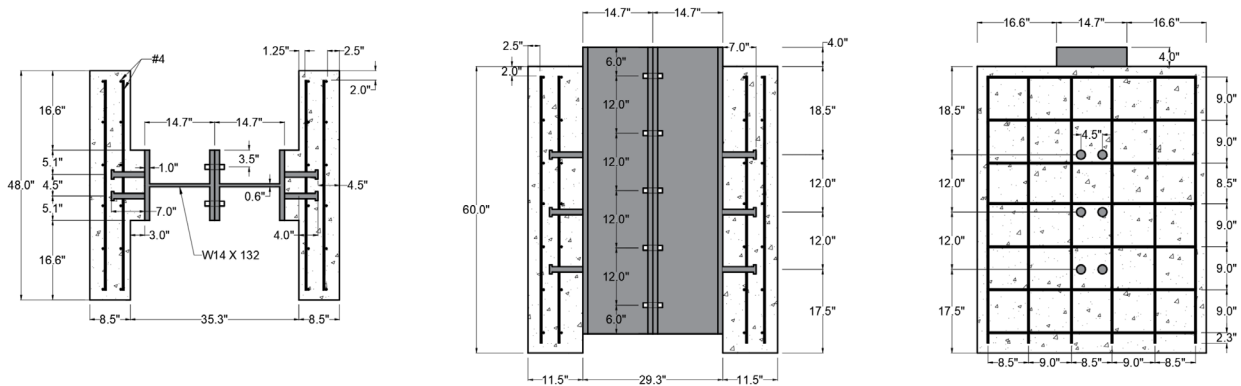


Figure 5.3 - Details of CIP Standard Push-Out Specimen (Specimen No. 7)

Figure 5.6 shows design drawings for the PCPs, which follow the TxDOT Bridge Design Manual (TxDOT 2023) and two standard drawings, namely TxDOT PCP Deck Details (TxDOT 2019b) and TxDOT PCP Fabrication Details (TxDOT 2019c). The PCP has a dimension of 60" × 20" × 4". The reinforcement consists of #4@6" transverse reinforcement, #3@5.3" longitudinal reinforcement, and two #3 R-bars for lifting purposes. The top surface of each PCP was roughened and other surfaces had no special surface preparation. A 0.75" chamfer was used in each PCPs at its inner corner, which follows the design requirements in TxDOT (2019b). All PCPs used in this study were produced by a commercial precast plant that supplies PCPs for actual bridge construction projects in Texas. Photos of the PCPs are in Figure 5.7 (a).

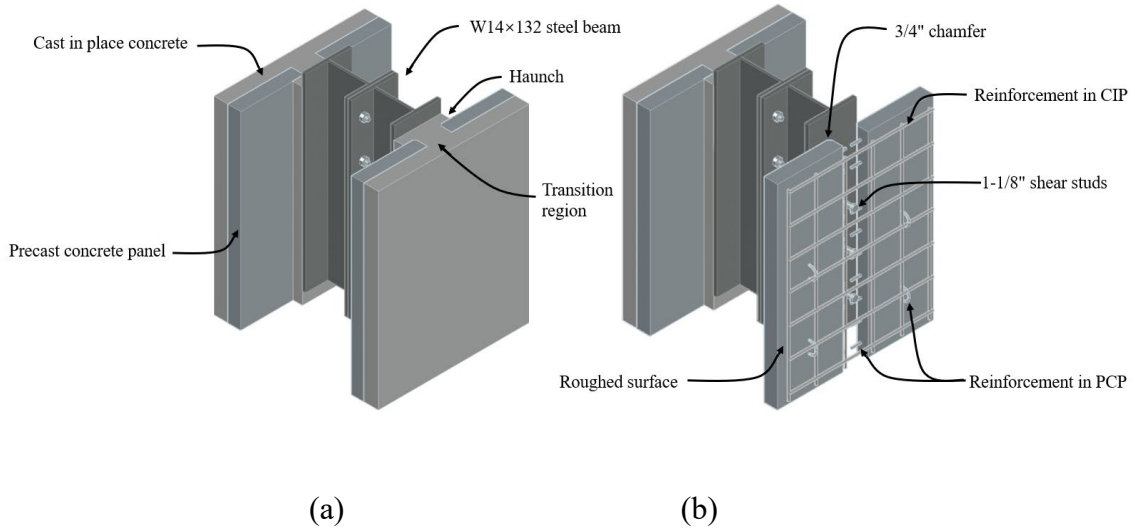


Figure 5.4 - PCP Standard Push-Out Specimen (Specimen No. 4) (a) 3D Schematic (b) View with Cast-in-Place Concrete Omitted

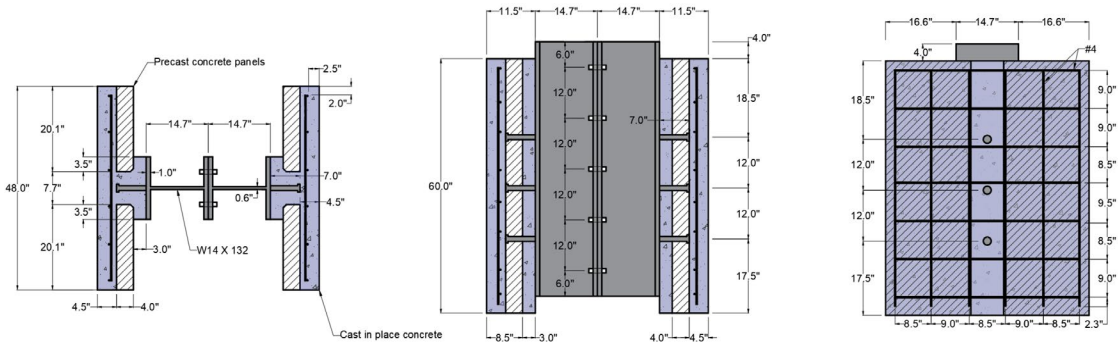


Figure 5.5 - Details of PCP Standard Push-Out Specimen (Specimen No. 4) (Reinforcement in PCP is Omitted)

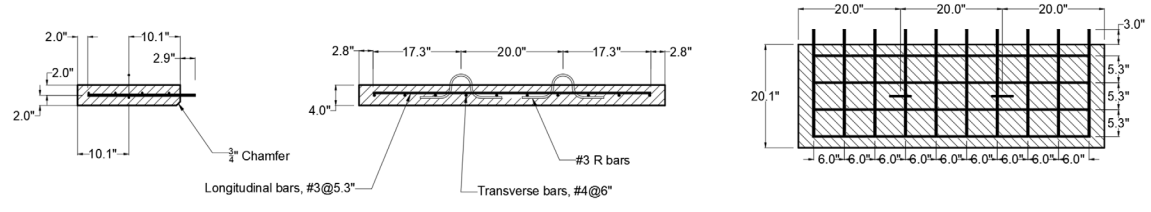


Figure 5.6 - Details of PCPs



(a)



(b)

Figure 5.7 - Photo of (a) PCPs (b) PCP Standard Specimen Before Casting

### 5.2.3. Remainder of Test Specimens

A review of previous research conducted on larger-diameter shear studs and push-out tests is included in Chapter 2. A brief review of key points is provided here. Past static push-out tests showed larger-diameter shear studs had inconsistent performance in static ultimate strength and ductility. (Badie, Tadros, et al. 2002, Shim, Lee and Yoon 2004, Lee, Shim and Chang 2005, Lin and Liu 2015, Hu, et al. 2020, Wang, et al. 2018). Key factors influencing the static ultimate strength are reported as transverse reinforcement ratio in the concrete deck (Shim, Lee and Yoon 2004, Badie, Tadros, et al. 2002), penetration depth of the shear stud into concrete deck (Shim, Lee and Yoon 2004), top concrete cover above the shear stud (Hu, et al. 2020), concrete compressive strength (Wang, et al. 2018), and shear stud layout (Lin and Liu 2015). Key factors influencing the ductility of shear studs were reported as concrete compressive and tensile strength (Wang, et al. 2018, Wang, et al. 2019, Hu, et al. 2020).

Findings from the literature review and input from the TxDOT project monitoring guided the design of the remainder of the test specimens, beyond the two standard specimens described above.

Table 5.1 provides the full test matrix for the static push-out tests. In the table, CIP means the concrete slab for this specimen is full-depth cast-in-place. PCP means partial depth precast concrete panels are used with a cast-in-place topping. Shear studs of two diameters were used, namely 7/8" and 1-1/8" diameters. For 1-1/8" diameter shear studs, three different stud layouts

were used, which are one stud per row without stagger, one stud per row with stagger, and two studs per row. For 7/8" studs, three studs per row were used.

As noted in Section 5.2.2, each specimen in the test matrix was derived from the two standard specimens. The difference between each specimen and the standard specimens is presented below, followed by a discussion on the purpose of each specimen.

Specimens No. 1 and No. 2 use 7/8" shear studs. Both specimens have three 7/8" diameter studs per row. The transverse spacing of the shear studs is 4 times the diameter which is equal to 3.5". For Specimen No. 2, the space between the PCPs was not enough for three 7/8" diameter studs. Therefore, the two outside studs were bent inward using a hammer. The clear distance between the outside studs and the PCPs was 5/8" after bending, which satisfies TxDOT design requirements (TxDOT 2019a). A photo of Specimen No. 2 before casting is in Figure 5.8. Other aspects of Specimens No. 1 and No. 2 are the same with the CIP and PCP standard specimens, respectively.



*Figure 5.8 - Shear Studs Bent Inward in Specimen No. 2*

Specimen No. 1 was considered as a reference specimen. It is intended to represent current practice using 7/8" studs. The results from other specimens can be compared with it to evaluate the relative performance. Figure 5.9 shows the details of Specimen No. 1. Specimen No. 2 is used to study the performance of 7/8" studs when PCPs are used. Based on the literature review, no previous push out tests using the partial depth PCPs were identified. Figure 5.10 shows the details of Specimen No. 2. The cast-in-place concrete in Figure 5.10 is shaded in blue and reinforcement from the PCPs is omitted for clarity.



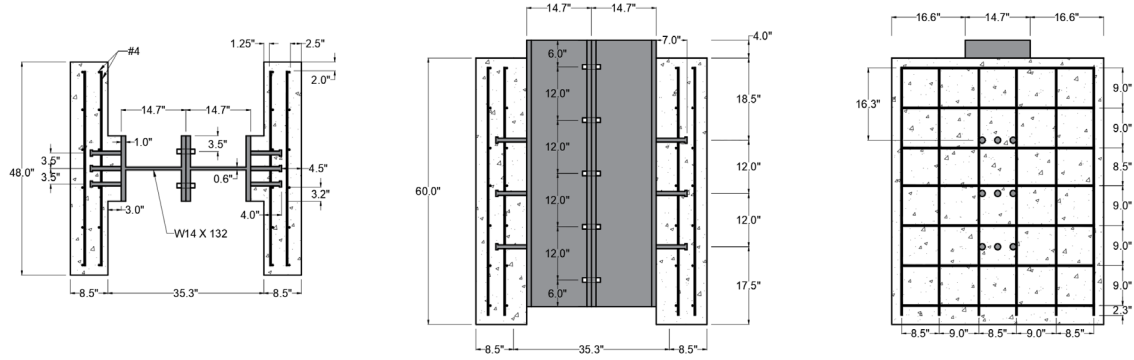


Figure 5.9 - Details for Specimen No. 1, Three 7/8" Studs Per Row, Fully CIP

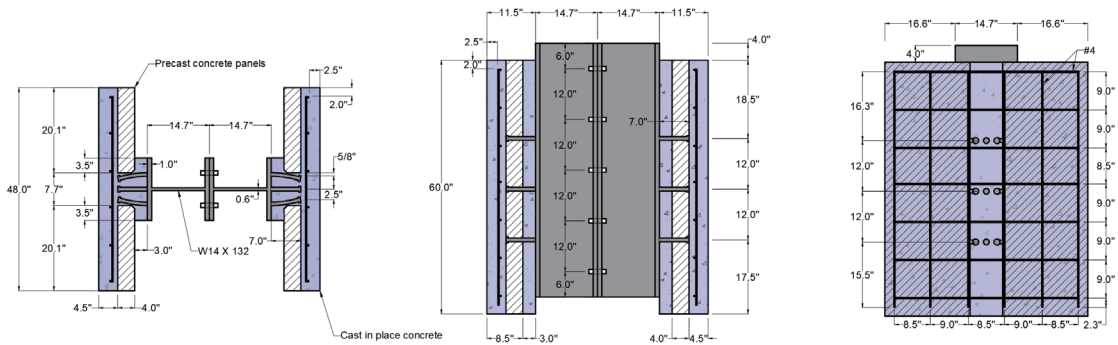


Figure 5.10 - Details for Specimen No. 2, Three 7/8" Studs Per Row, PCP

Specimen No. 3 has the same design as the standard CIP specimen except it has one 1-1/8" diameter shear stud per row without stagger. Specimen No. 3 provides a different stud layout from the standard specimen to evaluate the impact of this change in layout. Specimen No. 4 is the PCP standard specimen described earlier. Details of Specimen No. 3 and No. 4 are provided in Figure 5.11 and Figure 5.5.

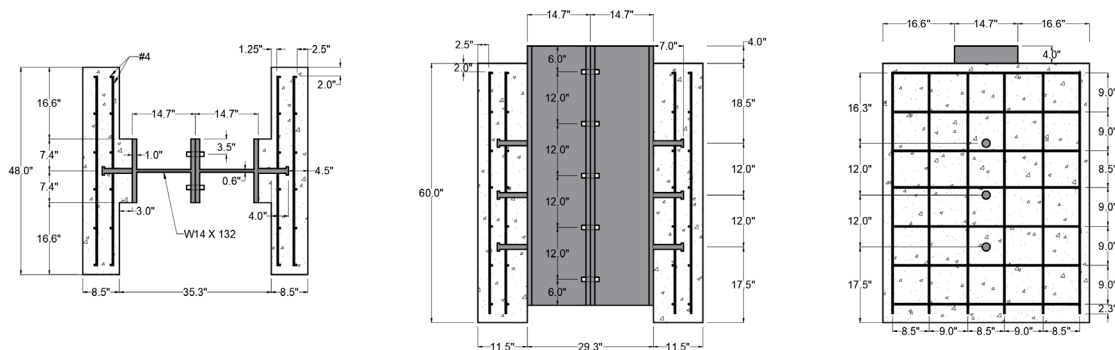


Figure 5.11 - Details for Specimen No. 3, One 1-1/8" Stud Per Row, No Stagger, Fully CIP

Specimens No. 5 and No. 6 have one stud per row with a staggered stud layout with fully CIP concrete deck and with PCPs, respectively. As shown Figure 5.12, the staggered layout means that shear studs are placed in a zigzag pattern and have four rows on each steel beam flange. The horizontal spacing between adjacent studs is 3 times the diameter, which equals 3.375". The staggered layout is intended to better spread the load transfer between studs and the concrete deck, as compared to a single line of studs without stagger. That is, the staggered layout avoids having a straight line of studs in the concrete deck that may create a crack along the length of the girder along the single line of studs. The horizontal distance of 3 times the stud diameter was chosen based on judgement. A photo showing a girder with a staggered layout of studs is in Figure 5.14. The details of Specimens No. 5 and No. 6 are in Figure 5.12 and Figure 5.13. The CIP concrete is shaded in blue and the reinforcement from the PCPs is omitted in Figure 5.13.

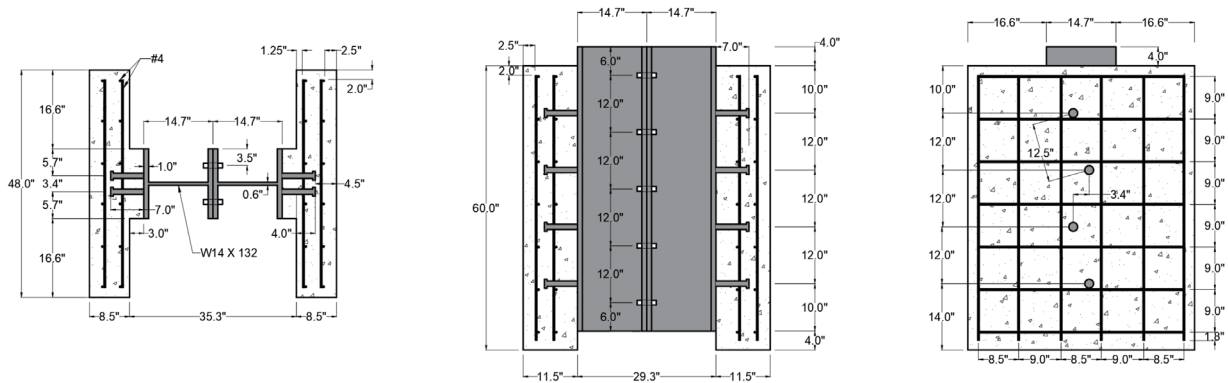


Figure 5.12 - Details for Specimen No. 5, One 1-1/8" Stud Per Row, Staggered Layout, Fully CIP

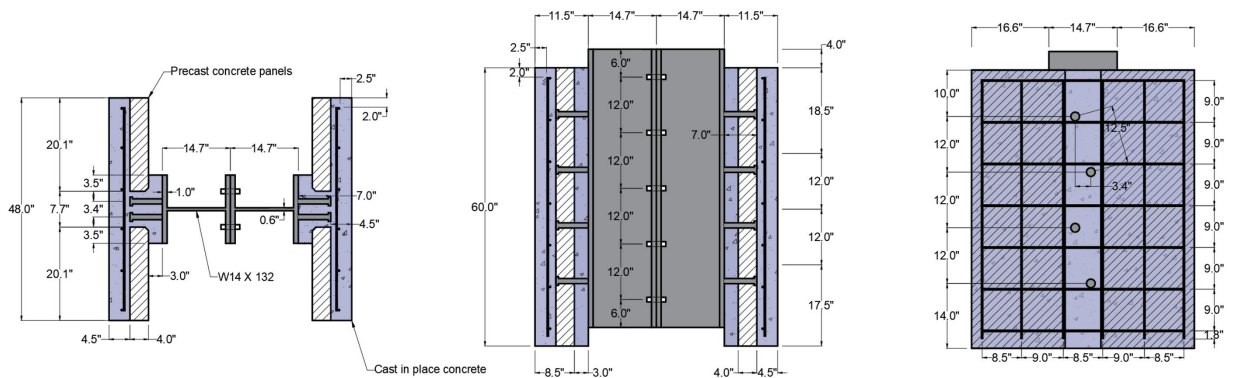


Figure 5.13 - Details for Specimen No. 6, One 1-1/8" stud Per Row, Staggered Layout, PCP





Figure 5.14 - Steel Girder for Specimen No. 5 with Staggered Layout of Shear Studs

Specimens No. 7 to No. 11 are all fully CIP specimens and have two 1-1/8" shear studs per row. Specimen No. 7 is the same as the standard CIP specimen and provides information on stud strength and ductility when two 1-1/8" shear studs per row is used. The details of Specimen No. 7 are shown in

Figure 5.3. Specimens No. 8 to No. 11 are called *special detailing specimens*. This group of specimens was used to study various factors that may influence the static performance of 1-1/8" shear studs.

Specimen No. 8 has two layers of #4@18" transverse reinforcement in the concrete deck, which is 50% less than that in the standard CIP specimen (Specimen No. 7). Preliminary tests showed #4@9" transverse reinforcement is enough to develop the full static strength and ductility of 1-1/8" shear studs. Specimen No. 8 was designed to get insights into the effects of the lower transverse reinforcement ratio on stud static loading behavior. In Figure 5.15, the top view of Specimen No. 8 is compared with the standard CIP specimen.

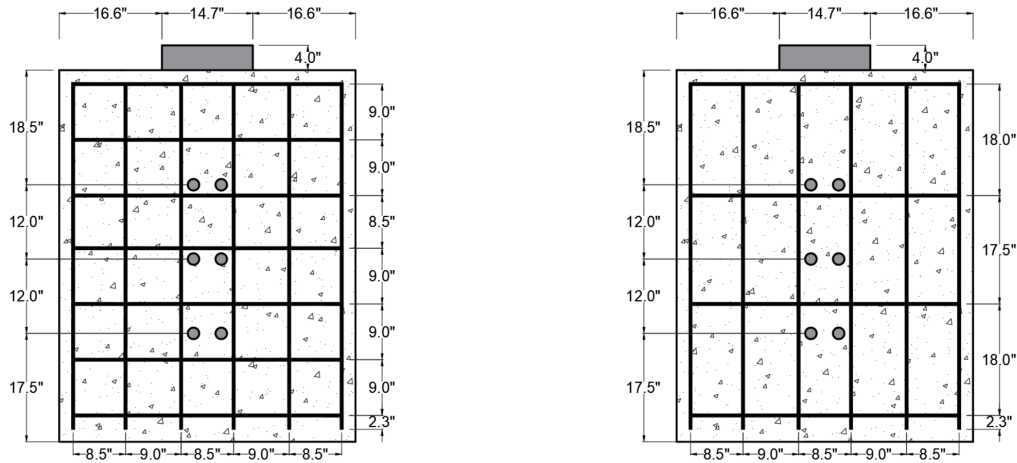


Figure 5.15 - Comparison of Standard CIP Specimen (Specimen No. 7, Left) with Specimen No. 8 (Right)

Specimen No. 9 was used to study the influence of stud penetration into the concrete deck. By using 5" long shear studs, the stud penetration into the concrete deck in Specimen No. 9 is 2", which is the smallest value allowed in the 9<sup>th</sup> Ed. AASHTO and TxDOT design requirements (TxDOT 2019a). The top of stud is now at the same level with the bottom mat reinforcement and does not penetrate any continuous reinforcement whereas the shear stud in standard CIP specimen, with a 4" penetration into the deck, extends 2.5" above the bottom mat of steel reinforcement. Photos of Specimen No. 5 and the standard CIP specimen are shown in Figure 5.17 to illustrate this point. In Figure 5.16, the cross-section of Specimen No. 9 is compared with the standard specimen.

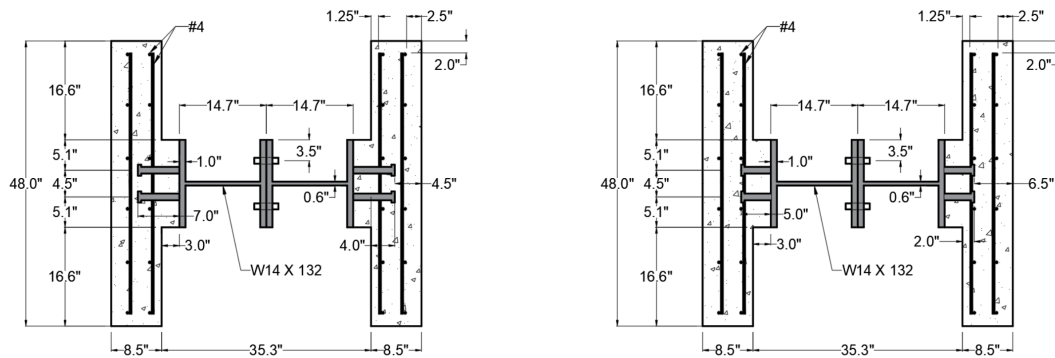


Figure 5.16 - Comparison of Standard CIP Specimen (Specimen No. 7, Left) with Specimen No. 9 (Right)



(a)



(b)

Figure 5.17 - Photos of (a) Specimen No. 9 (5" Long Stud) Before Casting (b) Standard CIP Specimen (7" Long Stud) Before Casting

Specimen No. 10 uses a 1" deep haunch to achieve a small top concrete cover above the 1-1/8" shear studs to investigate the influence of concrete cover. As shown in Figure 5.18, the top cover is 2.5" in Specimen No. 10, which is the minimum allowable value in TxDOT design standards (TxDOT 2019a). The smallest value for clear cover at the top of the deck in the 9<sup>th</sup> Ed. AASHTO is 2". Figure 5.18 shows a comparison between the cross-section of the standard CIP specimen and Specimen No. 10. In comparison, the top clear cover in the standard CIP specimen is 4.5".

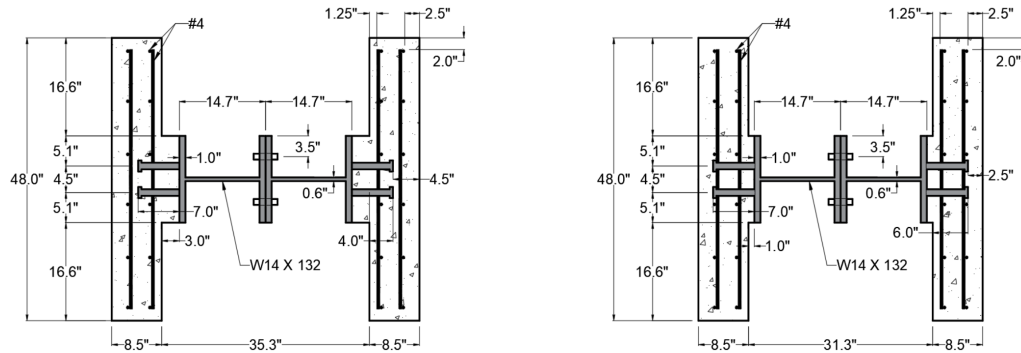


Figure 5.18 Comparison of Standard CIP Specimen (Specimen No. 7, Left) with Specimen No. 10 (Right)

Specimen No. 11 uses a W14 × 99 steel beam instead of a W14 × 132. The W14 × 99 has a flange thickness equal to 0.75", compared to a flange thickness of 1" for the W14 × 132. The 0.75" flange thickness in the W14 × 99 coincides with the minimum flange thickness recommended in Texas bridges (TxDOT 2021). This specimen was proposed to address the concern that when 1-1/8" diameter shear studs are used on top of a thin flange, the force

transferred from the stud into the beam flange may cause localized bending of the flange. Cross-section comparisons between the standard CIP specimen and Specimen No. 11 are given in Figure 5.19.

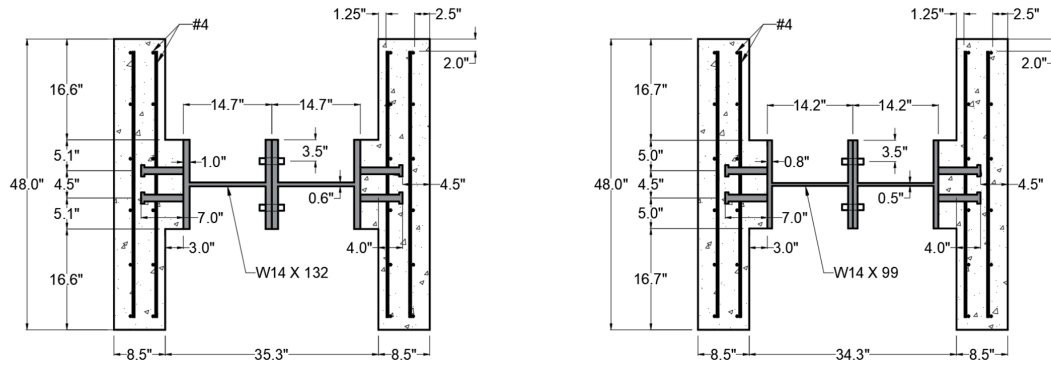


Figure 5.19 - Comparison of Standard CIP Specimen (Specimen No. 7, Left) with Specimen No. 11 (Right)

Table 5.2 lists the total number of studs used in each specimen. This total includes studs in each of the two slabs of a specimen. Later in this chapter, when the results of the push-out tests are reported, the average load per stud will be computed by taking the total load on the test specimen and dividing by the total number of studs, as listed in Table 5.2

Table 5.2 - Total Number of Studs in Each Push-Out Specimen

Specimen No.	Total Number of Studs in Specimen
1	18
2	18
3	6
4	6
5	8
6	8
7	12
8	12
9	12
10	12
11	12

## 5.3. Test Setup, Specimen Fabrication, and Instrumentation

### 5.3.1. Test Setup

The test setup for the push-out tests consisted of a self-reacting frame, loading assembly, and lateral support system. Figure 5.20 provides a 3D schematic of the test setup and its components. The setup has two bays allowing two specimens being placed inside simultaneously. The test setup was primarily designed and constructed by the research team for TxDOT Research Project 0-7016 – *Develop Guidance for Structural Behavior of Tall Haunches in TxDOT Beam and Girder Bridges*. Project 0-7016 also conducted an extensive series of static push-out tests, and the test setup was designed to accommodate the testing needs both of Project 0-7016 and 0-7042, and was shared among these two projects.

In Figure 5.20, components enclosed in the solid line box (gray color) make up the self-reacting frame. The self-reacting frame consists of six W12×72 columns, three W14×132 supporting girders, eight W18×130 coped beams, and two W30×211 load beams. The load capacity of the frame is 1600 kips per specimen, which is controlled by the bearing strength of the A490 bolts connecting the coped beams and columns.

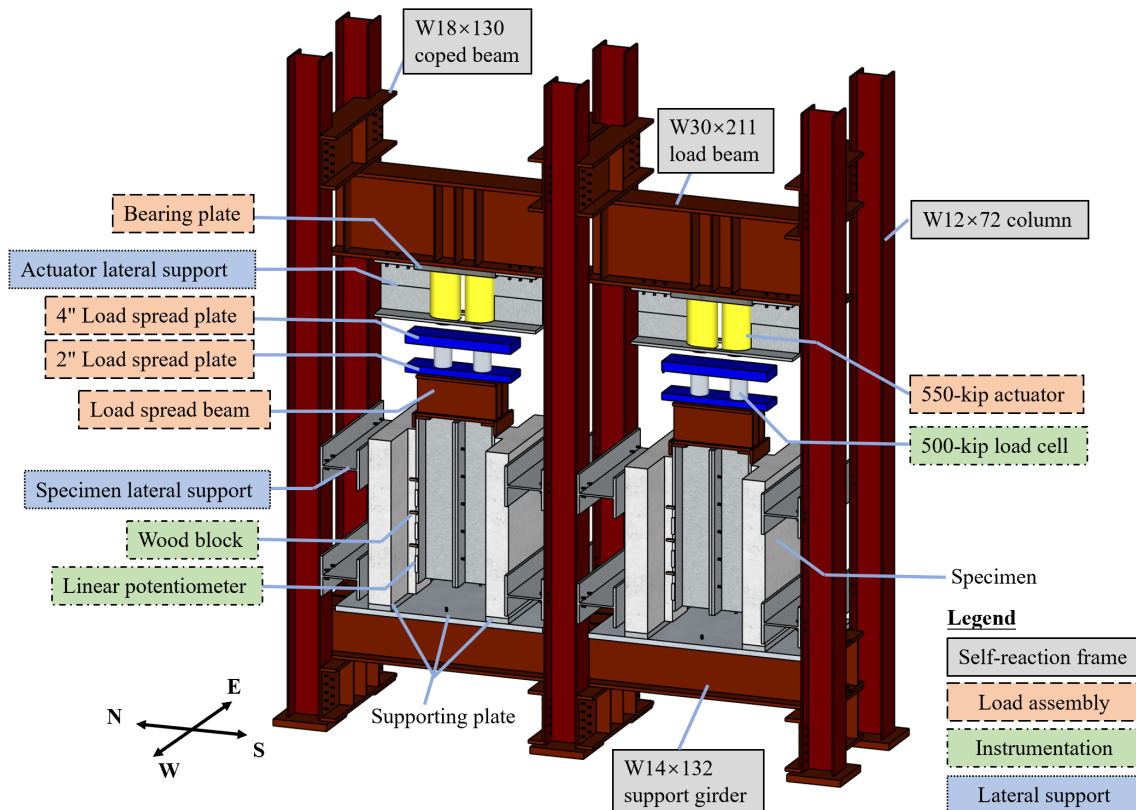


Figure 5.20 - 3D Schematic of Test-Setup and the Components



The load assembly consisted of a 2" bearing plate, two 550-kip actuators, a 4" thick load spreader plate, a 2" thick load spreader plate, and a W14×132 load spreader beam. These components are enclosed in the dash line boxes (orange color) in Figure 5.20. Preliminary analysis indicated the strongest specimen had a strength of about 900 kips. Therefore, two 550-kip actuators were used. The actuators are connected to the W30×211 load beam with a bearing plate. The 4" thick load spreader plate is used to transfer the point load from the actuators to top of load cells. The 2" thick load spreader plate transfers the load from the load cells to the top of the spreader beam. The spreader beam is in contact with the specimen at the steel beam outer flanges only (the flanges in contact with the concrete slabs), to minimize the moment in the specimen caused by the moment arm between the applied load and reaction force at the base of the concrete slabs. Safety measures as shown in Figure 5.21 were provided between the load assembly and the W30×211 load beam to prevent portions of the loading assembly from falling out of the test setup.



*Figure 5.21 - Photo of Specimens in the Test Setup with Enlarged View of the Haunch Bottom - Safety Measures for Load Assembly Can Be Seen (With Arrows) Between 4" Thick Load Spreader Plate and W30×211 Load Beam*

Initial tests demonstrated a potential safety hazard if no lateral support is provided for the actuators. When shear stud failure occurs, movement in the specimen transfers through the load assembly and can break the connection between the actuators and the W30×211 load beam, causing failure of the test setup. Components of the lateral support system are shown in Figure 5.20 in dotted line boxes (in blue color). The lateral support system has two parts. These are the actuator lateral support and the specimen lateral support. The actuator lateral was fabricated from one W14×132 beam where the middle part is cut to accommodate the actuators. In Figure 5.22, gaps between the lateral support and the actuator on the left are filled by Devcon 10210 epoxy. All gaps were filled with epoxy to minimize lateral movement of the actuators. Lateral support of each specimen consisted of four W14×132 girders bolted on to the frame columns, which prevented excessive movement of the specimen at failure of the shear studs.



*Figure 5.22 - Epoxy is Used to Fill the Gap Between Actuators and Lateral Support*

The specimen sits on two supporting plates where the haunch is not vertically supported, as shown in Figure 5.21. In the static tests, the two 550-kip actuators were connected to one hydraulic oil pump powered by air pressure, shown in Figure 5.23. The pump can output a maximum pressure of 10,000 psi to each actuator. One actuator will exert 550 kips when 10,000 ksi pressure is reached.



Figure 5.23 - Air Powered Hydraulic Pump

### 5.3.2. Specimen Fabrication

Shear studs were welded to the steel beams using the welding parameters established in the welding investigation described in Chapter 4, and are listed below in Table 5.3. Ferrules used in welding were examined to have no defects. Two welding trials and two 90° bend tests were performed each time before welding the studs for the specimens. All bend tests for 1-1/8" studs were performed on the flange of steel girders. The steel girders used for stud bend tests were the same size (W14×132) as those used in push-out specimens, but were not used in the push-out specimens. All bend tests for 7/8" studs were performed on 1'×1' ASTM A709 Grade 50W steel plate of 1" thickness. Figure 5.24 shows the 90° bend test result for 7/8" studs and 1-1/8" studs.

Table 5.3 - Stud Welding Parameters used for Push-out Specimens

Specimen Nos.	Stud Diameter (in)	Current (amps)	Time (s)	Plunge (in)	Lift (in)	Polarity
1-2	7/8	1700	1.0	1/4	3/16	Straight
3-11	1-1/8	2250	1.55	5/16	1/4	Reverse

Note: No surface preparation and no cable looping were used





(a)



(b)

*Figure 5.24 - 90° Bend Tests on (a) 7/8" Studs on 1'x1' Plate (b) 1-1/8" Studs on W14x132 girder Flange*

Figure 5.25 provides a 3D illustration and cross-section view of the casting formwork. Photos describing the specimen fabrication process are given in Figure 5.26. The formwork consists of two steel side pieces and several wood dividers. The presence of the steel side pieces allowed all PCP specimens to be cast without using bedding strips. Two specimens (four half-specimens) can be cast at the same time and all concrete is cast horizontally, as it is in an actual bridge deck. Slump tests were performed before casting and water was added to concrete mix, if needed, until the slump was at least 4". The two halves of one specimen were always cast at the same time. For specimens with PCPs, prior to placement of the cast-in-place concrete, the PCP surface was thoroughly wet but had no free-standing water.

Concrete cylinder strength tests showed the concrete developed a compressive strength over 3 ksi within 3 days, allowing the specimens to be safely lifted out of the formwork. Therefore, specimens were typically removed from the formwork 3 days after casting and then cured in an outdoor environment. Grease was applied between the formwork and the concrete to help remove the specimen. No grease was applied between the steel girder and the concrete haunch.

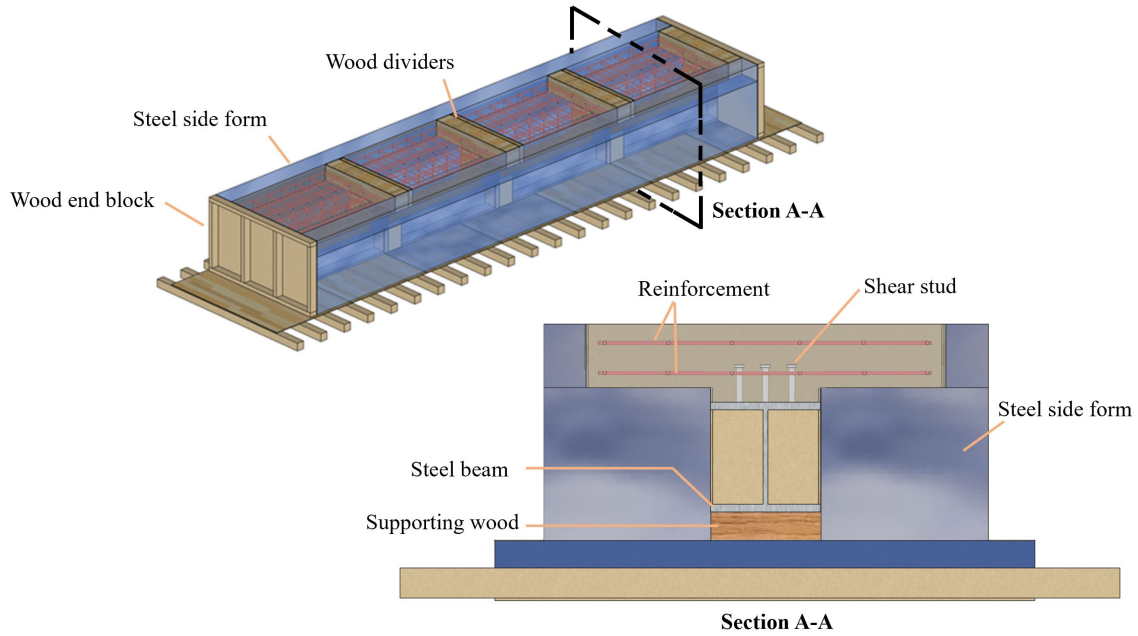


Figure 5.25 - 3D Schematic of Casting Formwork



Figure 5.26 - Fabrication Process for Specimen (1) Steel Beam and Reinforcement Placed in the Formwork (2) Concrete Being Cast and Vibrated (3) Concrete Being Cured Inside the Formwork (4) Specimens Removed from the Formwork

### 5.3.3. Instrumentation

Instrumentation used for the static push-out tests are enclosed in the dash-dot boxes (in green color) in Figure 5.20. Load was measured by two 500-kip load cells that were placed symmetrically with respect to the middle plane of the specimen. The difference in the two load cell readings was taken as the load difference in the north and south sides of the specimen, namely the load eccentricity. The relative displacement between the steel beam flange and the haunch was measured, and is also referred to as the slip between the steel beam flange and the concrete haunch. The slip was measured by eight linear potentiometers (LP) in Specimen No. 5 and No. 6. Six LPs were used in all other specimens. The LPs were mounted on the steel beam flange with double sided tape. A wood block was attached to the concrete haunch by glue and kept the tip of the LP always at the same height of shear studs during the tests. Figure 5.27 and Figure 5.28 illustrate the location of the LPs and the wood blocks. Photos of the LPs are provided in Figure 5.29.

The shear force on a stud was computed by dividing the total applied load on the specimen by the number of studs (see Table 5.1). This assumes that the studs share the applied load equally and that no load is transferred from the steel beam to the concrete slab by friction. Neither of these assumptions is likely correct, as it is shown later by the deformation of shear stud after the test and by the finite element simulations of the push-out tests in Chapter 7. Nonetheless, this method of computing the shear force applied to a stud is consistent with past push-out tests that form the basis of the shear stud strength provisions in the AASHTO LRFD Bridge Design Specifications. The slip in load-slip curves was derived by averaging the reading from all working LPs. It is important to note that LP readings are sensitive to the horizontal cracks in the haunch regions. Ideally, slip should only reflect the relative deformation of the steel beam and the concrete slab resulting from deformation of the shear stud and/or localized deformation of the concrete in the region of the shear stud. In this study, a contribution to the LP readings also occurred due to cracks opening in the concrete haunch. Therefore, the slip measurements tended to be larger than the actual deformation of the stud and the localized deformations of the concrete at the stud. Further, the wider the crack opens; the larger the overestimation will be in the slip measurement.

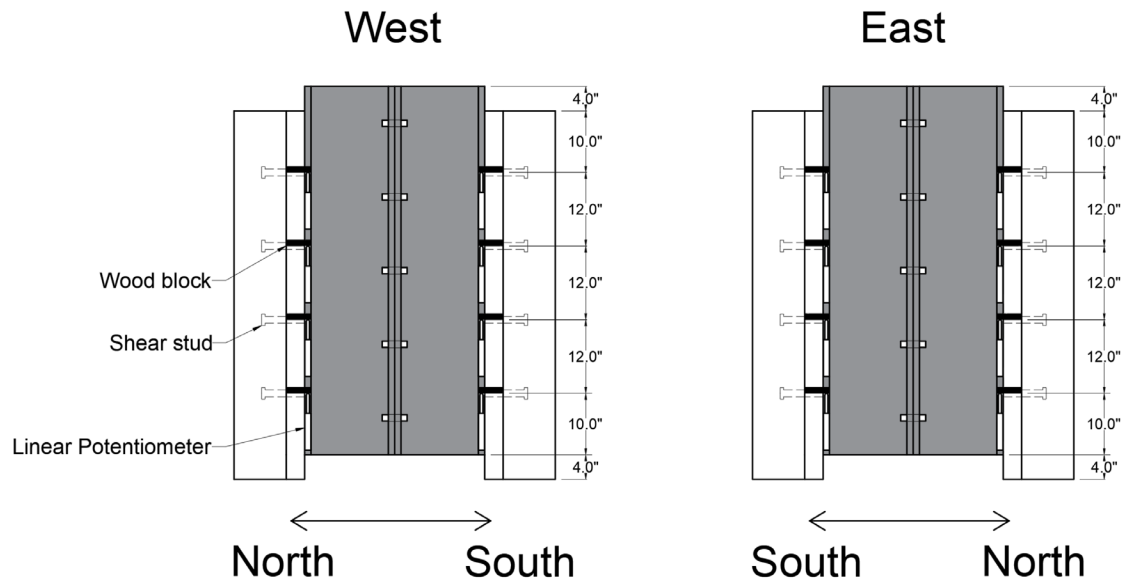


Figure 5.27 - Location of LPs and Wood Blocks on Specimen No. 5 and Specimen No. 6

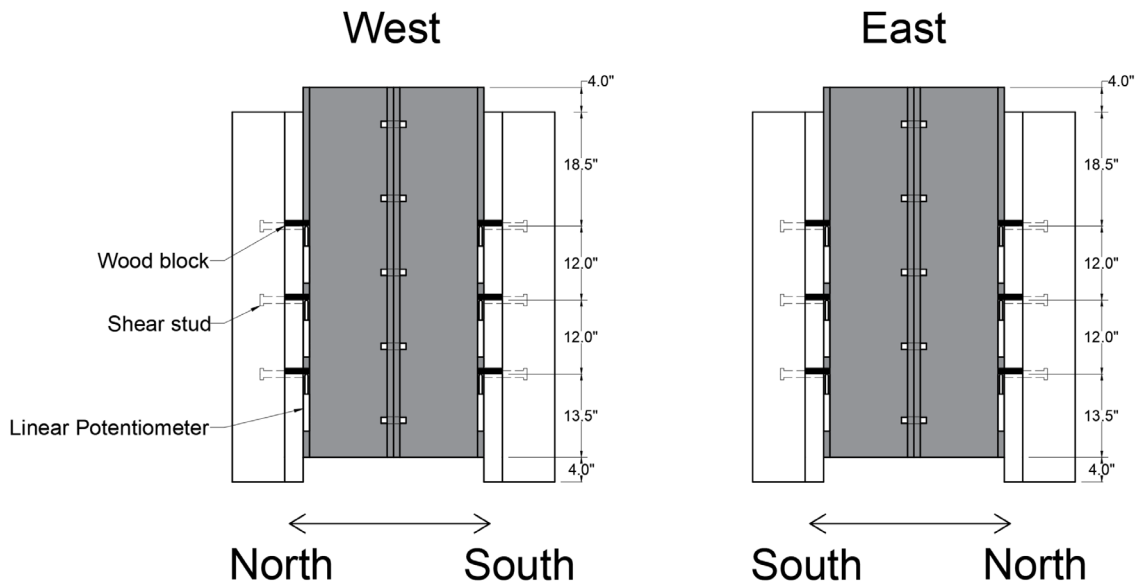


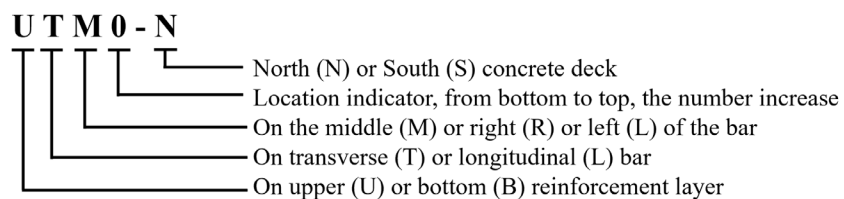
Figure 5.28 - Location of LPs and Wood Blocks on Specimens other than Specimen No. 5 and No. 6.



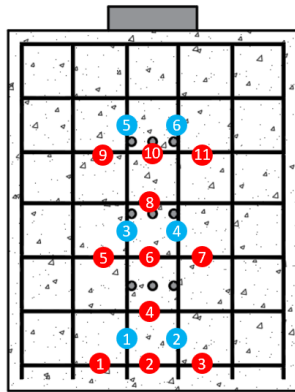


Figure 5.29 - Photo of LPs and the Wood Blocks on Specimen No. 11

Strain gauges were used in all CIP specimens except Specimen No. 10 and No. 11. The designation of each gauge was as follows:



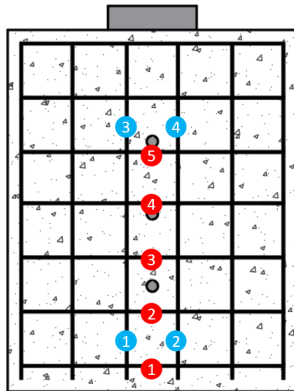
Strain gauge configurations and notation are shown for each specimen in Figure 5.30 to Figure 5.34. In these figures, gauges are only shown for upper layer of the reinforcement mesh. The bottom mesh shares the same gauge layout. In addition, the strain gauge arrangement in the north and south concrete decks are identical.



Specimen #1

Gauge ID	Notation	Gauge ID	Notation
1 (R)	(B)UTL0-N(S)	10 (R)	(B)UTM4-N(S)
2 (R)	(B)UTM0-N(S)	11 (R)	(B)UTR4-N(S)
3 (R)	(B)UTR0-N(S)	1 (B)	(B)ULL0-N(S)
4 (R)	(B)UTM1-N(S)	2 (B)	(B)ULR0-N(S)
5 (R)	(B)UTL2-N(S)	3 (B)	(B)ULL1-N(S)
6 (R)	(B)UTM2-N(S)	4 (B)	(B)ULR1-N(S)
7 (R)	(B)UTR2-N(S)	5 (B)	(B)ULL2-N(S)
8 (R)	(B)UTM3-N(S)	6 (B)	(B)ULR2-N(S)
9 (R)	(B)UTL4-N(S)		

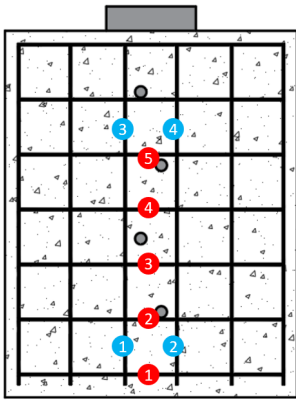
Figure 5.30 - Strain Gauge Locations and Notations for Specimen No. 1



Specimen #3

Gauge ID	Notation	Gauge ID	Notation
1 (R)	(B)UTM0-N(S)	1 (B)	(B)ULL0-N(S)
2 (R)	(B)UTM1-N(S)	2 (B)	(B)ULR0-N(S)
3 (R)	(B)UTM2-N(S)	3 (B)	(B)ULL1-N(S)
4 (R)	(B)UTM3-N(S)	4 (B)	(B)ULR1-N(S)
5 (R)	(B)UTM4-N(S)		

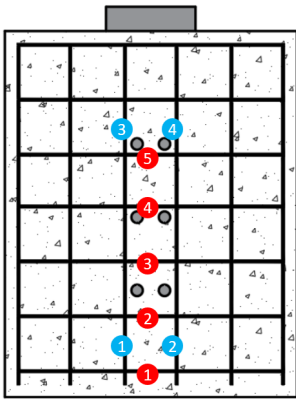
Figure 5.31 - Strain Gauge Locations and Notations for Specimen No. 3



Specimen #5

Gauge ID	Notation	Gauge ID	Notation
1 (R)	(B)UTM0-N(S)	1 (B)	(B)ULL0-N(S)
2 (R)	(B)UTM1-N(S)	2 (B)	(B)ULR0-N(S)
3 (R)	(B)UTM2-N(S)	3 (B)	(B)ULL1-N(S)
4 (R)	(B)UTM3-N(S)	4 (B)	(B)ULR1-N(S)
5 (R)	(B)UTM4-N(S)		

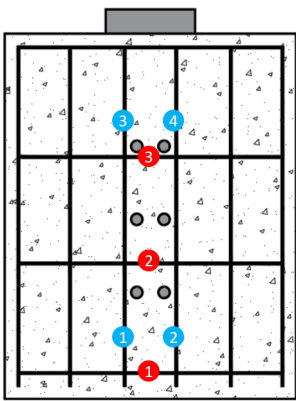
Figure 5.32 - Strain Gauge Locations and Notations for Specimen No. 5



Specimen #7 & #9

Gauge ID	Notation	Gauge ID	Notation
1 (R)	(B)UTM0-N(S)	1 (B)	(B)ULL0-N(S)
2 (R)	(B)UTM1-N(S)	2 (B)	(B)ULR0-N(S)
3 (R)	(B)UTM2-N(S)	3 (B)	(B)ULL1-N(S)
4 (R)	(B)UTM3-N(S)	4 (B)	(B)ULR1-N(S)
5 (R)	(B)UTM4-N(S)		

Figure 5.33 - Strain Gauge Locations and Notations for Specimen No. 7 and No. 9



Specimen #8

Gauge ID	Notation	Gauge ID	Notation
1 (R)	(B)UTM0-N(S)	1 (B)	(B)ULL0-N(S)
2 (R)	(B)UTM1-N(S)	2 (B)	(B)ULR0-N(S)
3 (R)	(B)UTM2-N(S)	3 (B)	(B)ULL1-N(S)
		4 (B)	(B)ULR1-N(S)

Figure 5.34 - Strain Gauge Locations and Notations for Specimen No. 8



## 5.4. Material Properties

### 5.4.1. Shear Studs

Table 5.4 lists the dimensions of the shear studs used in the push-out specimens. All studs and ferrules were supplied by Nelson. All studs of a given diameter and length came from the same production lot. The 7/8" and 1-1/8" studs (7" long) were from the same production lots as the studs used in the stud welding investigation reported in Chapter 4.

For each size stud, tension coupon tests were conducted to establish the stress-strain curve and the yield stress, ultimate tensile strength and elongation of the stud material. The test procedure is described in Section 4.4.2. Results for the 7/8" and 1-1/8" studs (7" long) were reported in Section 4.4.2. (See Figure 4.11 and Figure 4.13). The stress-strain curves for the 5" long 1-1/8" studs were not reported in Section 4.4.2, and are shown in Figure 5.35.

**Table 5.4 - Dimensions of Shear Studs Used in Push-Out Specimens**

Specimen Nos.	Stud Diameter (in)	Stud Length After Welding (in.)	Stud Length Before Welding (in.)	Stud Head Diameter (in)	Stud Head Height (in)
1-2	7/8	7	7-3/16	1-3/8	7/16
3-8, 10, 11	1-1/8	7	7-5/16	1-7/8	9/16
9	1-1/8	5	5-5/16	1-7/8	9/16

The measured yield stress, tensile strength and elongation (strain at fracture) for each diameter and length of stud used in the push-out tests is listed in Table 5.5. Four coupons were tested for each diameter and length of stud. The dynamic yield and ultimate strength refer to the values measured while the machine cross-heads were in motion at the rate of 0.02 inches per minute. The lowest value for dynamic yielding stress range among all tension coupons from each type of shear stud was taken as the dynamic yielding value. The average of tensile strength values was taken as the dynamic ultimate strength. The failure point in the stress-strain curve was determined by averaging the tensile fracture point of each coupon for studs of same type. The tension coupons showed tensile strength values (static and dynamic) greater than 60 ksi, as required by AWS D1.5. However, none of the studs satisfied the elongation requirement of 20 percent specified in AWS D1.5.

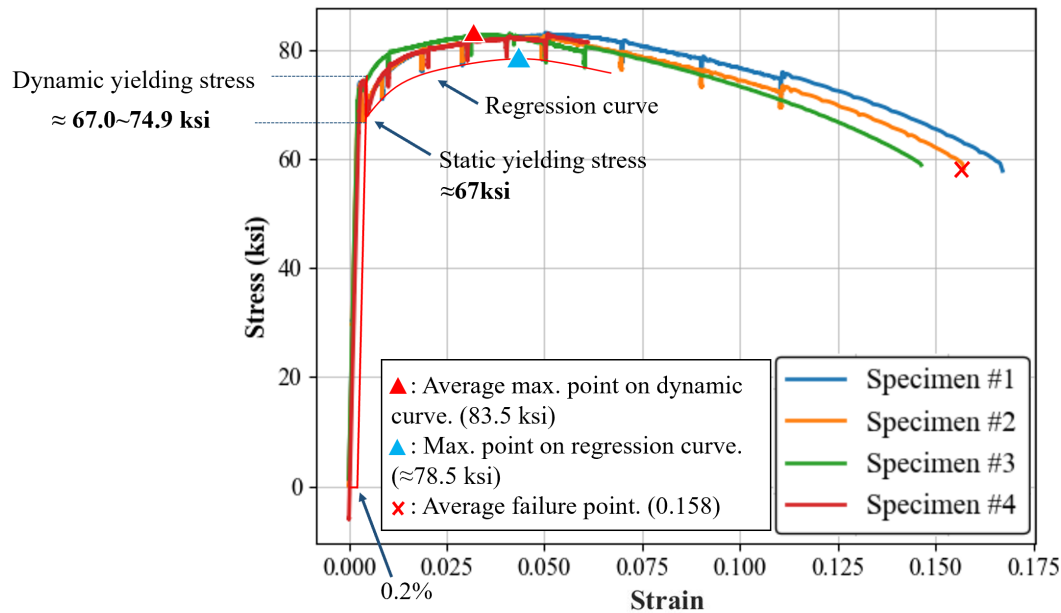


Figure 5.35 - Stress-Strain Curves for 5" Long 1-1/8" Diameters Stud Coupons

Table 5.5 - Tension Coupon Test Results for Studs Used in Push-out Specimens

Specimen Nos.	Stud Diameter and Length	Dynamic Yield Stress (ksi)	Static Yield Stress (ksi)	Dynamic Tensile Strength (ksi)	Static Tensile Strength (ksi)	Elongation (Strain at Fracture) (%)
1-2	7/8" dia. 7" length	61	59	75.2	70	17.5
3-8,10,11	1-1/8" dia. 7" length	75	74	83.5	76	15.4
9	1-1/8" dia. 5" length	67	67	83.5	83	15.8

### 5.4.2. Steel Reinforcement and Steel Girders

ASTM A615 Grade 60 #4 reinforcing bars of two different lengths (44" and 56") were used in this study, as shown in Figure 5.36. Three bars of each length were tested in tension in a 220-kip MTS machine using a crosshead displacement rate of 0.1" per minute based on ASTM A370. No extensometer was used due to the limitations of available equipment. Like the tension coupon tests for the shear studs, static yielding strength was measured in the test. However, no regular strain increment could be used to control the test so the static strength test was done by pausing the crosshead movement manually for 2 minutes at certain axial displacements. Figure 5.37 shows stress versus crosshead displacement for the reinforcement with the data processing information.



Figure 5.36 - Reinforcing Bars Used in Push-Out Specimens

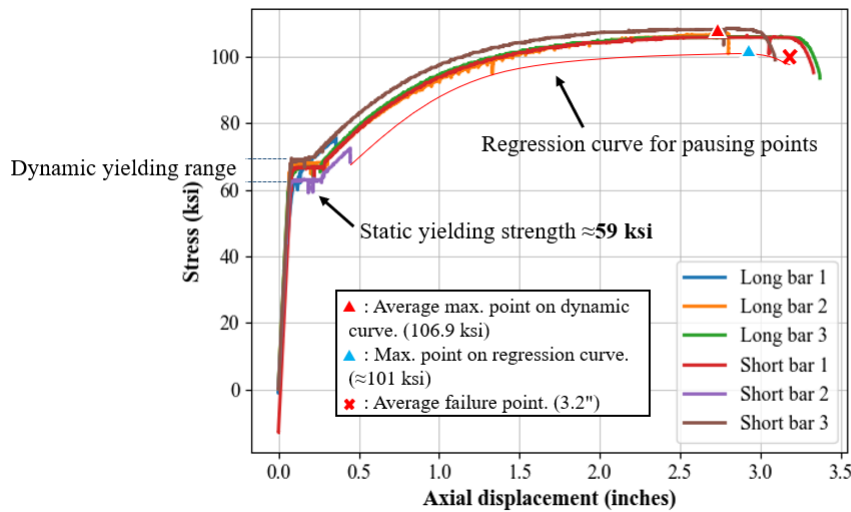


Figure 5.37 - Stress-Displacement Curves for Reinforcing Bars

It can be observed that the stress-displacement curves are similar for the 56" long (long bar) and 44" long (short bar) reinforcement. Therefore, the mechanical properties of the long bars and short bars are reported together. Stress-displacement response showed a clear yielding plateau so no 0.2% offset line was needed for determining yielding strength. The dynamic yielding strength was obtained by taking the average of the yielding plateau stresses. The tensile strength and ultimate displacement were obtained by averaging the maximum stress in the stress-displacement curves and the failure displacements, respectively. The lowest static yielding strength points (load dropping points on yielding plateau), which were obtained from specimen No. 2 of the short bars, was taken as the static yielding strength for the reinforcement. The static ultimate strength was obtained by curve fitting the lowest load dropping points after the plateau and finding the maximum point on this regression curve. It should be noted that four specimens were tested until fracture. Table 5.6 summarizes the mechanical properties for reinforcement used in the push-out specimens

**Table 5.6 - Tensile Properties for Reinforcement Used in Push-Out Specimens**

<b>Static Yield Stress (ksi)</b>	<b>Dynamic Yield Stress (ksi)</b>	<b>Static Tensile Strength (ksi)</b>	<b>Dynamic Tensile Strength (ksi)</b>
59.2	66.6	101.1	106.9

W14×132 and W14×99 steel girders of ASTM A992 steel were used in the push out test specimens. Mechanical properties for the two steel girders from certified mill test reports are listed in Table 5.7. W14×132 girders used in this project are made with four different heat numbers. Mill reports of each heat number were reviewed and Table 5.7 reports the smallest value. Tension coupon tests were not conducted for the girders, as they were for the studs, as the yield stress and tensile strength of the girders was not expected to play a role in the tests. That is, the girders are expected to remain essentially elastic in the push-out tests.

**Table 5.7 - Tensile Properties for Steel Girders (From Certified Mill Test Reports)**

<b>Steel Beam Section</b>	<b>Yield Stress (ksi)</b>	<b>Tensile Strength (ksi)</b>	<b>Elongation (%)</b>
W14×132	53.9	69.0	25.5
W14×99	55.0	72.0	27.0

### 5.4.3. Concrete Material Properties

TxDOT Class S concrete (TxDOT 2023) with a design compressive strength of 4 ksi was used for all push-out specimens. Concrete cylinders with 4" diameter were made when casting each specimen. For CIP concrete, strength tests were performed at 3-days, 7-days, 14-days, 21-days, and 28-days after casting and on the push-out test day. For PCP concrete, concrete strength tests were only performed on the push-out test day. Three concrete cylinders were tested for each strength test and then averaged. Based on ASTM C39, if the results from three cylinders had a variance more than 10%, more cylinders were tested until any three of them had a strength variance less than 10%. Then, the three with the highest average value were used. Table 5.8 provides the 28-day concrete strength and test day strength for the push-out specimens.

The top and bottom surfaces of concrete cylinders need preparation before running a compressive strength test. Most cylinders were prepared by the sulfur cap method (ASTM C617). Some cylinders were prepared with a grinding method. It was observed that the strength of the cylinder was related to the preparation method. The grinding method gave a smaller strength compared to the sulfur cap method.

**Table 5.8 - Concrete Strength for Push-Out Specimens**

Specimen No.	28-Day (psi)	Test Day CIP (psi)	Test Day PCP (psi)	Days from Casting to Push-Out Test Day
1	5383	5388	N/A	105
2	4293*	4647	7640	45
3	5090	5233	N/A	70
4	4535	4472	6825	71
5	4810	4721	N/A	27
6	4928	5105	6922	36
7	4537	4832	N/A	50
8	5500	5493*	N/A	53
9	4773	4758	N/A	44
10	5045	4213*	N/A	103
11	4475	4318	N/A	96

Note: \*: results obtained with cylinders prepared by the grinding method.

## 5.5. Test Procedures and Observations

The push-out tests always began with two relatively low loading cycles to check if the test setup and instrumentations were working properly. After the initial cycles, the specimens were loaded from zero load until the end of the test, which is called the *ramp loading stage* herein. Loading of the specimens was continued until failure of the shear studs, or until the load resistance of the specimen dropped 20% or more from the peak value. The static test used an air pressured hydraulic pump to control the loading. The loading rate was controlled manually by opening or closing an air pressure valve. The rate of loading was in the approximate range of 0.5 kips/sec to 1 kip/sec. As the peak resistance was reached and the load-slip curve flattened, loading was based on displacement (slip) control. The load eccentricity (difference between the readings of the two load cells) was monitored throughout each test. During the entire test program, the eccentricity was under 10%. The specimens were examined for the presence of cracks in the following circumstances: before the test began, after the initial two loading cycles, when the specimen emitted a sound, during the ramp loading, and after completion of the test. Unless noted otherwise, cracks found before the test are not shown in the crack mapping plots. A detailed description of the test process and observations is provided for each test in this section. A 3D schematic of a fully CIP push-out model is provided in Figure 5.38 to illustrate specimen surface notations that are used in the following sections.

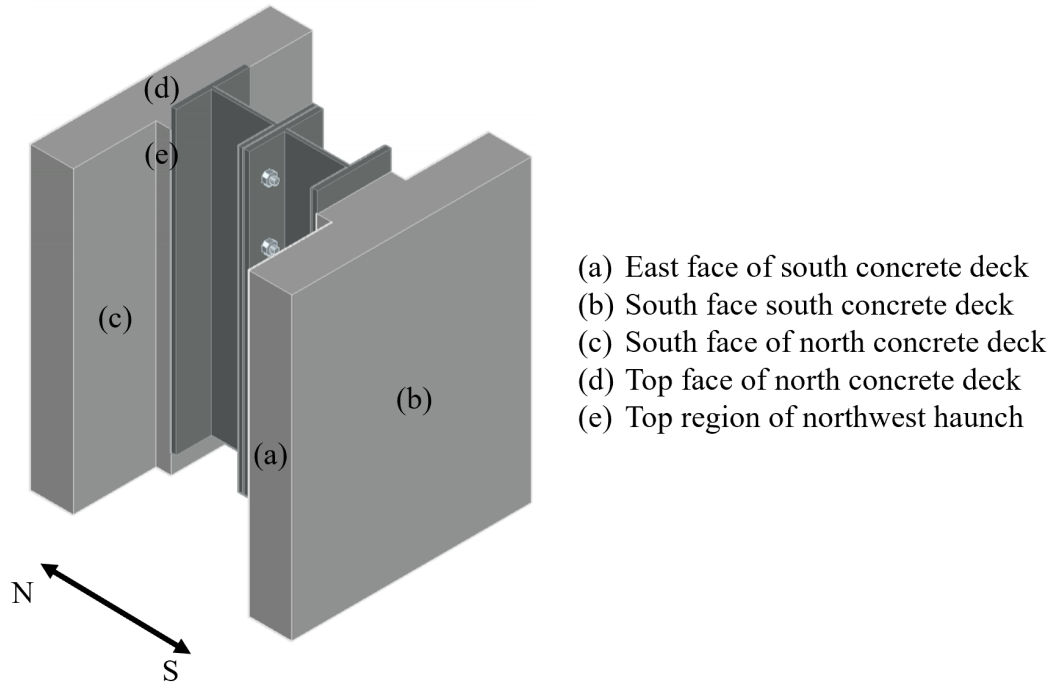


Figure 5.38 - Surface Notations on Push-Out Specimens

### 5.5.1. Specimen No. 1, Three 7/8" Studs Per Row, CIP

Two 0 to 150 kip cycles were performed at the beginning of the test. A sound was noticed in the first cycle when the load reached 150 kips and a sudden increase in LP readings was noticed although there was no drop in the load reading. Ramp loading began after these cycles. Loading was paused and cracks on the specimen were checked at 200 kips, 300 kips, 400 kips, 500 kips, and 600 kips. The first cracks were found at 400 kips in the northeast haunch near the top wood block and in northwest haunch at the top. More cracks developed in the haunch as the load increased. At 600 kips, concrete spalling was noticed on the top of the haunch on the northwest side, which is an indication of local compression force between the steel beam and the concrete. The specimen had no contact with the lateral support before failure. The specimen failed with shear stud fracture and both sides failed essentially simultaneously. Large pieces of concrete in the east haunch spalled off when the failure event occurred. No cracks were found on the west and east surfaces of the concrete deck. A mapping of the concrete damage and photos of the concrete spalling on the west and east surfaces are provided in Figure 5.39 for Specimen No. 1.

Photos showing the north concrete deck after failure and after removal of the steel beam are in Figure 5.40. The concrete is relatively intact with limited cracking and spalling and all shear studs embedded in the concrete are fractured. Close-up photos for the stud identified by the arrow are provided from two directions, one from the concrete side, the other from the steel beam side. The stud was fractured in the shank, and the fracture surface was smooth. Local



concrete crushing can be seen below each shear stud, on the side where the concrete is under compression.

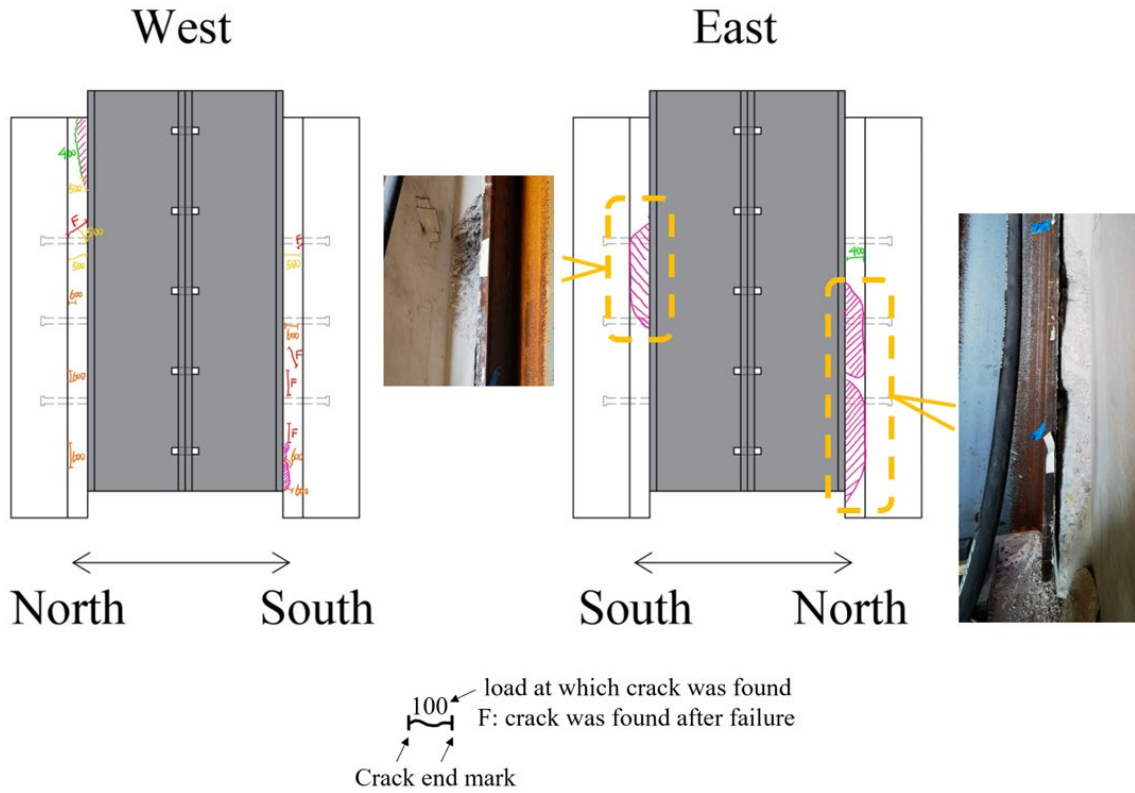


Figure 5.39 - Concrete Damage on Specimen No. 1

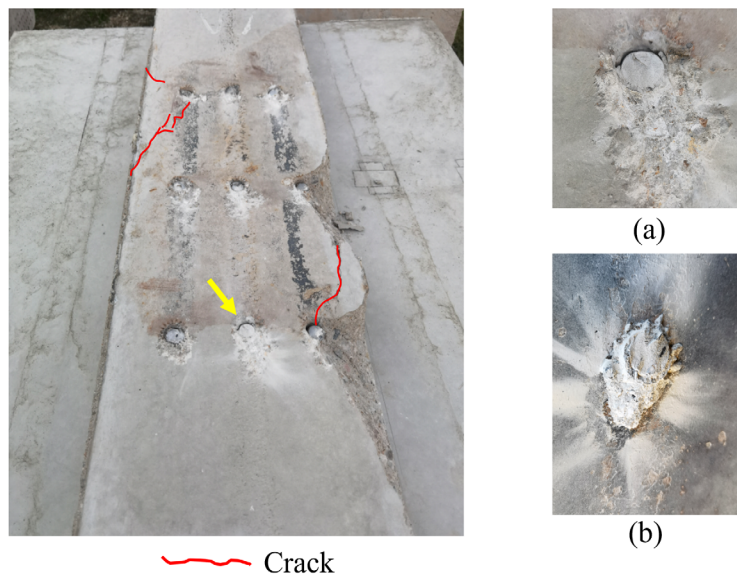


Figure 5.40 - Specimen No. 1: Concrete Deck After Failure with Enlarged Photos of the Stud Identified by the Arrow (a) Taken from Concrete Side (b) Taken from Steel Beam Flange Side



### 5.5.2. Specimen No. 2, Three 7/8" Studs Per Row, PCP

Small cracks were observed on the PCP surfaces before the test. Two load cycles were performed at the beginning of the test. The first cycle ranged from 0 to 150 kips. The second cycle ranged from 0 to 200 kips. Cracks were checked at the end of each loading cycle and the first crack was observed at 200 kips in the haunch region. During the ramp loading, cracks on the specimen were checked at 250 kips, 350 kips, 450 kips, and 550 kips. At 240 kips, a sound from the specimen was heard. At 284 kips, another sound was noticed. A sudden increase in the LP readings was noticed in both sound events but no load-drop occurred during either event. The cracks first observed at 200 kips widened during the test and a few more cracks were observed at 250 kips. No new cracks were observed until the failure. Large horizontal and splitting cracks were developed in the haunch region during the failure event. The specimen failed in a concrete controlled mode; that is, the shear studs did not fracture. The haunch concrete was displaced laterally from its original position due to splitting cracks in the middle portion of the CIP concrete directly over the steel beam. No cracks were observed at the west and east surfaces of the CIP concrete deck. Photos showing concrete damage are provided in Figure 5.41. A mapping of crack development is provided in Figure 5.42.

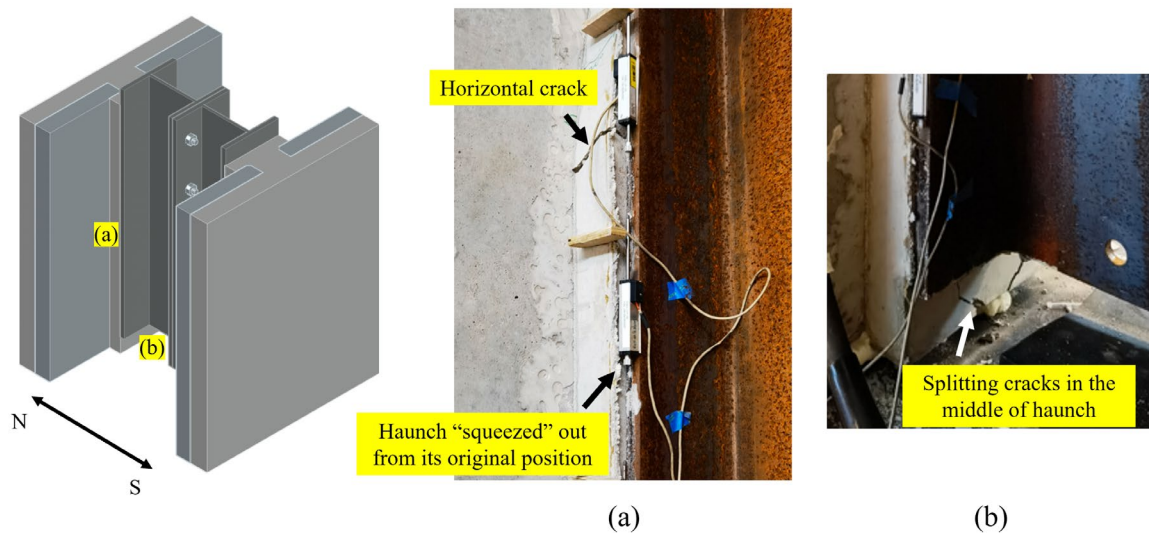


Figure 5.41 - Concrete Damage on Specimen No. 2. Location of Photos (a) and (b) are Shown in the Left Diagram

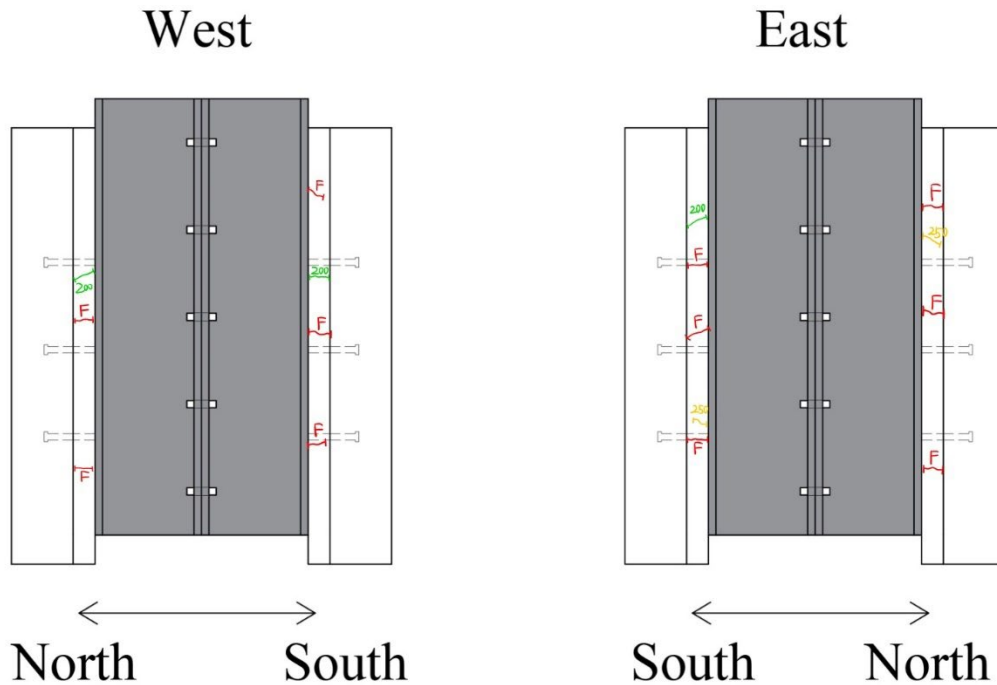


Figure 5.42 - Concrete Crack Mapping on Specimen No. 2

As mentioned earlier, readings of the LPs are sensitive to the concrete cracking in the haunch region. Figure 5.41 (a) can help illustrate this point. The wide horizontal crack in the haunch obviously contributes to the probe movement of the LP and thus leads to an overestimation in the slip readings.

### 5.5.3. Specimen No. 3, One 1-1/8" Stud Per Row, No Stagger, CIP

Two 0-to-50-kip load cycles were performed at the beginning of the test. Some cracks along the interface between the haunch and the concrete deck were observed after the two cycles and are believed to have developed before the test. These cracks did not widen during the test. Ramp loading was paused at 75 kips, 150 kips, 225 kips, 300 kips, 375 kips, and 450 kips to check for cracks on the specimen. The first and only crack on Specimen No. 3 was found at 375 kips between the top and middle wood blocks in the northwest haunch region. At 450 kips, contact between the lateral support and the specimen was observed, indicating horizontal and/or torsional movement in the specimen. But the load eccentricity was small and below 10%. The specimen failed with shear stud fracture and both sides failed essentially simultaneously. A mapping of crack development is provided in Figure 5.43. The north concrete deck after completion of the test is shown in Figure 5.44. As the enlarged photos show, the studs fractured in the shank with crushed concrete below each shear stud. The fracture surface of the stud appeared smooth. Almost no cracks were found in the concrete deck after the test.

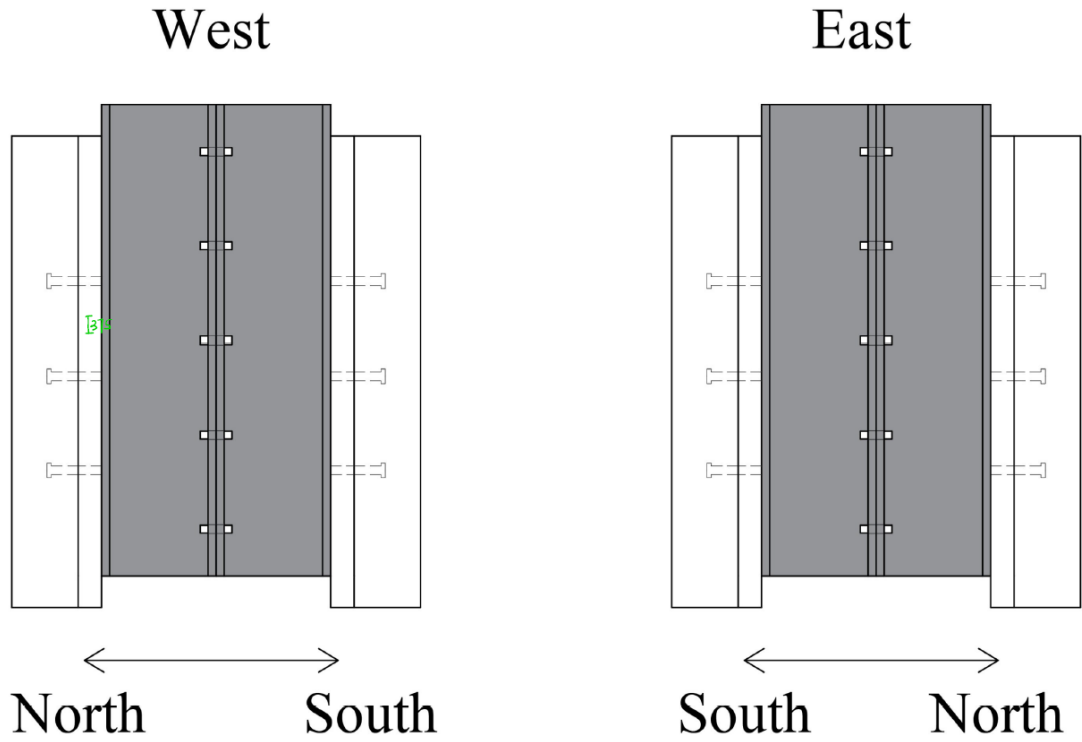


Figure 5.43 - Concrete Crack Mapping on Specimen No. 3

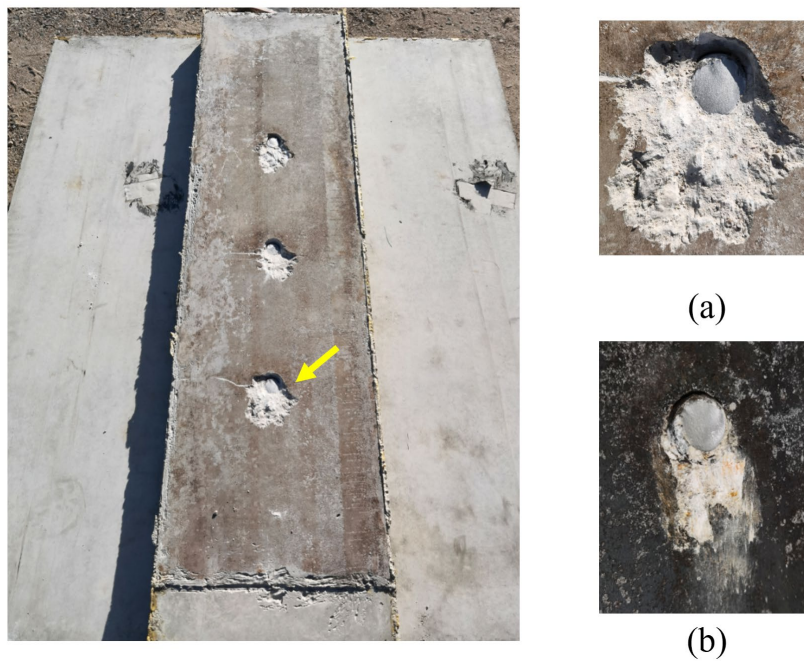


Figure 5.44 - Specimen No. 3: Concrete Deck After Failure with Enlarged Photos of the Stud Identified by the Arrow (a) Taken from Concrete Side (b) Taken from Steel Beam Flange Side

#### 5.5.4. Specimen No. 4, One 1-1/8" Stud Per Row, No Stagger, PCP

Some cracks were observed in the haunch on the north side before the test. These cracks widened during the loading. Two 0-to-75-kip cycles were performed at the beginning. The ramp loading was paused at 100 kips, 200 kips, 300 kips, and 400 kips to check for cracks. At a load of 181 kips, a sound was heard from the specimen and a 5-kip load drop was observed. A sudden increase in LP readings was observed at the same time. The first cracks in the south haunch were observed at 400 kips. No new cracks were found until the failure occurred. The specimen failed in a concrete failure mode with large splitting cracks and horizontal cracks. The shear studs did not fracture. Photos showing concrete cracking after the test are in Figure 5.45. As Figure 5.45 (c) shows, cracks developed from the corner of the haunch and propagated into the PCP and the transition region. No cracks were found in west and east CIP concrete surfaces. A mapping of crack development is provided in Figure 5.46. In the mapping, the cracks found before the test are shown because they grew during the test.

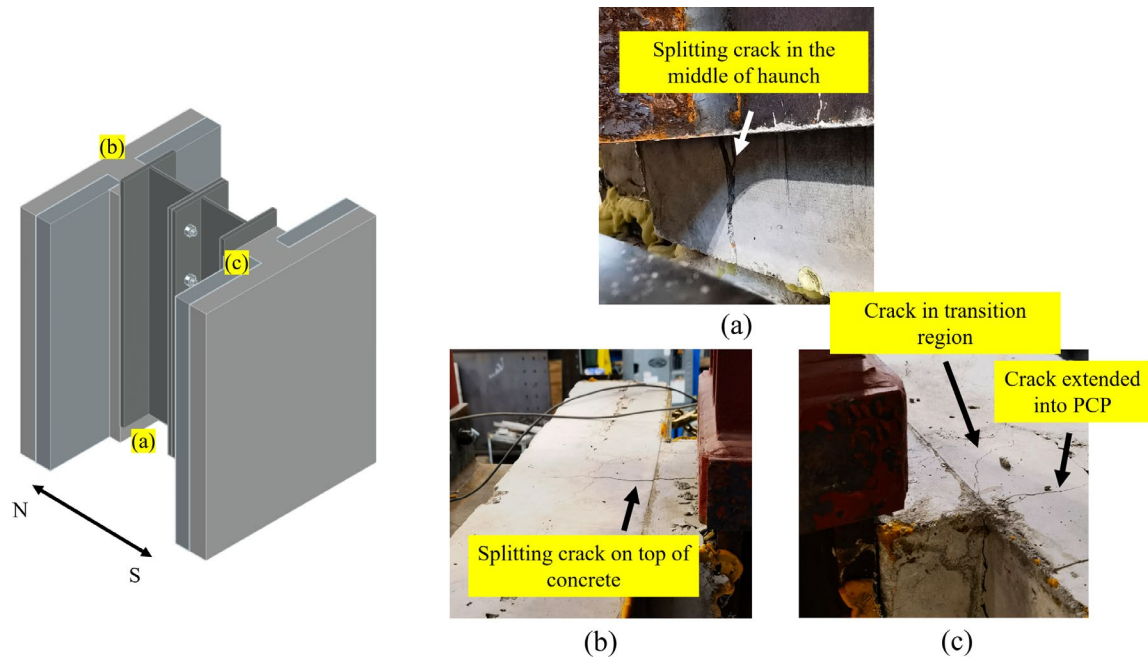


Figure 5.45 - Concrete Damage on Specimen No. 4. Locations of Photos are Shown in the Left Diagram

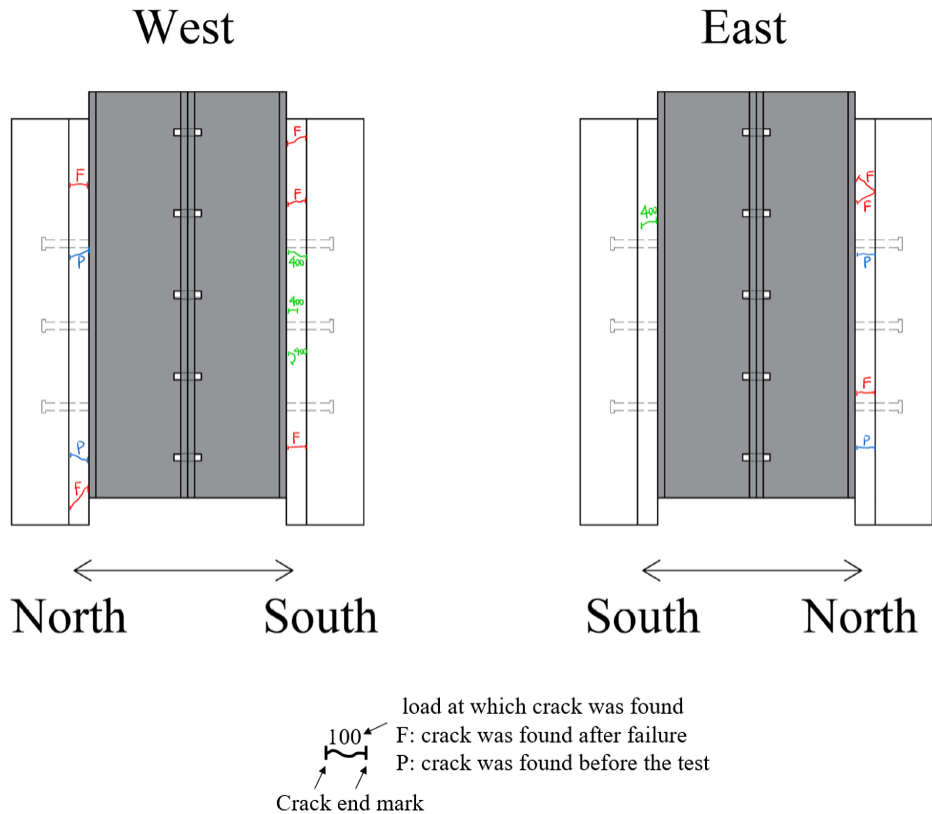


Figure 5.46 - Concrete Crack Mapping on Specimen No. 4

### 5.5.5. Specimen No. 5, One 1-1/8" Stud Per Row, Staggered, CIP

Two 0 to 100 kip cycles were applied at the beginning of the test. A crack at the northeast haunch near the top wood block was observed when the load reached 100 kips in these cycles. However, this crack is believed to have been present before the test based on its appearance so it is not shown in the crack mapping. The test paused at 150 kips, 250 kips, 350 kips, and 450 kips in ramp loading to check for cracks. Two sounds from the specimen were heard at 285 kips and 380 kips, respectively. Both sounds were accompanied with a sudden increase in the LP readings. Load drops at the 285 kip sound and the 380 kip sound was about 10 kips and 20 kips, respectively. The first cracks were observed at 285 kips, when the first sound occurred. Multiple new cracks along the interface between the haunch and the concrete deck developed at 350 kips. The specimen failed with shear stud fracture on the south side. No cracks were found on the east and west surfaces of the concrete deck. A mapping of crack development is provided in Figure 5.47.

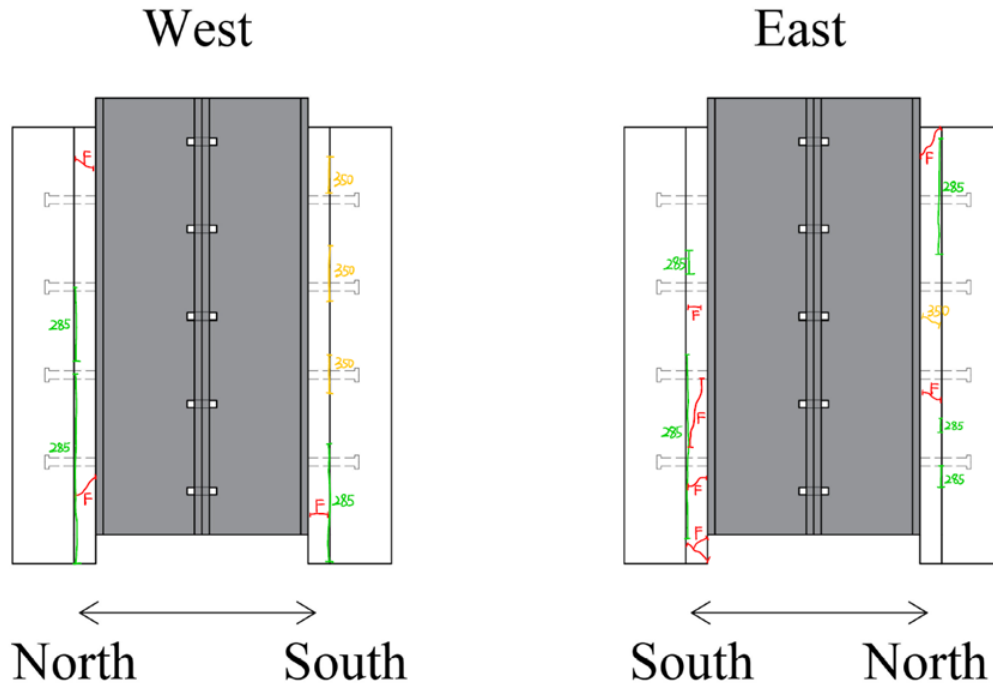


Figure 5.47 - Concrete Crack Mapping on Specimen No. 5

Photos of the south concrete deck and stud fracture surfaces are in Figure 5.48. A continuous crack starting from the top of the haunch connecting all studs can be seen. The enlarged photos of the stud identified by the arrow reveals that the stud fractured at the weld. Considerable porosity was visible at the fractured cross section. Concrete crushing was seen on the compression side of the studs.

### 5.5.6. Specimen No. 6, One 1-1/8" Stud Per Row, Staggered, PCP

The test began with two 0 to 100 kip cycles. When the specimen reached the second 100 kip load, a sound emitted from the specimen. An increase in LP readings was observed at the sound but no change occurred in the load. Hairline cracks were found at various locations after the sound. Ramp loading was paused at 150 kips, 250 kips, 350 kips, and 450 kips to check for cracks. Another big sound from the specimen was heard at 316 kips. This sound caused a 10 kip load drop accompanied with a sudden increase in slip. The first crack during ramp loading was noticed at 350 kips near the top wood block in the northeast haunch. At 450 kips, multiple new horizontal cracks formed on the northwest haunch region. The specimen failed in a concrete controlled mode, without fracture of shear studs. Horizontal and splitting cracks were developed in the haunch and extended into the PCPs, as shown in Figure 5.49 (a). No cracks were found in the east and west surfaces of the CIP concrete. A mapping of crack development is provided in Figure 5.50.



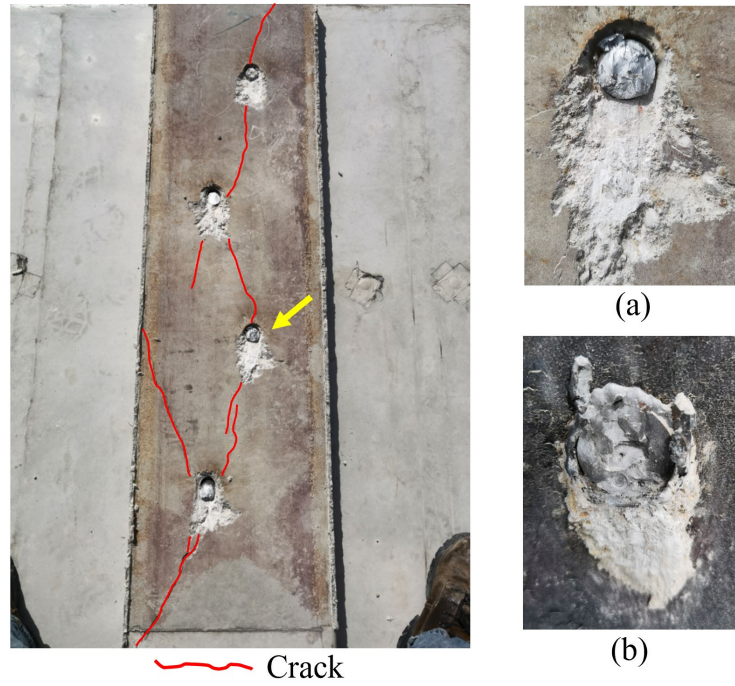


Figure 5.48 Specimen No. 5: Concrete Deck After Failure with Enlarged Photos of Stud Identified by the Arrow (a) Taken from Concrete Side (b) Taken from Steel Beam Flange Side

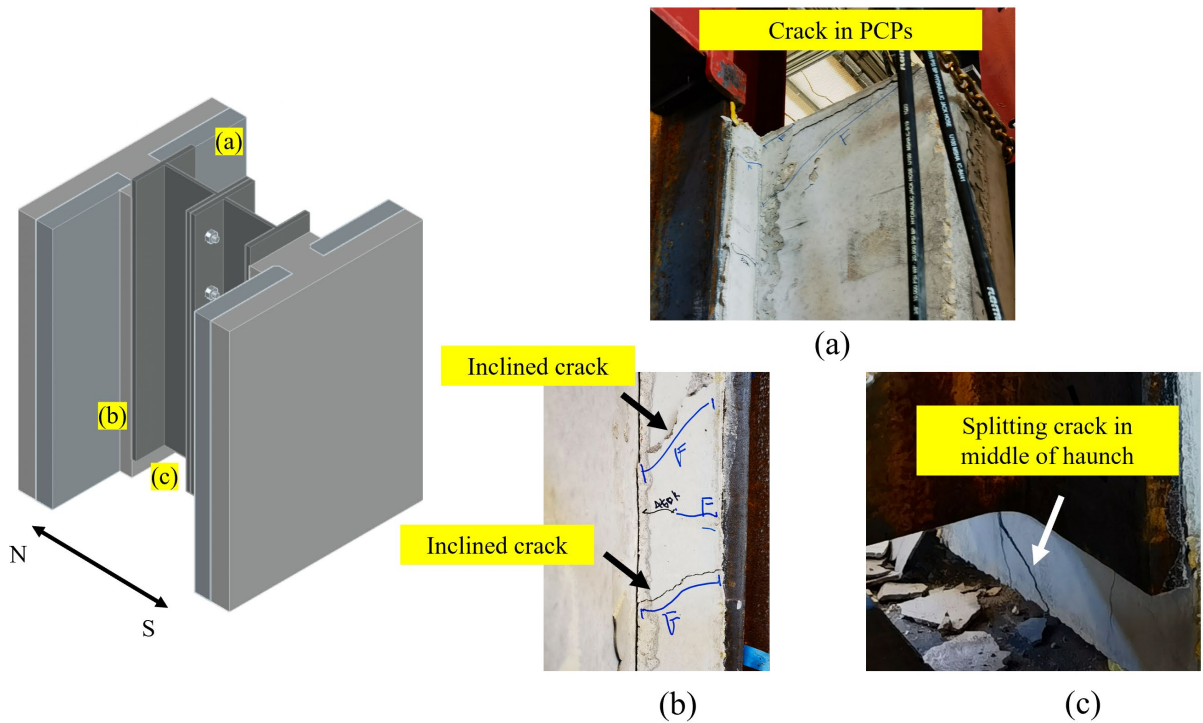


Figure 5.49 - Concrete Damage on Specimen No. 6. Locations of Photos Shown in the Left Diagram



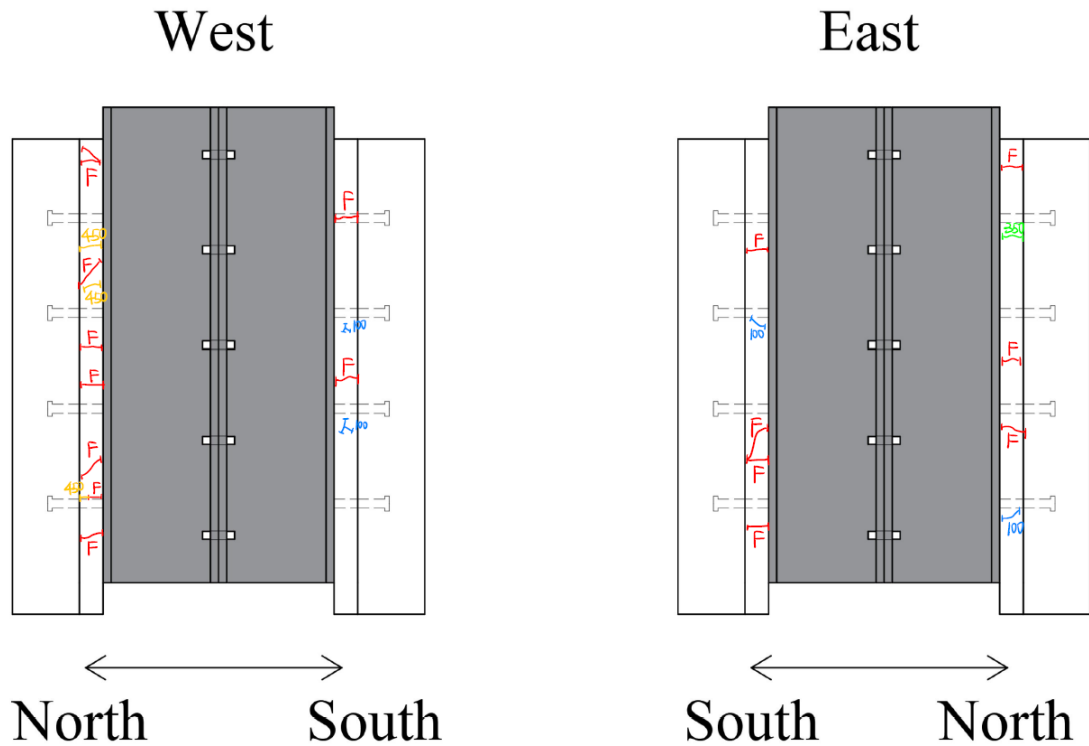


Figure 5.50 - Concrete Crack Mapping on Specimen No. 6

### 5.5.7. Specimen No. 7, Two 1-1/8" Studs Per Row, CIP

Two 0 to 150 kip loading cycles were applied to the specimen at the beginning of the test. Checks for cracks were conducted during the ramp loading stage at 200 kips, 300 kips, 400 kips, 500 kips, 600 kips, 650 kips, 700 kips, and 750 kips. At 600 kips, it was observed that the specimen contacted the lateral support. The first crack was observed at 600 kips near the haunch top. Horizontal cracks in the haunch were observed to develop at 650 kips. At 700 kips, more new cracks were observed and the existing crack in the lower haunch started to extend into the concrete deck, as shown in Figure 5.51. At 750 kips, more cracks were found that extended into the concrete deck and new inclined cracks were observed in the northeast haunch. The specimen failed with shear stud fracture on the north side. Large pieces of concrete in the northwest haunch spalled off at the failure. A mapping of crack development and photos are provided in Figure 5.51.

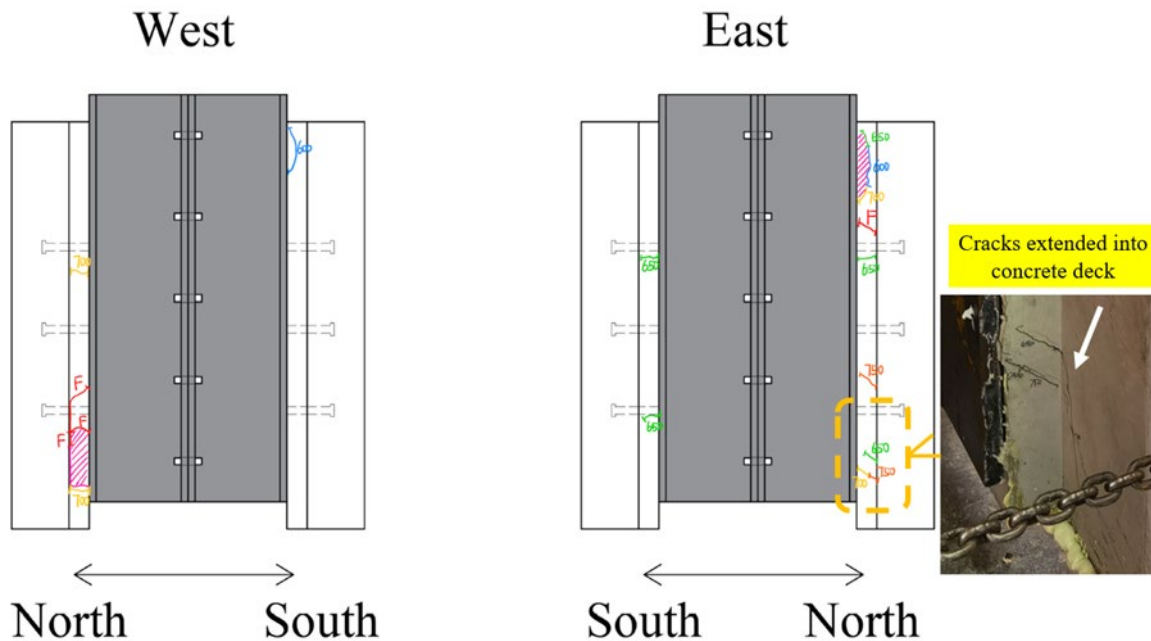


Figure 5.51 - Concrete Crack Mapping on Specimen No. 7

The north concrete deck after the failure is shown in Figure 5.52. Extensive cracks developed in the haunch region and in the concrete deck for this specimen. Pieces of concrete in the lower haunch around the bottom row of studs spalled off. The enlarged views of the stud identified by the arrow shows a weld fracture and porosity in the weld. Concrete crushing is apparent below the stud where the concrete is under compression. In Figure 5.52 (b), a piece of steel can be seen besides the fractured weld. This small steel piece is formed by leaked metal during the welding.

### 5.5.8. Specimen No. 8, Two 1-1/8" Studs Per Row, CIP, Half Transverse Reinforcement

Two 0 to 100 kip cycles of load were applied to the specimen at the beginning of the test. Some cracks along the haunch deck interface were observed and were believed to be present before the test. The specimen was checked for cracks at 200 kips, 300 kips, 400 kips, 500 kips, 600 kips, and 700 kips during the ramp loading. The first crack was observed at the southwest haunch, near the top wood block at 200 kips. At 245 kips, a sound was heard from the specimen. A sudden increase in the LP readings was noticed and the load decreased about 5 kips. No new cracks were found when the sound was heard. At 300 kips, a new crack was observed at the top corner of the haunch at the southwest side. New cracks were observed at 400 kips, 500 kips, and 600 kips and the cracks concentrated around the top wood block region, as shown in Figure 5.54. At 600 kips, cracks from the haunch started to extend into the concrete deck. These deck cracks kept growing at 700 kips. The specimen did not contact the lateral support prior to failure. When the maximum reading from the LPs reached 0.5", it was decided to increase the loading rate to finish the test faster. The highest load rate in this test was about 2 kips/sec. The specimen

eventually failed in a concrete failure mode. Specimen No. 8 had the most severe concrete deck cracking of all the specimens. A large number of cracks developed in the concrete deck and in the concrete haunch. Photos showing the damage on concrete deck are provided in Figure 5.53. A mapping of crack development is provided in Figure 5.54.

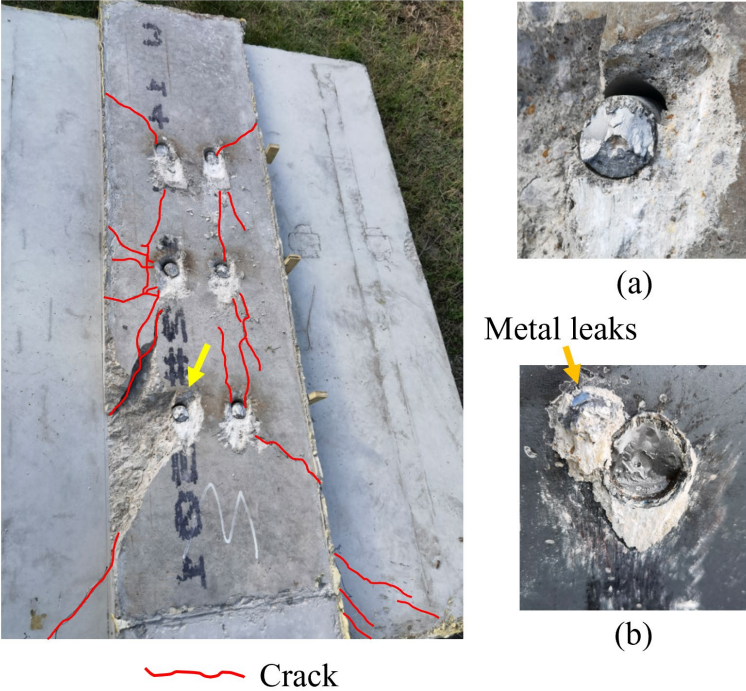
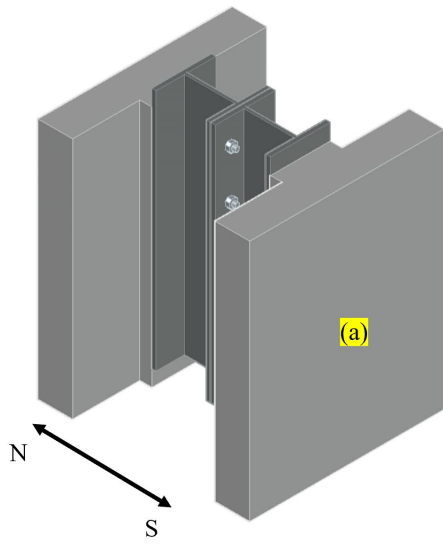


Figure 5.52 - Specimen No. 7: Concrete Deck After Failure with Enlarged Photos of Stud Identified by the Arrow (a) Taken from Concrete Side (b) Taken from Steel Beam Flange Side



(a)

Figure 5.53 - Concrete Deck Cracking on Specimen No. 8. Locations of Photos are Shown in Left Diagram

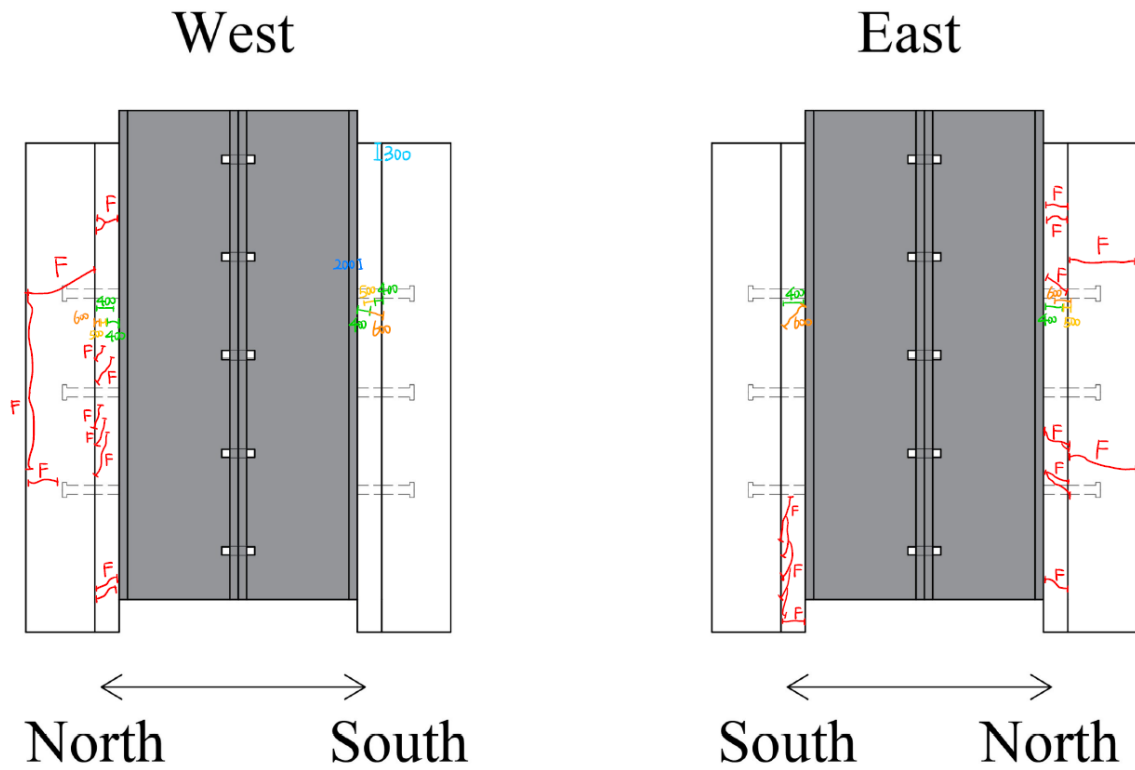


Figure 5.54 - Concrete Crack Mapping on Specimen No. 8

### 5.5.9. Specimen No. 9, Two 1-1/8" Studs Per Row, CIP, 5" Long Shear Studs

Two load cycles were applied to the specimen before the ramp loading. The first load cycle ranged from 0 to 100 kips. The second cycle ranged from 0 to 150 kips. No cracks were noticed after these cycles. Ramp loading stopped at 200 kips, 300 kips, 400 kips, 500 kips, 600 kips and 700 kips to check for cracks. At 200 kips and 240 kips, sounds from the specimen were noticed. These sound events were accompanied with an increase in the LP readings but no change in the load readings. Before reaching 400 kips, the load eccentricity was more than 10%, indicating the specimen was not placed at the center of the setup. Ramp loading was terminated and the specimen was re-centered. Ramp loading then went directly to 400 kips from zero after the adjustment. The first cracks were observed at 400 kips, and were visible on both sides of the haunch near the top wood block. As the load increased, the width of the existing cracks increased. However, no new cracks were observed until 700 kips. Multiple new inclined cracks in the haunch were found at 700 kips and these cracks eventually extended into the concrete deck at failure, as illustrated in Figure 5.55. The specimen failed in a concrete controlled failure mode without fracture of shear studs. The haunch had essentially been torn from the concrete deck with large cracks. A mapping of crack development and a photo of the torn off haunch after the test is provided in Figure 5.55.

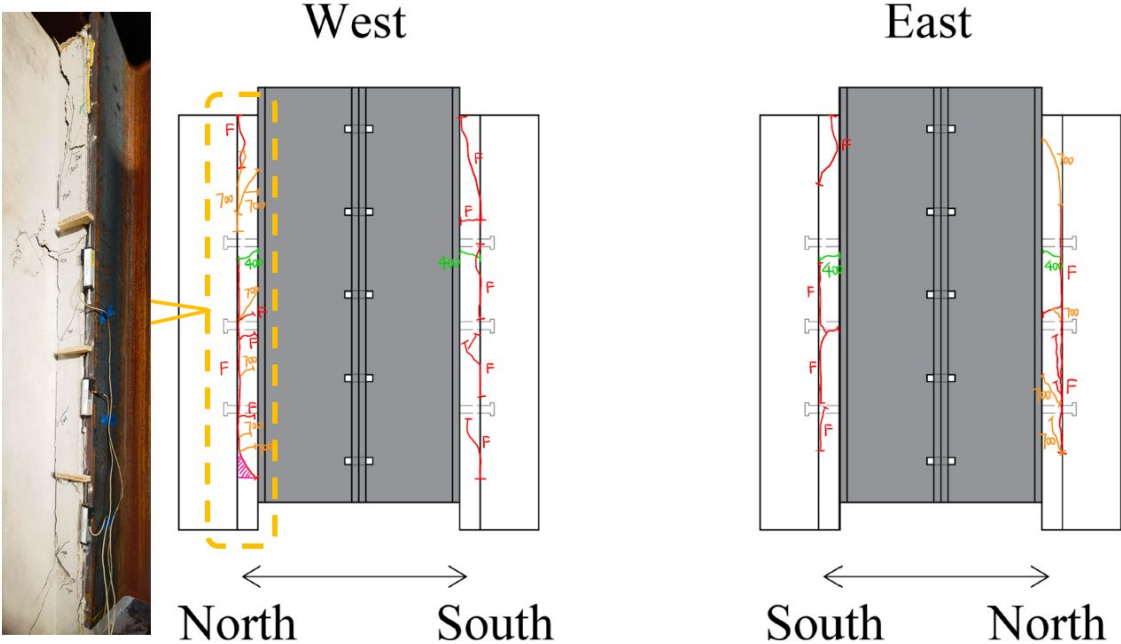


Figure 5.55 - Concrete Crack Mapping and Photo After Test on Specimen No. 9

### 5.5.10. Specimen No. 10, Two 1-1/8" Studs Per Row, CIP, 1" Haunch

Two 0 to 150 kip load cycles were conducted at the beginning of the test. No cracks were found after these cycles. Ramp loading was stopped at 300 kips, 450 kips, 600 kips, and 750 kips to check for cracks. At around 245 kips, a sound from the specimen was heard but no cracks were observed. A sudden increase in LP readings but no change in load occurred with the sound. The first crack was observed at 450 kips at the southeast top wood block. More cracks developed at 600 kips and most of them formed near the common edges between north/south deck and west/east deck surface. Additional cracks in the haunch were observed at 750 kips. The specimen failed with shear stud fracture and both sides failed essentially simultaneously. A small piece of concrete cover spalled off near the southeast base of the concrete deck, as shown in Figure 5.56. There was no contact between the specimen and the lateral support during the test prior to failure. A mapping of crack development and a photo of the spalled concrete deck is provided in Figure 5.56.

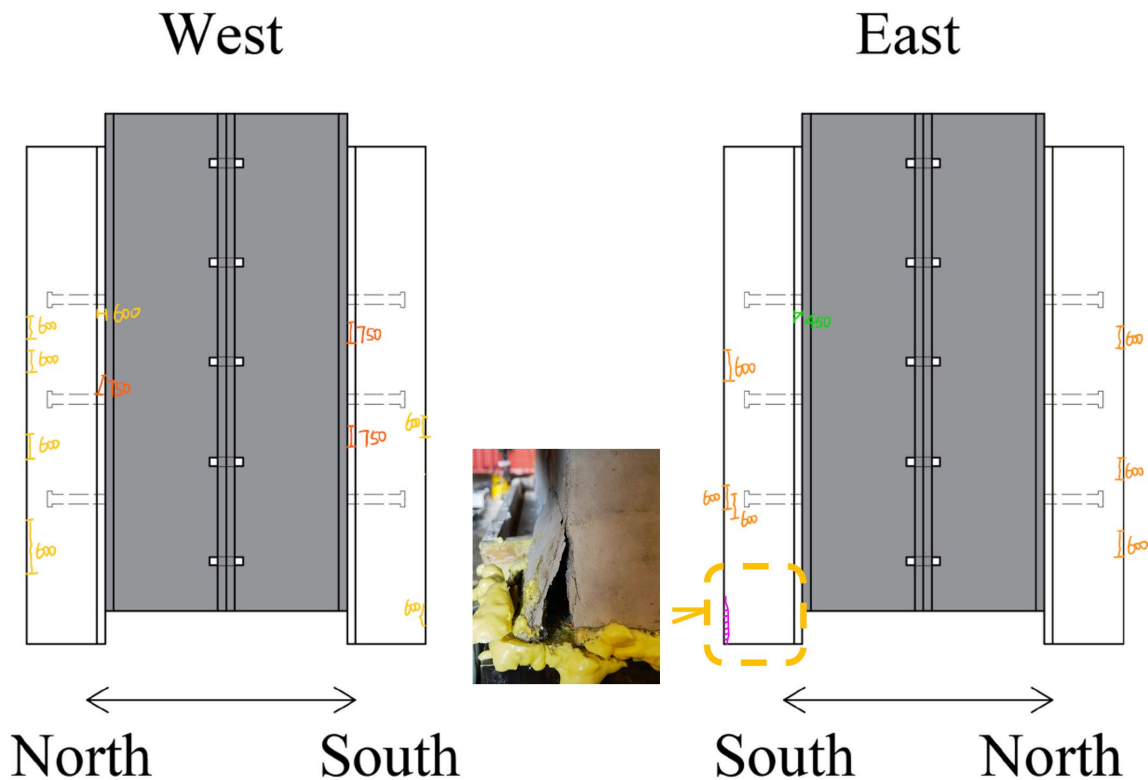


Figure 5.56 - Concrete Crack Mapping and Photo of Spalled Concrete on Specimen No. 10

Photos showing the south concrete deck after the failure are provided in Figure 5.57. The concrete deck showed local crushing of the concrete near the studs. No visible cracks were observed on the deck. All studs fractured in their shank away from the weld, as is shown by the enlarged photos.



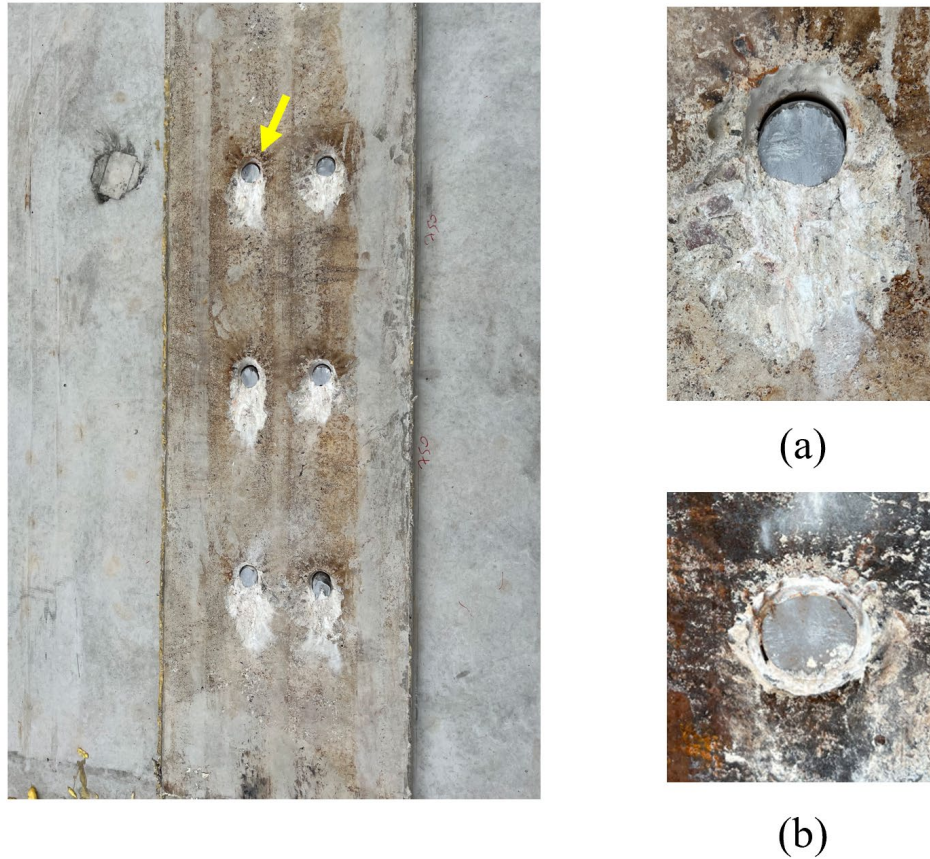


Figure 5.57 - Specimen No. 10: Concrete Deck After Failure with Enlarged Photos of Stud Identified by Arrow (a) Taken from Concrete Side (b) Taken from Steel Beam Flange Side

### 5.5.11. Specimen No. 11, Two 1-1/8" Studs Per Row, CIP, W14×99

Two 0 to 150 kip load cycles were performed at the beginning of the test. At 130 kips and 150 kips during the first cycle, sounds from the specimen were noticed. A sudden increase in LP readings but no change in load readings was observed with the sounds. A crack was found at 150 kips at the middle wood block in the southwest haunch. Ramp loading began after the initial load cycles. The test was paused at 300 kips, 450 kips, 600 kips, and 750 kips to check for cracks. The first crack in the ramp loading was found at 300 kips between the top and middle wood blocks. Then, each crack check revealed several new cracks in the haunch. The specimen ultimately failed with shear stud fracture on the north side. The failure generated some cracks that extended from the haunch region into the concrete deck. In addition, a vertical crack was observed at the east face of north concrete deck after failure, which is shown in Figure 5.58. No localized bending or distortion was observed in the steel beam flange. A mapping of crack development is provided in Figure 5.58.



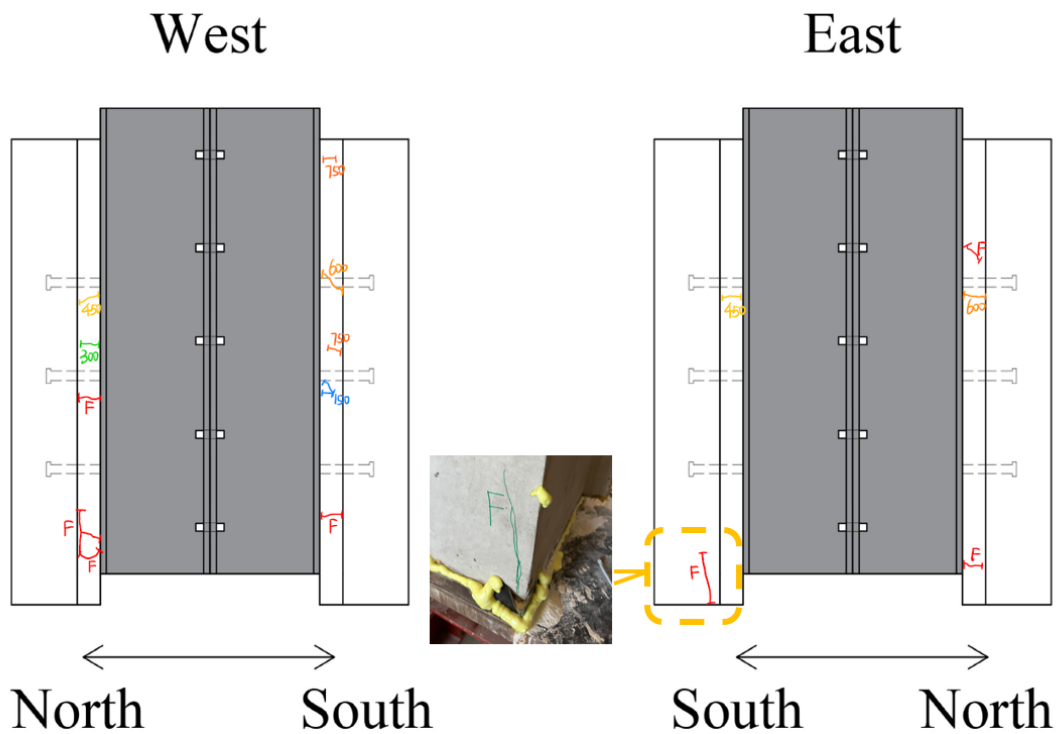


Figure 5.58 - Concrete Crack Mapping and Photo of Vertical Crack on Specimen No. 11

Photos showing the north concrete deck after the failure are provided in Figure 5.59. The cracking pattern in the concrete the in haunch region is similar to that in specimen No. 7. Enlarged photos of the stud identified by the arrow show the fracture occurred in the weld with large holes observed at the fracture surface. Concrete crushing was visible at the compression side of each shear stud.

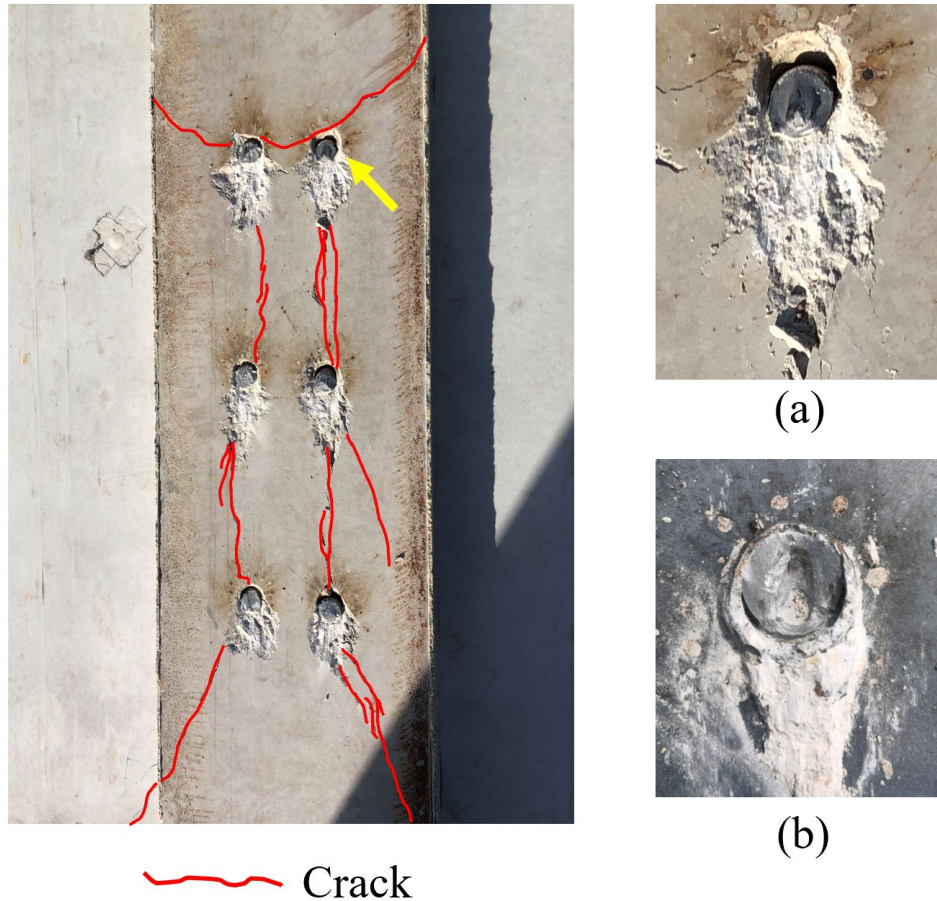


Figure 5.59 - Specimen No. 11: Concrete Deck After Failure with Enlarged Photos of Stud Identified by Arrow (a) Taken from Concrete Side (b) Taken from Steel Beam Flange Side

### 5.5.12. Summary of Test Observations

Based on the observations from the static push-out tests, when compared with 7/8" studs, there is no indication that using 1-1/8" studs will cause more concrete cracking under service level loads and under ultimate loads when one stud per row with no stagger or a 1" deep haunch was used. When two studs per row and a 3" deep haunch was used at the same time, cracking at ultimate load seemed more extensive. Specimens with the staggered layout of 1-1/8" studs showed cracks at earlier loads compared to 7/8" studs. For specimens with PCPs, the CIP part of the concrete always had severe damage and the specimens always failed in the concrete failure mode (as opposed to stud fracture). The specimens with less transvers reinforcement (Specimen No. 8) and less penetration of the stud into the deck (Specimen No. 9) compared to the standard specimen, exhibited more severe concrete cracking at both early and final loading stages. The specimen with less top cover (Specimen No. 10) compared to the standard specimen showed cracking near the concrete deck surface, although these cracks were observed at load levels likely well above service loading. Otherwise, in most specimens, cracks mostly developed in the haunch region.

Due to the presence of the specimen lateral supports, cracks on the north and south concrete deck surfaces were not checked during the test, but were checked after completion of the test. Table 5.9 provides a summary of the failure mode for each specimen.

**Table 5.9 – Failure Modes of Push-Out Specimens**

Specimen No.	Failure mode*	Failure side	Comment
1	S	Both	
2	C	-	w/PCP
3	S	Both	
4	C	-	w/PCP
5	S	South	
6	C	-	w/PCP
7	S	North	
8	C	-	Special detailing
9	C	-	
10	S	Both	
11	S	North	

Note: \*S: stud fracture. C: concrete damage

Shear studs of one special specimen were taken out from the concrete slab after the test. This special specimen is identical to Specimen No. 3 but not the same one. It was first tested under 2.3 million cycles of fatigue loading at a 15 ksi stress-range and then loaded to failure by static test. (See Chapter 6 for fatigue push-out tests). Both sides of the specimen failed essentially simultaneously with stud fracture in the static test. All studs in north side concrete deck were taken out and the deformation of the three studs are illustrated in Figure 5.60. From the left to the right, the shear studs are the top stud, middle stud, and the bottom stud in the push-out specimen, where the top stud is closest to the loading rams. The deformation of shear stud is concentrated at the base of the studs. The deformation of the studs appears to increase slightly when going from top to the bottom, indicating studs at the lower in the push-out specimen bear higher load.



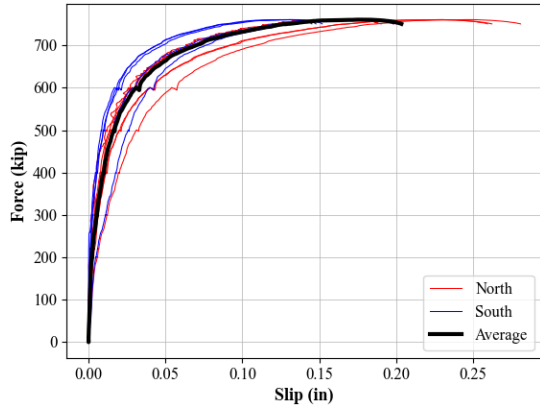
*Figure 5.60 – Deformation of Studs After Testing*

## 5.6. Test Results and Discussion

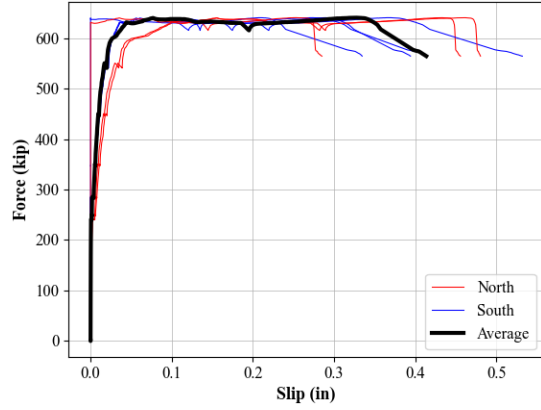
---

### 5.6.1. Load-Slip Response

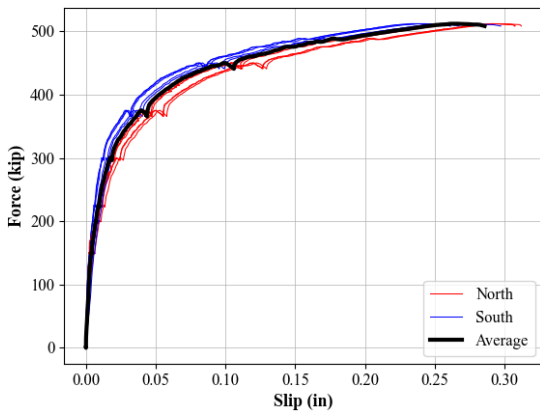
Load-slip curves for all specimens are given in Figure 5.61. The load-slip curve only illustrates the ramp loading stage; it does not include the two initial lower-level load cycles. The plots show the output from all LPs on the north and south sides of the specimen. The plots also show an average curve, which was derived by taking the average of all LP readings. In presenting this data, any LP that malfunctioned during a test was not included. In Figure 5.61, the end of each load-slip curve is given by either a sudden strength loss or reaching approximately 80% of the peak strength. For specimens with a sudden strength loss, the load-slip curve is ended one data point before the failure occurred. Observations from the load-slip curves are summarized below.



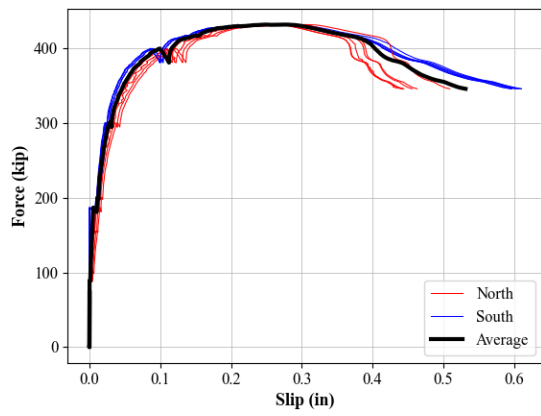
Specimen No. 1



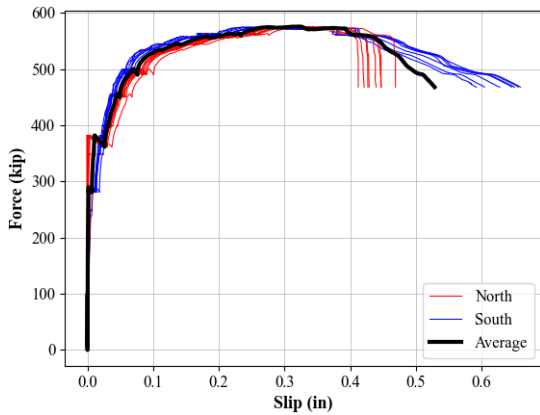
Specimen No. 2



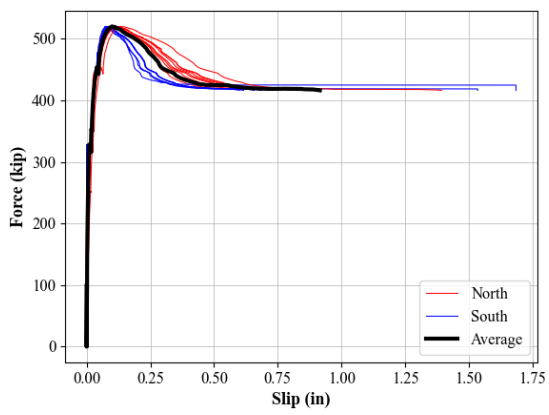
Specimen No. 3



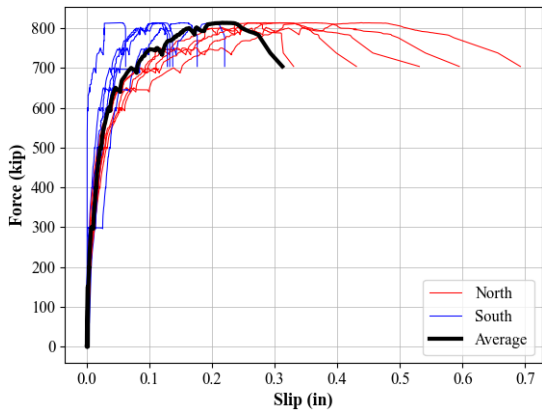
Specimen No. 4



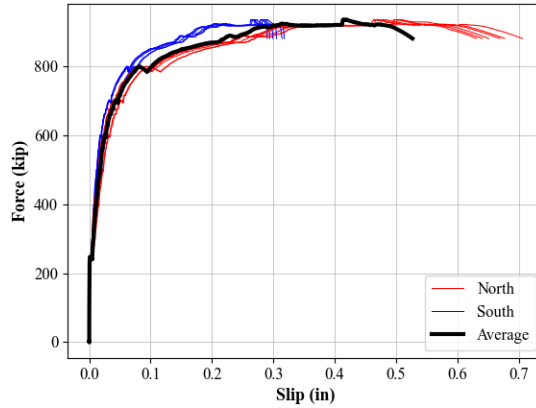
Specimen No. 5



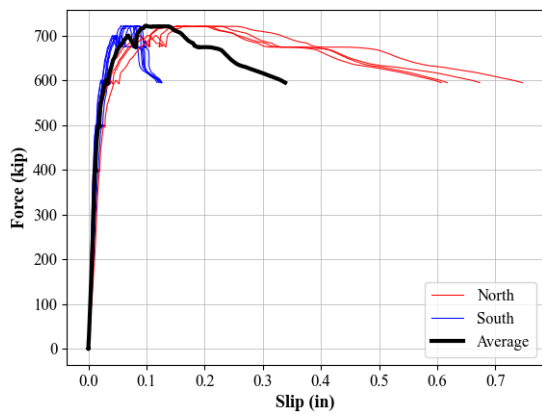
Specimen No. 6



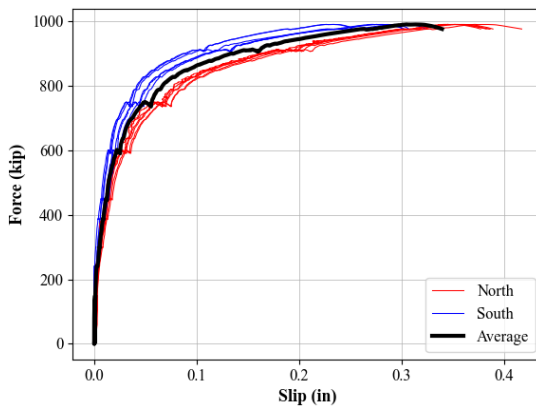
Specimen No. 7



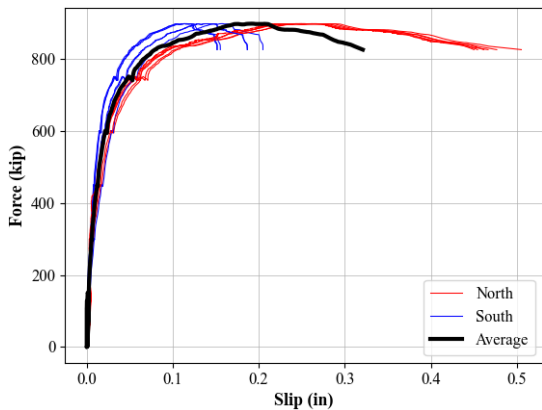
Specimen No. 8



Specimen No. 9



Specimen No. 10



Specimen No. 11

Figure 5.61 - Load-Slip Curves for Static Push-Out Tests

There is difference between north and south slip measurements in every test. As mentioned in Section 5.3.3, a limitation of instrumentation in this study is that the LP readings are somewhat sensitive to the cracks in the haunch region, and these cracks differ on the north and south sides. In general, however, the difference between slip measurements on the north and south sides reflects the fact that the initiation of damage in the concrete and/or stud will not likely occur on

both the north and south sides simultaneously, due to inevitable small differences in material properties, stud weld quality, load eccentricity, and other factors. Once damage is initiated on one side, it seems reasonable that slip will increase at a faster rate on that side. The tests showing the largest north and south slip differences were Specimen No. 8 and Specimen No. 9, which failed in a concrete controlled mode.

There are six specimens that failed by stud fracture, as indicated in Table 5.9. Of these, Specimen Nos. 5, 7, and 11 failed on one side. For one-side failure specimens, the north and south slip difference is more prominent than those specimens that failed on both sides. The side that eventually failed always had larger slip. This suggests that stud fracture is accompanied by more concrete cracking and deformation.

Several small load drops on the load slip curves are seen for all specimens. Most of these load drops occur while the loading was paused to check for cracks, reflecting relaxation of materials and possibly some leakage in the hydraulic loading system. Other drops occurred while sounds were heard during the test. Most sound-related drops are negligible. The sound from the specimen is believed to be the indication of breaking of the initial bond between the steel beam flange and the concrete haunch since bond-breakers were not used between the steel and concrete. Figure 5.62 provides an enlarged view of the early ramp loading stage of the Specimen No. 5, which had the largest sound-related load drop of about 20 kips. For Specimen No. 5, the slip on the south side had near zero readings until the sound occurs at 285 kips. Similarly, the slip on the north side had near zero readings until the sound occurred at 380 kips. After the sound, the slip at the north and south sides had similar values and started to increase normally.

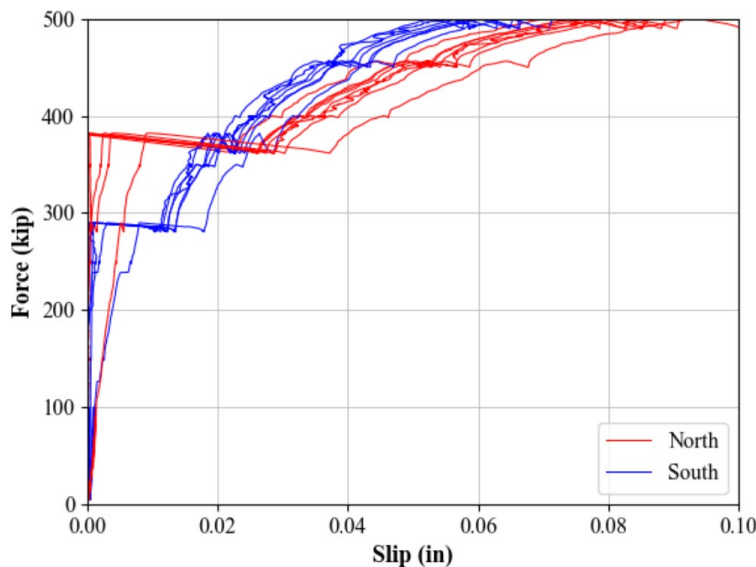


Figure 5.62 - Initial Portion of Load-Slip Curve for Specimen No. 5



Table 5.10 lists the maximum load, average slip corresponding to the maximum load, and the average failure slip obtained in each test. Failure slip has the same definition as the stopping point in Figure 5.61. Table 5.11 compares the stud strength in each test with the 9<sup>th</sup> Ed. AASHTO and the proposed 10<sup>th</sup> Ed. AASHTO design strength equations. The maximum load per stud was computed by taking the maximum load on a specimen from Table 5.10 and dividing by the total number of studs in the specimen from Table 5.2. Equations for stud factored shear resistance from the 9<sup>th</sup> Ed. AASHTO and the proposed 10<sup>th</sup> Ed. AASHTO can be found in Eq. 2-7 and Eq. 2-8 in Chapter 2.

As described in Chapter 2, the proposed 10<sup>th</sup> Ed. AASHTO removed the term related to the concrete strength. Only the stud material properties are involved in the strength calculation. It should be noted that this change does not mean 10<sup>th</sup> Ed. AASHTO excludes the possibility of a concrete failure mode at a shear stud. According to Pallares and Hajjar (2010), which is the basis for the proposed 10<sup>th</sup> Ed. AASHTO shear stud strength equation, even if stud strength is controlled by concrete failure (rather than stud fracture), the stud strength equation based only on stud fracture should still be conservative. Another important change is the design resistance factor,  $\phi$ . In the 9<sup>th</sup> Ed. AASHTO,  $\phi = 0.85$ , while in the proposed 10<sup>th</sup> Ed. AASHTO,  $\phi = 1.00$ . In general, the stud factored shear resistance is often lower in the proposed 10<sup>th</sup> Ed. AASHTO compared to the 9<sup>th</sup> Ed. AASHTO, although this is not always the case as indicated by the values in Table 5.11.

The values of  $f_{n1}$  and  $f_{n2}$  listed in Table 5.11 used measured values of  $f_c'$  and  $F_u$  determined by concrete cylinder tests and tensile coupon tests (see Section 5.4), as opposed to minimum specified values used in design. The tensile strength of the stud material was taken as the dynamic value listed in Section 5.2.1, as this reflects the strength determined using ASTM tensile coupon testing procedures. It must be mentioned that Specimen No. 9 did not satisfy the stud height to diameter ratio requirement ( $h/d \geq 5$ ) in the proposed 10<sup>th</sup> Ed. AASHTO.

As indicated in Table 5.11, the measured ultimate strength for all 1-1/8" shear studs were greater than predicted by the AASHTO design equations, for both the 9<sup>th</sup> Ed. AASHTO and the proposed 10<sup>th</sup> Ed. AASHTO. This suggests the AASHTO design equations can be directly used to predict the ultimate strength of 1-1/8" shear studs without any modification. Further, the average slip at failure for the 1-1/8" shear studs are comparable to and in most cases greater than that of 7/8" studs. And the ultimate slip requirement from EC-4 of 6 mm (0.24") was satisfied in every push-out test with 1-1/8" diameter shear studs. Based on a review of the literature, there is no established criterion for slip capacity of shear studs in U.S. standards. However, since the 1-1/8" studs exhibited slip capacities similar to or greater than the 7/8" studs in this test program, it may be inferred that the 1-1/8" shear studs have adequate slip capacity for use in composite steel bridge girders.

**Table 5.10 - Key Values in Load-Slip Curves**

Specimen No.	Maximum Load (kips)	Avg. Slip at Max. Load (in)	Load at Failure (kips)	Average Slip at Failure (in)
1	760.6	0.18	750.5	0.20
2	640.4	0.33	564.3	0.41
3	512.0	0.26	508.4	0.28
4	432.2	0.28	346.1	0.53
5	575.9	0.32	468.0	0.53
6	520.2	0.10	416.4	0.92
7	813.6	0.22	703.8	0.32
8	936.4	0.42	881.5	0.53
9	722.1	0.10	594.8	0.34
10	991.1	0.31	976.8	0.34
11	897.4	0.19	825.3	0.31

**Table 5.11 - Load Per Stud from Push-Out Tests and AASHTO Stud Factored Shear Resistance**

Specimen No.	Max. Load per Stud $f_s$ (kips)	9 <sup>th</sup> Ed. AASHTO $f_{n1}$ (kips, $\phi=0.85$ )	$f_s/f_{n1}$	10 <sup>th</sup> Ed. AASHTO $f_{n2}$ (kips, $\phi=1.0$ )	$f_s/f_{n2}$
1	42.3	38.4	110%	31.7	133%
2	35.6	35.7	100%		112%
3	85.3	63.8	134%	58.1	147%
4	72.0	57.5	125%		124%
5	72.0	59.6	121%		124%
6	65.0	62.7	104%		112%
7	67.8	60.5	112%		117%
8	78.0	66.3	118%		134%
9	60.2	59.9	101%		104%
10	82.6	62.3	133%		142%
11	74.8	56.1	134%		129%

## 5.6.2. Discussion of Results

### 5.6.2.1. Influence of Special Details

The push-out test program studied various factors mentioned in the literature that may influence stud performance. Specimens tested for this purpose are called special detail specimens. Figure 5.63 illustrates comparisons between the special detail specimens and the standard CIP specimen.

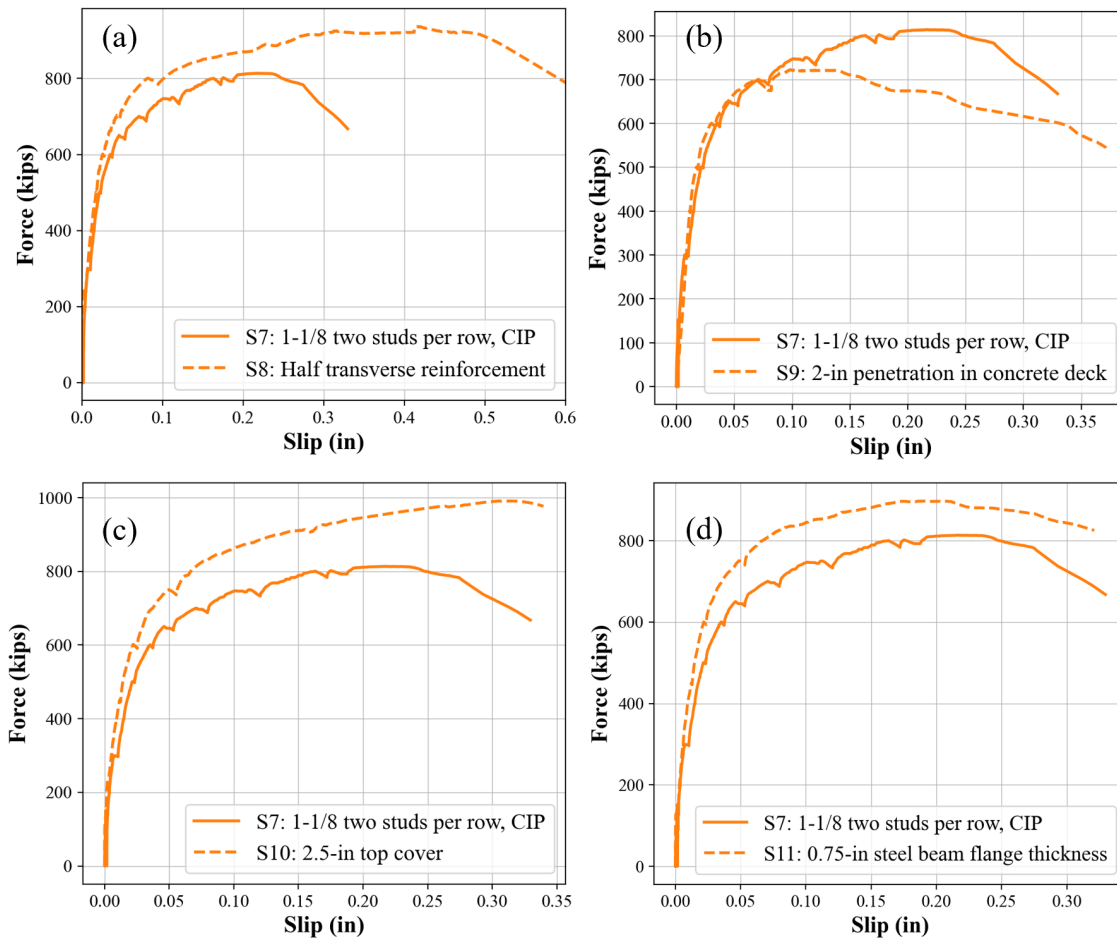


Figure 5.63 - Comparison Between Special Detail Specimens and the Standard CIP Specimen

Based on Figure 5.63 and Section 5.5, the smaller top clear cover (Specimen No. 10) and the smaller steel beam flange thickness (Specimen No. 11) resulted in no change to the failure mode and achieved slightly better load-slip response. On the other hand, less transverse reinforcement (Specimen No. 8) and less stud penetration into the deck (Specimen No. 9) reduced the specimen's load and/or deformation capacity and changed the failure mode from stud fracture to concrete failure.

The push-out test program results show that the typical deck reinforcement used in TxDOT bridges for full depth cast-in-place decks (two mats of #4@9"), is sufficient for 1-1/8" shear studs to develop their full strength and deformation capacity. When transverse reinforcement was reduced by 50% in Specimen No. 8, the 1-1/8" studs still developed good strength but had less slip capacity and worse crack controls. This is because the under-reinforced concrete cracked and lost load bearing capacity before the stud developed its full deformation capacity. The failure mode changed to a less ductile concrete failure for Specimen No. 8. It is important to note that the slip in Specimen No. 8 is considerably overestimated due to large cracks formation so the slip values should not be used solely to reflect the deformation capacity of shear stud.

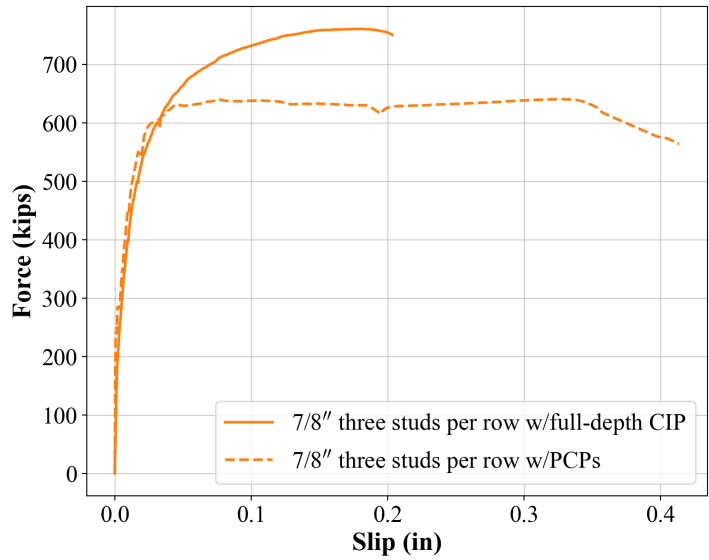
Specimen No. 9 had 5" long studs with a 2" stud penetration into the concrete deck. The 5" long stud has no penetration into any mat of continuous reinforcement. Both load and deformation capacity of the 1-1/8" shear studs decreased. This indicates that the 2" stud penetration into the concrete deck, which is the minimum requirement for 7/8" studs in 9<sup>th</sup> Ed. AASHTO and TxDOT standards (TxDOT 2019a), may not be adequate for 1-1/8" studs. The finite element study in Chapter 7 exams this issue in greater detail. Nonetheless, based on these push-out tests, it appears that a penetration distance into the concrete deck greater than 2" is preferable for 1-1/8" studs.

Specimen No. 10 with 2.5" top cover achieved a higher strength and the same ductility compared to the standard CIP specimen. This is likely due to the fact that the stud is embedded deeper in the concrete deck. Therefore, the 2.5" top cover required by current Texas design standards (TxDOT 2015a) appears sufficient for 1-1/8" shear studs.

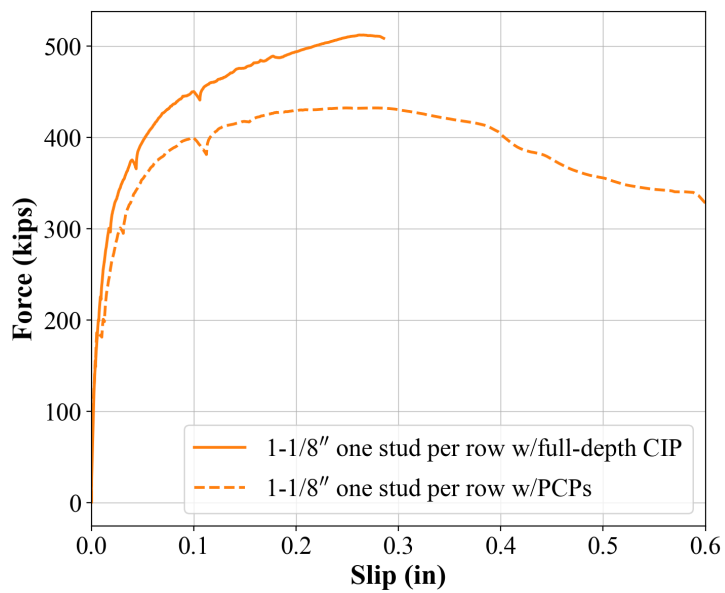
Specimen No. 11 has a steel beam flange thickness equal to 0.75". No signs of flange bending or distortion were noticed during the test. This indicates that 1-1/8" shear studs can be safely used on beams with flanges as thin as 0.75". Other than the beam flange thickness, Specimen No. 11 was nominally identical to the standard CIP specimen. Interestingly, however, specimens No. 11 showed higher strength than the standard CIP specimen, as can be seen in the load-slip curve from Figure 5.63 (d). The reason for this difference is not clear, but may reflect inherent variations in material properties and weld quality.

### **5.6.2.2. Influence of PCPs**

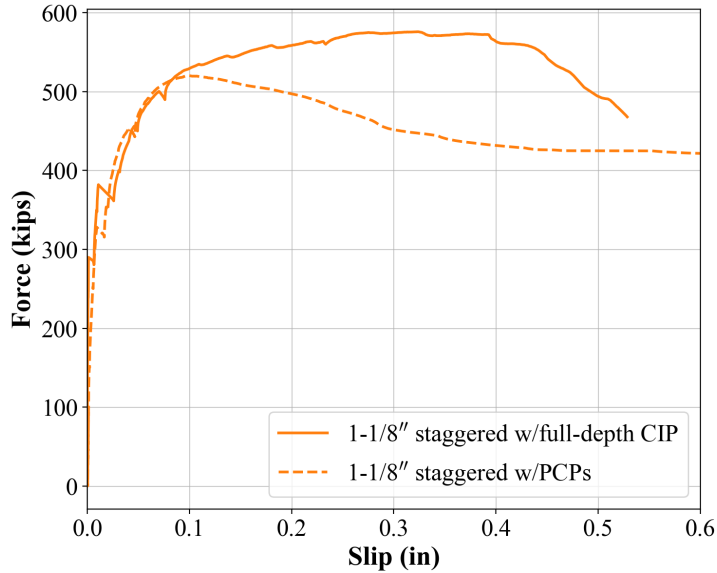
Figure 5.64 provides comparisons between specimens having PCPs versus full-depth CIP decks. For the 7/8" stud specimens, the ultimate strength decreased 18.8% when PCPs were used compared to the full-depth CIP deck. For 1-1/8" stud specimens, the strength decreased 15.6% and 9.7% for one stud per row and the staggered layout specimens, respectively, when PCPs were used. As noted in Section 5.5, all PCP specimens exhibited a concrete failure mode, whereas their counterpart specimens with full-depth CIP decks all failed by stud fracture. For the PCP specimens, the studs did not penetrate continuous reinforcement in the deck, which may, at least in part, account for the lower strength and different failure mode for the PCP specimens. Note that this concern regarding lower shear stud strength in decks with PCPs applies both to 7/8" and 1-1/8" shear studs.



(a)



(b)



(c)

Figure 5.64 - Push-Out Test results Comparison: PCPs Versus Full-Depth CIP Decks

### 5.6.2.3. Influence of stud layout

Figure 5.65 shows comparisons of the push-out test results for different layouts of 1-1/8" shear studs. One stud per row achieved the highest single-stud strength but showed the smallest slip capacity. The staggered layout had the intermediate single-stud strength but the highest slip capacity. Two studs per row have about the same single-stud strength as the staggered layout and a slightly better slip capacity compared to the one-stud case. As described in Section 5.5.3, Specimen No. 3 has the least concrete damage among all specimens, which indicates a positive correlation between good concrete integrity and high stud strength. Little damage in the concrete can also explain why Specimen No. 3 had the smallest slip capacity since slip contribution from concrete cracking was minimal. The staggered layout is a promising layout since it allows good strength and ductility development. Since there was only one specimen for each layout, it is unclear if the trends shown in Figure 5.65 truly reflect the influence of stud layout, or simply reflect variability in test results. The influence of stud layout is examined in more detail in the Chapter 7 by finite element studies.

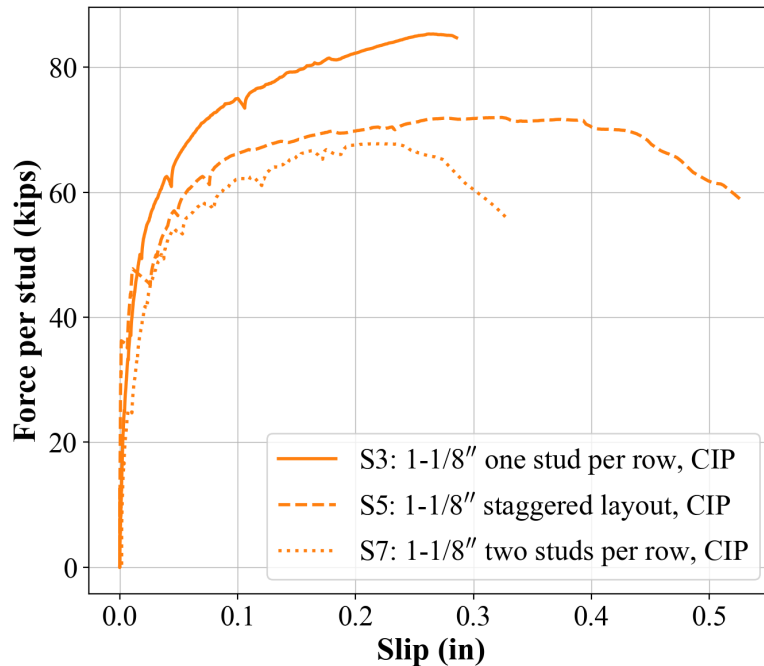


Figure 5.65 - Comparison Between Different Layouts for 1-1/8" Shear Studs

#### 5.6.2.4. Reinforcement Strain

Strains at various reinforcement locations were measured during the test. The strain values measured in the push-out tests were generally small. Some trends observed in the strain data will be discussed here.

Figure 5.66 shows the peak strain in the middle of the transverse bar, and Figure 5.67 shows the peak strain in the longitudinal bar for Specimen No. 1. The peak strain is the strain with the highest absolute value measured during the test. The color scale is given in the plots to reflect the intensity of strain. As Figure 5.66 shows, for both south and north sides, the peak strain in the transverse reinforcement increases in tension as the reinforcement gets closer to the base of the concrete deck. Conversely, the strain in the longitudinal reinforcement increases in compression as the location gets closer to the base of the deck. The two observations show that the base of the concrete is subject to a large compression force in the vertical direction, which makes the concrete expand in the transverse direction due to Poisson's effect. This might explain why large splitting cracks are developed in the middle of the haunch in specimens without continuous reinforcement near the haunch region. The same trend is found in the readings from TR and TL gauges in other specimens. (See Figure 5.30 for gauge designation).



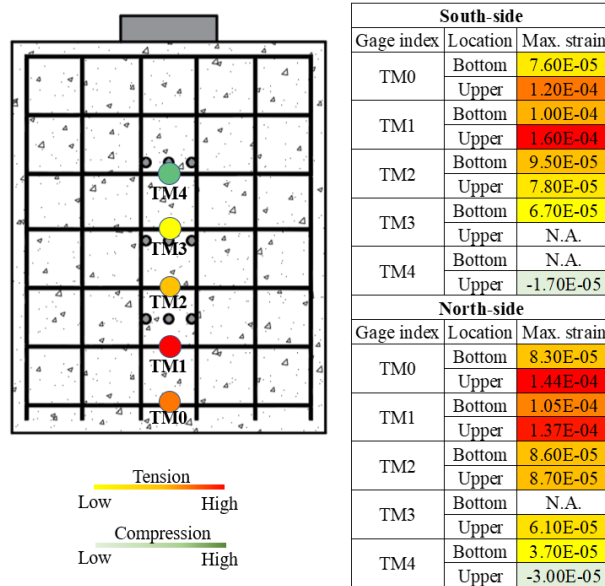


Figure 5.66 - Peak Strain in the Middle of the Transverse Reinforcement for Specimen No. 1

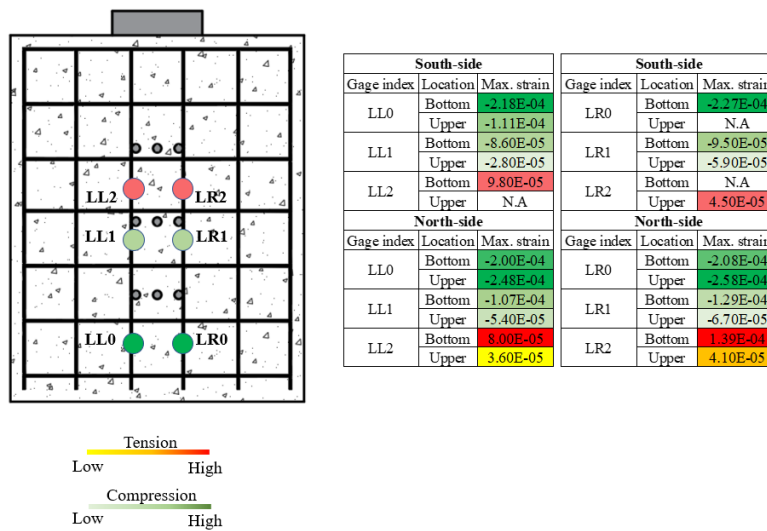


Figure 5.67 - Peak Strain in the Longitudinal Reinforcement for Specimen No. 1

It is well recognized that concrete cracking is related to tensile strain in the reinforcement. Specimen No. 8, which had one-half of the transverse reinforcement of the standard CIP specimen, had about twice the peak strains in its reinforcement when compared to the standard CIP specimen and had the highest recorded tensile strain in all specimens, which was equal to 0.0027. This value is beyond the yield strain of the reinforcing steel. In Figure 5.68, strain development at the same location between Specimen No. 8 and Specimen No. 7 (standard CIP specimen) is shown. Based on the plot, the majority of the strain in the reinforcement develops after the crack opens. The increase in strain due to crack opening is more significant in Specimen No. 8 because it had much more severe and wider cracks compared to Specimen No. 7.

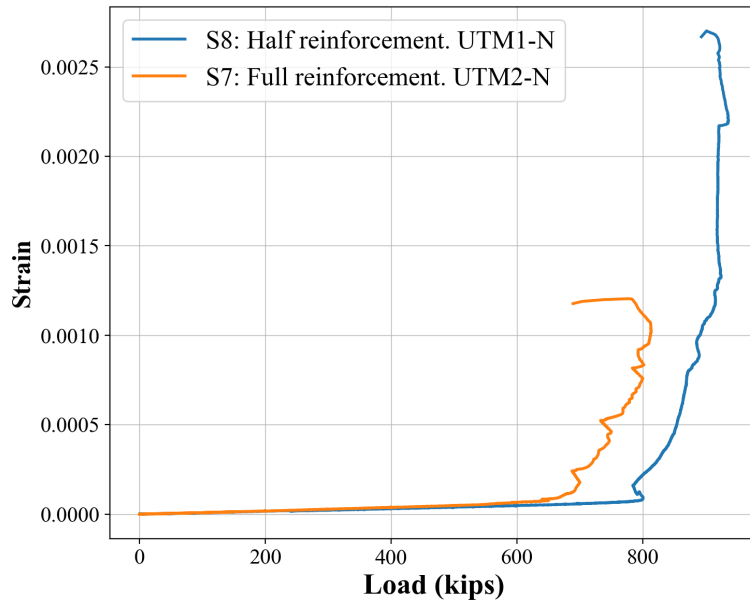


Figure 5.68 - Strain Development at the Same Location in Specimen No. 8 and Specimen No. 7

Specimen No. 3 has the overall smallest strains among the 1-1/8" stud specimens, as seen in Figure 5.69. In Figure 5.69, strain development is shown between different 1-1/8" stud layouts. Since Specimen No. 3 had the least cracking, the strain obtained with crack opening is the smallest, resulting in a small final strain.

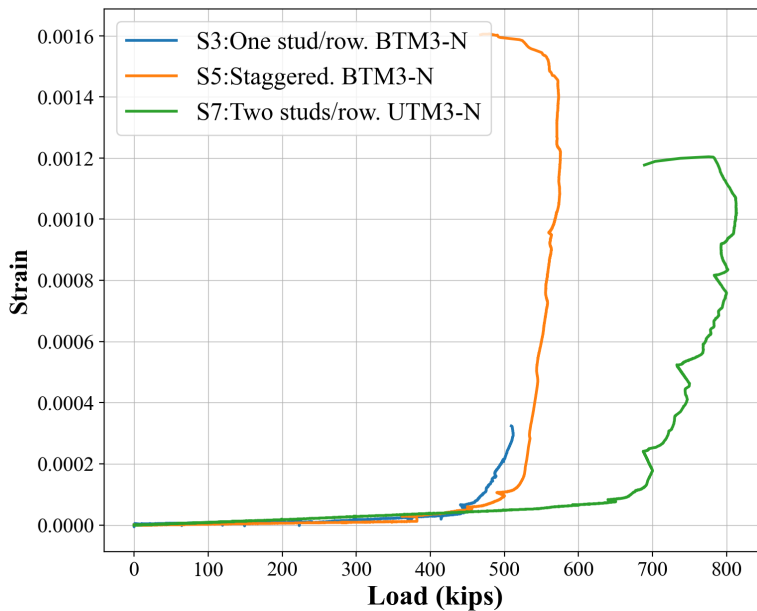


Figure 5.69 - Strain Development in Specimen Nos. 3, 5, and 7

The strain development shown in Figure 5.68 and Figure 5.69 generally matches the concrete crack observations in Section 5.6. Interestingly, the order of maximum strain in three specimens coincided with the order of failure slip observed in the push-out tests. This indicates that the slip is related to concrete damage and concrete damage is related to strain in reinforcement. However, it is noted that specimens with stud fracture can also develop relatively high strain in the reinforcement. Strain data alone cannot be used to distinguish between stud fracture and concrete failure mode.

## 5.7. Conclusions

---

Static push-out tests were conducted to investigate the ultimate strength and slip capacity of the shear studs, and included both 1-1/8" studs as well as 7/8" studs for comparisons. The test program included specimens with 8-1/2" thick full-depth cast-in-place decks as well as specimens where the deck was constructed using 4" thick PCPs with 4-1/2" cast-in-place topping. The deck details, including reinforcing details, were constructed in accordance with TxDOT standards and preferred practices.

A goal of the push-out test program was to determine if the AASHTO LRFD provisions for ultimate strength of shear studs can be safely used for 1-1/8" studs, or if some modifications of these provisions are needed. When comparing the results of the push-out test program with AASHTO LRFD shear stud provisions, two comparisons were made. One comparison is with the current 9<sup>th</sup> Ed. AASHTO (AASHTO 2020). The shear stud ultimate strength provisions in the 9<sup>th</sup> Ed. AASHTO are the same as those in past editions of AASHTO LRFD, going back many years. In the proposed 10<sup>th</sup> Ed. AASHTO (AASHTO 2021), which has not yet been released at this report was prepared, significant changes were made to both the ultimate strength and fatigue strength requirements for shear studs.

The results of the push-out tests showed excellent performance of 1-1/8" shear studs. The ultimate strength of 1-1/8" shear studs in all tests exceeded the stud ultimate strength requirements of both the 9<sup>th</sup> Ed. AASHTO and the proposed 10<sup>th</sup> Ed. AASHTO. In addition to providing data on ultimate strength, the push-out tests also provided data on the slip capacity of the shear studs. Slip capacity is a measure of stud ductility. Adequate slip capacity is needed to permit redistribution of forces among shear studs along the length of a bridge girder to permit the development of the full composite flexural strength of the girder. AASHTO LRFD does not specify a minimum slip capacity for shear studs. However, the slip capacity of the 1-1/8" shear studs measured in this test program were comparable to and sometimes larger than the slip capacity of the 7/8" shear studs measured in this test program. Thus, if 7/8" shear studs are considered to have adequate slip capacity for use in bridge girders, then 1-1/8" studs should also be acceptable.

An issue of concern arising from the static push-out tests is the ultimate strength of shear studs in decks constructed using PCPs. For decks with PCPs, the ultimate strength of both 7/8" and 1-1/8" shear studs was less than the corresponding specimens constructed with full-depth CIP decks. For the specimens with full-depth CIP decks constructed in accordance with TxDOT standards and with a 4" penetration of the stud into the deck, all studs failed by fracture of the shear studs. However, for specimens with PCP decks, not only was the ultimate strength reduced, but the ultimate strength was controlled by concrete failure, which appeared to be associated with the development of splitting cracks along the length of the deck in the region of the shear studs. This reduction in strength and change in failure mode occurred for specimens both with 7/8" as well as 1-1/8" shear studs, so this is not an issue related to the shear stud diameter. In a deck with PCPs, the shear stud is embedded in CIP concrete in the region between PCPs directly above the girder. This region has no reinforcing steel, and the lack of reinforcing steel in the region may be the reason for the reduction in shear stud strength and change in failure mode. However, even with the reduction in strength and change in failure mode, the measured ultimate strength of all shear studs in PCP decks exceeded the stud ultimate strength requirements in the 9<sup>th</sup> Ed. AASHTO and the proposed 10<sup>th</sup> Ed. AASHTO. Nonetheless, the ultimate strength of shear studs in decks constructed with PCPs merits further investigation in future research. The behavior of shear studs in decks with PCPs will be a major topic of study in the finite element analyses in Chapter 7.

Most of the push-out tests were constructed with studs penetrating 4" into the concrete deck. However, the 9<sup>th</sup> Ed. AASHTO and TxDOT standards specify a minimum penetration of 2" into the concrete deck. One of the push-out specimens with 1-1/8" studs was constructed with a 2" penetration of the stud into the deck. This specimen showed lower strength and lower slip capacity than the specimens with a 4" penetration of the stud into the deck. Based on this test, it appears that a minimum deck penetration greater than 2" may be preferable for 1-1/8" studs. This issue will also be studied further in the finite element analysis in Chapter 7.

Another question about using larger-diameter shear stud is can they be used on steel girders with a thin flange. One push-out specimen was constructed with two rows of 1-1/8" studs welded on to the flange of W14×99, which has a flange thickness of 0.75". Result from this test showed that no local bending or distortion was developed on 0.75" flange when ultimate strength of shear studs was reached. Thus, 1-1/8" studs can be safely used on girders with flanges as thin as 0.75".

A concern regarding larger-diameter shear studs is that such shear studs may cause cracking and other distress in the bridge deck at service level loads. This might occur because larger forces are being transferred between the stud and the surrounding concrete when larger-diameter shear studs are used, causing potentially larger localized stress levels in the concrete. However, no such distress was observed in the static push-out test program. The concrete cracking observed in specimens with 1-1/8" studs was no more severe than for specimens with 7/8" studs, at any load level for one 1-1/8" stud per row or two 1-1/8" per row with 1" haunch. Further, at load levels on

the order of one-half of the ultimate strength, no significant concrete cracking or other distress was observed any of the specimens. This indicates that reinforcing provided in bridge decks constructed in accordance with TxDOT standards, both for full-depth CIP decks as well as with PCP decks, is adequate to control concrete cracking at shear studs under service level loading.

## Chapter 6. Fatigue Push-Out Tests

### 6.1. Introduction

---

This chapter describes a series of push-out tests conducted to determine the fatigue resistance of 1-1/8" diameter shear studs. As described in the literature review in Chapter 2, past fatigue push-out tests on larger-diameter shear have shown consistently good fatigue performance. The data from previous research indicated that shear stud diameter did not have a significant effect on fatigue life. The fatigue resistance exhibited by larger-diameter shear studs has been similar to and often better than that of 7/8" studs. Essentially all previous fatigue tests on larger-diameter shear studs have shown performance that satisfies both the 9<sup>th</sup> Ed. AASHTO and the proposed 10<sup>th</sup> Ed. AASHTO S-N curves. Because of the consistently good fatigue performance of larger-diameter shear studs in past studies, only a limited number of fatigue tests were performed in this current study to confirm these previous results.

This chapter describes the fatigue test program. The same push-out test setup and specimen configuration used for the static push-out test program described in Chapter 5 were also used for the fatigue tests.

### 6.2. Test Specimens

---

Previous research has shown that the fatigue performance of larger-diameter shear studs is as good or better than that of 7/8" shear studs (Kakish 1997, Badie, Tadros, et al. 2002, Shim, Lee and Yoon 2004, Lee, Shim and Chang 2005, Mundie 2011). The test matrix was chosen to confirm these previous findings and to confirm that the 1-1/8" shear studs used in this test program satisfied the fatigue requirements in the 9<sup>th</sup> Ed. AASHTO and proposed 10<sup>th</sup> Ed. AASHTO.

A total of four fatigue push-out tests were constructed and tested. Table 6.1 lists key characteristics of the fatigue push-out specimens. The deck type of the all-fatigue push-out specimens was full-depth cast-in-place concrete. The specimens were tested under four different stress ranges varying between 15 ksi and 30 ksi. The stress ranges were chosen so that each fatigue test could be completed in a reasonable time in the laboratory and also to provide some variation in the tested stress ranges. Push-out specimens with one and two shear studs per row were also tested to investigate the influence of shear stud configuration on fatigue performance. Detailed descriptions of the specimens are provided in Section 5.2. As indicated in Table 6.1, Fatigue Specimen Nos. 1F and 2F were nominally identical to Specimen No. 3 in the static push-out test program. Similarly, fatigue Specimen Nos. 3F and 4F were nominally identical to Specimen No. 7 in the static push-out test program.

As described later, cyclic testing on Specimen Nos. 1F and 3F was stopped before fatigue failure, but well after the specimens' fatigue resistance exceeded the S-N curves in the 9<sup>th</sup> Ed. AASHTO

and proposed 10<sup>th</sup> Ed. AASHTO. Fatigue specimens that are not tested to failure are referred to as “runout” specimens. After fatigue testing, runout specimens 1F and 3F were tested to failure under static loading to investigate their residual static strength.

**Table 6.1 – Fatigue Push-Out Specimens**

Spec. No.	Stud Arrangement	Stress Range	Comments
1F	1 stud/row; no stagger x 3 rows	15 ksi	Same as Static Push-Out Spec. No. 3
2F		30 ksi	
3F	2 studs per row X 3 rows	20 ksi	Same as Static Push-Out Spec. No. 7
4F		25 ksi	

Note: For all specimens: 1-1/8" studs; 7" stud length after welding  
Full-depth cast-in-place deck; 3" haunch; W14×132 beams

## 6.3. Test Setup, Specimen Fabrication, Instrumentation and Closed-Loop Control

### 6.3.1. Test Setup and Specimen Fabrication

The same test setup described in Section 5.3.1 was used for the fatigue tests. However, a different system was used to apply and control the hydraulic pressure to the 550-kip actuators for cyclic loading. For the fatigue tests, a computer-controlled closed-loop system was adopted. It consisted of an MTS controller, a 30 gpm MTS hydraulic power unit, two servo valves, two linear potentiometers, and two 550-kip actuators. The details of the closed-loop control system are described later Section 6.3.3.

The same procedures were used to fabricate the static test specimens and the fatigue test specimens. Specimen fabrication details are described in Section 5.3.2.

### 6.3.2. Instrumentation

Two 500 kip load cells were used to monitor the load for the fatigue specimens. This assembly was positioned in the same manner as used in the static tests. The load cells were connected to the MTS controller as part of the closed-loop control as well as the data acquisition system. Load-slip data was recorded throughout the fatigue tests.

Unlike the static tests, the fatigue test specimens were instrumented with a total of four linear potentiometers (LPs) to measure the relative slip between the steel beam flange and the concrete haunch. The LPs were attached to the steel beam, and a wood block was also glued to the concrete haunch following the same approach as in the static tests. Figure 6.1 shows the placement of the LPs and wood blocks for the fatigue tests.



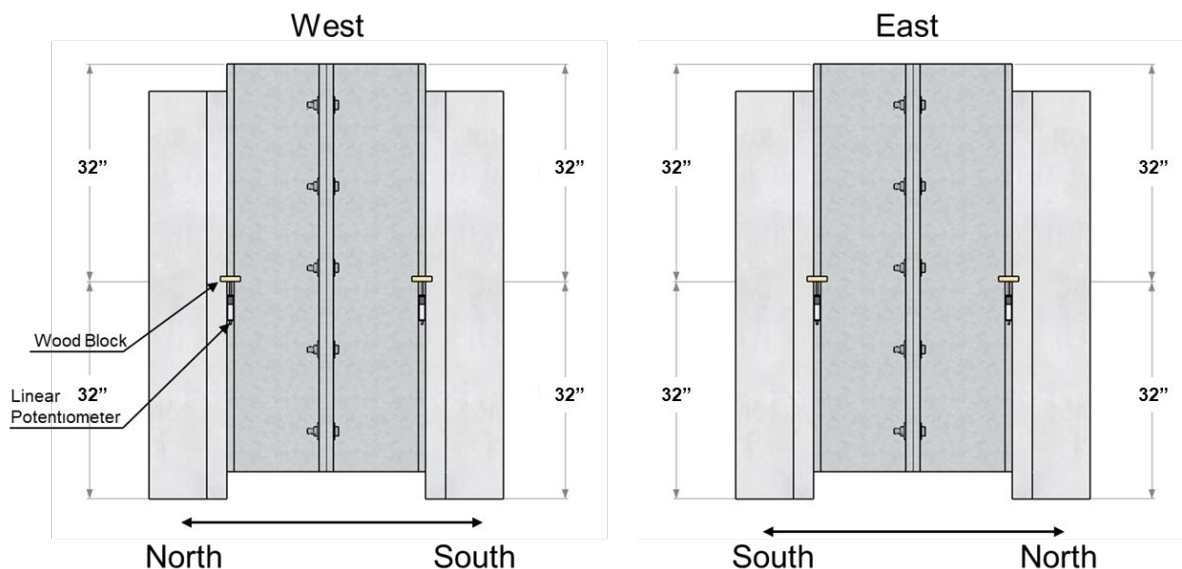


Figure 6.1 – Location of Linear Potentiometers on Fatigue Push-Out Specimens

Slip values were collected from two LPs on each steel beam flange. These slip values were intended to be representative of the slip between the steel beam flange and the concrete deck. In the static tests, a larger number of slip measurements were made over the height of the specimen and showed that slip varied over the height. In the case of the fatigue tests, the slip measurements were of secondary interest, so fewer measurements were made. The data of primary interest in the fatigue tests were the applied stress range and the number of load cycles.

For the residual static push-out strength tests of runout Specimen Nos. 1F and No. 3F, six LPs were mounted on the specimen in the same configuration as described in Section 5.3.3 for the static specimens. These were intended to provide a direct comparison with the load-slip response of their counterpart specimens in the static push-out tests reported in Chapter 5.

### 6.3.3. Closed-Loop Control

The closed-loop control system allowed application of the cyclic loading essentially 24 hours a day. This system consisted of an MTS controller, a 30 gpm MTS hydraulic power unit, two servo valves, two 550-kip actuators, and two linear potentiometers to measure the displacement of the actuator piston. The controller was an MTS FlexTest 60.

Figure 6.2 shows the key components of the closed-loop control system used for the fatigue tests. The target load range and the loading frequency were entered by the user as input on the MTS controller. The software that allows the user to input the commands is MTS TestSuite Multipurpose Elite. The controller provides a signal that characterizes the amount and direction of the load and the loading frequency the actuators need to apply. Then the command is sent to the servo-valve. This signal determines how much hydraulic fluid, incoming from the hydraulic

power unit, passes through the servo-valve spool to enter and exit the actuator. Through load cells, the load applied by the actuator is determined and sends feedback to the controller to be compared to the original command input by the user. The subsequent command signal is modified based on the feedback and then sent to the servo-valve.

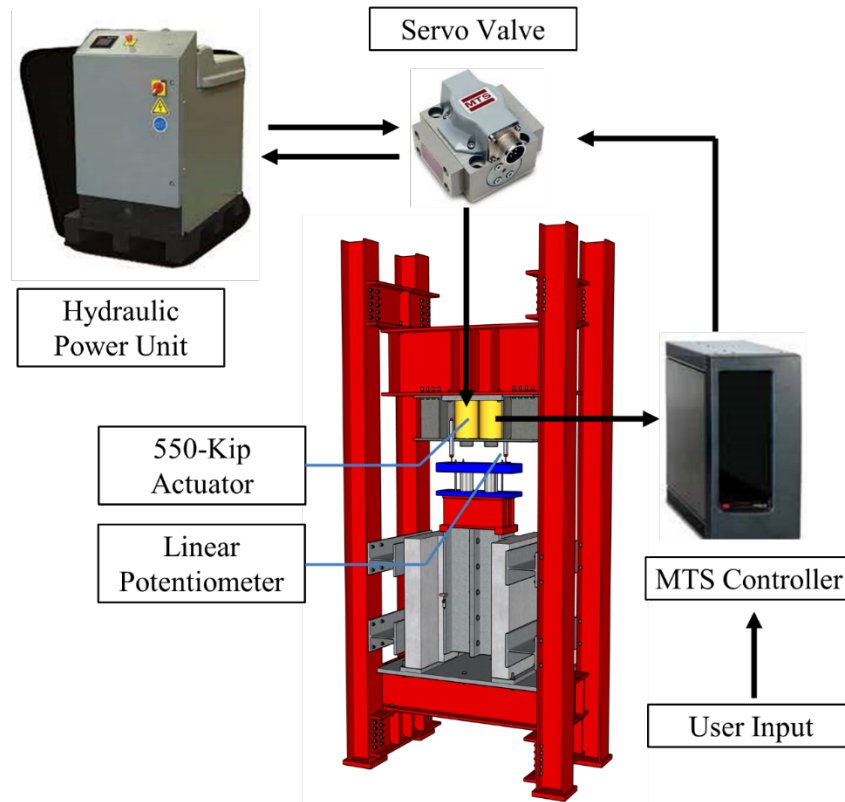


Figure 6.2 - Flow Chart of the Closed-Loop Control System

The MTS controller allows the operator to specify the load sequence applied to the specimen, and to specify limits to detect the failure of the specimen, enabling the controller to automatically stop the test. These limits for the fatigue tests were actuator stroke length tolerance and peak load change tolerance. The actuator stroke displacement is determined by linear potentiometers attached to the actuators and characterizes the displacement range of the actuator within a loading cycle. One indicator of failure is when the stroke length exceeds a specified value. A drop in the peak load sustained by the specimen was also used as an indicator of failure. When either one of these limits is exceeded, the automatic shutoff system interlocks the hydraulic pump and stops pressure. Through this capability of the controller, it was possible to safely continue fatigue loading essentially 24 hours a day.

## 6.4. Material Properties

---

### 6.4.1. Shear Studs

The shear studs used for the fatigue specimens were all 1-1/8" diameter and 7" long after welding. These shear studs came from the same production lot as the 7" long 1-1/8" diameter studs used in the static push-out tests. Tension coupon test results for these studs are listed in Table 5.5. The same stud welding procedures were used for the static push-out specimens and the fatigue push-out specimens and are listed in Table 5.3.

### 6.4.2. Concrete Material Properties

Similar to the static push-out specimens, the fatigue push-out specimens were constructed using TxDOT Class S concrete (TxDOT 2023) with a design compressive strength of 4 ksi. The fatigue specimens were constructed using a full-depth cast-in-place deck. The details of casting concrete cylinders and the compressive strength tests were described in Section 5.4.3. Cylinders were prepared by the sulfur cap method (ASTM C617). Table 6.2 lists the 28-day concrete compressive strength and test-day compressive strength for the fatigue specimens.

**Table 6.2 - Concrete Strength for Fatigue Specimens**

<b>Specimen No.</b>	<b>28-Day Strength (psi)</b>	<b>Test Day Strength (at start of fatigue testing) (psi)</b>	<b>Days from Casting to Start of Fatigue Testing</b>
1F	4882	5250	208
2F	4792	5492	124
3F	4801	4988	182
4F	4783	4996	143

## 6.5. Test Procedures and Observations

---

Table 6.3 lists the details of the applied fatigue loads and stress ranges for each fatigue specimen. A minimum load greater than zero was selected to prevent the separation of the actuators and the specimen at the minimum load point. The stress range was computed by taking the load range and dividing by the cross-sectional area of the stud and the total number of studs in the specimen. The stress ranges varied from 15 ksi to 30 ksi among the four specimens and were selected in part to permit completion of the fatigue tests in a reasonable amount of time and also to provide some variation in stress range.

The loading procedure can be divided into three main steps, as follows:

1. Pre-loading
2. Cyclic loading

3. Monotonic loading to failure for run-out specimens

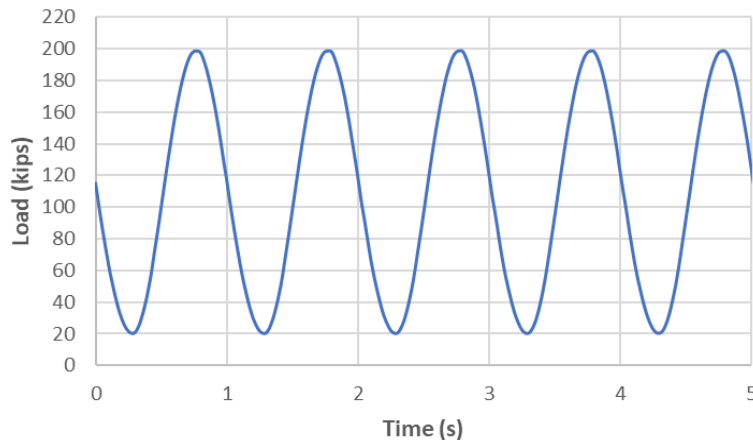
**Table 6.3 - Load and Stress Ranges for Fatigue Specimens**

Specimen No.	Minimum Load (kips)	Maximum Load (kips)	Load Range (kips)	Stress Range on Stud, S (ksi)	Load Frequency (Hz)
1F	18	108	90	15	3
2F	18	197	179	30	1
3F	36	275	239	20	1-2
4F	6	304	298	25	1

The pre-loading step consisted of a single loading and unloading cycle of the specimen. The pre-loading was applied at a rate of approximately 1 kip per second up to the peak load of the cyclic loading, as listed in Table 6.3. The purpose of this loading step was to attempt to break the bond that may have been present between the steel surface and the concrete. When the load reached the peak load, the specimen was unloaded at the rate of approximately 1 kip per second.

After the pre-loading stage, cyclic loading of the specimen commenced. During the cyclic loading stage, the load was varied for each cycle between the minimum and maximum values listed in Table 6.3 to achieve the desired stress range. The minimum load level was chosen to provide a minimum stress of 3 ksi on the studs for Specimens Nos. 1F to 3F. For Specimen No. 4F, a smaller minimum stress of 0.5 ksi was chosen to keep the maximum load within the capacity of the loading system.

The cyclic loading as a function of time was sinusoidal with a constant amplitude and a constant mean load. The loading frequency was chosen to provide the highest possible frequency to minimize testing time while still maintaining accurate loading control. Figure 6.3 shows the sinusoidal loading pattern at 1 Hz used for Specimen No. 2F. The cyclic loading was stopped automatically by the MTS controller in the case of failure or was stopped manually in the case of runout specimens.



*Figure 6.3 – Sinusoidal Loading Pattern for Specimen No. 2F*

To complete fatigue testing in a reasonable amount of time, a specimen was declared a runout if the fatigue failure event did not occur at a specified number of cycles which significantly exceeded the fatigue life requirements of the 9<sup>th</sup> Ed. AASHTO or the proposed 10 Ed. AASHTO. When a specimen was declared a runout, a single monotonic loading was applied to the specimen until failure to examine the residual static strength after the fatigue loading.

The presence of cracks on the concrete was checked before the test began and after the failure occurred due to the cyclic loading or after the cyclic loading was terminated as a runout. According to past research done in fatigue tests, a dull or shiny failure surface on shear studs is commonly observed. While a dull surface primarily indicates the propagation of fatigue cracks, a static failure surface tends to be shiny. In some tests, after failure, some of the studs showed a dull surface and some showed a shiny surface. This suggests that at the time of complete failure (all studs fractured) enough studs failed by fatigue that the applied loading exceeded the static fracture capacity of the remaining studs. A detailed description of the test process and observations is provided for each test in the following sections.

## 6.5.1. Cyclic Loading Observations

### 6.5.1.1. Specimen No. 1F: 15 ksi Stress Range, One Shear Stud Per Row

The specimen was checked for cracks in the concrete before the test, and there were no noticeable cracks on the concrete surfaces. No sound was heard from the specimen on the pre-loading stage indicating that the bond between the steel flange and concrete had not broken in this load cycle. However, a plot of slip versus number of loading cycles (see Figure 6.13) shows slip occurring from the start of cyclic loading, indicating that the bond was broken prior to the start of cyclic loading. Specimen No.1F was declared a runout after 2.3 million cycles. After the runout, there were no noticeable cracks on the surface.

### 6.5.1.2. Specimen No. 2F: 30 ksi Stress Range, one Shear Stud Per Row

The specimen was checked for cracks in the concrete before the test, and there were no noticeable cracks on the concrete surfaces. During the pre-loading stage, a sound from the specimen was heard accompanied by a sudden increase in slip, which was an indication of a broken bond between the steel flange and the concrete. The north side of the specimen failed with fracture of all shear studs after 156,473 cycles of load, and the steel beam flange and concrete slab were completely separated, as can be seen in Figure 6.4. Other than the separation, no crack development was observed on the concrete.

The bottom side of the north concrete deck after the failure is shown in Figure 6.5. While two of the three studs fractured through their shanks, one shear stud fractured near the weld. Enlarged photos of the studs identified by the arrows show that while the stud at the top exhibited a dull-



colored surface which is indicative of fatigue cracking, the other two studs have shiny failure surfaces suggesting a static failure rather than a fatigue crack.

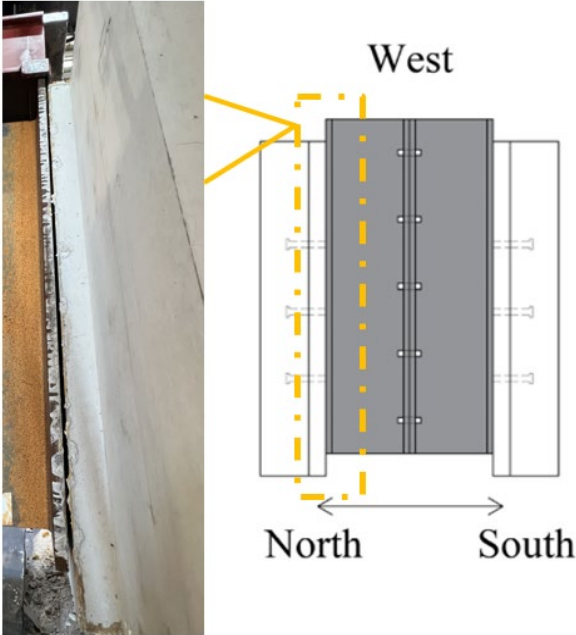


Figure 6.4 - Specimen No.2F: Photo of Separation Between Steel Flange and Concrete After Failure



Figure 6.5 - Specimen No.2F: Concrete Deck After Failure with Enlarged Photos of Studs

### 6.5.1.3. Specimen No. 3F: 20 ksi Stress Range, Two Shear Studs Per Row

The specimen was checked for cracks in the concrete before the test, and there were no noticeable cracks on the concrete surfaces. A sound was heard from the specimen during the pre-loading stage, which was accompanied by a significant rise in slip, indicating that the bond between the steel flange and the concrete had broken. Specimen No. 3F was declared a runout after 2.3 million cycles. Crack mapping of the specimen after runout is shown in Figure 6.6. Only minor cracks were observed.

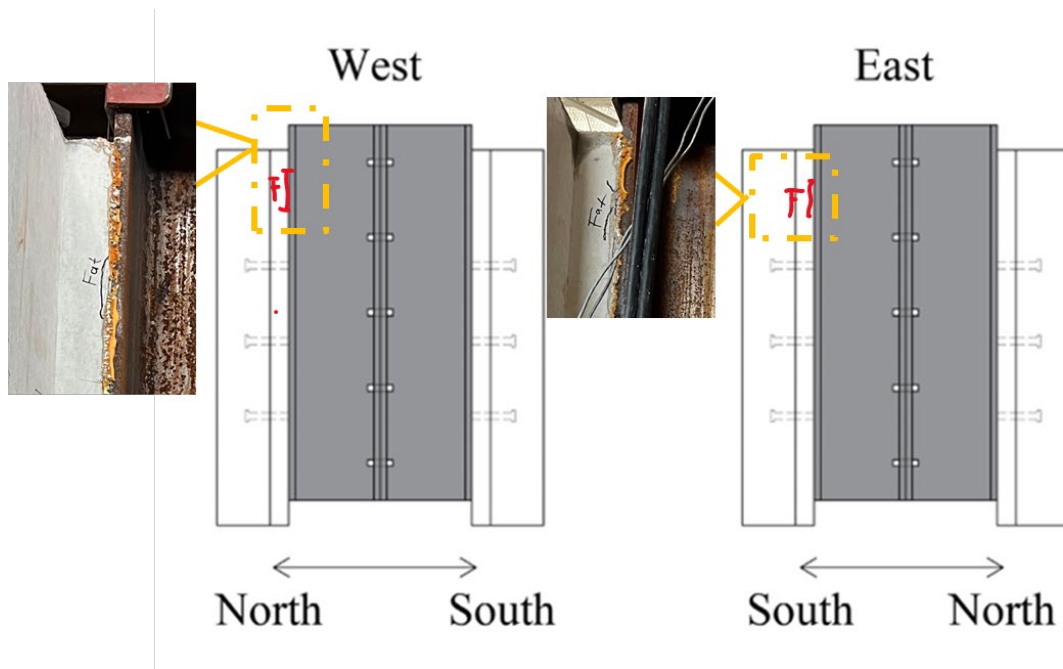


Figure 6.6 - Specimen No.3F: Crack Mapping After Runout

### 6.5.1.4. Specimen No. 4F: 25 ksi Stress Range, Two Shear Studs Per Row

The specimen was checked for cracks before the test, and there were no noticeable cracks on the concrete surfaces. No sound was heard during the pre-loading stage. However, a plot of slip versus number of load cycles (see Figure 6.16) does not show any sudden increases in slip during cyclic loading, indicating the bond between the steel flange and the concrete was broken prior to the start of cyclic loading. The specimen failed with fracture of all shear studs on the north side after 147,470 cycles of load, and the steel beam flange and concrete slab were completely separated from each other. After the failure occurred, the specimen was checked for cracks in the concrete, and a mapping of the cracks is provided in Figure 6.7.

The bottom side of the north concrete deck after the failure is shown in Figure 6.8. All the shear studs on the steel flange beam fractured near the weld for this specimen. Enlarged photos of the studs identified by the arrows show that the fracture surface of the stud at the top exhibited porosity in the weld. Since the fatigue life of Specimen No. 4F was comparatively shorter than Specimen No. 2F despite the higher stress range in Specimen No. 2F, the fatigue cracks may



have propagated at a faster rate due to the presence of the weld porosity. The fracture surface of the stud at the bottom was shiny, indicating static failure that might happen at the end of the test.

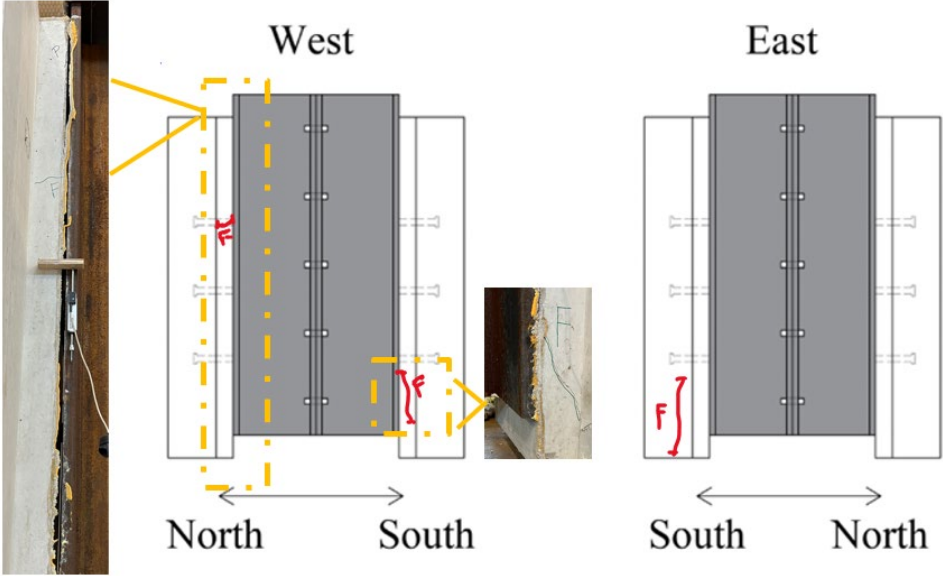


Figure 6.7 - Specimen No.4F: Photo of the Separation and Crack Mapping After Failure



Figure 6.8 - Specimen No.4F: Concrete Deck After Failure with Enlarged Photos of Studs

### 6.5.2. Monotonic Loading Observations

After cyclic loading of Specimen Nos. 1F and 3F was stopped and the specimens were declared runouts, the specimens were subject to a final monotonic load cycle to characterize their residual strength after fatigue loading. The following sections describe observations made during the final monotonic loading of these specimens.

#### 6.5.2.1. Specimen No. 1F: Monotonic Loading

The monotonic load was applied to the specimen until the specimen failed. The specimen failed with fracture of all shear studs on the north side, and the steel beam flange and concrete slab were completely separated from each other. After the failure, the separation surface of the specimen is shown in Figure 6.9.

Figure 6.10 shows photos of the bottom side of the north concrete deck after the failure. All the shear studs on the steel flange beam fractured near the weld for this specimen. The fracture surfaces of all shear studs showed areas of both dull and shiny surfaces, suggesting that fatigue cracks extended partially through the stud cross-section and the propagated through the complete section under the final monotonic load. Significant porosity in the weld was also present at one of the failed shear stud cross-sections.

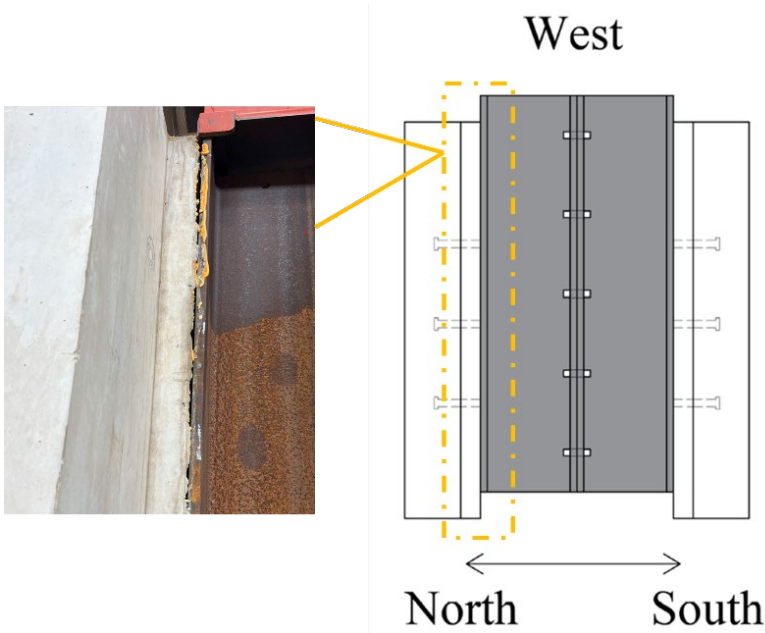


Figure 6.9 - Specimen No.1F: Photo of the Separation Between Steel Beam Flange and Concrete After Failure Under Monotonic Loading



Figure 6.10 - Specimen No.1F: Concrete Deck After Failure Under Monotonic Loading with Enlarged Photos of Studs

### 6.5.2.2. Specimen No. 3F: Monotonic Loading

The monotonic load was applied to the specimen until the specimen failed. The specimen failed with fracture of all shear studs on the north side, and the steel beam flange and concrete slab were completely separated from each other, as can be seen in Figure 6.11.

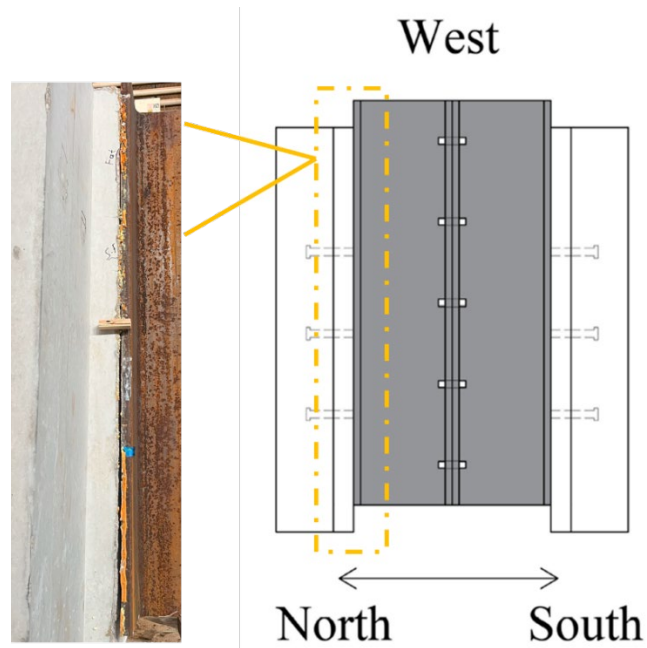


Figure 6.11 - Specimen No.3F: Photo of the Separation Between the Steel Beam Flange and Concrete After Failure



Figure 6.12 shows photos of the bottom side of the north concrete deck after the failure. While four of the shear studs fractured in their shank away from the weld, two shear studs fractured in the weld with significant porosity visible on the fracture surfaces. All fractures surfaces were shiny indicating that the fractures were almost entirely the result of the static loading rather than propagation of fatigue cracks.



Figure 6.12 - Specimen No.3F: Concrete Deck After Failure with Enlarged Photos of Studs

## 6.6. Fatigue Test Results

---

### 6.6.1. S-N Results

The applied stress range (S) and number of cycles to failure or to runout (N) are listed in Table 6.4. The table also notes on which side of the push-out specimen the shear studs failed. For the runout specimens, the failure side shown in parenthesis in Table 6.4 indicates the failure side under the final monotonic loading cycle.

As expected, as the stress range decreased, the fatigue life of the specimen increased. However, the fatigue life of Specimen No. 4F was shorter than that of Specimen No. 2F even though Specimen 4F had a smaller stress range. The reason behind that may be differences in weld quality or may simply reflect typical variability in fatigue test results.

**Table 6.4 - Fatigue Test Results**

Specimen No.	Minimum Stress (ksi)	Maximum Stress (ksi)	Stress Range, S (ksi)	Number of Cycles	Failure side
1F	3	18	15	2,390,000	Runout (North)
2F	3	33	30	156,473	North
3F	3	23	20	2,359,000	Runout (North)
4F	0.5	25.5	25	147,470	North

### 6.6.2. Slip Versus Number of Cycles

Curves plotting slip versus number of loading cycles for Specimen Nos. 1F to 4F are shown in Figure 6.13 to Figure 6.16. As described earlier, a total of four linear potentiometers (LPs) were placed on each specimen to measure the relative slip between the steel beam flange and the concrete. The slip shown in Figure 6.13 to Figure 6.16 was computed by averaging the two LPs on each slab. The slip values shown in the figures the maximum slip measurement during the cyclic loading at 10-second intervals. Thus, a slip value for a given number of cycles represents the maximum slip for a range of 10 to 30 cycles depending on the frequency that the specimen was tested. Due to the longer fatigue life of Specimen Nos. 1F and 3F, during the test, the LPs needed to be repositioned to avoid dead spots in the active region of the track, and due to this reason, local drops in the plots are the indication of repositioning.

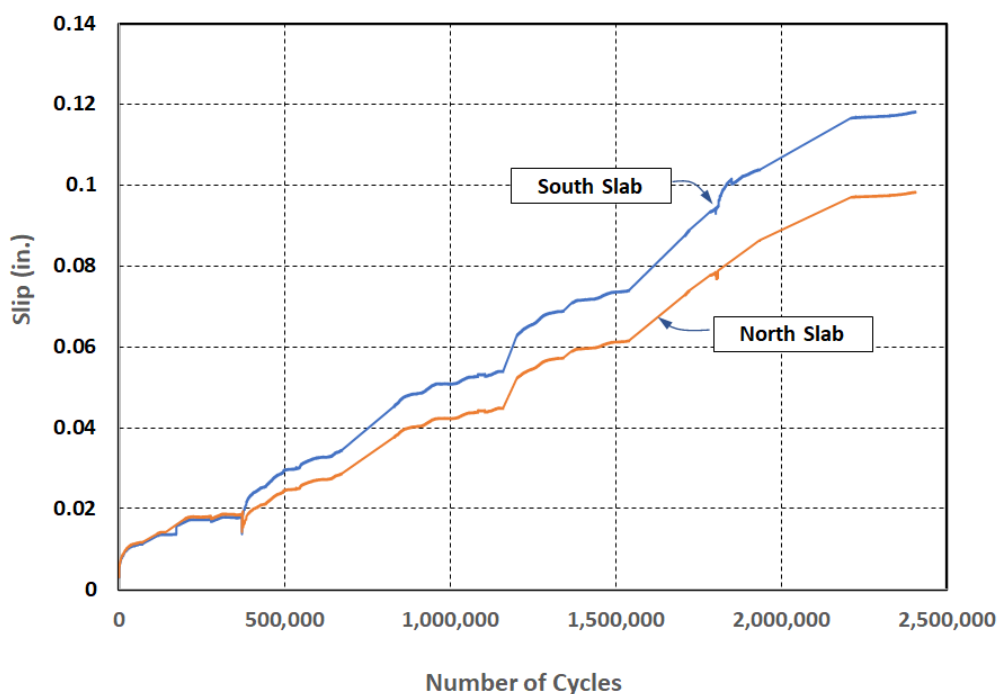


Figure 6.13 – Slip Versus Number of Cycles for Specimen No. 1F

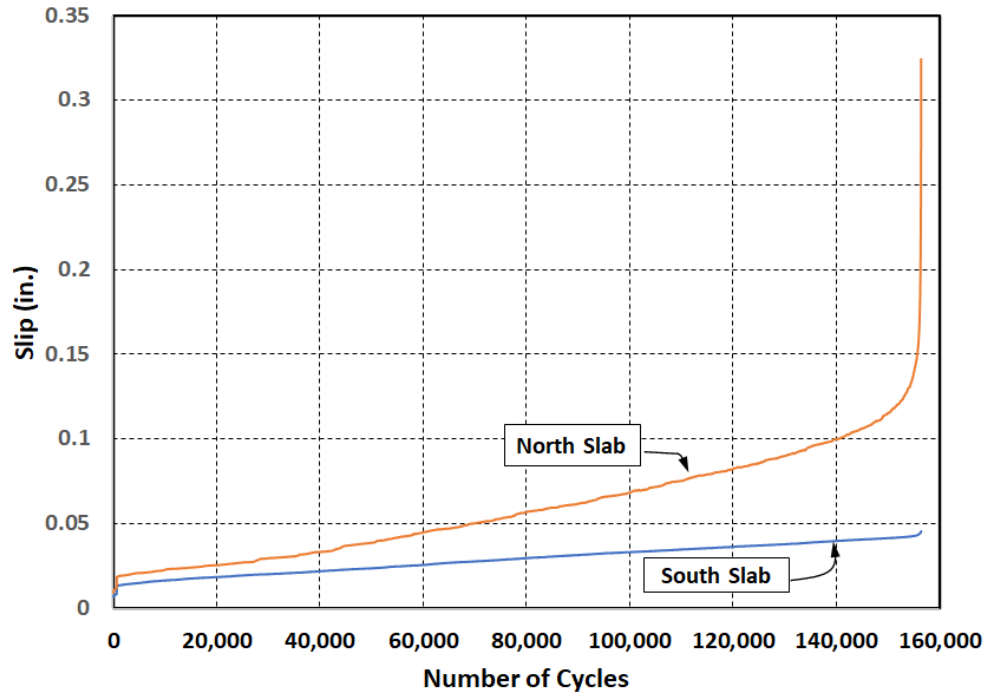


Figure 6.14 – Slip Versus Number of Cycles for Specimen No. 2F

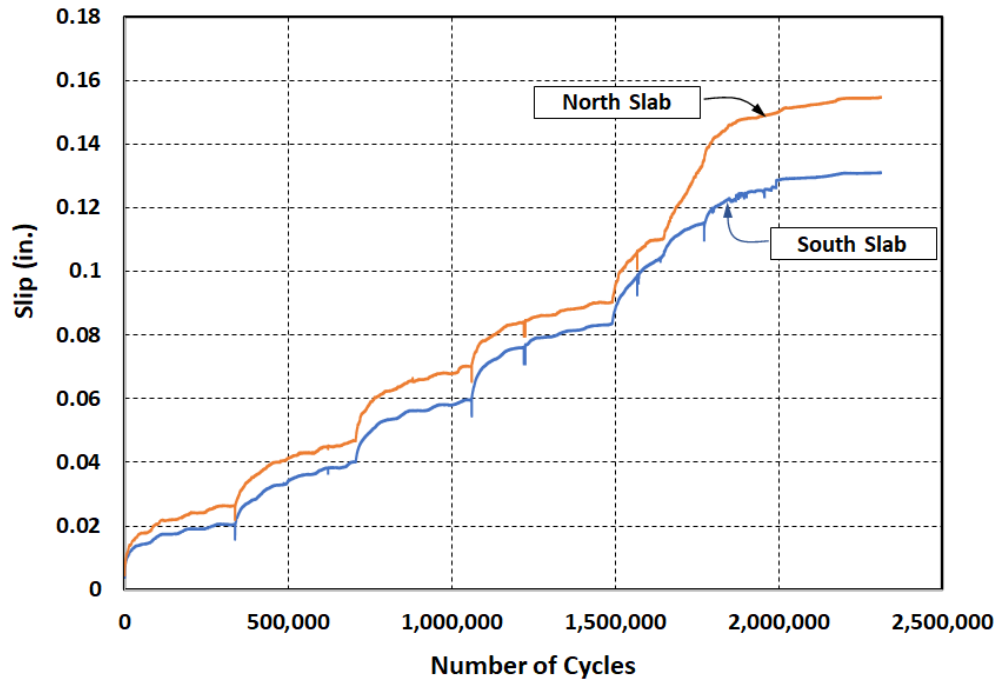


Figure 6.15 – Slip Versus Number of Cycles for Specimen No. 3F

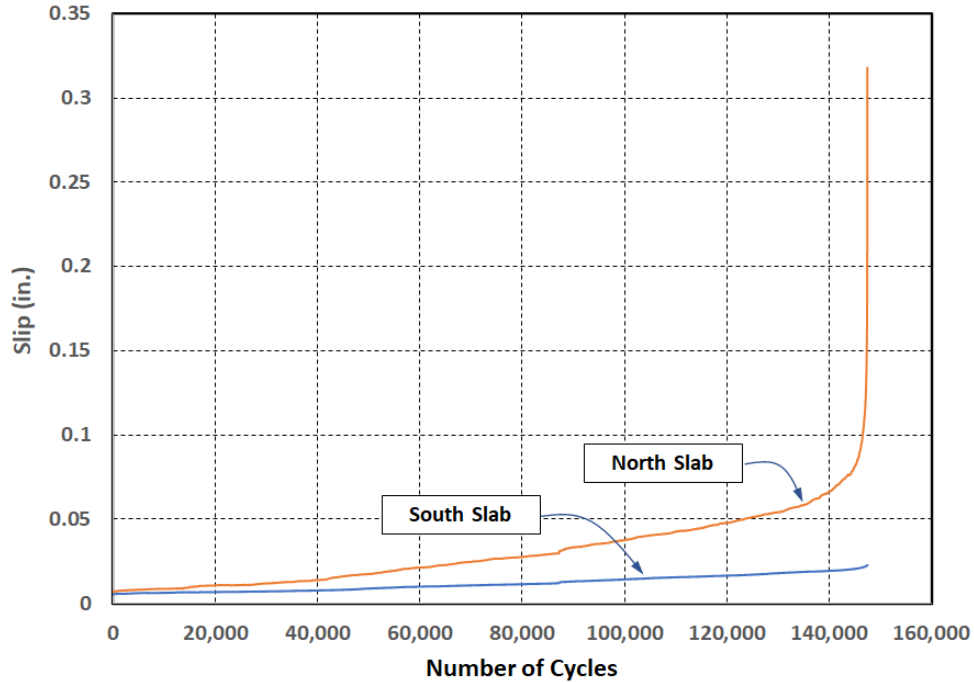


Figure 6.16 – Slip Versus Number of Cycles for Specimen No. 4F

Slip versus number of loading cycles is shown for all specimens in a single plot in Figure 6.17. In order to compare the largest slips, only the side of the specimen with the larger slip was plotted. For all specimens, there is a continual increase in slip with the number of loading cycles. This slip may reflect both damage to the concrete as well as damage to the stud. However, for the specimens that were subjected to fatigue loading to failure (Specimen Nos. 2F and 4F), there was a very rapid increase in slip just prior to complete failure. For example, Specimen No. 4F (Figure 6.16) showed a relatively small slip of 0.07" at 140,000 cycles but experienced complete fracture of all studs at approximately 147,000 cycles. Consequently, in an actual bridge girder, there may be little apparent sign of distress, such as larger girder deflections, prior to fatigue failure of shear studs. However, as discussed in Chapter 2, information in the literature suggests that the fatigue performance of shear studs in girders is better than that of shear studs in push-out specimens. This may be due to the larger number of shear studs in a girder than in a push-out specimen, thereby permitting a greater degree of force redistribution among studs in a girder, as shear studs experience a reduction in stiffness due to fatigue cracking.



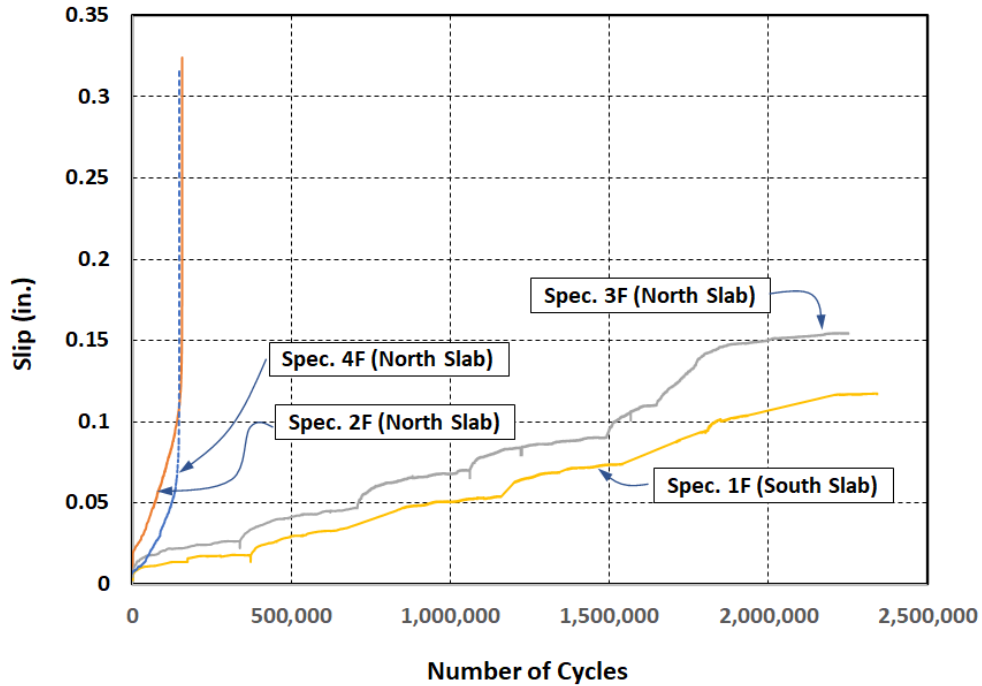


Figure 6.17 – Slip Versus Number of Cycles for All Specimens

### 6.6.3. Comparison with AASHTO S-N Curves

Results of fatigue tests are normally displayed in the form of S-N plots. These plots show the stress range (S) on the vertical axis and the number of cycles to failure (N) on the horizontal axis. Each fatigue test shows as a single point on the S-N plot. The plots can also show the S-N curves used for fatigue design in various design standards.

Figure 6.18 is an S-N plot in a semi-log format and shows data points from this TxDOT 0-7042 fatigue test program as well as from previous test programs. The arrows on two of the 1-1/8" stud tests denote runouts. Also shown in Figure 6.18 is the S-N curve from the 9<sup>th</sup> Ed. AASHTO (AASHTO 2020). As can be seen from this figure, the 1-1/8" studs tested in this research project showed fatigue performance that is similar to or better than 7/8" studs and similar or better than larger-diameter shear studs tested by others. Further, all of the studs tested in this program exceeded the S-N curve of the 9<sup>th</sup> Ed. AASHTO.

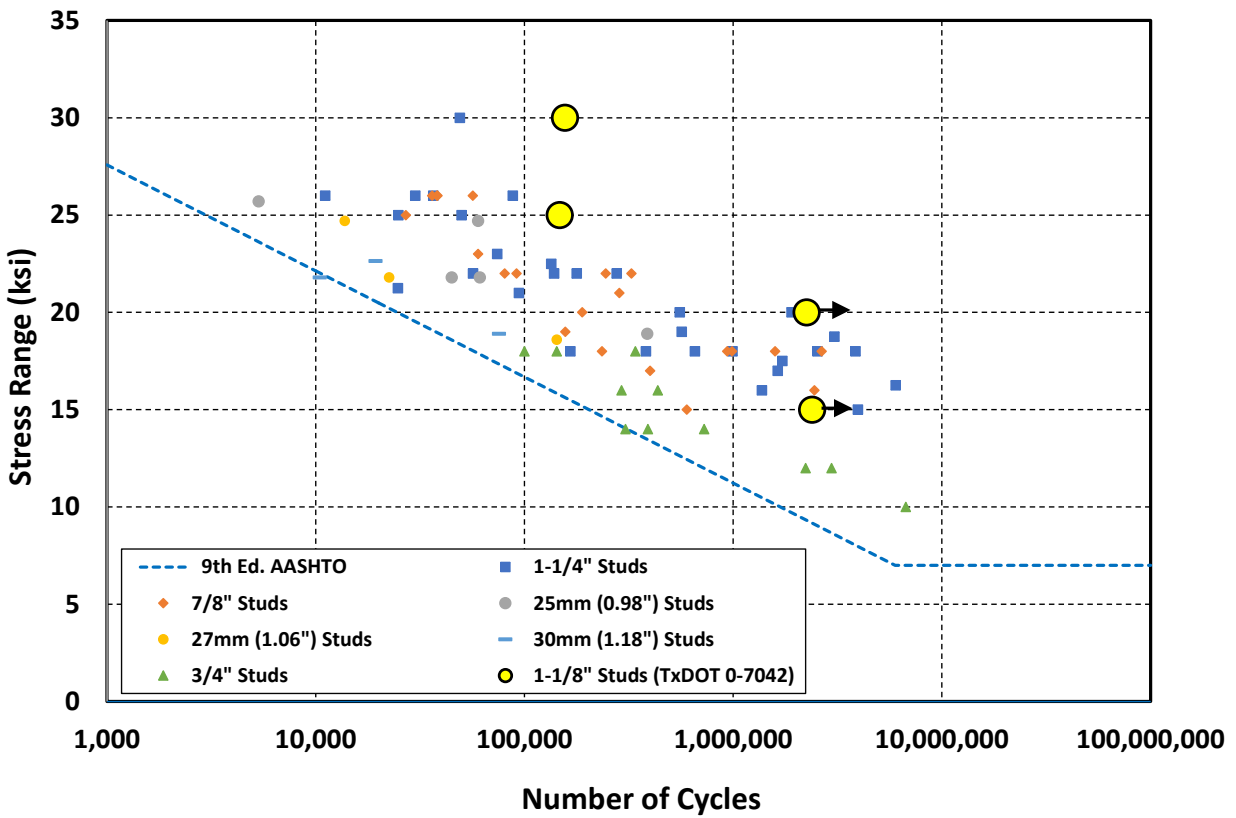


Figure 6.18 – 9<sup>th</sup> Ed. AASHTO S-N Curve for Shear Studs and Fatigue Test Results

In Figure 6.19, the current 9<sup>th</sup> Ed. AASHTO and the proposed 10<sup>th</sup> Ed. AASHTO S-N curves for shear studs are plotted in a log-log format along with the test results from this TxDOT 0-7042 fatigue test program. The fatigue performance of the 1-1/8" shear studs tested in this research project exceeded the requirements of both specifications.

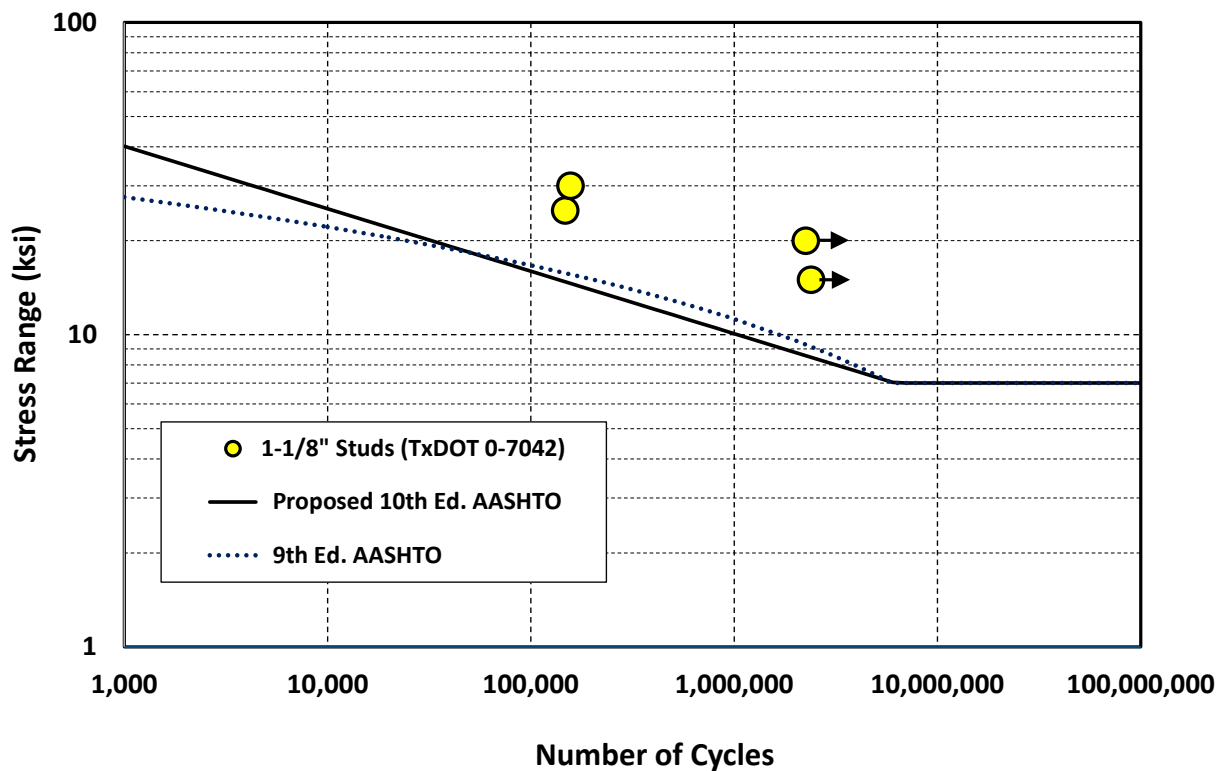


Figure 6.19 - Comparison of 9<sup>th</sup> Ed. and Proposed 10<sup>th</sup> Ed. AASHTO S-N Curves and Fatigue Results for 1-1/8" Studs Tested in TxDOT 0-7042 Research Project

## 6.7. Residual Static Strength Results

As described earlier, after cyclic loading was terminated for runout Specimen Nos. 1F and 3F, these specimens were subjected to a final monotonic loading cycle to failure, to investigate their residual static strength after extensive fatigue loading.

Load-slip curves for the final monotonic loading cycle for Specimen Nos. 1F and 3F are shown in Figure 6.20 and Figure 6.21. These curves were constructed in the same manner as described in Section 5.6. The figures show the measurement from all LPs on the north and south sides of the specimen, and an average curve, which was derived by taking the average of all LP readings.

Table 6.5 lists the maximum loads achieved in the final monotonic load cycle for the fatigue specimens and the corresponding static push-out specimens. Fatigue Specimen No. 1F was nominally identical to Specimen No.3 in the static push-out program. Fatigue Specimen No. 3F was nominally identical to Specimen No.7 in the static push-out program. The data in Table 6.1 show that Specimen Nos. 1F and 3F had a residual static strength of 63% and 87%, respectively, compared to the corresponding static specimens. That is, despite the extensive fatigue loading, Specimen Nos. 1F and 3F still retained a substantial residual static strength.

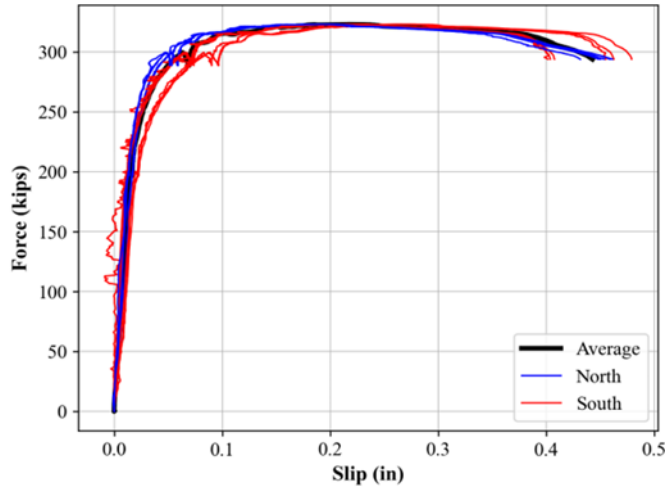


Figure 6.20 – Load-Slip Curve for Specimen No. 1F for Final Monotonic Loading

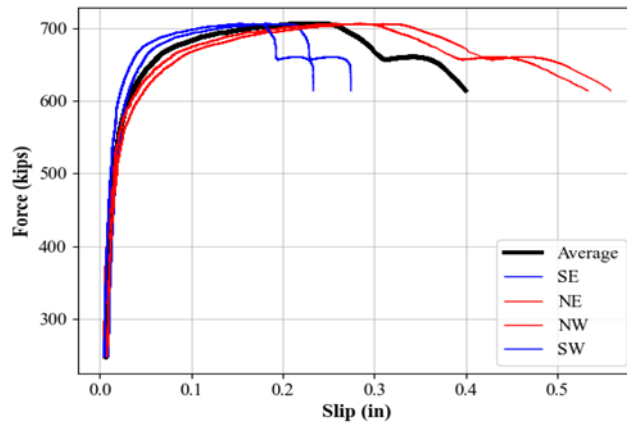


Figure 6.21 - Load-Slip Curve for Specimen No. 3F for Final Monotonic Loading

Table 6.5 – Maximum Load in Monotonic Loading Cycle and Residual Strength

Fatigue Specimen No.	Maximum Load $P_{\max\text{-fatigue}}$ (kips)	Corresponding Static Specimen No.	Maximum Load $P_{\max\text{-static}}$ (kips)	Residual Strength $P_{\max\text{-fatigue}} / P_{\max\text{-static}}$
1F	322.2	3	512.0	63%
3F	705.6	7	813.6	87%

Table 6.6 lists the maximum average load per stud developed in fatigue Specimen Nos. 1F and 3F in the final monotonic load cycle. These values were computed by taking the maximum load on the specimen, listed in Table 6.5, and dividing by the total number of studs in each specimen. Specimen No. 1F had a total of six studs and Specimen No. 3F had a total of twelve studs. Also listed in Table 6.6 is the factored shear resistance for one stud using both the 9<sup>th</sup> Ed. AASHTO and the proposed 10 Ed. AASHTO. The AASHTO factored shear resistance values were

computed using measured material properties rather than nominal specified values. For stud tensile strength,  $F_u = 83.5$  ksi was used (see Table 5.5) and for concrete compressive strength, the test day measured values were used, as listed in Table 5.8 and Table 6.2. Concrete modulus of elasticity, needed for the 9<sup>th</sup> Ed. AASHTO stud strength calculation, was determined using Eq. 5.4.2.4-1 in the 9<sup>th</sup> Ed. AASHTO.

**Table 6.6 – Load Per Stud and AASHTO Stud Factored Resistance**

Fatigue Specimen No.	Max. Load per Stud $f_s$ (kips)	9 <sup>th</sup> Ed. AASHTO $f_{n1}$ (kips, $\phi=0.85$ )	$f_s/f_{n1}$	10 <sup>th</sup> Ed. AASHTO $f_{n2}$ (kips, $\phi=1.0$ )	$f_s/f_{n2}$
1F	53.7	64.0	84%	58.1	92%
3F	58.8	61.8	95%		101%

As indicated by Table 6.6, even after extensive fatigue loading, the studs retained on the order of 85 to 95-percent of the static strength specified in the 9<sup>th</sup> Ed. AASHTO and on the order of 90 to 100-percent of the static strength specified in the proposed 10<sup>th</sup> Ed. AASHTO.

## 6.8. Conclusions

Four fatigue push-out tests were conducted on specimens with 1-1/8" shear studs with full-depth cast-in-place decks. For all specimens, the deck details, including reinforcing details, were constructed in accordance with TxDOT standards and preferred practices.

The fatigue push-out specimens were tested using stress ranges of 15, 20, 25 and 30 ksi. For two of the specimens, cyclic loading was continued until fatigue failure, corresponding to complete fracture of all studs on one side of the push-out specimen. For the other two specimens, cyclic loading was continued to 2.3 million cycles without failure. The cyclic loading was then stopped, and these specimens were classified as runout specimens.

The primary objective of the push-out test program was to determine if the AASHTO provisions for fatigue resistance of shear studs can be safely used for 1-1/8" studs, or if some modification of these provisions are needed. The test results showed that all four specimens exceeded the fatigue resistance requirements in both the 9<sup>th</sup> Ed. AASHTO and the proposed 10<sup>th</sup> Ed. AASHTO. The literature review from past fatigue push-out tests described in Chapter 2 has shown consistently good fatigue performance for larger-diameter shear studs. This previous data indicated that shear stud diameter did not have a significant effect on fatigue life. Essentially all previous fatigue tests on larger-diameter shear studs have shown performance that satisfies both the 9<sup>th</sup> Ed. AASHTO and the proposed 10<sup>th</sup> Ed. AASHTO S-N curves. The fatigue tests conducted for Project 0-7042 have confirmed these previous findings. These results indicate that the fatigue strength provisions in both the 9<sup>th</sup> Ed. AASHTO and the proposed 10<sup>th</sup> Ed. AASHTO can be safely used for 1-1/8" studs.

The two runout fatigue specimens in this test program, after completion of cyclic loading, were subjected to one final monotonic loading cycle to failure. The purpose of this final monotonic loading cycle was to characterize the residual static strength of shear studs that had previously been subjected to extensive fatigue loading. These tests showed that the studs retained on the order of 85 to 95-percent of the static strength specified in the 9<sup>th</sup> Ed. AASHTO and on the order of 90 to 100-percent of the static strength specified in the proposed 10<sup>th</sup> Ed. AASHTO. Consequently, despite extensive prior fatigue loading, these studs retained very substantial residual static strength.

# Chapter 7. Finite Element Studies: Static Push-Out Behavior

## 7.1. Introduction

---

Finite element (FE) analyses were performed to study the behavior of 7/8" and 1-1/8" diameter shear studs in push-out specimens. The objective was to supplement the static push-out test program by investigating variables not considered in the experimental tests. A particular focus of the FE study was to examine the behavior of 7/8" and 1-1/8" shear studs in bridge decks constructed using partial depth precast concrete deck panels (PCPs), since as described in Chapter 5 the results of the experimental push-out tests raised some concerns about shear stud ultimate strength and failure mode in bridge decks constructed using PCPs. The analyses were conducted using the commercial program Abaqus (Abaqus 2016) run on the Texas Advanced Computing Center (TACC) supercomputer Stampede2. Python scripting was extensively used for both preprocessing and postprocessing.

The first phase of the FE study was the development and validation of a modeling technique that reasonably captured the experimental load-slip response and failure modes of the eleven static push-out test specimens reported in Chapter 5. Specific aspects examined in this phase included the model material properties, contact properties and constraints, boundary conditions, element size and formulation, and solver parameters. The development and validation of the modeling technique relied on the data from the tests. To ensure a modeling scheme with optimized predictive capability, a single set of modeling parameters was established that provided good correlation with all experiments, rather than adjusting the modeling techniques on a specimen-by-specimen basis to obtain better agreement for any given specimen. The FE model validation phase is described in Section 7.2.

The second phase of the FE study was parametric studies. In this phase, a series of simulated push-out tests were conducted to study variables of interest, including the impact of PCPs on shear stud behavior. The simulated push-out tests in the parametric studies represented cases that were not tested in the experimental program. Results from the parametric studies were used to better understand the key factors influencing the strength of large diameter shear studs. The parametric studies are described in Section 7.3.

## 7.2. FE Model Description and Validation

---

### 7.2.1. Model Geometry and Components

The FE models developed in the validation process are listed in Table 7.1, and they represent all eleven specimens in the experimental push-out test program.



**Table 7.1 - FE Models for Validation**

<b>Model No.</b>	<b>Corresponding Push-Out Test Specimen</b>	<b>Symmetry Consideration</b>
1	7/8", three/row, CIP	Quarter
2	7/8", three/row, PCP	
3	1-1/8", one/row, no stagger, CIP	
4	1-1/8", one/row, no stagger, PCP	
5	1-1/8", one/row, staggered, CIP	Half
6	1-1/8", one/row, staggered, PCP	
7	1-1/8", two/row, CIP	Quarter
8	1-1/8", two/row, CIP Half reinforcement	
9	1-1/8", two/row, CIP 5" long stud	
10	1-1/8", two/row, CIP 1" deep haunch	
11	1-1/8", two/row, CIP 0.75" steel beam flange thickness	

As described in Chapter 5, the push-out specimens, test setup, and instrumentation were all designed in a symmetric way. The presence of symmetry was exploited in the FE studies by modeling a half or a quarter of the actual specimen with proper symmetric boundary conditions applied. The geometry of the FE models is the same as that of the corresponding specimens, described through detailed drawings found in Chapter 5. To illustrate the overall geometry and components of the FE models, Models No. 6 and No. 7 are shown in Figure 7.1 and Figure 7.2 as typical examples. Model No. 6 is one-half of the actual specimen and Model No. 7 is a quarter of the actual specimen. Model No. 6 consists of concrete, PCPs, steel beam, shear studs, reinforcement, and a rigid foundation. Model No. 7 has everything in Model No. 6 except PCPs since it represents the fully cast-in-place specimen. The following items that were present in the actual specimens were omitted in the FE models to achieve better computational efficiency: R bars in PCPs for lifting purposes, the opposite half of the steel beam, and the lifting devices in the CIP concrete deck. These items are not expected to influence the behavior of the FE model. In Figure 7.1 and Figure 7.2, the CIP concrete in the right plot is omitted to show the studs and reinforcement.

As described in Section 5.2.3, the shear studs in Specimen No. 2 of the push-out program were bent by hammer to satisfy the clear distance requirement between the edge of the stud and the edge of the PCP. The geometry of the bent shear studs is somewhat irregular. This geometry was simplified in the corresponding FE models by having straight shear studs with a clear distance of 5/8" between the stud head and the PCP. This simplification makes the concrete deck of the FE model 1.8" (i.e., 4-percent) wider than that in the test.

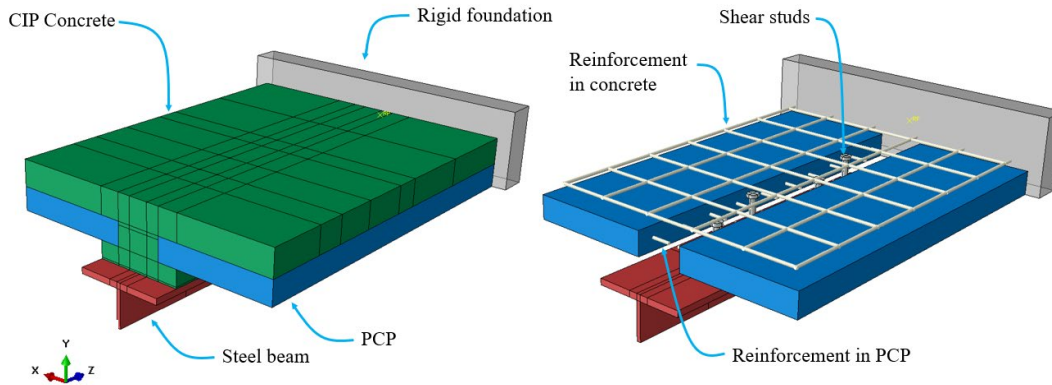


Figure 7.1 - FE Model No. 6

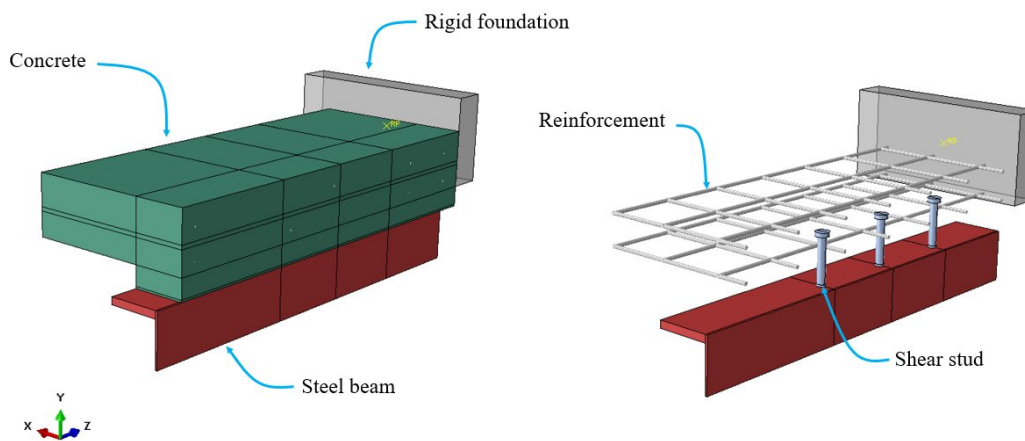


Figure 7.2 - FE Model No. 7

Based on information in the literature, including the weld collar at the base of the stud in an FE model can significantly affect the FE results (El-lobody 2002, Dara 2015, Kruszewski, Zaghi and Wille 2019, Cao and Shao 2019). Therefore, the weld collars of the shear studs were included in all FE models, as illustrated in Figure 7.3. Table 7.2 below provides the weld collar dimensions used in the models for 1-1/8" and 7/8" studs. These dimensions were obtained by measuring the actual stud weld collars in the push-out test specimens.

Table 7.2 - Dimensions of Weld Collars

Stud Diameter (in)	Height (in)	Diameter (in)	Comments
7/8	0.19	1.05	Average height based on 6 actual weld collars. Average diameter based on 14 actual weld collars.
1-1/8	0.28	1.23	Average height based on 20 actual weld collars. Average diameter based on 25 actual weld collars.

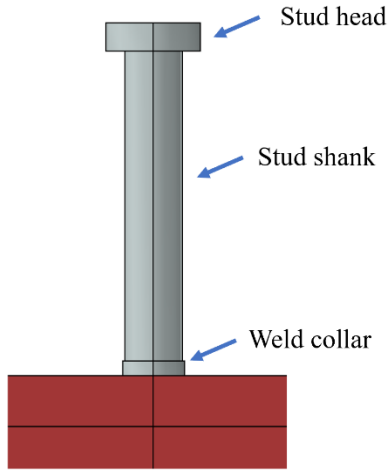


Figure 7.3 - Enlarged View of FE Model of Shear Stud

## 7.2.2. Material Properties

### 7.2.2.1. Material Properties in Nonlinear FE Analysis

For nonlinear material models in FE analysis, in addition to uniaxial stress-strain curves, a yield function and a plastic flow rule must be defined. If material damage is included, damage models also need to be defined.

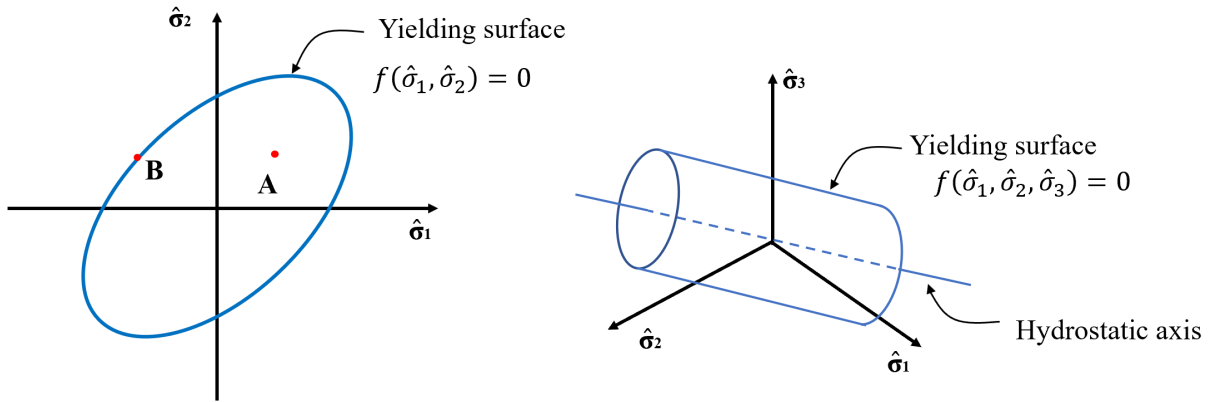
The yield function,  $f$ , defines the state of stress at yielding of a material. In the 1-dimensional case, yielding of the material can be determined by simply comparing the instantaneous stress with the uniaxial yield stress. For 2- and 3-dimensional models, stress is not a scalar but a tensor. Yielding of the material needs to consider multiple stress terms in the stress tensor. This can be done by using invariants of the stress tensor. For metals, yielding is usually related to the second invariant of the deviatoric stress tensor (Koutromanos 2014), which is called  $J_2$  plasticity or the Von Mises yield criterion. Eq. 7-1 provides the expression for the Von Mises yield function (Koutromanos 2014).

$$\begin{aligned}
 f(\{\sigma\}) &= \sqrt{\frac{1}{2} \left[ (\sigma_{11} - \sigma_{22})^2 + (\sigma_{22} - \sigma_{33})^2 + (\sigma_{33} - \sigma_{11})^2 \right] + 3(\sigma_{12}^2 + \sigma_{23}^2 + \sigma_{31}^2)} - \sigma_y(\tilde{\epsilon}^{pl}) \\
 &= \sqrt{3J_2} - \sigma_y(\tilde{\epsilon}^{pl})
 \end{aligned} \tag{7-1}$$

In Eq. 7-1,  $\sigma_y$  is the uniaxial yield strength of the material. For elastic perfect plastic material (i.e., no strain hardening)  $\sigma_y$  is a constant. For material with hardening,  $\sigma_y$  is determined by the current hardening variable and the equivalent plastic strain,  $\tilde{\epsilon}^{pl}$ . The equivalent plastic strain  $\tilde{\epsilon}^{pl}$

expresses the accumulation of plastic deformation (hardening variable).  $J_2$  is the second invariant of the deviatoric stress tensor.

The assembly of stress states that satisfy the yield function,  $f(\{\sigma\}) = 0$ , creates a yield surface in higher dimensional space. Figure 7.4 illustrates the Von Mises yield surface in 2D and 3D principal stress space. Two points are depicted in the 2D diagram showing the stress states corresponding to not yielded (Point A) and yielded (Point B), respectively.



Stress state A:  $f(\{\sigma\}_A) < 0$ , material is not yielded

Stress state B:  $f(\{\sigma\}_B) = 0$ , material is yielded

Figure 7.4 - Von Mises Yield Surface in 2D Principal Stress Space and 3D Principal Stress Space

For concrete, several yield functions have been proposed, including those by Drucker and Prager (1952) and Lubliner et al. (1989). In Abaqus, the concrete damaged plasticity (CDP) material model uses the yield function proposed by Lee and Fenves (1998), which combines the Drucker-Prager and Lubliner yield functions. Expressions for the CDP yield function are given in Eq. 7-2 to Eq. 7-5. The  $\langle \rangle$  symbol in Eq. 7-2 represents the Macaulay bracket. When  $K=2/3$  is used, the CDP yield function is the Lubliner yield function. When  $K=1.0$ , the CDP yield function becomes the Drucker-Prager yield function. A schematic of CDP yield surface in 3D principal stress space is shown in Figure 7.5.

$$f(\{\hat{\sigma}\}, \tilde{\epsilon}^{pl}) = \frac{1}{1-\alpha} (\alpha I_1 + \sqrt{3J_2} + \beta \langle \hat{\sigma}_{max} \rangle - \gamma \langle -\hat{\sigma}_{max} \rangle) - \sigma_{yc}(\tilde{\epsilon}^{pl}) \leq 0 \quad (7-2)$$

$$\alpha = \frac{f_b - f_c}{2f_b - f_c} \quad (7-3)$$

$$\beta = \frac{\sigma_{yc}(\tilde{\epsilon}^{pl})}{\sigma_{yt}(\tilde{\epsilon}^{pl})} (1 - \alpha) - (1 + \alpha) \quad (7-4)$$

$$\gamma = \frac{3(1 - K)}{2K - 1} \quad (7-5)$$

where:

- $I_1$  = first invariant of the stress tensor;
- $\hat{\sigma}_{max}$  = maximum principal stress;
- $\sigma_{yc}$  = uniaxial yield strength of concrete in compression;
- $f_b$  = initial biaxial compressive strength;
- $f_c$  = initial uniaxial compressive strength;
- $\sigma_{yt}$  = uniaxial yield strength of concrete in tension;
- $K$  = material constant,  $0.5 < K < 1.0$ .

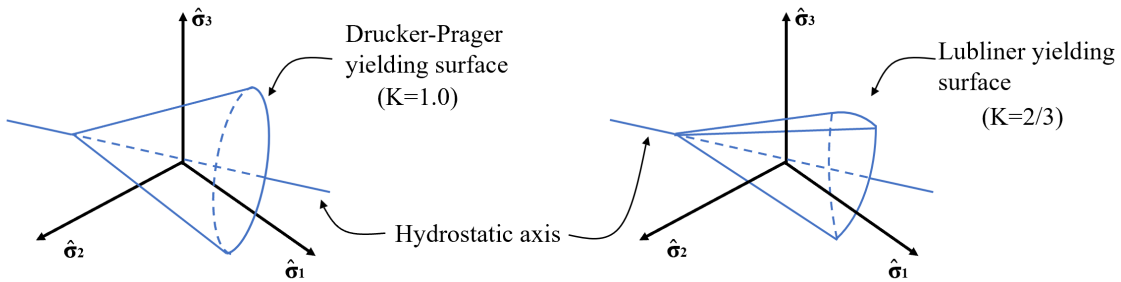


Figure 7.5 - CDP Yield Surface for Different Values of  $K$  in 3D Principal Space

Plastic flow means changes in material plastic strain. Plastic flow exists only if the material is already yielded (point B in Figure 7.4). A flow rule is the expression of plastic strain rate. Eq. 7-6 presents the general form of the flow rule. The evolution of plastic strain is related to the derivative of the function  $G$  and the parameter  $\lambda$ .

$$\dot{\varepsilon}_{ij}^{pl} = \lambda \frac{\partial G}{\partial \sigma_{ij}} \quad (7-6)$$

where:

- $\dot{\varepsilon}_{ij}^{pl}$  = component in the plastic strain rate tensor;
- $\lambda$  = plastic multiplier;
- $G$  = plastic potential function;
- $\sigma_{ij}$  = component in the stress tensor.

When the plastic potential function  $G$  is the same as the yield function  $f$ , the material has an associated flow rule, which is usually the case for metals. When the plastic potential function is different from the yield function, the material has a non-associated flow rule, which is usually the case for concrete.

The constitutive model for the concrete includes softening, which is known to create a propensity for spurious mesh size effects in FE models (Burchnall 2014, Lu and Panagiotou 2014, Deng, et al. 2021) associated with strain localization. The spurious mesh size effect makes numerical

models lack objectivity, and may negatively impact the convergence behavior of finite element approximations. This point can be best explained with the aid of a simple model like the one shown in Figure 7.6, focused on a rectangular bar under axial tension. The bar is made of a quasi-brittle material, where the behavior is linearly elastic until a tensile strength is reached; after this point, the material exhibits strain softening. The finite element mesh includes multiple elements, and each element is assigned the uniaxial tensile stress-strain response shown in Figure 7.6 (c). Figure 7.7 gives the strain contour for two analysis steps. The step in Figure 7.7 (a) corresponds to the instant that the bar stress reaches the tensile strength. As expected, the axial strain distribution at that instant is homogeneous, i.e., all elements have the same value of strain, equal to the ratio of the tensile strength over the elastic modulus. The step in Figure 7.7 (b) reflects when the material starts to soften. In this step, deformation concentrates at one location while all other locations elastically unload, which is shown by the fact that strain in element A at step (b) is smaller than that in step (a).

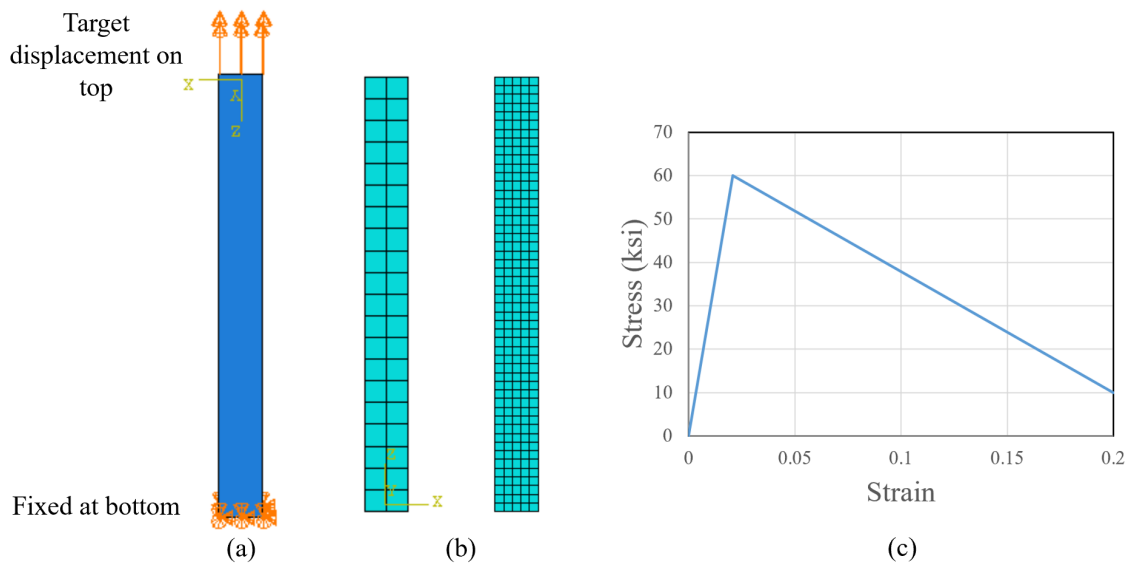


Figure 7.6 - Rectangular Bar Model (a) Boundary Conditions (b) Two Different Mesh Schemes (c) Stress-Strain Behavior for Each Element

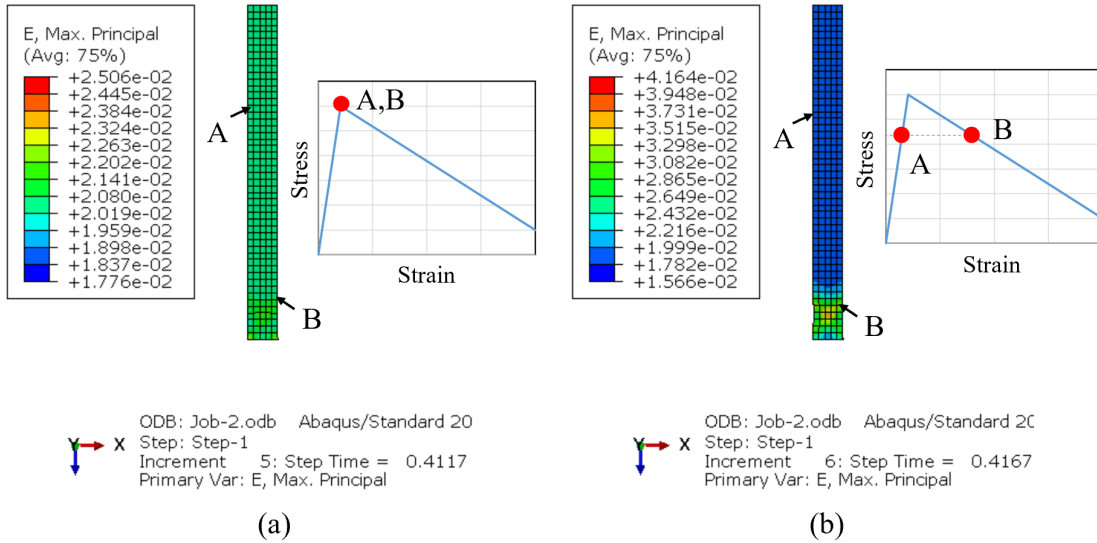


Figure 7.7 - FE Results for Bar Under Tension (a) When Bar Reaches the Peak Tensile Strength (b) When Bar Starts Softening

The issue with strain localization is that large deformations will eventually concentrate in a single layer of elements. When elements become smaller and smaller, the energy dissipated during the softening process also gets smaller, resulting in changes in the model behavior. Figure 7.8 illustrates the input stress-strain curve and resulting load-displacement curve for two different mesh schemes. It can be noticed that the post-peak portion in the load-displacement curve for the finer mesh has a steeper slope than the coarser mesh; the smaller area under the post-peak curve for the finer mesh reflects the reduction in dissipated energy.

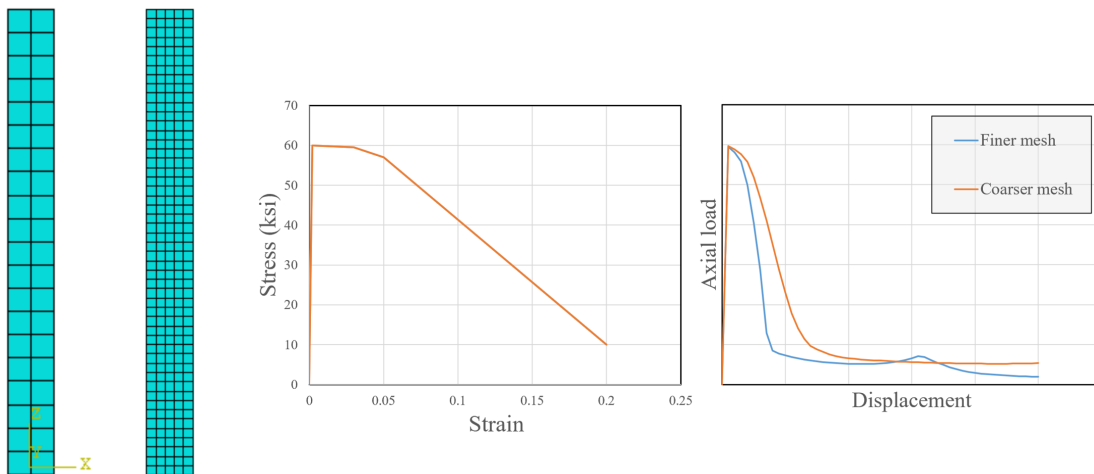


Figure 7.8 - Axial Load versus Axial Displacement for Two Mesh Schemes with the Same Stress-Strain Input



To eliminate spurious mesh size effects, a regularization process must be employed. The most common regularization process, also adopted herein, is to adjust the softening branch in the stress-strain curve based on element size, so that the energy dissipation for full fracture is identical for different mesh sizes. Figure 7.9 shows the stress-strain curve of the example uniaxial tension analysis, after regularization. The finer mesh appears to have a more ductile post-peak behavior. However, the area under the stress-strain curve multiplied by the element characteristic length is the same for the two mesh schemes. Figure 7.9 also presents the analysis results obtained for a regularized stress-strain response. It can be noticed that the load-displacement responses for the two mesh schemes are similar now. In Abaqus, strain regularization can be done by inputting stress-displacement relationships or by inputting fracture energy. For this study, fracture energy was used for concrete tensile material response and for the steel damage model. If stress-strain is the only available input, then manual adjustment is needed by choosing a reference characteristic length, which is the case for concrete compression response in this study. The next section illustrates the process of manually adjusting concrete compression stress-strain curves based on element size.

#### **7.2.2.2. Concrete Material Properties**

The uniaxial stress-strain response for concrete used in the Abaqus model is shown in Figure 7.10. The entire stress-strain response can be defined once the concrete compressive strength  $f_c$  is known. The value of  $f_c$  for each FE model is the test day measured strength given in Chapter 5. It should be noted that for Specimen No. 8 and Specimen No. 10 in the push-out tests, the test day concrete strength was obtained with a different concrete cylinder preparation method, which gave a questionable concrete compressive strength. Therefore, the test day strength was discarded and the 28-day strength was used in FE model for these two specimens, as the 28-day strength was considered more reliable.

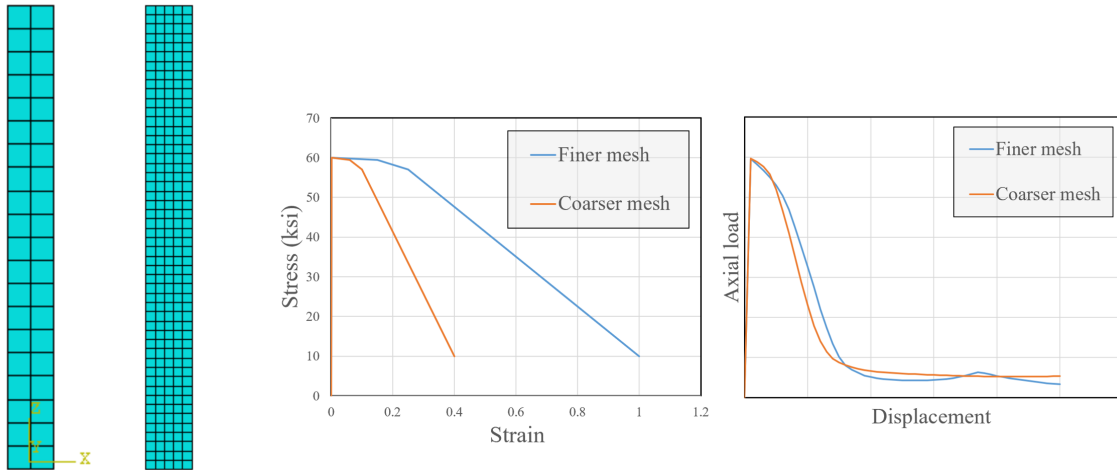


Figure 7.9 - Bar Analysis Results After Regularization of Tensile Softening Rule

The stress-strain curve for uniaxial compression is linearly elastic up to a stress value of  $0.2f_c$ . After this point, the curve is governed by the equations in (Mander, Priestley and Park 1988, Karthik and Mander 2011) and the expressions are given in Figure 7.10. The corresponding curve for uniaxial tension is bilinear. The stress-strain curve first increases linearly up to the modulus of rupture  $f_t$  and then decreases linearly. The value of  $f_t$  is taken as  $\sqrt{5f_c}$  ( $f_c$  and  $f_t$  in psi) in this study based on the parametric study described in Section 7.2.8.2. The decreasing branch is called tension softening and is controlled by the concrete fracture energy  $G_f$ , which is taken as 1.2 lb/in (energy per unit area). The area under the linear decay branch equals  $G_f/L$ , in which  $L$  is the characteristic length of the element. For line (e.g., truss) elements,  $L$  is the element length. For hexahedral solid elements,  $L$  can be taken as the cubic root of the element volume. The elastic modulus of concrete  $E_c$  was calculated based on the 9<sup>th</sup> Ed. AASHTO Equation 5.4.2.4-1. For the strain range in Figure 7.10, the stress-strain curve given by Mander's model can be regarded as the true stress-strain curve.

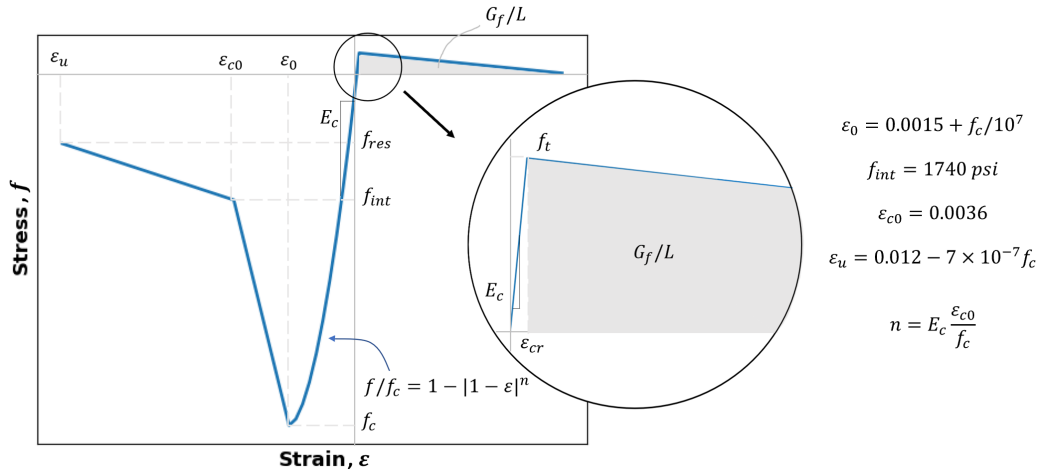


Figure 7.10 - Uniaxial Stress-Strain Behavior of Concrete

The softening branch of the concrete material compressive response is also regularized to eliminate spurious mesh size effects. Specifically, a reference value for parameters  $\varepsilon_{c0}$  and  $\varepsilon_u$  is established, by considering the average response of a prism with a size  $L_R$  equal to 450mm, which was also gauge length in the concrete experiments by Mander et al. (1988). If the actual element size  $L$  differs from  $L_R$ , then the two compressive strain parameters are adjusted based on the following two equations.

$$\varepsilon'_{c0} = \frac{\varepsilon_{c0} L_R}{L} \quad (7-7)$$

$$\varepsilon'_u = \frac{\varepsilon_u L_R}{L} \quad (7-8)$$

where:

- $\varepsilon'_{c0}$  = regularized ultimate strain from Mander model;
- $\varepsilon_{c0}$  = original ultimate strain from Mander model;
- $L_R$  = reference length, equals to 450 mm;
- $L$  = characteristic length of element, mm;
- $\varepsilon'_u$  = regularized failure strain;
- $\varepsilon_u$  = original failure strain from Mander model.

The finite element meshes used in the present study are non-uniform, in the sense that the various solid elements generally have different size  $L$ . Each element should therefore have its own adjusted stress-strain curve, which introduces large amounts of pre-processing work. Two strategies are used in this study to simplify the pre-processing work. First, since the spurious mesh size effect only impacts the softening behavior, no adjustment was made for elements that remain elastic throughout the analysis. Second, a single characteristic length was used for all elements that need adjustment, which was taken as the mean value of the characteristic length of all elements that enter the softening stage during the analysis. Therefore, to adjust the stress-strain curve, each FE model needs to be run twice. In the first analysis, the concrete is given the unadjusted stress-strain

curve. Abaqus monitors and records the characteristic length of elements entering the softening stage. The stress-strain curve is then adjusted based on this information and the model with the adjusted strain-strain curve is run again to obtain final results.

In this study, the concrete uniaxial stress-strain curve is used with the Concrete Damaged Plasticity (CDP) model in Abaqus, which provides the definition for the yield function and plastic flow rule. The yield function and yield surface schematic for CDP are given in Eq. 7-2 and Figure 7.5.

There are two parameters Abaqus allows the user to modify in the yield function, namely  $K$  and  $f_b/f_c$ . It can be noticed from Figure 7.5 that for both Drucker-Prager and Lubliner, the yield surface expands along the negative direction of the hydrostatic axis. This means when concrete is under multiaxial compression, the yield strength of the material will increase, which is true for concrete. However, the Lubliner function is reported to have a much faster strength increase rate under multiaxial compression compared to Drucker-Prager and is reported to overestimate the hysteretic strength of shear walls (Moharrami and Koutromanos 2016). Nonetheless, most previous research uses the default value of  $K=2/3$  and this value was adopted in this study.

The value of  $f_b/f_c$  is the ratio between the initial biaxial compressive strength and the initial uniaxial compressive strength. The values of  $f_b$  and  $f_c$  will change when the material yields. The term “initial” refers to their values before yielding.  $f_c$  is given in the uniaxial stress-strain curve and  $f_b$  can be obtained by drawing the projection of the initial yield function in the plane of the principal stress space. The default value of  $f_b/f_c$  is given as 1.16 by Abaqus. Dara (2015) reported that FE models of push-out specimens were not sensitive to this parameter. The default value of 1.16 was used in this study.

The CDP model in Abaqus uses a non-associated flow rule, in which the plastic potential function  $G$  is the Drucker-Prager hyperbolic function (Abaqus 2016). The CDP plastic potential function is given in Eq. 7-9.

$$G = \sqrt{(\varepsilon f_t \tan \psi)^2 + 3J_2} + \frac{1}{3}I_1 \tan \psi \quad (7-9)$$

where:

- $\varepsilon$  = material constant called eccentricity;
- $f_t$  = uniaxial tensile strength of concrete;
- $\psi$  = material constant called dilation angle.

There are two parameters in the CDP plastic flow rule that Abaqus allows the user to modify. These are the dilation angle  $\psi$  and the eccentricity  $\varepsilon$ . The dilation angle controls the material volumetric expansion under plastic deformation. Abaqus does not provide a default value for dilation angle. Dara (2015) performed a parametric study on  $\psi$  in Abaqus and found the strength of push-out FE models increased and the ductility decreased when  $\psi$  changed from 35° to 56°.

An intermediate value of  $\psi=40^\circ$  was used in this study. Figure 7.11 illustrates the FE model created by Dara and the influence on load-slip curve when different values of  $\psi$  are used.

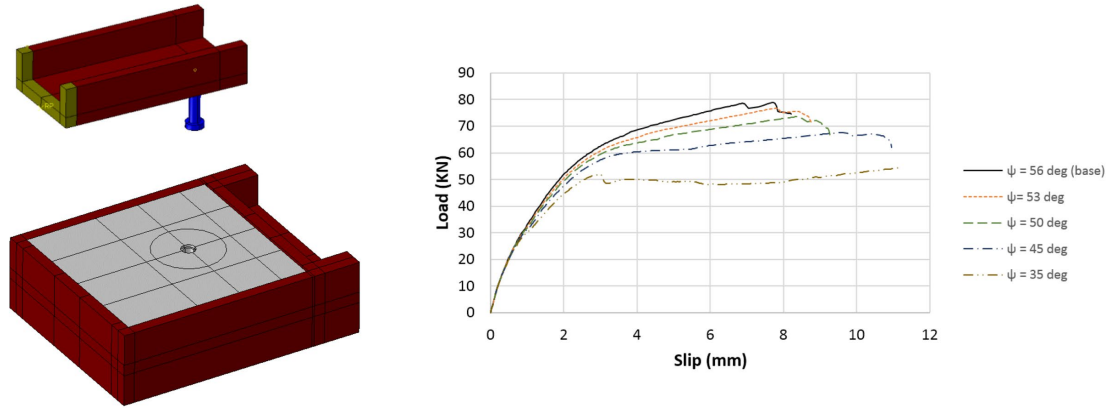


Figure 7.11 - FE Models and Parametric Study on Impact of Dilation Angle  $\psi$  (Dara 2015)

The eccentricity defines the curvature of the plastic potential hyper-surface. Wosatko et al. (2019) created plots of the plastic potential surface,  $G=0$ , when different values of eccentricity are used, as shown in Figure 7.12. The default value of eccentricity in Abaqus is given as 0.1. Dara (2015) reported that push-out models in Abaqus were not sensitive to this parameter and so the default value was used in the present study.

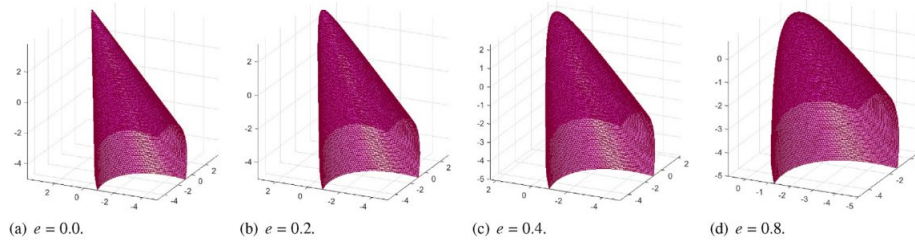


Figure 7.12 - Effect of Eccentricity on Plastic Potential Surface (Wosatko, et al. 2019)

In summary, for the CDP parameters, Abaqus default values were used in this study. The use of these default values is common in previous FE studies on push-out specimens using CDP (Nguyen and Kim 2009, Kruszewski, Zoghi and Wille 2019). These previous studies included not only normal strength concrete, but also high-performance concrete. The default values for CDP plasticity parameters show a wide range of application on concrete materials.

### 7.2.2.3. Steel Material Properties

The uniaxial true stress-strain curve for the stud material is given in Figure 7.13. Only the tensile branch is shown in the plot since the compression behavior is the same. The engineering stress-strain curve for the 1-1/8" shear studs was obtained by tension coupon tests reported in Chapters 4 and 5. The true stress-strain curve before the onset of necking at the peak engineering stress was derived from the engineering stress-strain curves using standard conversions (Jones 2019). The post-necking true stress-strain curve was obtained using a trial-and-error procedure in Abaqus. A true stress-strain curve with an assumed post-necking portion was input to a FE model of a tension coupon. This tension coupon FE model underwent the same loading process as the experimental tension coupon. Results between analysis and experiment were compared, using a procedure similar to that recommended by Jones (2019). If there was significant discrepancy between the experimental and simulated engineering stress-strain curves, the post necking true stress-strain curve was adjusted in the simulation until reasonable agreement was achieved. In Figure 7.14, the FE result using the true stress-strain curve given in Figure 7.13 is compared with experimental data. As the figure shows, good agreement was obtained between the experimental and the FE load-deformation response. The FE model also captured the experimental engineering stress-strain curves.

For simplicity, the steel beam in the FE model has an elastic-perfectly-plastic stress-strain response with a yield strength of 50 ksi. Steel reinforcement in the FE model has a yield strength of 60 ksi and a linear hardening to 90 ksi at 0.14 strain and perfectly plastic afterwards. For all steel material in this FE study, the metal plasticity model in Abaqus was used, which provides the yield function and plastic flow rule. The metal plasticity model has  $J_2$  plasticity (Von Mises yield criterion) and has an associated flow rule.

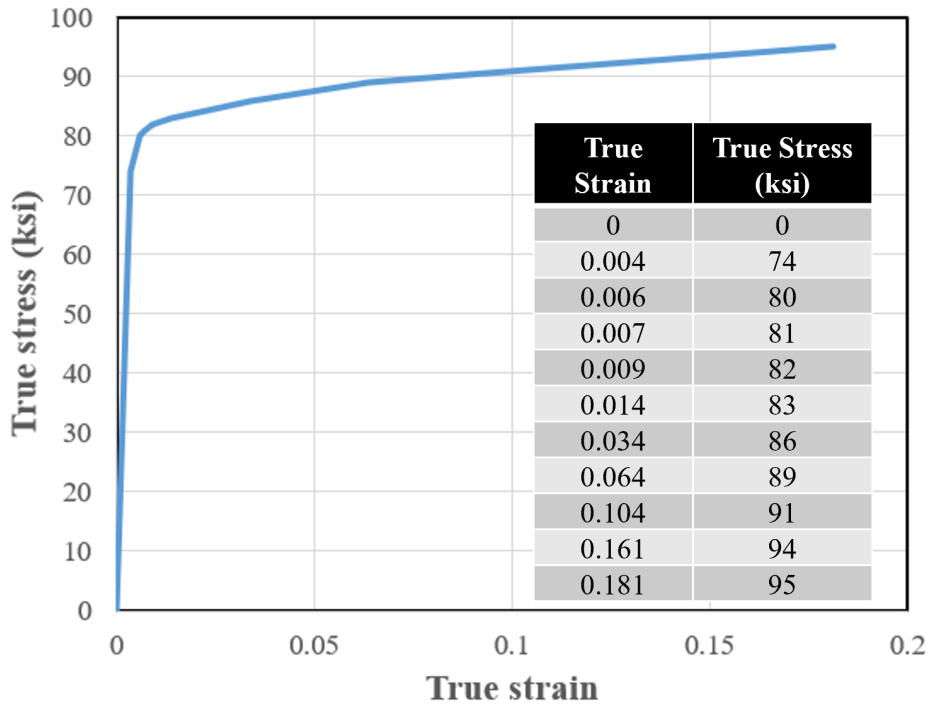


Figure 7.13 - True Stress-Strain Curve for Stud Material

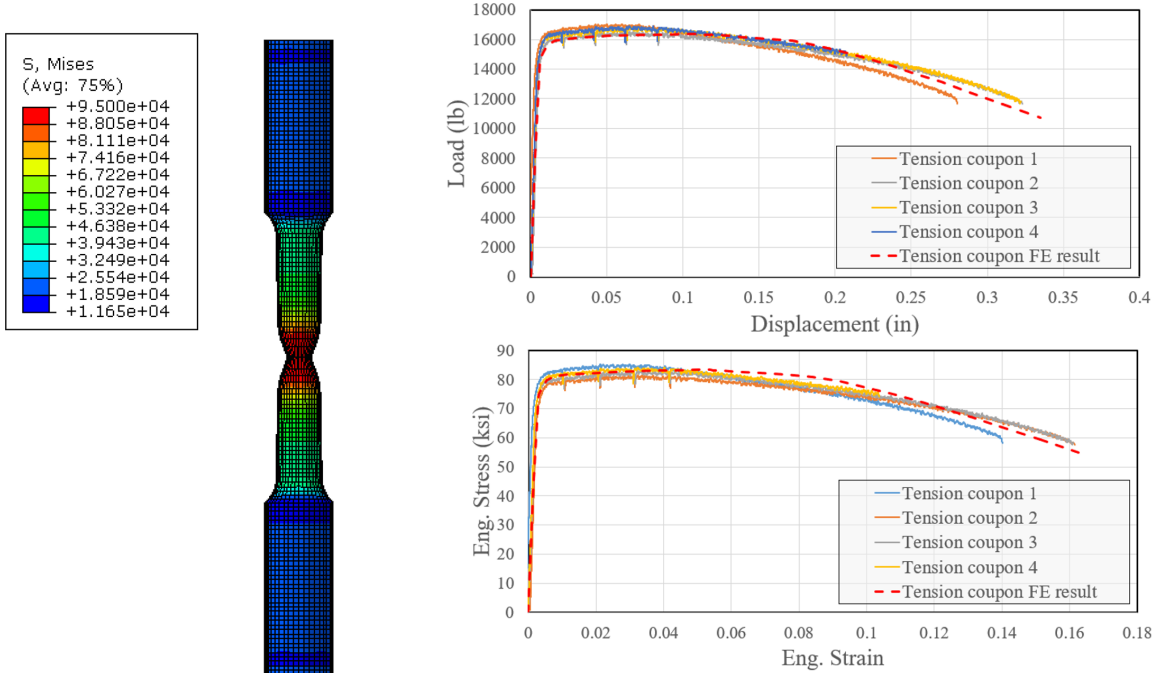


Figure 7.14 – FE analysis of steel tension coupon and comparison with experiments

The true stress-strain response for the stud material has no softening. In order to capture the progressive steel damage in the stud, damage properties need to be defined. Material damage in



Abaqus consists of two parts, the damage initiation criterion and the damage evolution rule, as shown in Figure 7.15. In Abaqus, material damage is reflected by a scalar  $D$ . When the damage initiation criterion is met at stress  $\sigma_{y0}$ , the value of  $D$  starts accumulating. The yield stress of the material without damage,  $\bar{\sigma}$ , is reduced to  $(1-D)\bar{\sigma}$  and the unloading stiffness is also reduced. When  $D$  reaches 1, the material point is completely failed and when all material points in one element fail, this element can be removed from the mesh, as shown in Figure 7.16. Element removal for the studs was enabled in all FE models in this study.

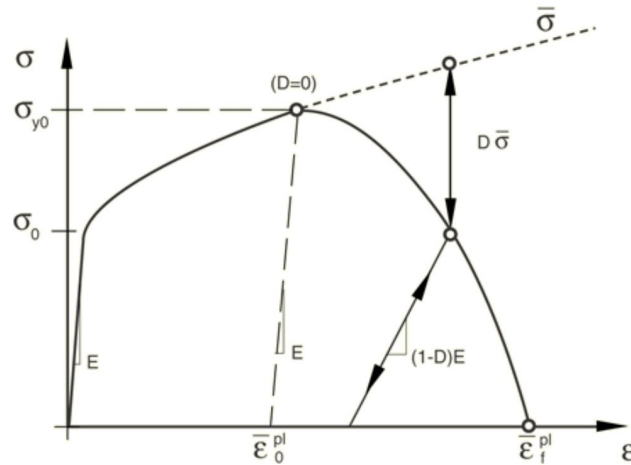


Figure 7.15 - Stress-strain curve for material with ductile damage (Abaqus 2016)

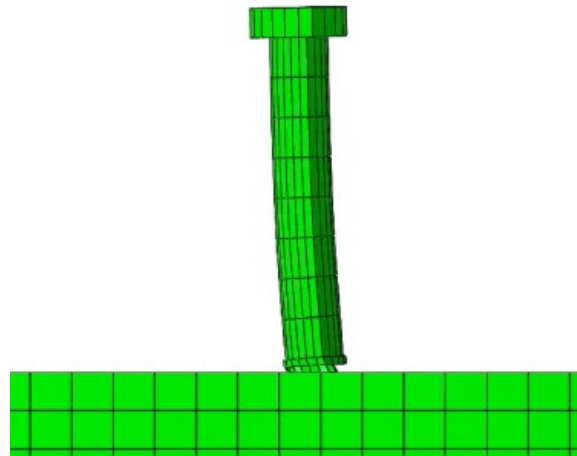


Figure 7.16 - Element Removal at the Weld of Shear Stud

The commonly used damage initiation criteria for shear studs in the literature includes the ductile damage model, the shear damage model, and the porosity damage model (Nguyen and Kim 2009, Cai 2015). Preliminary analysis showed using any one of the above damage models could not describe the experimentally observed response with sufficient accuracy. Therefore, a combination of the ductile damage and the shear damage models in Abaqus was used.

The ductile damage model in Abaqus is essentially the material damage criterion proposed by Hancock and Mackenzie (1976). Eq. 7-10 provides the description of this damage initiation criterion. Defining the ductile damage model requires calibration of material constants  $\alpha$  and  $\beta$ .

$$\bar{\varepsilon}_{critical}^{pl} = \alpha \exp(-\beta\eta) \quad (7-10)$$

where:

$\bar{\varepsilon}_{critical}^{pl}$  = equivalent plastic strain at the initiation of damage initiation;

$\alpha$  = material constant;

$\beta$  = material constant;

$\eta$  = ratio between hydrostatic stress and the Von Mises stress called stress triaxiality.

The expression for stress triaxiality is given in Eq. 7-11.

$$\eta = \frac{I_1}{\sqrt{3J_2}} \quad (7-11)$$

The shear damage model in Abaqus is the material damage criterion proposed by Hooputra et al. (2004). Eq. 7-12 provides the description of this damage initiation criterion. Defining the shear damage model requires calibration of  $\bar{\varepsilon}_s^+$ ,  $\bar{\varepsilon}_s^-$ , and  $f$ .

$$\bar{\varepsilon}_{critical}^{pl} = \frac{\varepsilon_s^+ \sinh[f(\theta - \theta^-)] + \varepsilon_s^- \sinh[f(\theta^+ - \theta)]}{\sinh[f(\theta^+ - \theta^-)]} \quad (7-12)$$

$$\theta = \frac{\sqrt{3J_2} - k_s I_1}{\tau_{max}} \quad (7-13)$$

where:

$\bar{\varepsilon}_{critical}^{pl}$  = equivalent plastic strain at the initiation of damage initiation;

$\bar{\varepsilon}_s^+$  = equivalent plastic strain under equiaxial tensile loading when shear damage initiates;

$f$  = material constant;

$\bar{\varepsilon}_s^-$  = equivalent plastic strain under equiaxial compression loading when shear damage initiates;

$\theta$  = shear stress ratio;

$\theta^+$  =  $2 - 4k_s$ ;

$\theta^-$  =  $2 + 4k_s$ ;

$k_s$  = material constant equal to 0.1 for metals;

$\tau_{max}$  = maximum shear stress.

Cai (2015) performed a comprehensive study on material constants in the ductile damage model and the shear damage model for structural steel both at room temperature and at elevated temperature. Material constants reported by Cai (2015) were shown to be able to successfully capture experimental results for tension coupon tests and shear tests. Therefore, in this study, the material constants in the ductile damage and shear damage models reported by Cai (2015) were initially adopted. Preliminary analysis showed a better match of the push-out experimental data was achieved if  $\alpha$ ,  $\bar{\epsilon}_s^+$ , and  $\bar{\epsilon}_s^-$  calibrated by Cai are divided by 2. The final material constants in this study for the two damage models are summarized in Table 7.3.

**Table 7.3 - Ductile and Shear Damage Model Parameters**

Damage Model	Input Material Constant
Ductile damage	$\alpha = 1.275$
	$\beta = 2.11$
Shear damage	$\epsilon_s^+ = 0.2$
	$\epsilon_s^- = 4.5$
	$f = 4.0$

Damage evolution in Abaqus is represented by the damage scalar  $D$ , which can be defined as a function of either equivalent plastic displacement at failure or fracture energy to account for the spurious mesh size effect. When  $D$  is defined as a function of displacement, the function can be linear, exponential, or tabular. When  $D$  is defined as a function of fracture energy, the function can be linear or exponential (Abaqus 2016). Equivalent plastic displacement and fracture energy are related. When linear damage evolution is used, the fracture energy,  $G_f$ , can be converted to equivalent plastic displacement at failure,  $\bar{u}_f^{pl}$ , by the equation given in Figure 7.17.

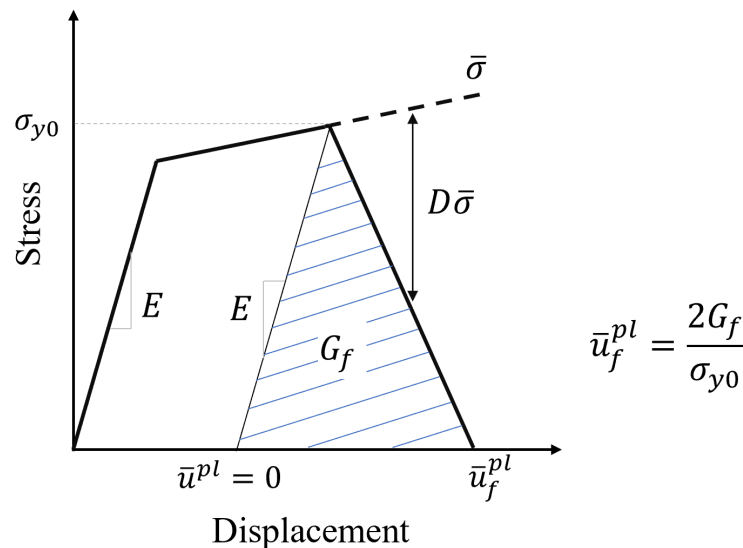


Figure 7.17 - Relationship Between Fracture Energy and Plastic Equivalent Displacement at Failure

In this study, equivalent plastic displacement was used for damage evolution with a linear relationship. The equivalent plastic strain at failure,  $\bar{\varepsilon}_f^{pl}$ , in Figure 7.15 is obtained by Eq. 7-14. Since the element characteristic length,  $L$ , is included,  $\bar{\varepsilon}_f^{pl}$  is calibrated based on the element size and the spurious mesh size effect is reduced.

$$\bar{\varepsilon}_f^{pl} = \frac{\bar{u}_f^{pl}}{L} + \bar{\varepsilon}_0^{pl} \quad (7-14)$$

Hull and Clyne (1996) reported that the fracture energy for metals ranges from 8 kJ/m<sup>2</sup> to 1000 kJ/m<sup>2</sup>, which can be translated to  $\bar{u}_f^{pl}$  of 0~0.15" using the equation in Figure 7.17. Preliminary analysis showed that there was no single value for  $\bar{u}_f^{pl}$  that worked well for eleven push-out specimen FE models. To have stud fracture failure reasonably correlate with experimental observations,  $\bar{u}_f^{pl}$  varied between 0" and 0.03" in the FE models. This is the only modeling parameter that varied between FE models without supporting data from experiments.

When  $n$  damage models are used, Abaqus will combine the effect of each damage model using Eq. 7-15. The overall damage index  $D$  is given by Eq. 7-16.

$$D_{combined} = 1 - \prod_{k=1}^n (1 - D_k) \quad (7-15)$$

$$D = \max[D_{combined}, \max(D_k)] \quad (7-16)$$

### 7.2.3. Constraints and Contact Conditions

The FE models contain the following surface interactions: interaction between the shear stud and the concrete, interaction between the steel beam and the concrete, interaction between concrete and the rigid foundation, and interaction between the PCP and CIP concrete (for models with PCP only). Figure 7.18 shows the surface interactions in Model No. 4, which contains all surface interactions mentioned above.

The first three interactions exist in all FE models and the last one exists in the PCP models. The first three interactions are steel-concrete interaction, and the same interaction property is used for all three. In the normal direction, surfaces cannot penetrate each other, which is called "hard" contact in Abaqus. In the tangential direction, frictional movement is allowed between surfaces, where a friction coefficient equal to 0.5 was used. These interactions properties are applied to the model using the General Contact algorithm in Abaqus.

Abaqus implements contact in a way that the model is first analyzed as if there is no contact. When the two surfaces overlap, a correction force is imposed on one surface to "push" it back to the interface with the other. The pushed-back surface is called the "slave" surface while the other is called the "master" surface (Abaqus 2016). Therefore, "hard" contact does not really prevent

two surfaces from penetrating each other. The “master” surface can penetrate the “slave” surface. This phenomenon is especially prominent when the “master” surface has a finer mesh compared to the “slave” surface, as Figure 7.19 illustrates. In order to minimize this numerical error, the General Contact algorithm is used. General Contact implements the abovementioned procedure twice and makes each surface the “slave” surface, which is called the balanced method. Therefore, there are no pure “master” and “slave” surfaces in the General Contact case and the penetration is reduced.

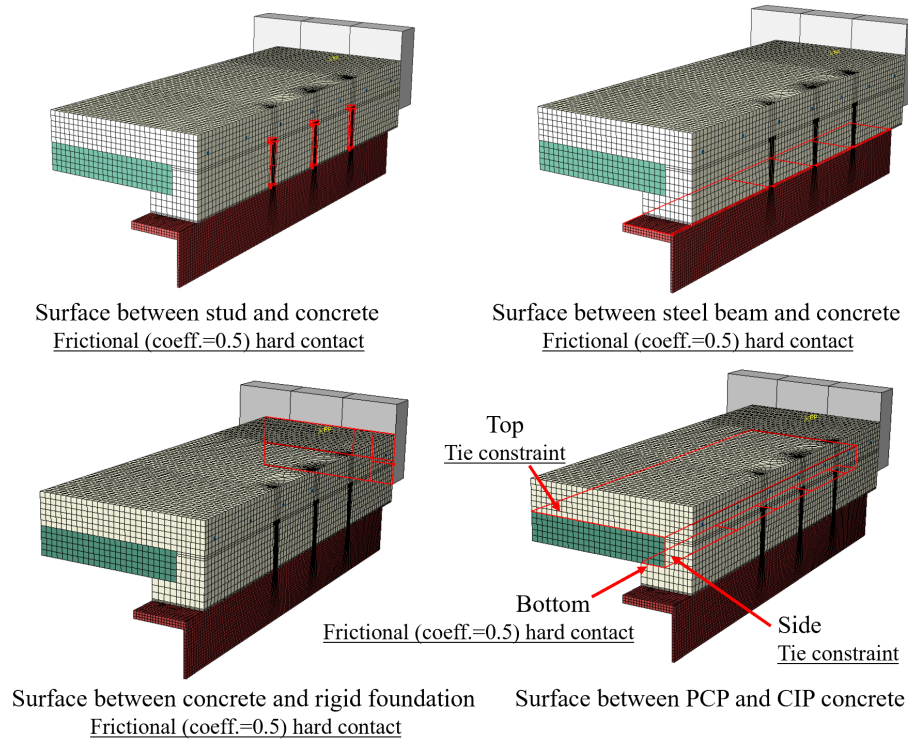


Figure 7.18 - Surface Interactions in Model No. 4

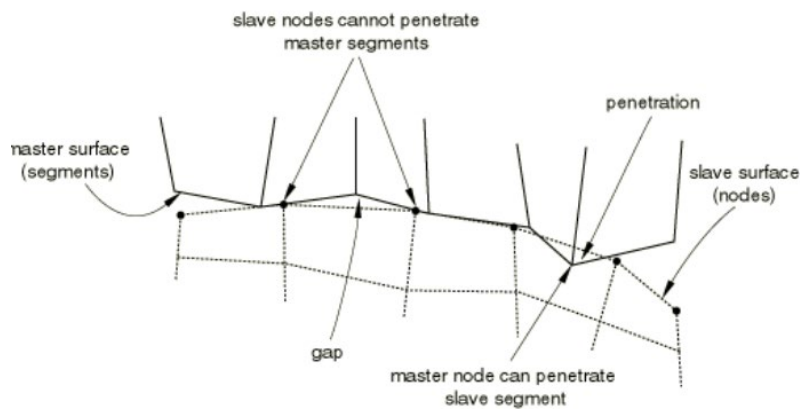


Figure 7.19 - Surface Penetration Between Master and Slave Surfaces (Abaqus 2016)

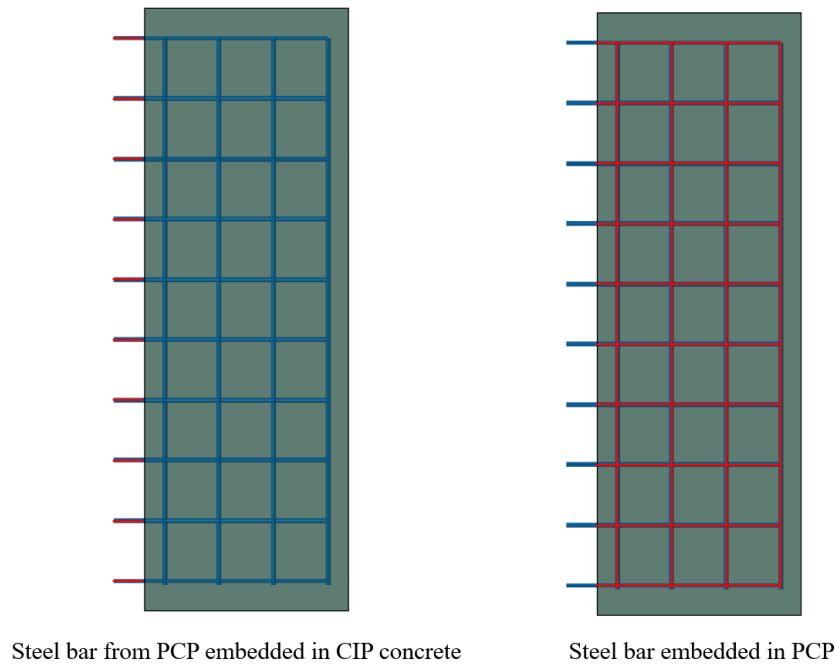
The mesh tie constraint was applied to surfaces between the PCP and the CIP concrete except at the bottom surface of the PCP in Figure 7.18. In the real specimen, surface preparation was provided on top of the PCP to provide an improved bond with the CIP concrete. In the experiments, no visible movement was noticed at the top and side interfaces between PCP and CIP concrete, which suggests using the mesh tie constraint is reasonable. The mesh tie constraint requires defining “master” and “slave” surfaces as well. Degrees-of-freedom (DOFs) of nodes on the “slave” surface are given by interpolating DOFs of nearby nodes on the “master” surface. The two surfaces under tie constraints will have no relative movement. In the model, the PCP side surface is also under the tie constraint with the CIP concrete, in which no surface preparation was made. The bottom PCP surface has the normal “hard” contact and frictional interaction with CIP concrete with a coefficient of friction equal to 0.5. The frictional coefficient of 0.5 used here was based on a parametric study presented in Section 7.2.8.1.

Besides surface interactions, an embedment interaction was applied between the reinforcement and the concrete. The embedment interaction is a representation of a perfect bond between a steel reinforcing bar and concrete. Similar to the mesh tie constraint, nodal displacements of the reinforcement truss elements become the interpolation of nearby concrete element nodes. Like the real specimen, for models with PCPs, the reinforcement in the PCP is partially embedded in the PCP and partially embedded in CIP concrete, as shown in Figure 7.20.

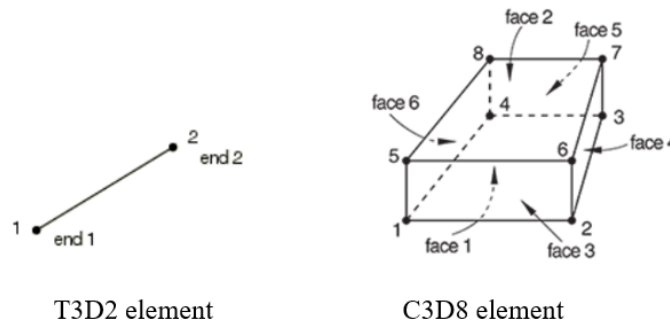
#### **7.2.4. Element Formulation and Mesh**

Two types of elements were used in the FE models. These are linear 1D truss elements and linear 3D hexahedron elements. The 1D truss element is named T3D2 in Abaqus, and was used for steel reinforcing bars.

Preliminary analysis showed considerable hourglass deformation when reduced integration 3D elements were used. The hourglass mode is a deformation of the element caused by rank deficiency of the stiffness matrix when reduced integration is used and is not representative of actual deformations. In other words, the stiffness matrix from reduced integration cannot describe all DOFs of the element. The undescribed DOFs of the element can have unlimited deformation. To remove the hourglass mode, selective reduced integration 3D elements named C3D8 in Abaqus were used (Abaqus 2016). C3D8 elements were used in all parts of the model other than the reinforcement. Figure 7.21 illustrates the T3D2 element and C3D8 element in Abaqus.



*Figure 7.20 - PCP Reinforcement Embedment Interaction*



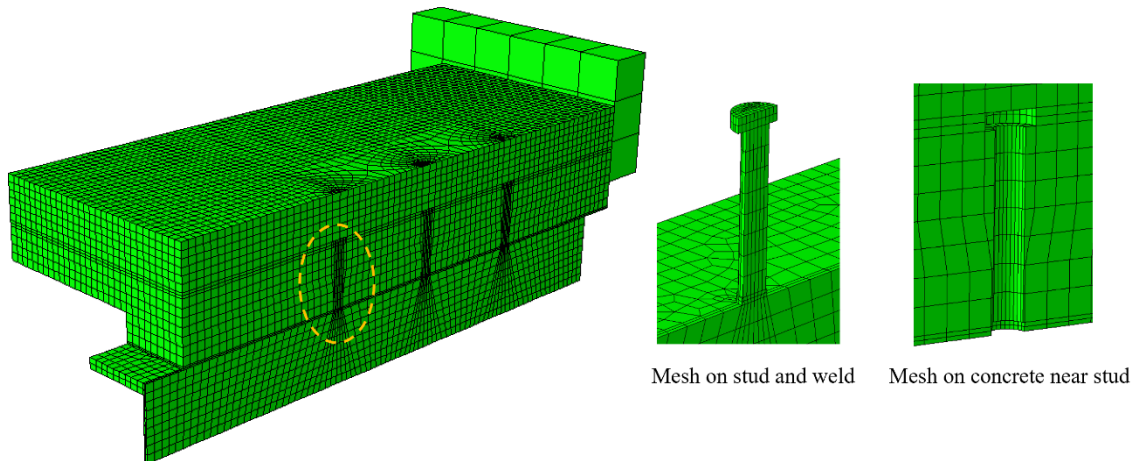
*Figure 7.21 - Abaqus Elements Used in FE Model (Abaqus 2016)*

The selective reduced integrated elements in Abaqus employ the so-called B-bar method (Abaqus 2016). A full description of that method can be found in FE textbooks (Koutromanos 2018). A brief introduction is provided here. The B-bar method is employed for problems where locking might be a concern. The most notable class of locking problems involves incompressible materials, for which the volumetric strain is negligible compared to the deviatoric strain. This is the case for metals, where plastic strains are purely deviatoric. For such cases, the need to satisfy material incompressibility conditions tacitly introduces additional constraints to a solution, potentially leading to overly stiff numerical response unless a very fine mesh is used. The B-bar method addresses this issue by separating the strain-displacement matrix into the locking and non-locking parts, namely the parts giving the volumetric and deviatoric strains, respectively.



The deviatoric (non-locking) part of the matrix is calculated in accordance with the piecewise approximation, while the volumetric (locking) part of the matrix is constant throughout each element, and equal to the value at the element centroid. By using the B-bar method, there will be no shear locking issue. At the same time, the stiffness matrix will have no rank deficiency and thus no hourglass mode will occur either.

An important issue in FE modeling is mesh refinement. The mesh needs to be fine enough to provide accurate results while avoiding excessive computational costs. The general practice is to use a combination of fine and coarse meshes in different parts of the model. A relatively fine mesh should be used in regions of high stress or strain gradients and at sharp changes in geometry while a coarser mesh is used in other locations to achieve better computational efficiency. This strategy is adopted in this study. Figure 7.22 shows the mesh on Model No. 3, which represents the mesh strategy for all FE models in this study. Preliminary analysis showed high stress and strain gradients concentrated in regions like the shear stud shank, the weld collar, and their surrounding concrete. Thus, the finest mesh was used in these regions. Regions in the concrete and the steel beam away from these regions were given a coarser mesh.



*Figure 7.22 – Mesh for Model No. 3*

To find a mesh size that provided accurate load-slip curves, three different mesh schemes were implemented for Model No. 3. As shown in Figure 7.23, for the weld collar, the stud shank and head, and the surrounding concrete, mesh sizes of 0.8", 0.2", and 0.1" were considered. For other regions, the mesh size was always taken as 0.8". Figure 7.24 provides the load-slip curve comparisons. The load-slip curve was not sensitive to the key region mesh size once the mesh was smaller than 0.8". However, damage initiation was significantly delayed with the 0.8" mesh. Using a mesh equal to or finer than 0.2" gave consistent damage behavior. Hence, a 0.2" mesh was regarded as adequate. Since Model No. 3 contains 1-1/8" studs, all FE models with 1-1/8"

studs used a 0.2" mesh in key regions. In regions far away from key regions of high stress and strain gradients and material damage, the mesh size ranged from 0.4" to 0.8".

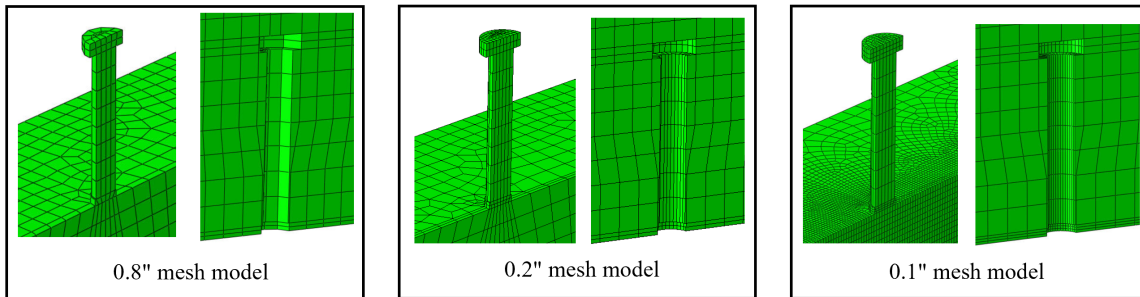


Figure 7.23 - Mesh Schemes for Sensitivity Study on Model No. 3

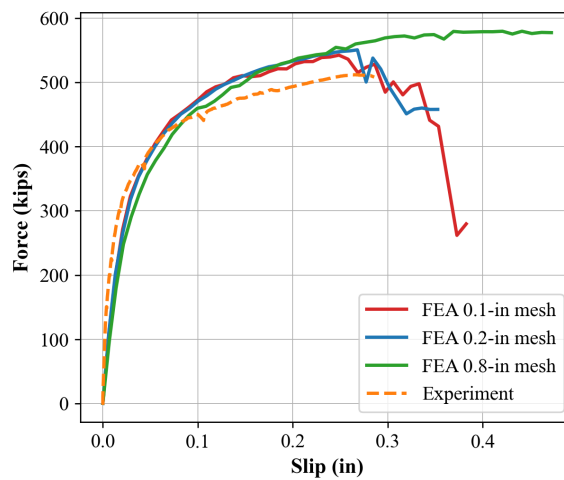


Figure 7.24 - Load-Slip Response for Different Mesh Sizes for Model No. 3

For FE models using 7/8" studs, a finer mesh scheme may be needed due to the smaller stud and weld collar in the key regions. Mesh sizes of 0.2", 0.1", and 0.05" were tried in key regions, as shown in Figure 7.25. Because the element size of 0.05" required an extremely long analysis time, a mass scaling technique was used for the mesh sensitivity study. Materials density was increased 100 times for the 0.05" mesh model, which sped up the analysis 10 times (see Section 7.2.7). To ensure the increased density will not impose a significant dynamic effect on the load-slip response, a case study on Model No. 1 using 0.1" mesh was carried out and the results are presented in Figure 7.26 (a). Increasing density 100 times did not change the load-slip response of Model No. 1 under 0.1" mesh but delayed steel damage initiation. The comparison of different mesh schemes for Model No. 1 is presented in Figure 7.26 (b). The 0.2" mesh, which gave good results for the 1-1/8" stud model was not small enough for the 7/8" stud model. Further, for the 7/8" stud model, the load-slip response did not change once the mesh was smaller than 0.1". Stud fracture failure occurred earlier in the 0.05" case but the change was deemed acceptable

considering mass scaling. Therefore, a 0.1" mesh was used in key regions for FE models with 7/8" studs. For other regions, a coarser mesh up to 0.8" is used.

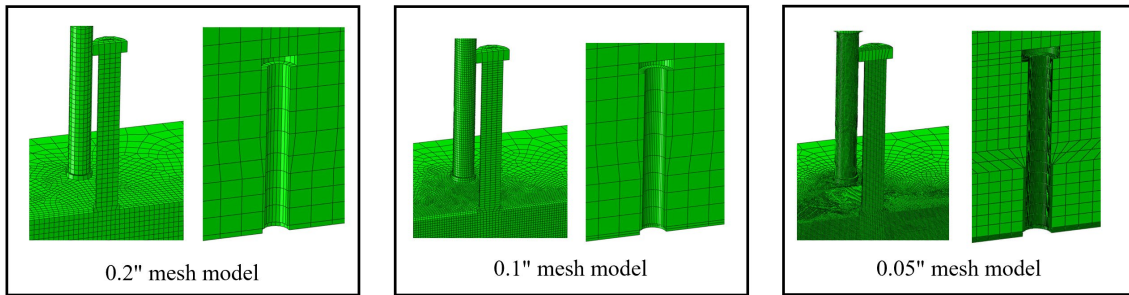


Figure 7.25 - Mesh Schemes for Sensitivity Study for Model No. 1

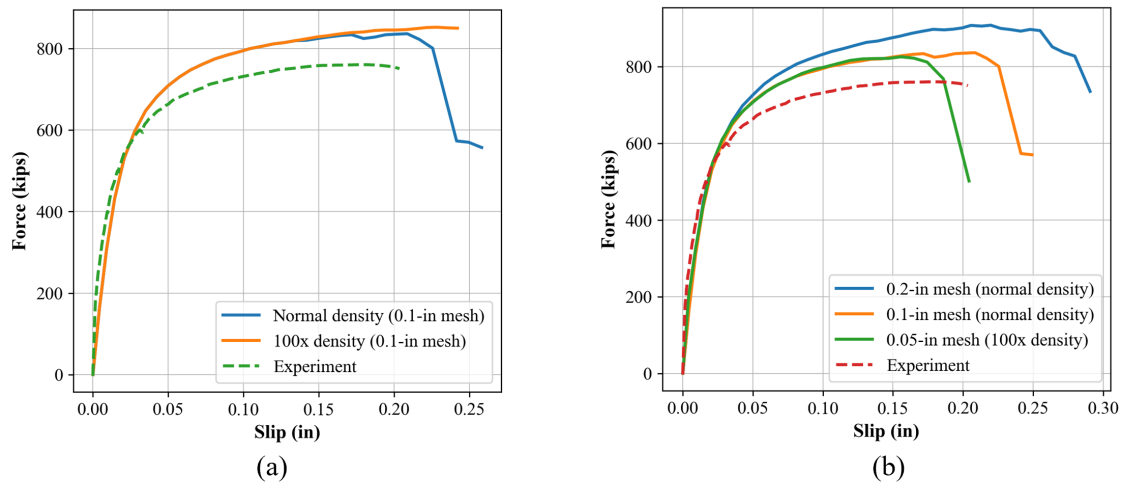


Figure 7.26 - Load-Slip Response for (A) With and Without Mass Scaling for 0.1" Mesh Scheme (B) Under Different Mesh Sizes for Model No. 1

Preliminary analysis showed that the element size used in the steel beam flange significantly changed the model behavior. When only one element was used through the thickness of the flange, the flange exhibited a distorted shape as shown in Figure 7.27, which did not occur in the actual specimens. This phenomenon can be attributed to the fact that one layer of C3D8 elements does not accurately reflect the bending stiffness of the flange. When more than two elements were used through the thickness of the beam flange, this buckling type of deformation was eliminated.

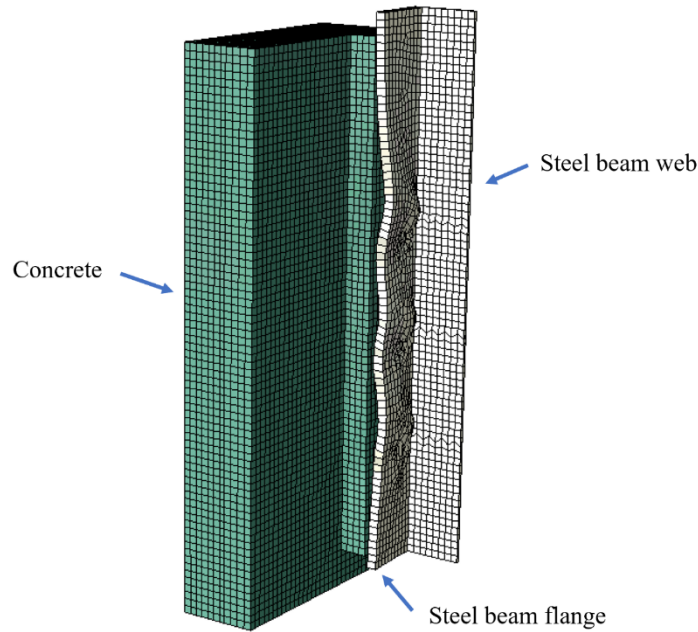


Figure 7.27 - Deformation of Steel Beam Flange When One Element Is Used Through the Thickness

On the other hand, when the element size is small in the steel beam flange, it may develop strain localization in the layer of elements directly under the shear stud. Figure 7.28 illustrates the strain localization. Options to avoid this are to include strain hardening in the steel beam material property or make the steel beam purely elastic. In this study, a purely elastic beam is used in some FE models showing the strain localization issue.

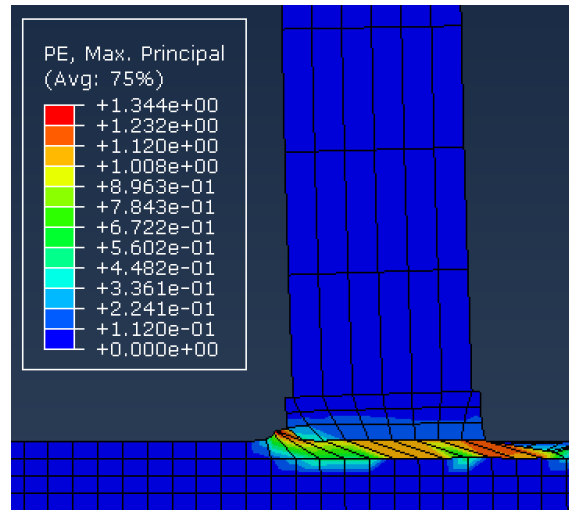


Figure 7.28 - Strain Localization in Top Layer of Elements in Steel Beam

## 7.2.5. Boundary Conditions

Since FE models only include a quarter or a half of the real specimen, symmetric boundary conditions were applied on the corresponding surfaces. A target displacement was applied on top

of the steel beam to represent the displacement imposed on the specimen by the hydraulic rams. The value of the target displacement depends on the slip recorded in the experiments, which ranged from 0.5" to 1.0". The rigid foundation was fixed on all DOFs. Figure 7.29 shows the boundary conditions applied on Model No. 7, which represents the boundary conditions for FE models with quarter symmetry. For models with half symmetry, no X-axis symmetry condition was needed.

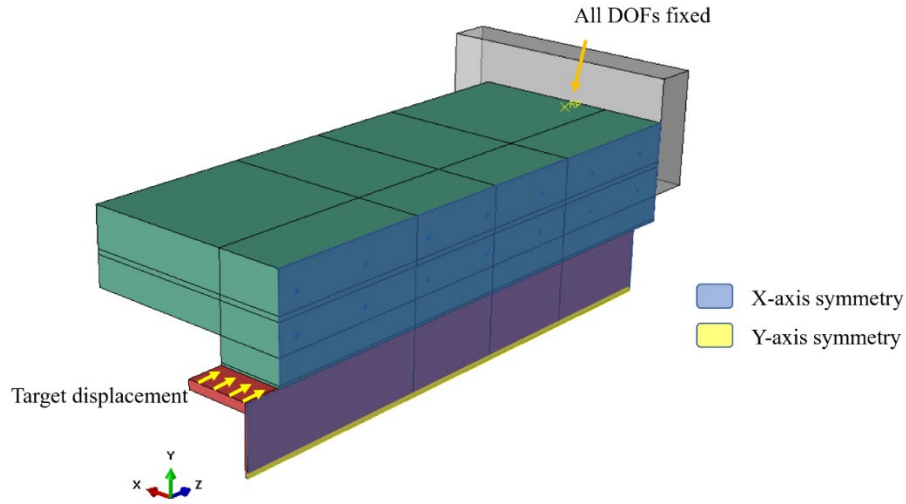


Figure 7.29 - Boundary Conditions for Model No. 7

## 7.2.6. Solver and Large Deformation Algorithm

The dynamic explicit solver in Abaqus was selected in this study. A brief introduction is provided here. The time domain of the numerical analysis is divided into multiple time increments. At the beginning of each time increment, quantities like nodal displacement, nodal velocity, and nodal acceleration are known from the previous time increment. The method of deriving these quantities at the end of the time increment is called the time-marching scheme. Abaqus provides various solvers that have different time-marching schemes. For the explicit solver, quantities at the end of the time increment can be computed with explicit expressions using quantities at the beginning of the increment. In Abaqus, the expressions used in the dynamic explicit solver are called the central difference method (CDM), where a lumped mass matrix is used. Equations 7-17 to 7-19 provides the CDM expressions for a given DOF.

$$\dot{U}_{n+\frac{1}{2}} = \dot{U}_{n-\frac{1}{2}} + \frac{\Delta t_{n+1} + \Delta t_n}{2} \ddot{U}_n \quad (7-17)$$

$$U_{n+1} = U_n + \Delta t_{n+1} \dot{U}_{n+\frac{1}{2}} \quad (7-18)$$

$$\ddot{U}_n = M^{-1}(F_n^{ext} - F_n^{int}) \quad (7-19)$$

where:

- $U_n$  = displacement at time increment  $n$ ;
- $\dot{U}_n$  = velocity at time increment  $n$ ;
- $\ddot{U}_n$  = acceleration at time increment  $n$ ;
- $\Delta t_n$  = stable time increment at time increment  $n$ ;
- $M$  = mass matrix;
- $F_n^{ext}$  = exterior force vector;
- $F_n^{int}$  = interior force vector.

Once the general displacement and general velocity at time increment  $n$  are known, these values for the time increment  $n+1$  can be directly calculated. The advantage of using the explicit method is that it does not require iteration to update physical quantities nor requires a tangent stiffness matrix. For the FE model in this study with large deformations, material nonlinearity, and contact constraints, the explicit solver provides better computational efficiency compared to the implicit solver, which uses iterations to update physical quantities. The disadvantage of using the explicit method is that the time increment  $\Delta t$  must be smaller than the stable time increment, which is controlled by the element size and material properties. This can result in the need for a large number of time increments. A typical stable time increment is given below, which is valid for truss element with linear elastic material and size  $L$ .

$$\Delta t = \frac{L}{\sqrt{\frac{E}{\rho}}} \quad (7-20)$$

where:

- $L$  = element size;
- $E$  = modulus of elasticity;
- $P$  = density.

When explicit dynamic schemes are used for quasi-static loading scenario, care must be taken to ensure that inertial effects are insignificant. A measure of the significance of inertial effects is the value of the kinetic energy as compared to the total internal energy. Mia and Bhowmick (2017) report that for a quasi-static test, the ratio of kinetic energy over internal energy should be less than 5%. Abaqus documentation (Abaqus 2015) recommends values between 1% and 5% for the specific ratio. At very early loading stages, kinetic energy will be almost equal to the internal energy since the model does not have much deformation and all energy is contributed by movement. The kinetic energy should be compared with the total energy after the first few time increments. It can be observed from Eq. 7-20 that if a faster analysis is needed, the density of the material can be given a higher value. This technique is called mass scaling. This study does not include any mass scaling except that used in the mesh sensitivity study described earlier, to avoid having undesirable dynamic effects. However, mass scaling in Section 7.2.4 showed that load-slip response of the FE models did not have remarkable changes when the material density increases 100 times.

Nonlinear geometry is considered in all FE models in this study. The dynamic explicit solver in Abaqus considers nonlinear geometry by default. For large deformation problems, physical quantities like displacement, velocity, and acceleration can be described by the initial coordinates (material coordinates) or current coordinates (spatial coordinates). For C3D8 and T3D2 elements used in this study, Abaqus uses the updated Lagrangian to formulate the governing equations (strong form) and weak forms. That is for each time increment, the initial coordinates are updated to the current coordinates, which avoids having a convective term in the strong form. More details on the FE formulation of large deformation problems can be found in Koutromanos (2014).

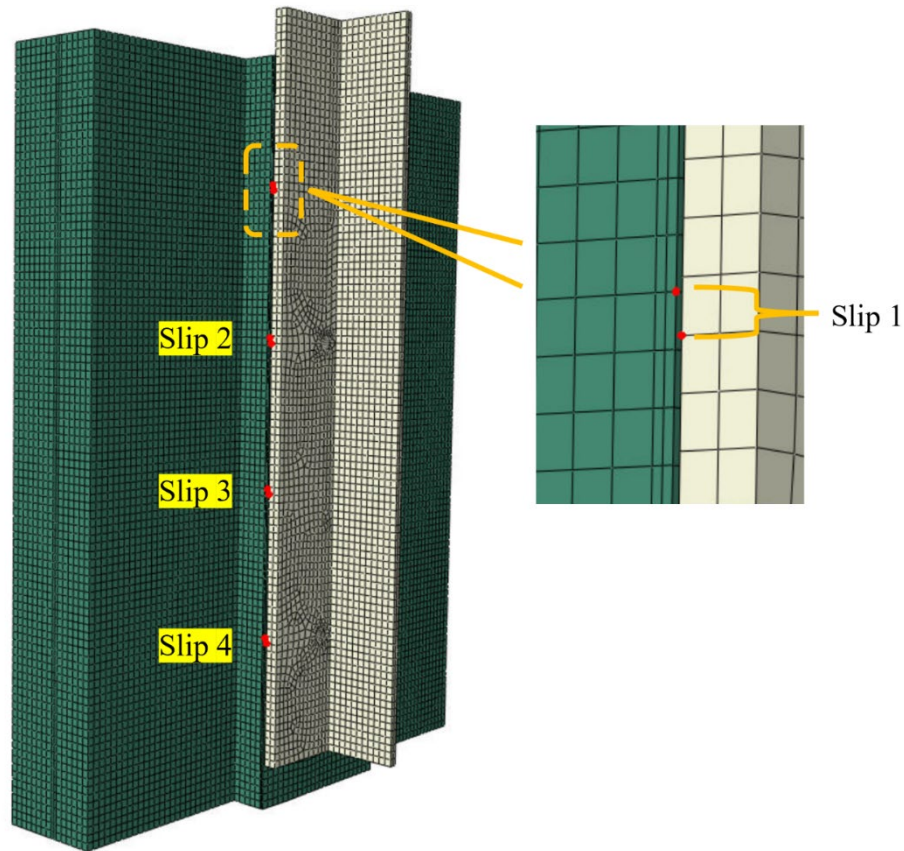
## **7.2.7. Validation Results and Discussion**

Results of FE models developed based on the above procedures, called modeling techniques, were compared with experiments. First, the load-slip response is compared and discussed. Then, the detailed damage patterns are compared and discussed.

### **7.2.7.1. Load-Slip Response**

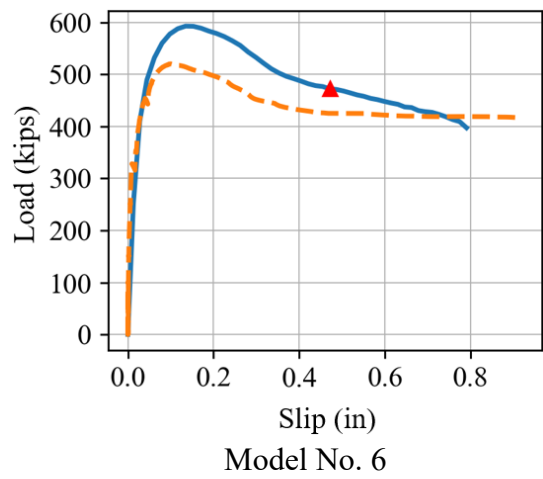
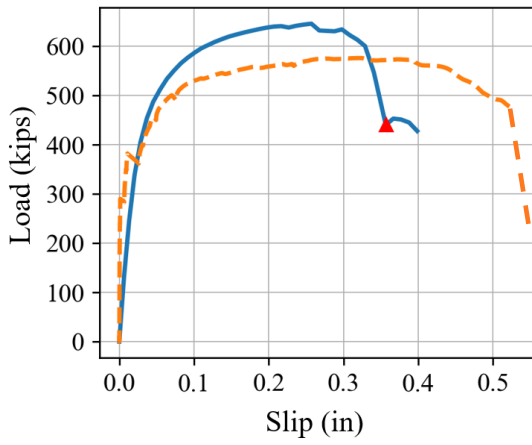
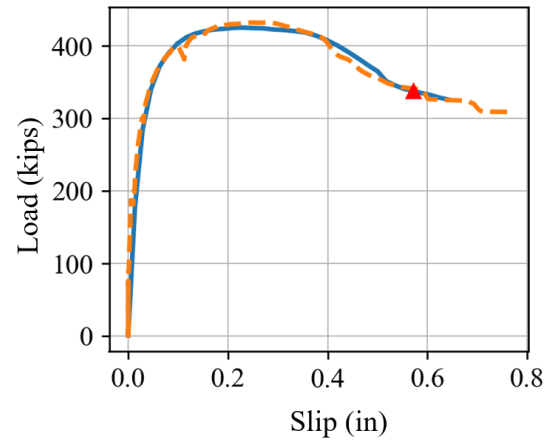
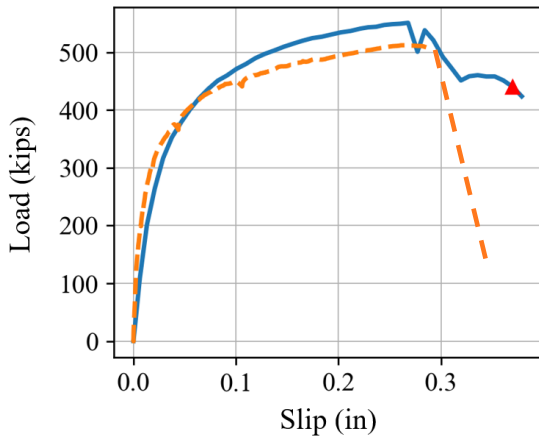
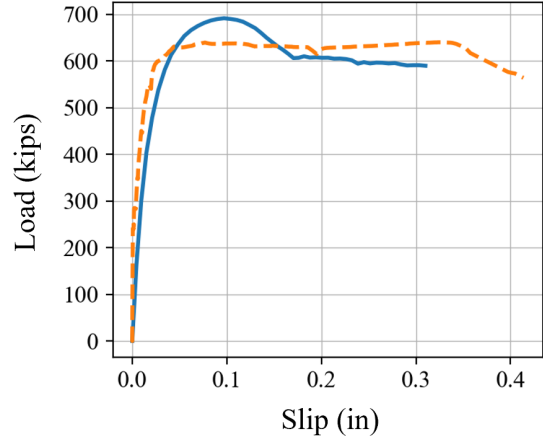
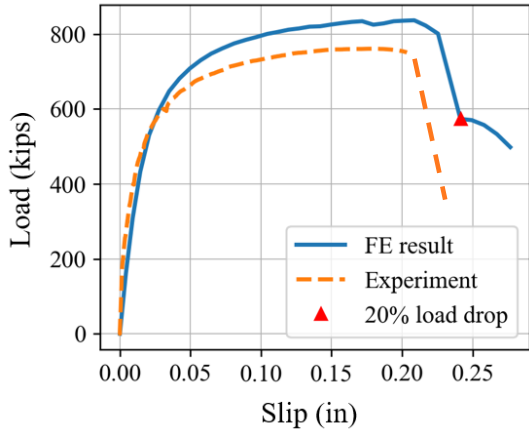
In the FE study, slip was measured using a similar method as that used for the experiments. The relative displacement between nodes on the concrete and on the steel flange at various locations were recorded and averaged, as shown in Figure 7.30. The load was obtained by summing the reaction forces of nodes at the top of the steel section where the target displacement was applied.





*Figure 7.30 - Slip Measurement in Model No. 5*

Comparisons of the load-slip curves between the eleven FE models and experiments are given in Figure 7.31. For FE models with stud fracture, a sudden decrease of the load is observed. The first analysis step for which the strength is less than 80% of the peak strength is shown as a red triangle. If the FE model has a 20% drop from the peak strength without a sudden decrease, the model is regarded as concrete failure. Model No. 2 never had a load drop more than 20% during the entire analysis. As noted in Chapter 5, the experimental load-slip behavior after the stud fracture point was not reliable due to instrumentation limitations. For experimental load slip-curves with stud fracture, an illustrative post-fracture decreasing branch is given in Figure 7.31 for comparison purposes.



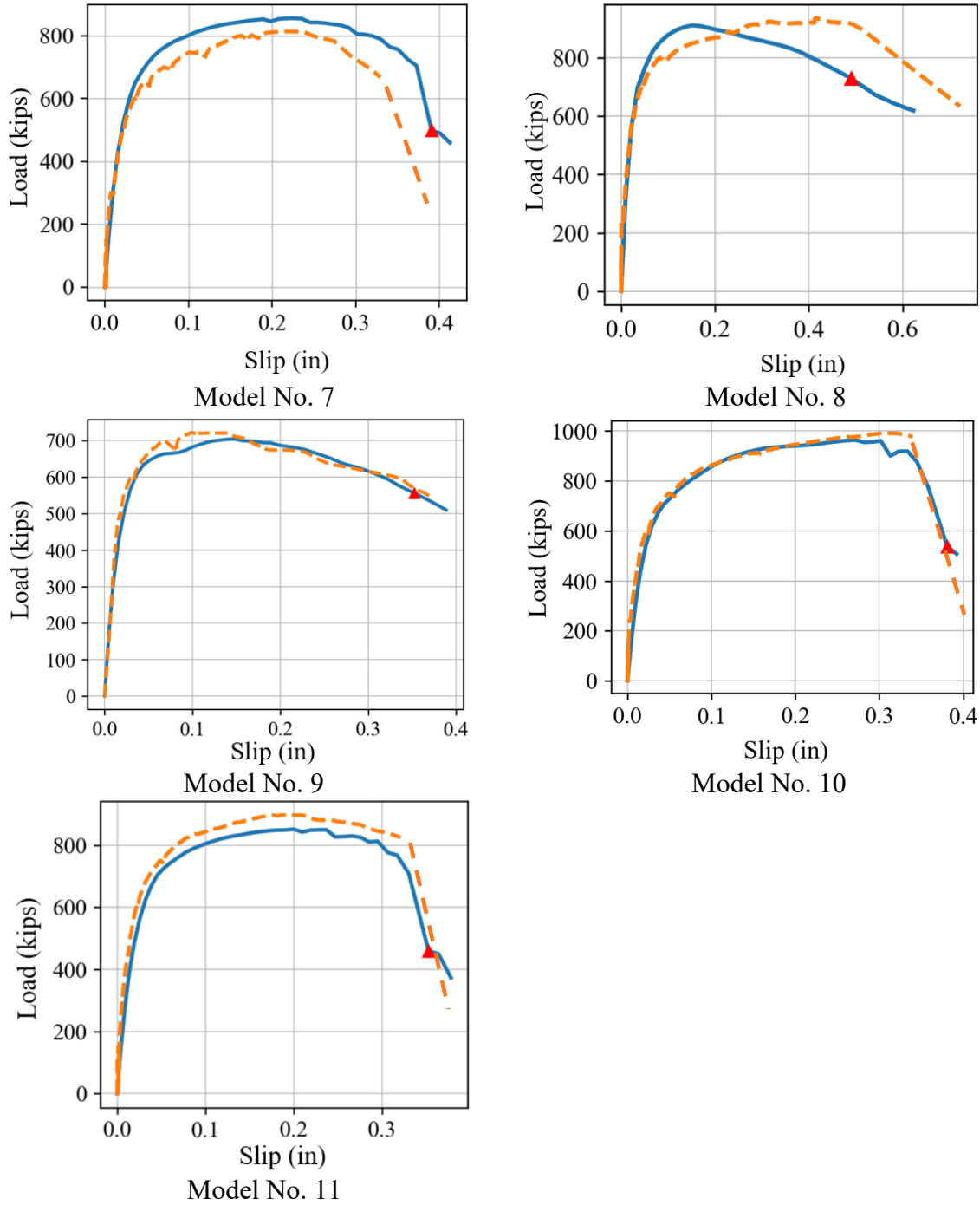


Figure 7.31 - Load-Slip Curves for FE Models and Corresponding Experiments

Table 7.4 lists the peak strength from the FE models and the experiments. The relative error of each model is calculated. Based on Figure 7.31 and Table 7.4, the FE models tend to overestimate the strength for specimens using a staggered stud layout. The two staggered layout models both have a strength error more than +10%. Model No. 6, which reflects the staggered layout specimen with PCPs, has the highest error of +13.9%. Other than those, the error in peak strength is generally no larger than  $\pm 10\%$ . Overall, the average arithmetic and absolute error in

peak strength of the eleven FE models is 3.7% and 6.3%, respectively, which suggests reasonable strength predictions by the FE models. Additionally, each FE model captured the correct failure mode.

**Table 7.4 - Strength Comparisons Between FE Models and Experiments**

Model No.	Experimental Max. Load (kips)	FE Max. Load (kips)	Error	Failure mode
1	761	836	10.0%	S*
2	640	692	8.0%	C*
3	512	540	5.6%	S
4	432	425	-1.6%	C
5	576	646	12.1%	S
6	520	593	13.9%	C
7	814	855	5.1%	S
8	936	912	-2.6%	C
9	722	704	-2.5%	C
10	991	964	-2.8%	S
11	897	852	-5.1	S

Note: S: stud fracture. C: concrete damage

Table 7.5 provides comparisons of slip between FE models and the experimental results. For FE models with stud fracture, the ultimate slip is taken at one analysis step before the sudden strength decrease. This is because this sudden strength decrease may introduce a large slip, which is not representative of ductility of the stud and concrete. For FE models with concrete failure, the slip is taken at the point where the strength has dropped 20% from the peak strength.

**Table 7.5 - Slip Comparisons Between FE Models and Experiments**

Model No.	Experimental Slip at Max. Load (in)	FE Slip at Max. Load (in)	Error	Experimental Ultimate Slip (in)	FE Ultimate Slip (in)	Error
1	0.18	0.21	16.6%	0.20	0.23	11.2%
2	0.33	0.10	-70.4%	0.41	N.A.	N.A.
3	0.26	0.24	-6.7%	0.28	0.32	12.9%
4	0.28	0.23	-17.6%	0.53	0.55	4.1%
5	0.32	0.26	-20.6%	0.53	0.34	-35.4%
6	0.10	0.13	36.3%	0.92	0.45	-50.3%
7	0.22	0.23	4.6%	0.32	0.37	16.5%
8	0.42	0.15	-63.7%	0.53	0.47	-10.2%
9	0.10	0.15	48.8%	0.34	0.34	1.4%
10	0.31	0.27	-11.0%	0.34	0.36	6.8%
11	0.19	0.20	4.1%	0.31	0.33	6.2%

The discrepancy in slip between FE models and experiments is more prominent compared to strength. Models with the highest slip difference are Model Nos. 2, 5, 6, and 8. All of them show a considerable underestimation of the experimental slip. Chapter 5 described the limitations of the experimental instrumentation. It is believed that the slip is overestimated in the experiments for specimens with large cracks in the concrete haunch. Specimens Nos. 2, 6, and 8 are those with the most severe haunch cracking in the experiments. Thus, overestimation in the slip is likely to be large. Concrete cracking in the experiments is an uncertain event related to the inevitable variations in material properties and loading conditions. It is impractical to track each crack in the FE model precisely. As a result, the FE model cannot reflect the overestimation of slip accurately. Nonetheless, the average arithmetic and absolute error in the ultimate slip of the eleven FE models are -5.6% and 16.4%, respectively. The average arithmetic and absolute error in the slip at the maximum load of the eleven FE models are -7.2% and 27.3%, respectively. Considering the complexity and uncertainty in modeling concrete and steel nonlinear material response and damage, both are deemed acceptable.

#### **7.2.7.2. Concrete and Stud Damage**

As noted above, individual cracks in concrete cannot be tracked in the FE model. However, tensile damage in concrete can be reflected by the contour plot of the maximum principal strain. Figure 7.32 presents the contour plot of the Model No. 5 concrete deck, in which bands with high tensile strain can be observed and the development of these bands resembles the crack development in the experiment. The compression damage on concrete can be illustrated by looking at the contour plot of minimum principal strain. Figure 7.33 provides a comparison between the contour plot in Model No. 3 and the concrete damage in the experiment. The damage captured in the FE models agrees well with the experiment. A high concentration of compression strain is located below the stud region, which resembles the concrete crushing pattern observed in the experiment. Once again, the FE model cannot capture the exact concrete damage pattern observed in the experimental specimens. The strain contour plots only provide an indication of regions with high strain concentration.

One important observation from the experimental program is that when PCPs were used, more severe concrete cracking developed. Figure 7.34 shows the maximum principal strain contour plot on the CIP concrete in Model Nos. 7, 2, 4, and 6 using the same color scale. The fully CIP Model No. 7 is included as a reference to show the change in concrete tensile damage when PCPs are used. Horizontal cracking in the haunch is noticed in all four FE models. But the three FE models with PCPs have a higher tensile strain in the horizontal crack, reflecting a larger and wider horizontal crack. FE Model No. 6 in Figure 7.34 (d) can be compared with Figure 7.32. The PCP specimens developed more severe cracking compared to the fully CIP Model No. 5. These observations from the FE models agree with the experimental observations.

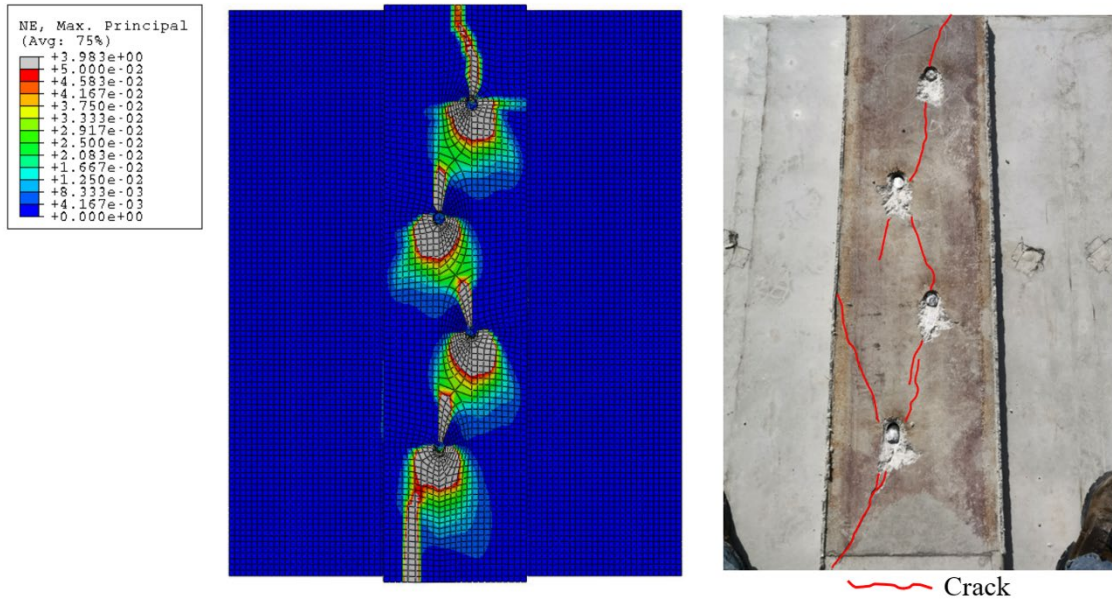


Figure 7.32 - Comparison Between Maximum Principal Strain Contours in FE Model No. 5 and Cracks Observed in Experiment

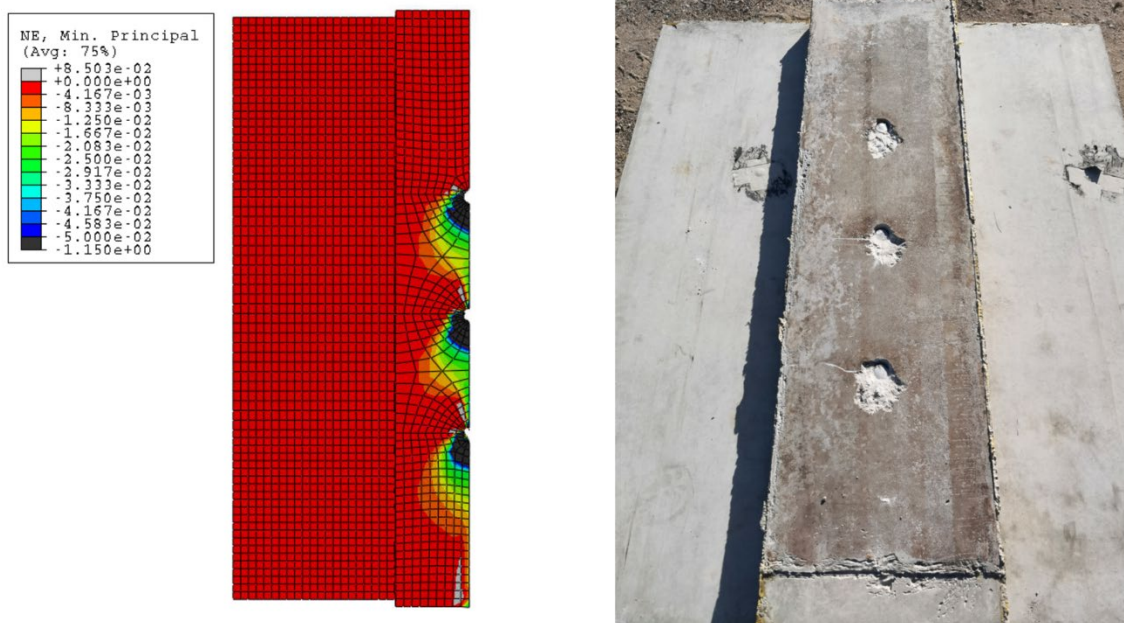


Figure 7.33 - Comparison Between Minimum Principal Strain Contours in FE Model No. 3 and Compression Damage Observed in Experiment

For PCP specimens, besides horizontal cracks in the haunch, splitting cracks in the CIP concrete between the PCPs were always observed in the experiments. As Figure 7.34 shows, all four FE models captured the splitting cracks. The splitting crack in Model No. 2 ( Figure 7.34 b) is



developed away from the middle of the haunch. The corresponding experimental specimen for Model No. 7 does not have a splitting crack.

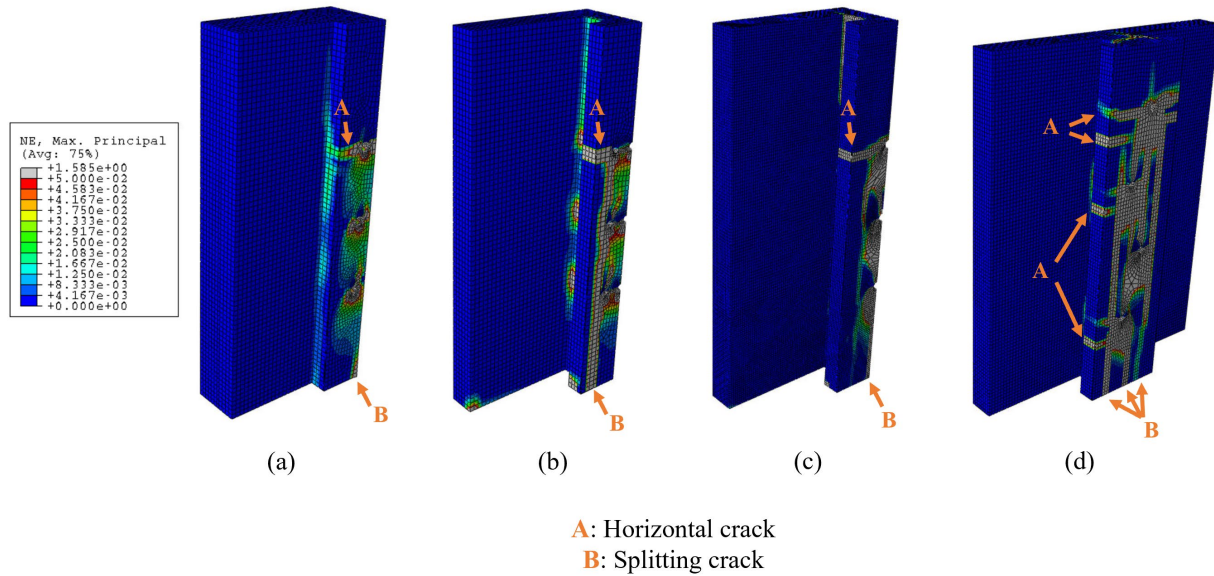


Figure 7.34 - Maximum Principal Strain Contours for (a) Model No. 7, (b) Model No. 2, (c) Model No. 4, and (d) Model No. 6

When only half transverse reinforcement is used, the experimental Specimen No. 8 showed several cracks on the concrete deck. Figure 7.35 shows the maximum principal strain contours on Model No. 8. The high tensile strain band is observed to develop extensively on the concrete deck surface and resembles the experimental observation. However, a splitting cracking is also noticed in the FE model, which was not observed in the experiment.

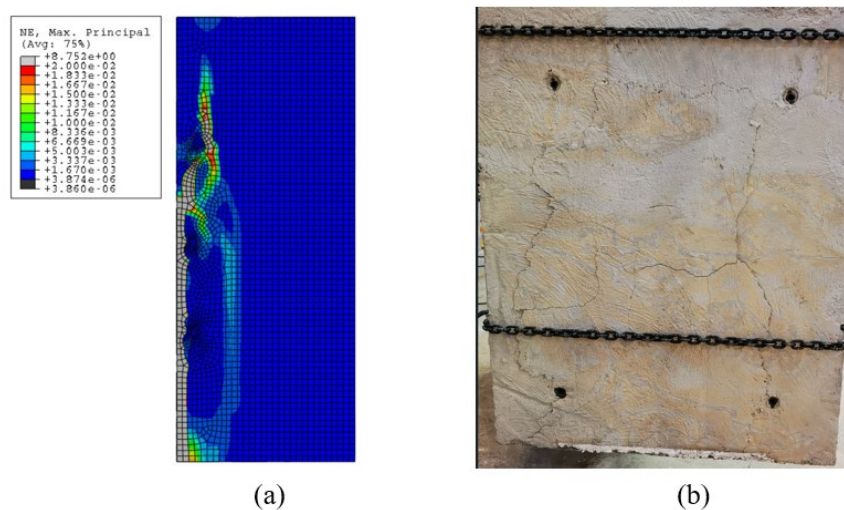
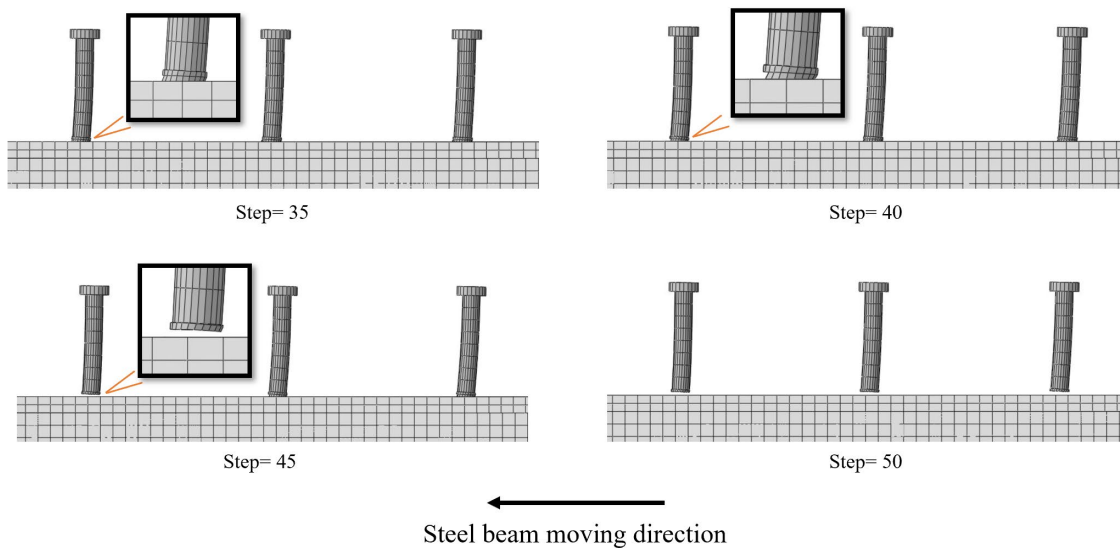


Figure 7.35 - (a) Maximum Principal Strain Contour on Model No. 8 Concrete Deck, and (b) Photo of Specimen No. 8 Concrete Deck after the Test



Shear stud fracture is seen in the FE models as the removal of elements. Figure 7.36 shows the sequence of element removal in Model No. 7, which is representative for all FE models with stud fracture. The element removal starts at the weld collar on the side of the stud facing the steel beam movement direction in the left shear stud. At analysis step 45 in Figure 7.36, the shear stud on the left is completely sheared off while the other two studs developed different levels of damage. All shear studs sheared off at the end of the analysis, which is step 50. All element removal occurs at the weld collar region, indicating concentration of forces in this region. The shear stud on the left represents the shear stud closest to the bottom of the push-out specimen. These observations are consistent with the experimental findings reported in Chapter 5, in which shear studs after the test showed larger deformations for the stud close to the bottom of the specimen.



*Figure 7.36 - Element Removal at Base of Shear Studs at Different Analysis Steps*

Overall, the FE models reproduced the load-slip response for the eleven push-out specimens in the experimental program with reasonable accuracy. The failure mode was correctly captured for all eleven specimens and the damage patterns in the concrete in the FE models are comparable to the experimental observations. The next step was to conduct simulated push-out tests using the validated FE models and modeling techniques to study issues of interest that were not studied in the experimental program.

## 7.2.8. Discussion on Selected Modeling Parameters

### 7.2.8.1. Friction Coefficient

Previous FE studies report a wide range of friction coefficients between steel and concrete, ranging from 0.15~0.4. Rabbat and Russell (1985) reported the friction coefficient to be 0.57 to

0.70 between steel and concrete. Additionally, an observation from the push-out tests reported in Chapter 5 is that the stud shear strength obtained in these tests was often close to the tensile strength of the stud, which is contradictory to the shear test results reported in Chapter 4. It is believed that friction between steel beam and concrete contributed to the total resistance of the push-out specimens.

Model No. 7 was re-analyzed with various friction coefficients. Results are presented in Figure 7.37. It can be observed that friction contributes a significant portion of the total load resistance in the push-out model. When no friction is included in the model, the peak strength drops about 200 kips compared to the 0.6 friction coefficient case. This means the friction provides about 24% of the shear resistance in the push-out models. If the contribution from friction is excluded, the shear strength for each stud is 53.9 kips, which is close to the shear strength of 53.6 kips obtained by the shear test reported in Chapter 4. As a reminder, the friction coefficient is used for all surfaces under contact in the FE model. If the friction coefficient is equal to zero, not only will the surface between the steel beam flange and concrete have no friction, but also the surfaces between the stud and concrete, and the concrete and rigid steel foundation will have no friction.

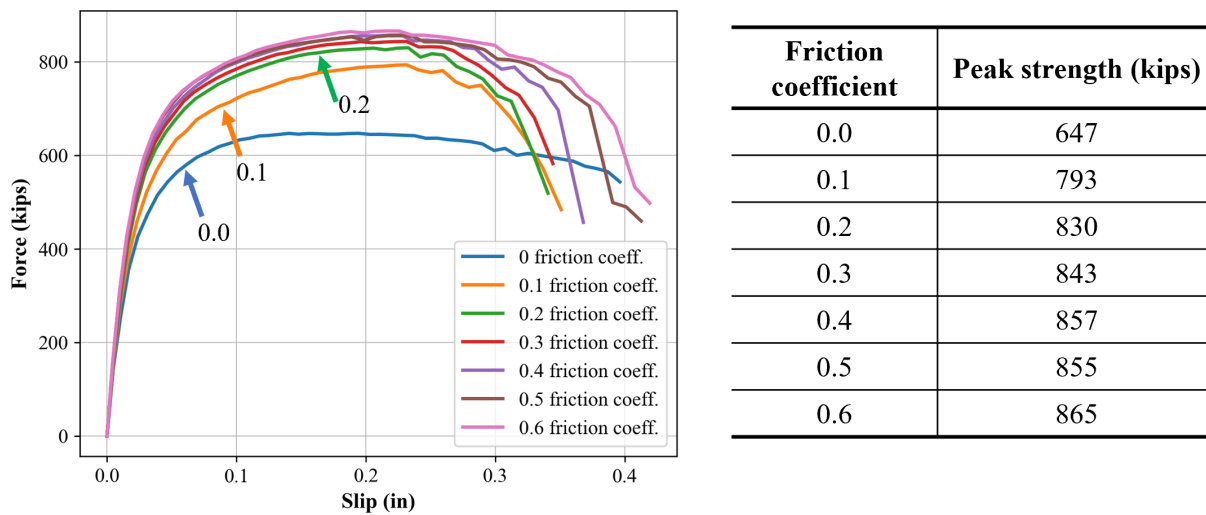


Figure 7.37 - Model No. 7 Results Using Various Friction Coefficients

When the friction coefficient is more than 0.2, the increase in peak strength is much less significant. There is less than a 5% strength increase when the friction coefficient is increased from 0.2 to 0.6. Therefore, the common range of friction coefficients used in previous research of 0.3~0.4 will give mostly the same results as 0.5, which is used in this study.

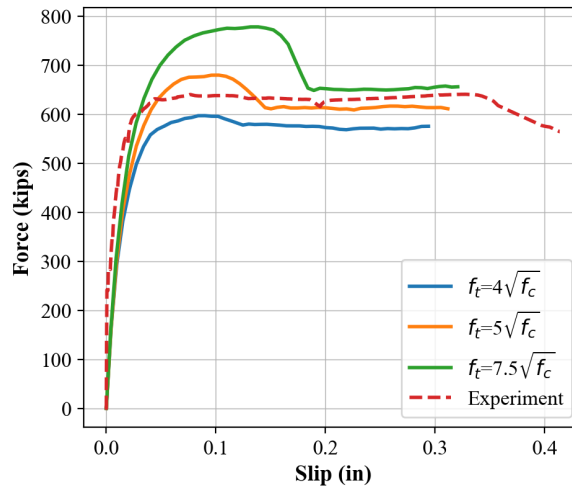
### 7.2.8.2. Concrete Tensile Strength

The tensile strength for normal strength concrete, in psi, ranges from  $\sqrt{4f_c}$  to  $\sqrt{7.5f_c}$  (Dara 2015). Table 7.6 presents the average arithmetic error for eleven FE models when different concrete tensile strength equations are used. The concrete tensile strength has significant influence on the

strength for all FE models. Model No. 2 is used here as an example. Figure 7.38 shows Model No. 2 load-slip response using different values of concrete tensile strength. When higher concrete tensile strength is used, a peak in the load-slip curve is seen, which does not exist in the experimental result. The shape of the load-slip curve matches the experiment best for the  $\sqrt{4f_c}$  case. However, a concrete tensile strength of  $\sqrt{5f_c}$  resulted in the overall smallest error for the eleven FE models and therefore,  $\sqrt{5f_c}$  is adopted for all FE models including Model No. 2.

**Table 7.6 - Average Error for Different Concrete Tensile Strengths**

Concrete tensile strength (psi)	Average Absolute Error of Eleven FE Models
$\sqrt{4f_c}$	7.4%
$\sqrt{5f_c}$	6.3%
$\sqrt{7.5f_c}$	15.6%



*Figure 7.38 - Load-Slip Curves for Model No. 2 Using Various Values of Concrete Tensile Strength*

### 7.2.8.3. Concrete Compressive Strength

As noted in Section 8.2.2.2, the concrete compressive strength,  $f_c$ , used for each FE model was based on the test-day concrete cylinder strength for each corresponding experimental specimen, except Model No. 8 and No. 10 which used the measured 28-day strength. The specified value of the 28-day compressive strength for the concrete used in all push-out specimens was 4 ksi. The actual values of  $f_c$  varied from 4.3 ksi to 5.5 ksi among the eleven push-out FE models. Model No. 7, which has  $f_c = 4.8$  ksi, was re-analyzed with different values of  $f_c$  to examine the impact of this variation. Figure 7.39 presents the results and it is clear that  $f_c$  plays a significant role in the strength of the push-out model. With  $f_c = 4$  ksi, the peak strength of Model No. 7 was reduced

6% and 11% compared to the 4.8 ksi and 5.6 ksi cases, respectively. Stud fracture was also delayed when lower strength concrete was used. Model No. 7's strength based on AASHTO design equations is also reported in Figure 7.39. The decreasing rate of the 9<sup>th</sup> Ed. AASHTO stud design strength is greater than that of the FE model. When  $f_c = 4$  ksi is used, the AASHTO design strength reduced 11% and 20% compared to the 4.8 ksi and 5.6 ksi cases, respectively. The design equation for stud strength in the 9<sup>th</sup> Ed. AASHTO becomes more conservative when lower strength concrete is used. In the proposed 10<sup>th</sup> Ed. AASHTO, stud strength is no longer a function of concrete strength, and only depends on the strength of the stud steel material, as described in Chapter 2. The same stud tensile strength,  $F_u$ , of 83.5 ksi, as reported in Chapter 5, was used for all AASHTO design strength calculations in Figure 7.39.

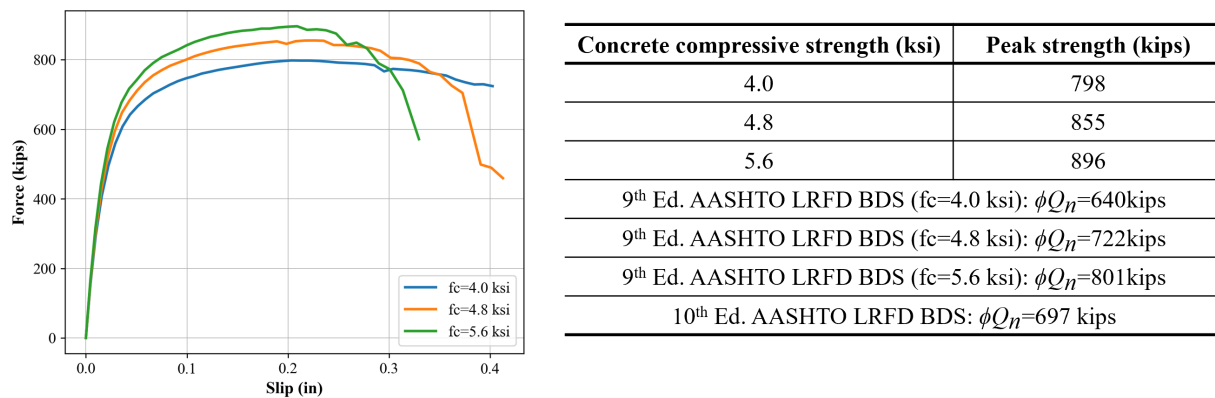


Figure 7.39 - Load-Slip Curves for Model No. 7 Using Various Values of Concrete Compressive Strength

### 7.3. Parametric Studies

Table 7.7 illustrates the matrix for the parametric study. For each point of interest, at least three FE models were investigated. The parametric study is separated into three major categories, namely the stud penetration into the deck, the clear distance between the stud and the PCP, and other details like the bedding strip size. Stud penetration was investigated by changing the stud length and alternatively, by changing the haunch depth. The clear distance between the stud and the PCP was studied by changing the total width of the concrete deck or by changing the overlap of PCP on the steel beam flange. The parametric studies included both full-depth CIP decks as well as decks using 4" PCPs with 4.5" CIP topping. Clearly, some of the variables in the parametric study apply only to decks with PCPs, such as the clear distance between the stud and the PCP and the dimensions of the bedding strip.

Observations and discussion for each point of interest are presented below. For most of the parametric studies, the strength of the push-out FE model is compared with the strength computed using the 9<sup>th</sup> Ed. AASHTO and the proposed 10<sup>th</sup> Ed. AASHTO. When computing the AASHTO design strength values, the values of  $f_c$  for the concrete and  $F_u$  for the stud are the same values that were used in the FE models. These values of  $f_c$  and  $F_u$  generally coincide with measured values from the actual push-out specimens listed in Table 7.8, unless noted otherwise.

For all specimens, including those with PCPs, AASHTO stud strength was computed using the  $f_c$  of the cast-in-place concrete, since the studs are always embedded in the cast-in-place concrete.

### 5.1.1 Stud Penetration into Concrete Deck

For this research, both in the experimental push-out tests and in the parametric studies, stud penetration is defined as the distance that the stud penetrates into the concrete deck. Penetration depth is measured starting at the base of the deck, which is the same as the top of the haunch. For example, if a 7" long stud is used with a 3" haunch, the stud penetration into the deck is 4".

The experimental program showed the importance of stud penetration into the concrete deck. As a reminder, in Chapter 5, Specimen No. 9 using 1-1/8" stud had a 2" penetration with a fully CIP concrete deck. The performance of Specimen No. 9 changed significantly compared to Specimen No. 7 using a 4" penetration. In this parametric study, the stud penetration investigation was extended to 7/8" studs when the fully CIP concrete deck is used and extended to 1-1/8" studs when PCPs are used. The range of penetration depths was also expanded compared to the experimental program.

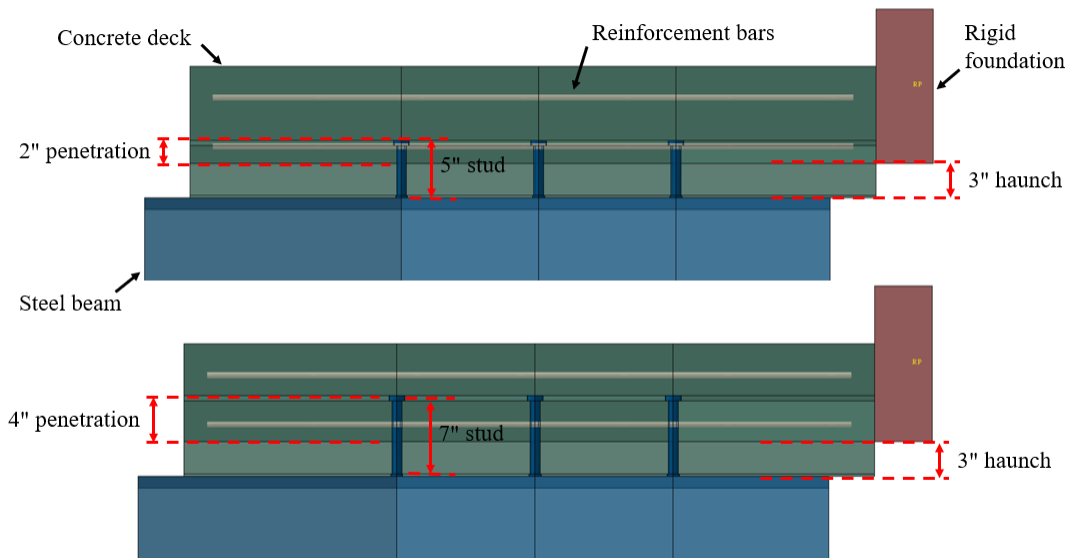
**Table 7.7 - Parametric Study Matrix**

Category	Description	Parametric matrix
Stud Penetration	Stud Penetration into Concrete Deck	2", 3", 4", 5", 6"
	Haunch Depth	0", 0.5", 1", 1.5", 2", 3"
Clear Distance Between Stud and PCP	Beam Flange Width	15", 20", 24"
	Clear Distance Between Stud and PCP	5/8", 9/8", 13/8"
	PCP Overlap with Steel Beam Flange	3.5", 5", 8.1"
Others	Bedding Strip Size	0", 1.5", 3"
	Transverse Reinforcement	#4@27", #4@18", #4@9"

**Table 7.8 - Concrete Compressive Strength and Stud Tensile Strength Used in FE Models and to Compute AASHTO Stud Strength (Unless Noted Otherwise)**

Model No.	$f_c$ (ksi)		$F_u$ (ksi)
	CIP	PCP	
1	5.39	N/A	83.5
2	4.65	7.64	
3	5.23	N/A	
4	4.47	6.83	
5	4.72	N/A	
6	5.11	6.92	
7	4.83	N/A	
8	5.50	N/A	
9	4.76	N/A	
10	5.05	N/A	
11	4.32	N/A	

Changes in the stud penetration depth were achieved first in the parametric study by changing the height of the shear stud while keeping the haunch depth fixed, which is the same as the laboratory procedure. Figure 7.40 shows a side view of two FE models with the same haunch depth but with different stud penetrations. For the 2" penetration case, a shorter stud is used compared to the 4" penetration case.



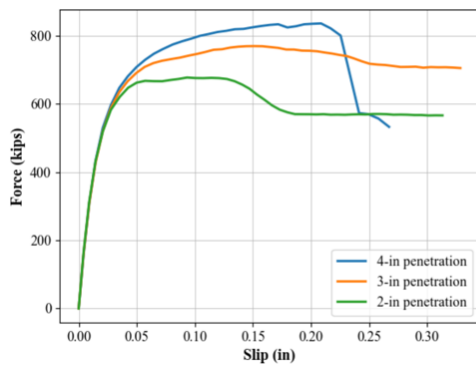
*Figure 7.40 - FE Models with Different Stud Penetrations into a Fully CIP Concrete Deck*

### 7.3.1.1. Fully CIP Concrete Deck, 7/8" Studs

Figure 7.41 illustrates the results of different penetration depths for 7/8" studs. Three penetration depths were studied, namely 2", 3", and 4". Model No. 1 in Section 7.2 is used as the basis for

this parametric study. Load-slip response of Model No. 1 is directly plotted in Figure 7.41 as “4-in penetration”. The other two FE models are derived based on Model No. 1 with the same concrete compressive strength,  $f_c$ , and equivalent plastic displacement at failure,  $\bar{u}_f^{pl}$ . The only difference between models is the stud length.

The failure mode of each case can be determined by looking at the load-slip response. When penetration is smaller than 4”, no stud fracture occurred within 0.3” slip and concrete controls the failure mode for the 2” case. The table in Figure 7.41 presents stud ultimate strength and ductility. Ultimate strength of the FE models decreases when smaller penetration is used. When penetration reaches 2”, which is the minimum allowable value in AASHTO and in TxDOT design standards (TxDOT 2019), the strength of the stud does not satisfy the 9<sup>th</sup> Ed. AASHTO stud strength design equation. The table in Figure 7.41 also provides the slip at 80% and 90% of peak load (20% drop and 10% drop from the peak load). The slip at 90% peak load can be compared with the ductile criterion of 0.26” (6.67mm) from Eurocode 4 (CEN 2004). It can be observed that the models with 2” and 4” penetration do not satisfy the EC-4 requirement.



Penetration (inches)	Peak strength (kips)	Ultimate slip (inches) 80%/90%
2	678	0.32/0.16
3	770	>0.33/>0.33
4	836	0.23/0.23
9 <sup>th</sup> Ed. AASHTO LRFD BDS: $\phi Q_n=691$ kips		
10 <sup>th</sup> Ed. AASHTO LRFD BDS: $\phi Q_n=571$ kips		
Eurocode 4-2 2005: slip at 90% peak load: 0.26" (6.67mm)		

Figure 7.41 - Parametric Study on Penetration of 7/8” Studs into Fully CIP Concrete Deck

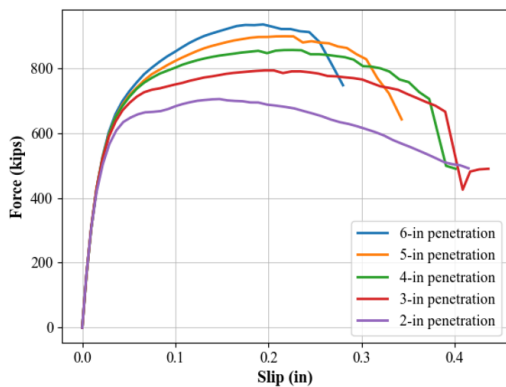
### 7.3.1.2. Fully CIP Concrete Deck, 1-1/8” Studs

Parametric study results are shown in Figure 7.42. FE models reflecting stud penetrations of 2” and 4” are existing Models No. 7 and No. 9 in Section 7.2. Their results are directly adopted in Figure 7.42 as “4-in penetration” and “2-in penetration”. Concrete compressive strength,  $f_c$ , is different in Model No. 7 and No. 9 but very close to each other. For other FE models in this parametric study, concrete compressive strength is taken as the average of the two. Model No. 7 and No. 9 have the same  $\bar{u}_f^{pl}$  and this is used in other FE models for comparison.

Like the 7/8” studs, the 1-1/8” stud had smaller ultimate strength when smaller penetration is used. The failure mode is stud fracture except for the 2” penetration case, which showed concrete failure. The model with 2” penetration is also the only one that does not satisfy the strength from the 9<sup>th</sup> Ed. AASHTO design equation. For those models that showed failure by stud fracture, the



ultimate slip is reduced when a larger penetration is used. This is because the higher resistance developed when larger values of penetration are used cause earlier stud fracture.



Penetration (inches)	Peak strength (kips)	Ultimate slip (inches) 80%/90%
2	704	0.34/0.27
3	792	0.39/0.35
4	855	0.37/0.33
5	898	0.33/0.31
6	934	0.27/0.25
9 <sup>th</sup> Ed. AASHTO LRFD BDS: $\phi Q_n=722$ kips		
10 <sup>th</sup> Ed. AASHTO LRFD BDS: $\phi Q_n=697$ kips		
Eurocode 4-2 2005: slip at 90% peak load: 0.26" (6.67mm)		

Figure 7.42 - Parametric Study on Penetration of 1-1/8" Studs into Fully CIP Concrete Deck

### 7.3.1.3. Concrete Deck with PCP, 1-1/8" Studs

Model No. 4 was used as the basis for this parametric study. Its load-slip curve is shown in Figure 7.44 as "4-in penetration". The other two FE models were derived based on Model No. 4 with the same  $f_c$  and  $\bar{u}_f^{pl}$ . Figure 7.43 illustrates two FE models in this parametric study.

All models show a concrete controlled failure mode and decreased strength when smaller penetration depths are used. For the model with 2" penetration, the ultimate strength does not satisfy the 9<sup>th</sup> or 10<sup>th</sup> Ed. AASHTO requirements. The slip at 90% peak load is higher than the EC-4 requirement for all FE models in this group. Some of the predicted slip may be due to large horizontal cracks in the haunch region that may not reflect the true slip capacity of the shear stud.

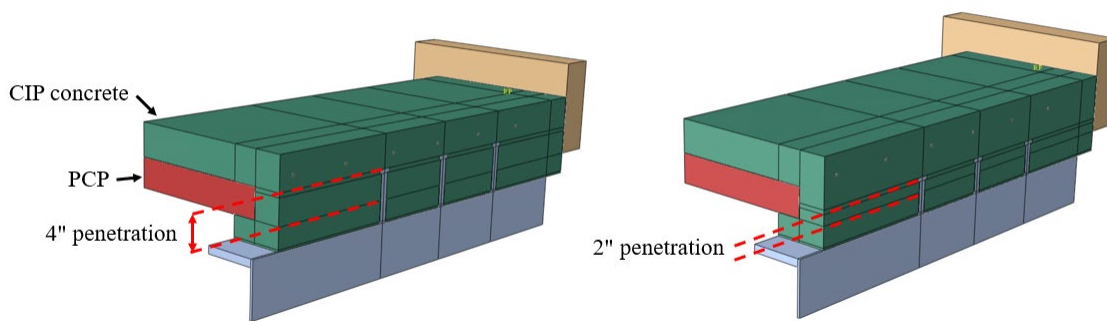
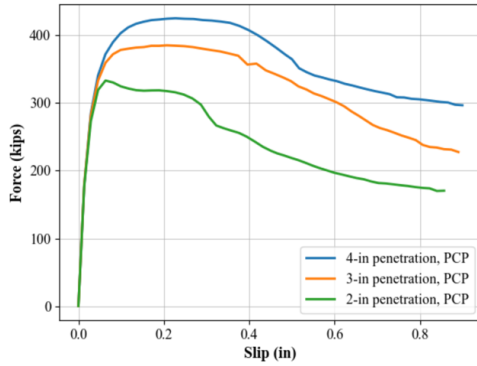


Figure 7.43 - FE Models with PCP and with Different Stud Penetrations



Penetration (inches)	Peak strength (kips)	Ultimate slip (inches) 80%/90%
4	425	0.52/0.42
3	385	0.57/0.44
2	333	0.32/0.27
9 <sup>th</sup> Ed. AASHTO LRFD BDS: $\phi Q_n=345$ kips		
10 <sup>th</sup> Ed. AASHTO LRFD BDS: $\phi Q_n=349$ kips		
Eurocode 4-2 2005: slip at 90% peak load: 0.26" (6.67mm)		

Figure 7.44 - Parametric Study on Penetration of 1-1/8" Studs into Concrete Deck with PCP

### 7.3.2. Haunch Depth

In the laboratory experiments, ten of the eleven specimens had a haunch depth of 3". However, one of the specimens, specifically Specimen No. 10 had a 1" haunch and this specimen showed a higher strength compared to the specimens with a 3" haunch. The reduction in haunch depth in Specimen No. 10 also resulted in an increased penetration of the stud into the deck. Therefore, the reason for the strength increases in Specimen No. 10 may have been related to the smaller haunch depth, or to the increased penetration depth, or possibly to other factors. This part of the parametric study will examine the effect of haunch depth in greater detail. The FE models includes a wider range of haunch depths and special consideration for stud penetration. FE models with PCPs are also studied using various haunch depths.

#### 7.3.2.1. Fully CIP Concrete Deck, 1-1/8" Studs of Same Length

Figure 7.45 presents two FE models with different haunch depths while the shear stud length is fixed at 7". As a consequence, the reduction in haunch depth simultaneously increases the stud penetration into the concrete deck. This is the same as Specimen No. 10 in the experimental push-out test program. It should be noted that when a 0" haunch is used, the top clear cover above the shear stud is only 1.5", which does not satisfy the requirements in AASHTO and TxDOT design standards.

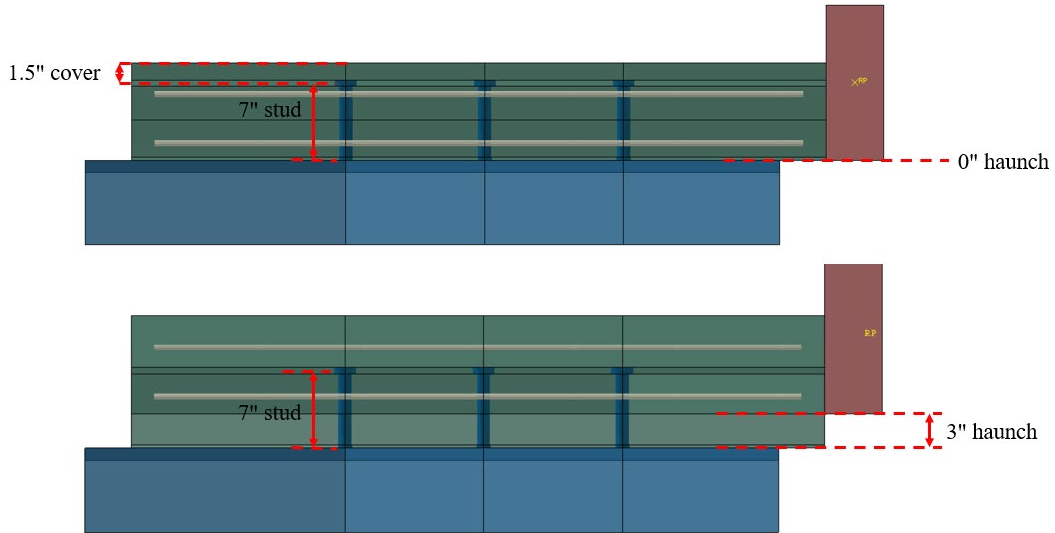
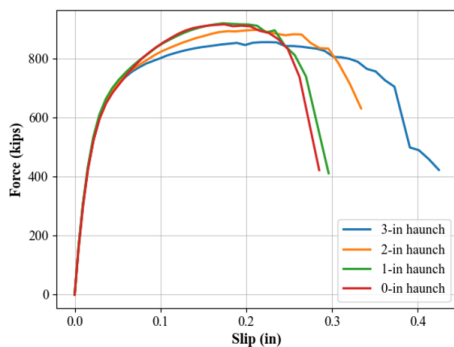


Figure 7.45 - FE Models with Different Haunch Depths and with Fixed Stud Length of 7"

Figure 7.46 presents the results of the parametric study. FE models reflecting 3" and 1" haunches were already developed in Section 7.2, which are Model No. 7 and Model No. 10, respectively. Model No. 7 is selected as the basis for this parametric study. Its result is given as "3-in haunch" in Figure 7.46. Model No. 10 has different  $f_c$  and  $\bar{u}_f^{pl}$  from Model No. 7. For comparison purposes, Model No. 10 is analyzed again with the same  $f_c$  and  $\bar{u}_f^{pl}$  as Model No. 7 and the results are plotted as "1-in haunch" in Figure 7.46.

Based on the results in Figure 7.46, the stud ultimate strength increases and ultimate slip decreases when haunch depth gets smaller. The FE model with 0" haunch has almost identical response as the 1" haunch model, indicating the strength gain from decreasing haunch depth has an upper limit. Top concrete cover above the stud seems to have no obvious effect on strength and ductility. The FE models with a 1" and 0" haunch do not satisfy the EC-4 slip requirements, although only by a very small amount, due to earlier fracture of the studs.



Haunch depth (inches)	Peak strength (kips)	Ultimate slip (inches) 80%/90%
0	916	0.26/0.25
1	919	0.27/0.25
2	897	0.31/0.30
3	855	0.37/0.33
9 <sup>th</sup> Ed. AASHTO LRFD BDS: $\phi Q_n=722$ kips		
10 <sup>th</sup> Ed. AASHTO LRFD BDS: $\phi Q_n=697$ kips		
Eurocode 4-2 2005: slip at 90% peak load: 0.26" (6.67mm)		

Figure 7.46 - Parametric Study on Haunch Depth for 1-1/8" Studs in Fully CIP Concrete Deck and with Fixed Stud Length of 7"

In Figure 7.46, the ultimate slip for the 1" haunch model is considerably smaller than in Model No. 10 described in Section 7.2. This is because  $\bar{u}_f^{pl}$  in the models of this parametric study adopted the value from Model No. 7. If the  $\bar{u}_f^{pl}$  value from Model No. 10 is used in this parametric study, the load-slip response is given by Figure 7.47. As noted in Section 7.2.2.3,  $\bar{u}_f^{pl}$  is not a constant across FE models and ranges between 0"~0.03".

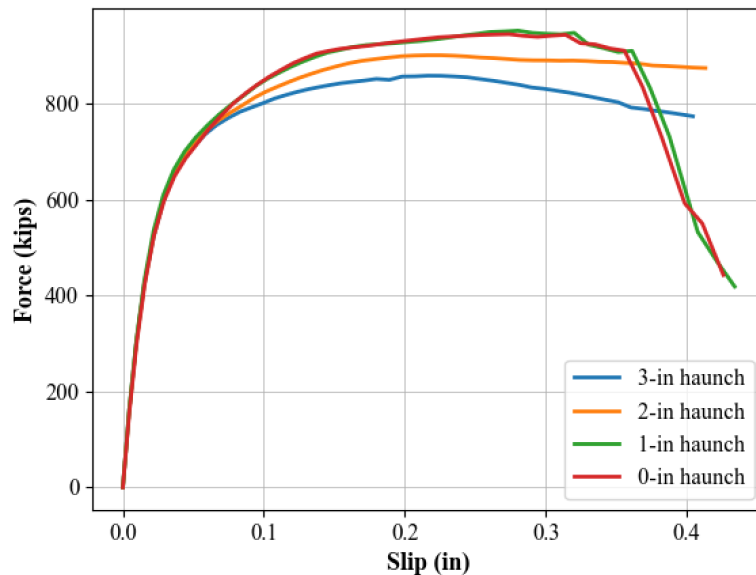


Figure 7.47 - Parametric Study on Haunch Depth for 1-1/8" Studs in Fully CIP Concrete Deck, Using  $\bar{U}_F^{Pl}$  from Model No. 10

### 7.3.2.2. Fully CIP Concrete Deck, 1-1/8" Studs with the Same Deck Penetration

Since the prior section changed haunch depth and stud penetration simultaneously, in order to better isolate the effect of haunch depth, another group of parametric studies was performed. Figure 7.48 illustrates the FE models for this purpose. When haunch depth decreases, the stud length also decreases to keep the deck penetration constant at 4". Model No. 7 is used as the basis for this group of FE models and its result is shown as "3-in haunch" in Figure 7.49. For the model with 0" haunch, the stud is only 4" long and no longer satisfies the length to diameter ratio requirement ( $h/d \geq 4$ ) in 9<sup>th</sup> Ed. AASHTO. When 10<sup>th</sup> Ed. AASHTO is considered, both the 0" and 1" haunch models do not satisfy the stud length to diameter ratio requirement ( $h/d \geq 5$ ).

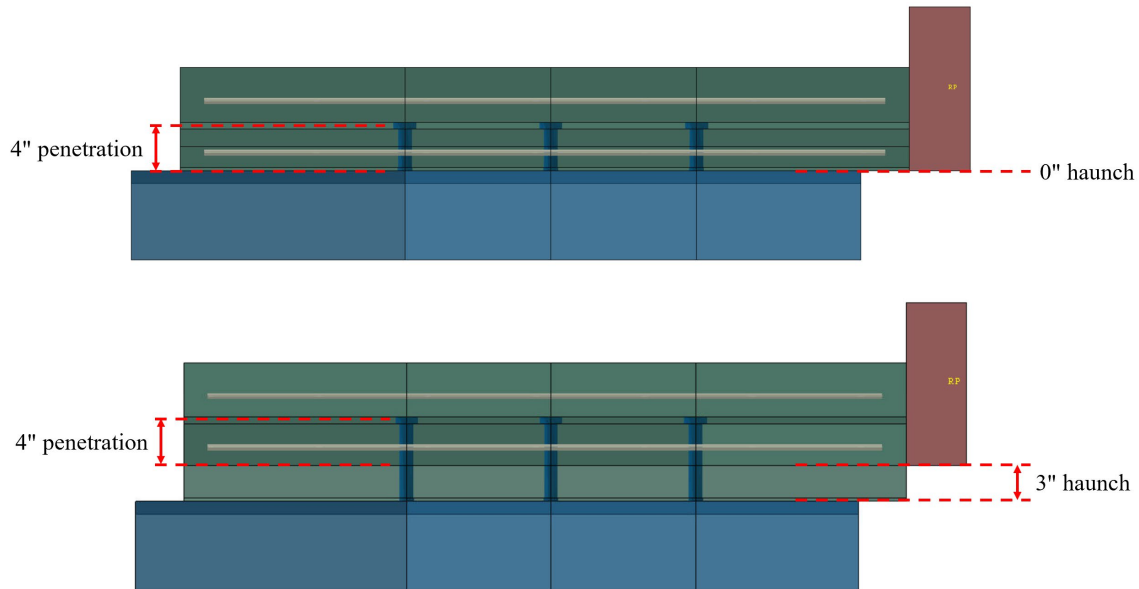
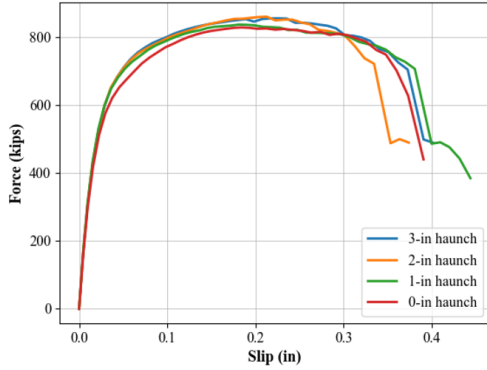


Figure 7.48 - FE Models with Different Haunch Depths and with Stud Penetration Fixed at 4"

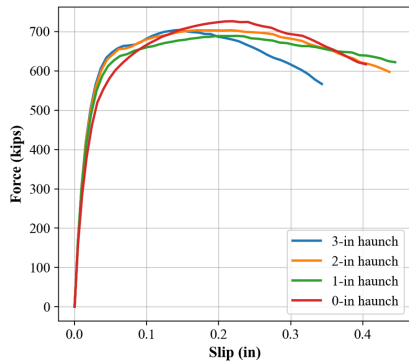
Based on Figure 7.49, the strength and ductility of 1-1/8" studs do not have significant changes when different haunch depths are used. This indicates that it is the stud penetration controlling the behavior of push-out FE models. The length to diameter ratio of the stud does not appear to influence the load-slip curves in these analyses even though some of the cases violated AASHTO requirements. Even these cases, however, developed strength values that exceeded AASHTO requirements. It is believed that the minimum length to diameter ratio in AASHTO may be intended to ensure adequate penetration of the stud into the deck. If this is the case, this requirement may be better stated as a minimum ratio of stud penetration to stud diameter.

Figure 7.50 illustrates one additional group of parametric studies. Model No. 9 is used as the basis and its result is shown as "3-in haunch" in Figure 7.50. These FE models have the same stud penetration into the concrete deck equal to 2", which is the minimum allowable stud penetration in both the 9<sup>th</sup> and proposed 10<sup>th</sup> Ed. AASHTO and TxDOT design standards. The haunch depth decreases from 3" to 0". The strength difference between FE models is minor. However, only the model with a 0" haunch satisfies the stud strength requirement from the 9<sup>th</sup> Ed. AASHTO.



Haunch depth (inches)	Peak strength (kips)	Ultimate slip (inches) 80%/90%
0	828	0.36/0.35
1	836	0.38/0.35
2	860	0.33/0.31
3	855	0.37/0.33
9 <sup>th</sup> Ed. AASHTO LRFD BDS: $\phi Q_n=722$ kips		
10 <sup>th</sup> Ed. AASHTO LRFD BDS: $\phi Q_n=697$ kips		
Eurocode 4-2 2005: slip at 90% peak load: 0.26" (6.67mm)		

Figure 7.49 - Parametric Study on Haunch Depth for 1-1/8" Studs in Fully CIP Concrete Deck and with a Fixed Deck Penetration Of 4"



Haunch depth (inches)	Peak strength (kips)	Ultimate slip (inches) 80%/90%
0	726	0.42/0.35
1	689	0.45/0.45
2	703	0.45/0.38
3	704	0.35/0.28
9 <sup>th</sup> Ed. AASHTO LRFD BDS: $\phi Q_n=722$ kips		
10 <sup>th</sup> Ed. AASHTO LRFD BDS: $\phi Q_n=697$ kips		
Eurocode 4-2 2005: slip at 90% peak load: 0.26" (6.67mm)		

Figure 7.50 - Parametric Study on Haunch Depth for 1-1/8" Studs in Fully CIP Concrete deck and with a Fixed Stud Penetration of 2"

### 7.3.2.3. Concrete Deck with PCP, 1-1/8" Studs of the Same Length

The parametric studies on haunch depth also considered decks with PCPs. For this type of deck, the minimum haunch depth was not taken as 0". This is because in actual bridge construction, PCPs are placed on bedding strips, which have a minimum height of 0.5". Figure 7.51 depicts two PCP FE models with different haunch depths. Model No. 4 is used as the basis in the parametric study. Therefore, all FE models have one 1-1/8" stud per row and the same  $f_c$  and  $\bar{u}_f^{pl}$  as Model No. 4. The result of Model No. 4 is shown as "3-in haunch PCP" in Figure 7.52. The model with a 0.5" haunch does not satisfy the top cover requirements in AASHTO and TxDOT design standards, because 7" long studs were used in the models.

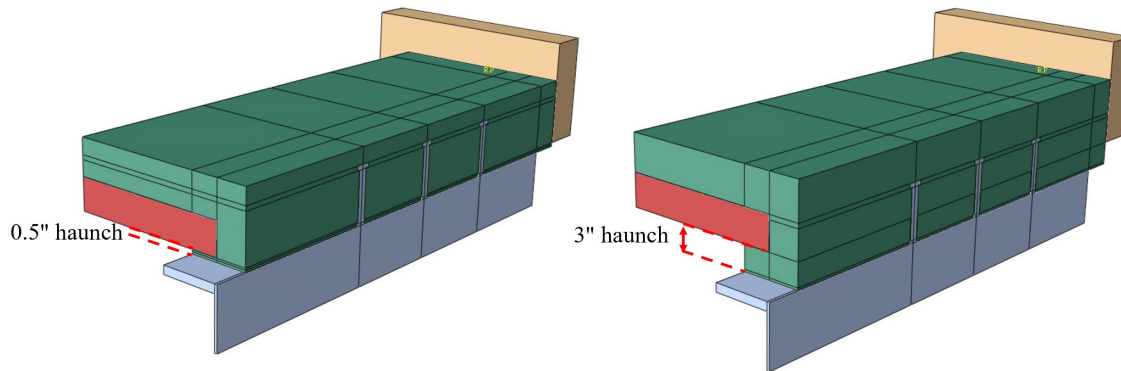
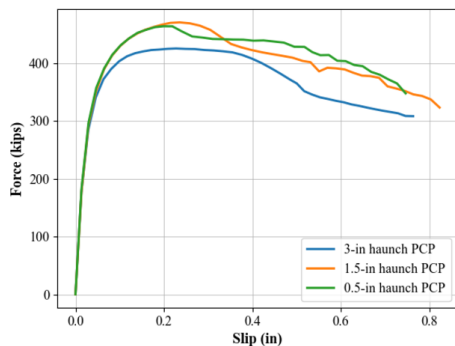


Figure 7.51 - FE Models with Different Haunch Depths; Concrete Deck Has PCP and Stud Length Is Fixed at 7"

Results of the parametric study are presented in Figure 7.52. The ultimate strength increases when haunch depth decreases from 3" to 1.5". When haunch depth continues decreasing from 1.5" to 0.5", stud ultimate strength no longer increases. All FE models failed in a concrete controlled mode. No obvious trend is observed in the ultimate slip. The increase in strength is believed to be due, at least in part, to the increase in stud penetration as the haunch depth decreases.



Haunch depth (inches)	Peak strength (kips)	Ultimate slip (inches) 80%/90%
0.5	464	0.71/0.54
1.5	470	0.67/0.37
3	425	0.55/0.44
9 <sup>th</sup> Ed. AASHTO LRFD BDS: $\phi Q_n=345$ kips		
10 <sup>th</sup> Ed. AASHTO LRFD BDS: $\phi Q_n=349$ kips		
Eurocode 4-2 2005: slip at 90% peak load: 0.26" (6.67mm)		

Figure 7.52 - Parametric Study on Haunch Depth for 1-1/8" Studs in Concrete Deck with PCP and with a Fixed Stud Length of 7"

### 7.3.3. Beam Flange Width

The steel beam used in the push-out tests had a flange width of about 15". However, actual bridge girders typically have wider flanges than this. For example, the two bridges studied in Chapter 3 each had 24" wide flanges. A parametric study was carried out to investigate the effects of having a wider beam flange for decks with and without PCPs.



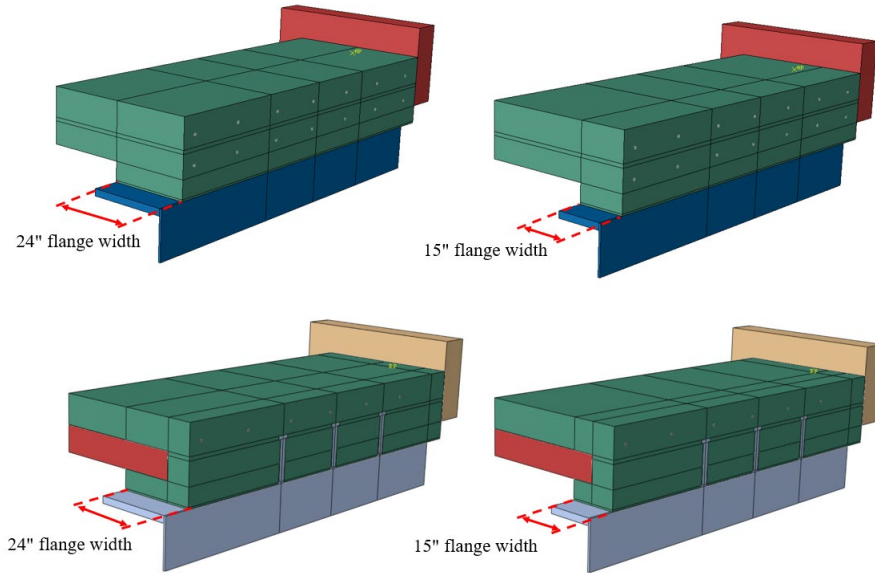
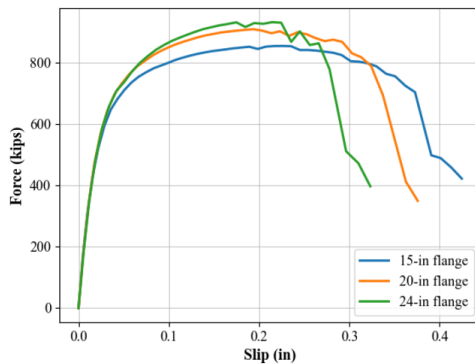


Figure 7.53 - FE Models with Different Beam Flange Widths

Figure 7.53 presents the FE models with different beam flange widths. The fully CIP models are based on Model No. 7 and have two studs per row. When the steel beam flange gets wider, the haunch also gets wider. The models with PCPs are based on Model No. 4 and have one stud per row. Since the total width of the concrete deck does not increase with a wider flange, the PCP will take up more space on the steel beam flange and the clear distance from studs to the PCP is the same when increasing the beam flange width.

### 7.3.3.1. CIP Concrete Deck, 1-1/8" Studs

As noted above, Model No. 7 was used as the basis for this parametric study. All FE models had two 1-1/8" studs per row and the same  $f_c$  and  $\bar{u}_f^{pl}$  as Model No. 7.



Flange width (inches)	Peak strength (kips)	Ultimate slip (inches) 80%/90%
15	855	0.37/0.33
20	910	0.32/0.30
24	933	0.28/0.27
9 <sup>th</sup> Ed. AASHTO LRFD BDS: $\phi Q_n=722$ kips		
10 <sup>th</sup> Ed. AASHTO LRFD BDS: $\phi Q_n=697$ kips		
Eurocode 4-2 2005: slip at 90% peak load: 0.26" (6.67mm)		

Figure 7.54 - Parametric Study on Steel Beam Flange Width for Fully CIP Concrete Deck and 1-1/8" Studs

Figure 7.54 presents the analysis results and result of Model No. 7 is directly used as the “15-in flange”. The ultimate strength of the shear stud increases as the steel beam flange gets wider. The ultimate slip decreases because the higher strength results in earlier stud fracture. These observations indicate that the volume of CIP concrete surrounding the shear stud has an impact on the stud strength and ductility. With more concrete, the stud gets better confinement and higher ultimate strength but lower ductility is developed.

### 7.3.3.2. Concrete Deck with PCP, 1-1/8" Studs

Results for concrete decks with PCPs are shown in Figure 7.55. The Model No. 4 result is shown as “15-in flange 1stud/PCP”. The load-slip response between models is almost identical with slight variation in the value of slip corresponding to initiation of steel damage. It is believed that since the clear distance between the stud and the PCP did not change among FE models, the width of CIP concrete surrounding the shear stud did not increase. Therefore, the confinement effect on shear stud is almost the same among FE models. This indicates the PCP does not provide confinement to the shear stud.

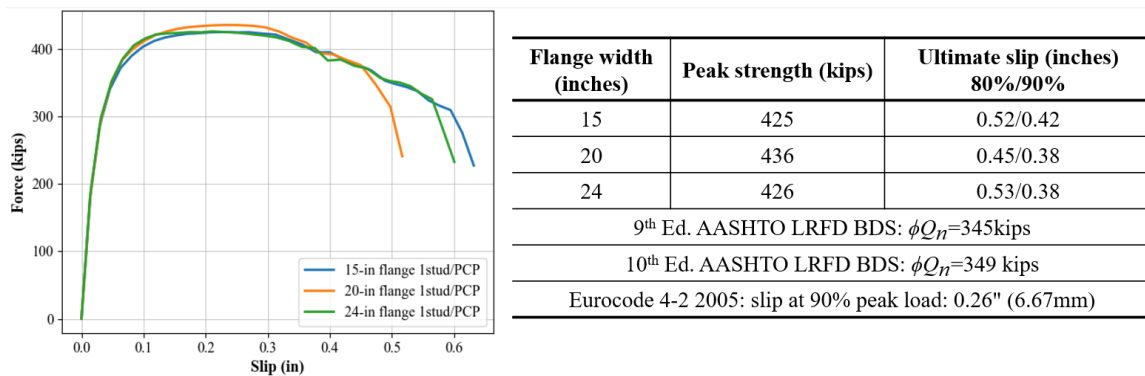


Figure 7.55 - Parametric Study on Steel Beam Flange Width for Concrete Deck with PCP and 1-1/8" Studs

### 7.3.4. Clear Distance Between Stud and PCP with 7/8" Studs

The parametric study on beam flange width raises the question about the impact of the clear distance between the stud and the PCP. When this value was fixed, increasing the flange width did not give higher ultimate strength. A group of FE models were therefore developed to study the impact of clear distance on the stud load-slip response.

TxDOT standard drawings: *Miscellaneous Details Steel Girders and Beams* (TxDOT 2019) specify that the clear distance between stud head and the nearby PCP should be at least 5/8", which was used in the experimental program for Specimen No. 2. Figure 7.56 presents two FE models with different values of clear distance between the PCP and the shear stud head, where the CIP concrete deck is omitted for visual clarity. The change in clear distance was accomplished by increasing the total width of the concrete deck. The dimensions of the PCPs are the same in all FE models. Model No. 2 was used as the basis for this parametric study and is

shown as “0.625-in clear distance” in Figure 7.57. All other FE models share the same  $f_c$  and  $\bar{u}_f^{pl}$  with Model No. 2.

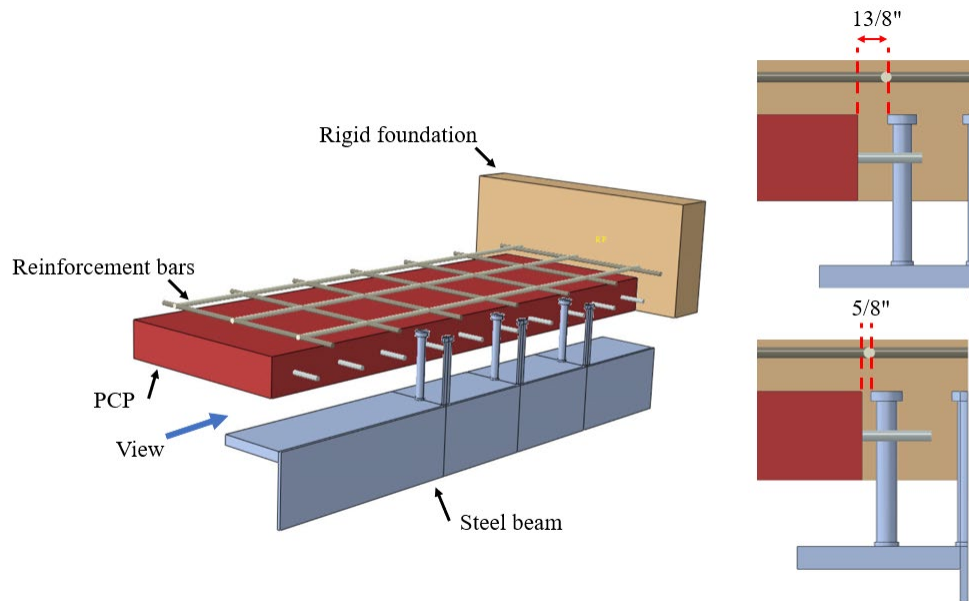
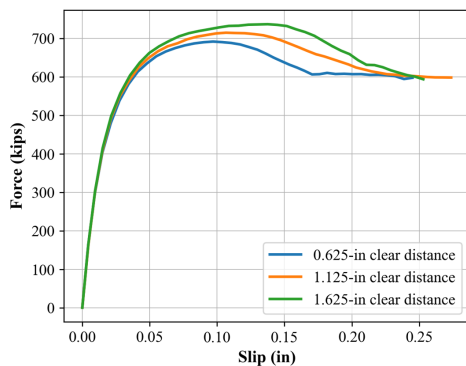


Figure 7.56 - FE Models with Different Clear Distances Between Stud Head and PCP (CIP Concrete Omitted from View)

Results of the parametric study are given in Figure 7.57. The ultimate strength of the models increases with a larger clear distance. When the clear distance is greater than or equal to 5/8", the strength of the model is more than the design strength from the 9<sup>th</sup> Ed. AASHTO. The ultimate slip for all models was small due to the strength drop at the early yielding stage.



Clear distance (inches)	Peak strength (kips)	Ultimate slip (inches) 80%/90%
5/8	692	>0.25/0.16
9/8	715	>0.28/0.19
13/8	737	>0.26/0.19
9 <sup>th</sup> Ed. AASHTO LRFD BDS: $\phi Q_n=641$ kips		
10 <sup>th</sup> Ed. AASHTO LRFD BDS: $\phi Q_n=571$ kips		
Eurocode 4-2 2005: slip at 90% peak load: 0.26" (6.67mm)		

Figure 7.57 - Parametric Study on Clear Distance Between 7/8" Stud and PCP

### 7.3.5. PCP Overlap on Steel Beam Flange with 1-1/8" Studs

Another way to study the clear distance between the stud and the PCP is by modifying the distance that the PCP overlaps the steel beam flange. Figure 7.58 shows two FE models with different PCP overlap distances. The overlap distance was varied from 3.5" to 8" in this study. The models for this parametric study were based on the "24-in flange" model in Figure 7.54, which has the same  $f_c$  and  $\bar{u}_f^{pl}$  as Model No. 4. Results of this FE model are shown in Figure 7.59 as "8-in PCP overlap". Variations in the PCP overlap were achieved by changing the total width of the concrete deck. This means that the dimensions of the PCPs are the same for all FE models.

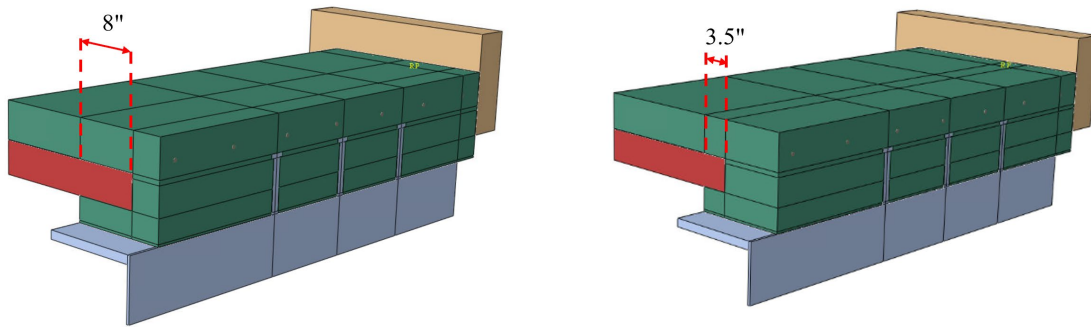


Figure 7.58 - FE Models with Different PCP Overlap Distance with Steel Beam Flange

Results for these analyses are shown in Figure 7.59. The ultimate strength of the models increases when the PCP overlap is reduced from 8" to 5". The failure mode also changed from concrete controlled failure to stud fracture. When the PCP overlap is further reduced to 3.5", the load-slip response did not change. This parametric study can be viewed as an extension of the clear distance investigation. Less PCP overlap on the steel beam means more clear distance and more CIP concrete surrounding the stud, which provides a higher confinement effect to the stud. As a result, the strength of the stud increases.

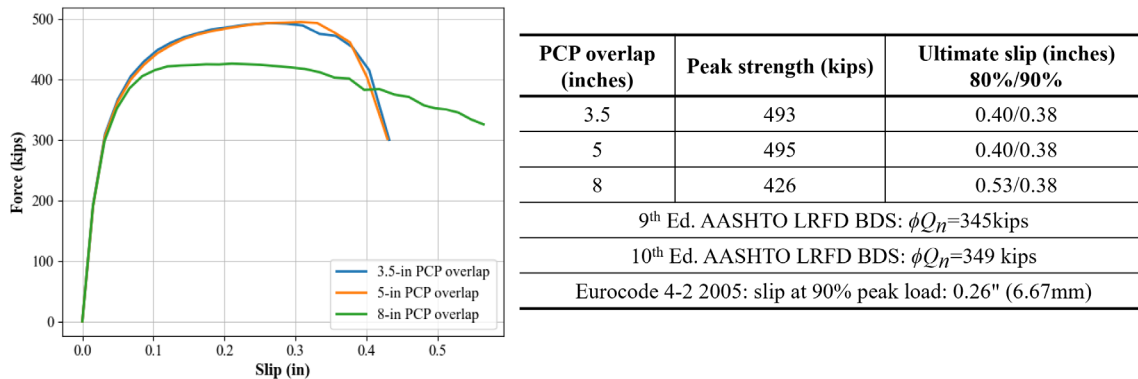


Figure 7.59 - Parametric Study on PCP Overlap Distance with Steel Beam Flange for 1-1/8" Studs

### 7.3.6. Bedding Strip Size

In the experimental study, the design of casting formwork (see Chapter 5) allowed the PCP specimens to be constructed without a bedding strip. The FE models also did not include the bedding strip. However, in actual bridge construction, bedding strips must be used to support the PCPs. The space occupied by the bedding strip will reduce the amount of CIP concrete under the PCP. A group of FE models were developed to study the influence of the presence of a bedding strip. Figure 7.60 shows two FE models with different bedding strip dimensions. For simplicity, the bedding strip is not explicitly modeled and the region with the bedding strip is left empty. This is reasonable since the bedding strip is very flexible and weak compared to concrete and is therefore not expected to have any impact on the stud behavior. The base model for this parametric study is the same as the one used in Section 7.3.5. The base model results are shown in Figure 7.61 as “No bedding strip”. The effect of having bedding strips is illustrated in Figure 7.61. No obvious change in strength and ductility is observed.

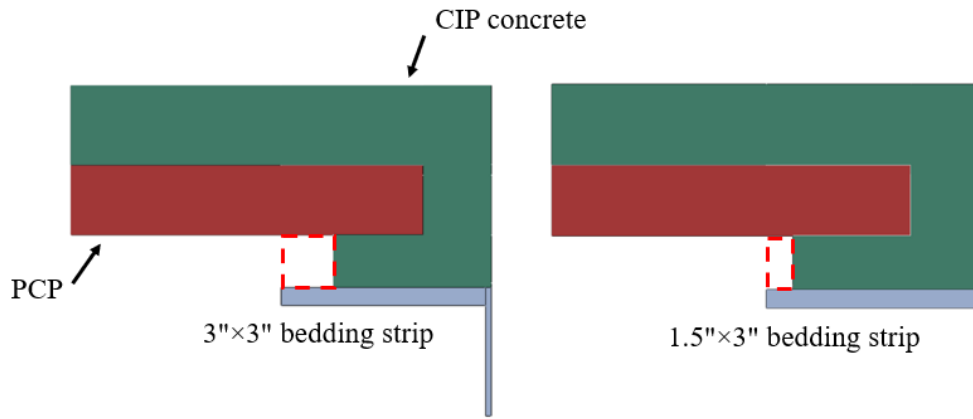
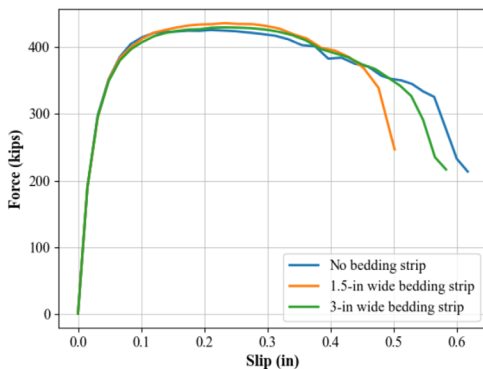


Figure 7.60 - FE Models with Different Size of Bedding Strips



Bedding strip width (inches)	Peak strength (kips)	Ultimate slip (inches) 80%/90%
0	426	0.53/0.38
1.5	436	0.45/0.41
3.0	429	0.49/0.41
9 <sup>th</sup> Ed. AASHTO LRFD BDS: $\phi Q_n=345$ kips		
10 <sup>th</sup> Ed. AASHTO LRFD BDS: $\phi Q_n=349$ kips		
Eurocode 4-2 2005: slip at 90% peak load: 0.26" (6.67mm)		

Figure 7.61 - Parametric Study on Size of Bedding Strips

### 7.3.7. Transverse Reinforcement Ratio with 1-1/8" Studs

Specimen No. 8 in the experimental study had only 50% transverse reinforcement compared to the standard CIP specimen. As discussed in Chapter 2, the transverse reinforcement ratio is reported in the literature as one important factor for strength development of large diameter shear studs. However, the test results showed that the strength of 1-1/8" studs in Specimen No. 8 was well developed, but was accompanied with severe cracking in the concrete. This parametric study investigates the transverse reinforcement ratio. A new model was developed with transverse reinforcement of #4@27", which is only 25% of that provided in the standard CIP specimen (Model No. 7). Figure 7.62 illustrates two FE models, where the one with #4@9" transverse reinforcement is Model No. 7 and the other one has #4@27" transverse reinforcement. Model No. 7 is used as basis for this parametric study. Results of Model No. 7 are shown as "#4@9"" in Figure 7.63. The FE model with #4@18" transverse reinforcement was developed in Section 7.2 but these results are not used since Model No. 8 had different  $f_c$  and  $\bar{u}_f^{pl}$ . The results shown as #4@18" in Figure 7.63 is Model No. 8 re-run with the same  $f_c$  and  $\bar{u}_f^{pl}$  as Model No. 7.

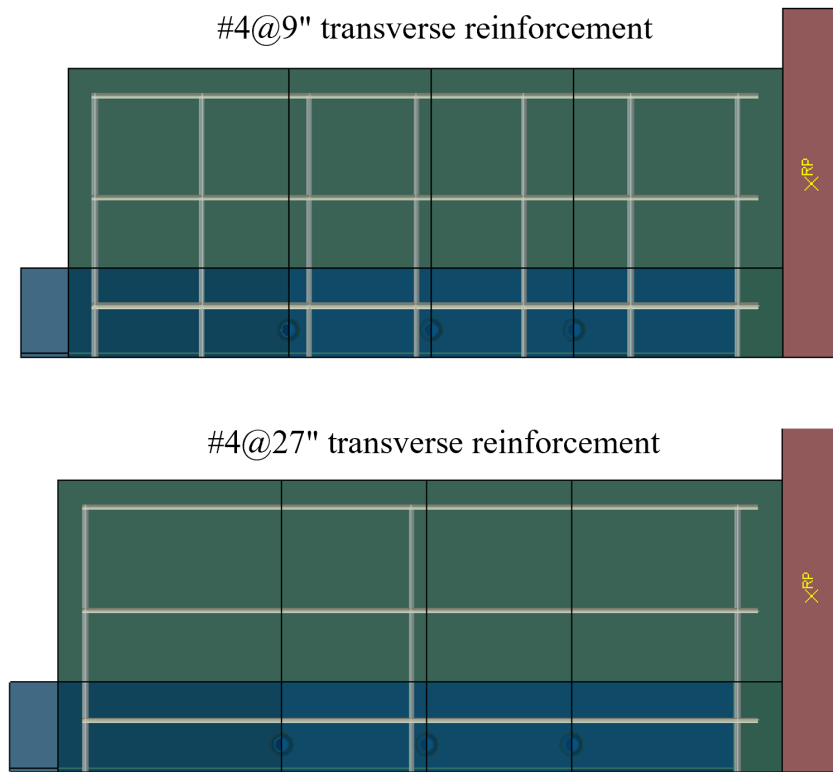


Figure 7.62 - FE Models with Different Transverse Reinforcement Ratios

Based on Figure 7.63, the ultimate strength of 1-1/8" studs is not sensitive to the transverse reinforcement ratio, which might be caused by the size of the concrete deck. The concrete deck in this study is relatively larger compared to previous studies (Badie, Tadros, et al. 2002, Lee, Shim and Chang 2005) that concluded the transverse reinforcement ratio is important. The larger size of the concrete deck may be sufficient to provide adequate confinement even with less transverse reinforcement.

On the other hand, the strength of the push-out models starts to decline earlier when less transverse reinforcement is used. This means the concrete gets damaged earlier. Although stud fracture is seen in the model with #4@18" transverse reinforcement, the stud fractured after the load dropped more than 20%. Therefore, the FE models with less transverse reinforcement than model No. 7 all exhibited concrete controlled failure.

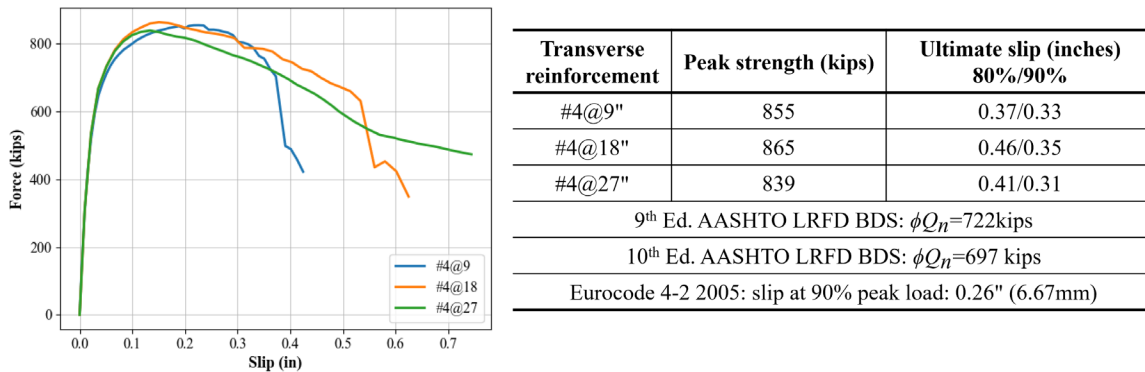


Figure 7.63 - Parametric Study on Transverse Reinforcement Ratio

## 7.4. Development of Design Recommendations Based on FE Studies of Push-out Tests

The experimental push-out tests described in Chapter 5 and the simulated push-out tests described in this chapter showed that some of the current provisions in AASHTO and in TxDOT design standards do not always allow 1-1/8" studs to develop the specified stud ultimate strength in the 9<sup>th</sup> Ed. AASHTO or the proposed 10<sup>th</sup> Ed. AASHTO. In some cases, the design strength for 7/8" studs could not be developed either. When decks with PCPs were used, lower ultimate strength was observed in comparison with full-depth CIP decks. Further, the specimens with PCPs showed splitting cracks running along the length of the beam, and such cracks were not observed in the full-depth CIP deck specimens. Additional FE analyses were therefore conducted and are reported in this section to further support the development of design recommendations that are intended to allow the studs to develop the design strength specified in AASHTO.

### 7.4.1. Fully CIP Concrete Decks

The parametric study reported in Section 7.3 showed that, other than the factors in the AASHTO design equations, the strength of a stud in fully CIP concrete deck is significantly affected by the



stud penetration into the concrete deck and by the beam flange width. Other design considerations like haunch depth, transverse reinforcement ratio, and top clear cover showed less effect on stud strength and slip capacity. The current minimum requirement of stud penetration depth into the deck of 2" may not allow 7/8" studs and 1-1/8" studs to develop the design strength specified in the 9<sup>th</sup> Ed. AASHTO. Based on Figure 7.41 and Figure 7.42, to satisfy 9<sup>th</sup> Ed. AASHTO design strength for 7/8" and 1-1/8" studs, the stud penetration should be at least 3".

It should be emphasized that the concrete compressive strength,  $f_c$ , for results shown in Figure 7.41 and Figure 7.42 is higher than 4 ksi. Section 7.2.8.3 showed that  $f_c$  has significant impact on stud strength. Therefore, the peak strengths for FE models shown in Figure 7.41 and Figure 7.42 are expected to be higher compared to the cases where  $f_c = 4$  ksi. To consider this effect, the FE model for "3-in penetration" in Figure 7.41 and the FE model for "3-in penetration" in Figure 7.42 were re-analyzed with  $f_c = 4$  ksi. The results are shown in Figure 7.64. It can be observed that the peak strength for the two FE models decreased compared with values reported in Figure 7.41 and Figure 7.42. However, the decreasing rate of the 9<sup>th</sup> Ed. AASHTO design strength with the reduction in  $f_c$  is faster than that of the FE models. This is the same observation made in Section 7.2.8.3. The 9<sup>th</sup> Ed. AASHTO design equation become more conservative when lower strength concrete is used. Eventually, a 3" deck penetration allows 7/8" and 1-1/8" studs to satisfy the 9<sup>th</sup> Ed. AASHTO and 10<sup>th</sup> Ed. AASHTO design strength when  $f_c = 4.0$  ksi. Since the proposed 10<sup>th</sup> Ed. AASHTO equation for shear stud strength is independent of  $f_c$ , the strength for both 7/8" and 1-1/8" studs satisfy the proposed 10<sup>th</sup> Ed. AASHTO stud strength equation. However, as shown in Figure 7.41 and Figure 7.42, increasing the deck penetration from 2" to 3" results in a significant increase in stud strength. Therefore, a 3" penetration is recommended here for all shear studs embedded in fully CIP concrete decks.

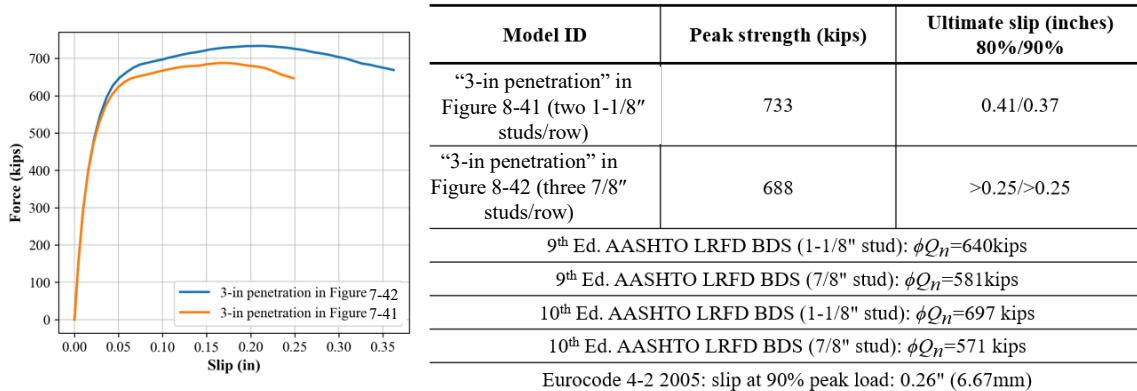


Figure 7.64 - Re-analysis for FE Models with 3" Penetration Using  $f_c = 4.0$  ksi

## 7.4.2. Concrete Decks with PCPs

### 7.4.2.1. Design Recommendations for the 9<sup>th</sup> Ed. AASHTO

A major observation from both the experimental tests and FE simulations is that stud ultimate strength is reduced when PCPs are used, in comparison to fully CIP decks. The concrete also has more cracking and loses load bearing capacity earlier in push-out specimens with PCPs. Section 7.3 studied the factors influencing the strength of shear studs in concrete decks with PCPs. The conclusion was that the stud penetration into the concrete deck and the clear distance between the stud and the PCP strongly influence the strength. Figure 7.65 illustrates all the FE models in the parametric study related to these two factors. Two examples are given in Figure 7.65. Data point A represents the FE model in Section 7.3.1.3, which has 1-1/8" studs with 3" penetration into the concrete deck and 3" clear distance from the PCP. Data point B represents the FE model in Section 7.3.4, which has 7/8" studs with 4" penetration into concrete deck and 5/8" clear distance from the PCP. The red data point indicates this FE model has a stud strength satisfying the 9<sup>th</sup> Ed. AASHTO. The grey point indicates this FE model has stud strength lower than required by the 9<sup>th</sup> Ed. AASHTO. The required minimum clear distance of 5/8" and minimum stud penetration of 2" are shown by the dashed lines in Figure 7.65.

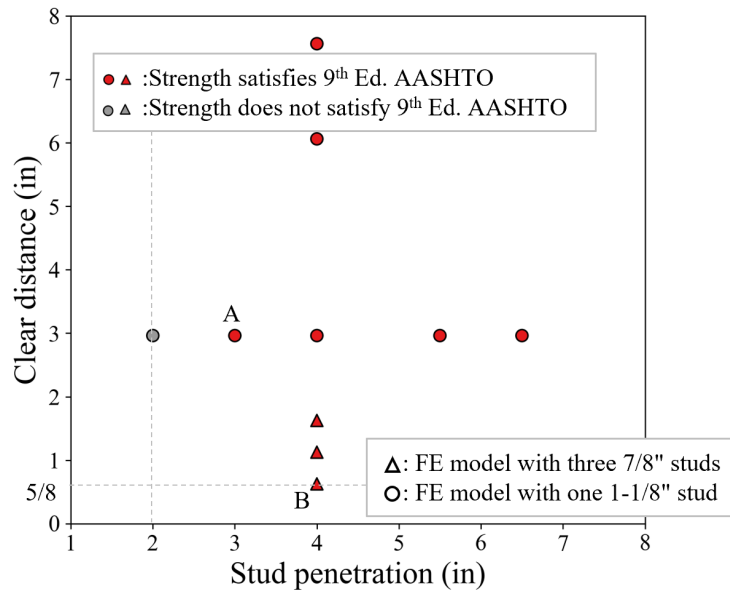


Figure 7.65 - Parametric Study Results on Stud Penetration and Clear Distance

The data in Figure 7.65 indicates that to have a stud strength higher than the 9<sup>th</sup> Ed. AASHTO requirement, both the stud penetration and clear distance must be sufficient. The criteria for sufficient penetration and clear distance were further examined by conducting additional parametric studies.

Additional FE models were developed and analyzed, and results are shown in Figure 7.66. These new models were based on the models in the parametric study. For example, a series of additional FE models were developed based on Model A (see Figure 7.65) but with reduced PCP clear distance. It can be observed that the strength of the stud no longer satisfies the 9<sup>th</sup> Ed. AASHTO when the clear distance is reduced to 2".

The boundary between red data points and grey data points can be found using machine learning algorithms. Based on Figure 7.66, 7/8" stud strength is only sensitive to the reduction in clear distance while 1-1/8" stud strength is sensitive to the reduction both in stud penetration and in clear distance. Since the strength sensitivity to these factors is different, FE models with 1-1/8" studs and FE models with 7/8" were analyzed in machine learning separately. For this study, the simple support vector machine (SVM) method was used. A detailed mathematical description of SVM can be found in Murphy (2012). Here, only a brief introduction of SVM is provided.

The SVM method is a supervised machine learning method and is used for classification problems. Its goal is to find the boundary between groups of data. SVM calculates the distance of each data point to the boundary and locates the boundary that divides the data evenly. In other words, the boundary will be the "middle" line between groups of data. This feature ensures the boundary is not too close to either side to avoid misclassification.

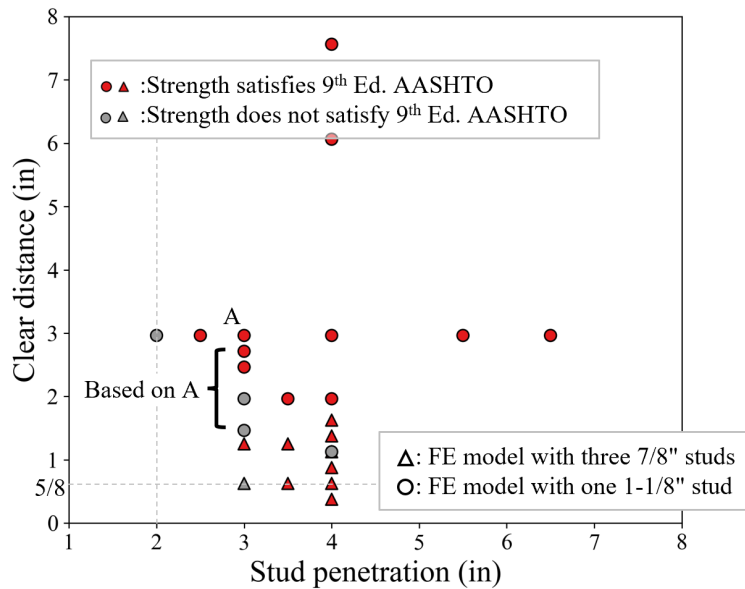


Figure 7.66 - Additional Parametric Study Results on Stud Penetration and Clear Distance

The classification results plus the boundary equation are provided in Figure 7.67 for 1-1/8" studs. Selective data points are presented with the ratio between stud strength from the FE model and the design strength from the 9<sup>th</sup> Ed. AASHTO in parentheses. Linear SVM is used. The 2D space defined by stud penetration ( $x_1$ ) and clear distance ( $x_2$ ) has been divided into two regions. The region with orange color means the 9<sup>th</sup> Ed. AASHTO is likely to overestimate the stud strength.

The region with blue color means the 9<sup>th</sup> Ed. AASHTO is likely to give a conservative prediction of stud strength. The expression for the boundary is given in Figure 7.67. Based on the equation, if a 2" stud penetration is used, the 9<sup>th</sup> Ed. AASHTO is likely to give a conservative stud strength prediction when the clear distance is larger than 3.2". For design purposes, it is recommended that for 1-1/8" studs with PCPs, the minimum stud penetration is taken as 4" and the minimum clear distance between the stud and PCP is taken 2". However, in cases where these dimensions cannot be accommodated, Figure 7.67 can be used to identify other acceptable combinations of penetration and clear distance. For example, if a clear distance of only 1" can be provided, the stud penetration should be increased to 4.5" to provide a stud strength that satisfies the 9<sup>th</sup> Ed. AASHTO.

In Figure 7.68, the classification result for 7/8" studs and the boundary equation is provided. The ratio between stud strength in the FE model and design strength from the 9<sup>th</sup> Ed. AASHTO is given in parentheses for selective data points. If the stud penetration of 2" is used, the clear distance needs to be larger than 2.5" to make 9<sup>th</sup> Ed. AASHTO likely to be conservative. It is recommended in design that for 7/8" studs, the penetration into the concrete deck should be at least 4" and the clear distance from shear stud head to PCP should be at least 1".

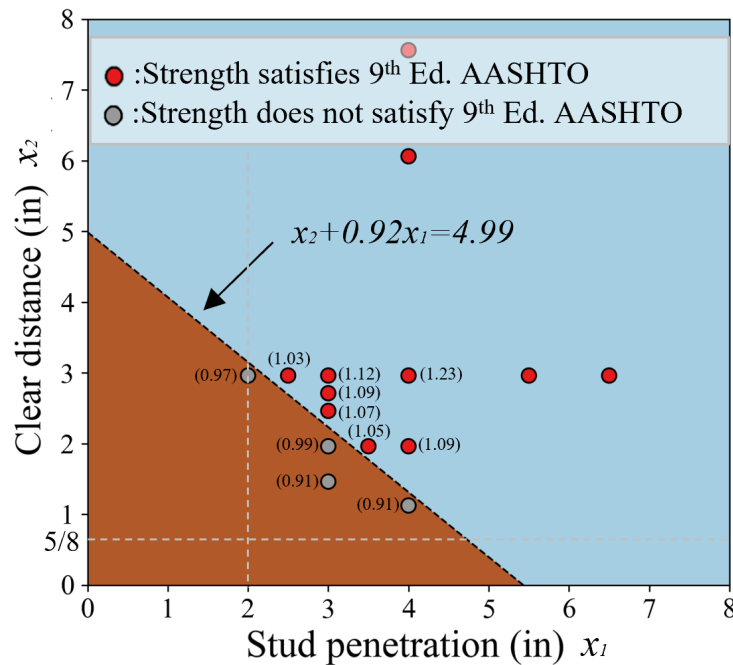


Figure 7.67 - Classification and Boundary Equation for 1-1/8" Studs using Linear SVM

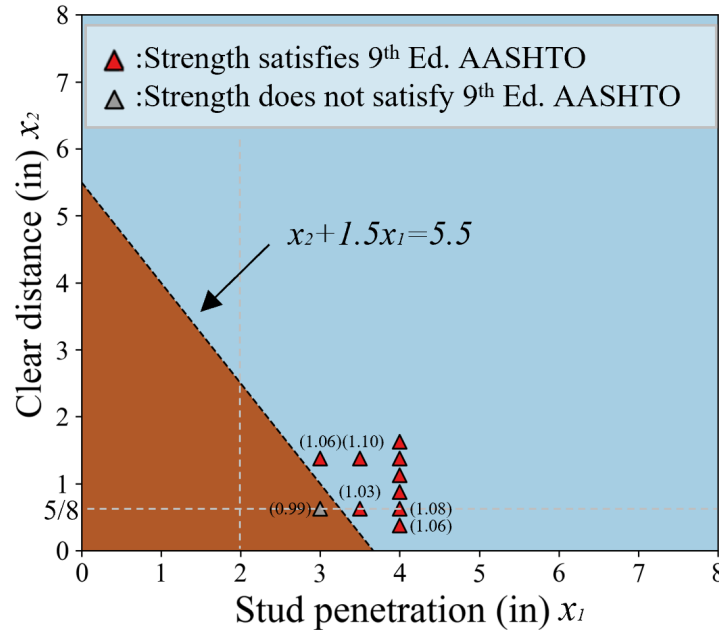


Figure 7.68 - Classification and Boundary Equation for 7/8" Studs using Linear SVM

Data points used here are based on FE models with different values of concrete compressive strength,  $f_c$ . However, all of the models have  $f_c$  higher than 4.0 ksi. Section 7.2.8.3 and Section 7.4.1 show that when a smaller  $f_c$  is used, the 9<sup>th</sup> Ed. AASHTO design equation will become more conservative compared to the FE models. In other words, if all FE models use the same  $f_c = 4.0$  ksi, more data points in Figure 7.67 and Figure 7.68 are likely to be red. Therefore, results presented in this section are conservative.

#### 7.4.2.2. Design Recommendations for the Proposed 10<sup>th</sup> Ed. AASHTO

Stud ultimate strength design equations in the proposed 10<sup>th</sup> Ed. AASHTO (AASHTO 2021), described in Chapter 2, are significantly changed from the 9<sup>th</sup> Ed. AASHTO. Consequently, an additional series of analyses were conducted to evaluate the influence of stud penetration and clear distance relative to the requirements of the proposed 10<sup>th</sup> Ed. AASHTO. As described in Chapter 2, the proposed 10<sup>th</sup> Ed. AASHTO no longer considers concrete properties in the stud strength design equation. Classification using FE models with  $f_c$  higher than 4.0 ksi will therefore give unconservative results. Consequently, the FE models used to generate the data points in Figure 7.67 and Figure 7.68 were re-analyzed with  $f_c = 4.0$  ksi. The results are presented in Figure 7.69.

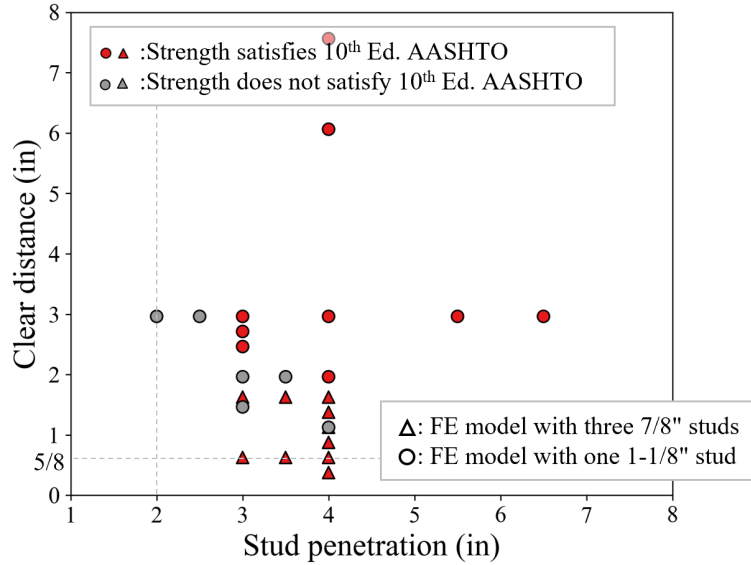


Figure 7.69 - Additional Parametric Study Results on Stud Penetration and Clear Distance with  $f_c=4.0$  ksi (proposed 10<sup>th</sup> Ed. AASHTO)

The stud strength design equation in the proposed 10<sup>th</sup> Ed. AASHTO tends to be more conservative compared to the 9<sup>th</sup> Ed. AASHTO. However, according to Figure 7.69, this statement is valid only for 7/8" studs and for the case where  $f_c > 4.0$  ksi. Comparing to Figure 7.66, more FE models with 1-1/8" studs have stud strength less than the proposed 10<sup>th</sup> Ed. AASHTO requirement in Figure 7.69.

Figure 7.70 provides the classification result and boundary equation for 1-1/8" studs when the 10<sup>th</sup> Ed. AASHTO is considered and when  $f_c = 4.0$  ksi. The ratio between stud strength in the FE model and the design strength in the proposed 10<sup>th</sup> Ed. AASHTO is provided in parentheses for selective data points. The orange region is considerably larger than that in Figure 7.67, indicating that the 9<sup>th</sup> Ed. AASHTO is more conservative for 1-1/8" studs. The boundary equation given in Figure 7.70 shows that if 2" penetration is used, the proposed 10<sup>th</sup> Ed. AASHTO is likely to be conservative once the clear distance is more than 3.6". For design purposes, the stud penetration is recommended to be larger than 4" and the clear distance is recommended to be larger than 2".

For 7/8" studs, only a limited number of parametric studies were performed. Since no FE model had stud strength less than the proposed 10<sup>th</sup> Ed. AASHTO equation, no classification can be performed. Nonetheless, the same design recommendation in Section 7.4.2.1 is proposed here for improved strength performance. The stud is recommended to have at least 4" penetration into the concrete deck while the clear distance is at least 1".

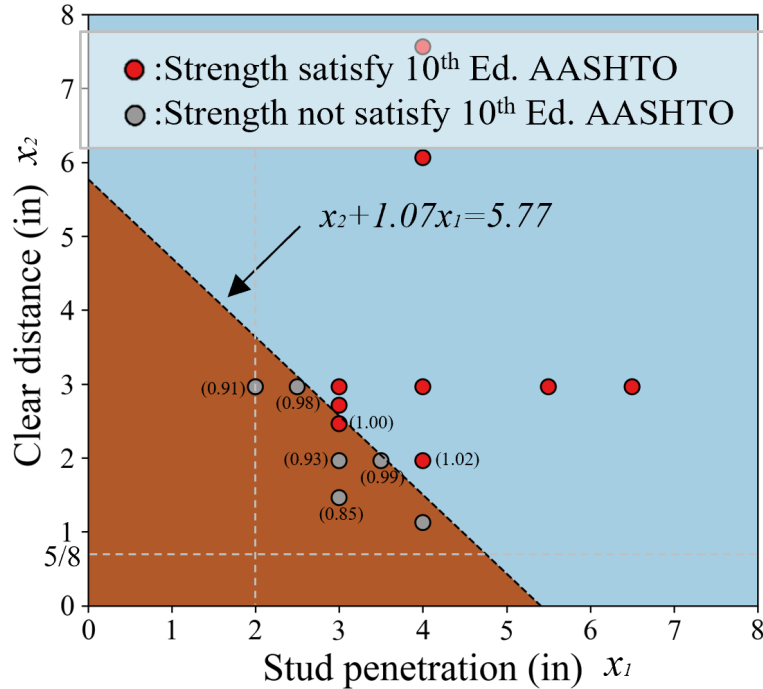


Figure 7.70 - Classification and Boundary Equation for 1-1/8" Stud using Linear SVM (proposed 10<sup>th</sup> Ed. AASHTO)

## 7.5. Conclusions

The finite element (FE) method was used to study the behavior of push-out specimens. All push-out test specimens described in Chapter 5 were modeled in the FE software Abaqus. FE models were developed as either a quarter or a half of a push-out specimen based on the symmetry in the specimens and the setup. Material properties for concrete and steel in the models were based on material test data for the test specimens described in Chapter 5 and necessary adjustments were made to counter the spurious mesh size effect. Material parameters that were not available from the material tests were either given the same values (plasticity parameters in CDP) or calibrated in the same way (concrete tensile strength) for all FE models. Damage parameters to simulate stud fracture were selected to match the experimental results best. The damage initiation criterion was the same in all FE models, but the damage evolution was shown to be a variable across FE models. Surface contact properties were defined as frictional hard contact except those between CIP and PCP, which were tied together. A frictional coefficient of 0.5 was used for all FE models and this was shown to be reasonable based on the discussion in Section 7.2.8.1. The mesh size and element formulations were selected based on extensive mesh sensitivity studies. Models of the 1-1/8" studs and the 7/8" studs were given different mesh schemes based on their own mesh sensitivity study results. The element size was shown to be sufficiently small giving converged FE results while common numerical issues like the hourglass mode were excluded. Boundary conditions mimic the actual loading setup in the experiments. The dynamic explicit solver in Abaqus was used but the dynamic effect was controlled to be small. The updated Lagrangian method was adopted in Abaqus for large deformation problems.



This model development process produced FE models that reasonably captured the load-slip response and the failure mode of the experimental specimens. Concrete compression and tensile damage patterns predicted by the FE models were comparable to damage patterns observed in the experiments. In FE models that predicted stud fracture, the shear stud closest to the bottom of the FE model (i.e., at the bottom of the push-out specimen) fractured first. All fractures concentrated in the weld collar region, which is similar to the experimental observations. Based on these findings, the FE modeling technique was deemed reasonable. New FE models outside the eleven FE models for the experimental push-out specimens were developed following the same modeling technique. These simulated push-out models were used to study various issues of interest in greater depth in an extensive parametric study.

The parametric study expanded the variables studied in the experimental push-out tests. The parametric study investigated stud penetration distance into the deck, haunch depth, steel beam flange width, clear distance between the stud and the PCP, the overlap distance of the PCP with the steel beam, bedding strip size, and transverse reinforcement ratio. The clear distance between the stud and the PCP, and the PCP overlap distance with the steel beam essentially studied the same variables.

Results of the parametric study showed that stud penetration distance into the concrete deck significantly influenced the load-slip response of the push-out models, both for fully CIP decks and for decks with PCPs. Haunch depth had little effect on stud ultimate strength if the stud penetration was kept the same. Increasing steel beam flange width significantly improved stud behavior for fully CIP models. For FE models with PCPs, increasing beam flange width without providing more CIP concrete near the stud had minimal impact on stud strength and ductility. This observation agrees with the results obtained from studies on the clear distance between the stud the edge of the PCP. All of these observations indicate that with more CIP concrete surrounding the shear stud, the shear stud will develop a higher ultimate strength and likely to have stud fracture failure mode rather than a concrete controlled failure.

The size of the bedding strip had little impact on stud strength and ductility of the push-out models. The transverse reinforcement ratio was shown to be not consequential when the concrete deck size has adequate width.

The parametric studies showed that stud strength in decks with PCPs is significantly influenced by two factors, namely stud penetration into the concrete deck and the clear distance between the stud head and the PCP. For the AASHTO design equations to be conservative, sufficient penetration and clear distance must be provided. By using additional FE models, criteria for required penetration and clear distance were found. Studs of 1-1/8" diameter and 7/8" diameter were considered separately. Recommendations for stud penetration and clear distance between the stud head and the PCP were developed based on the additional FE studies combined with engineering judgement.

# Chapter 8. Large-Scale Beam Tests

## 8.1. Introduction

---

This chapter describes tests on two large-scale composite beam specimens constructed using 1-1/8" diameter shear studs. The overall goal of these tests was to evaluate the performance of 1-1/8" studs in composite steel girder specimens and to extend information learned in the push-out tests to a more realistic representation of an actual bridge girder. Specific objectives of the tests included the following:

- Investigate if 1-1/8" shear studs cause unusual or excessive deck cracking in negative moment regions under service level loads.
- Evaluate the strength and slip capacity of 1-1/8" shear studs in a composite girder under positive moment.
- Evaluate the strength and ductility of composite steel bridge girders constructed using 1-1/8" shear studs.
- Evaluate the performance of 1-1/8" shear studs in full-depth cast-in-place decks and in decks constructed with partial depth precast concrete deck panels (PCPs).
- For decks with PCPs, evaluate the design criteria developed in Chapter 7 for minimum stud penetration into the deck and minimum clear distance between the head of the stud and the edge of the PCP.
- Compare deck cracking in the negative moment region under service loads for full-depth cast-in-place decks versus decks constructed with PCPs.

The large-scale beam tests considered only static loading. No fatigue tests were conducted on the large-scale beam specimens. Past fatigue tests on larger-diameter shear studs in push-out specimens, as described in Chapter 2, have shown consistently good performance. The fatigue push-out tests on 1-1/8" studs reported in Chapter 6 confirmed this good fatigue performance showing fatigue lives that exceeded the requirements of both the 9<sup>th</sup> Ed. AASHTO and the proposed 10<sup>th</sup> Ed. AASHTO S-N curves. Further, as noted in Chapter 2, past research indicates that the fatigue performance of shear studs is typically better in beam specimens compared to push-out specimens. As a result, given the considerable cost and time for the large-scale beam tests, the focus of the tests was on static loading behavior as there were more questions on the static strength and slip capacity of 1-1/8" shear studs in beam specimens for both full-depth cast-in-place decks and for decks constructed with PCPs.

This chapter summarizes the details of both beam specimens, the test setup, the construction process, material properties, instrumentation, loading procedures, and test results. Conclusions are provided at the end of the chapter.

## 8.2. Beam Specimens

---

This section introduces the two beam specimens with information on span arrangement, shear stud dimensions, and layouts, cross-section details, deck reinforcement, and welded splice details. Both specimens used a W40×199 steel girder, an 8.5" thick deck, and a 2" haunch. Beam Specimen No. 1 used an 8.5" thick full-depth cast-in-place deck whereas Beam Specimen No. 2 used a deck consisting of 4" PCPs with a 4.5" cast-in-place topping.

### 8.2.1. Span Arrangements

The overall length of each beam specimen was 100'. This was the largest span length that could be practically accommodated within the laboratory. As described in the literature review in Chapter 2, the majority of past laboratory composite beam tests, either for building or bridge applications, have used span lengths on the order of 30' to 40'. Information in the literature (Zona and Ranzi 2014) indicates the slip demand, i.e., the required ductility of shear studs, increases with span length. Consequently, the largest span length that could be accommodated in the laboratory was used for this test program. Each 100' long girder was constructed from two pieces of W40×199 sections with a welded splice provided at 40' from the north support.

Each beam specimen was tested using two different span arrangements: a two-span arrangement and a single-span arrangement. The two-span arrangement used for both beam specimens is illustrated in Figure 8.1. For this arrangement, an interior support was placed 40' from one end. The interior support created a two-span condition that allowed testing of the negative moment region of the beams. In the two-span condition, the beams were subject to lower levels loads intended to be representative of service loads on a bridge. The purpose of the two-span test was to determine if the use of 1-1/8" shear studs resulted in excessive cracking in negative moment regions under service loads.

Once the two-span testing was completed on each specimen, the interior support was removed to provide a 100' single-span. Both beam specimens were tested to failure in the single-span configuration. The purpose of the single-span test was to establish the ultimate flexural strength, overall ductility, and controlling failure mode of each beam specimen. The single-span arrangement is illustrated for Beam Specimen No. 1 in Figure 8.2 and for Beam Specimen No. 2 in Figure 8.3. For Beam Specimen No. 1, load was applied by two hydraulic rams centered on the span and placed 8' apart. For Beam Specimen No. 2, load was applied by a single hydraulic ram located at mid-span. The different arrangement of hydraulic rams for the single-span tests was the result of differing availability of laboratory equipment at the time the two different beam

specimens were tested. Both arrangements of hydraulic rams, however, produce a large positive moment at midspan of each beam specimen.

For both specimens, the steel girders and the concrete deck extend beyond the end supports. The specific overhang lengths are shown in Figure 8.4.

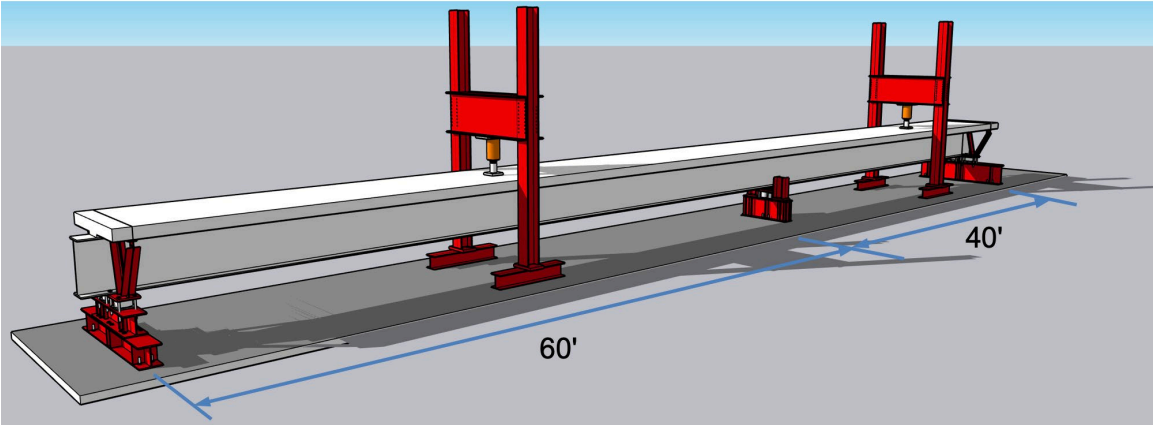


Figure 8.1 – Two-Span Loading Arrangement for Beam Specimen Nos. 1 and 2

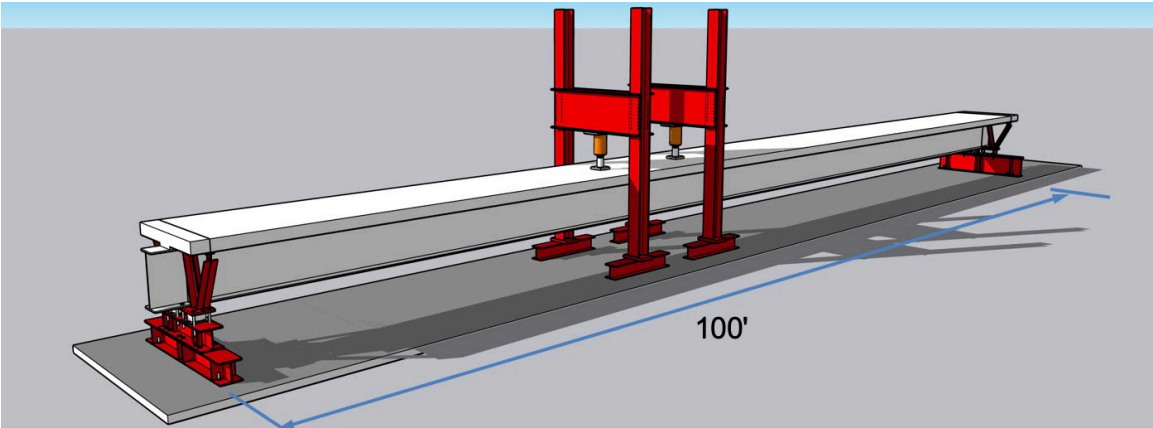


Figure 8.2 – Single-Span Loading Arrangement for Beam Specimen No. 1

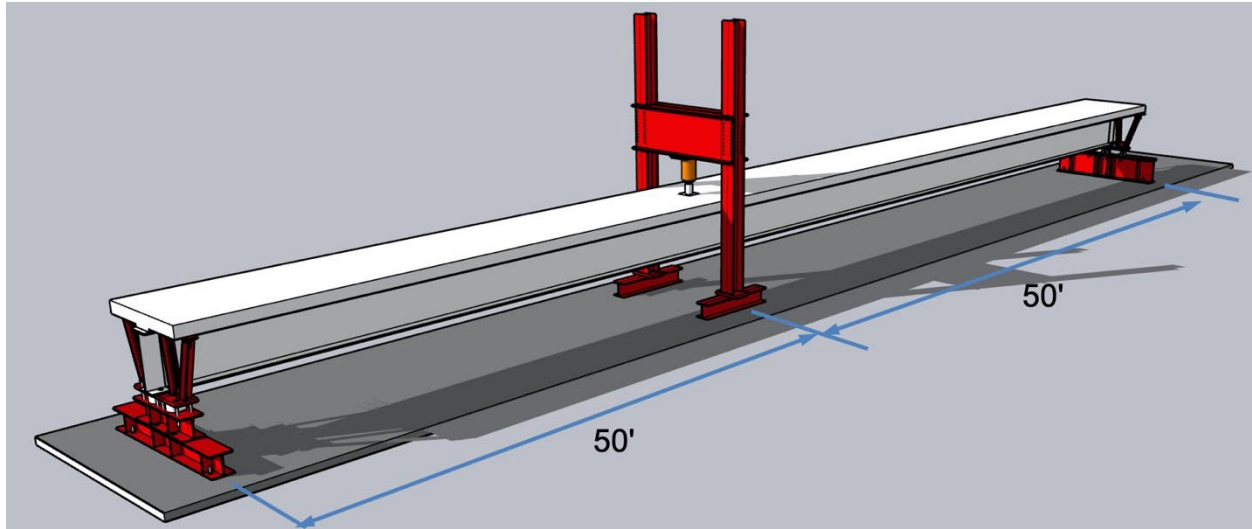


Figure 8.3 – Single-Span Loading Arrangement for Beam Specimen No. 2

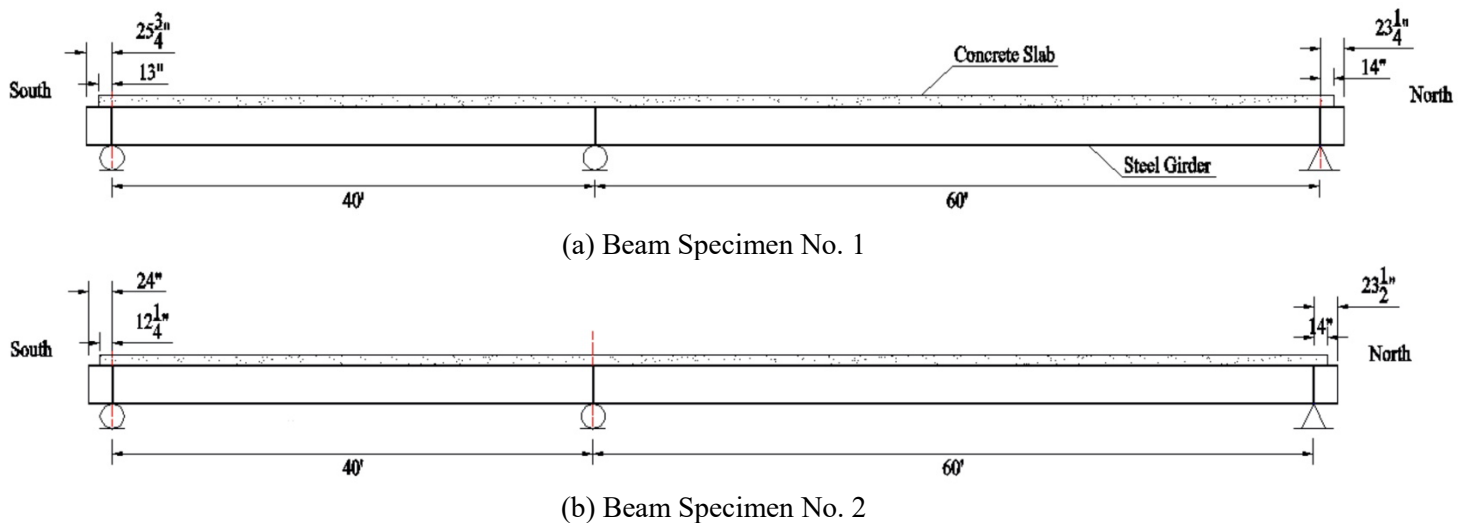


Figure 8.4 – Overhang Lengths of Beam Specimens

### 8.2.2. Specimen Cross-Sections

The cross-section of both beam specimens consisted of a W40×199 steel girder, an 8.5" concrete slab, a 2" height haunch, deck reinforcement, and shear studs in a staggered layout. The W40×199 girders were specified and supplied in accordance with ASTM A709 Gr. 50W steel.

The nominal depth of the W40×199 is 38.7" and the depth of the composite beam (steel section + haunch + deck) is 49.2". For the 100' single-span, the span-to-depth ratio is 31 for the steel

section alone and 24.5 for the composite section including the deck. Table 2.5.2.6.3-1 in the 9<sup>th</sup> Ed. AASHTO (AASHTO 2020) suggests a maximum span-to-depth ratio for simple spans of 30 for the steel beam alone and 25 for the composite beam including the deck. Thus, the span-to-depth ratios for the beam specimens are close to the limits specified by AASHTO.

The cross-section of Beam Specimen No. 1 is shown in Figure 8.5. The concrete deck is 78" wide and 8.5" thick with a 2" haunch. The deck reinforcement design is based on TxDOT requirements (TxDOT 2023) and typical practices as represented by the three bridges evaluated in Chapter 3. Additional reinforcing bars, designated as E bars (#5@9") are provided in the negative moment region where 1% reinforcement is required per Section 6.10.1.7 of the 9<sup>th</sup> Ed. AASHTO. More deck reinforcement details are provided later.

The cross-section of Beam Specimen No. 2 is shown in Figure 8.6. Following current TxDOT practices for PCP applications, the concrete deck consists of a 4.5" cast-in-place layer over 4" PCPs. The width of the concrete slab of Beam Specimen No. 2 is slightly larger than for Beam Specimen No. 1 due to the manufacturing size limit of the PCPs. The PCPs are supported on foam bedding strips that are 2" high by 1.5" wide, providing for a 2" haunch. The bedding strip dimensions are within the acceptable limits specified by TxDOT standards (TxDOT 2019b). The overlap distance between the PCPs and the girder flange is 4" which is in accordance with TxDOT standards (TxDOT 2019c). There is one mat of reinforcement in the cast-in-place layer. In the negative moment region of the beam, the reinforcement ratio is 1.18% of the CIP portion of the deck and is based on recommendations from TxDOT Research Project 0-6909 (Ge, et al. 2021).

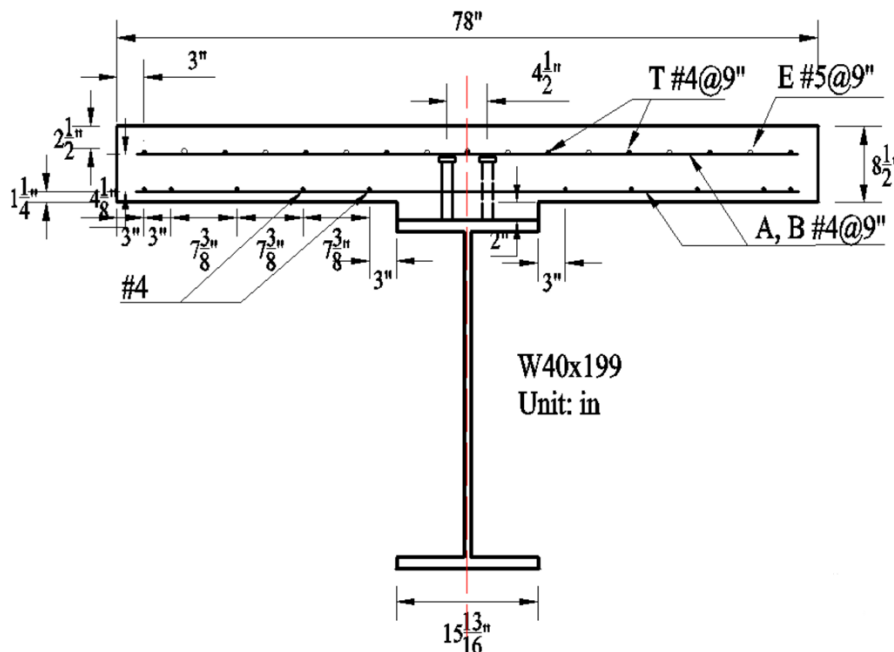


Figure 8.5 – Cross-Section of Beam Specimen No. 1  
(Deck Reinforcement Shown for Negative Moment Region)

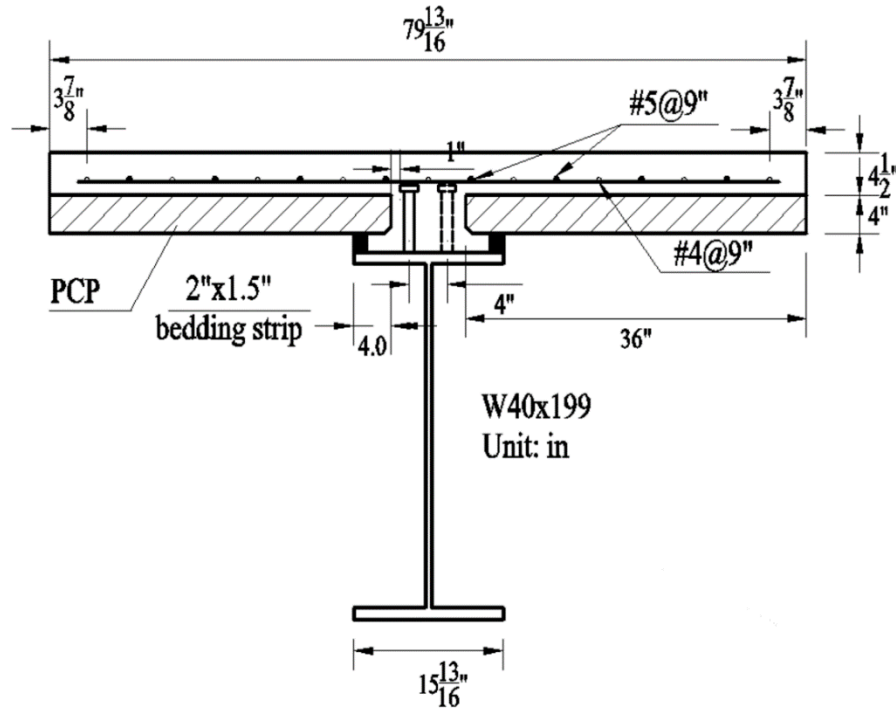


Figure 8.6 – Cross-Section of Beam Specimen No. 2  
(Deck Reinforcement Shown for Negative Moment Region)

### 8.2.3. Stud Layouts

Both beam specimens used 1-1/8" shear studs placed in a staggered layout. All studs were detailed to be 7" long after welding. Shear stud dimensions are shown in Figure 8.7 Both specimens had a 2" haunch so the studs penetrated 5" into the deck. Figure 8.10 shows photos of the studs welded to each beam specimen.

For Beam Specimen No. 1, 68 shear studs were used over the full length of the beam. The longitudinal spacing of studs was 18" and the transverse spacing was 4 1/2" as shown in Figure 8.8. The number of studs was chosen to achieve partial composite behavior in the single-span test. Partial composite design is not permitted in AASHTO. However, for partial composite design, the ultimate flexural strength of the girder is controlled by the strength of the shear studs. Beam Specimen No. 1 was designed as partially composite to evaluate the strength and slip capacity of 1-1/8" studs in a beam specimen, for comparison with the strength and slip capacity measured in the push-out tests described in Chapter 5.



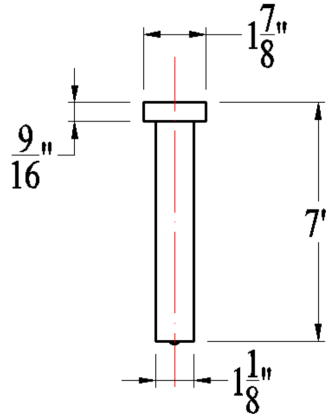


Figure 8.7 – Shear Stud Dimensions

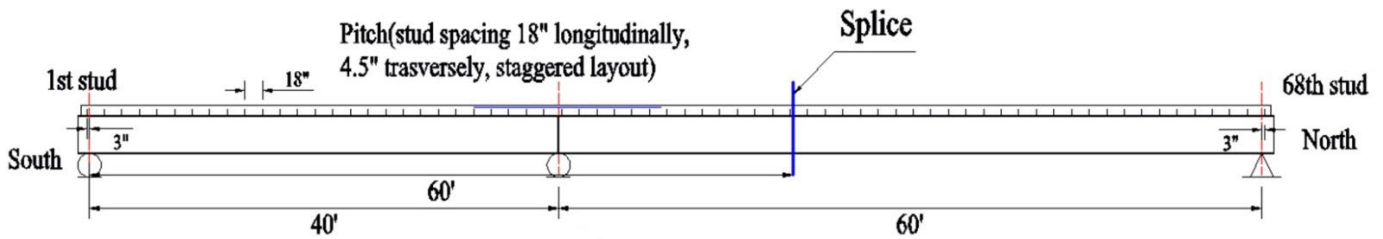


Figure 8.8 – Shear Stud Layout for Beam Specimen No. 1

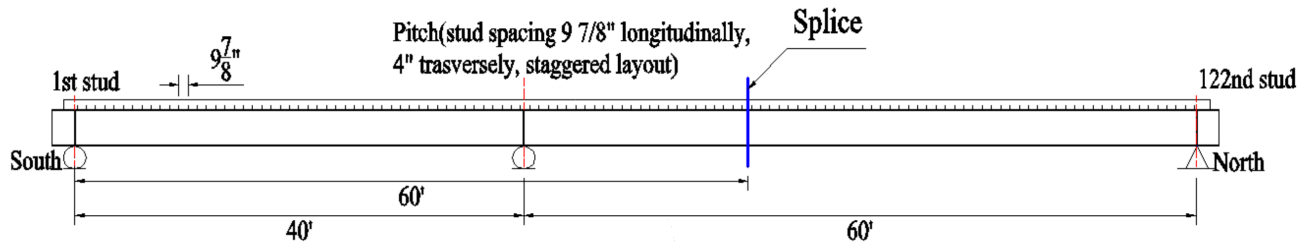


Figure 8.9 – Shear Stud Layout for Beam Specimen No. 2

For Beam Specimen No. 2, 122 shear studs were provided over the full length of the beam. The longitudinal spacing of the studs was  $9 \frac{7}{8}$ " and the transverse spacing was 4" as shown in Figure 8.9. The number of studs was chosen to achieve fully composite behavior in the single-span test. Beam Specimen No. 2 had a deck constructed with PCPs. The 4" transverse spacing was chosen to provide a clear distance between the head of the stud and the edge of the PCP of about 1". Based on the finite element studies presented in Chapter 7, the use of 1" clear distance between the head of the stud and the edge of the PCP combined with a 5" deck penetration should allow the stud to develop the strength specified in both the 9<sup>th</sup> Ed. AASHTO and the proposed 10<sup>th</sup> Ed. AASHTO. The finite element studies also showed that a deck penetration distance of 4" and a clear distance between the head of the stud and the PCP of 2" should provide

adequate stud strength. The 15.8" flange width for the W40×199 beams did not allow for a 2" clear distance between the stud and the PCP, so the specimen was designed with a 5" deck penetration and a 1" clear distance between the stud and the PCP.

Both beam specimens had fewer shear studs than what would typically be used in an actual bridge girder. In an actual bridge girder, the number of shear studs are normally controlled by fatigue, resulting in more shear studs than required for strength. This was demonstrated by the preliminary design studies reported in Chapter 3. Fatigue was not considered in the design of the two beam specimens, as the primary interest in the beam tests was the behavior, strength, and slip capacity of 1-1/8" studs under static loading.

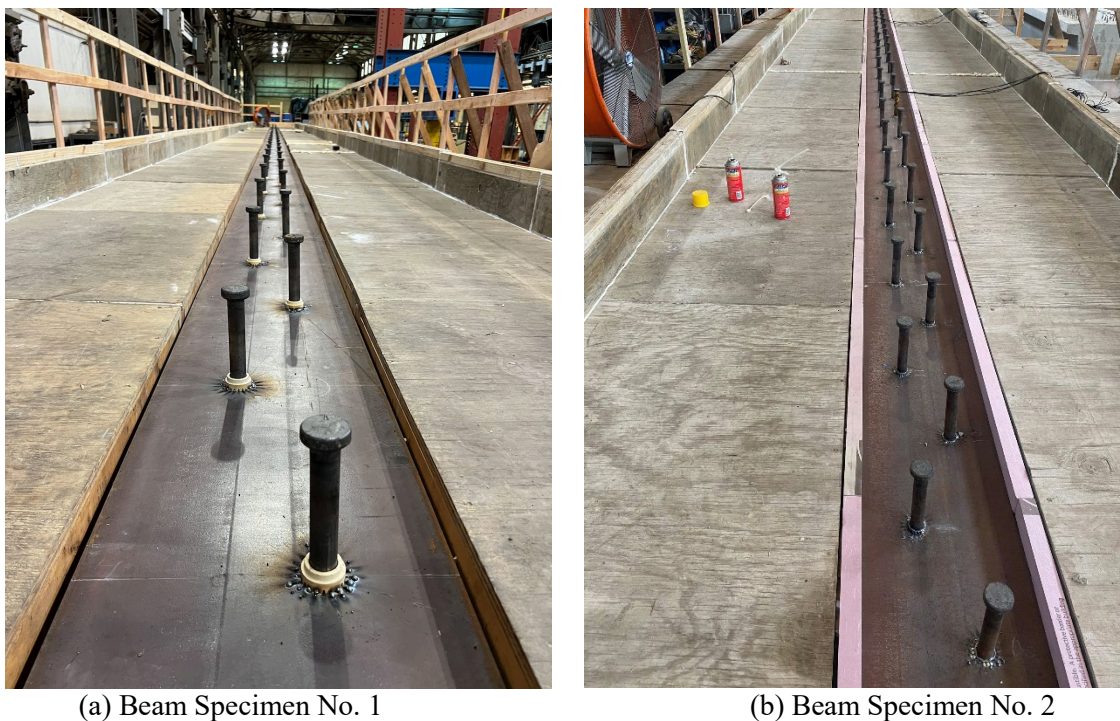


Figure 8.10 – Layout of Studs

## 8.2.4. Deck Reinforcement

The deck reinforcement used in the beam specimens of this study are ASTM A615 Grade 60 #4 and #5 reinforcing bars. The reinforcement cage consists of longitudinal reinforcement going through the whole length of the girder, transverse reinforcement and additional #5 reinforcement in the negative moment regions.

### 8.2.4.1. Deck Reinforcement for Beam Specimen No. 1

Since Beam Specimen No. 1 had a full-depth cast-in-place concrete slab, two reinforcement mats were used in the deck as shown in Figure 8.5. The longitudinal rebar was designed to be #4@9",

and the transverse rebar was also #4@9". As noted above, additional #5@9" rebar (E) in the negative moment region was provided to provide the 1% reinforcement requirement of AASHTO. The plan view of the top mat of Beam Specimen No. 1 is shown in Figure 8.11. The region of additional #5 reinforcing bars was determined by the maximum applied load, and 1'-5" development length at each end was also included per TxDOT Bridge Detailing Guide (TxDOT 2022) . The plan view of the bottom mat is shown in Figure 8.12.

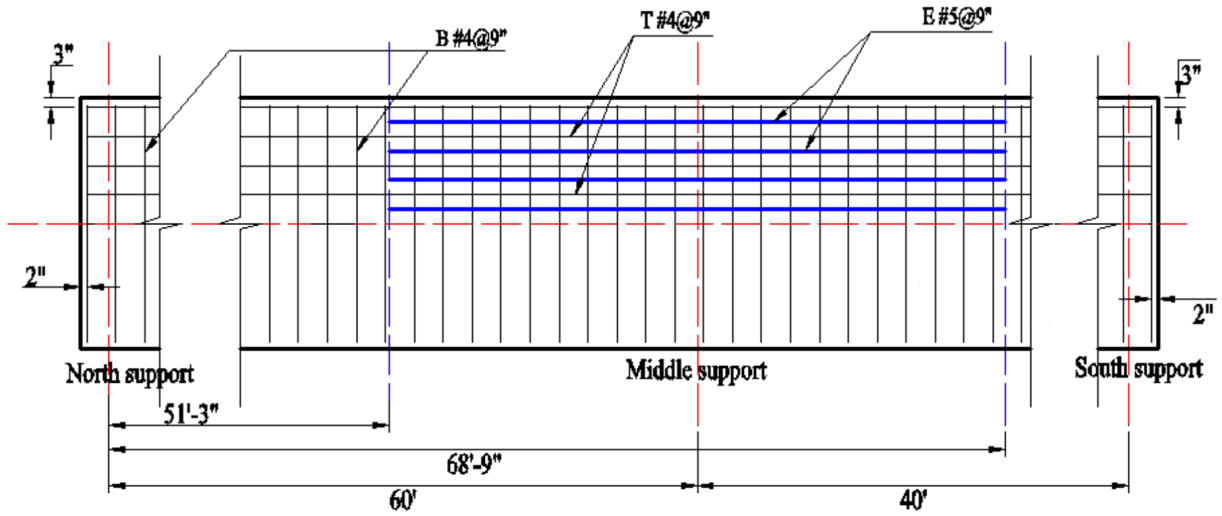


Figure 8.11 – Plan View of Top Mat of Reinforcing Bars for Beam Specimen No. 1

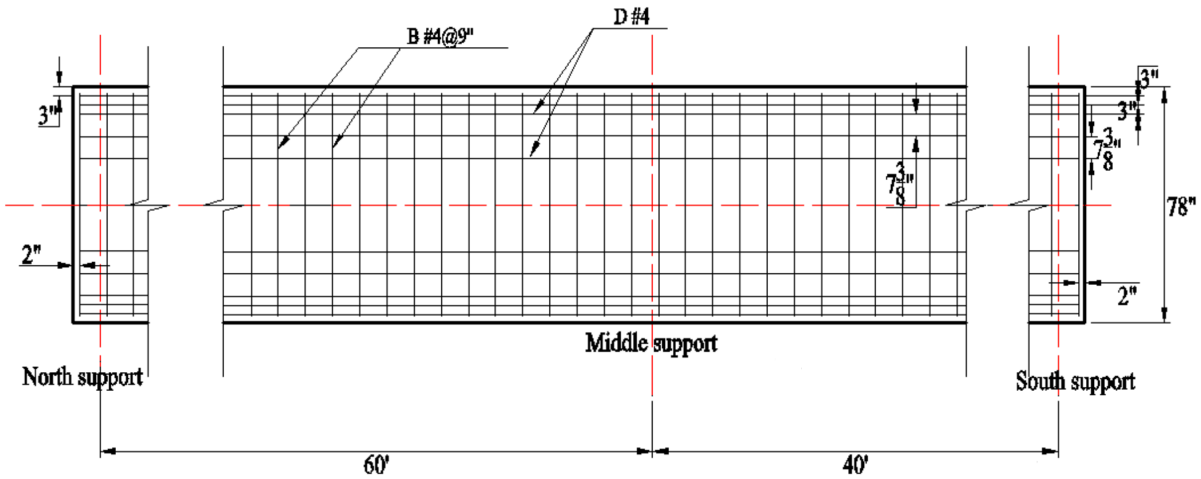


Figure 8.12 – Plan View of Bottom Mat of Reinforcing Bars for Beam Specimen No. 1

Since the length of the concrete slab is approximately 100', the #4 longitudinal reinforcing bars were spliced at 30' and 70' away from south support, as shown Figure 8.13. The splice length for #4 longitudinal reinforcement is 1'-7" based on the TxDOT Bridge Detailing Guide (TxDOT

2022). The same splice locations were used for the #4 longitudinal reinforcing bars in both the top and bottom mats.

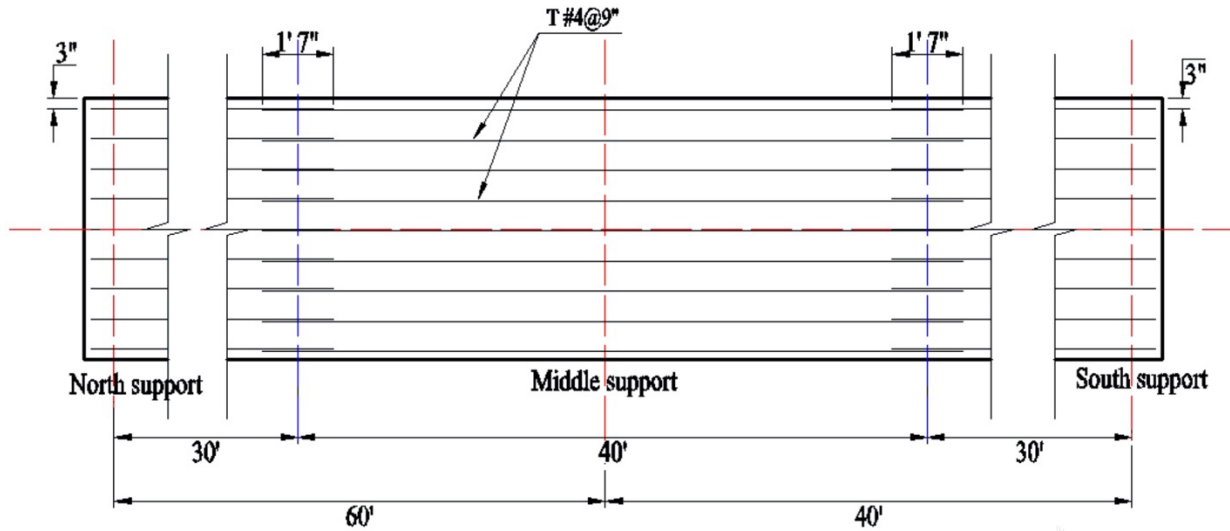


Figure 8.13 – Location of Splices in #4 Longitudinal Reinforcing Bars for Beam Specimen No. 1

#### 8.2.4.2. Deck Reinforcement for Beam Specimen No. 2

Since PCPs were used in Beam Specimen No. 2, only one layer of reinforcement was placed in the cast-in-place concrete layer above the PCPs. The longitudinal reinforcement was #4@9" and transverse reinforcement was #4@9". As described above, in the negative moment region, additional #5 longitudinal reinforcement was used based on recommendations from TxDOT Research Project 0-6909 (Ge, et al. 2021). For the #4 longitudinal reinforcing bars, the splice length and splice locations were the same as for Beam Specimen No. 1. The additional #5 reinforcing bar length in the negative moment region also includes the 1'-5" development length per the TxDOT Bridge Detailing Guide (TxDOT 2022). Figure 8.14 shows a plan view of the longitudinal reinforcing bars in Beam Specimen No. 2.

#### 8.2.5. Precast Concrete Panels

The precast concrete panels used in the study were produced at Bexar Concrete in San Antonio, Texas in accordance with TxDOT standards (TxDOT 2019c). The dimensions of a PCP panel are shown in Figure 8.15, where the panel length is 6' and the width is 3'. The thickness of the PCP is 4". The reinforcement used is ASTM A615 Gr 60 rebar and the reinforcement plan was specified as #3@5" longitudinal reinforcement, #4@6" transverse reinforcement and #3 U bars. Dimensions of the U bars are shown in Figure 8.16. The #4 transverse reinforcing bars extended 3.5" beyond the edge of the PCP closest to the steel girder, as shown in Figure 8.15.

All the panels had a 3/4" chamfer at the edge closest to the steel girder per TxDOT standards (TxDOT 2019c). A total of 34 panels were used on Beam Specimen No. 2 and those panels were cast on the same day from three trucks. Photos of the PCP fabrication process are shown in Figure 8.17, Figure 8.18, and Figure 8.19.

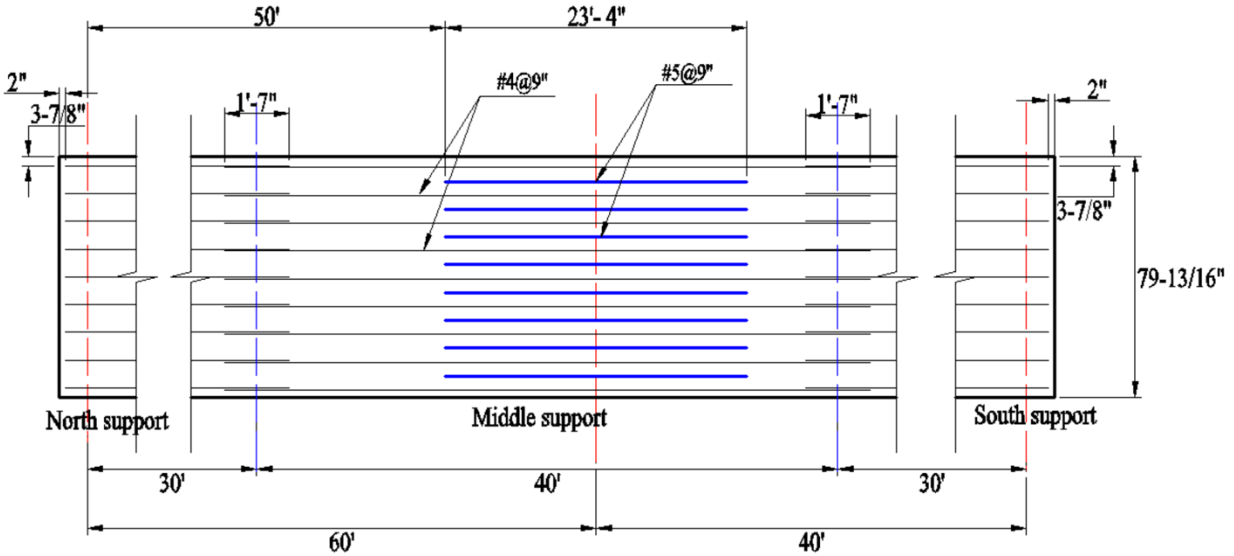


Figure 8.14 – Plan View of Longitudinal Reinforcing Bars for Beam Specimen No. 2

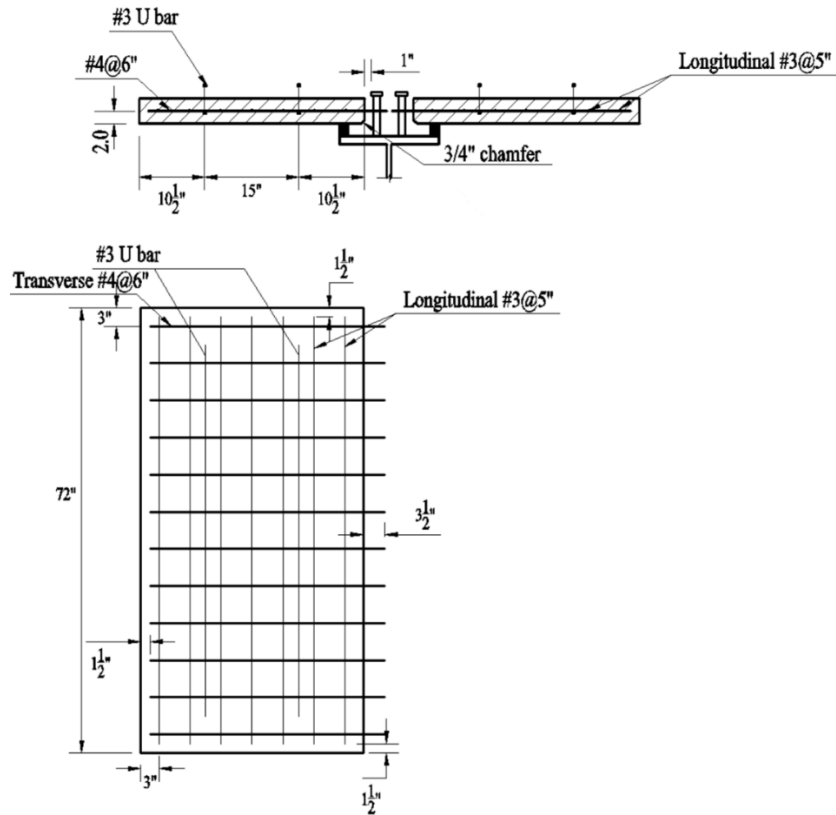


Figure 8.15 – Dimensions of a PCP Panel



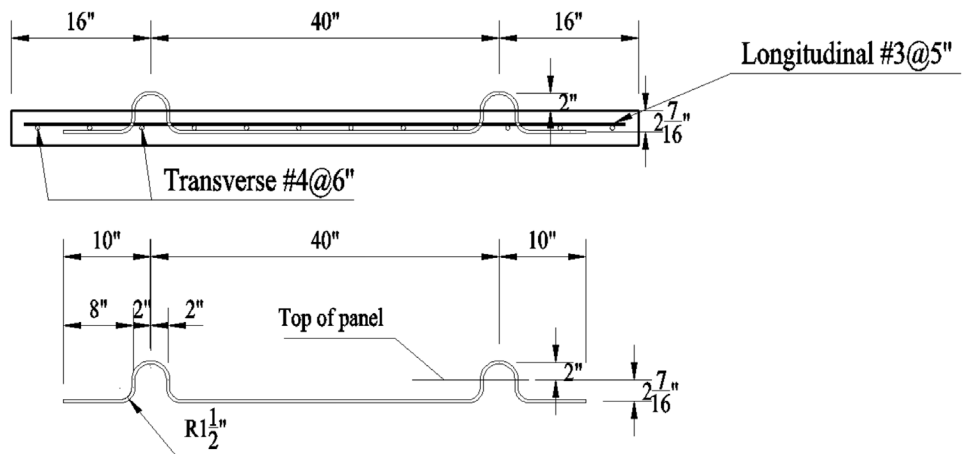


Figure 8.16 – U-Bar Dimensions



Figure 8.17 – Formwork and Reinforcing for PCPs



*Figure 8.18 – Broom Finishing of Top Surface of PCPs*



*Figure 8.19 – Finished PCP Panels*



## 8.3. Test Setup

This section presents details of the test setup for the large-scale beam tests. An overview of the setup for the two-span tests is shown Figure 8.1 and for the single-span tests in Figure 8.2 and Figure 8.3. Test setup components included the girder supports, the loading towers, lateral restraints and end braces. Each component of the setup is introduced in the following paragraphs.

### 8.3.1. Girder Supports

Three girder supports were needed; one at each end of the 100' long girder and the interior support for the two-span test. Photos of the three supports are shown in Figure 8.20. For the two-span tests, all the three supports were in place and for the single-span test, the interior support was removed. The north support was designed to be a pin connection with a roller welded to the plate of the support. The interior and south supports were designed to be a roller connection where the girder can rotate and translate freely. Each of the three supports incorporated load cells to measure the girder reactions.



Figure 8.20 – Girder Supports (From Left to Right: North, Interior, South)

### 8.3.2. Loading Towers

The loading towers were used to apply vertical load to the girder with hydraulic rams. Two nominally identical loading towers were constructed, as two load application points were needed for the two-span tests on both beam specimens (see Figure 8.1) and for the single span test on Beam Specimen No. 1 (see Figure 8.2). The single-span test for Beam Specimen No. 2 required only one loading tower (see Figure 8.3).

Each loading tower consisted of two columns, two coped beams and an 800 kip ram as shown in Figure 8.21. A 500 kip load cell was placed on top of a 2" thick steel plate beneath the ram and the bottom surface of the plate was cast on top of hydrostone to level the load cell surface. During the single-span tests, additional plates and a short beam were added to fill the gap due to

the limited stroke length of the ram (12.8"). A spacer beneath the load cell and the additional spacer plates can be seen in Figure 8.21.

Figure 8.22 shows the location of the loading towers for the two-span tests on Beam Specimen No. 1 and 2. Figure 8.23 and Figure 8.24 show the location of the loading towers for the single-span tests on Beam Specimen No. 1 and Beam Specimen No. 2. For the single-span tests, as noted earlier, a single loading tower was used at midspan for Beam Specimen No. 2 as compared to a pair of loading towers centered at midspan for Beam Specimen No. 1. The different arrangements were used because of limitations of availability laboratory equipment at the times these tests were run.



Figure 8.21 – Photos of Loading Tower

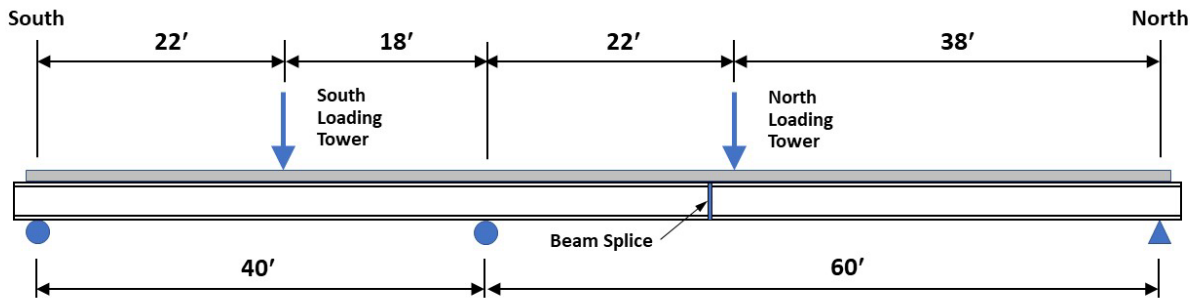


Figure 8.22 – Location of Loading Towers for Two-Span Test on Beam Specimen Nos. 1 and 2

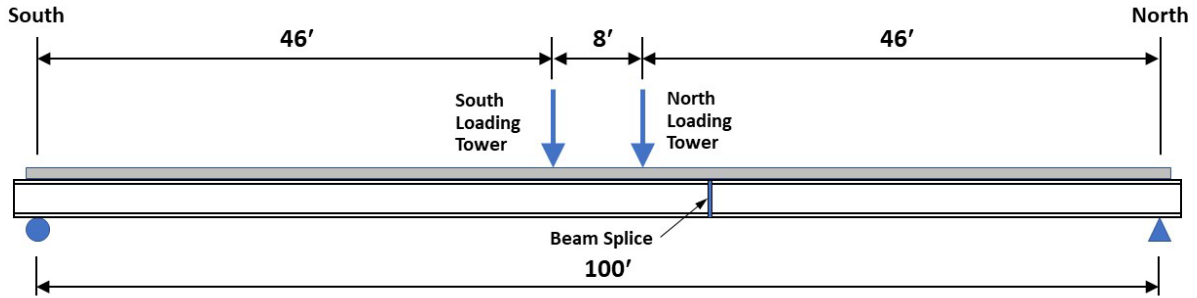


Figure 8.23 – Location of Loading Towers for Single-Span Test on Beam Specimen No. 1

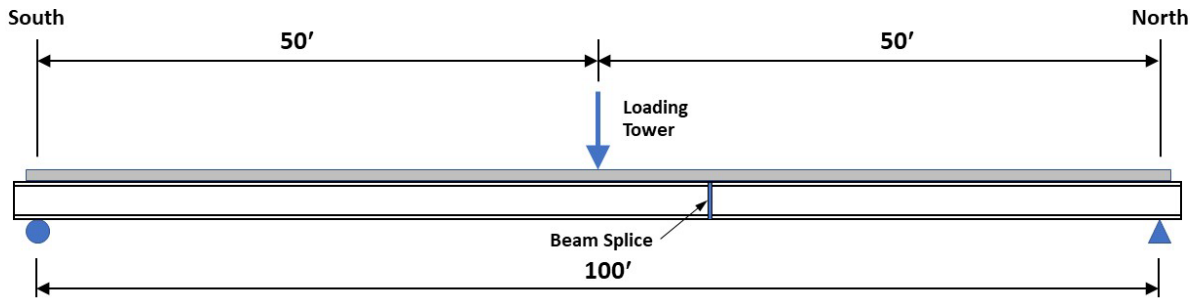


Figure 8.24 – Location of Loading Tower for Single-Span Test on Beam Specimen No. 2

### 8.3.3. Lateral Restraints

Lateral restraints were bolted to each column of the loading towers as a safety precaution to prevent excessive lateral movement of the beam specimen. A lateral restraint is highlighted in Figure 8.25. The lateral restraints were installed to leave a gap of about 1/2" between the restraint and the slab, to avoid any restraint to vertical motion of the specimen. None of the specimens came into contact with the lateral restraints in any of the tests.

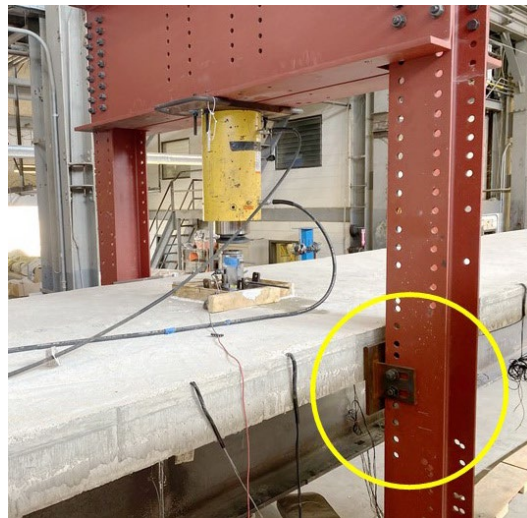


Figure 8.25 – Beam Specimen Lateral Restraint



### 8.3.4. End Braces

End braces were provided at each end of the beam. The end braces provided lateral restraint to the bare steel beam during specimen construction. The end braces also prevented tilting of the concrete slab in the finished specimen. Figure 8.26 (a) shows an end brace before the concrete deck was placed and cured. Figure 8.26 (b) shows an end brace in the finished specimen.

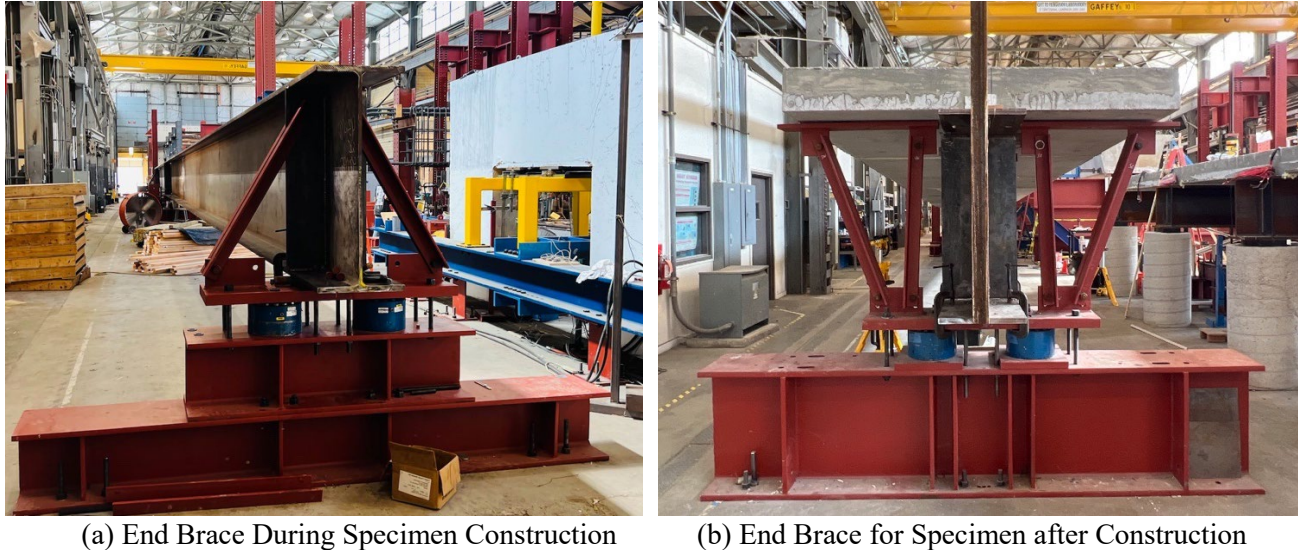


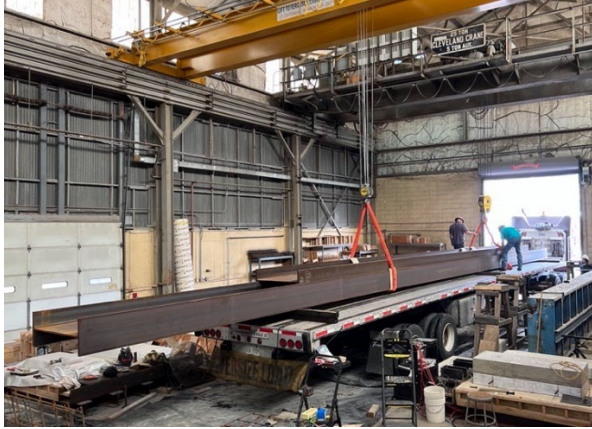
Figure 8.26 – Beam Specimen End Braces

## 8.4. Specimen Construction

The two specimens were constructed in almost the same way except that Beam Specimen No. 2 had one more step of PCP placement. The construction process is summarized as steel girder erection, formwork work fabrication and assembly, shear stud welding, reinforcement cage fabrication, instrumentation, concrete casting and curing. The details of the construction process are described in the following sections.

### 8.4.1. Erection of Steel Girder

Due to the shipping and handling constraints, the steel girders of both specimens were constructed from two pieces of W40×199 sections that were welded together to form a single test specimen girder. Figure 8.27 shows the process of lifting the two pieces of W40×199 and also shows the girder on its supports.



(a) Girder unloading



(b) Girder on the supports

Figure 8.27 – Unloading and Erection of Steel Girder

The two pieces of W40×199 were spliced at 40' from the north support. A welded splice was used instead of a bolted splice to avoid the bolts and splice plate at the top flange from working as an additional shear transfer device between the concrete deck and the steel beam. The splice consisted of complete joint penetration groove welds for both the top and bottom flanges and the web, as shown in Figure 8.28. Photos of a welded splice are shown in Figure 8.29.

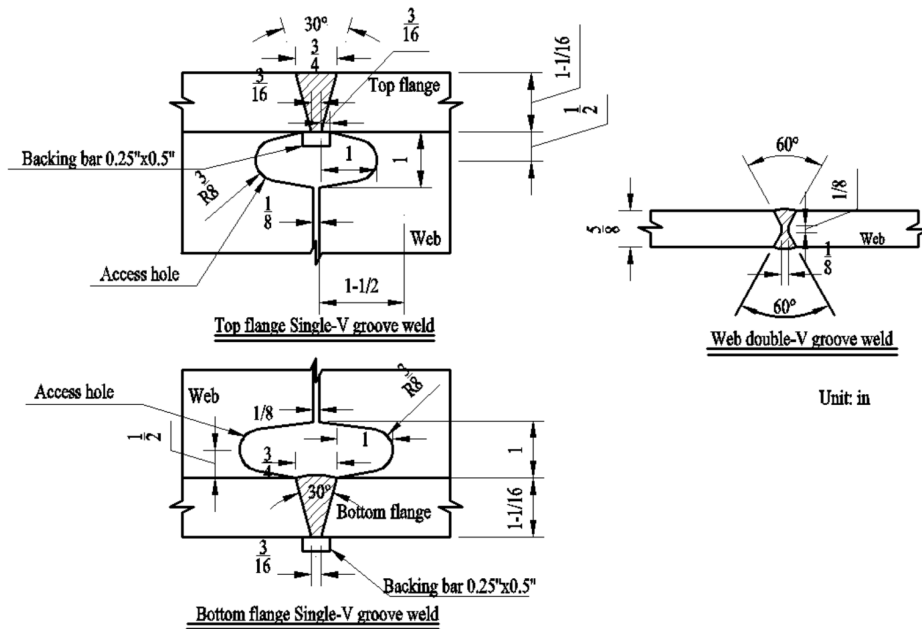
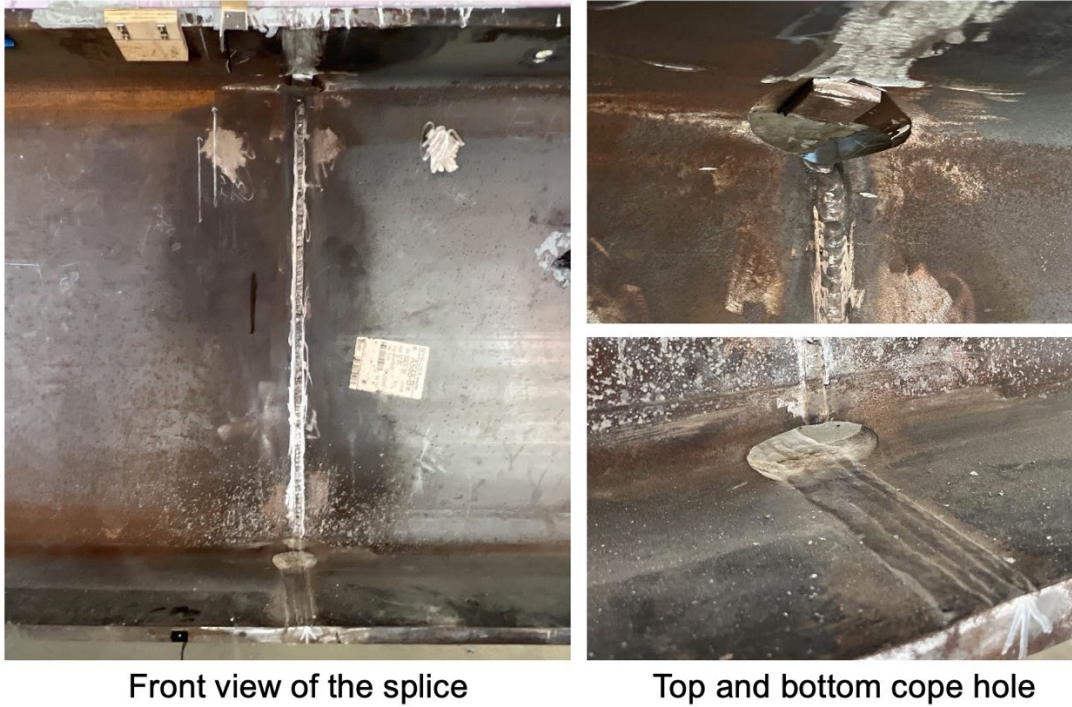


Figure 8.28 – Welded Splice Detail



Front view of the splice

Top and bottom cope hole

Figure 8.29 – Photos of Welded Splice

#### 8.4.2. Formwork

After the steel girder was in place on its supports, the formwork was constructed and installed. A 3D sketch of the formwork is shown in Figure 8.30. Figure 8.31 shows a cross-section view of the formwork. Photos of the assembled formwork are in Figure 8.32. The top of the plywood surface that supported the bottom of the deck was 2" above the girder flange to provide a 2" haunch for both specimens.

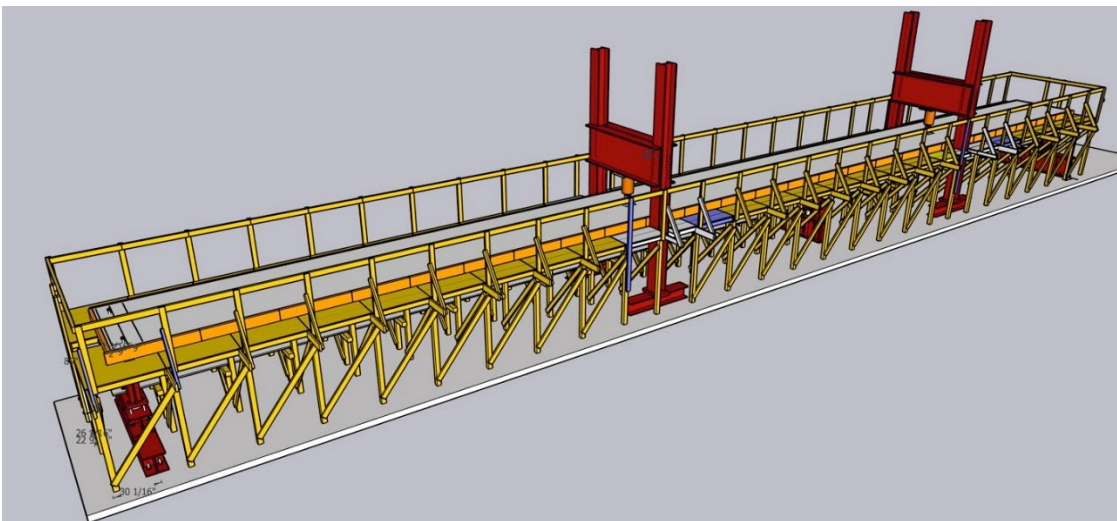
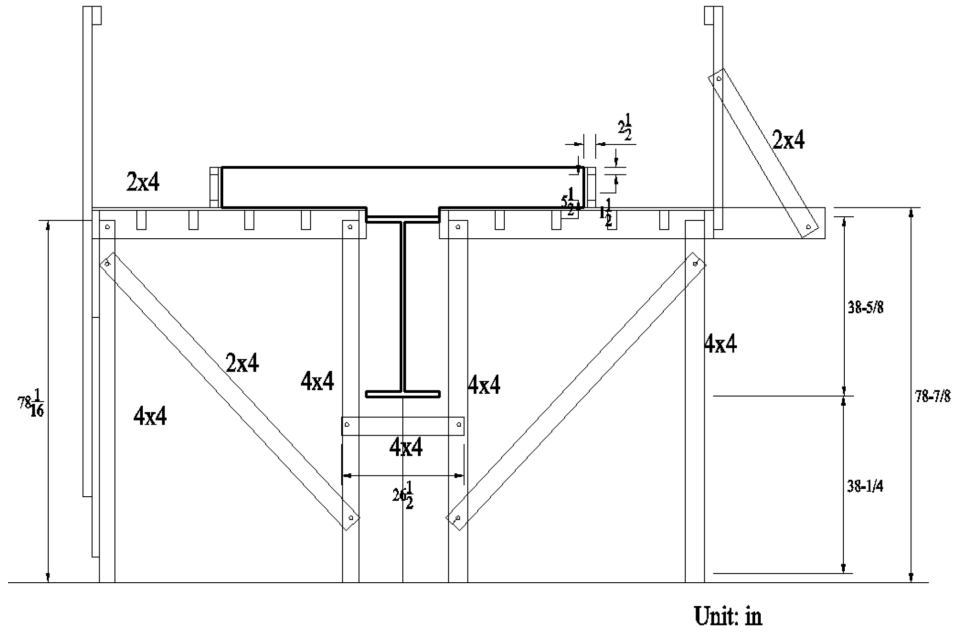
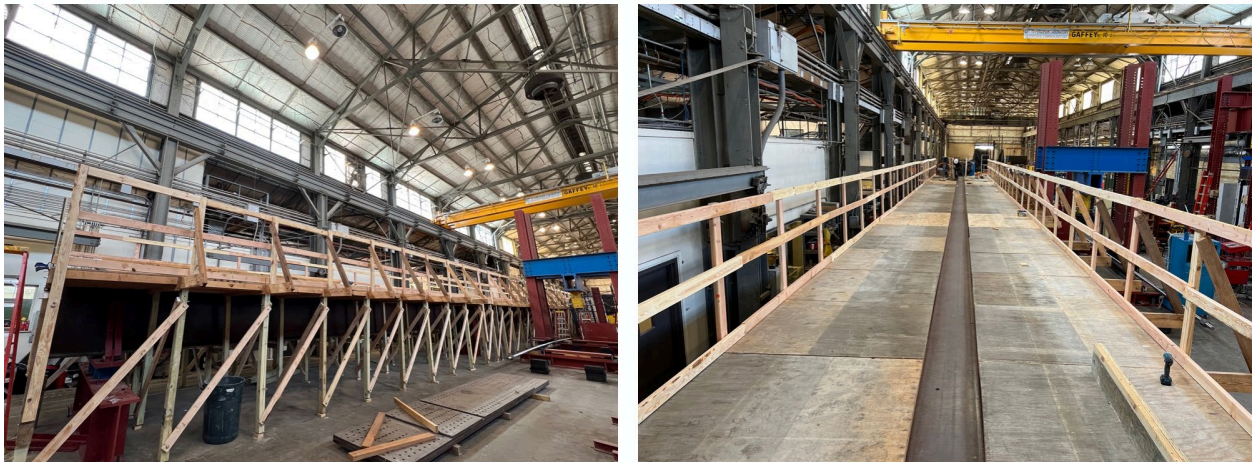


Figure 8.30 - 3D Sketch of the Formwork





*Figure 8.31 - Cross-Section of Formwork*



*Figure 8.32 – Assembled Formwork*



### 8.4.3. Shear Stud Welding

The welding parameters used for the beam specimens are the same as the parameters used on push-out specimen. The welding parameter setting for 1-1/8" studs are listed in Table 8.1. Figure 8.33 shows a photo of the stud welding gun with a stud installed in the gun prior to welding. Figure 8.34 shows studs being welded on Beam Specimen No. 2.

**Table 8.1 – Stud Welding Parameters used for Beam Specimens**

<b>Current (amps)</b>	<b>Time (s)</b>	<b>Plunge (in)</b>	<b>Lift (in)</b>	<b>Polarity</b>
2250	1.55	5/16	1/4	Reverse

Note: No surface preparation and no cable looping was used

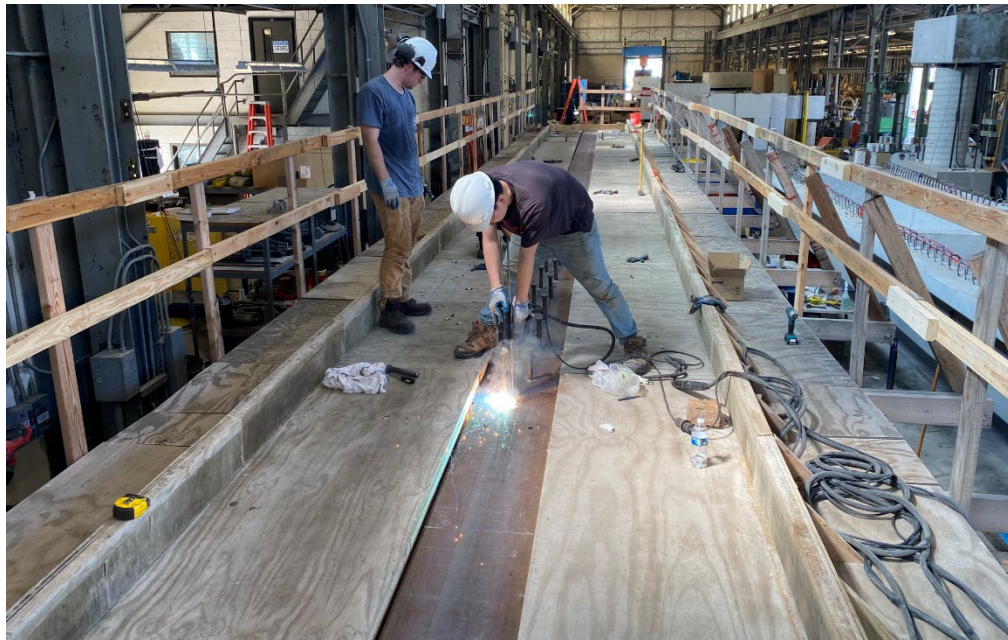
The 1-1/8" shear studs used for both beam specimens were all from the same production lot supplied by Nelson Stud Welding. For Beam Specimen No. 1, three trial studs were welded at the south end of the specimen and were subjected to 90° bend tests, and all three studs passed this test without failure of the weld. These three studs were then cut off just above the beam flange, and the flange surface was then ground smooth. On the day all of the studs were welded to the beam, two 1-1/8" shear studs were first welded on the steel girder at midspan and were subject to 30° bend tests. Both studs, shown in Figure 8.35, successfully passed this test. These bent studs were left in-place as permitted by AWS D1.5 (AWS 2020).

For Beam Specimen No. 2, three studs were welded along the length of the 100ft long girder (south end, midspan and north end) and all three passed 90° bend tests as shown in Figure 8.36. These three studs were then cut off just above the beam flange, and the flange surface was then ground smooth.

For both beam specimens, the length reductions for welded studs were above 1/4" which met the suggested length reduction value listed in Table 4.6. Figure 8.37 shows examples of the weld collar appearance of studs in both specimens which have a bluish color and even height. The successful 90° bend tests, successful 30° beam tests, good length reduction and good weld collar appearance provide indications of good weld quality.



*Figure 8.33 – Shear Stud Welding Gun with Stud Installed*



*Figure 8.34 – Welding Studs on Beam Specimen No. 2*





Figure 8.35 – 30 Degree Bend Tests of Studs on Beam Specimen No. 1



Figure 8.36 – 90 Degree Bend Tests of Studs on Beam Specimen No. 2

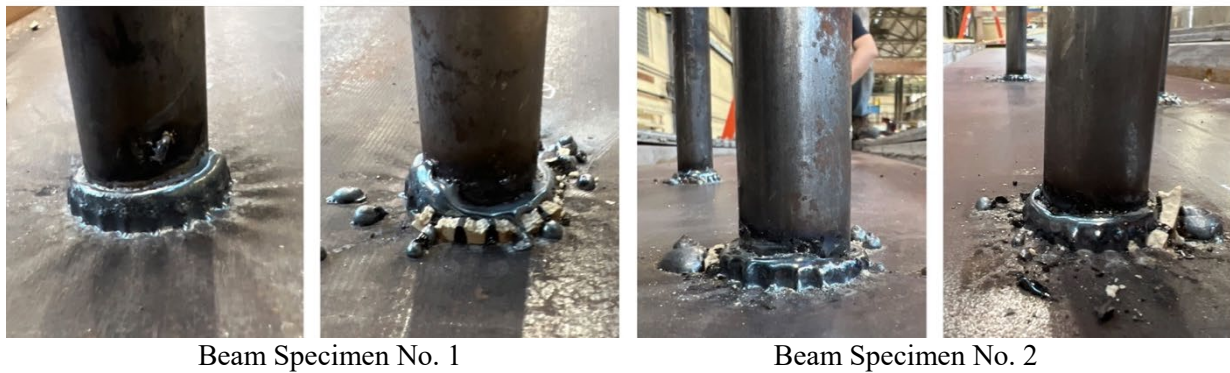


Figure 8.37 – Examples of Weld Collars



#### 8.4.4. Placement of Deck Reinforcement

Deck reinforcement for each specimen was described in Section 8.2.4. Figure 8.38 shows the finished deck reinforcement for Beam Specimen No. 1. Figure 8.39 shows the finished deck reinforcement over the PCP panels for Beam Specimen No. 2.

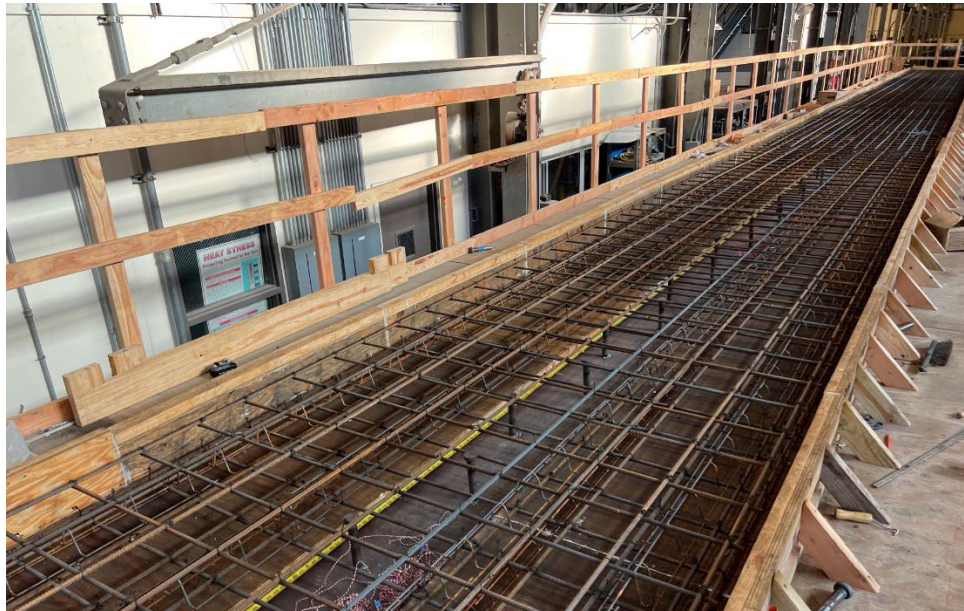


Figure 8.38 – Finished Deck Reinforcement for Beam Specimen No. 1

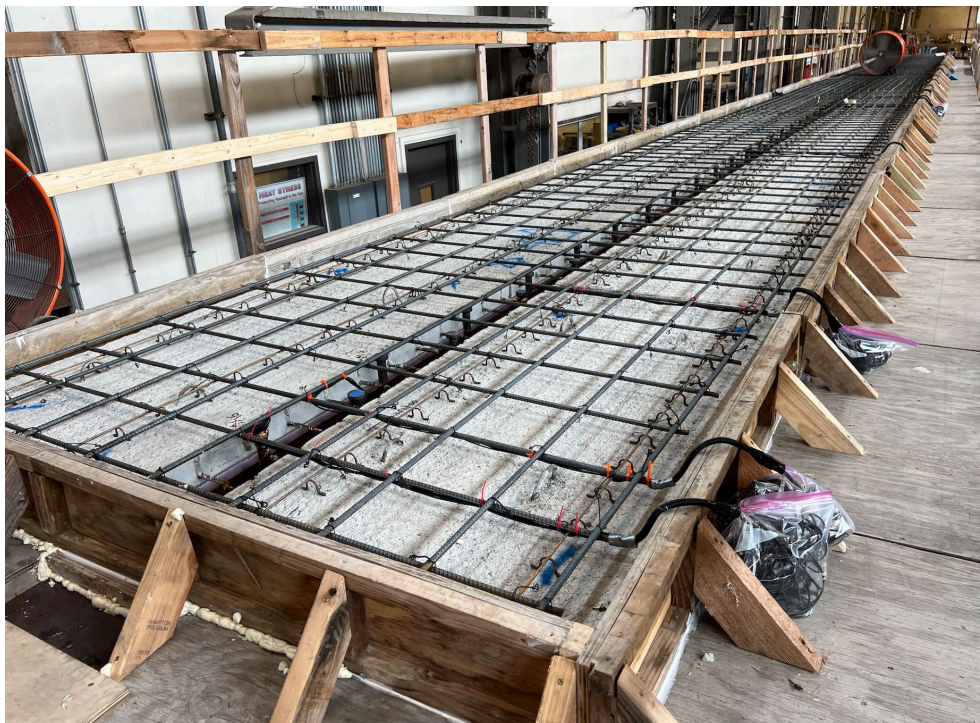


Figure 8.39 – Finished Deck Reinforcement for Beam Specimen No. 2



### 8.4.5. PCP Placement

In total 34 PCP panels were used in Beam Specimen No. 2 with 17 panels on each side of the top flange of the steel girder. Details of the panels were provided in Section 8.2.5, and a photo of the panels prior to placement is in Figure 8.40.



Figure 8.40 – PCP Panels Prior to Placement

Prior to placement of the PCP panels, 2" high by 1.5" wide foam bedding strips were placed at the outer edges of the beam flange. The bedding strips were attached to the beam flange with an adhesive, and adjacent strips were glued together at the butt joints. V-notches were cut into the top of the bedding strips in accordance with TxDOT standards (TxDOT 2019b). A photo of the bedding strips is in Figure 8.41. The top of the bedding strips were nominally at the same elevation as the formwork.

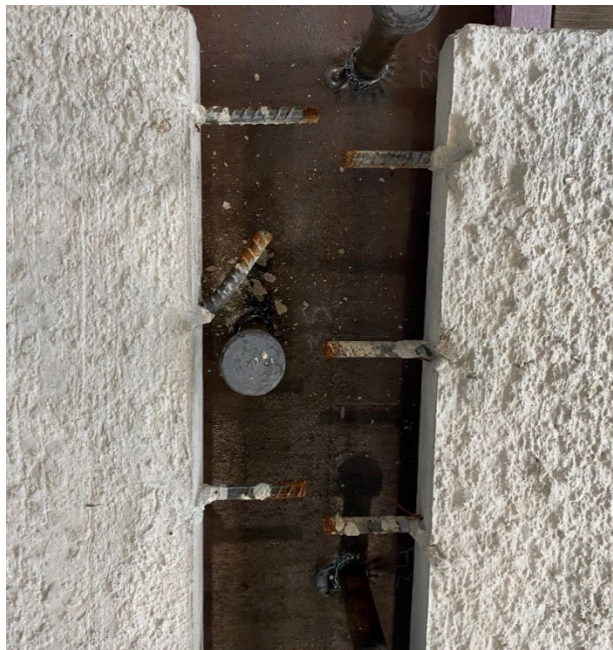
The PCP panels were placed starting at the south end of the girder and continued to be placed moving towards the north end. The panels were supported by both the formwork and by the bedding strips. In some cases, when a panel was placed, the short segment of a transverse reinforcing bar protruding from the edge of the PCP interfered with a shear stud. In these cases, the protruding reinforcing bar was either bent to avoid the shear stud or was cut off. A photo of a bent reinforcing bar is shown in Figure 8.42.

As noted in Section 8.2.5, the panels were fabricated using three different trucks of concrete. The location of the panels along the length of the girder and the corresponding truck batches is shown

in Figure 8.43. The length of each panel was 6', and so there was a seam between panels every 6'. The panels were placed so that the center of a panel was located at midspan of the beam, i.e., 50' from the end of the beam. Consequently, there was not a seam located at midspan, but there were seams located at 3' on each side of midspan.



*Figure 8.41 – Foam Bedding Strips*



*Figure 8.42 – Reinforcing Bar Protruding from PCP Bent to Avoid Shear Stud*

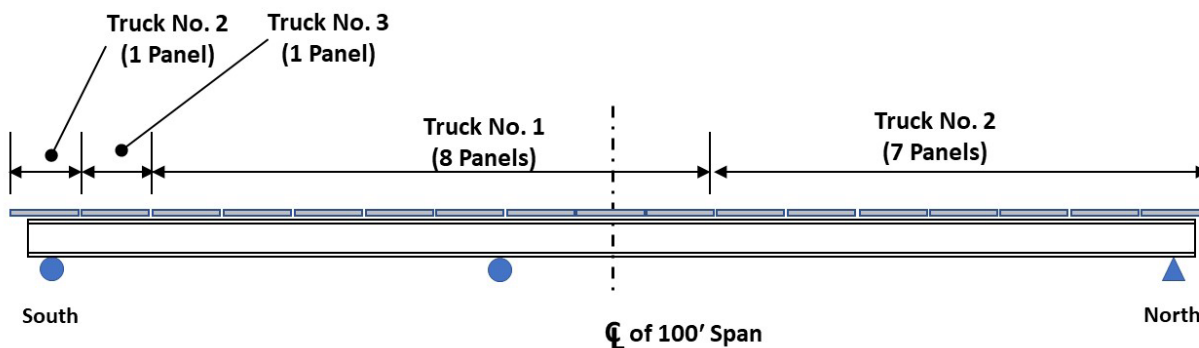


Figure 8.43 – Location of Panels and Corresponding Concrete Truck Numbers

The flange width of the W40×199 girder is 15.8". According to TxDOT standards (TxDOT 2019c), the minimum overlap distance between PCPs and top flange of the steel girder, for girder flange widths from 15" to 18" should 4", but may be as large as 4.75" or as small as 3". The panels were placed to provide an overlap distance as close as practical 4". The panels were also placed to provide a clear distance of about 1" between the head of the stud and the edge of the PCP. As described in Section 8.2.3, the 1" clear distance combined with the 5" stud penetration into the deck was based on recommendations developed in the finite element studies described in Chapter 7.

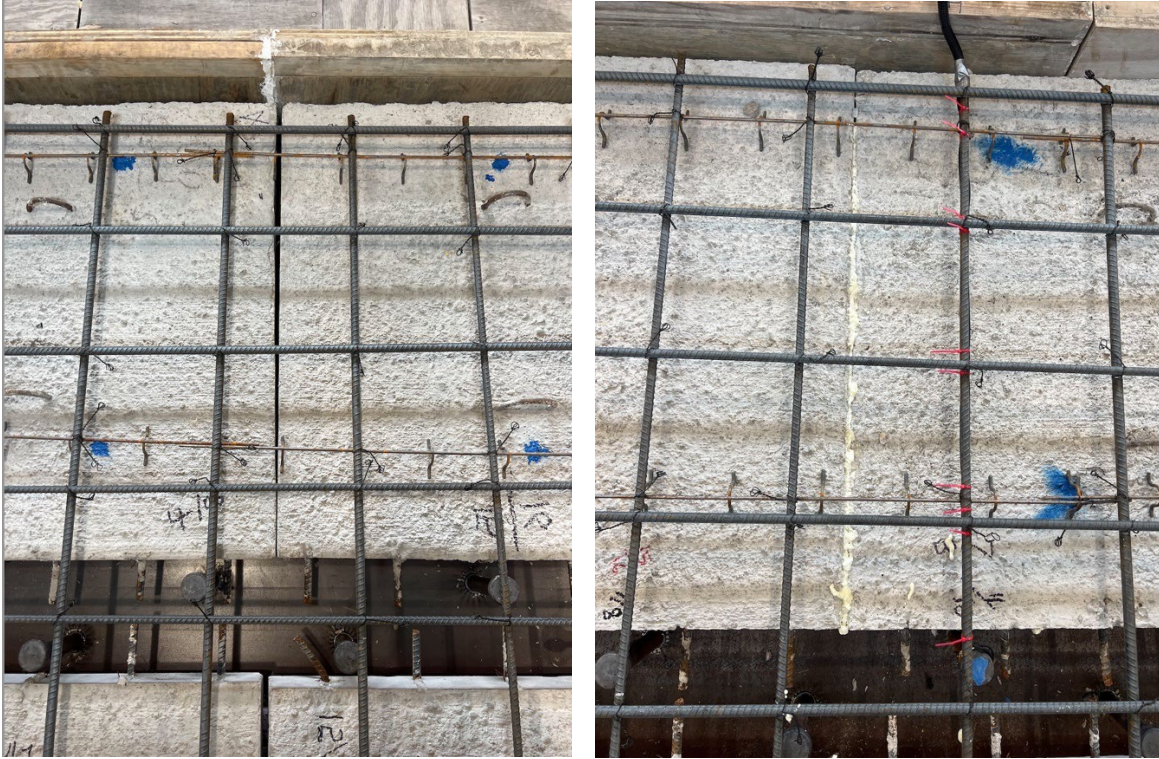
When placing the PCPs, adjacent panels were butt up against each other to minimize the gap between panels. However, due to geometric tolerances on the panel dimensions, squareness variations and edge straightness variations, there were small gaps between most panels. Table 8.2 lists the gaps between adjacent panels. The minimum gap was 0 and the maximum gap was 1/2". For gaps wider than 1/4", foam spray was used to seal the gap. Figure 8.44 shows examples of gaps between PCP panels.

Table 8.2 – Gaps Between PCP Panels

Location	East Side Gap (in.)	West Side Gap (in.)	Location	East Side Gap (in.)	West Side Gap (in.)
P1	3/8	5/16	P9	5/16	1/8
P2	3/16	0	P10	1/16	7/16
P3	1/8	5/16	P11	1/8	3/16
P4	1/8	3/16	P12	1/4	1/2
P5	1/8	1/8	P13	7/16	1/2
P6	1/8	1/8	P14	3/16	1/8
P7	1/4	1/8	P15	1/4	3/16
P8	1/8	1/16	P16	7/16	1/8

Notes: In the location column, P1 represents the end panel: the joint between panel 1 and panel 2. The gap value listed is the maximum gap width along one gap.





(a) The maximum gap (1/2")

(b) Sealed gap using foam spray

Figure 8.44 – Examples of Gaps Between PCP Panels

#### 8.4.6. Concrete Placement

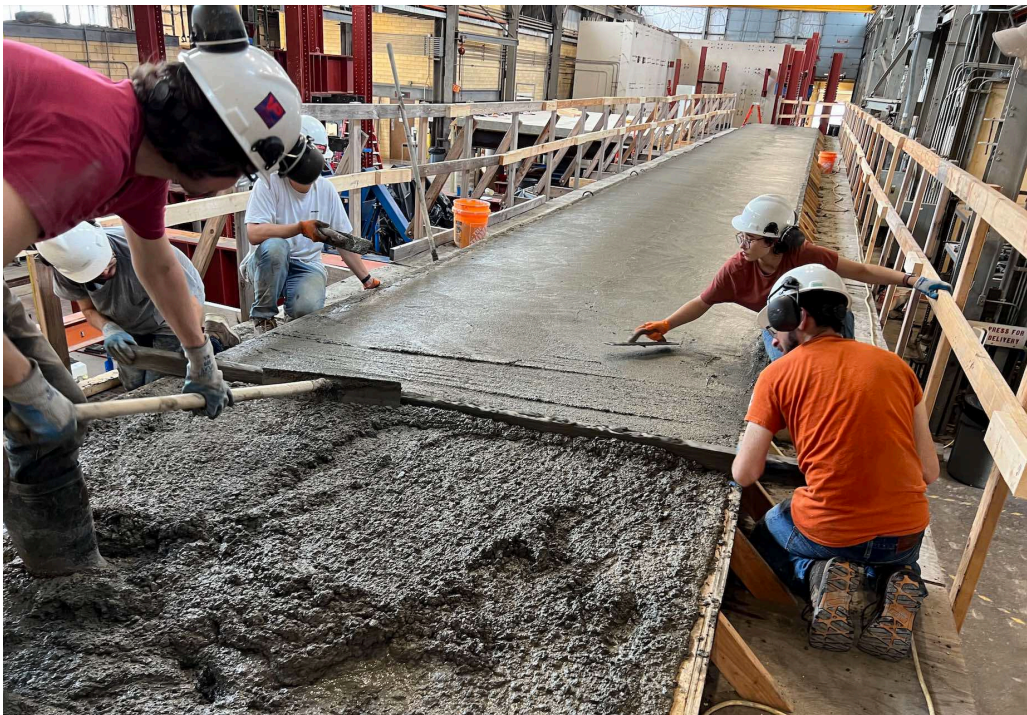
The cast-in-place concrete used for both specimens was TxDOT Class S concrete with a specified 28-day compressive strength of 4000 psi. Figure 8.45 and Figure 8.46 show photos of the concrete placement operations. For Beam Specimen No. 2, prior to placing the concrete, the PCPs were thoroughly wet but had no free water on the surface. After placement, the concrete was covered with a plastic sheeting for curing.

Beam Specimen No. 1 required three trucks of concrete. The approximate sections of the deck cast with each truck is shown in Figure 8.47. The cast-in-place concrete for Beam Specimen No. 2 required two concrete trucks. The approximate sections of the deck cast with each truck is shown in Figure 8.48.





*Figure 8.45 – Concrete Placement for Beam Specimen No. 1*



*Figure 8.46 – Concrete Placement for Beam Specimen No. 2*

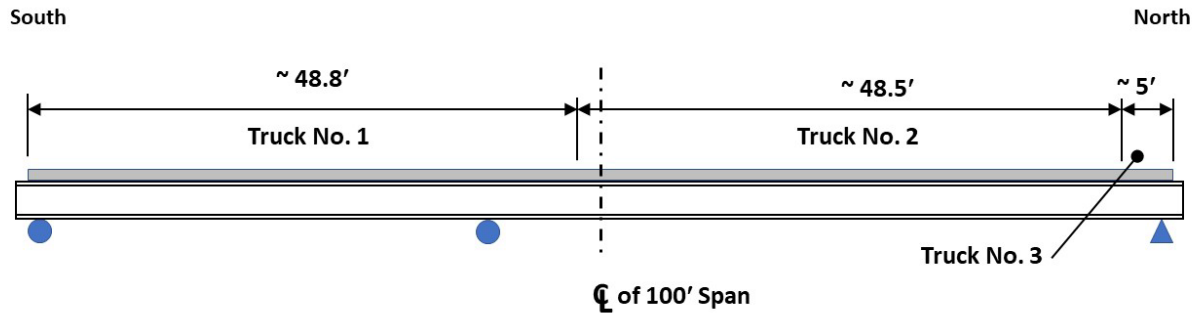


Figure 8.47 – Beam Specimen No. 1: Sections of Concrete Deck Cast from Different Concrete Trucks

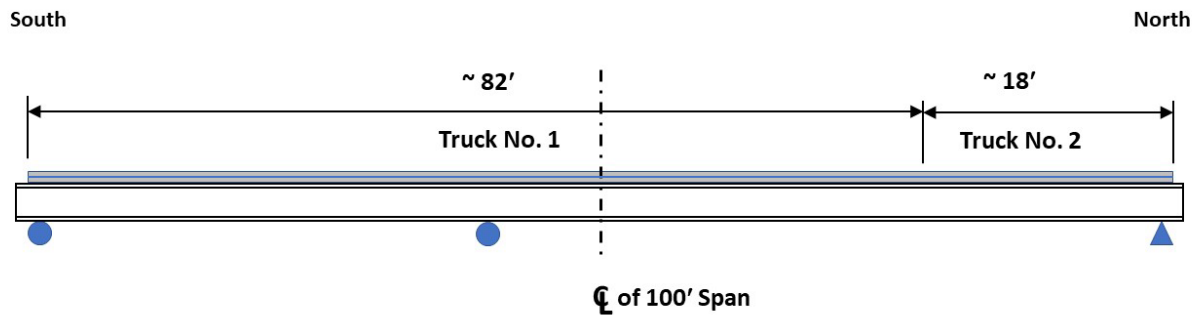


Figure 8.48 – Beam Specimen No. 2: Sections of CIP Portion of Deck Cast from Different Trucks

## 8.5. Material Properties

### 8.5.1. Shear Studs

#### 8.5.1.1. Tension Coupon Tests

The shear studs used on both specimens were from a single production lot and were supplied by Nelson Stud Welding. To obtain tensile properties, three tension coupons were machined from the 1-1/8" studs and tested in a 22 kip MTS test machine at Ferguson Laboratory. Figure 8.49 is a photo of a tension coupon during testing and Figure 8.50 shows coupons before and after testing.





Figure 8.49 – Tension Test on Coupon Machined for 1-1/8" Stud



Figure 8.50 – Tensile Coupons from 1-1/8" Studs Before and After Testing

The extensometer was kept on the coupon through fracture to obtain the entire stress-strain curve. The cross-head loading rate was 0.02 in. per minute for the entire duration of the test. The static yield and ultimate strength of the studs were also measured by adopting a loading procedure that has a 2 minute pause at strains of 0.01, 0.02, 0.03, 0.05, 0.07, 0.09, 0.11. Then the static yield strength can be obtained from the intersection of the 0.2% strain offset line and the regression curve of first three pause points in the stress strain curve. The static ultimate strength was also obtained from the regression curve.

The stress strain curves of the three tests are plotted in Figure 8.51. From the plot it can be seen that the three test results match closely. Tension coupon test results are summarized in Table 8.3. The dynamic yield stress and ultimate strength values are based on the stress-strain curves while the cross-heads are in motion at 0.02 in. per minute. The static yield stress and ultimate strength values are based on a regression curve fit to the data points after the 2 minute load holds. All values are based on an average of the three tension coupons.

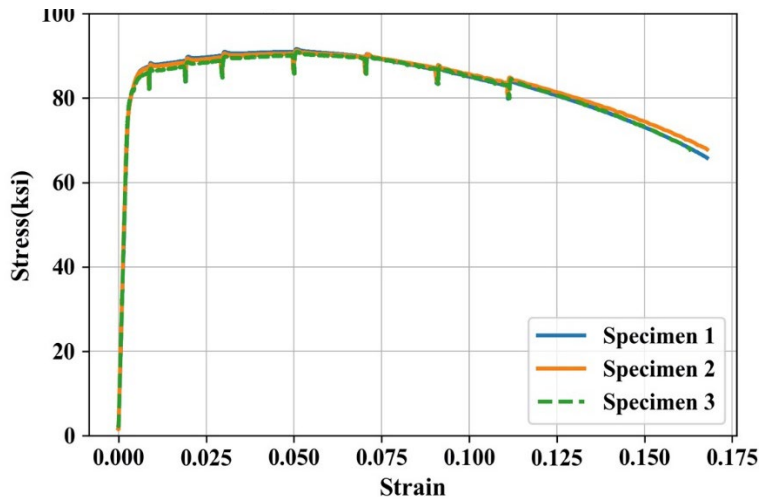


Figure 8.51 – Stress-Strain Curves for 1-1/8" Stud Tension Coupons

Table 8.3 – Tensile Properties of 1-1/8" Studs Used in Beam Tests

Dynamic Yield Stress	Static Yield Stress	Dynamic Ultimate Strength	Static Ultimate Strength	Strain at Fracture
83.9 ksi	80.7 ksi	90.9 ksi	85.8 ksi	17-percent

The 7" long 1-1/8" studs used in the beam tests were from a different production lot than the 7" long 1-1/8" studs used in the push-out tests. The tensile coupon properties for the 7" long 1-1/8" studs used in the push-out tests are listed in Table 4.3. The 1-1/8" studs used in the beam tests have significantly higher strength than those used in the push-out tests. For example, the dynamic ultimate strength of the 1-1/8" studs used in the push-out tests was 83.5 ksi, compared to 90.9 ksi for the studs used in the beam tests.

### 8.5.1.2. Charpy V-Notch Tests

In addition to tension coupon tests, Charpy V-notch (CVN) tests were conducted on samples machined from the 1-1/8" studs used for the beam tests. The CVN tests were conducted by Chicago Spectro Service Laboratory, Inc. The tests were performed at two temperatures: 30 deg. F and 70 deg. F. Nine tests were conducted at each temperature. Results are listed in Table 8.4. As is typical of CVN testing, there is considerable scatter in the data. However, with an average CVN of 37 ft.-lbs. at 70 deg. F, it may be concluded that the stud material has acceptable toughness.

## 8.5.2. Steel Girders – Material Properties and Section Dimensions

For each beam specimen, the steel girder was fabricated by welding an approximately 62' long piece of W40x199 to an approximately 42' long piece of W40x199. These lengths were chosen to provide an approximately 2' long overhang beyond the end supports for the 100' long span of

the test specimen, as shown in Figure 8.4. Consequently, a total of four different pieces of W40×199 were used to fabricate the girders for the two test specimens. All four pieces were produced to ASTM A709 Gr 50W steel, and all four pieces came from different heats of steel and therefore had different tensile properties. The length of each piece of W40×199 was several feet longer than needed for the test specimen beams, and the excess length was cut and used to make tension coupons.

**Table 8.4 – CVN Test Results for 1-1/8" Studs Used in Beam Tests**

Temperature	Absorbed Energy (ft-lbs)	Temperature	Absorbed Energy (ft-lbs)
30 deg F	17	70 deg F	14
	9		8
	24		86
	15		18
	7		64
	5		9
	15		68
	10		50
	7		20
Avg at 30 deg F	12	Avg at 70 deg F	37

Four plate tension coupons were cut from each of the four W40×199 sections. The location of the coupons is illustrated in Figure 8.52. Tension coupon tests for the W40×199 sections used in Beam Specimen No. 1 were conducted at Ferguson Structural Engineering Laboratory using a 220kips MTS test machine. The cross-head loading rate was 0.02 in. per minute for the entire duration of the test. Also, the static yielding strength and was measured by adopting a loading procedure that has a 2-minute pauses at several strain levels along the yield plateau. Static ultimate strength values were not measured. Tension coupon test results for the W40×199 sections used in Beam Specimen No. 1 are listed in Table 8.5

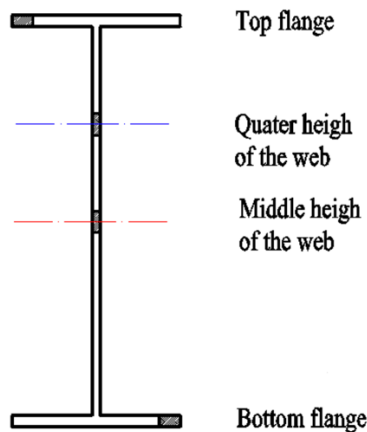


Figure 8.52 – Location of Tension Coupons in W40x199 Sections

Table 8.5 – Tension Coupon Test Results for Beam Specimen No. 1

W40x199 Section	Coupon Location	Static Yield Stress (ksi)	Dynamic Yield Stress (ksi)	Dynamic Ultimate Strength (ksi)	Strain at Fracture (%)
60' Section	Top Flange	53.5	55.5	74.2	28
	Web-Center	58.8	61.6	76.1	25
	Web-Quarter	59.2	63.2	77.6	25
	Bottom Flange	-	57.7	73.7	27
40' Section	Top Flange	53.4	55.3	70.5	32
	Web-Center	62.6	65.3	77.8	24
	Web-Quarter	61.9	66.1	78.1	22
	Bottom Flange	54.0	56.9	71.2	29

Tension coupons for the W40×199 sections used in Beam Specimen No. 2 were tested by Chicago Spectro Service Laboratory, Inc. A cross-head rate of 0.02 in. per minute was used from the start of the test up through the initiation of strain hardening. The cross-head rate was then increased to 0.5 in. per minute for the remainder of the test up through fracture. Static yield stress values were not measured. Results are summarized in Table 8.6.

Table 8.6 - Tension Coupon Test Results for Beam Specimen No. 2

W40x199 Section	Coupon Location	Dynamic Yield Stress (ksi)	Dynamic Ultimate Strength (ksi)	Strain at Fracture (%)
60' Section	Top Flange	56.5	72.2	26
	Web-Center	65.9	79.4	21
	Web-Quarter	64.9	78.4	22
	Bottom Flange	58.8	73.1	25
40' Section	Top Flange	60.7	76.5	22
	Web-Center	66.6	80.5	21
	Web-Quarter	68.1	81.7	22
	Bottom Flange	59.7	76.0	24

In addition to conducting tension coupon tests, cross-section dimensions of the W40×199 sections were measured. The various dimensions that were measured are shown in Figure 8.53. For each W40×199 section, each dimension shown in Figure 8.53 was measured at several points along the length of the girder, and then averaged. For web thickness measurement, an ultrasonic thickness measuring device was used. The measured dimensions are listed in Table 8.7. For reference, this table also lists the nominal dimensions of the W40×199 listed in the AISC Steel Construction Manual (AISC 2017).



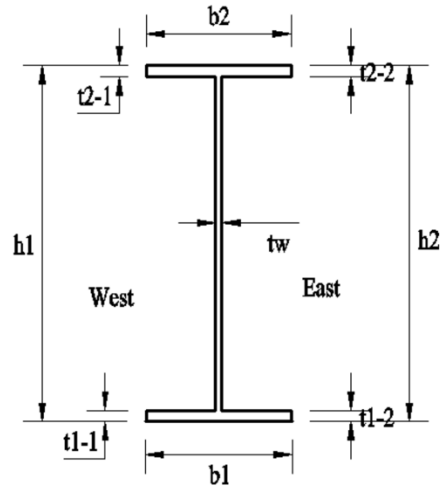


Figure 8.53 – Cross-Section Measurement Locations

Table 8.7 – Measured Cross-Section Dimensions

Location	W40x199 Cross-Section Dimensions (in.)				AISC Dimensions
	Beam Specimen No. 1		Beam Specimen No. 2		
	60' Section	40' Section	60' Section	40' Section	
tw	0.65	0.62	0.71	0.68	0.65
t1_1	1.04	1.05	1.06	1.06	1.07
t1_2	1.12	1.10	1.06	1.12	1.07
b1	15.75	15.75	15.88	15.69	15.8
t2_1	1.03	1.05	1.13	1.15	1.07
t2_2	1.07	1.06	1.13	1.25	1.07
b2	15.88	15.75	15.94	15.83	15.8
h1	38.75	38.88	38.88	38.94	38.7
h2	38.94	38.88	38.81	38.88	38.7

### 8.5.3. Concrete

The concrete used for Beam Specimen No. 1 and the cast-in-place concrete used for Beam Specimen No. 2 was specified as TxDOT Class S concrete with minimum 28-day strength of 4000 psi. The concrete used for the PCP panels of Beam Specimen No. 2 was TxDOT Class H concrete with minimum 28-day strength 5000 psi.

For the cast-in-place concrete, compressive cylinder tests were performed at 28 days after casting and on the day the single-span test on the beam specimen was completed. For the PCPs, cylinders were cast at the PCP fabrication plant and transported to Ferguson Lab for testing 28 days after casting and on the day the single span test on the beam specimen was completed. All

cylinder tests were conducted at Ferguson Lab and the cylinder ends were prepared by grinding. The cylinder compressive strength test results are listed in Table 8.8 and Table 8.9. The portions of the concrete deck cast with each truck is shown in Figure 8.47 and Figure 8.48. The PCPs cast from each truck are shown in Figure 8.43.

**Table 8.8 – Concrete Compressive Strength for Beam Specimen No. 1**

	Concrete Compressive Strength (psi)		
	Truck 1	Truck 2	Truck 3
28th day	5100	5917	4479
Test day	4951	5555	4817

**Table 8.9 – Concrete Compressive Strength for Beam Specimen No. 2**

	Concrete Compressive Strength (psi)				
	CIP		PCP		
	Truck 1	Truck 2	Truck 1	Truck 2	Truck 3
28th day	5572	5525	8647	9486	9196
Test day	6060	5840	8272	9242	/

### 8.5.4. Reinforcement

ASTM A615 Grade 60 #4 and #5 reinforcing bars were used in the beam specimens. Tensile tests were performed on samples of the reinforcing bars. For Beam Specimen No. 1, the rebar tensile tests were performed at the Ferguson Laboratory using a 220 kips MTS test machine. An extensometer with an 8" gauge length was attached to the rebar up through fracture.

For Beam Specimen No 1, the components of the deck reinforcement (see Figure 8.12 and Figure 8.13) are: approximately 30ft #4 longitudinal rebars in the south span (A), 40ft long #4 longitudinal rebar in the middle (B), transverse rebar (C), bottom layer of 30ft #4 longitudinal rebars in the north span (D), top layer of 30ft #4 longitudinal rebar in the north span (E) and #5 rebar in the negative moment region(F). Those reinforcement came from two different rebar orders: rebar order A, B, C, D were from the 1st order, and rebar E, F came from the 2nd order. Four types of rebar were tested: the 40ft long #4 longitudinal rebar in the middle(B), top layer of 30ft #4 longitudinal rebars in the north span (E), #5 reinforcement in the negative moment region (F) and transverse rebar(C). Typical tensile test stress strain curves are shown in Figure 8.54. Both static and dynamic yield stress values were obtained, whereas only dynamic ultimate strength values were measured. Test results are listed in Table 8.10. Three specimens were tested for each type of reinforcement and the value listed in the table is the average of three results. From Table 8.10, rebar B and C have similar yield strength and ultimate strength. Since rebar A

and D also came from the 1st order as for rebar B and C, they are expected to have similar properties as rebar B and C.

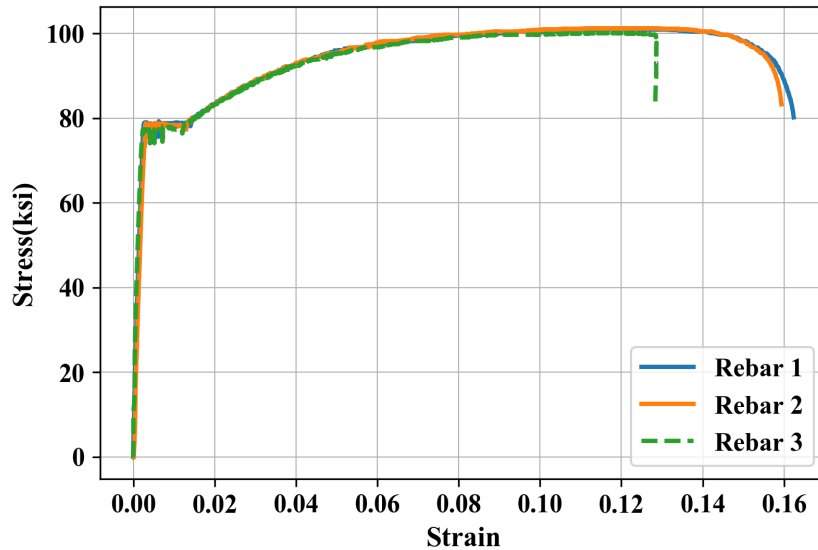


Figure 8.54 - Typical Reinforcement Tensile Test Results for Beam Specimen No. 1

Table 8.10 – Reinforcing Bar Tensile Test Results for Beam Specimen No. 1

Rebar	Static Yield Stress (ksi)	Dynamic Yield Stress (ksi)	Dynamic Ultimate Strength (ksi)	Strain at Fracture (%)
B	78.5	83.3	106.3	14.5
C	78.3	82.2	106.0	16.0
E	64.4	68.8	107.1	12.5
F	60.0	62.7	105.7	11.0

For Beam Specimen No. 2, tensile tests of the transverse and longitudinal rebars used in the CIP portion of the deck were conducted by Chicago Spectro Service Laboratory, Inc. Only dynamic values of yield stress and ultimate strength were measured. Results are listed in Table 8.11.

Table 8.11 - Reinforcing Bar Tensile Test Results for Beam Specimen No. 2

Rebar	Dynamic Yield Stress (ksi)	Dynamic Ultimate Strength (ksi)	Strain at Fracture (%)
Transverse #4	65.1	106.7	15.5
Longitudinal #4	62.8	104.2	15.3
Negative #5	63.0	103.8	16.1

## 8.6. Instrumentation

This section describes the instrumentation plan adopted for the beam tests. To capture the behavior of the composite girders during testing, applied forces and reactions, vertical deflections, end slip and slip at several shear stud locations, and strain on the steel section and reinforcement were measured. Cracks during the two-span serviceability tests were also carefully tracked and measured.

### 8.6.1. Applied Loads and Girder Reactions

Each loading tower included a 500 kip load cell to measure the forces applied to the test specimens. A load cell can be seen in Figure 8.21(b). To measure the girder reactions, the two end supports were each provided with two 200 kips load cells. The interior support used for the two-span tests were provided with two 750 kip load cells for Beam Specimen No. 1 and two 500 kip load cells for Beam Specimen No. 2. The load cells in the girder supports can be seen in the photos in Figure 8.20 and Figure 8.26.

### 8.6.2. Vertical deflection

String potentiometers (SP) were used to measure the vertical deflection of the composite girders. The locations of deflection measurements are shown in Figure 8.55. The same locations were used for Beam Test No. 1 and for Beam Test No. 2. The top drawing is the elevation view for the two-span test and the lower one is for the single-span test. In each figure short lines at the top of the girder represent shear studs. Red dashed lines are the center of the supports while gray dashed lines indicate tenth points along the length of the girder. Blue line above the middle support indicates additional reinforcement. For the two-span test, one SP was attached to the bottom surface of the steel girder beneath each loading tower. One was placed at the middle span and one was placed at the tenth point from the north support. For single-span test, one SP was placed at each quarter point and two were arranged at midspan of the specimen as shown in Figure 50.

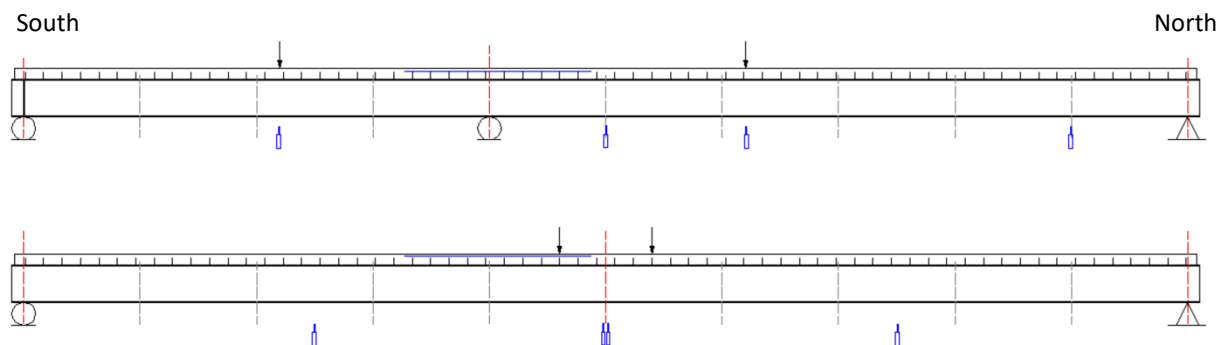


Figure 8.55 – Locations of Vertical Deflection Measurements  
(Top: Two-Span Test; Bottom: Single Span Test)



At quarter point

Two SPs at middle span

Figure 8.56 - String Potentiometers at the Quarter Point and at Midspan

### 8.6.3. Slip

The relative slip between the top flange of the steel girder and the bottom of the concrete deck was measured at various locations along the length of the girder. In total 15 linear potentiometers (LP) were used to measure slip along the length of the specimen. The LPs designated as LP1 to LP15 from south to north at approximately 10' intervals were attached to the specimen as shown in Figure 8.57. In this figure, the small red symbols represent linear potentiometers. At the other side of each LP location, one manual dial gauge was attached as a check on the LP readings. A manual dial gauge was also provided at each end of the specimen. Figure 8.58 provides photos of the linear potentiometers and dial gauges.

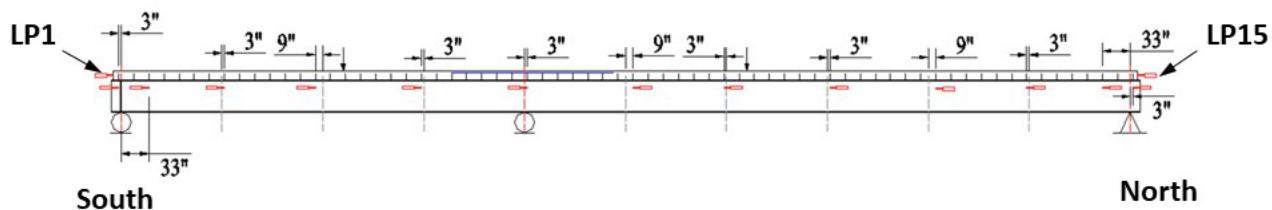


Figure 8.57 – Location of Slip Measurements



Linear Potentiometer

Dial gauge

LP & Dial gauge at end

Figure 8.58 – Linear Potentiometers and Dial Gauges Used to Measure Slip

### 8.6.4. Strain

Strain measurements were made to investigate various aspects of the behavior of the composite girders such as tracking the change of neutral axis location at various load levels and in both positive and negative moment regions. Strain measurements were also made in an attempt to estimate the shear force in specific studs by tracking strains at section in front of and behind the specific stud. There are mainly four strain gauge arrangements on cross sections which are depicted by colored lines in Figure 8.59.

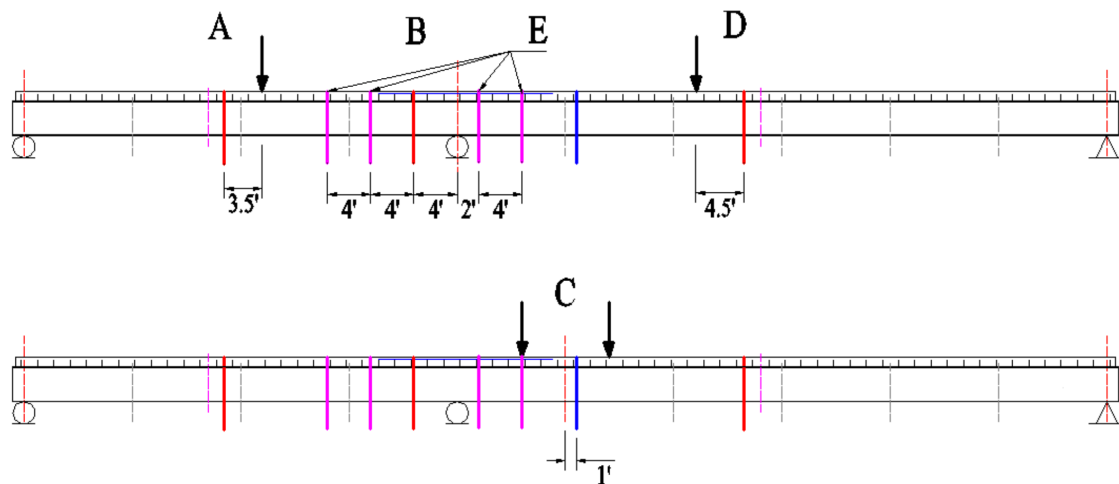


Figure 8.59 – Specimen Cross-Sections with Strain Gauges

For the positive moment region (A, C, D), the strain gauge arrangement is shown in Figure 8.60 where 6 strain gauges were attached to steel girder and 3 were attached to the longitudinal reinforcement. Sections A and D are 3.5' and 4.5' away from the loading towers to avoid local effects due to the concentrating loading.



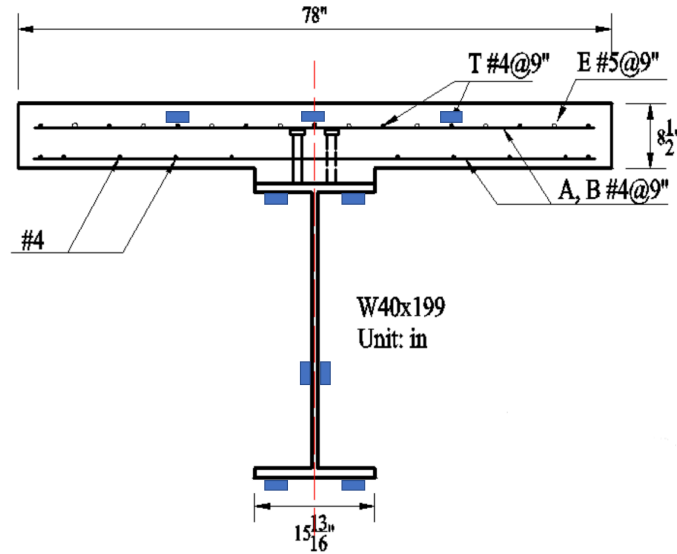


Figure 8.60 - Strain Gauge Locations in Positive Moment Region (Sections A, C, D)

For the negative moment region, there are two types of strain gauge sections: Section B and Section E. Section B had the most strain gauges to investigate the girder behavior and cracking behavior in the negative moment region. This section is 4' away from the interior support to avoid local effects caused by concentrated loading from the support. The strain gauge arrangement on Section B is shown in Figure 8.61. There were four strain gauges on the steel girder, 4 gauges on the transverse rebar, and one gauge on each longitudinal reinforcing bar (not shown in the figure).

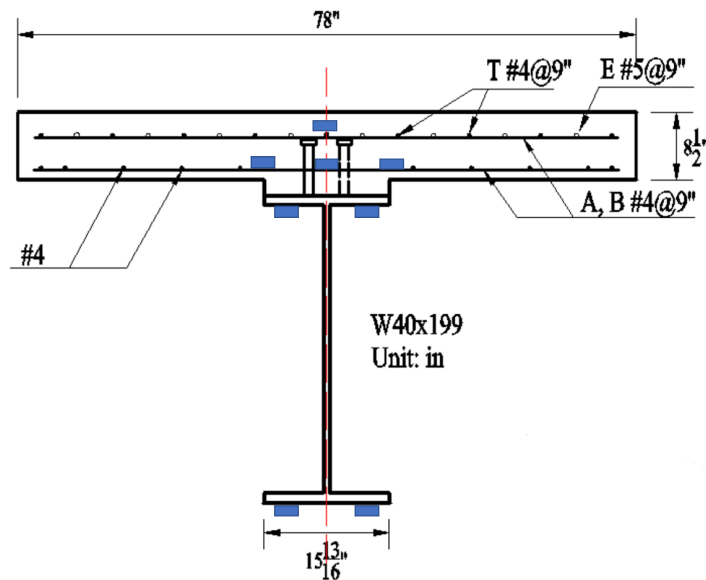


Figure 8.61 - Strain Gauge Locations in Negative Moment Region (Section B)



To track the change of the neutral axis location in the negative moment region, additional strain gauges were attached at Section E as shown in Figure 8.62. There are only 4 strain gauges on steel section to track neutral axis location.

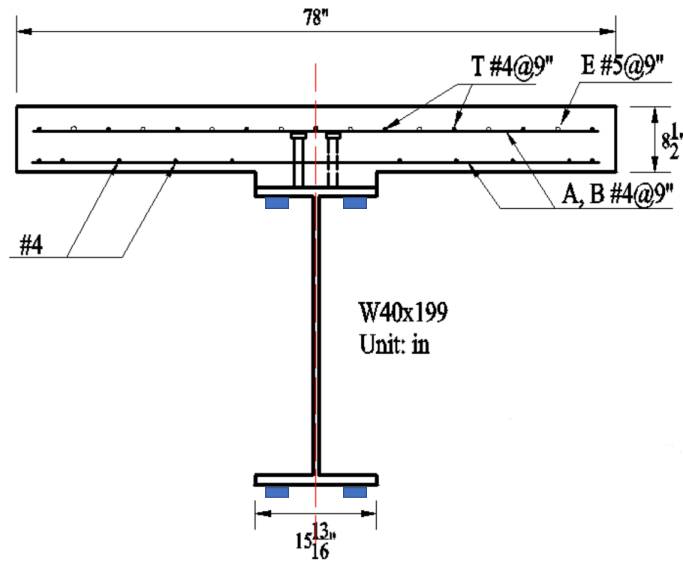


Figure 8.62 - Strain Gauge Locations in Negative Moment Region (Section E)

Strain gauges were also attached at the sections depicted as dashed pink lines in Figure 8.59 and are located Sections A and D. The location of gauges at these sections is shown in Figure 8.63. Together with the strain data obtained from Sections A and D, the strain data from these sections were intended to be used to estimate the shear force in selected studs. The strain data can be used to estimate the net axial force in the beam section as long as that section remains elastic. Knowing the net axial force in the beam on either side of a shear stud, the difference in the axial force values provides an estimate of the shear force in the stud.

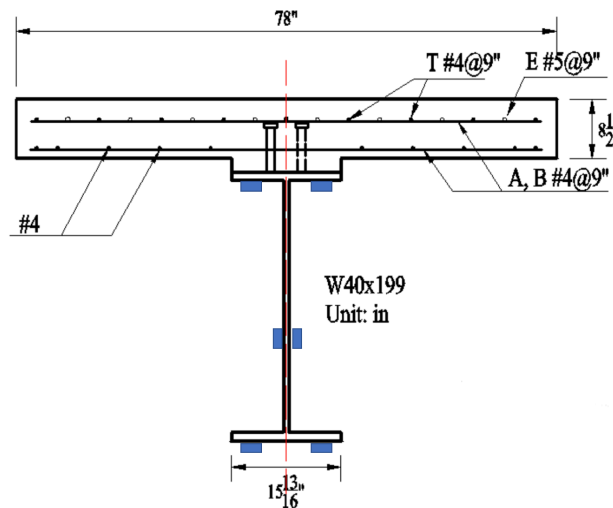


Figure 8.63 - Strain Gauge Locations to Estimate Shear Stud Forces

## 8.7. Loading Procedures

### 8.7.1. Two-Span Tests

The primary purpose of the two-span test was to evaluate deck cracking behavior in the negative moment region. The key issue of interest was whether the use of 1-1/8" studs promoted excessive deck cracking under service level loading. For the two-span tests, loads were applied on either side of the interior support to generate negative moment, as shown in Figure 8.1 and Figure 8.22. Throughout the two-span tests, equal loads were applied at the north and south load towers.

#### 8.7.1.1. Beam Specimen No. 1

For Beam Specimen No. 1, the sequence and magnitudes of the applied loads are listed in Table 8.12. Multiple cycles were applied at several of the load levels to evaluate crack growth under repeated load cycles. This table also lists the negative moment at the interior support for each load level.

**Table 8.12 – Loading Sequence for Two-Span Test of Beam Specimen No. 1**

Applied Load (per ram)	50k	150k	225k	300k	350k	400k	450k
Load cycles	7	7	7	3	3	1	1
Moment at Interior Support (k-ft)	-415	-1128	-1739	-2294	-2664	-3033	-3353

According to the 9<sup>th</sup> Ed. AASHTO (AASHTO 2020) Section 5.6.7 and Commentary C5.6.7, reinforcing bar stress should be controlled under 60% of yield at the service limit state to avoid excessive deck cracking. Assuming no concrete contribution to the section, the moment required to develop rebar stress 60% of yield is -2237 k·ft, which corresponds approximately to the applied load level of 300 kips per ram. Larger loads were also applied to evaluate deck cracking under these larger loads. The maximum load was limited to 450 kips per ram to avoid any permanent damage (other than deck cracking) that might affect the subsequent single span test.

#### 8.7.1.2. Beam Specimen No. 2

For Beam Specimen No. 1, the sequence and magnitudes of the applied loads are listed in Table 8.13. The loading sequence was the same as that used for Beam Specimen No. 1. However, for Beam Specimen No. 2, the applied loading did not exceed 300 kips per ram to further limit any possible damage to the specimen that might affect the subsequent single-span test of this specimen.

**Table 8.13 - Loading Sequence for Two-Span Test of Beam Specimen No. 2**

<b>Applied Load (per ram)</b>	<b>50k</b>	<b>150k</b>	<b>225k</b>	<b>300k</b>
Load cycles	7	7	7	3
Moment at Interior Support (k-ft)	-415	-1128	-1739	-2294

### 8.7.2. Single-Span Tests

For both beam specimens, after completion of the two-span tests, the interior support was removed, resulting in a single simple span of 100'. In this single span configuration, the specimens were tested to failure under positive moment. For the single-span tests, loads were applied at midspan. The load application points for Beam Specimen No.1 are shown in Figure 8.2 and Figure 8.23. Two load towers that were 8' apart were centered at midspan, resulting in an 8' length of the girder subject to uniform moment. The load application points for Beam Specimen No. 2 are shown in Figure 8.3 and Figure 8.24. For this test, a single load tower was placed at midspan. This change in loading arrangement was the result of limitations in available laboratory equipment in the time between tests on Beam Specimen No. 1 and Beam Specimen No. 2. It is not anticipated that this change in loading arrangement for the single-span tests had any significant impact on the results.

For the singles span tests, the load was increased to failure. For Beam Specimen No. 1, the specimen was loaded, unloaded and reloaded at lower load levels to evaluate deck cracking under positive moment and to evaluate repeatability of the load-deflection response. Essentially no decking was observed and the load-deflection response was found to be highly repeatable. Consequently, these repeated loads were not applied for Beam Specimen No. 2.

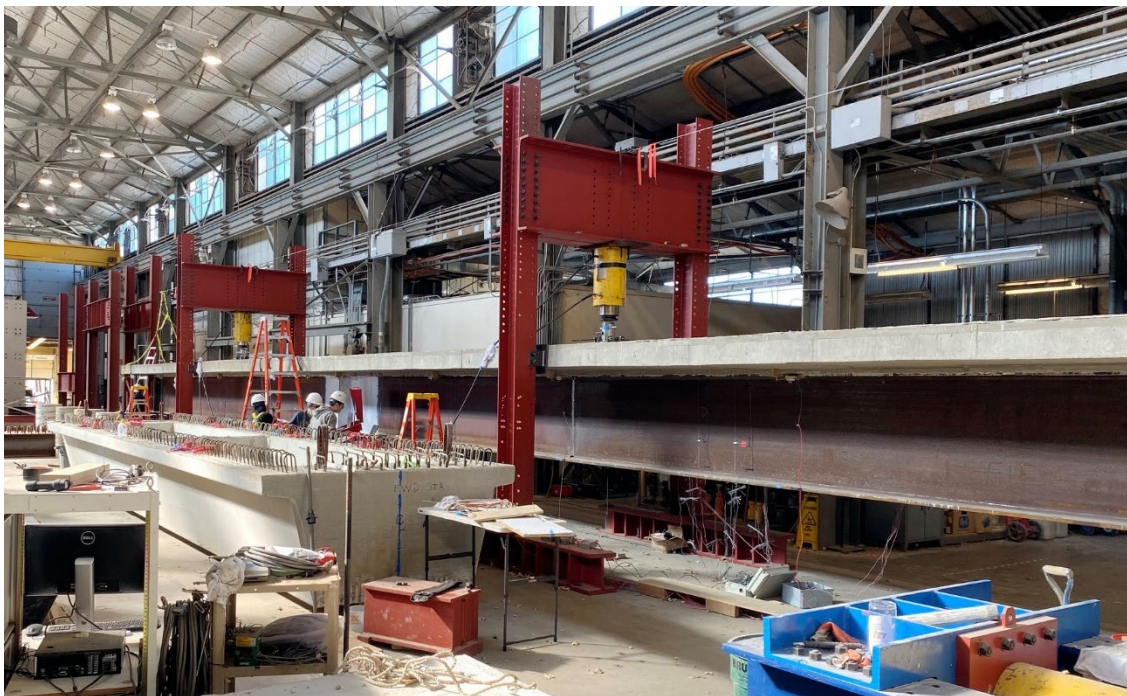
However, for both Beam Specimen No. 1 and 2, the specimen was periodically unloaded in the inelastic range of behavior. This is because the loading rams did not have enough stroke to take the specimens to failure. Typically, as the rams reached their stroke limit, the specimen was unloaded and exhibited permanent deflection. This permanent deflection provided additional space between the bottom of the ram and the top of the girder deck. This space was then filled with steel spacers (see Figure 8.21(b)) which allowed the application of additional load and deflection to the specimen. This procedure was repeated until failure of the specimen.

## 8.8. Beam Specimen No. 1 – Test Results, Analysis, and Discussion

---

### 8.8.1. Two-Span Test

The two-span test for Beam Specimen No. 1 used the loading arrangement shown in Figure 8.22 and the loading sequence listed in Table 8.12. Since the focus of this test was to evaluate deck cracking in the negative moment region around the interior support, the cracks were tracked in the region of the deck that extended 6' on either side of the interior support. The crack tracking region was painted with white primer as shown in Figure 8.65. The short dark lines at the edges of the slab mark every foot in the region and the dashed line at the center of the region is directly above the interior support. The locations of shear studs are marked by black dots. The crack distribution under different load levels is presented in Figure 8.66 to Figure 8.69. The location of cracks were marked with a felt pen line immediately next to the crack. The maximum crack width under each load level is listed in Table 8.14.



*Figure 8.64 – Beam Specimen No. 1 – Overall View During Two-Span Test*





Figure 8.65 – Beam Specimen No. 1 - Portion of Deck over Interior Support Prepared for Tracking Cracks

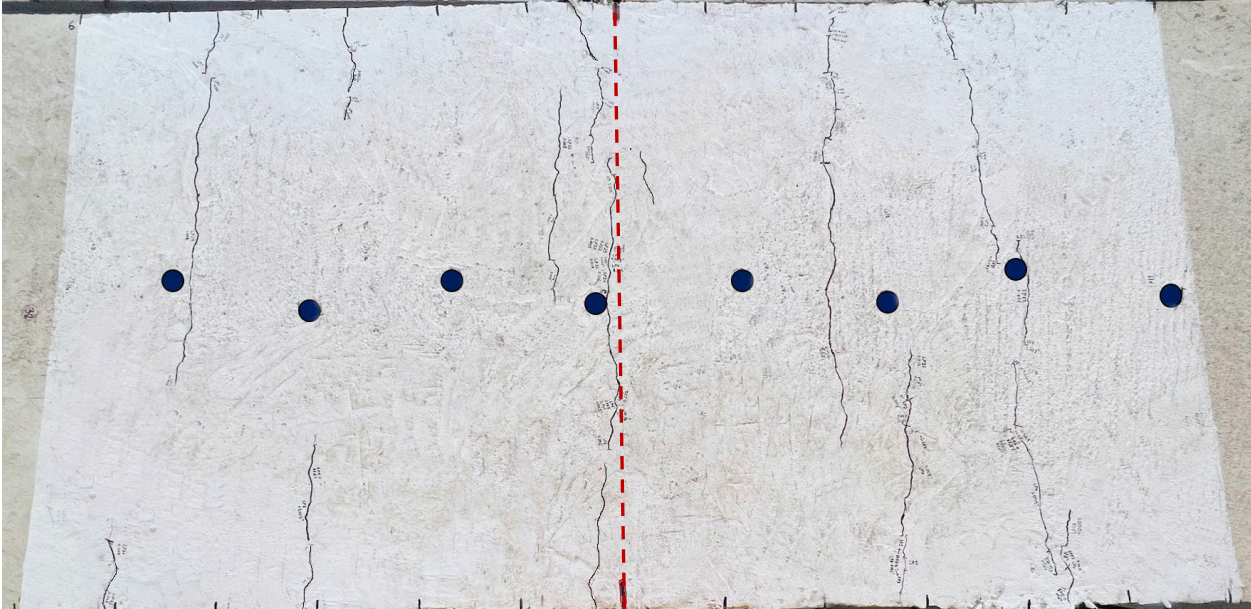
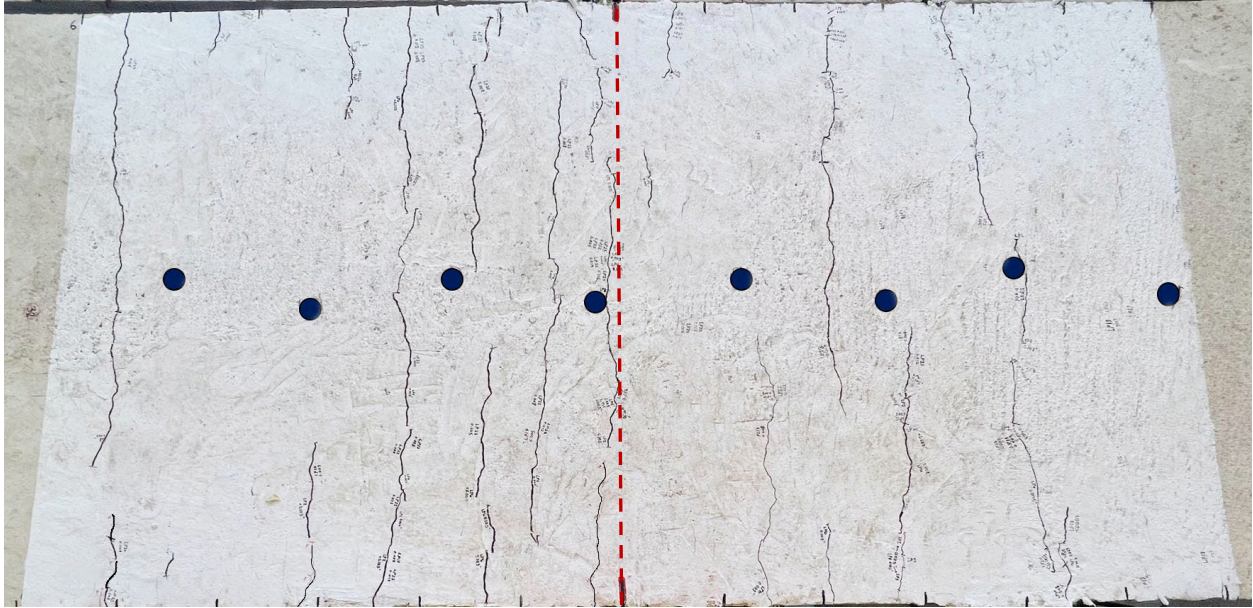
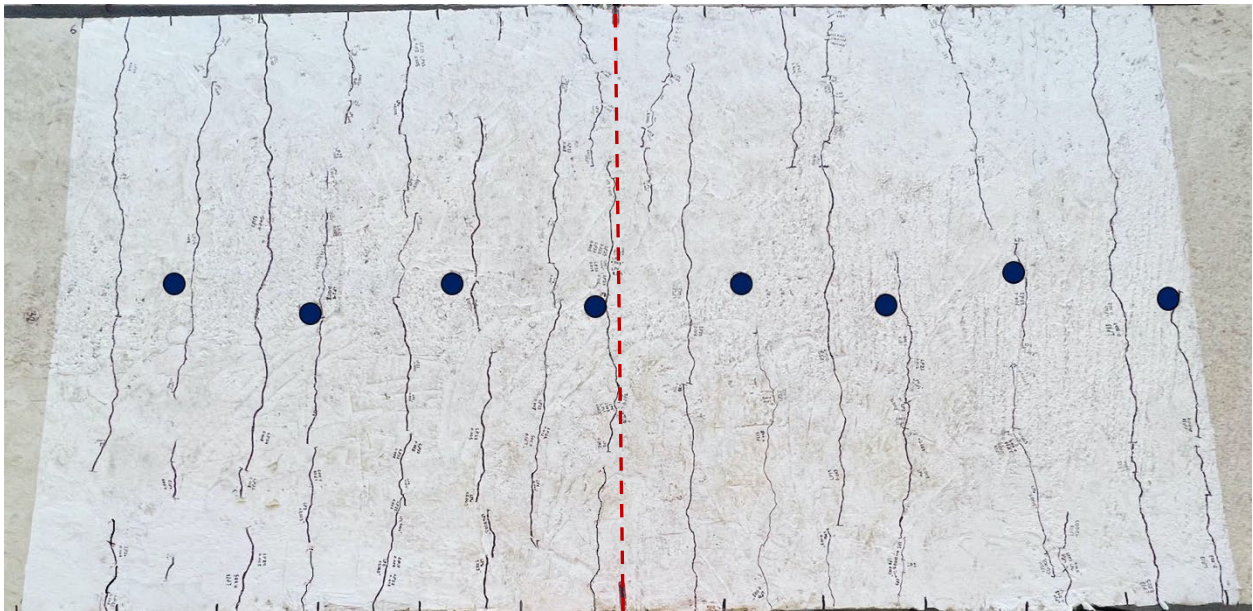


Figure 8.66 – Beam Specimen No. 1 - Crack Distribution after 7 Cycles of 50 kips Load per Ram



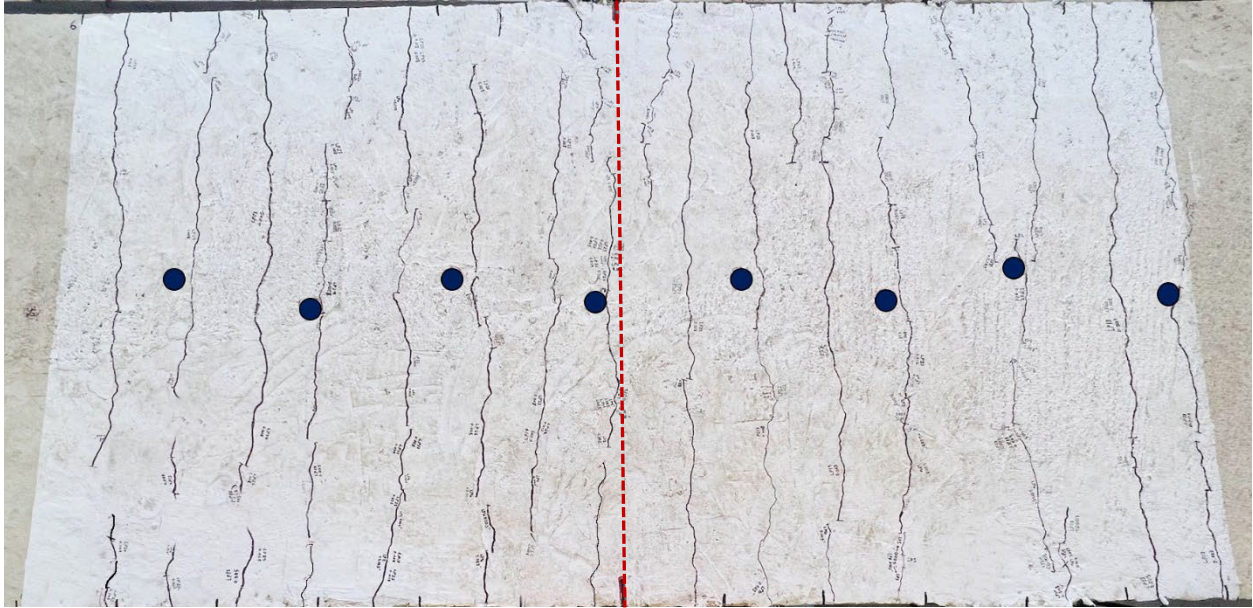


*Figure 8.67 - Beam Specimen No. 1 - Crack Distribution after 7 Cycles of 150 kips Load per Ram*

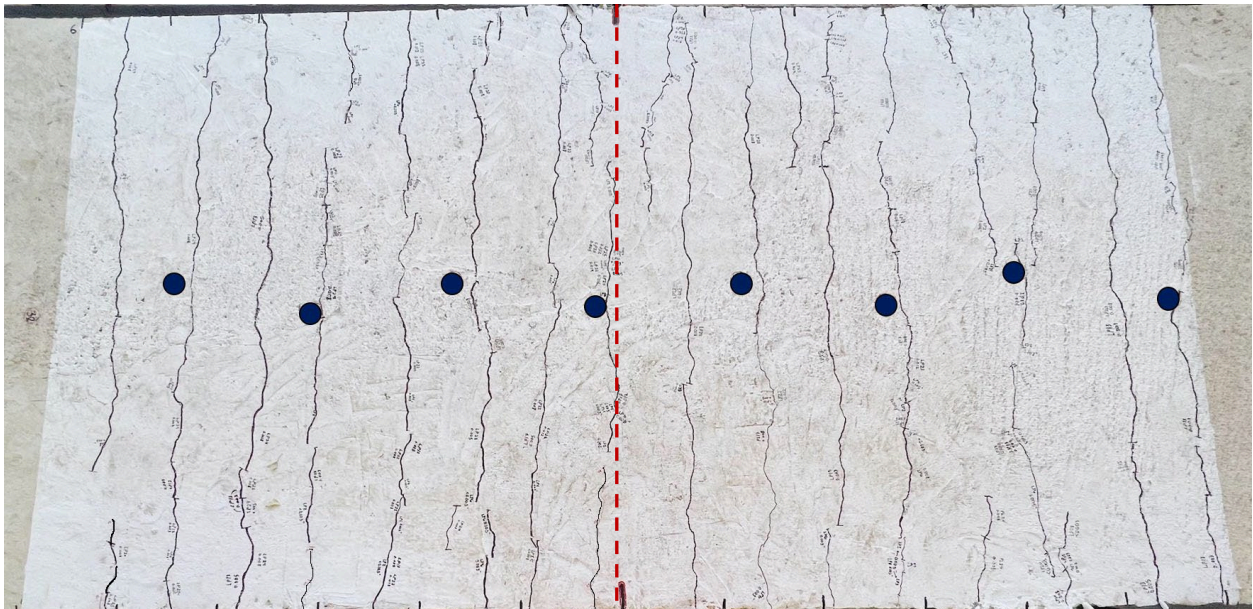


*Figure 8.68 - Beam Specimen No. 1 - Crack Distribution after 7 Cycles of 225 kips Load per Ram*





*Figure 8.69 - Beam Specimen No. 1 - Crack Distribution after 7 Cycles of 300 kips Load per Ram*



*Figure 8.70 – Beam Specimen No. 1 - Crack Distribution After Completion of Two-Span Test*

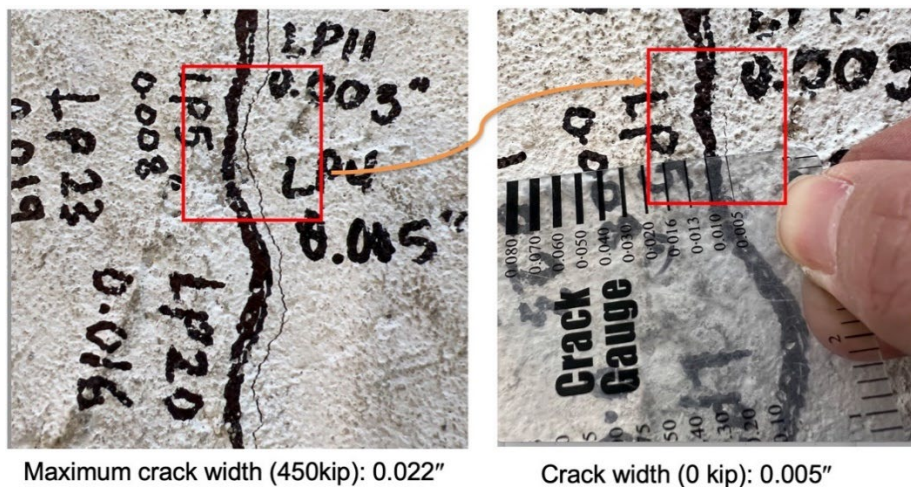


**Table 8.14 – Beam Specimen No. 1 - Maximum Crack Width under Different Load Levels**

Applied Load (per ram)	50k	150k	225k	300k	350k	400k	450k
Load cycles	7	7	7	3	3	1	1
Moment at Interior Support (k-ft)	-415	-1128	-1739	-2294	-2664	-3033	-3353
Max crack width (in)	0.008	0.008	0.013	0.016	0.016	0.02	0.025

Figure 8.70 shows the crack distribution after all the load cycles listed in Table 8.12 were applied. The crack spacing is from 8" to 12" and the average spacing is 9". As shown in Table 8.14 the maximum crack width under the 450 kips load per ram is 0.025" and it occurred directly over the interior support. After the unloading, the width of the crack at the same location reduced to 0.005". Figure 8.71 illustrate the maximum crack width under 450 kips load per ram and after removing this load. As noted earlier, 300 kips load per ram was the load that generates a stress in the longitudinal reinforcing of 60 percent of yield based on simplified hand calculation, and provides an estimate of the maximum permissible service load on the composite girder per AASHTO. The loading was continued beyond 300 kips per ram up to 450 kips per ram. In going beyond 300 kips per ram, there is almost no new crack formation and only a few crack extensions were observed with crack widths increasing from 0.016" to 0.025".

An important observation is that large transverse cracks were not generated at the shear studs. Further, no cracking was observed in the longitudinal direction of the deck indicating that the shear studs did not cause the development of splitting cracks along the length of the beam. Overall, these test results indicate that the 1-1/8" shear studs in a full-depth cast-in-place deck with reinforcing in accordance with AASHTO and TxDOT standards do not cause unusual or excessive deck cracking in negative moment regions under service loads.



**Figure 8.71 – Beam Specimen No. 1 – Maximum Crack Width under 450 kips per Ram and After Unloading**

## 8.8.2. Single-Span Test

After completion of the two-span test, the interior support was removed to provide for a single simply supported span of 100'. Two loading towers were arranged symmetrically around midspan and the spacing between the two loading towers was 8' as shown in Figure 8.23. Figure 8.72 is a photo of the specimen prior to the start of the single-span test.

### 8.8.2.1. Overall Response

A plot of the total applied load versus midspan deflection is shown in Figure 8.73. The total applied load on this plot is the sum of the applied loads at the two load towers. The load at each tower was essentially identical throughout the test. The midspan deflection in the plot is the average of the string potentiometers (SP2 and SP3) attached to the bottom flange of the steel girder at midspan.

The initial cycles at 50 kips, 100 kips and 150 kips total load were repeated several times to examine the deck for cracking under these lower level loads and to evaluate the repeatability of the load-deflection response. No cracks were observed in the deck at these load levels and the load-deflection response was found highly repeatable, indicating no development of damage in the specimen under these repeated loads. At total loads above 100 kips, the specimen was periodically unloaded, as seen in Figure 8.73. As described earlier, this was done because the hydraulic rams did not have adequate stroke to accommodate the large deflections of this specimen. After entering the inelastic range of behavior, when the specimen was unloaded there was a permanent deflection. The space beneath the ram provided by this permanent deflection was filled with steel spacers, allowing the specimen to be reloaded to larger deflections. This procedure was repeated several times until failure of the specimen. The plot in Figure 8.73 shows a short vertical drop in load just below 12" of displacement at about 220 kips of load. This anomaly in the load-deflection curve was the result of some difficulties encountered controlling the load at this point, and does not reflect the actual response of the specimen.

From the load-deflection plot, it can be seen that the specimen began exhibiting significant inelastic behavior beyond about 150 kips of total load. Beyond this, the specimen exhibited excellent ductility, showing very large inelastic deformations with continued loading. The peak total load sustained by the specimen was 235 kips. The specimen failed when the midspan deflection was approximately 18.5", showing a sudden drop in load capacity accompanied by a very loud sound corresponding to fracture of shear studs. After complete unloading, the specimen showed a permanent midspan deflection of about 15". A photo of the specimen after completion of testing and unloading is shown in Figure 8.74, where the large permanent deflection is apparent.



Figure 8.72 – Beam Specimen No. 1 Prior to Single-Span Test

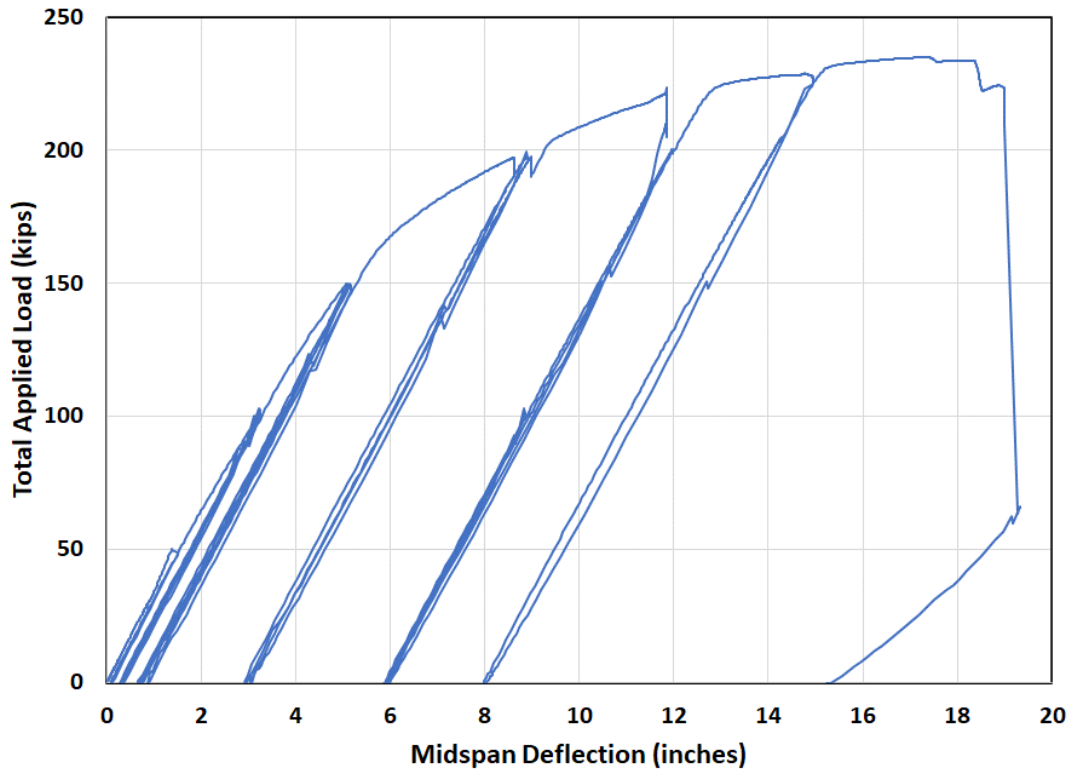


Figure 8.73 – Beam Specimen No. 1 – Total Load vs. Midspan Deflection





*Figure 8.74 – Beam Specimen No. 1 After Completion of Single-Span Test*

### **8.8.2.2. Failure Mode**

The failure mode for Beam Specimen No. 1 was the fracture of all shear studs over the south half of the beam. Since Beam Specimen No. 1 was designed as partially composite, shear stud failure was the expected failure mode for the composite beam specimen. Figure 8.75 is a photo of the south half of the beam after the concrete deck was removed. On the north half of the beam, all shear studs were still intact and attached to the beam flange after completion of testing. Figure 8.76 is a photo of shear studs on the north half of the beam after removal of the concrete.



*Figure 8.75 – Beam Specimen No. 1 – View of Top Flange for South Half of the Girder After Removal of Concrete Deck*



*Figure 8.76 – Beam Specimen No. 1 – Shear Studs on North Half of Beam After Removal of Concrete Deck*

After the removal of the concrete slab, the failure mode of each fractured shear stud in the south span was studied and documented, including the fractured part on the steel flange, the fractured part left inside the concrete slab, macro-etch tests of selected studs, and the shape of fractured studs. The observed failure modes were classified into 5 categories, as shown in Table 8.15. This table also lists the number of studs in each category and the corresponding percentage of fractured studs exhibiting each mode. Some of the failure mode classifications in Table 8.15 correspond to terminology used in ISO 14555 (ISO 2017b). Figure 8.77 presents representative photos of each stud failure mode observed in Beam Specimen No. 1.

**Table 8.15 – Shear Stud Failure Modes – Beam Specimen No 1**

Failure mode	Quantity	Percentage (%)
Shank failure	15	40.5
Bright spot	4	10.8
Flat fracture	5	13.5
Deep fracture	8	21.6
Wide crater	5	13.5

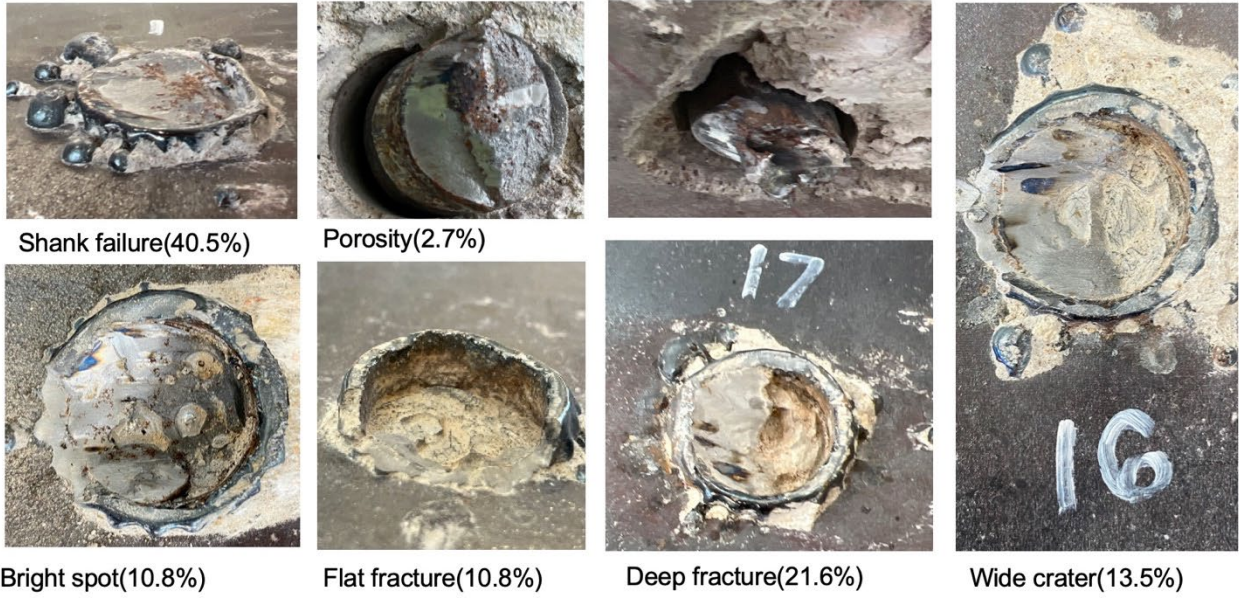


Figure 8.77 – Photos of Shear Stud Failure Modes for Beam Specimen No. 1

Macro etch tests were also performed on cross-sections cut through the weld of fractured shear studs, for the portion of the stud or weld left on the steel girder. These results are shown in Figure 8.78 to Figure 8.82.

Shank failure(40.5%)

• Weld collar height 5/16" , width 1-5/8"

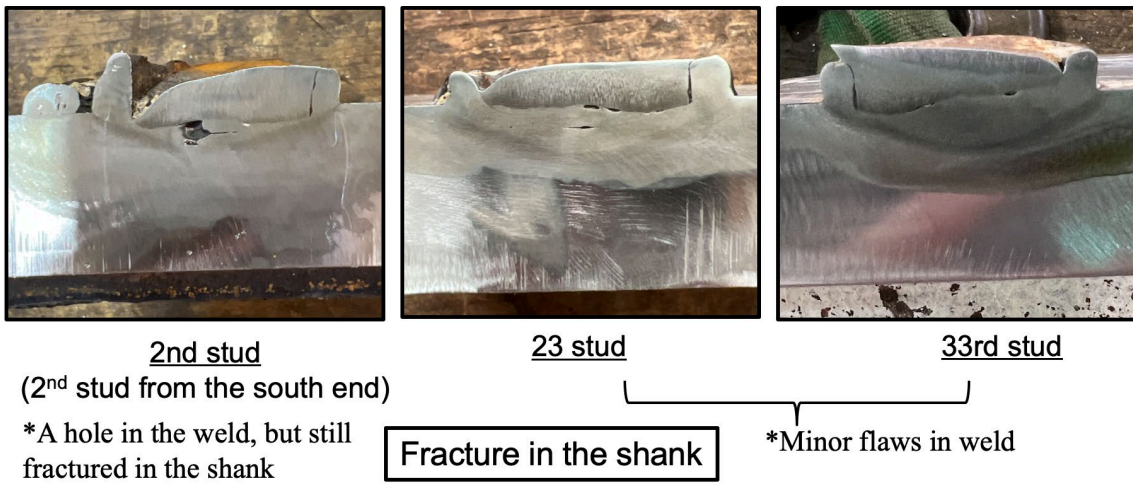


Figure 8.78 – Macro-Etch Test Results for Shank Failure Mode



Bright spot (10.8%)

Fracture between heat affected zone(HAZ) & weld



13th stud

24th stud

Figure 8.79 - Macro-Etch Test Results for Bright Spot Failure Mode

Flat fracture(13.5%)

Fracture in the weld or in HAZ



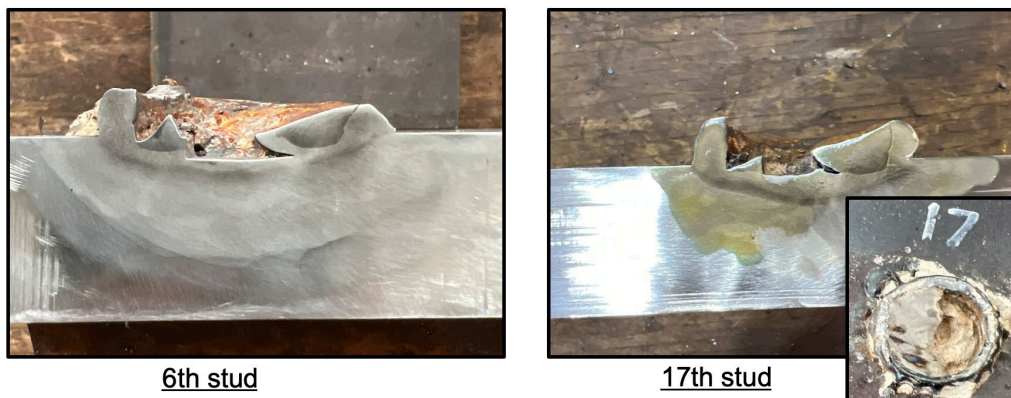
7th stud

15th stud

Figure 8.80 – Macro-Etch Test Results for Flat Fracture Failure Mode

Deep fracture(21.6%)

Fracture in the weld or between HAZ and weld



6th stud

17th stud

Figure 8.81 – Macro-Etch Test Results for Deep Fracture Failure Mode

Wide crater(13.5%)



Fracture in the weld or between HAZ and weld 16th stud

Figure 8.82 – Macro-Etch Test Results for Wide Crater Failure Mode

Selected fractured shear studs in the south half span were cored from the concrete slab and removed from the slab. The deformed shape of those studs is shown in Figure 8.83. From left to right in both figures are 1st, 2nd, 8th, 14th, 35th, and 36th stud from south end of the specimen. The 1st and 2nd studs are the first two studs at the south end of the beam and exhibit the largest deformation. It is also observed that the deformation is mainly concentrated in a short region near the base of the stud, with the remainder of the stud remaining almost straight. The deformed shapes reflect localized shear deformation at the base of the stud, with little evidence of bending.



Figure 8.83 – Deformed Shape of Fractured Shear Studs

From the above observations of stud failure modes, shank failure was the most common failure modes, occurring in approximately 41-percent of the fractured studs. All three of the shank failures selected for macro-etching exhibited some flaws/holes inside the weld indicating that minor flaws/holes inside the weld will not significantly reduce stud strength. Further, the macro-etch sections for studs that fractured in the weld have intact sections, suggesting that weld quality for studs with other failure modes should be similar or better than the studs with shank failure

that had flaws in the welds. Based on the stud welding investigation in Chapter 4, welded studs that failed the 90° bend test typically showed severe porosity or bright spots inside the weld and flaws on the macro-etch sections. Therefore, it is believed that inadequate weld quality did not likely adversely affect stud performance in Beam Specimen No. 1. Rather, it is expected that the studs fractured as a result of reaching their shear fracture strength.

### 8.8.2.3. Slip

The relative slip between the concrete slab and the steel girder was measured using linear potentiometers (LPs) at the girder ends and at selected locations along the length of the girder, as shown in Figure 8.57. Table 8.16 lists the slip measured at each LP just prior to failure of the specimen, when the load was at its peak value and the midspan deflection was approximately 18". The missing slip measurements in this table correspond to LPs that malfunctioned during the test.

**Table 8.16 – Slip Just Prior to Specimen Failure**

Linear Potentiometer	Slip (inches)
1	0.41
2	0.40
3	/
4	0.43
5	0.45
6	0.42
7	0.28
8	0.02
9	0.09
10	0.10
11	0.09
12	0.08
13	0.06
14	/
15	0.06

From the data in Table 8.16, the slip at the south half span (LP1 to LP7) is larger than the slip at the north half span (LP9 to LP15), and the midspan slip (LP8) has the lowest value of 0.02". The maximum slip of 0.45" occurred at the LP5 location and the slip values in the 30ft region (LP1 to LP6) at the south end are similar and are at or above 0.4". A typical load slip curve, taken at LP5, is shown in Figure 8.84. The slip data from this test indicates that the 1-1/8" studs in this specimen had a slip capacity of approximately 0.4". This is similar to the slip capacities exhibited by the 1-1/8" studs in the static push-out tests in Chapter 5. As noted in Chapter 5, the slip capacity of the 1-1/8" studs was typically larger than the slip capacities exhibited by 7/8"



studs, and also exceeds the minimum specified slip capacity of 0.26" in Eurocode 4 (CEN 2004). Thus, the combined evidence from the static push-out tests and from Beam Specimen No. 1 indicates that 1-1/8" studs have adequate slip capacity for use in composite steel bridge girders.

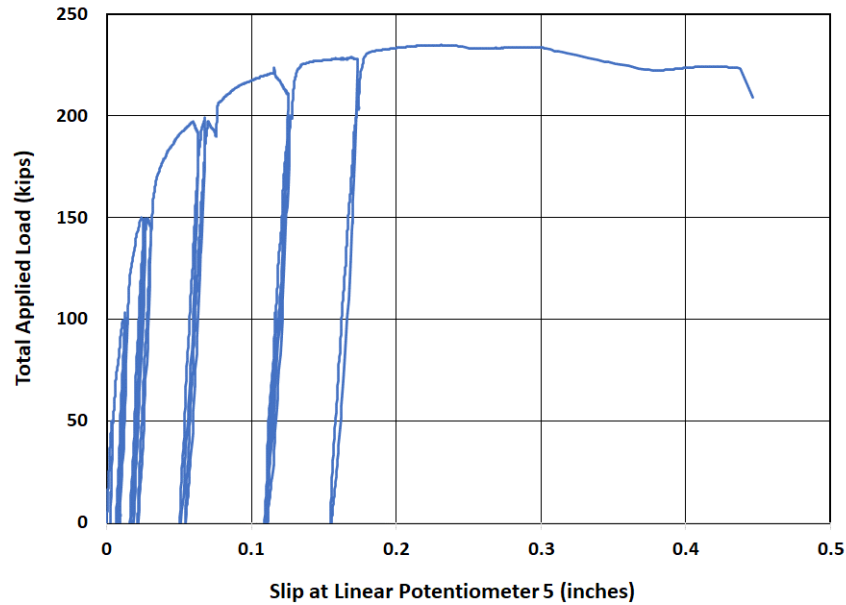


Figure 8.84 - Typical Load Slip Curve for Beam Specimen No. 1 (LP5)

#### 8.8.2.4. Composite Girder Flexural Capacity

This section discusses the maximum moment sustained by Beam Specimen No. 1 and compares this to values computed for full composite flexural strength. The maximum moment sustained by the specimen had two components: the moment due to self-weight and the moment due to the loads applied by the rams. These values are listed in Table 8.17. The self-weight of the specimen, including the steel girder and concrete deck, was estimated at 924 lbs./ft. For the 100' long simply support beam, this results in a self-weight moment of 1155 kip-ft. The peak load applied by the loading rams was a total of 235 kips or 117.5 kips per load tower. The moment due to this applied loading is 5405 kip-ft. The total moment sustained by Beam Specimen No. 1 is the sum of these, which is 6560 kip-ft.

Table 8.17 – Maximum Moment Sustained by Beam Specimen No. 1

Component of Moment	Moment
Moment due to Self-Weight	1155 kip-ft
Moment Due to Maximum Loads Applied by Rams	5405 kip-ft
Total Moment	6560 kip-ft

For comparison, the plastic moment capacity was computed for full composite behavior of Beam Specimen No. 1. The calculations were done using standard composite beam cross-sectional

analysis as specified in AASHTO (AASHTO 2020) and in AISC (AISC 2022) for composite beam design. Two different calculations were done; one using measured material properties and section dimensions and the second using nominal material properties and section dimensions. Results are listed in Table 8.18.

For the calculation using measured properties, the dynamic yield stress of the top flange, web, and bottom flange of the 60' long section of W40×199 listed in Table 8.5 as well as the measured cross-section dimensions listed in Table 8.7 were used. The yield stress values and dimensions for the 60' long section of the W40×199 were used since this was the section at the location of maximum moment in the beam. For concrete compressive strength, the results of the cylinder tests run on the same day as the single-span test were used, as listed in Table 8.8. The average of the Truck 1 and Truck 2 strength were used, since concrete from both trucks were used in the maximum moment region of the beam.

For the calculation using nominal properties,  $F_y = 50$  ksi was used for the W40×199, and  $f_c = 4$  ksi was used for the concrete. The cross-section dimensions of the W40×199 were based on the handbook dimensions listed in the AISC Steel Construction Manual.

The actual moment of 6560 kip-ft sustained by the Beam Specimen No. 1 is approximately 90-percent of the full composite strength of 7245 kip-ft based on measured properties. As described earlier, Beam Specimen No. 1 was intentionally designed as partially composite, i.e., designed not to develop the full composite strength of the girder. For full composite design, the flexural strength of the composite girder is controlled by the strength of the concrete slab and the steel girder, not by the strength of the shear studs. On the other hand, for partial composite design, the flexural strength of the composite girder is controlled by the strength of the steel girder and by the strength and slip capacity of the shear studs. Thus, Beam Specimen No. 1 was designed as partially composite to ensure that shear stud failure would occur in the test, to evaluate the strength and slip capacity of the studs.

**Table 8.18 – Computed Full Composite Moment Capacity of Beam Specimen No. 1**

Basis for Plastic Moment Capacity Calculation	Plastic Moment Capacity for Full Composite Behavior
Measured Material Properties and Measured W40x199 Section Dimensions	7245 kip-ft
Nominal Material Properties and Nominal W40x199 Section Dimensions	5965 kip-ft

### 8.8.2.5. Shear stud strength

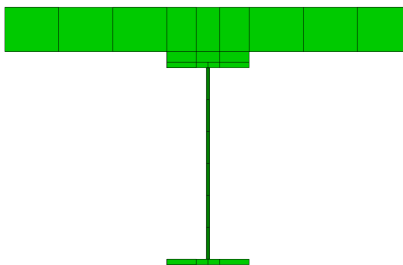
To estimate the strength of the shear studs in Beam Specimen No. 1, a finite element (FE) model of the specimen was created using the software Abaqus. The concrete deck and the W40×199 section were modeled using 4-node shell elements, designated as “S4” in Abaqus. The shell

elements used for the concrete deck incorporated the reinforcing bars. The steel was modeled as an elastic-plastic material. The concrete stress-strain curve in compression was represented by a modified Hognestad (1951) model. In tension, the concrete model included tension stiffening. For concrete and steel, material strength values in the model were chosen on measured material properties rather than nominal properties.

The Abaqus CARTESIAN element was used to model the shear studs. This element acts as a nonlinear spring, connection the top of the steel flange to the bottom of the concrete deck. The load-deflection response of this element can be input to represent the load-slip relationship at a shear stud. The load-slip relationship input into the CARTESIAN element is the relationship developed by Ollgaard et al. (1971). The model did not include a representation of shear stud fracture. However, the model includes a plateau in the load-slip relationship at a selected level that represents the shear stud strength.

To estimate the strength of the shear studs in Beam Specimen No. 1, a trial and error process was used. Different models were run with different assumptions of shear stud strength. For each model, the self-weight of the specimen was first applied. Then, load was applied at the location of the two loading towers and increased until a plateau was reached in the overall load-deflection response of the model or the analysis stopped due to lack of convergence. The process was repeated using different value of shear stud strength until the predicted load-deflection response reasonably matched to experimental response. Figure 8.85 shows a cross-section of the FE model, with the shell elements extruded to show their thickness. Figure 8.86 shows a three-dimensional view of the model under load.

The trial and error process described above resulted in a good match between the predicted and experimental load-deflection responses for an assumed shear stud strength of 65 kips. Figure 8.87 plots the load-deflection response for the FE analysis assuming a 65 kip shear stud strength and the experimental result. As is apparent, the match is quite close. An attempt was made to derive shear stud forces from strain gauge data from the beam, however the results were inconsistent and inconclusive. Consequently, it is believed that the shear stud strength estimate of 65 kips from the FE analysis is the most reliable estimate of shear stud strength in Beam Specimen No. 1.



*Figure 8.85 – Cross-Section of FE Model of Beam Specimen No. 1*



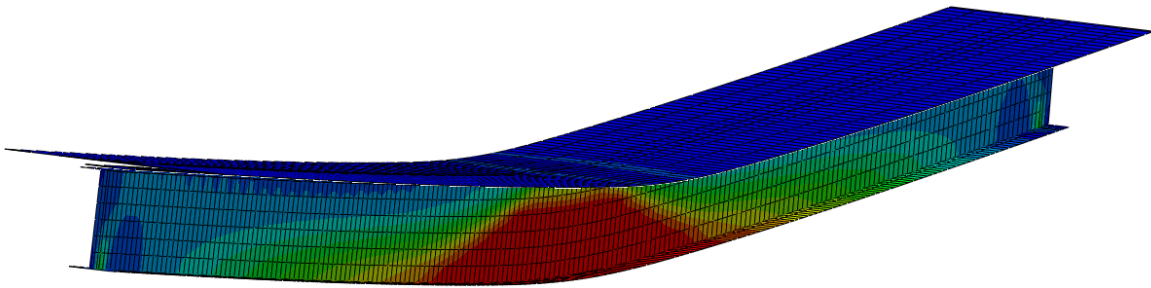


Figure 8.86 – FE Model of Beam Specimen No. 1 Under Load

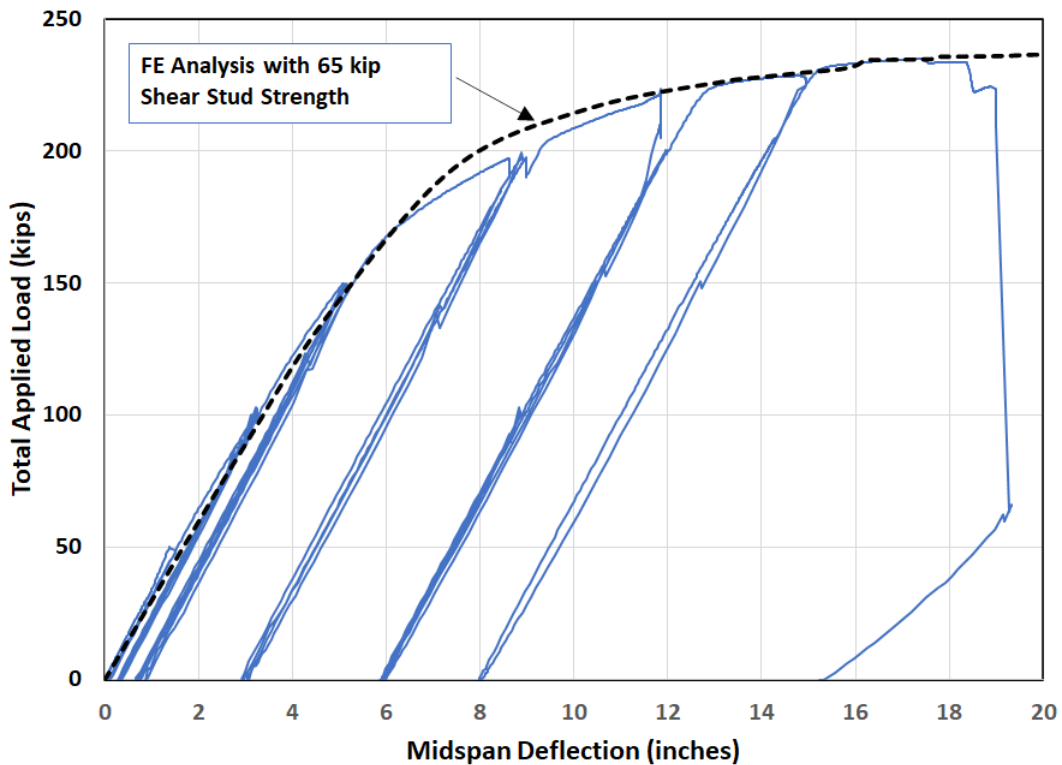


Figure 8.87 – FE and Experimental Load-Deflection Responses for Beam Specimen No. 1

Table 8.19 lists the AASHTO factored shear resistance for the 1-1/8" studs in Beam Specimen No. 1. Values are included both for the 9<sup>th</sup> Ed. AASHTO and the proposed 10<sup>th</sup> Ed. AASHTO stud strength equations. Further, for each edition of AASHTO, factored shear stud strength was computed using both nominal material properties and measured material properties. Concrete modulus, needed for the 9<sup>th</sup> Ed. AASHTO stud strength equation, was computed using Eq. 5.4.2.4-1 in the 9<sup>th</sup> Ed. AASHTO. The stud factored shear resistance for nominal material properties used  $f_c = 4$  ksi for the concrete and  $F_u = 60$  ksi for the stud. The stud factored shear

resistance for measured properties used  $f_c = 5.25$  ksi (average of Trucks 1 and 2 in Table 8.8) and  $F_u = 90.9$  ksi (see Table 8.3) for the stud. The estimated actual shear strength of 65 kips for the studs in Beam Specimen No. 1 exceed all of the values in Table 8.19, although the values are quite close when using measured material properties.

**Table 8.19 – AASHTO Factored Shear Resistance for 1-1/8" Studs in Beam Specimen No. 1**

AASHTO Edition	Material Properties	AASHTO Factored Shear Connector Resistance
9 <sup>th</sup> Ed.	Nominal	50.7 kips
	Measured	63.9 kips
Proposed 10 <sup>th</sup> Ed.	Nominal	41.7 kips
	Measured	63.2 kips

## 8.9. Beam Specimen No. 2 – Test Results, Analysis and Discussion

---

### 8.9.1. Two-Span Test

The two-span test for Beam Specimen No. 2 used the same loading arrangement as for Beam Specimen No. 1. The loading sequence for Beam Specimen No. 2, listed in Table 8.13, was the same as for Beam Specimen No. 1, except that loading did not extend beyond 300 kips per ram. Cracks were tracked in the region of the deck that extended 6' on either side of the interior support. The crack tracking region was painted with white primer as shown in Figure 8.89. The short dark lines at the edges of the slab mark every foot in the region and the dashed line at the center of the region is directly above the interior support. The locations of shear studs are marked by black dots. The crack distribution under different load levels is presented in Figure 8.90 to Figure 8.93. The location of cracks were marked with a felt pen line immediately next to the crack. Figure 8.94 shows the crack distribution at the completion of the two-span test. Superimposed on this figure are lines that show the boundaries of the PCPs. The maximum crack width under each load level is listed in Table 8.20. As discussed earlier, 300 kips load per ram was the load that generates a stress in the longitudinal reinforcing of 60 percent of yield based on simplified hand calculation, and provides an estimate of the maximum permissible service load on the composite girder per AASHTO.

As with Beam Specimen No. 1, the cracks in Beam Specimen No. 2 were well distributed and with small widths. It appears that large transverse cracks were not generated by the shear studs, and little cracking was observed in the longitudinal direction of the deck indicating that the shear studs did not cause splitting cracks along the length of the beam. Further, there was no evidence of any significant reflective cracking at the edges of the PCPs. The crack widths in Beam Specimen No. 2 were very similar to those in Beam Specimen No. 1. Overall, these test results

indicate that the 1-1/8" shear studs in a deck constructed with PCPs do not cause unusual or excessive deck cracking in negative moment regions under service loads.

As discussed in Section 8.2.2, in the negative moment region of the Beam Specimen No. 2, the reinforcement ratio was 1.18% of the CIP portion of the deck based on recommendations from TxDOT Research Project 0-6909 (Ge, et al. 2021). Since the cracking in the negative moment region of Beam Specimen No. 2 (deck with PCPs) was very similar to that in Beam Specimen No. 1 (full-depth cast-in-place deck), these test results provide data that support the deck reinforcing recommendations from TxDOT Research Project 0-6909.



Figure 8.88 – Beam Specimen No. 2 Prior to Two-Span Test

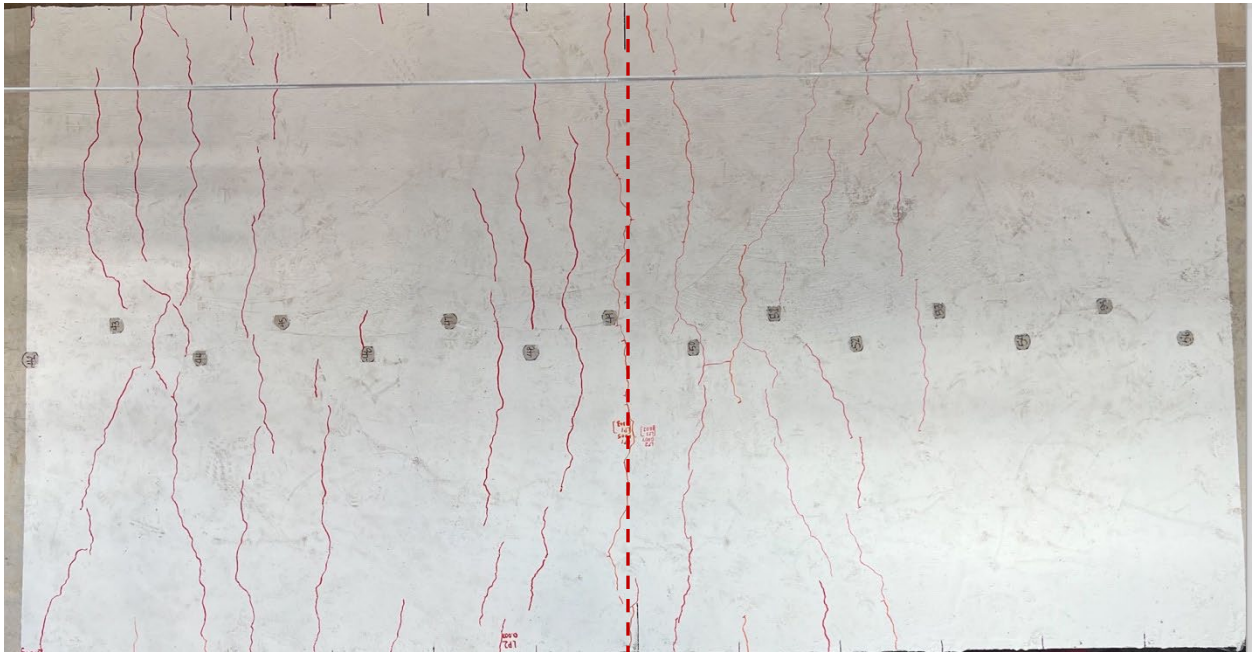


Figure 8.89 - Beam Specimen No. 2 - Portion of Deck over Interior Support Prepared for Tracking Cracks

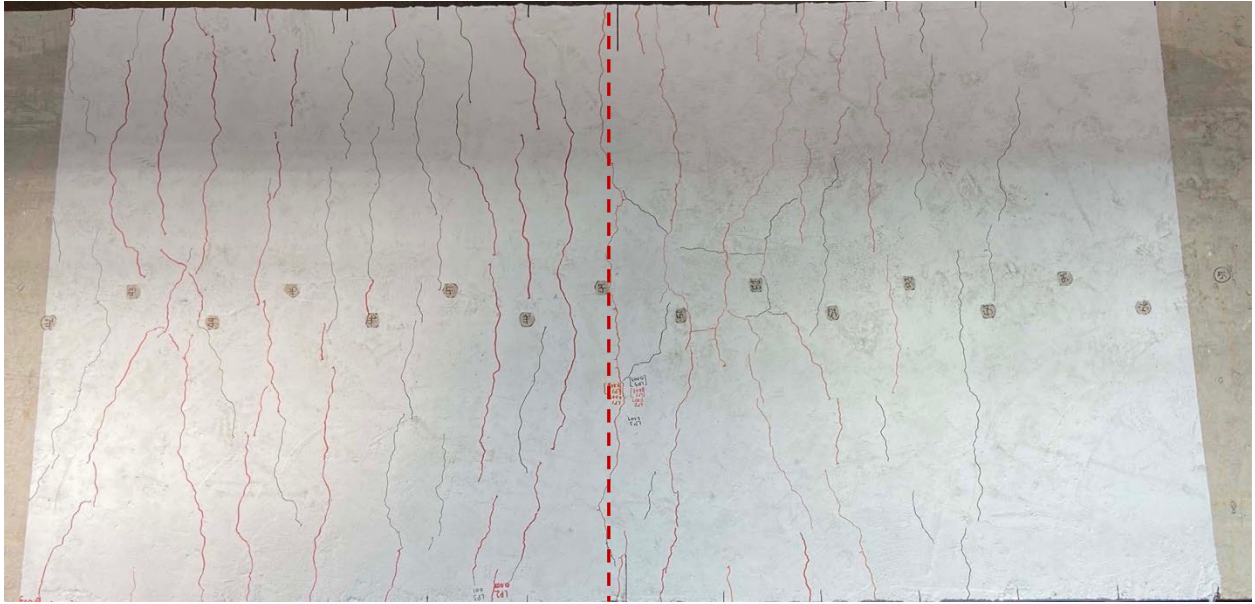




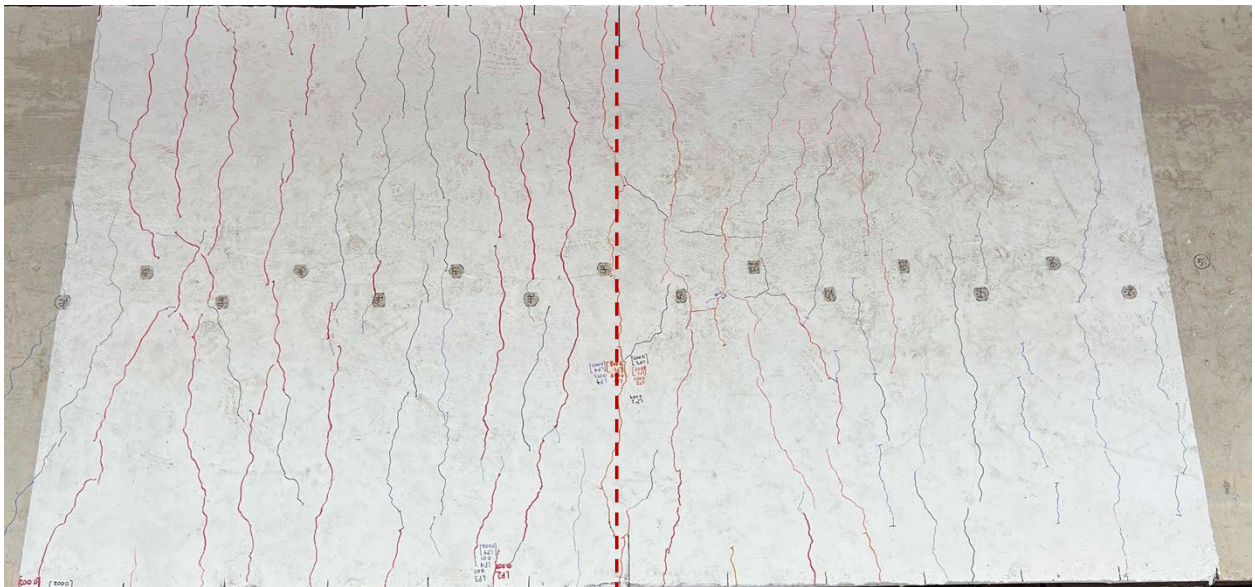
*Figure 8.90 – Beam Specimen No. 2 – Crack Distribution after 7 Cycles of 50 kips Load per Ram*



*Figure 8.91 - Beam Specimen No. 2 - Crack Distribution after 7 Cycles of 150 kips Load per Ram*



*Figure 8.92 - Beam Specimen No. 2 - Crack Distribution after 7 Cycles of 225 kips Load per Ram*



*Figure 8.93 - Beam Specimen No. 2 - Crack Distribution after 7 Cycles of 300 kips Load per Ram*





Figure 8.94 - Beam Specimen No. 2 - Crack Distribution After Completion of Two-Span Test and Boundaries of the PCPs

Table 8.20 – Beam Specimen No. 2 – Maximum Crack Width under Different Loads

Applied Load (per ram)	50k	150k	225k	300k
Load cycles	7	7	7	3
Moment at Interior Support (k-ft)	-415	-1128	-1739	-2294
Max crack width (in)	0.007	0.007	0.013	0.013

### 8.9.2. Single-Span Test

After completion of the two-span test, the interior support was removed to provide for a single simply supported span of 100'. A single loading tower was placed at midspan as shown in Figure 8.24. This change in loading arrangement compared to the single-span test of Beam Specimen No. 1 was the results of limitations in available laboratory equipment in the time between tests of Beam Specimen No. 1 and 2. Figure 8.95 is a photo of Beam Specimen No. 2 prior to the start of the single-span test.





*Figure 8.95 – Beam Specimen No. 2 Prior to Single-Span Test*

### **8.9.2.1. Overall Response**

A plot of applied load versus midspan deflection is shown in Figure 8.96. The specimen was unloaded four times during the test to place steel spacers beneath the loading ram to extend its stroke. From the load-deflection plot, it can be seen that the specimen began exhibiting significant inelastic behavior beyond about 150 kips of load. Beyond this, the specimen exhibited excellent ductility, showing very large inelastic deformations with continued loading. The peak total load sustained by the specimen was 252 kips. The specimen failed when the midspan deflection was approximately 21", showing a sudden drop in load capacity due to crushing of the concrete slab near midspan, as described in the next section. A photo of the specimen after completion of testing and unloading is shown in Figure 8.97, where the large permanent deflection is apparent.

### **8.9.2.2. Failure Mode**

The failure mode of the Beam Specimen No. 2 was concrete crushing at the section approximately 3' away from midspan, which is also the joint between the 9th and 10th PCP panels from the south end. Photos of the crushed section of deck are provided in Figure 8.98 to Figure 8.101. As noted above, the crushed section of deck is at joint between PCP panels. There was no evidence of stud failure in this specimen.

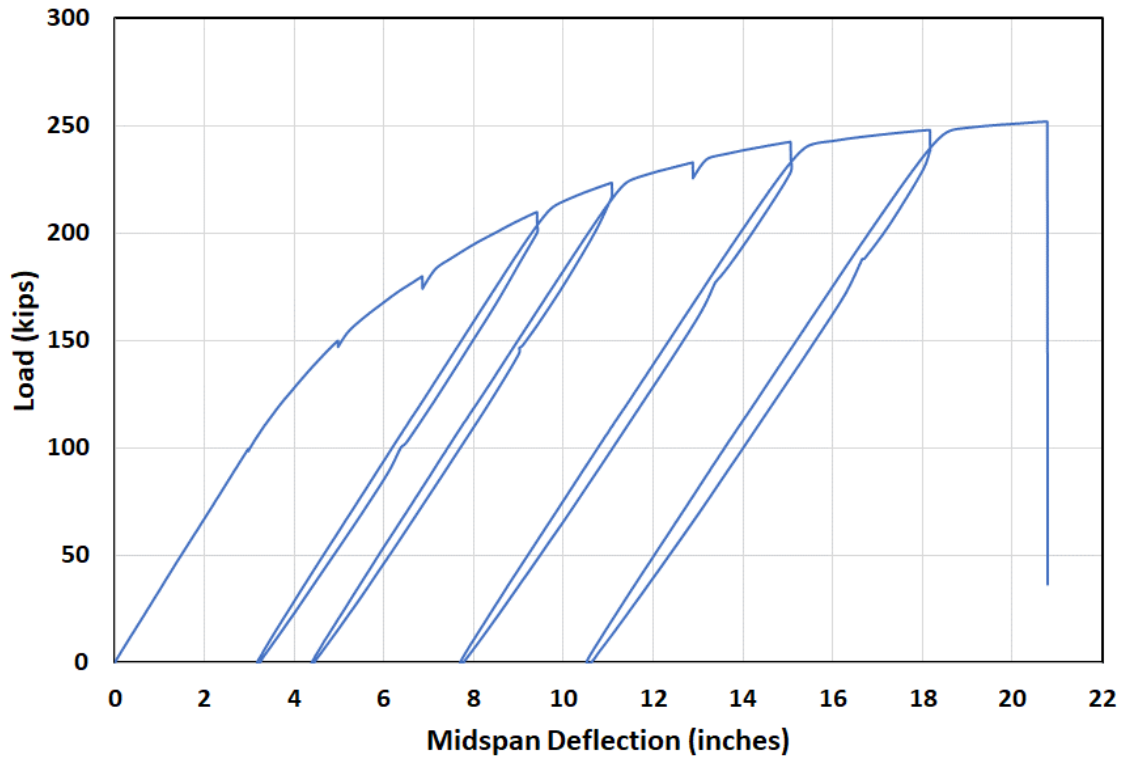


Figure 8.96 – Beam Specimen No. 2 – Load vs Midspan Deflection

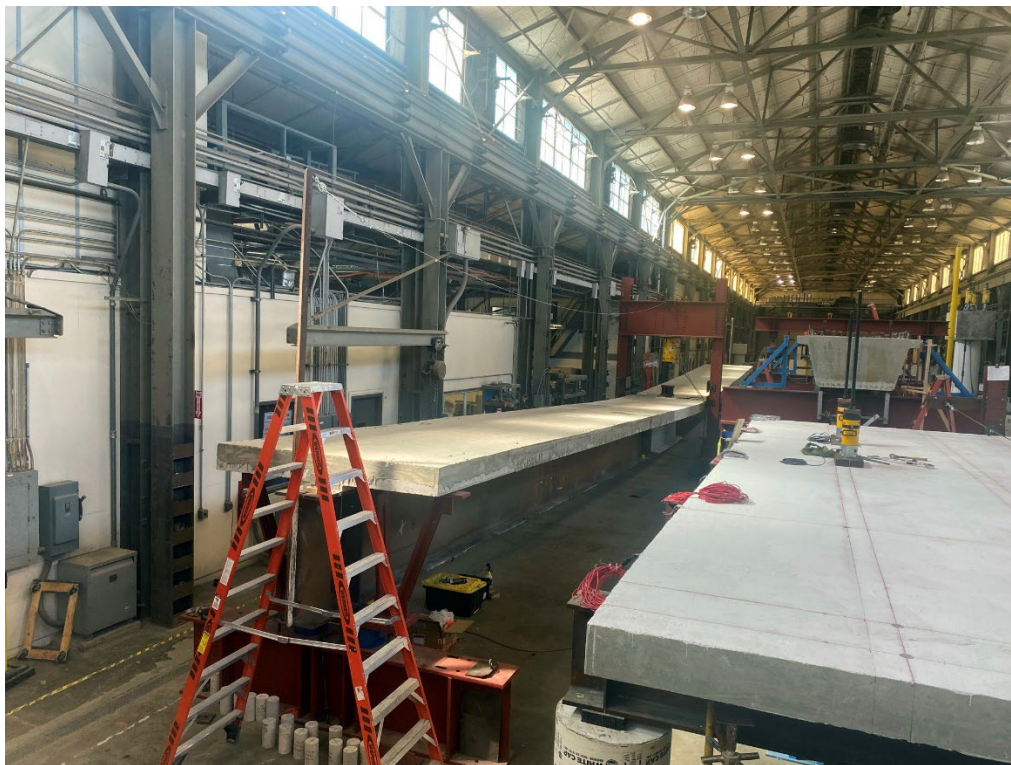


Figure 8.97 – Beam Specimen No. 2 After Completion of Single-Span Test





Figure 8.98 – Beam Specimen No. 2 – View Looking Down on Crushed Section of Deck



Figure 8.99 – Beam Specimen No. 2 – East Side of Crushed Section of Deck



Figure 8.100 – Beam Specimen No. 2 -West Side of Crushed Section of Deck





*Figure 8.101 – Beam Specimen No. 2 – View Looking Up at the Bottom Side of Deck Showing Crushing at Boundary of PCPs*

As the concrete deck was removed during demolition of Beam Specimen No. 2, dozens of studs were exposed and all were found to be intact and still connected to the top flange. Figure 8.102 shows photos of the first stud at each end of the specimen and 13th stud that was 10' from the south end. The studs were nearly straight at the end of the test, with no visible signs of cracks or damage.



1st stud at south end

10ft from south end

1st stud at north end

*Figure 8.102 – Beam Specimen No. 2 – Photos of Studs After Concrete Deck Removal*

In the static push-out tests on 1-1/8" studs for decks constructed with PCPs reported in Chapter 5, stud failure always occurred by the development of longitudinal splitting cracks in the cast-in-place concrete between the PCPs, rather than by fracture of the shear studs. In Beam Test No. 2, there was no evidence of splitting cracks in the concrete. Figure 8.103 is a photo of a section of the concrete deck cut near a shear stud and this section corresponds to the cast-in-place portion

between the PCPs. No splitting cracks or other concrete distress is visible at this sectional cut. Figure 8.104 is a photo of a similar cut made at the end of the beam, close to the first shear stud at that end of the beam. Again, there is no evidence of splitting cracks or other concrete distress at this sectional cut.



*Figure 8.103 – Beam Specimen No. 2 – Section Cut Through Slab Near Shear Stud*



*Figure 8.104 – Beam Specimen No. 2 – Section of Slab Cut Near End of Beam*

### 8.9.2.3. Slip

The relative slip between the concrete slab and the steel girder was measured using linear potentiometers (LPs) at the girder ends and at selected locations along the length of the girder, as shown in Figure 8.57. The maximum slip was approximately 0.07" at the LP7 location. Figure 8.105 is a plot of load versus slip at LP7. The small slip values for Beam Specimen No. 2 and the observations of the studs after the test, as described in the previous section, indicate that stud failure did not occur in Beam Specimen No. 1. Further, the maximum slip demand of 0.07" in Beam Specimen No. 2 is well within the slip capacities measured in the static push-out tests and in Beam Specimen No. 1.

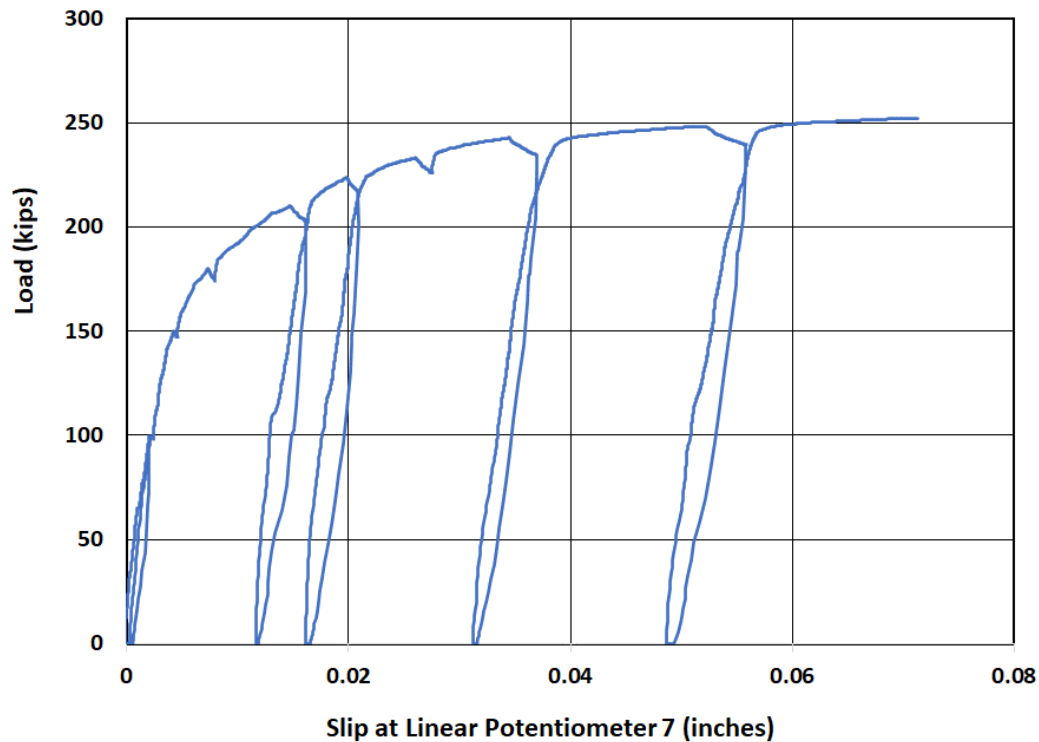


Figure 8.105 – Load-Slip Curve at LP7 for Beam Specimen No. 2

### 8.9.2.4. Composite Girder Flexural Capacity

This section discusses the maximum moment sustained by Beam Specimen No. 2 and compares this to values computed for full composite flexural strength. The maximum moment sustained by the specimen had two components: the moment due to self-weight and the moment due to the load applied by the ram. These values are listed Table 8.21. The self-weight of the specimen, including the steel girder and concrete deck, was estimated at 932 lbs./ft. For the 100' long simply support beam, this results in a self-weight moment of 1165 kip-ft. The peak load applied



by the loading ram was a total of 252 kips. The moment due to this applied loading is 6300 kip-ft. The total moment sustained by Beam Specimen No. 2 is the sum of these, which is 7465 kip-ft.

**Table 8.21 - Maximum Moment Sustained by Beam Specimen No. 2**

Component of Moment	Moment
Moment due to Self-Weight	1165 kip-ft
Moment Due to Maximum Load Applied by Ram	6300 kip-ft
Total Moment	7465 kip-ft

For comparison, the plastic moment capacity was computed for full composite behavior of Beam Specimen No. 2. The calculations were done using standard composite beam cross-sectional analysis as specified in AASHTO (AASHTO 2020) and in AISC (AISC 2022) for composite beam design. Two different calculations were done; one using measured material properties and section dimensions and the second using nominal material properties and section dimensions. Results are listed in Table 8.22.

For the calculation using measured properties, the dynamic yield stress of the top flange, web, and bottom flange of the 60' long section of W40×199 listed in Table 8.6 as well as the measured cross-section dimensions listed in Table 8.7 were used. The yield stress values and dimensions for the 60' long section of the W40×199 were used since this was the section at the location of maximum moment in the beam. For concrete compressive strength, the results of the cylinder tests run on the same day as the single-span test were used, as listed in Table 8.9. A value of 6 ksi for the compressive strength of the entire concrete deck was used, rather than incorporating a higher value for the PCP portion of the deck.

For the calculation using nominal properties,  $F_y = 50$  ksi was used for the W40×199, and  $f_c = 4$  ksi was used for the concrete. The cross-section dimensions of the W40×199 were based on the handbook dimensions listed in the AISC Steel Construction Manual.

Beam Specimen No. 2 was designed as fully composite. The observed failure mode of crushing of the concrete slab rather than shear stud failure reflects fully composite behavior. However, the actual moment sustained by the specimen of 7465 kip-ft is only 94-percent of the full composite flexural strength of 7985 kip-ft.

**Table 8.22 – Computed Full Composite Moment Capacity for Beam Specimen No. 2**

Basis for Plastic Moment Capacity Calculation	Plastic Moment Capacity for Full Composite Behavior
Measured Material Properties and Measured W40x199 Section Dimensions	7985 kip-ft
Nominal Material Properties and Nominal W40x199 Section Dimensions	5980 kip-ft

Similar to Beam Specimen No. 1 a finite element (FE) model of Beam Specimen No. 2 was developed in Abaqus. However, for Beam Specimen No. 2, the deck model included separate elements for the PCP and CIP portions of the deck, although no attempt was made to model the gaps between PCP panels. The material strength values in the FE model were based on measured values, including using different strength values for the CIP and PCP portions of the deck, as listed in Table 8.9. Figure 8.106 shows the FE model mesh and Figure 8.107 plots the load-deflection response for the FE model and the experimental result. The FE Model did not converge beyond a midspan deflection of about 18.5". Nonetheless, it is clear that the FE model, similar to the cross-section strength calculations described above, predicts a higher strength than observed in the experiment.

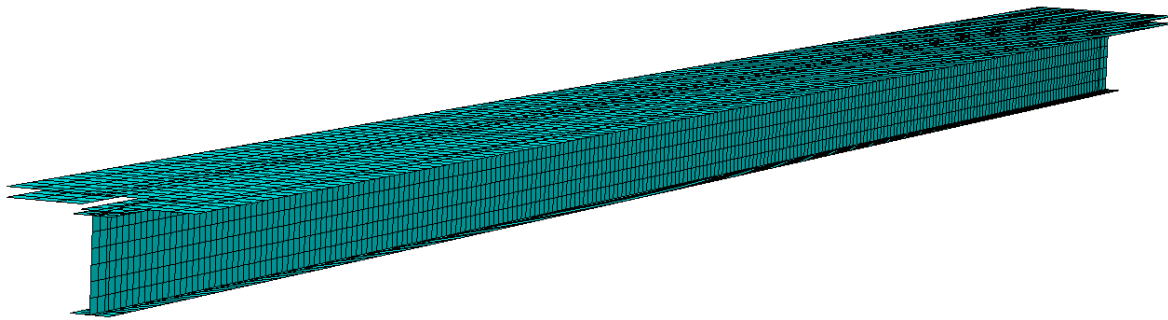


Figure 8.106 – Mesh of FE Model for Beam Specimen No. 2

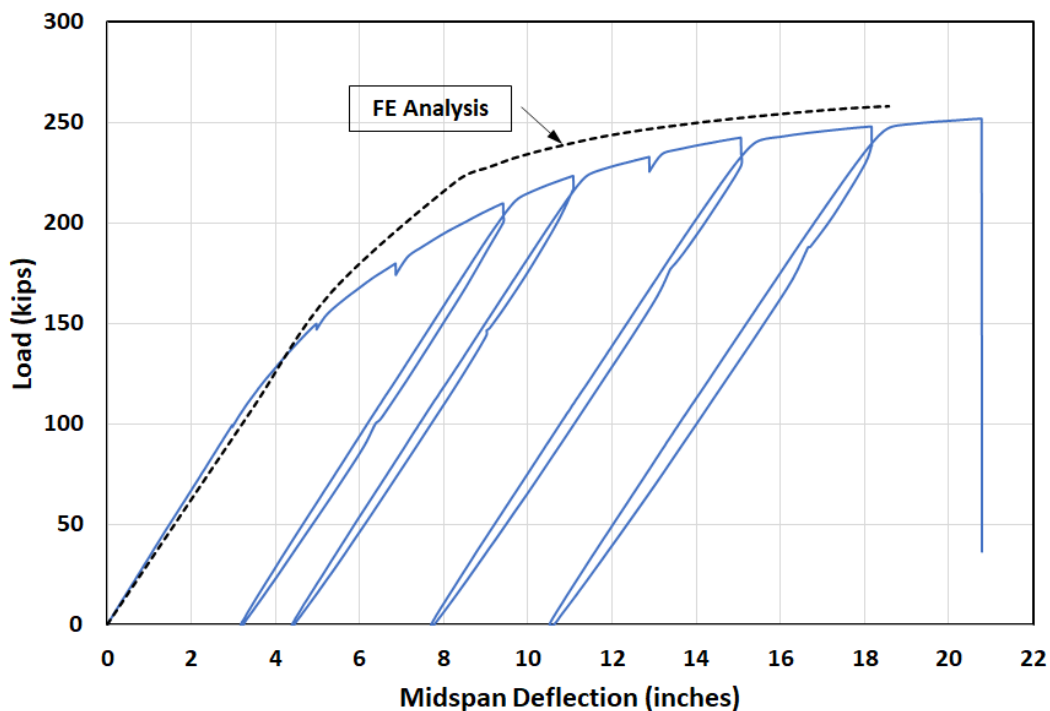


Figure 8.107 - FE and Experimental Load-Deflection Responses for Beam Specimen No. 2

Since the shear studs did not fail in Beam Specimen No. 2, the somewhat lower strength observed in the test of Beam Specimen No. 2 cannot be attributed to inadequate strength of the shear studs. It is believed this reduction in strength was attributable to the PCPs. The cross-section strength calculation for Beam Specimen No. 2 showed that the plastic neutral axis was located in the top flange of the W40×199 section, indicating that the entire depth of the concrete deck was in compression at the development of the full flexural strength of the composite girder. The gap between PCP panels may have prevented the development of a full compression block in the slab. This is supported by the observation that the failure of the concrete deck in the test occurred at the location of a gap between two adjacent PCP panels.

## 8.10. Summary and Conclusions

---

This chapter described tests on two large-scale composite beam specimens constructed using 1-1/8" diameter shear studs. The two beam specimens are referred to as Beam Specimen No. 1 and Beam Specimen No. 2.

Both specimens were 100' in length and both were constructed using 1-1/8" shear studs. Beam Specimen No. 1 was constructed using an 8.5" thick full-depth CIP deck whereas Beam Specimen No. 2 was constructed using a deck with 4" PCPs with a 4.5" CIP topping.

In addition to different types of decks, the two beam specimens also had a different number of 1-1/8" studs. Beam Specimen No. 1 was designed a partially composite, where the flexural strength of the composite beam is controlled by the strength and ductility of the shear studs. AASHTO does not allow partial composite design for bridge girders. However, partial composite design was used for Beam Specimen No. 1 to evaluate the strength and slip capacity of 1-1/8" shear studs in a beam specimen as compared to a push-out specimen. Beam Specimen No. 2 was designed as fully composite and had nearly twice as many 1-1/8" shear studs as Beam Specimen No. 1. The purpose of Beam Specimen No. 2 was to demonstrate that a composite steel bridge girder constructed with 1-1/8" shear studs can develop the full composite flexural strength in accordance with AASHTO. An additional purpose of Beam Specimen No. 2 was to determine if the use of PCPs affected the behavior of a composite steel bridge girder.

Both beam specimens were tested in two configurations. In the first configuration, an interior support was provided 40' from the end of the 100' long beam. This interior support created a two-span condition that allowed testing of the negative moment region of the beam. In the two-span condition, the beams were subject to lower levels loads intended to be representative of service loads on a bridge. The purpose of the two-span test was to determine if the use of 1-1/8" shear studs resulted in excessive cracking in negative moment regions under service loads. Once the two-span testing was completed, the interior support was removed to provide a 100' simple span. Both beam specimens were tested to failure in the simple span configuration. The purpose

of the simple span test was to establish the ultimate flexural strength, overall ductility, and controlling failure mode of each beam specimen.

For each beam specimen, testing in the two-span configuration showed no indication of excessive deck cracking in negative moment regions under service level loads. The 1-1/8" shear studs did not appear to generate large cracks in the region of the shear studs. While deck cracking was observed in the negative moment region of the beams, the cracks were well distributed and with small widths. Consequently, the conclusion from both beam tests is that the 1-1/8" studs are not likely to generate deck cracking serviceability problems.

In the negative moment region of Beam Specimen No. 2, the reinforcement ratio was 1.18% of the CIP portion of the deck based on recommendations from TxDOT Research Project 0-6909 – *Designing for Deck Stress Over Precast Panels in Negative Moment Regions* (Ge, et al. 2021). Since the cracking in the negative moment region of Beam Specimen No. 2 (deck with PCPs) was very similar to that in Beam Specimen No. 1 (full-depth cast-in-place deck), these test results provide data that support the deck reinforcing recommendations from TxDOT Research Project 0-6909.

After testing was completed in the two-span configuration for Beam Specimen No. 1, the interior support was removed and the beam was tested to failure as a 100' long simple span. Beam Specimen No. 1 was designed as partially composite and with an 8.5" thick full-depth cast-in-place deck. The ultimate strength of the beam was controlled by failure of the shear studs, as intended by the partial composite design. The estimated ultimate strength of the studs in the beam specimen was less than that of the studs in the push-out specimens. However, the estimated ultimate strength of the studs in the beam specimen still satisfied the stud strength requirements in the 9<sup>th</sup> Ed. AASHTO and the proposed 10<sup>th</sup> Ed. AASHTO. Measurements of slip between the beam flange and the concrete slab in the beam test showed the slip capacity of the 1-1/8" studs was approximately 0.4". This is similar to the slip capacities measured for 1-1/8" studs in the static push-out tests and indicates a slip capacity that is similar to or somewhat larger than that of 7/8" studs. The overall conclusion from Beam Specimen No. 1 is that 1-1/8" studs can develop the strength required by the 9<sup>th</sup> Ed. AASHTO and the proposed 10<sup>th</sup> Ed. AASHTO and also exhibit adequate slip capacity.

After testing was completed in the two-span configuration for Beam Specimen No. 2, the interior support was removed and the beam was tested to failure as a 100' long simple span. Beam Specimen No. 2 was designed as fully composite with a deck consisting of 4" thick PCPs and a 4.5" cast-in-place topping. The ultimate strength of the beam was controlled by crushing of the concrete deck near the point of maximum moment. No shear stud failure was observed in the test and there was no indication of splitting cracks in the cast-in-place concrete in the region of the shear studs. Consequently, the 1-1/8" shear studs performed well in this test. The penetration distance of the stud into the deck and the clear distance between the head of the stud and the

edge of the PCP in the test specimen was based on the design recommendations developed in the finite element studies in Chapter 7. The satisfactory behavior of the shear studs in Beam Specimen No. 2 provides at least some degree of validation of these recommendations.

The maximum moment developed by Beam Specimen No. 2 was approximately 6-percent less than the predicted value based on full composite behavior. It is believed this reduction in strength was attributable to the PCPs. The gap between PCP panels may have prevented the development of a full compression block in the slab. This is supported by the observation that the failure of the concrete deck in the test occurred at the location of a gap between two adjacent PCP panels.

In the single-span tests, both beam specimens exhibited excellent ductility. Very large inelastic deformations were developed prior to ultimate failure.

# Chapter 9. Summary, Key Findings, and Recommendations

## 9.1. Introduction

---

This report documents the research tasks and findings from Texas Department of Transportation Research Project 0-7042 – *Use of Larger Diameter Shear Studs for Composite Steel Bridges*. The overall goal of the project was to evaluate the feasibility of using larger-diameter shear studs for composite steel bridges in Texas. The term *larger-diameter* refers to studs with a diameter greater than 1". Studs with a diameter greater than 1" are not currently permitted by the AASHTO LRFD Bridge Design Specifications nor by the AWS D1.5 Bridge Welding Code. The research initially considered both 1-1/8" and 1-1/4" diameter shear studs, but the majority of testing and finite element analysis ultimately focused on 1-1/8" studs. The research considered the use of 1-1/8" studs in two types of bridge deck systems. The first was a deck constructed using 8.5" full-depth cast-in-place (CIP) concrete. The second was a deck constructed using 4" thick precast concrete deck panels (PCPs) with a 4.5" CIP concrete topping.

As described in Chapter 1, the specific objectives of Project 0-7042 were as follows:

- Determine if good quality welds can be consistently achieved for larger-diameter shear studs using commercially-available stud welding equipment.
- Determine if current equations in the AASHTO LRFD Bridge Design Specifications for stud ultimate strength and fatigue resistance can be safely used for larger-diameter shear studs, or if modifications to these equations are needed.

When evaluating the applicability of stud ultimate strength and fatigue strength equations in the AASHTO LRFD Bridge Design Specifications for use with 1-1/8" studs, the research considered both the 9<sup>th</sup> Ed. AASHTO (AASHTO 2020) as well as the proposed 10<sup>th</sup> Ed. AASHTO (AASHTO 2021).

- Determine if larger-diameter shear studs cause excessive cracking of the concrete deck under service level loading for fully CIP decks or decks with PCPs and a CIP topping.

The following section summarizes the major research tasks undertaken in this project and key findings for each task.



## 9.2. Summary of Research Tasks and Key Findings

---

### 9.2.1. Background and Literature Review

A review was conducted of previous research on shear studs, in general, and more specifically on larger-diameter shear studs. This includes previous work both on stud ultimate strength and on stud fatigue resistance. In addition, all design and detailing requirements for shear studs pertinent to bridge construction were summarized, including those in the 9<sup>th</sup> Ed. AASHTO, the proposed 10<sup>th</sup> Ed. AASHTO, AWS D1.5, and pertinent TxDOT standards and guidance documents. This work is summarized in Chapter 2. Key findings from this task are as follows:

- Shear stud strength and fatigue requirements in the current 9<sup>th</sup> Ed. AASHTO are essentially the same as those found in several previous versions of AASHTO. However, significant changes to shear stud strength and fatigue requirements have been balloted and approved for the upcoming 10<sup>th</sup> Ed. AASHTO. A summary of the proposed changes in the 10<sup>th</sup> Ed. AASHTO is provided in Chapter 2.
- A limited number of studies were identified that experimentally evaluated the static and fatigue loading behavior of larger-diameter shear studs. This includes research conducted in the U.S. at the University of Nebraska and at Auburn University, as well as research conducted in Korea and China.
- The literature review from past static push-out tests indicates that larger-diameter studs have exhibited highly-variable strength and ductility. Contradictory conclusions regarding the strength and ductility are reported in the literature. Test results have shown strength values both well above and well below predictions from the AASHTO LFRD design equations (both 9<sup>th</sup> Ed. AASHTO and proposed 10<sup>th</sup> Ed. AASHTO). The ductility of larger-diameter shear studs is commonly reported as better than that of 7/8" studs, but lower ductility is also reported. On the other hand, data on the impact of factors such as deck reinforcement ratio and stud penetration into the deck on the strength and ductility of larger-diameter shear studs is limited. Based on the available data on static loading behavior, the suitability of larger-diameter shear studs for use in composite steel bridges is unclear. Additional testing and analysis are needed to establish the performance of larger-diameter shear studs in bridge decks representative of Texas bridge design standards and practices.
- The literature review from past fatigue push-out tests has shown consistently good fatigue performance for larger-diameter shear studs. This data indicates that shear stud diameter does not have a significant effect on fatigue life. The fatigue resistance exhibited by larger-diameter shear studs has been similar to and often better than that of 7/8" studs.

Essentially all fatigue tests on larger-diameter shear studs have shown performance that satisfies both the 9<sup>th</sup> Ed. AASHTO and the proposed 10<sup>th</sup> Ed. AASHTO S-N curves.

- No previous studies were identified that evaluated the behavior of shear studs of any diameter in concrete decks constructed using partial depth precast concrete panels with a cast-in-place topping as used in Texas bridges.
- A review of the literature identified two bridges in the U.S. that were constructed with larger-diameter shear studs. Both bridges were constructed in Nebraska using 1-1/4" shear studs. The first bridge was constructed in 1999 with a full-depth cast-in-place deck. The second bridge was constructed in 2004 using a full-depth precast concrete deck system. Based on recent information obtained from the Nebraska Department of Transportation, the decks of both bridges are performing well.

### 9.2.2. Preliminary Design Studies

Three existing TxDOT bridges constructed with 7/8" diameter shear studs were redesigned using 1", 1-1/8", and 1-1/4" shear studs. The purpose of these redesigns was to quantify the reduction in the number of shear studs that can be achieved when using larger-diameter studs for realistic bridges. An additional purpose of this exercise was to determine if existing stud geometric requirements and limitations (minimum and maximum pitch, transverse spacing requirements, minimum and maximum stud length requirements, etc.) may be problematic for larger-diameter shear studs. Key findings from the preliminary design studies are as follows:

- The redesign process for larger diameter shear studs was very similar to that of 7/8" diameter shear studs. Stud diameter up to 1-1/4" can be successfully designed without violating any geometric requirements or limitations in the 9<sup>th</sup> Ed. AASHTO, the proposed 10<sup>th</sup> Ed. AASHTO, or TxDOT specifications.
- The reduction in the number of shear studs was found to be significant when larger-diameter shear studs are used. The actual percentage reduction in the required number of studs varied somewhat among the three bridges, based on the stud diameter, and based on the number of studs per row used in the design. However, compared to 7/8" shear studs, the reduction in the number of studs was found to be on the order of 25%, 40%, and 50% for 1", 1-1/8", and 1-1/4" diameter shear studs, respectively, for both the current 9<sup>th</sup> Ed. AASHTO and the proposed 10<sup>th</sup> Ed. AASHTO.

### 9.2.3. Stud Welding Investigations

A significant effort was dedicated to determining if larger-diameter shear studs can be welded with consistent quality using commercially available stud welding equipment. As part of this effort, hundreds of trial welds were made using a wide range of welding parameters and then

evaluated for quality using a variety of evaluation and testing methods. Trial welds were made on small plates as well as on girders with various flange thickness values. Welding trials were conducted both on 1-1/8" and 1-1/4" studs. All stud welds were made using a Nelson Nelweld 6000 stud welding machine. Nelson provided the equipment needed to modify the stud-welding gun of the machine to accommodate the larger-diameter shear studs. Nelson also manufactured the 1-1/8" and 1-1/4" shear studs and welding ferrules for use in this research project, as well as providing extensive technical advice on stud welding variables. Key findings from the study are as follows:

- A large number of parameters affect the stud welding process and the quality of a stud weld. These include welding current, welding time, lift, plunge, polarity, free travel, location of ground cable attachments, use of cable looping, surface preparation, and the addition of steel masses to control arc blow.
- Both the 1-1/8" and 1-1/4" shear studs could be successfully welded using a commercially-available stud welding machine with relatively simple and inexpensive modifications to the welding gun to accommodate the larger-diameter studs.
- Determining a suitable combination of welding parameters that resulted in consistent good quality stud welds required hundreds of trial welds. However, welding parameters were ultimately identified that provided consistent good quality for 1-1/8" and 1-1/4" studs.
- Stud welding trials were conducted on 1' × 1' plates that were 1" thick and 2" thick. Stud welding trials were also conducted on the flanges of longer rolled beams with flange thicknesses varying from 3/4" to 3-1/2". It was found that welding parameters that provided good quality welds on the 1' × 1' plates did not necessarily provide good quality welds on the flanges of significantly longer beams. Further, the welding parameters providing good quality stud welds on beams with thinner flanges were not suitable for beams with thicker flanges. However, it was found that the parameters that provided good quality welds on beams with a 3-1/2" thick flange also worked well for beams with thinner flanges, down to a 3/4" flange thickness.
- The welding parameters that provided consistent good quality welds on beam flanges for 1-1/8" and 1-1/4" studs are listed in Table 4.12.
- Based on the welding investigations, the welding of 1-1/4" studs was highly sensitive to the selected welding parameters and base metal conditions. The welding of 1-1/8" studs, on the other hand, was more robust with a single set of welding parameters providing consistent good quality welds over a wide range of base-metal conditions. Thus, it is believed that the use of 1-1/8" studs is more likely to provide consistent good quality stud welds in actual bridge construction.

- A common technique used to verify weld quality is conducting bend tests on welded studs. This includes 90° bend tests to verify weld quality as well as 30° bend tests used in the field for routine quality control. For 7/8" studs, bend tests can be conducted using a lever-action with a length of pipe section placed over the stud to bend the stud, or by striking the stud with a hammer. For the 1-1/8" and 1-1/4" studs used in this research project, using a pipe to bend the studs was not feasible due to the significantly higher strength of these studs compared to 7/8" studs. Consequently, the bend tests on 1-1/8" and 1-1/4" studs were done by striking them with a heavy sledgehammer. In conducting the bend tests, it was found that bending a 1-1/4" diameter shear stud with a hammer was much more difficult and physically demanding than for a 1-1/8" diameter shear stud. Thus, it is believed that conducting bend tests in the field is more feasible for 1-1/8" studs compared to 1-1/4" studs.
- Based on the results of the stud welding investigations, the decision was made to proceed with the use of 1-1/8" studs for the remainder of this research project. Consequently, the push-out tests, the finite element studies, and the large-scale beam tests conducted in subsequent tasks all used 1-1/8" studs, and there was no further consideration of 1-1/4" studs in these subsequent research efforts. Future research may show greater feasibility for the use of 1-1/4" shear studs in bridges. However, based on currently available information from this research and from previous research, it is believed that using 1-1/8" shear studs is the most practical and implementable choice at this time.

#### 9.2.4. Static Push-Out Tests

Static push-out tests were conducted on eleven specimens to investigate the ultimate strength and slip capacity of the shear studs and included both 1-1/8" studs as well as 7/8" studs for comparisons. The test program included specimens with 8-1/2" thick full-depth cast-in-place decks as well as specimens where the deck was constructed using 4" thick PCPs with 4-1/2" cast-in-place topping. The deck details, including reinforcing details, were constructed in accordance with TxDOT standards and preferred practices. Key findings from this task are as follows:

- The results of the push-out tests show excellent performance of 1-1/8" shear studs. The ultimate strength of 1-1/8" shear studs in all tests exceeded the stud ultimate strength requirements of both the 9<sup>th</sup> Ed. AASHTO and the proposed 10<sup>th</sup> Ed. AASHTO.
- The slip capacities of the 1-1/8" shear studs measured in this test program are comparable to and sometimes larger than the slip capacity of the 7/8" shear studs measured in this test program.
- For decks with PCPs, the ultimate strength of both 7/8" and 1-1/8" shear studs was less than the corresponding specimens constructed with full-depth CIP decks. For the

specimens with full-depth CIP decks constructed in accordance with TxDOT standards and with a 4" penetration of the stud into the deck, all studs failed by fracture of the shear studs. However, for specimens with PCP decks, not only was the ultimate strength reduced, but the ultimate strength was controlled by concrete failure, which appeared to be associated with the development of splitting cracks along the length of the deck in the region of the shear studs. This reduction in strength and change in failure mode occurred for specimens both with 7/8" as well as 1-1/8" shear studs, so the reduction is not associated with the shear stud diameter. However, even with the reduction in strength and change in failure mode, the measured ultimate strength of all shear studs in PCP decks exceeded the stud ultimate strength requirements in the 9<sup>th</sup> Ed. AASHTO and the proposed 10<sup>th</sup> Ed. AASHTO.

- An uncertainty with the use of larger-diameter shear stud is application to steel girders with thin flanges. One push-out specimen was constructed with two rows of 1-1/8" studs welded on to the flange of W14×99, which has a flange thickness of 0.75". Result from this test showed that no local bending or distortion was developed in the 0.75" flange when the ultimate strength of the shear studs was reached. Thus, 1-1/8" studs can be safely used on girders with flanges as thin as 0.75".
- A concern regarding larger-diameter shear studs is that such shear studs may cause cracking and other distress in the bridge deck at service-level loads. This might occur with 1-1/8" studs because, relative to smaller studs, larger forces are transferred between the stud and the surrounding concrete, causing potentially larger localized stress levels in the concrete. However, no such distress was observed in the static push-out test program. This indicates that reinforcing provided in bridge decks constructed in accordance with existing TxDOT standards, both for full-depth CIP decks as well as with PCP decks, is adequate to control concrete cracking at shear studs under service-level loading.

### 9.2.5. Fatigue Push-Out Tests

Fatigue tests were conducted on four push-out specimens constructed with 1-1/8" shear studs, with stress ranges varying from 15 ksi to 30 ksi. A relatively small number of fatigue tests were conducted in this research project because all previous fatigue test programs on larger-diameter shear studs reported in the literature consistently showed good performance, with fatigue lives of the larger-diameter shear studs that were at least as good as and often better than that of 7/8" shear studs. Key findings and observations from fatigue experiments on the shear studs are as follows:

- All four fatigue specimens exhibited fatigue lives that exceeded the requirements of both the 9<sup>th</sup> Ed. AASHTO and the proposed 10<sup>th</sup> Ed. AASHTO S-N curves.

- For two of the specimens, fatigue loading was stopped once the number of loading cycles significantly exceeded the requirements of the 9<sup>th</sup> Ed. AASHTO and the proposed 10<sup>th</sup> Ed. AASHTO. These two specimens were then subject to static loading to failure, to evaluate their residual static strength. These tests showed that the studs retained on the order of 85 to 95-percent of the static strength specified in the 9<sup>th</sup> Ed. AASHTO and on the order of 90 to 100-percent of the static strength specified in the proposed 10<sup>th</sup> Ed. AASHTO. Consequently, despite extensive prior cyclic loading to investigate fatigue performance, these studs retained very substantial residual static strength.

### 9.2.6. Finite Element Studies of Static Push-Out Behavior

Finite element (FE) analyses were performed to study and compare the behavior of 7/8" and 1-1/8" diameter shear studs in push-out specimens. The objective of these studies was to extend information developed in the static push-out test program and to investigate variables not considered in the test program. While this FE study considered the impact of a number of design variables on shear stud behavior, a particular focus of the FE study was to examine the behavior of both 7/8" and 1-1/8" shear studs in bridge decks constructed using partial-depth precast concrete deck panels.

The FE studies were divided into two phases. The first phase was FE model development and validation and the second phase was parametric FE studies examining a wide range of design and detailing variables. For the model development and validation phase, all eleven experimental push-out specimens were modeled, and FE predictions were compared to the experimentally measured load-slip response and also compared to the observed failure modes and concrete damage patterns. The FE models simulated both damage in the concrete as well as fracture of the studs. This model development process produced FE models that reasonably captured the load-slip response and the failure mode of the experimental specimens.

The parametric FE study expanded the variables studied in the experimental push-out tests. The parametric study investigated stud penetration distance into the deck, haunch depth, steel beam flange width, clear distance between the stud and the PCP, the overlap distance of the PCP with the steel beam, bedding strip size, transverse reinforcement ratio, the clear distance between the stud and the PCP, and the PCP overlap distance with the steel beam. Key findings from the parametric FE studies are as follows:

- Stud penetration distance into the concrete deck significantly influenced the load-slip response of the push-out models, both for full-depth CIP decks and for decks with PCPs. Larger penetration distances generally increased the predicted stud strength.
- Haunch depth had little effect on the stud ultimate strength if the stud penetration distance into the deck was kept the same.



- Increases in the steel beam flange width significantly improved stud behavior for full-depth CIP models. For FE models with PCPs, increasing beam flange width without providing more CIP concrete near the stud had minimal impact on stud strength and ductility. Conversely, for decks with PCPs, providing more CIP concrete surrounding the shear stud resulted in higher stud strength.
- For FE Models with PCPs, the size of the bedding strip had little impact on stud strength and ductility.
- Stud strength in decks with PCPs was significantly influenced by two factors, namely stud penetration into the concrete deck and the clear distance between the stud head and the PCP. Based on a series of additional FE studies, recommendations were developed for these two parameters for both 1-1/8" and 7/8" shear studs. These recommendations are presented later in this chapter.

### 9.2.7. Large-Scale Composite Beam Tests

In this task, two large-scale composite beams were constructed and tested. Both beams were 100' in length and both beams were constructed using 1-1/8" shear studs. The first beam specimen was constructed using an 8.5" thick full-depth cast-in-place deck whereas the second beam specimen was constructed using a deck with 4" PCPs with a 4.5" cast-in-place topping.

In addition to different types of decks, the two beam specimens also had a different number of 1-1/8" studs. The first beam specimen was a partially-composite design, where the flexural strength of the composite beam is controlled by the strength and ductility of the shear studs. Although not permitted by AASHTO, a partial-composite design was used for the first beam specimen to evaluate the strength and slip capacity of 1-1/8" shear studs in a beam as compared to a push-out specimen. The second beam specimen was designed as fully composite and had nearly twice as many 1-1/8" shear studs as the first specimen. The purpose of the second beam specimen was to demonstrate that a composite steel bridge girder constructed with 1-1/8" shear studs can develop the full composite flexural strength in accordance with AASHTO. An additional purpose of the second beam specimen was to determine if the use of PCPs affected the behavior of a composite steel bridge girder.

Both beam specimens were tested in two configurations. In the first configuration, an interior support was provided 40' from the end of the 100' long beam. This interior support created a two-span condition that allowed testing of the negative moment region of the beam. In the two-span condition, the beams were subject to lower levels loads intended to be representative of service level conditions on a bridge. The purpose of the two-span test was to determine if the use of 1-1/8" shear studs resulted in excessive deck cracking in negative moment regions under service loads. Once the two-span testing was completed, the interior support was removed to

provide a 100' simple span. Both beam specimens were tested to failure in the simple-span configuration. The purpose of the simple-span test was to establish the ultimate flexural strength, overall ductility, and controlling failure mode of each beam specimen. Key findings and observations from these tests are as follows:

- For each beam specimen, testing in the two-span configuration showed no indication of excessive deck cracking in negative moment regions under service level loads. The 1-1/8" shear studs did not appear to generate large cracks in the region of the shear studs. While deck cracking was observed in the negative moment region of the beams, the cracks were well distributed and with small widths. Consequently, the conclusion from both beam tests is that the 1-1/8" studs are not likely to generate deck cracking serviceability problems.
- In the negative moment region of Beam Specimen No. 2, the reinforcement ratio was 1.18% of the CIP portion of the deck based on recommendations from TxDOT Research Project 0-6909 – *Designing for Deck Stress Over Precast Panels in Negative Moment Regions* (Ge, et al. 2021). Since the cracking in the negative moment region of Beam Specimen No. 2 (deck with PCPs) was very similar to that in Beam Specimen No. 1 (full-depth cast-in-place deck), these test results provide data that support the deck reinforcing recommendations from TxDOT Research Project 0-6909.
- After testing was completed in the two-span configuration for Beam Specimen No. 1, the interior support was removed and the beam was tested to failure as a 100' long simple span. Beam Specimen No. 1 was designed as partially composite and with an 8.5" thick full-depth cast-in-place deck. The ultimate strength of the beam was controlled by failure of the shear studs, as intended by the partial composite design. The estimated ultimate strength of the studs in the beam specimen was less than that of the studs in the push-out specimens. However, the estimated ultimate strength of the studs in the beam specimen still satisfied the stud strength requirements in the 9<sup>th</sup> Ed. AASHTO and the proposed 10<sup>th</sup> Ed. AASHTO. Measurements of slip between the beam flange and the concrete slab in the beam test showed the slip capacity of the 1-1/8" studs was approximately 0.4". This is similar to the slip capacities measured for 1-1/8" studs in the static push-out tests and indicate a slip capacity that is similar to and somewhat larger than that of 7/8" studs. The overall conclusion from Beam Specimen No. 1 is that 1-1/8" studs can develop the strength required by the 9<sup>th</sup> Ed. AASHTO and the proposed 10<sup>th</sup> Ed. AASHTO and also exhibit adequate slip capacity.
- After testing was completed in the two-span configuration for Beam Specimen No. 2, the interior support was removed and the beam was tested to failure as a 100' long simple span. Beam Specimen No. 2 was designed as fully composite with a deck consisting of 4" thick PCPs and a 4.5" cast-in-place topping. The ultimate strength of the beam was

controlled by crushing of the concrete deck near the point of maximum moment. No shear stud failure was observed in the test and there was no indication of splitting cracks in the cast-in-place concrete in the region of the shear studs. Consequently, the 1-1/8" shear studs performed well in this test. The penetration distance of the stud into the deck and the clear distance between the head of the stud and the edge of the PCP in the test specimen was based on the design recommendations developed in the finite element studies in Chapter 7. The satisfactory behavior of the shear studs in Beam Specimen No. 2 provide at least some degree of validation of these recommendations.

- The maximum moment developed by Beam Specimen No. 2 was approximately 6-percent less than the predicted value based on full composite behavior. It is believed this reduction in strength was attributable to the PCPs. The gap between PCP panels may have prevented the development of a full compression block in the slab. This is supported by the observation that the failure of the concrete deck in the test occurred at the location of a gap between two adjacent PCP panels.
- In the single-span tests, both beam specimens exhibited excellent ductility. Very large inelastic deformations were developed prior to ultimate failure.

## 9.3. Recommendations

---

### 9.3.1. General Recommendations

The results of this research project have shown that 1-1/8" shear studs can be safely used in composite steel bridges in Texas. The use of 1-1/8" studs, compared to conventional 7/8" studs, can significantly reduce the number of shear studs on a steel girder, thereby enhancing safety during construction and providing more space on the flange of a girder for placement of PCPs. 1-1/8" shear studs can be used both for I girders and for trapezoidal box girders. However, their use is not recommended for steel twin tub girder bridges designed for system redundancy, as the current methodology for assessing system redundancy (TxDOT 2023) is based on the use of 7/8" shear studs.

The following sections provide more specific recommendations resulting from this research project.

### 9.3.2. Welding of 1-1/8" Shear Studs

The research conducted in this project showed that 1-1/8" studs can be welded with consistent good quality using commercially-available stud welding equipment. Based on numerous trial welds, the following parameters were found to provide good quality welds for 1-1/8" studs on beams with flange thickness values ranging from 3/4" to 3-1/2":

- Current: 2250 amps
- Time: 1.55 seconds
- Plunge: 5/16"
- Lift: 1/4"
- Polarity: Reverse

No special surface preparation was applied to the base metal before welding, other than sweeping away loose dirt. In addition, no cable looping around the studs was done to facilitate the welding.

For future applications of 1-1/8" studs on steel bridge girders, the contractor responsible for stud welding, working with the stud manufacturer, must determine welding parameters and inspection procedures that provide good quality welds in accordance with the requirements of AWS D1.5 (AWS 2020) Chapter 9 and Annex D. While the parameters listed above can be used as a starting point, there are likely other combinations of parameters that will provide good quality welds. Further, the parameters listed above may not provide quality welds for studs with different material properties, head geometries, aluminum flux ball characteristics, or ferrule characteristics in comparison with the studs used in this research. These welding parameters may also not be suitable for different base metal conditions than those used in this research.

AWS D1.5 Annex D (*Manufacturer's Stud Base Qualification Requirements*) permits the qualification of welding procedures to be done using trial welds made on steel plates. Experience with welding of 1-1/8" studs in this research project showed that welding parameters that provided good quality welds on 1' x 1' plates do not necessarily provide good quality welds on beam flanges, even when the plate thickness and the beam flange thickness are the same. Consequently, it is recommended that welding parameters be developed using trial welds on members representative of the girders and using the full range of flange thickness values expected on a project. In developing welding parameters, it is recommended that 90° bend tests be conducted to evaluate weld quality. In this research, it was found that many studs could be bent 30° without failure. However, upon further bending, welds often failed before achieving a 90° bend, exposing weld defects such as excessive porosity on the fracture surface. Thus, while 30° bend tests may be suitable for routine quality control as specified in AWS D1.5, 90° bend tests or direct tension tests should be used when developing or confirming parameters for stud welding to girders.

For initial bridge projects that will use 1-1/8" studs, it is recommended that TxDOT work closely with the contractor in developing and verifying welding and inspection procedures. The lessons learned on stud welding in this research project, as described in Chapter 4 of this report, can be used as a guide on issues to consider in welding 1-1/8" studs. After adequate experience and confidence are gained in welding 1-1/8" studs to girders, the level of TxDOT oversight can likely be moderated.

### 9.3.3. Head Dimensions for 1-1/8" Studs

At the time this research was conducted, 1-1/8" studs were not available as an "off-the-shelf" product from stud manufacturers. However, 1-1/8" studs can be procured on a custom-order basis from some stud manufacturers. An issue in ordering 1-1/8" studs is the head dimensions. Head dimensions for shear studs are specified in AWS D1.5 (AWS 2020). Since 1-1/8" studs are not currently recognized in AWS D1.5, no head dimensions are specified. Thus, the purchaser of the studs must specify head dimensions.

The 1-1/8" shear studs used in this project had a head diameter of 1-7/8" and a head height of 9/16". These head dimensions were selected by Nelson based on their experience as described in Section 4.4.1 of this report. There is nothing in this research to suggest that the head dimensions played a critical role in the ultimate strength or fatigue strength of the studs. Nonetheless, since the studs used in this research performed well in both ultimate strength and fatigue tests, it is recommended these same head dimensions be used in the future.

### 9.3.4. Design of 1-1/8" Studs for Ultimate Strength and Fatigue

The stud ultimate-strength tests in push-out specimens and in large-scale beam specimens, and the stud fatigue tests in push-out specimens indicate that both the current 9<sup>th</sup> Ed. AASHTO equations as well as the proposed 10<sup>th</sup> Ed. AASHTO equations for stud ultimate strength and fatigue can be used for 1-1/8" studs, subject to stud length, deck penetration distance, and other detailing requirements presented in the next section. However, it is recommended that 1-1/8" studs be designed for ultimate strength and fatigue using the proposed 10<sup>th</sup> Ed. AASHTO stud provisions. The proposed 10<sup>th</sup> Ed. AASHTO represents the most up-to-date provisions on stud design for composite steel bridges and also provides a more conservative approach to the calculation of stud ultimate strength compared to the 9<sup>th</sup> Ed. AASHTO.

The static push-out tests described in Chapter 5 and the finite element simulations of static push-out tests described in Chapter 7 indicated that stud strength is lower in decks constructed with PCPs as compared with full-depth cast-in-place decks. However, the data show that even with the lower strength, studs in decks with PCPs still satisfy the ultimate strength requirements of the 10<sup>th</sup> Ed. AASHTO as long as the penetration of the stud into the deck and the clear distance between the stud head and the PCP satisfy the limitations presented in the next section.

### 9.3.5. Stud Penetration into Deck and Clear Distance to PCP for 7/8" and 1-1/8" Studs

The static push-out tests described in Chapter 5 showed that the ultimate strength of 1-1/8" studs is sensitive to the penetration distance into the deck. The parametric finite element studies presented in Chapter 7 further confirm that the ultimate strength of both 7/8" studs and 1-1/8" studs was sensitive to the stud penetration distance into the deck, with larger penetration

distances providing for increased stud strength. This was the case both for full-depth cast-in-place decks as well as for decks constructed with PCPs.

Based on the static push-out test results, the parametric finite element studies, and the judgment of the research team, for full-depth cast-in-place decks, a minimum deck penetration distance of 3" is recommended, both for 7/8" studs and 1-1/8" studs. This recommendation is shown graphically in Figure 9.1.

For decks with PCPs, in addition to the ultimate strength of 7/8" studs and 1-1/8" studs being sensitive to penetration distance into the deck, stud strength was also sensitive to the clear distance between the head of the stud and the edge of the PCP. Recommendations for stud penetration and clear distance between the stud head and the PCP were developed based on the static push-out tests and the finite element studies combined with the judgment of the research team. These recommendations are presented in Table 9.1 and are also shown graphically in Figure 9.2. For 1-1/8" studs, two options are provided. The first option is to provide a minimum penetration of 4" combined with a clear distance from the head of the stud to the PCP of 2". This combination of minimum penetration distance and clear distance should be suitable for most typical girder flange widths and overlap distances between the girder flange and the PCP. However, in cases where the 2" minimum clear distance between the head of the stud and the PCP cannot be achieved, for example in the case of a narrow girder flange, a minimum clear distance between the head of the stud and the PCP of 1" is acceptable if the stud penetration distance is increased to 5".

Penetration distance into the deck is measured from the base of the deck, which is the same as the top of the haunch, as illustrated in Figure 9.1 and Figure 9.2.

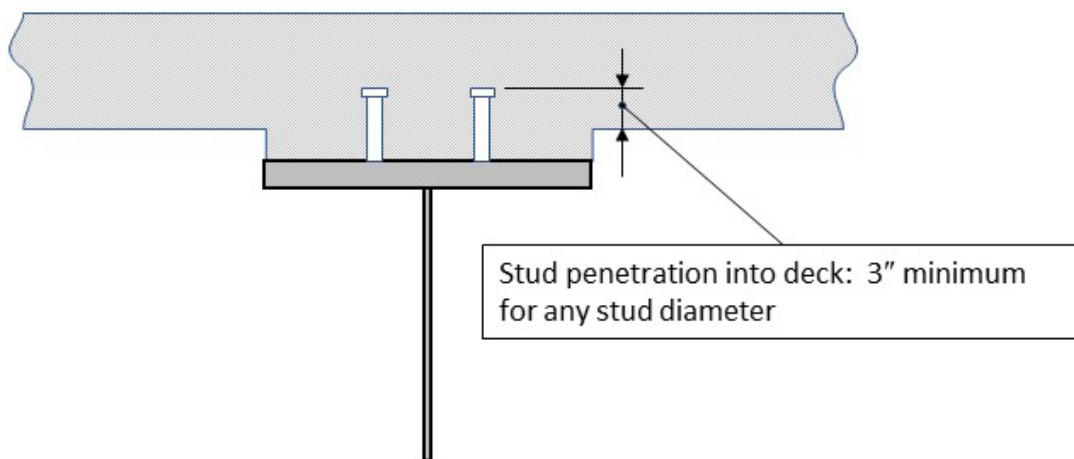


Figure 9.1 – Recommended Stud Penetration into Deck for Full-Depth Cast-in-Place Decks



**Table 9.1 – Recommendations for Stud Penetration into Concrete Deck and Clear Distance Between Stud Head and PCP for Decks Constructed with PCPs**

<b>Stud Diameter</b>	<b>Stud Penetration into Deck</b>	<b>Clear Distance Between Head of Stud and PCP</b>
7/8"	≥ 4"	≥ 1"
1-1/8"	≥ 4"	≥ 2"
	≥ 5"	≥ 1"

The stud penetration distances recommended in Table 9.1, Figure 9.1, and Figure 9.2 combined with the haunch depth will control the minimum required length of the stud. In addition, the total stud length must meet the requirements of the proposed 10<sup>th</sup> Ed. AASHTO, which specifies a minimum stud length to diameter ratio of 5 for normal weight concrete and 7 for lightweight concrete. Thus, for normal weight concrete, as is usually used in TxDOT bridge decks, satisfying the length to diameter ratio of 5 requires a minimum stud length of 4-3/8" for 7/8" studs, and 5-5/8" for 1-1/8" studs. Current TxDOT standards (TxDOT 2019a) specify a minimum stud length of 5" which will satisfy the minimum length to diameter ratio of 5 for 7/8" studs but will not for 1-1/8" studs. The maximum stud length will be controlled by the TxDOT requirement for a minimum clear cover of 2.5" between the top of the stud and the top of the concrete deck (TxDOT 2019a).

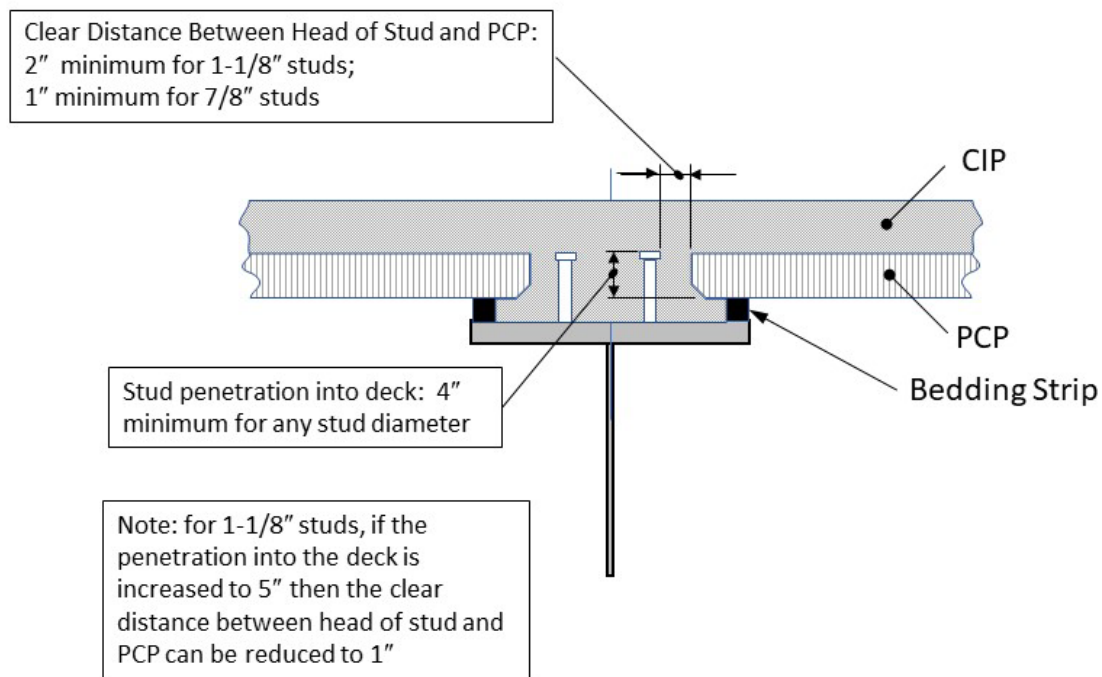


Figure 9.2 – Recommended Stud Penetration into Deck and Clear Distance from Stud to PCP for Decks with PCPs

For 7/8" studs, current AASHTO (AASHTO 2020) and TxDOT standards (TxDOT 2019a) require a minimum 2" penetration into the deck. The recommendations presented above increase the deck penetration for 7/8" studs from 2" to 3" in full-depth cast-in-place decks and to 4" for decks with PCPs. For full-depth cast-in-place decks, the finite element studies in Chapter 7 indicate that 2" penetration may not be adequate to meet the stud strength requirements in the 9<sup>th</sup> Ed. AASHTO, but will likely meet the stud strength requirements in the proposed 10<sup>th</sup> Ed. AASHTO. Nonetheless, the finite element studies show there is a significant benefit in increased stud strength and ductility by increasing the deck penetration from 2" to 3". Consequently, it was the judgment of the research team to recommend a minimum deck penetration of 3".

For 7/8" studs in decks with PCPs, the finite element studies indicate that the current minimum deck penetration of 2" combined with the minimum clear distance between the stud and the PCP of 5/8" is not adequate to satisfy the stud strength requirements in the 9<sup>th</sup> Ed. AASHTO. However, these minimum dimensions may be adequate for the proposed 10<sup>th</sup> Ed. AASHTO, although the data is incomplete on this point. Consequently, it was the judgment of the research team to recommend a minimum deck penetration of 4" and a minimum clear distance of 1" from the stud to the edge of the PCP, for 7/8" studs in decks with PCPs.

### 9.3.6. Additional Detailing Recommendations for 1-1/8" Studs

The preliminary design studies reported in Chapter 3 suggest that in many cases, one stud per row is adequate to satisfy AASHTO stud strength and fatigue requirements when using 1-1/8" studs. That is, a single line of studs along the length of the girder may be adequate for many bridges. When using one stud per row, it is recommended to stagger the studs, as shown in Figure 9.3.

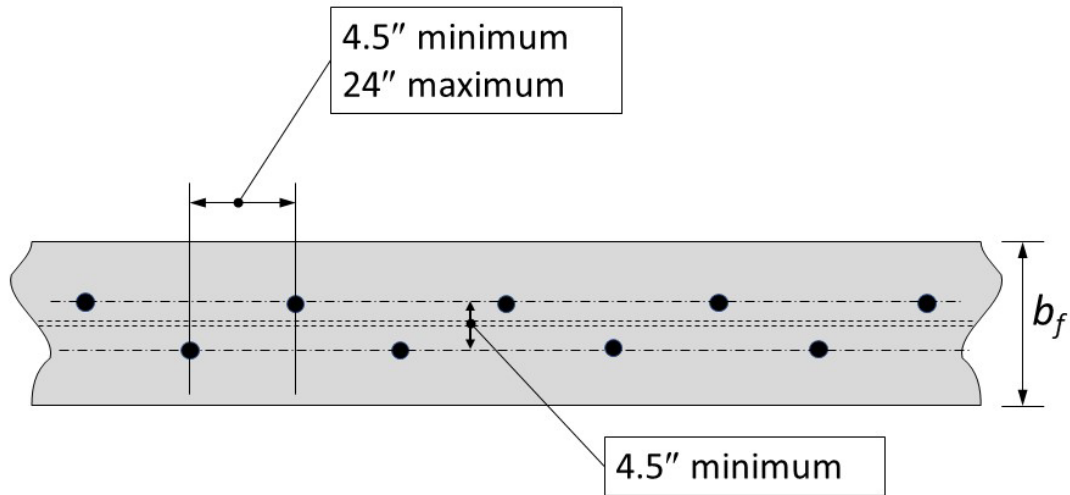


Figure 9.3 – Plan View of Girder Top Flange with Staggered Stud Arrangement

In the static push-out test program reported in Chapter 5, two arrangements of studs with a single stud per row were tested. In one arrangement, no stagger was provided and all studs were placed directly over the web of the girder. In the second arrangement, the studs were staggered. Both showed acceptable performance, although the staggered arrangement showed somewhat better slip capacity. A staggered layout of studs was also used on the large-scale beam specimens described in Chapter 8.

Based on limited data and the judgment of the research team, the staggered layout is recommended. The staggered layout is believed to provide an improved spread of the load transfer between studs and the concrete deck, as compared to a single line of studs without stagger. That is, the staggered layout reduces the likelihood of developing a longitudinal crack along the length of the girder along the single line of studs that is more likely with a single line of studs.

In the push-out tests and in the large-scale beam tests, the transverse distance between lines of studs in the staggered arrangement varied from 3.375" (three stud diameters) to 4.5" (four stud diameters). There was no noticeable difference in performance over this range of transverse spacing. As shown in Figure 9.3, a transverse spacing of 4.5" is recommended for the staggered layout as this satisfies the minimum transverse spacing of four times the stud diameter specified

in both the 9<sup>th</sup> Ed. AASHTO and the proposed 10<sup>th</sup> Ed. AASHTO. Figure 9.3 also shows a minimum pitch of 4.5" which corresponds to the requirement of four stud diameters specified in the proposed 10<sup>th</sup> Ed. AASHTO. The maximum pitch of 24" corresponds to the maximum pitch specified in TxDOT standards (TxDOT 2023).

In cases where one stud per row is not adequate to satisfy AASHTO fatigue or strength requirements, a conventional arrangement of two studs per row can be used, with a minimum transverse spacing of 4.5" (four stud diameters).

### **9.3.7. Effects of PCPs on Composite Steel Girders**

In this research project, both full-depth cast-in-place bridge decks, as well as bridge decks constructed with 4" thick PCPs with a 4.5" cast-in-place topping, were considered. This was the case for the static push-out tests, the parametric finite element studies, and the large-scale beam tests. To the knowledge of the research team, no previous research reported in the literature considered the behavior of composite steel girders constructed with PCP bridge decks of the type used in Texas.

During the course of this research project, two issues were identified in relation to the use of PCPs. These issues pertain not only to 1-1/8" shear studs but also to 7/8" shear studs.

The first issue identified was the impact of the PCPs on the ultimate strength of shear studs. The static push-out tests showed that for decks with PCPs, the ultimate strength of both 7/8" and 1-1/8" shear studs was less than the corresponding specimens constructed with full-depth CIP decks. Further, whereas the strength of the studs in full-depth CIP decks was controlled by stud fracture, the strength of studs in PCP decks was controlled by the development of splitting cracks in the CIP portion of the deck surrounding the shear studs. The effect of PCPs on stud strength was studied in detail in the parametric finite element studies. These studies indicate that studs in decks with PCPs provide an ultimate strength that satisfies both the 9<sup>th</sup> Ed. AASHTO and the proposed 10<sup>th</sup> Ed. AASHTO as long as adequate deck penetration distance and adequate clear distance between the stud and the PCP are provided. The recommended stud penetration distance and clear distance between the stud and the PCP were presented above in Section 9.3.5. These recommendations were followed in the design of large-scale Beam Specimen No. 2 and the studs performed well in this test, with no stud fracture or deck splitting cracks observed in the test, thereby providing at least some degree of validation of these recommendations. Consequently, following the recommendations in Section 9.3.5 is expected to mitigate issues related to the effect of PCPs on stud strength.

The second issue identified concerning the use of PCPs is the impact of the PCPs on the flexural strength of composite steel bridge girders under positive bending moment. The issue of concern is that gaps between PCP panels may prevent the development of a full compressive stress block in the concrete deck as the girder approaches its composite flexural strength. Figure 9.4 shows

qualitative representations of the compressive stress block in a bridge deck constructed with PCPs. In the region away from the gap between PCP panels, a compressive stress block can develop over the full depth of the deck, as typically assumed in the calculation of composite girder flexural strength. However, at the location of a gap between PCP panels, the gap hinders the transfer of compressive stress between adjacent panels. This results in the development of larger compressive stresses in the CIP portion of the deck, and is likely to reduce the flexural strength of the girder.

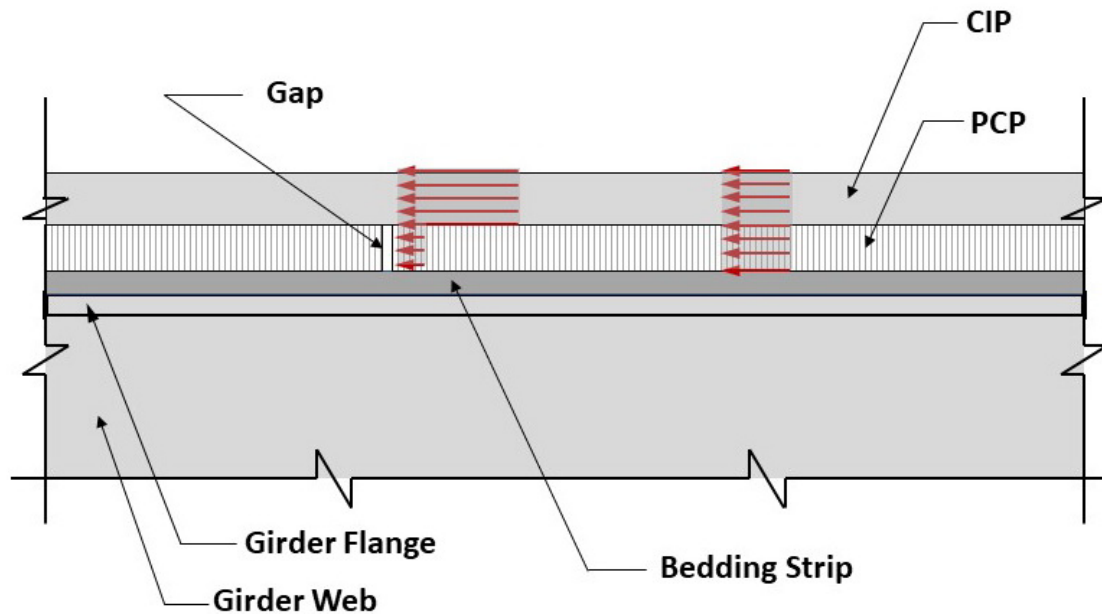


Figure 9.4 – Idealized Representation of the Compressive Stress Block in a Bridge Deck with PCPs

Large-scale Beam Specimen No. 2 in this project was constructed using PCPs. As described in Chapter 8, the ultimate strength of the beam was controlled by crushing of the concrete deck at the location of a gap between PCP panels. The maximum moment developed by the composite beam was approximately 6-percent less than the predicted value for full composite behavior based on standard design equations for composite beams. It is believed this reduction in strength was attributable to the gap between PCP panels. Different geometries in composite steel or prestressed concrete girders may result in larger reductions due to the gap. Note that in the construction of Beam Specimen No. 2, the PCP panels were placed as close to each other as possible, essentially butting up one panel against another. However, because the panels were not perfectly rectangular and because the panel edges were not perfectly straight, it was not possible to completely eliminate the gap.

## 9.4. Proposed Changes to the AASHTO LRFD Bridge Design Specifications

---

This section provides suggested changes to the AASHTO LRFD Bridge Design Specifications (hereinafter referred to as “AASHTO”) to incorporate findings from this research project. These suggested changes are intended for discussion within the appropriate AASHTO technical committees and to support the development of ballot items.

Neither the current 9<sup>th</sup> Ed. AASHTO nor the proposed 10<sup>th</sup> Ed. AASHTO specify any limits on shear stud diameter. Consequently, no changes to AASHTO are needed to enable the use of 1-1/8” shear studs. However, changes are needed to AASHTO to incorporate the detailing recommendations presented in Sections 9.3.5 and 9.3.6 above.

At the time this report was prepared, the 10<sup>th</sup> Ed. AASHTO had been fully balloted, but not yet published. However, the research team had access to ballot items pertaining to changes to shear stud requirements (AASHTO 2021) and it is the understanding of the research team that these ballot items have been approved and are therefore likely to appear in the 10<sup>th</sup> Ed. AASHTO. Thus, the changes proposed below are intended to be changes to the 10<sup>th</sup> Ed. AASHTO as shown in the draft changes provided in AASHTO 2021.

### AASHTO 6.10.10.1.3 – Transverse Spacing

10<sup>th</sup> Ed. AASHTO:

Stud shear connectors placed transversely across the top flange of the steel section shall not be closer than 4.0 stud diameters center-to-center transverse to the longitudinal axis of the supporting member.

The clear distance between the edge of the top flange and the edge of the nearest shear connector shall be not less than 1.0 in.

Proposed change:

Stud shear connectors placed transversely across the top flange of the steel section shall not be closer than 4.0 stud diameters center-to-center transverse to the longitudinal axis of the supporting member.

When one shear connector per row is used, the shear connectors shall be placed using a staggered pattern, where the distance between lines of shear connectors shall be at least 4.0 stud diameters transverse to the longitudinal axis of the supporting member.

The clear distance between the edge of the top flange and the edge of the nearest shear connector shall be not less than 1.0 in.



### AASHTO C6.10.10.1.3

10<sup>th</sup> Ed. AASHTO:

Large- and small scale experimental testing has shown that shear studs can be spaced at a 4.0 stud diameter center-to-center transverse spacing with no reduction in strength or fatigue resistance (Provines et al. 2019).

Proposed change:

Large- and small scale experimental testing has shown that shear studs can be spaced at a 4.0 stud diameter center-to-center transverse spacing with no reduction in strength or fatigue resistance (Provines et al. 2019).

Recent research (reference to 0-7042 final report) on 1-1/8" diameter shear studs has shown that in many cases, AASHTO stud strength and fatigue requirements can be met using one stud per row. For such cases, a staggered arrangement of studs is preferred, as shown in Figure C6.10.10.1.3.1. The staggered layout is believed to better spread the load transfer between studs and the concrete deck, as compared to a single line of studs without stagger. That is, the staggered layout avoids having a straight line of studs in the concrete deck that may create a longitudinal crack along the length of the girder along the single line of studs.

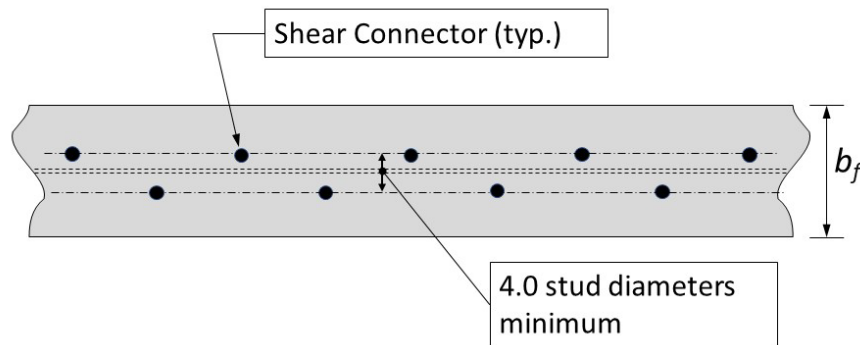


Figure C6.10.10.1.3.1 – Plan View of Top Flange of Girder with Staggered Shear Connector Layout

### AASHTO 6.10.10.1.4 – Cover and Penetration

10<sup>th</sup> Ed. AASHTO:

The clear depth of concrete cover over the tops of the shear connectors should not be less than 2.0 in. Shear connectors should be detailed to penetrate at least 2.0 in. into the concrete deck. Shear connectors on members in structures that are not load-path

redundant shall be detailed to penetrate at least above the bottom mat of deck reinforcement.

Proposed change:

The clear depth of concrete cover over the tops of the shear connectors ~~should~~ shall not be less than 2.0 in. Shear connectors ~~should~~ shall be detailed to penetrate at least ~~2.0~~ 3.0 in. into the concrete deck. Shear connectors on members in structures that are not load-path redundant shall be detailed to penetrate at least above the bottom mat of deck reinforcement.

When the bridge deck consists of partial-depth precast deck panels with a cast-in-place topping, shear connectors shall be detailed to penetrate at least 4.0 in. into the concrete deck relative to the bottom of the partial-depth precast deck panels. In addition, shear connectors shall be detailed so that the horizontal clear distance between the head of the stud and the edge of the precast panel is at least 1.0 in. for 7/8 in. diameter shear connectors and at least 2.0 in. for shear connector diameters greater than 7/8 in. For shear connector diameters greater than 7.8 in., the horizontal clear distance between the head of the stud and the edge of the precast panel may be reduced to 1.0 in. if the shear connectors are detailed to penetrate at least 5.0 in. into the concrete deck.

## 9.5. Proposed Changes to the AASHTO/AWS D1.5 Bridge Welding Code

---

This section provides suggested changes to the AASHTO/AWS D1.5 Bridge Welding Code (hereinafter referred to as “AWS D1.5”) to incorporate findings from this research project. These suggested changes are intended for discussion within the appropriate AASHTO and AWS technical committees and to support the development of ballot items. Suggested changes are in reference to the 2020 version of AWS D1.5 (AWS 2020).

Table 9.1 – Footnote b:

AWS D1.5: 2020:

Type B studs shall be studs that are headed, bent, or of other configuration in 12 mm [1/2 in] through 23 mm [7/8 in] diameter that are used as an essential component in composite beam design and construction.

Proposed change:

Type B studs shall be studs that are headed, bent, or of other configuration in 12 mm [1/2 in] through ~~23 mm [7/8 in]~~ 29 mm [1-1/8 in] diameter that are used as an essential component in composite beam design and construction.

Figure 9.1

Proposed change:

Add the following row to the table in Figure 9.1:

<b>Standard Dimensions, mm [in]</b>				
<b>Shank Diameter (C)</b>		<b>Length Tolerance (L)</b>	<b>Head Diameter (H)</b>	<b>Minimum Head Height (T)</b>
28.6	+0.00	$\pm 1.6$	$47.6 \pm 0.4$	14.3
[1-1/8]	-0.38 [-0.015]	[ $\pm 1/16$ ]	[1-7/8 $\pm 1/64$ ]	[9/16]

As described in Section 9.3.3 above, there is nothing in this research project to suggest that the head dimensions played a critical role in the ultimate strength or fatigue resistance of the studs. Thus, the head dimensions as well as all tolerances suggested above for 1-1/8" studs should be considered as an initial starting point but require the input of stud manufacturers to determine what is practical considering stud manufacturing processes.

## 9.6. Value of Research

This section provides a discussion of the value of research for Project 0-7042, as required by the Texas Department of Transportation. The primary outcome of Project 0-7042 is the information, technology, and detailed design recommendations needed to implement the use of 1-1/8" diameter shear studs in composite steel bridges in Texas. Based on the outcome of this project, the research team believes that 1-1/8" diameter shear studs can be implemented immediately in the design and construction of new composite steel girder bridges in Texas, using the design recommendations presented earlier in this chapter.

As discussed in Chapter 1 of this report, the primary motivation for pursuing research on larger-diameter shear studs was to reduce the number of shear studs needed on a composite steel girder. Currently, composite steel girder bridges in Texas and most of the U.S. use 7/8" diameter shear studs. A very large number of 7/8" diameter shear studs are typically needed to satisfy shear stud strength and fatigue requirements in the AASHTO LRFD Bridge Design Specifications. Using 1-1/8" diameter shear studs will reduce the number of studs on a steel girder by about 40-percent, as compared to the use 7/8" diameter shear studs. This will significantly reduce the congestion of shear studs on the top flange of a steel girder.

An important benefit of reducing the number of shear studs on a girder is that additional space is available on the top flange to support partial-depth precast concrete deck panels (PCPs). Texas has not traditionally used PCPs in the construction of the decks of composite steel girder bridges. Rather, full-depth cast-in-place decks have typically been used. Prior to placing a full-depth cast-in-place deck, permanent metal deck forms (PMDF) are first installed. The PMDF spans between girders and serves as the formwork to support the concrete deck during placement. The PMDF is attached to the girders through the use of cold-formed angles that are attached to the edge of the girder top flanges. The cold-formed angles are used to control the elevation of the PMDF. The PMDF and cold-formed angles are costly items that serve no purpose once the concrete hardens. That is, after construction is completed, the PMDF serves no structural purpose or other purpose for the service life of the bridge.

Constructing a bridge deck with PCPs can reduce both the time and cost of constructing a bridge. PMDF and cold-formed angles are not needed when PCPs are used. PCPs, which span between girders, are placed on relatively inexpensive foam bedding strips attached to the edge of the top flange of a girder. The foam bedding strips support the PCPs during construction and can be used to adjust the elevation of the PCPs. After placement of the PCPs, a layer of cast-in-place concrete is placed over the PCPs to complete the bridge deck. Like PMDF, the PCPs serve as formwork to support the cast-in-place layer of concrete. However, unlike PMDF, the PCPs become a structurally integral part of the bridge deck. Thus, the PCPs serve the dual purpose of acting as formwork and also as serving a structural portion of the bridge deck.

Bridge decks constructed using PCPs have been successfully used for many years in Texas for prestressed concrete girder bridges. The majority of these applications have been for straight simple-span bridges. In contrast, steel girder bridges in Texas are often curved and often have multiple continuous spans with regions of negative moment over interior supports. Both of these characteristics raised concerns regarding the use of PCPs on steel girder bridges. Previously, there were concerns regarding the stability of PCPs on curved bridges during construction. These concerns were addressed through research conducted in TxDOT Project 0-6816 (*Partial Depth Concrete Panels on Curved Steel Bridges*) which developed recommendations for the use of PCPs on curved steel bridges. For continuous multiple-span bridges, there was previously inadequate guidance on the amount of deck reinforcement needed in the cast-in-place layer above the PCPs in regions of negative moment to control deck cracking. This issue was addressed in TxDOT Project 0-6909 (*Designing for Deck Stress Over Precast Panels in Negative Moment Regions*) which developed guidelines for designing reinforcement in negative moment regions for decks constructed with PCPs.

An additional issue of concern regarding the use of PCPs on steel girder bridges is the space needed on the girder top flange to support the PCPs. The recommended overlap distance between the edge of the PCP and the outer edge of a steel girder flange is 5" for girder flange widths greater than 18". With a PCP supported from both edges of the flange, 10" of the flange is

covered by PCPs, leaving less space for the placement of shear studs. The use of 1-1/8" shear studs, as developed in this research project, essentially eliminates space conflicts on the top flange between the shear studs and the PCPs, thereby facilitating the use of PCPs on steel girder bridges.

The results of Project 0-7042, combined with the results of previous TxDOT Projects 0-6816 and 0-6909, enable the use of PCPs on a wide range of steel girder bridges in Texas. This includes straight and curved bridges, simple and continuous span bridges, and I-girder and tub-girder bridges. The use PCPs on steel girder bridges in Texas is expected to reduce the cost and construction time for steel girder bridges.

Facilitating the use of PCPs is considered to be the primary benefit of Project 0-7042. However, the significant reduction in the number of shear studs on steel girder flanges when 1-1/8" diameter shear studs are used is also expected to enhance construction worker safety. During erection and the early stages of construction, before PMDF or PCPs have been placed, workers must walk on the top flange of the steel girders. Shear studs are tripping hazards for workers, and large numbers of studs make walking safely on the girder flanges more difficult. Reducing the number of shear studs reduces the number of tripping hazards, thereby enhancing construction worker safety.

An additional benefit of using 1-1/8" diameter shear studs is expected to be a reduction in the time required to attach shear studs to the girder flange. The time required to weld a shear stud is largely independent of the diameter of the shear stud. Thus, the 40-percent reduction in the number of studs when 1-1/8" diameter shear studs are used will reduce the time needed to weld studs on a steel girder flange.

More broadly, Project 0-7042 has added to the body of knowledge and the tools available to designers of steel girder bridges. Also, while the focus of this project was composite steel girder bridges in Texas, the results of this project should benefit the design and construction of composite steel girder bridges in other states.

## References

- AASHTO. 2021. *Bridge Committee Agenda Item, LRFD Bridge Design Specifications: Section 6, Various Articles, T-14 Structural Steel Design, June 2, 2021*. American Association of State Highway and Transportation Officials.
- . 2020. *LRFD Bridge Design Specifications*. 9th. American Association of State Highway and Transportation Officials.
- Abaqus. 2016. *Abaqus Analysis User's Guide Version 6.16*. Dassault Systemes.  
<http://130.149.89.49:2080/v2016/books/usb/default.htm>.
- . 2015. *Abaqus Lecture 5: Quasi-Static Analysis*. Accessed May 10, 2023.  
<https://imechanica.org/files/l5-quasi-static.pdf>.
- AISC. 2022. *Specification for Structural Steel Buildings. ANSI/AISC 360-22*. American Institute of Steel Construction.
- . 2017. *Steel Construction Manual, 15th Edition*. American Institute of Steel Construction.
- ASTM. 2022. *Standard Test Methods and Definitions for Mechanical Testing of Steel Products, ASTM 370-22*. American Society for Testing and Materials.
- AWS. 2020. *Bridge Welding Code. AASHTO/AWS D1.5*. American Welding Society.
- . 2020. *Structural Welding Code - Steel. AWS D1.1/D1.1M:2020*. American Welding Society.
- . 1991. *Welding Handbook*. 8th Edition. American Welding Society.
- Badie, S., A. Girgis, M. Tadros, and N. Nguyen. 2007. "Development and Application of Large-Size Shear Studs to Steel Girder Bridges." *Engineering Journal* (American Institute of Steel Construction) (Second Quarter): 79-90.
- Badie, S., A. Morgan Girgis, M. Tadros, Sriboonma, and K. 2011. "Full-Scale Testing for Composite Slab/Beam Systems Made with Extended Stud Spacing." *Journal of Bridge Engineering* 16 (5): 653-661.
- Badie, S., M. Tadros, H. Kakish, D. Splittgerber, and M. Baishya. 2002. "Large Studs for Composite Action in Steel Bridge Girders." *Journal of Bridge Engineering* (American Society of Civil Engineers) 7 (3).
- Bonilla, J., L. Bezerra, and B. Massicotte. 2018. "Review of stud Shear Resistance Prediction in Steel-Concrete Composite Beams." *Steel and Composite Structures* (Techno Press) 27 (3): 355-370.
- Burchnall, D. 2014. *Formulation and Validation of a Nonlinear Shell Element for the Analysis of Reinforced Concrete and Masonry Structures*. Ph.D. Dissertation, Virginia Tech University.
- Cai, W. 2015. *Steel Fracture Modeling at Elevated Temperature for Structural-Fire Engineering Analysis*. Ph.D. Dissertation, University of Texas at Austin.
- Cao, J., and X. Shao. 2019. "Finite Element Analysis of Headed Studs Embedded in Thin UHPC." *Journal of Constructional Steel Research* 161 (2): 355-368.
- CEN. 2004. "Eurocode 4: Design of Composite Steel and Concrete Structures, Part 1-1: General Rules for Buildings; EN 1994-1-1." Brussels, Belgium: European Committee on Standardization (CEN), Brussels, Belgium.
- Chambers, H. 2001. "Principles and Practices of Stud Welding." *PCI Journal* (Pecast-Prestressed Concrete Institute).
- Chapman, J.C., and S. Balakrishnan. 1964. "Experiments on Composite Beams." *The Structural Engineer* 42 (11): 369-383.
- CSI. 2022. *CSI Bridge Users Manual*. Computers & Structures, Inc.



- Dara, S. 2015. *Behavior of Shear Studs in Composite Beams at Elevated Temperatures*. Ph.D. Dissertation, University of Texas at Austin.
- Deng, X., I. Koutomanos, J. Murcia-Delso, and M. Panagiotou. 2021. "Nonlinear Truss Models for Strain-Based Seismic Evaluation of Planar RC Walls." *Earthquake Engineering and Structural Dynamics* 50 (11): 2939-2960.
- Driscoll, G., and R. Slutter. 1961. "Research on Composite Design at Lehigh University." *AISC National Engineering Conference*. Minneapolis: American Institute of Steel Construction.
- Drucker, D., and W. Prager. 1952. "Soil Mechanics and Plastic Analysis for Limit Design." *Quarterly of Applied Mathematics* 10 (2): 157-165.
- El-lobody, E. 2002. *Finite Element Modeling of Shear Connection for Steel-Concrete Composite Girders*. Ph.D. Thesis, University of Leeds.
- Fallaha, S., C. Sun, M. Lafferty, and M. Tadros. 2004. "High Performance Precast Concrete NUDECK Panel System for Nebraska's Skyline Bridge." *PCI Journal* 49 (5): 40-50.
- Ge, X., K. Munsterman, X. Deng, M. Reichenbach, S. Park, T. Helwig, M. Engelhardt, E. Williamson, and O. Bayrak. 2021. *Designing for Deck Stress Over Precast Panels in Negative Moment Regions*. Report No. 0-6909-1/5-6909-01-1, Center for Transportation Research, University of Texas at Austin.
- Ghiami Azad, A.R. 2016. "Fatigue Behavior of Post-installed Shear Connectors used to Strengthen Continuous Non-Composite Steel Bridge Girders." Ph.D. Dissertation, University of Texas at Austin.
- Goble, G. 1968. "Shear Strength of Thin Flange Composite Specimens." *AISC Engineering Journal* (American Institute of Steel Construction) 5: 62-65.
- Hancock, J., and A. Mackenzie. 1976. "On the Mechanisms of Ductile Failure in High-Strength Steels Subjected to Multi-Axial Stress-States." *Journal of the Mechanics and Physics of Solids* 24 (2-3): 147-160.
- Hognestad, E. 1951. *A study of Combined Bending and Axial Load in Reinforced Concrete Members; Bulletin Series No. 399*. University of Illinois Engineering Experiment Station.
- Hooputra, H., H. Gese, H. Dell, and H. Werner. 2004. "A Comprehensive Failure Model for Crashworthiness Simulation of Aluminum Extrusions." *International Journal of Crashworthiness* 9 (5): 449-464.
- Hu, Y., H. Yin, X. Ding, S. Li, and J. Wang. 2020. "Shear Behavior of Large Stud Shear Connectors Embedded in Ultra-High-Performance Concrete." *Advances in Structural Engineering* 23 (16): 3401-3414.
- Hull, D., and T. Clyne. 1996. *An Introduction to Composite Materials*. 2nd. Cambridge University Press.
- ISO. 2017b. *Arc Stud Welding of Metallic Materials, ISO Standard 14555*. International Standards Organization.
- . 2017a. *Studs and Ceramic Ferrules for Arc Stud Welding, ISO Standard 13918*. International Standards Organization.
- Jones, C. 2019. *A Method for Developing the True Stress-Strain Relationship for Structural Steels based on Tension Coupon Tests*. Ph.D. Dissertation, University of Texas at Austin.
- Kakish, H. 1997. *Composite Action in Bridge Girder Systems*. Ph.D. Dissertation. University of Nebraska.

- Karthik, M., and J. Mander. 2011. "Stress-Block Parameters for Unconfined and Confined Concrete Based on a Unified Stress-Strain Model." *Journal of Structural Engineering* 137 (2): 270-273.
- Kayir, H. 2006. *Methods to Develop Composite Action in Non-Composite Bridge Floor Systems: Fatigue Behavior of Post-Installed Shear Connectors*. M.S. Thesis. University of Texas at Austin.
- Koutromanos, I. 2018. *Fundamentals of Finite Element Analysis: Linear Finite Element Analysis*. Wiley.
- . 2014. *Nonlinear Finite Element Analysis Notes*. Virginia Tech University.
- Kreitman, K., A. Ghiami Azad, H. Patel, M. Engelhardt, T. Helwig, E. Willaimson, and R. KLingner. 2016. *Strengthening Existing Continuous Non-composite Steel Girder Bridges using Post-installed Shear Connectors*. Research Report No. 0-6719-1, Center for Transportation Research, University of Texas at Austin.
- Kruszewski, D., E. Zaghi, and K. Wille. 2019. "Finite Element Study of Headed Shear Stud Embedded in Ultra-High Performance Concrete." *Engineering Structures* 188: 538-552.
- Kulak, G., J. Fisher, and J. Struik. 2001. *Guide to Design Criteria for Bolted and Riveted Joints*. Research Council on Structural Connections and American Institute of Steel Construction.
- Kwon, G., B. Hungerford, H. Kayir, B. Schaap, Y.K. Ju, R. Klingner, and M. Engelhardt. 2007. *Strengthening Existing Non-composite Steel Bridge Girders using Post-installed Shear Connectors*. Research Report No. 0-4124-1, Center for Transportation Research, University of Texas at Austin.
- Lee, J., and G. Fenves. 1998. "Plastic-Damage Model for Cyclic Loading of Concrete Structures." *Journal of Engineering Mechanics* 124 (8): 892-900.
- Lee, P., C. Shim, and S. Chang. 2005. "Static and Fatigue Behavior of Large Stud Shear Connectors for Steel-Concrete Composite Bridges." *Journal of Constructional Steel Research* 61 (9): 1270-1285.
- Lienert, T., V. Acoff, S. Babu Sudarsanam, and T. Siewart. 2011. *Stud Arc Welding, In ASM Handbook*. Vol. 06A. ASM International.
- Lin, Z., and Y. Liu. 2015. "Experimental Study on Shear Behavior of Large Stud Connectors." *Journal of Tongji University (Natural Science)* 43 (12): 1788-1793.
- Linnert, George, E. 1965. *Welding Metallurgy*. American Welding Society.
- Lu, Y., and M. Panagiotou. 2014. "Three-Dimensional Cyclic Beam-Truss Model for Nonplanar Reinforced Concrete Walls." *Journal of Structural Engineering* 140 (3).
- Lubliner, J., J. Oliver, and E. Onate. 1989. "A Plastic-Damage Model for Concrete." *International Journal of Solids and Structures* 25 (3): 299-326.
- Mander, J., N. Priestley, and R. Park. 1988. "Theoretical Stress-Strain Model for Confined Concrete." *Journal of Structural Engineering* 114 (8): 1804-1826.
- Mia, M., and A. Bhowmick. 2017. "Static Strength of Headed Shear Stud Connectors using Finite Element Analysis." *6th International Conference on Engineering Mechanics and Materials*. Vancouver, Canada: Canadian Society of Civil Engineering.
- Midwest Fasteners. 2019. "Arc Stud Weld Inspection (Visual)." Accessed June 2023. [https://midwestfasteners.wpenginepowered.com/wp-content/uploads/pdf/arc\\_stud\\_weld\\_visual\\_inspection.pdf](https://midwestfasteners.wpenginepowered.com/wp-content/uploads/pdf/arc_stud_weld_visual_inspection.pdf).
- Moharrami, M., and I. Koutromanos. 2016. "Triaxial Constitutive Model for Concrete under Cyclic Loading." *Journal of Structural Engineering* 142 (7).

- Mundie, D. 2011. *Fatigue Testing and Design of Large Diameter Shear Studs Used in Highway Bridges*. M.S. Thesis. Auburn University.
- Murphy, K. 2012. *Machine Learning: A Probabilistic Perspective*. The MIT Press.
- Nelson Stud Welding. 2008a. "Nelweld 4000 and 6000 Operations and Service Manual." June. Accessed June 2023. <https://www.stanleyengineeredfastening.com/-/media/Web/SEF/Resources/Docs/Nelson/Nelson-Nelweld-Operating-Manual.pdf>.
- . 2008b. "NS20A & NS20N Heavy Duty Floating Lift Weld Guns - Instruction and Maintenance Manual." Accessed June 2023. <https://www.stanleyengineeredfastening.com/-/media/Web/SEF/Resources/Docs/Nelson/Nelson-NS20-HD-Gun-Operating-Manual.pdf>.
- Nguyen, H., and S. Kim. 2009. "Finite Element Modeling of Push-Out Tests for Large Stud Shear Connectors." *Journal of Constructional Steel Research* 65 (10): 1909-1920.
- NSBA. 2022. *Steel Bridge Design Handbook*. National Steel Bridge Alliance. <https://www.aisc.org/nsba/design-and-estimation-resources/steel-bridge-design-handbook/>.
- Ollgaard, J., R. Slutter, and J. Fisher. 1971. "Shear Strength of Stud Connectors in Lightweight and Normal-Weight Concrete." *Engineering Journal - AISC* (American Institute of Steel Construction).
- Ollgaard, J., R. Slutter, and J. Fisher. 1971. "Shear Strength of Stud Connectors in Lightweight and Normal-Weight Concrete." *Engineering Journal - AISC* (American Institute of Steel Construction) 8 (No. 2): 55-64.
- Pallares, L., and J.F. Hajjar. 2010. "Headed Steel Stud Anchors in Composite Structures, Part I: Shear." *Journal of Constructional Steel Research* 66: 198-212.
- Patel, H.V. 2013. *Strengthening of Non-composite Steel Girders with Post-Installed Shear Connectors: Fatigue Behavior of the Adhesive Anchor*. M.S. Thesis - University of Texas at Austin.
- Provines, J.T., J.M. Ocel, and K. Zmetra. 2019. *Strength and Fatigue Resistance of Clustered Shear Stud Connectors in Composite Steel Girders, Report FHWA-HRT-20-005*. Federal Highway Administration.
- Rabbat, B., and H. Russell. 1985. "Friction Coefficient of Steel on Concrete and Grout." *Journal of Structural Engineering* 111 (3): 505-515.
- Shim, C., P. Lee, and T. Yoon. 2004. "Static Behavior of Large Shear Stud Connectors." *Engineering Structures* 26 (12): 1853-1860.
- Slutter, R.G., and J.W. Fisher. 1966. *Fatigue Strength of Shear Connectors, Report No. 316.2*. Fritz Engineering Laboratory, Lehigh University.
- Thurlimann, B. 1959. "Fatigue and Static Strength of Stud Shear Connectors." *Journal of the American Concrete Institute* (American Concrete Institute) 30 (12): 1287-1302.
- TxDOT. 2023. "Bridge Design Manual - LRFD." *Texas Department of Transportation - Bridge Division*. January. Accessed April 7, 2023. <http://onlinemanuals.txdot.gov/txdotmanuals/lrf/lrf.pdf>.
- TxDOT. 2022. *Bridge Detailing Guide*. Texas Department of Transportation.
- . 2019. "Miscellaneous Details: Steel Girders and Beams - SGMD." *Texas Department of Transportation - Bridge Division*. April. Accessed April 7, 2023. <https://ftp.dot.state.tx.us/pub/txdot-info/cmd/cserve/standard/bridge/spgdste1-19.pdf>.

- . 2019a. "Miscellaneous Details: Steel Griders and Beams - SGMD." *Texas Department of Transportation - Bridge Division*. April. Accessed April 7, 2023.  
<https://ftp.dot.state.tx.us/pub/txdot-info/cmd/cserve/standard/bridge/spgdste1-19.pdf>.
- . 2021. "Preferred Practices for Steel Bridge Design, Fabrication, and Erection, November 2021." *Texas Department of Transportation*. Accessed April 7, 2023.  
[https://ftp.dot.state.tx.us/pub/txdot-info/library/pubs/bus/bridge/steel\\_bridge.pdf](https://ftp.dot.state.tx.us/pub/txdot-info/library/pubs/bus/bridge/steel_bridge.pdf).
- . 2019b. "Prestressed Concrete Deck Panels - PCP." *Texas Department of Transportation - Bridge Division*. Accessed June 2023. <https://ftp.dot.state.tx.us/pub/txdot-info/cmd/cserve/standard/bridge/MS-PCP-23.pdf>.
- . 2015. "Prestressed Concrete Panel Fabrication Details - PCP-FAB." *Texas Department of Transportation - Bridge Division*. January. Accessed April 7, 2023.  
<https://ftp.dot.state.tx.us/pub/txdot-info/cmd/cserve/standard/bridge/pcpstde2.pdf>.
- . 2019c. "Prestressed Concrete Panel Fabrication Details - PCP-FAB." *Texas Department of Transportation - Bridge Division*. January. Accessed April 7, 2023.  
<https://ftp.dot.state.tx.us/pub/txdot-info/cmd/cserve/standard/bridge/pcpstde2.pdf>.
- Viest, I. 1956. "Investigation of Shear Stud Connectors for Composite Concrete and Steel T-Beams." *Journal of the American Concrete Institute* 27 (8): 875-891.
- Wang, J., X. Qizhi, Y. Yao, J. Qi, and H. Xiu. 2018. "Static Behavior of Grouped Large Headed Stud-UHPC Shear Connectors in Composite Structures." *Composite Structures* 206: 202-214.
- Wang, Q., T. Tong, Q. Xu, and H. Xiu. 2019. "Static Behavior of Large Stud Shear Connectors in Steel-UHPC Composite Structures." *Engineering Structures* 178: 534-542.
- Wosatko, A., A. Winnicki, M. Polak, and J. Pamin. 2019. "Role of Dilatancy Angle in Plasticity-Based Models of Concrete." *Archives of Civil and Mechanical Engineering* 19: 1268-1283.
- Xue, D., Y. Liu, Z. Yu, and J. He. 2012. "Static Behavior of Multi-stud Shear Connectors for Steel-Concrete Composite Bridge." *Journal of Construction Steel Research* (Elsevier) 74: 1-7.
- Zona, A., and G. Ranzi. 2014. "Shear Connection Slip Demand in Composite Steel-Concrete Beams with Solid Slabs." *Journal of Constructional Steel Research* 102: 266-281.